Springer Series on Fluorescence 17
Series Editor: Martin Hof

David M. Jameson *Editor*

Perspectives on Fluorescence

A Tribute to Gregorio Weber

Springer

17
Springer Series on Fluorescence

Methods and Applications

Series Editor: Martin Hof

Springer Series on Fluorescence

Series Editor: Martin Hof

Recently Published and Forthcoming Volumes

Perspectives on Fluorescence
A Tribute to Gregorio Weber
Volume Editor: David M. Jameson
Vol. 17, 2016

Fluorescence Studies of Polymer Containing Systems
Volume Editor: Karel Procházka
Vol. 16, 2016

Advanced Photon Counting
Volume Editors: Peter Kapusta, Michael Wahl and Rainer Erdmann
Vol. 15, 2015

Far-Field Optical Nanoscopy
Volume Editors: Philip Tinnefeld, Christian Eggeling and Stefan W. Hell
Vol. 14, 2015

Fluorescent Methods to Study Biological Membranes
Volume Editors: Y. Mély and G. Duportail
Vol. 13, 2013

Fluorescent Proteins II
Application of Fluorescent Protein Technology
Volume Editor: G. Jung
Vol. 12, 2012

Fluorescent Proteins I
From Understanding to Design
Volume Editor: G. Jung
Vol. 11, 2012

Advanced Fluorescence Reporters in Chemistry and Biology III
Applications in Sensing and Imaging
Volume Editor: A.P. Demchenko
Vol. 10, 2011

Advanced Fluorescence Reporters in Chemistry and Biology II
Molecular Constructions, Polymers and Nanoparticles
Volume Editor: A.P. Demchenko
Vol. 9, 2010

Advanced Fluorescence Reporters in Chemistry and Biology I
Fundamentals and Molecular Design
Volume Editor: A.P. Demchenko
Vol. 8, 2010

Lanthanide Luminescence
Photophysical, Analytical and Biological Aspects
Volume Editors: P. Hänninen and H. Härmä
Vol. 7, 2011

Standardization and Quality Assurance in Fluorescence Measurements II
Bioanalytical and Biomedical Applications
Volume Editor: Resch-Genger, U.
Vol. 6, 2008

Standardization and Quality Assurance in Fluorescence Measurements I
Techniques
Volume Editor: U. Resch-Genger
Vol. 5, 2008

Fluorescence of Supermolecules, Polymeres, and Nanosystems
Volume Editor: M.N. Berberan-Santos
Vol. 4, 2007

Fluorescence Spectroscopy in Biology
Volume Editor: M. Hof
Vol. 3, 2004

Fluorescence Spectroscopy, Imaging and Probes
Volume Editor: R. Kraayenhof
Vol. 2, 2002

New Trends in Fluorescence Spectroscopy
Volume Editor: B. Valeur
Vol. 1, 2001

More information about this series at http://www.springer.com/series/4243

Perspectives on Fluorescence

A Tribute to Gregorio Weber

Volume Editor:
David M. Jameson

With contributions by

L.A. Bagatolli · F.J. Barrantes · L. Betts · P. Bianchini · L. Brand · F. Cardarelli · M. Castello · P.L.-G Chong · R.N. Day · A.P. Demchenko · A. de Silva · A. Diaspro · E. Gratton · K. Jacobson · D.M. Jameson · T.M. Jovin · J.R. Knutson · L. Lanzanò · P. Liu · G. Marriott · G.D. Reinhart · M. Ridilla · C.A. Royer · L. Scipioni · R.P. Stock · N.L. Thompson · H. van Amerongen · A. van Hoek · G. Vicidomini · A.J.W.G. Visser · N.V. Visser · J. Xu

Springer

Volume Editor
David M. Jameson
John A. Burns School of Medicine
University of Hawaii at Manoa
Honolulu
Hawaii, USA

ISSN 1617-1306 ISSN 1865-1313 (electronic)
Springer Series on Fluorescence
ISBN 978-3-319-41326-6 ISBN 978-3-319-41328-0 (eBook)
DOI 10.1007/978-3-319-41328-0

Library of Congress Control Number: 2016949376

Printed on acid-free paper

This Springer imprint is published by Springer Nature
The registered company is Springer International Publishing AG Switzerland

Series Editor

Prof. Dr. Martin Hof

Academy of Sciences of the Czech Republic
J. Heyrovsky Institute of Physical Chemistry
Department of Biophysical Chemistry
Dolejskova 3
16223 Prague 8
Czech Republic
martin.hof@jh-inst.cas.cz

Aims and Scope

Fluorescence spectroscopy, fluorescence imaging and fluorescent probes are indispensible tools in numerous fields of modern medicine and science, including molecular biology, biophysics, biochemistry, clinical diagnosis and analytical and environmental chemistry. Applications stretch from spectroscopy and sensor technology to microscopy and imaging, to single molecule detection, to the development of novel fluorescent probes, and to proteomics and genomics. The *Springer Series on Fluorescence* aims at publishing state-of-the-art articles that can serve as invaluable tools for both practitioners and researchers being active in this highly interdisciplinary field. The carefully edited collection of papers in each volume will give continuous inspiration for new research and will point to exciting new trends.

Preface

During the last few decades, fluorescence spectroscopy has evolved from a narrow, highly specialized technique into an important discipline widely utilized in the biological, chemical, and physical sciences. As in all scientific disciplines, the development of modern fluorescence spectroscopy has benefited from the contributions of many individuals from many countries. However, one individual, *Gregorio Weber*, can be singled out for his outstanding and far-reaching contributions to this field.

Gregorio Weber was born in Argentina on July 4, 1916. He died of leukemia on July 18, 1996. His death ended a remarkable and amazingly productive scientific career, which began in Buenos Aires, developed in England at Cambridge and Sheffield, and flourished at the University of Illinois at Urbana-Champaign. His contributions to the fields of fluorescence spectroscopy and protein chemistry are still evident and significant yet many young people entering these fields may not realize the debt they owe to his pioneering efforts. This book is intended to recognize the 100th anniversary of his birth. This project began several years ago when I was approached by Martin Hof and Otto Wolfbeis to organize this volume. To this end, I invited a number of distinguished researchers to take time away from their already busy schedules and write a chapter outlining a particular aspect of fluorescence spectroscopy, indicating how Gregorio Weber had influenced the field and their own approach to the work. Many of these authors had worked directly with Gregorio Weber, either as students, postdocs, or scientists visiting his lab. I believe that these collected chapters will not only offer the reader valuable and informative insights into the application of fluorescence methodologies to a wide variety of systems but will also serve to emphasize the debt that all of us working with fluorescence owe to Gregorio Weber.

The first four chapters (Jameson, Barrantes, Jovin, Visser) focus largely on the life and science of Gregorio Weber. Jameson summarizes and recounts Weber's scientific career pointing out his contributions to fluorescence spectroscopy as well as to protein chemistry. Barrantes provides a marvelously detailed look into

Weber's formative years in Argentina – before he left for England. Jovin follows Weber's life from childhood to scientific eminence, discussing many of the major personalities and influences along the way. Visser gives a personal account of his time as a postdoc at UIUC in Weber's lab and his work there on the application of high pressure to flavinyl tryptophan compounds and flavodoxin proteins.

Several chapters focus on spectroscopy, in particular the application of fluorescence spectroscopy to biophysical subjects. Gratton presents a compelling personal account of the development of frequency domain fluorometry and the pivotal influence Gregorio Weber had on his approach to this research. Visser and his co-authors discuss the ultrafast decay of fluorescence anisotropy of NATA, while Demchenko gives an extensive and detailed account of Weber's red-edge effect and its significance to fluorescence spectroscopy in general and to protein dynamics in particular. Day discusses modern approaches to fluorescent lifetime imaging, while Xu and Knutson discuss the impact of laser developments on fluorescence spectroscopy.

Two chapters concern applications of fluorescence probes to study cell membranes as well as cellular interiors. Chong describes the use of fluorescence to elucidate membrane lateral organization, while Bagatolli and Stock apply 6-acyl-2-(dimethylamino)naphthalenes as relaxation probes of biological environments to elucidate aspects of water dynamics in cellular interiors.

Four chapters focus on proteins, in and out of cells. Reinhart presents an engaging discussion of his early connections to the Weber lab and how Weber's work on the thermodynamics of protein interactions inspired his own studies on allosteric enzymes. Royer describes how fluorescence can be applied to characterize the molecular and energetic basis for the role of protein interactions in the regulation of gene expression. Brand provides a detailed examination of relaxation processes, such as time-dependent spectral shifts, exhibited by solvatochromic probes including tryptophan, and how these processes can illuminate aspects of protein dynamics. Marriott describes a new class of genetically encoded fluorescent proteins based on the lumazine-binding protein (LUMP) and then discusses the potential of using LUMP and related encoded proteins to advance the application of fluorescence polarization to analyze target proteins and protein interactions in living cells.

Several chapters describe the use of fluorescence methodologies to elucidate aspects of cellular dynamics. Cardarelli and Gratton discuss spatiotemporal fluorescence correlation spectroscopy to follow movement of single molecules inside cells, while Diaspro and colleagues describe the use of STED microscopy to elucidate pico-nanosecond temporal dynamics in cells. Jacobson and colleagues discuss plasma membrane DC-SIGN clusters and their significance.

I hope you enjoy this overview of modern applications of fluorescence, and I hope you gain a better appreciation not only of Gregorio Weber's contributions to the field but also of his unique personality and character.

Kailua, HI, USA David M. Jameson

Contents

A Fluorescent Lifetime: Reminiscing About Gregorio Weber

David M. Jameson

Abstract During the last few decades, fluorescence spectroscopy has evolved from a narrow, highly specialized technique into an important discipline widely utilized in the biological, chemical, and physical sciences. As in all scientific disciplines, the development of modern fluorescence spectroscopy has benefited from the contributions of many individuals from many countries. However, one individual, *Gregorio Weber*, can be singled out for his outstanding and far-reaching contributions to this field. This chapter will briefly outline aspects of Gregorio Weber's life and times and discuss some of his more important contributions to the fluorescence field. Some of his more important contributions to the field of protein chemistry will also be discussed. In addition to the facts of Weber's life and work, I shall also interject several anecdotes from my personal experience with him, which will serve to illustrate his outstanding personality and character.

Keywords Anecdotes • Awards • Fluorescence • Gregorio Weber • Proteins • Scientific accomplishments

I began my graduate studies in the Chemistry Department at the University of Illinois at Urbana-Champaign (UIUC) in the fall of 1971. After hearing each faculty member discuss the research ongoing in their lab, I chose Gregorio Weber as a faculty advisor. I was particularly attracted by the concept that the interaction of light with matter could provide important information about the nature of biomolecules, especially proteins. During my graduate career I had to synthesize fluorescent probes as well as build the photon-counting instruments I was to use. I also was given the opportunity to work closely with many of the international

D.M. Jameson (✉)
Department of Cell and Molecular Biology, University of Hawaii, 651 Ilalo Street, BSB 222, Honolulu, HI 96734, USA
e-mail: djameson@hawaii.edu

D.M. Jameson (ed.), *Perspectives on Fluorescence: A Tribute to Gregorio Weber*, Springer Ser Fluoresc (2016) 17: 1–16, DOI 10.1007/4243_2016_13,

visitors to the lab. Needless to say, this level of training held me in good stead over the rest of my scientific career. In those early graduate student years I was very impressed with Gregorio Weber's huge store of knowledge and his ability to communicate that knowledge to others. With time I learned that he was one of the great pioneers in the fluorescence field. In the remaining pages I shall outline some of the more important aspects of Gregorio Weber's contributions to fluorescence spectroscopy and to protein chemistry.

I once asked Gregorio Weber how he first got interested in science. He told me that he had a very inspiring high school science teacher and that he told this teacher that he was interested to become a scientist. The teacher informed him that support of scientific careers in Argentina at that time (the late 1930s) was rather hit or miss and advised him to pursue a medical degree. In that way, if a scientific career did not work out at least he could support himself seeing patients. Gregorio Weber followed this advice and earned an MD degree from the University of Buenos Aires in 1943. He soon became an assistant to Bernardo Houssay, who was awarded the 1947 Nobel Prize in Physiology and Medicine for his discovery of the role of pituitary hormones in the regulation of glucose in the blood. Houssay was the first Argentine and Latin American to be awarded with a Nobel Prize in some field of the Sciences. Houssay was impressed with Weber's abilities and suggested that he apply for a prestigious British Council Fellowship to support graduate studies toward a PhD at Cambridge University. Gregorio Weber left Argentina for Cambridge England in 1943 and traveled in a convoy which took 44 days to complete the journey, due to precautions taken against the chance of U-boat attacks. Upon reaching England, Weber initially spent 6 months in the laboratory of Eric Rideal, a physical chemist, learning surface chemistry. But he soon became enamored of the work of Malcolm Dixon, the well-known enzymologist. Interestingly, from the point of view of Weber's future career, Malcolm Dixon had carried out some of the early work on the absorption spectrum of cytochrome c. This interest in spectroscopy may be part of the reason that Dixon suggested that Weber investigate the fluorescence of flavins and flavoproteins. As Weber related in 1986 at the first International Weber Symposium in Bocca di Magra, Italy, in honor of his 70th birthday, he knew very little about fluorescence at that time and nothing about flavins [1]. Needless to say, he did not stay ignorant for long! He soon discovered that many of the basic properties of fluorescence, such as lifetimes, quantum yields, and polarizations had been studied by physicists for several decades. The work that interested him the most, however, was that of Francis Perrin. He said that he read the famous paper of Francis Perrin, on the depolarization of fluorescence by Brownian rotations, not once but many times [2]. Interestingly, Weber commented "Argentine secondary education in the first half of the century included French language and literature so that I could not only understand the scientific content but also enjoy the literary quality of the writing. It was written in that transparent, terse style of XVIII century France, which I have tried, perhaps unsuccessfully, to imitate from then onwards." [1]. Throughout his life, Weber often commented that he was also attracted to fluorescence because of the counterpoint of the esthetic and scientific aspects. Specifically, he said that he was impressed by the fact that visual

observation of changes in the color or intensity of fluorescence could immediately be related to a molecular event. Even in those early days, Weber appreciated the need for a true quantitative understanding of the fluorescence phenomenon. In his PhD thesis he wrote "I feel that a knowledge, as deep as possible, of the physical principles concerned is indispensable. Even close collaboration with a physicist cannot spare this task to the biochemist. I am tempted to believe that a biologist having n ideas related to the biological side of the problem and a physicist possessing another n relating to the physical side would result in some 2n useful combinations whereas the same ideas collected in one brain would lead to a number of combinations more like n!" [3].

Needless to say, at that time, in the 1940s, Weber's fluorescence instrumentation had to be homebuilt. In his original instrument, the light source was a carbon arc, originally developed for use in searchlights during the war. The exciting light was first filtered through a layer of concentrated $NaNO_2$ to remove UV light (<420 nm) and then polarized by a Nicol prism (Fig. 1) (It is interesting to note that during my time as a graduate student in Weber's lab, during the 1970s, we still used these $NaNO_2$ filters routinely, although in our case we used these filters to help in isolating the emission from the exciting light). Weber then used additional glass filters to further remove the exciting light and to isolate the emission. The actual measurement of the polarization of the fluorescence was realized using visual compensation techniques involving observation of interference patterns as a "pile-of-plates" polarizer (the compensator of Arago) was rotated. At that time, photoelectric-based detectors were primitive and could only detect the strongest fluorescence signals, and consequently the eye was the detector of choice. With these visual methods, Weber was able to quantify levels of polarized light reaching

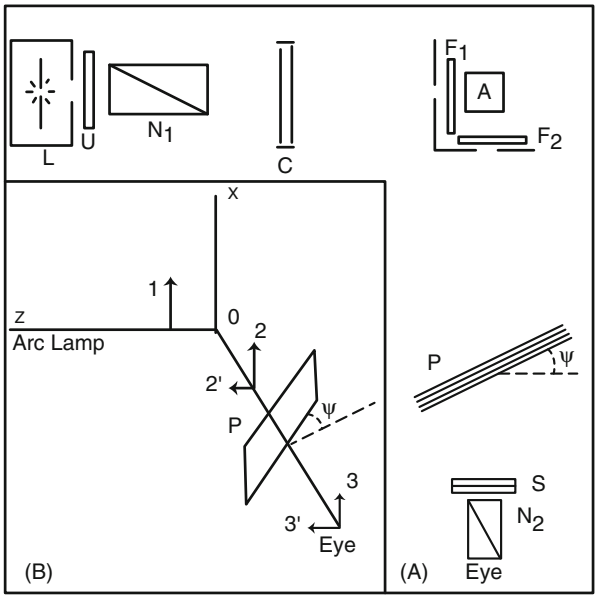

Fig. 1 Original drawing from Gregorio Weber's PhD thesis showing the optical arrangement of the instrument he constructed for polarization measurements

only 1 or 2%. However, he paid a price for these visual observations since, like many of the pioneering spectroscopists, he suffered acute eye ailments in later years as a result of excessive exposure to infrared and ultraviolet light, which led to removal of his lenses, detached retinas, and eventually corneal transplants. As a consequence of the photophobia these eye ailments caused, Weber had to wear sunglasses most of his latter life – those of us who knew him as "The Professor" considered his sunglasses almost as a trademark.

His first publication entitled: *The quenching of fluorescence in liquids by complex formation. Determination of the mean life of the complex* [4] was the first work to demonstrate that fluorescence quenching can take place after formation of molecular complexes of finite duration rather than collisions. (A complete list of Gregorio Weber's publications can be found on the website maintained by the Laboratory for Fluorescence Dynamics at http://www.lfd.uci.edu/weber/publications/). His second publication was entitled *Fluorescence of riboflavin and flavin-adenine dinucleotide* [5], and was the first demonstration of an internal complex in FAD. Some years later he published the first demonstration that NADH also formed an internal complex [6]. He continued to publish important papers on the excited state properties of FAD and NAD in the 1960s and 1970s.

After completing his PhD, awarded in 1947, Weber carried out independent investigations at the Sir William Dunn Institute of Biochemistry at Cambridge, supported by a British Beit Memorial Fellowship, from 1948 to 1952. This fellowship, founded in 1909, was one of the most prestigious and competitive fellowships for postdoctoral or medical degree research in the world. At Cambridge he began to delve more deeply into the theory of fluorescence polarization and also to develop methods which would allow him to study proteins which did not contain an intrinsic fluorophore (intrinsic protein fluorescence from tryptophan and tyrosine had not yet been discovered). He invested considerable time and effort in synthesizing a fluorescent probe which could be covalently attached to proteins and which possessed absorption and emission characteristics appropriate for the instrumentation available in post-war England. For example, as stated earlier, reliable and sensitive photodetectors had not yet been developed and visual observations were the norm, so the emission had to be observable with the eye. The result of 2 years of effort was dimethylaminonaphthalene sulfonyl chloride or dansyl chloride – a probe which is still utilized today. With dansyl chloride and with new instrumentation Weber began to investigate several protein systems, publishing his theory and experimental results in two classic papers published in Biochemical Journal in 1952 [7, 8].

In 1953, Hans Krebs recruited Weber for the new Biochemistry Department at Sheffield University. That same year, Krebs received the Nobel Prize for his elucidation of the metabolic reactions which produce energy in cells – the tricarboxylic acid or Krebs Cycle. David Lloyd, who was an undergraduate student at Sheffield and who was assigned to Gregorio Weber for first year tutorials, told the story (http://www.cf.ac.uk/biosi/staffinfo/lloyd/weber/): "My predecessor as Head of Microbiology in Cardiff, David Hughes, had previously been a member of the Medical Research Council Unit for the Study of Cell Metabolism established for Sir Hans Krebs in Sheffield and later in Oxford. When Gregorio went for interview

there in 1953, David Hughes was given the important duty of showing the already distinguished applicant around and reporting back to 'Prof' as everyone called Krebs. Hughes told me that he felt quite insignificant by comparison to this young genius, and that there was no one whom could question Gregorio's suitability. So his response to Krebs was: Let's not interview, but just appoint."

During his years at Sheffield Weber continued to lay the foundations of modern fluorescence spectroscopy developing both fluorescence theory and instrumentation. One of his significant discoveries during his Sheffield days was that anilinonaphthalene sulfonate (ANS) had a very weak fluorescence in water but this fluorescence increased very dramatically when ANS interacted with bovine serum albumin. Interestingly, more than 60 years after Weber's report (in 1954 with David Lawrence) ANS is still a popular probe and is often used in protein unfolding studies as an indicator of a "molten globular" state. (The emission properties of ANS provide one of my favorite handlamp demonstrations of fluorescence – one which I highly recommend to anyone teaching an introductory class on fluorescence. One simply takes two large test tubes, one containing ANS in water, the other containing BSA in buffer. The exact concentrations are not so important – as long as there is a reasonable amount of probe and protein. Using a UV handlamp to illuminate the samples, one demonstrates that the ANS/water solution exhibits a very weak, yellowish fluorescence, while the BSA exhibits no fluorescence (there is sometimes a weak blue fluorescence from impurities, but it is usually negligible). With the lights out, you then pour the contents of one tube into the other (either way) and the result is a huge increase in fluorescence and a dramatic blue shift, that is, from weak yellow to very bright sky blue (Fig. 2). This demonstration never fails to elicit "Oohs!" and "Aahs!" from the audience.)

During these early years at Sheffield, Weber also began his seminal studies on intrinsic protein fluorescence. Specifically, in 1957, with his postdoctoral fellow F.W.J. Teale, he published the first emission spectra of the aromatic amino acids and the first accurate excitation spectra. Figure 7 from their seminal paper [9] has been reproduced many times and is shown again here in Fig. 3. Weber and Teale published a series of important papers and communications on intrinsic protein fluorescence and the determination of absolute quantum yields. Interestingly, the

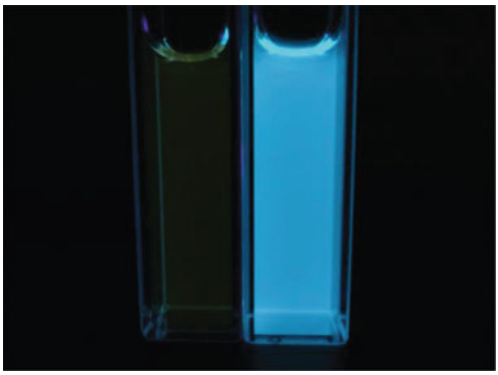

Fig. 2 Solution of ANS in PBS (*left*) and the same concentration of ANS in PBS after addition of bovine serum albumin (*right*). Solutions are illuminated using a UV handlamp set for the long wavelength (365 nm)

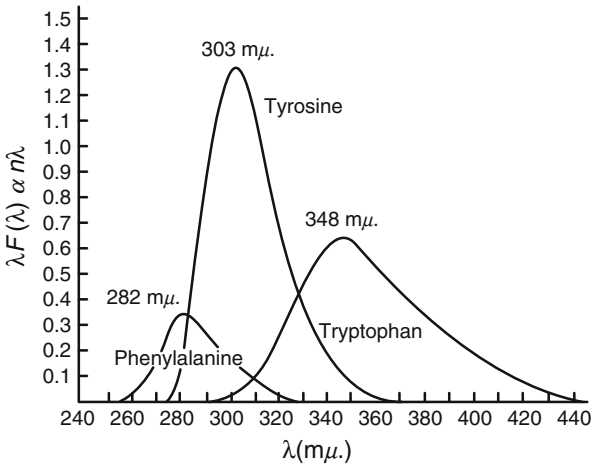

Fig. 3 Figure 7 from [9] giving the first emission spectra of the aromatic amino acids

Fig. 7. Fluorescence spectra of the aromatic amino acids in water. Abscissa: wavelength (mμ.). Ordinate: relative number of quanta.

quantum yield Weber and Teale reported for tryptophan, 0.20, was later found to be somewhat higher than the currently accepted value near 0.13. At the time when Weber and Teale carried out their experiments, the large temperature effect on tryptophan's lifetime and quantum yield was not appreciated. As Weber told me, their work, reported as done at "room temperature," was, in fact, carried out in England in the winter in a Quonset hut without central heating, which caused a marked increase in their tryptophan quantum yield relative to that expected for 25°C. Weber's interest in the photophysics of tryptophan continued over the years, eventually leading to a publication in 1977 of an important and often quoted paper with Bernard Valeur [10] on the ^1L_a and ^1L_b excitation bands of indole and tryptophan. The study of intrinsic protein fluorescence has become one of the most important techniques used in protein research and has been of great importance in establishing the dynamic nature of proteins. This potential was certainly not lost on Weber who presented a classic paper at the "Light and Life" conference held in 1960 and, in a true understatement, summarized his presentation in the Discussion held after the talk by saying "There are many ways in which the properties of the excited state can be utilized to study points of ignorance of the structure and function of proteins" [11]. In fact, in an earlier communication (presented at the annual meeting of the British Biochemical Society on April 3, 1959) Weber estimated that the excited state lifetime of tryptophan in proteins was on the order of 4 ns and commented "These values are too short to permit measurements of fluorescence polarization to be of value in the determination of the rotational relaxation times of proteins in solution, but can give useful information on local conditions about the tryptophan or tyrosine residues." Present day methods of site-directed mutagenesis, which permit the facile removal and/or addition of tryptophan residues to allow the creation of novel single-tryptophan containing

proteins, have led to the full realization of Weber's vision of the utility of intrinsic protein fluorescence.

In 1960, Weber spent a year as a visiting professor at Brandeis University and gave a series of lectures on fluorescence, inspiring several students and postdoctoral fellows with the potential of fluorescence methods. One of these, Ludwig Brand, went on to establish himself as one of the leading researchers in the biological applications of fluorescence spectroscopy. At around this time, I.C. "Gunny" Gunsalus, head of the Biochemistry Division of the Department of Chemistry at the University of Illinois at Urbana-Champaign, recruited Weber away from Sheffield. Gunny related to me the story that while he was convincing his colleagues that Gregorio Weber was an exceptional scientist, someone commented that Weber didn't have as many publications as one might expect from a senior professor. Gunny replied that while this was true, *Weber's ratio of outstanding papers to total papers was unity* and that this ratio – known thereafter as the Weber ratio – was certainly the more important consideration. In fact, when Weber left England several other Sheffield faculty members, who would later go on to establish distinguished careers elsewhere, also left. As related by David Lloyd in his tribute to Gregorio Weber: "In fact I was later to learn that discontent in the Department arose largely because of repeated refusals to promote Gregorio to the research Chair he so evidently deserved. Links with Urbana-Champaign, Illinois were already strong (Gibson, Massey and Weber had spent sabbaticals there; R.E. Hungate, Ralph Wolfe and Woody Hastings had been on sabbaticals in Sheffield. It was therefore no surprise when Gregorio announced his intended departure for that campus. He took with him Jim Longworth (his first research student) and Lorna Young (his technician). Then Vince Massey, Graham Palmer and their research students (Ben Swoboda, and Steve Mayhew who had worked with John Peel in Microbiology) left for Ann Arbor, Michigan; and Rod Bennett went to Dartmouth N.H. Theo Hofmann left for Toronto's Biochemistry Department. Keith Dalziel and Mark Dickinson went to Oxford. Quentin Gibson and Colin Greenwood went to the Johnson Foundation, University of Pennsylvania at Philadelphia." In later years, this exodus became known as the "great Sheffield brain drain."

In 1962, Gregorio Weber joined the University of Illinois and built a research program that continued actively until his death in 1997. During his early years in Urbana, Weber continued to develop novel fluorescence instrumentation and probes and extended his studies of protein systems. Among the fluorescence probes Weber developed in Urbana were pyrenebutyric acid (which had a lifetime of 100–150 ns and thus extended the polarization method to proteins with molecular weights of 10^6), bis-ANS (which binds to many proteins with much higher affinity than ANS and which also binds to many nucleotide binding sites), IAEDANS (the first sulfhydryl specific fluorescence probe), and PRODAN (2-dimethylamino-6-propionyl-naphthalene; a probe designed by Weber to have an exceptionally large excited state dipole moment and hence to possess an extreme environmental sensitivity). Weber also made derivatives of PRODAN such as LAURDAN, which included a lauric acid tail to render the probe lipid soluble (LAURDAN has been very extensively used in recent years as a probe of membrane dynamics)

Fig. 4 Gregorio Weber with his technician Fay Ferris (circa 1984)

and DANCA, which had a cyclohexanoic group attached that increased the affinity of the probe for heme-binding sites. Most of these probes were actually synthesized by Fay Ferris, Weber's lab technician for many years at UIUC, who acted as his eyes and hands in the lab (Fig. 4)

Much of Gregorio Weber's efforts during the last few decades of his life were focused on development of his ideas on protein dynamics and protein–protein interactions. In this regard, two of the research lines he developed were oxygen quenching of fluorescence and applications of elevated hydrostatic pressure. His initial foray into oxygen quenching was with his student W. M. Vaughan who studied oxygen quenching of pyrenebutyric acid, free in solution and associated with protein [12]. The low solubility of oxygen in aqueous solutions required that the targeted fluorophore had a very long lifetime, which in the case for pyrenebutyric acid was greater than 100 ns. In order to study intrinsic tryptophan fluorescence in proteins, Weber needed to use a cell capable of holding up to 100 atm of oxygen pressure. Joseph Lakowicz was the graduate student who worked on this project and the results showed that oxygen, an uncharged, nonpolar quencher, could reach tryptophan residues in protein interiors [13]. The last paragraph in their seminal paper stated, "The general conclusion to be derived from all the points mentioned above is that the functional properties of protein molecules are not properly represented by rigid molecules that do not include the rapid structural fluctuations necessary to explain the phenomena we have observed. Our experimental findings are fully consistent with the ideas on the character of protein conformation put forward by one of us (Weber, 1972) but not with the often expressed belief that proteins exist in a very small number of permissible conformations. Such models are, in our opinion, inconsistent with the weak forces that determine protein structure." One must appreciate that at this time, in the early 1970s, the popular view of proteins was that of rigid, dense structures that would not allow for small molecules such as oxygen to diffuse into the protein interior.

Weber had for years championed the view that proteins were highly dynamic structures. In his seminal review in Advances in Protein Chemistry in 1975 [14], Weber wrote that proteins were "kicking and screaming stochastic molecules."

In the mid-1970s Weber began to apply the method of elevated hydrostatic pressure, coupled with fluorescence, to the study of molecular complexes and proteins. His appreciation of the possibilities of hydrostatic pressure was no doubt influenced by his friendship with Harry G. Drickamer, a professor in Chemical Engineering at UIUC, whose laboratory was actually in the same building as Weber's lab. Drickamer was arguably one of the great pioneers in high pressure studies in condensed matter – in his life he was awarded 27 major awards for his research including the National Medal of Science awarded by President George H. Bush in 1989. Weber's first work on this topic, published in 1974, was a study of FAD, FMN, and the molecular complex of isoalloxazine and adenine [15]. Over the next three decades Weber applied hydrostatic pressure methods to the study of biomolecules ranging from small complexes to single chain proteins to oligomeric proteins and eventually to viruses. He also applied pressure to biological membranes. Eventually he published 48 articles on pressure effects on biomolecules. His review in 1983 with Drickamer in the Quarterly Review of Biophysics [16] was a landmark paper in the field – in the opening paragraph they stated: "... we concentrate here on the examination of the conceptual framework employed in the interpretation of high pressure experiments and in the critical discussion of our knowledge of selected areas of present interest and likely future significance." Weber's contributions to protein chemistry were recognized by the American Chemical Society in 1986, which named him as the first recipient of Repligen Award for the Chemistry of Biological Processes, whose purpose was "... to acknowledge and encourage outstanding contributions to the understanding of the chemistry of biological processes, with particular emphasis on structure, function, and mechanism."

In 1992, Weber published his book "Protein Interactions" in which he essentially summarized his ideas about proteins [17]. He dedicated this book to "Those who put doubt above belief," in keeping with his lifelong philosophy of wariness in accepting popular scientific theories. Gregorio Weber's scientific achievements were recognized by many honors and awards. These include election to the US National Academy of Sciences, election to the American Academy of Arts and Sciences, election as a corresponding member to the National Academy of Exact Sciences of Argentina, the first National Lecturer of the Biophysical Society, the Rumford Premium of the American Academy of Arts and Sciences, the ISCO Award for Excellence in Biochemical Instrumentation, the first Repligen Award for the Chemistry of Biological Processes, and the first International Jablonski Award for Fluorescence Spectroscopy. It is worth noting that the Rumford Premium is one of the oldest scientific awards given in the USA. It was created by a bequest to the Academy from Benjamin Thompson, Count Rumford, in 1796 – previous awardees include J. Willard Gibbs, A.A. Michelson, Thomas Edison, R.W. Wood, Percy Bridgman, Irving Langmuir, Enrico Fermi, S. Chandrasekhar, Hans Bethe, Lars Onsanger, and other highly original thinkers. The Rumford award

Fig. 5 Gregorio Weber receiving the Rumford Premium. Also receiving awards are Robert L. Mills and Chen Ning Yang

committee recommended that the 1979 award be given to two physicists, Robert L. Mills and Chen Ning Yang, for their joint work on the theory of gauge invariance of the electromagnetic field, and to Gregorio Weber, "Acknowledged to be the person responsible for modern developments in the theory and application of fluorescent techniques to chemistry and biochemistry" (Fig. 5).

In addition to these seminal contributions, Gregorio Weber also trained and inspired generations of spectroscopists and biophysicists who went on to make important contributions to their fields, including both basic research and the commercialization of fluorescence methodologies and their extension into the clinical and biomedical disciplines. Weber is honored today by several awards and meetings including the Gregorio Weber Award for Excellence in Fluorescence Theory and Applications, awarded annually by ISS, Inc (http://www.iss.com/events/weber.html) and the Gregorio Weber International Prize in Biological Fluorescence (Weber Prize) awarded every 3 years for research related to a doctoral (or equivalent) dissertation (http://www.lfd.uci.edu/weber/prize/). Approximately every 3 years (since 1986) an international symposium is held in his honor entitled the International Weber Symposium on Innovative Fluorescence Methodologies in Biochemistry and Medicine (http://www.lfd.uci.edu/weber/symposium/). These Weber Symposia were held in Italy in 1986 and 1991, and in Hawaii in 1995,

Fig. 6 Group photo for the first International Weber Symposium held in 1986 in Bocca di Magra, Italy

1999, 2002, 2005, 2008, 2011, and 2014. The group picture from the first meeting held in Bocca di Magra, Italy, is shown in Fig. 6 – I shall treat this as a "Where's Waldo" exercise and let the reader locate Gregorio Weber.

An important website, http://www.cf.ac.uk/biosi/staffinfo/lloyd/weber/, was established by David Lloyd at Cardiff University who was actually an undergraduate with Gregorio Weber in Sheffield. This website has short contributions from many of Weber's colleagues from his Cambridge and Sheffield days, including a marvelous and insightful article by David Lloyd, which offer illuminating insights into Weber's personality and his influence on young scientists. For example, one of the interesting anecdotes presented by David Lloyd from his time with Gregorio Weber is "It was a fast-track education to be with Gregorio Weber in those tutorials. He told us of his heroes: James Clark Maxwell, whose unification of the magnetic and electrical forces was perhaps the greatest leap forward in the physics of the 19th century, and the major achievements of the Americans, Willard Gibbs and G.N. Lewis in thermodynamics and solution chemistry. He set us interesting essay topics: 'The dynamics of life', 'The government and administration of cellular metabolism', and one which still puzzles me 'Does nature favour the survival of the fittest (Darwin) or conservation of the mean (Lotka-Volterra)?'". David Lloyd went on to write "As Krebs said of Warburg, so could we say of Gregorio: his influence has spread far and wide. He was an intellectual genius, a colossus who changed everyone he touched. I am told that he did not believe in an afterlife, but rather that we just stop. But as on a snooker table the cue ball that collides sends the others on into their separate trajectories."

In his contribution to this website, Fred Sanger (two-time Nobel Prize winner) wrote:

> I do not feel able to comment on Gregorio's published scientific work as it was in a rather different field from my own interests, but I do believe that his contribution to science was considerably more than has appeared in print. During the time that we were both working in the Cambridge Biochemical Laboratory he would frequently come over to my bench to see what I was doing, discuss my work and make useful suggestions. I found this stimulating and often helpful for my work. Gregorio had a considerably wider knowledge of science than I did, and was a wonderful person.

During the time that I was a graduate student in Weber's laboratory (1971–1977), I overlapped with graduate students, David Kolb, Jim Stewart, Moraima Winkler, Kathy Gibbons, Joe Lakowicz, Alex Paladini, Jr., J. Fenton Williams, John Wehrly, Bob Hall, Wayne Richards, and Tom Li, and with postdoctoral fellows Francisco Barrantes, Roberto Morero, Fumio Tanaka, I. Iweibo, Yueh-hsiu Chien, Louise Slade, Bob Mustacich, Richard Spencer, George Mitchell, Bernard Valeur, Antoine Visser, Bill Mantulin, and Enrico Gratton. Other individuals who spent formative periods in Weber's laboratory include Philippe Wahl, Meir Shinitzky, Sonia Anderson, John Olson, Ken Jacobson, Bob Clegg, Greg Reinhart, and George Fortes. In the 1980s and 1990s Weber's students included, Parkson Chong, Lan King, Catherine Royer, Suzanne Scarlata, Chris Luddington, Rob Macgregor, Peter Torgerson, and Gerard Marriott, and postdoctoral fellows included Maite Coppey, Frank Kaufman, Mohamed Rholam, Dave Edmundson, Kancheng Ruan, Andre Kasprzak, Gen-Jun Xu, Larry Morrison, Edith Miles, Don Nealon, Leonardo Erijman, Patricio Rodriguez, Susana Sanchez, Jerson Silva, and Debora Foguel. During my years in Gregorio Weber's laboratory (as a student and later as a postdoc), visitors who came to carry out experiments included Nicole Cittanova, Bill Cramer, Andy Cossins, Pierre Sebban, Serge Pin, Bernard Alpert, Christian Zentz, Patrick Tauc, Maurice Eftink, Tiziana Parasassi, and José Maria Delfino. No doubt I am missing some names and I apologize for my failing memory. Figure 7 is a picture taken at Enrico Gratton's house in the early 1980s where Enrico, Greg Reinhart, and I are presenting a computerized chess set to Gregorio Weber for his birthday. This chess computer actually was embedded in a full sized chess board that would detect the moves made on the board and indicate its response – a perfect present for "The Professor" who liked to play chess.

As I mentioned already, Weber had many eye problems due to excessive amount of UV and infrared radiation over the years. I was actually visiting him in the early 1990s when the hospital called to say that a cornea transplant was available and so I immediately drove him over. A couple of days later I was visiting him when a doctor came in to remove the bandage from his remaining bandaged eye, which had received a new cornea – the bandage had already been removed from the other eye. Weber's first words were "I have a homogeneous, clear, binocular visual field" – a statement conveying the maximum of information with the minimum of words.

Another memorable comment occurred when he was working on a mathematical solution for resolving multiple lifetime components from phase and modulation data given multiple light modulation frequencies. To accomplish this task Weber

Fig. 7 *Left to right*: Greg Reinhart, David Jameson, Gregorio Weber, and Enrico Gratton

devised a new (for him) mathematical procedure. Later, one of his friends in the mathematics department told him that this approach looked familiar and eventually helped to find a reference in the literature. I remember vividly going with Weber to Altgeld Hall on the UIUC campus, which housed the math library. There, we found the reference to an article by R. de Prony in Volume 1 of the 1795 issue of *J. Ecole Polytech*. When Weber wrote his article on this topic [18], one of the section headings was titled: "Computation of the Component Lifetimes from the Moments by Prony's Method." I asked Weber why he referenced de Prony's article – almost two centuries old – rather than simply state that he had developed the method himself. Weber replied that since de Prony had found the method first he must receive the credit!

An anecdote which demonstrates Weber's nurturing attitude toward students was given in my book "Introduction to Fluorescence" [19]. Namely: "When I was a graduate student, I was trying to improve the sensitivity of my measurements and I hit upon the idea of having two adjacent sides of a fluorescence cuvette coated with a mirror finish. My idea was that the excitation beam would then be reflected from the back side through the solution again, and the fluorescence reaching the side facing away from the detector would be reflected toward the detector. In fact, this arrangement improved my signal about threefold. I was, naturally, proud of this accomplishment and demonstrated it to Gregorio Weber who politely praised my ingenuity and then proceeded to show me an old article he had written (from the 1950s) in which he had also used mirror coatings on his cuvette. In that article, he also acknowledged that he was following the idea of Francis Perrin who published the same approach in the 1920s!" So Weber first praised me for my ingenuity and initiative – raising my self-confidence – but then later educated me by pointing out

that others, starting with Francis Perrin in 1929, had hit upon the same approach. Surely this is the manner in which professors should treat students and colleagues!

Another incident I well remember was when I was attending a NATO conference with Weber in the early 1980s in Sicily. At the cocktail party preceding the opening of the conference I was standing next to Weber when a young woman came up to him and asked if he was Meir Shinitzky (who had actually been a postdoc in Weber's lab years earlier and who was certainly a very distinguished scientist at the time of this incident). Weber replied "No, I am Gregorio Weber." The young woman next asked if he knew anything about fluorescence! Weber paused and clearly considered carefully his reply – which was "I know some things, but not everything." The young woman replied, "Well then, I had better go find Meir Shinitzky." I loved Weber's statement since it epitomized his intellectually honesty in his approach to science and to life in general. He might have replied, for example, that he probably knew more about fluorescence than anyone else on earth, but his actual reply captured simultaneously his humility and his honest appraisal that no matter how much he knew there was always a vastly greater amount that he did not know. Continuing with the theme of humility, I am reminded when Weber gave the final talk at the end of the 1986 Bocca di Magra meeting. Of course when he finished there was loud and unrelenting applause. Finally Weber said loudly "Please stop – you are celebrating the birthday of Gregorio Weber, not Josef Stalin!"

Modern students take the internet for granted and are accustomed to being able to retrieve information on just about any topic rapidly while at their desks. I have previously written that in my graduate student and postdoctoral days we did not have the internet or Google – but rather we had Weber. The difference being that Weber always gave us the *correct* answer. My point was that all of the people who knew Weber in those days considered him an authority, not only on fluorescence but also on all matters relating to science in general. His knowledge on a wide range of topics, including the scientific literature, was simply astonishing and saved many of us countless hours in the library that we would have spent digging out the information we needed – I may also add that it also settled many bets in the lab among the students!

I hope this chapter has given the reader some concept of the scientific insights of Gregorio Weber and his important and original contributions both to fluorescence and to protein chemistry. Those of us lucky enough to have known and worked with Gregorio Weber, however, can attest to his other qualities, including his humanity and simplicity. He inspired generations of young biophysicists from around the world, demonstrating by example how scientists ought to interact with each other, namely with courtesy, respect, selflessness, good humor, and generosity. Throughout his life Weber shared his resources, both professional and personal, with all. He became Professor Emeritus in 1986, at the age of 70. Although there was no mandatory retirement age at the university, Weber said that he wanted to retire to free up the faculty position for others just starting out. He was given a smaller lab and office and continued to work on his own – and with the occasional visitor – up until his death. I can attest to the fact that he maintained his scientific curiosity and intellectual honesty to the end of his life. Although he was too sick – from leukemia

Fig. 8 David Jameson and Gregorio Weber in Hawaii (circa 1990)

– to leave his hospice bed he still enjoyed discussing life and science with his visitors. While bed-ridden and in his final days he was reading a book on the history of the French Revolution – in French! I asked him why he was reading that particular book and he replied that it was because the French Revolution was so interesting.

As a final anecdote, I vividly recall a conversation I had with Weber in Hawaii in the early 1990s (Fig. 8). Weber was in his 70s at the time and he turned to me one day and said "You know David, when I was much younger an older colleague said to me that when I passed the age of 60 I would begin to notice that my students had more ideas than me and better ideas than me." To this statement I replied "Gee – really Professor?" After a rather long pause he said "I have not found this to be the case."

References

1. Weber G (1989) Final words at Bocca di Magra. In: Jameson DM, Reinhart GD (eds) Fluorescent biomolecules: methodologies and applications. Plenum Press, New York, pp 343–349
2. Perrin F (1926) Polarisation de la lumière de fluorescence. Vie moyenne des molécules dans l'etat excité. J Phys Sér 7:390–401
3. Weber G (1947) Fluorescence of riboflavin, diaphorase and related substances. PhD thesis, St. John's College, University of Cambridge
4. Weber G (1948) The quenching of fluorescence in liquids by complex formation. Determination of the mean life of the complex. Trans Faraday Soc 44:185
5. Weber G (1950) Fluorescence of riboflavin and flavin-adenine dinucleotide. Biochem J 47:114–121
6. Weber G (1957) Intramolecular transfer of electronic energy in dihydro diphosphopyridine nucleotide. Nature (London) 180:1409
7. Weber G (1952) Polarization of the fluorescence of macromolecules. 1. Theory and experimental method. Biochem J 51:145–155

8. Weber G (1952) Polarization of the fluorescence of macromolecules. 2. Fluorescent conjugates of ovalbumin and bovine serum albumin. Biochem J 51:155–167
9. Weber G, Teale FWJ (1957) Ultraviolet fluorescence of aromatic amino acids. Biochem J 65:476–482
10. Valeur B, Weber G (1977) Resolution of the fluorescence excitation spectrum of indole into the 1La and 1Lb excitations bands. Photochem Photobiol 25:441–444
11. Weber G (1961) Excited states of proteins. In: McElroy WD, Glass B (eds) Light and life. Johns Hopkins Press, Baltimore, pp 82-106
12. Vaughan WM, Weber G (1970) Oxygen quenching pyrenebutyric acid fluorescence in water. A dynamic probe of the microenvironment. Biochemistry 9:464–473
13. Lakowicz JR, Weber G (1973) Quenching of protein fluorescence by oxygen. Detection of structural fluctuations in proteins in the nanosecond time scale. Biochemistry 12:4171–4179
14. Weber G (1975) Energetics of ligand binding to proteins. Adv Protein Chem 29:1–83
15. Weber G, Tanaka F, Okamoto BY, Drickamer HG (1974) The effect of pressure on the molecular complex of isoalloxazine and adenine. Proc Natl Acad Sci U S A 71:1264–1266
16. Weber G, Drickamer HG (1983) The effect of high pressure upon proteins and other biomolecules. Q Rev Biophys 16:89–112
17. Weber G (1992) Protein interactions. Chapman and Hall, New York
18. Weber G (1981) Resolution of the fluorescence lifetimes in a heterogeneous system by phase and modulation measurements. J Phys Chem 85:949–953
19. Jameson DM (2014) Introduction to fluorescence. Taylor and Francis (CRC Press), New York

Gregorio Weber's Roots in Argentina

Francisco J. Barrantes

Abstract Professor Gregorio Weber was an outstanding, dedicated scientist, versed in a great variety of scientific subjects. But he was also an exceptional human being: of a reserved nature, he never placed himself above or before others, never put people down. He was a cultivated man with a brilliant intellect, amicable, generous, modest, and prone to listen. He had a real concern with the underlying social issues in all the countries where he lived. His childhood, youth, and university training up to his first doctoral degree took place in his home country, Argentina, and these periods of his life had a deep impact on the shaping of his persona, his cultural habits, and his scientific interests. His great mind and avid quest for knowledge in all spheres of life were undoubtedly nourished by the high standards of the educational system in Argentina at that time but were also fired by the crucial influence of his family and cultural environment, his circle of talented friends, and the informal training that he received in Buenos Aires.

Keywords Argentine science • G. Weber in Argentina • G. Weber medical studies • G. Weber ancestors

Contents

F.J. Barrantes (✉)
Laboratory of Molecular Neurobiology, Faculty of Medical Sciences, UCA-CONICET, Institute for Biomedical Research (BIOMED), Av. Alicia Moreau de Justo 1600, C1107AFF Buenos Aires, Argentina
e-mail: rtfjb1@gmail.com

D.M. Jameson (ed.), *Perspectives on Fluorescence: A Tribute to Gregorio Weber*, Springer Ser Fluoresc (2016) 17: 17–40, DOI 10.1007/4243_2016_9,

1 Introduction

Although the scientific community is well acquainted with Prof. Gregorio Weber's pioneer work and accomplishments in the fields of fluorescence, protein chemistry, and protein–ligand interactions, records of his formative years in Argentina are practically non-existent. When I first began trying to piece together Gregorio's early life in his home country, the task seemed intractable: his contemporaries in the scientific arena, also centennial, are no longer with us; trying to locate former colleagues who might have interacted with him in Argentina drew a blank; my literature search didn't come up with any written recollections associated with Gregorio's roots, and I realized that I was the only Argentine disciple who is still active in the field of fluorescence. However, talking to his daughters and some of his lifetime friends in the USA and the few contemporary family members still alive here in Argentina led me along a fascinating path of discovery and reconstruction as details of Gregorio's childhood, adolescence, and early scientific life began to unfold.

My search included visiting what remains of the old Faculty of Medical Sciences and the institute where Gregorio had read for his M.D. (the premises had been partly torn down decades ago and the remaining sections now form part of the Faculty of Economy of the University of Buenos Aires). Despite the frustration of not being able to find written records at the old building, I was pleased to discover a bronze plaque on an old classroom facing a restored patio with a central fountain (see illustration below) which reads: "These classrooms are the site of the Institute of Physiology of the Faculty of Medical Sciences of the University of Buenos Aires, which Prof. Bernardo A. Houssay directed between 1919 and 1946. Here were conducted the investigations in physiology that led to the award of the Nobel Prize in Medicine to Prof. Houssay in 1947. Dr. Luis F. Leloir, Nobel awardee in Chemistry 1971 also performed his biochemical investigations here. National Academy of Medicine. 1996." These were the laboratories where Gregorio Weber performed his experiments on fibrinogen for his first doctoral thesis at the University of Buenos Aires! Probably this was an inflexion point: I decided to leave aside the originally planned first part of this chapter on superresolution fluorescence microscopy and concentrate exclusively on Gregorio's personal and scientific life in Argentina.

I regret not ever overcoming my timidity and asking Gregorio more about this period of his life. My consolation, however, is that I have been able to embark on this most enjoyable historical research expedition which has renewed and enhanced my immense admiration for him, refueled by the warm memories transmitted by his nephews and nieces, his 100-year-old cousin, and the very few close acquaintances from his early years still alive. Reading the Ph.D. thesis he wrote after graduating as an M.D. and researching his origins, family, friends, tutors, and possible sources of inspiration has been a truly wonderful journey for me personally and one which, I hope, will fill a gap and supplement the excellent recollections of Prof. Weber's work and life in the northern hemisphere that Dave Jameson (e.g., [1] and [30]) has provided over the last decades.

2 Gregorio Weber's Family and Childhood in Buenos Aires

Prof. G. Weber was born in Buenos Aires on July 4th, 1916, son of Leon Weber and Rosa Gerchunoff, and named Gregorio after his maternal grandfather. Leon Weber was originally from Bessarabia, in more recent history a region under Russian rule up to World War I, united with Romania in 1918 and forming part of present-day Ukraine and Moldova. The Weber family lived for some time in Transylvania, the central part of Romania. When Leon Weber was about 18, he left Romania to escape from the 5-year military service ahead. He managed to stow away on a cargo ship belonging to the Dreyfus Armateurs Shipping Group, heading for the Caspian Sea. He was discovered on board before the ship reached port but was fortunately given the chance to work his way. Leon became a respected employee and the firm subsequently kept him in service, based in Hamburg. Thereafter Leon Weber accepted the company's offer to work in Argentina, where of course Gregorio was later born. He arrived on the ship "Santa María" on February 2nd 1908. Dreyfus currently accounts for about 10% of the world's agricultural commodity trade flows and one century ago the Buenos Aires branch was already a key outpost for grain commerce. It should be remembered that in the early twentieth century Argentina was ranked among the ten richest countries in the world. Once in Argentina, Leon became an expert in sampling grain for export, and was eventually head of the division for wheat quality control, a post he held until 1964.

Gregorio's mother, Rosa Gerchunoff, was the daughter of Rab Gershon Ben Abraham Gerchunoff and Anna Korenfeld. According to the 1895 last nominal census in Argentina, Rosa was 16 at that time, which puts her date of birth in 1879; her first name is written Rachila and the family surname appears as Herschenov. The family was originally from Proskurov, a town belonging to the Russian Empire (currently Jmelnítskiy, in the Ukraine). They later moved to Tulchyn, from where they emigrated in 1889 to Argentina together with another 135 families. When they arrived in Argentina they first of all settled in the Jewish colony Moisés Ville, in the

Fig. 1 Gregorio Weber's maternal branch of the family in a typical group pose. Rosa Gerchunoff, Gregorio's mother, is the one standing on the *right*, aged 16. To her *left*, her famous brother Abraham (Alberto) Gerchunoff. Buenos Aires, 1901

province of Santa Fe and later moved to Rajil in the province of Entre Ríos, one of the colonies founded by Baron Maurice de Hirsch as havens for exiles from the Pogrom. The Gerchunoffs were intellectuals with no experience in work on the land. Adapting to farm life in the colony was hard, even more so when in 1891 Rosa Gerchunoff's father was murdered by a gaucho, an episode described in "The Crimes of Moisés Ville[1]" [2]. I was impressed to hear Gregorio's cousin Anita – currently aged 100 – narrate the story of her grandfather's murder by a drunk gaucho, a historical fact which was also an oral tradition received via her mother Cecilia Gerchunoff, and which motivated their moving to the province of Entre Ríos (Fig. 1).

Rosa's brother Abraham was born in 1881 according to the above census – the year of the Great Pogrom – although there are still discrepancies about the exact date of his birth, partly because in order to be able to work formally while he was an adolescent he may have declared himself to be older. He later became a journalist for the prestigious La Nación newspaper and a well-known writer under the name of

[1] Moisés Ville, sometimes called "the Palestine of the Pampas," was the first Jewish agricultural colony in Argentina. The book by Javier Senay describes the circumstances surrounding the murder of 22 Ukrainian immigrants in this colony between 1889 and 1906. The gauchos felt that their livelihood and lifestyle were being threatened by the agricultural export model which involved the fencing off of land.

Alberto Gerchunoff. With his book "Los Gauchos Judíos," published in 1910 and translated into English in 1955 ("The Jewish Gauchos of the Pampas"), Alberto is widely considered to have successfully defended the ethnicity of the Jewish immigrants whilst at the same time assuring their "argentineness," showing the two to be compatible. It is reported that Jorge Luis Borges said Alberto Gerchunoff "was an indisputable writer, but his reputation transcends that of a man of letters. Unintentionally and perhaps unwittingly, he embodied an older type of writer . . . who saw the written word as a mere stand-in for the oral, not as a sacred object."

Rosa met Leon through her elder sister Sofía's husband, Enrique Halperín, who also worked at Dreyfus. After their marriage Rosa and Leon Weber lived in San Juan Av. in the San Telmo district, the heart of the city's oldest colonial area. Their eldest child, Ana Sofía, was born on 31st May 1913, Frida arrived on December 7th 1914, and Gregorio was the youngest child, born on July 4th 1916. Rosa worked as a volunteer at the Israeli Hospital in Buenos Aires. She died in 1923 at the early age of 44 of tuberculosis, a common cause of death in the pre-antibiotic era, and it is presumed that she had contracted the disease while working at the hospital. Leon then moved with his family to 636 Hipólito Yrigoyen St., a 400-year-old street in the quarter of Montserrat, where the city of Buenos Aires was founded, and less than two blocks away from the presidential palace. Family members recall that when Gregorio was a very small child he always referred to himself as "yo, yo" (me, me), and soon Yoyo was adopted as his official nickname by the family at large, a substitute name which lasts to this day in the inner family circle and among his closest friends. Gregorio and his sisters were very close, especially after their mother's tragic death. Her sudden absence must have had quite a strong impact on Gregorio at his tender age. His aunt Sofía and her seven children were frequent visitors at the Weber family home after the death of Rosa and played an understandably crucial role in Gregorio's childhood and adolescence (Figs. 2 and 3).

Fig. 2 An already recognizable Prof. Weber, aged 1. Buenos Aires, 1917

Fig. 3 Frida (12), Gregorio (10) and Ana (13) Weber. Buenos Aires, 1926

In the days when Gregorio attended primary school, calligraphy classes formed an important part of the curriculum during the first 2 years. Dip pens and ink-filled white porcelain pots were the tools of the time and children filled pages and pages of millimetrically equidistant cursive letters. Gregorio's tidy handwriting is definitely to be traced back to this early stage and stayed with him for his whole life.

Gregorio's eldest sister Ana studied chemistry at the Faculty of Exact Sciences, which in those days was a couple of blocks away from their Montserrat home. She worked for the National Roads System and later for the National Atomic Energy Commission (CNEA). Ana studied uranium compounds at the laboratory of Analytical Chemistry headed by Raquel Zukal. The CNEA had other laboratories working on radionucleids: the radiochemistry laboratory, headed by Walter Seelmann-Eggebert, a disciple of Otto Hahn, and the laboratory of general chemistry, under Arturo Cairo. Ana married Juan T. D'Alessio, a chemist who later undertook postgraduate studies in physics (the latter discipline did not exist as such in the Faculty of Exact Sciences when he was an undergraduate) and was a disciple of Teófilo Isnardi; as we'll see below, Juan had a great deal of influence on the shaping of Gregorio's scientific choices.

Frida, the second sister, studied philology and worked at the Institute of Spanish Literature. As a researcher she specialized in Spanish theater of the Golden (XVIth)

Century, drawing interesting and unsuspected links with Russian narrative when analyzing the structure of comedy [3]. She married a civil engineer, Alberto Kurlat. He was also the son of immigrants: Felix Kurlat was from a small town in the Ukraine, Krivoye Ozero, and his mother, Assa Liebeschütz, was from Odessa. Frida was a good friend of Aida Barenboim, mother of the famous pianist and conductor Daniel Barenboim. Frida's intellectual interests and her circle of friends may have been one of the influences on Gregorio's humanistic tastes and his permanent search for stylistic beauty and perfection in language.

One of Frida's daughters, Isabel, studied medicine, later specializing in neonatology. Before she had embarked on this specialization, while staying with his sister's family on one of his visits to Argentina in later years, Gregorio asked Isabel which branch of medicine she would like to follow. Isabel replied that she was thinking of specializing in pediatrics; with his characteristic wit and prescience Gregorio told her: "Don't worry, pediatrics is a malady that spontaneously gets resolved with time. . .". Before practicing her clinical specialization, Isabel worked for a few years at the chair of Biochemistry of the Faculty of Medicine with Prof. Andrés Stoppani, one of Gregorio's friends from university days.

Family life was very important for the extended Weber family. As mentioned, Gregorio's aunt Sofía Gerchunoff – married to Enrique Halperín – and her seven children often shared the family table with Leon Weber and his three offspring. Gregorio's mother's family played a decisive role in shaping his cultural tastes, if not his scientific inclinations. The Gerchunoff branch of the family was part of the rising intellectual middle-class in Buenos Aires, as were the Halperín cousins. By then Leon Weber had a well-paid job at Dreyfus, and the family enjoyed a relatively comfortable economic position with access to the rich cultural offerings of Buenos Aires, the literary links cultivated by his cousin Alberto Gerchunoff and the more affluent branch of the Halperín cousins, particularly Gregorio Weber's eldest cousin, Gregorio Halperín, who was a professor of Latin, married to the Italian Renata Donghi, professor of Spanish and Italian literature. The son of Gregorio Halperín and Renata Donghi, Tulio Halperín-Donghi (1926–2014), later became a source of pride for the family: he was probably one of the country's most respected scholars of nineteenth and twentieth century Argentine history who later taught at Oxford and became a professor at Berkeley.

3 The City: Buenos Aires – and the Countryside – La Cumbre, Córdoba

When Gregorio Weber was born, Argentina had 7.5 million inhabitants. On the political front, during Gregorio's childhood and early adolescence Argentina lived a period of political stability: the year before his birth the first national elections under universal (but only male!) suffrage took place; after decades of conservative administrations, three successive democratically elected presidents from the more

liberal Radical Civic Union, one of the two major political forces in Argentina, succeeded one another in office. In tune with the political front, Argentina was living its economic and cultural Belle Époque: in the preceding 40 years the GDP had grown at an annual rate of 6%, the fastest recorded in the world at that time, attracting immigrants by the thousands: when Gregorio was born, half of the population of Buenos Aires was foreign-born. Argentina was among the ten richest countries in the world, ahead of Germany, France, and Italy. In contrast, Gregorio's adolescence was marked by the 1930 coup that installed the first of a series of de facto military rulers and signified the commencement of economic decline for Argentina as a consequence of the Great Depression and the collapse of commodity trade.

In 1929 Leon Weber bought a small property at the foot of the hills on the outskirts of La Cumbre, a resort in the Mediterranean province of Córdoba, where he and the family spent 3-month-long summer holidays together with their extended family, who also had a property there. Gregorio's cousin Ana ("Anita") – now aged 100 – told me several anecdotes about Gregorio's adolescence that are worth narrating here. They did not have a car, and the rides to and from town required taxis. They soon discovered that the taxi driver also hired horses, and horse-riding became Gregorio's passion and main activity when on holidays. Anita laughed heartily when recalling that as a young adult Gregorio had a very elegant jacket, which was probably meant for formal occasions. Instead, the dark jacket became his uniform when riding his horse, normally at full gallop. The inhabitants of the small town of La Cumbre must have wondered at this tall, elegant young man, flashing by on horseback dressed in what must have seemed like an Olympic equestrian uniform!

Back in Buenos Aires, whilst still an adolescent, Gregorio was very fond of music. According to his cousin Anita, she, Mauricio Goldenberg, Gregorio, and a "gorgeous" girlfriend of his at that time were regulars up in the Gods at the Buenos Aires opera house, the Colón Theater. Gregorio continued this tradition until his final years at medical school, with classmate and girlfriend Carola (see below).

4 Medical School Days and the Forging of Lifelong Friendships

If one rolls back Gregorio's scientific life, one inevitably wonders how it is that he chose to study medicine of all disciplines. Dave Jameson mentions that Gregorio's science teacher at secondary school advised him to study medicine in view of the difficulties involved in finding steady employment as a scientist in those days in Argentina [4]. The death of Gregorio's mother, Rosa, from an incurable disease, must have been a very painful experience for a 7-year-old child, and may also have played a role. The family story is that Ana, his eldest sister, was the one who wanted to be a physician, but in the early 1930s few women studied medicine

in Argentina and Leon Weber was not happy at all with the idea. The family's recollection is that Gregorio told Ana "I will study medicine for you."

Being a student at the School of Medical Sciences of the University of Buenos Aires, dating back to 1852, was not a light endeavor; but Gregorio had a very bright intellect and was a hard-working student. In those days, medical studies took a total of 6 years, and included a very tough entrance examination. He became part of a group of outstanding classmates and friends: Miguel Podolski, Leon Berlin, Mauricio Goldenberg, Carola Blitzman, Isabel MacDonald, Amalia Ingenieros, and Andrés Stoppani. After graduating Miguel Podolski and Leon Berlin practiced medicine for some years but subsequently left clinical practice and engaged in a highly successful endeavor, as owners of the Argentine branch of Odol, a pharmaceutical-cosmetic firm currently belonging to GlaxoSmithKline.

Mauricio Goldenberg was already friends with Gregorio from pre-university days. He trained as a phenomenological psychiatrist and later became a psychoanalyst famous for installing a communitarian "straitjacket-free" psychiatric approach in general hospitals and brought pioneer reforms in mental health treatment not only to Argentina but also to other Latin American countries. Isabel Fernández Vega, Mauricio's widow, recalls that the last time she and Mauricio, who she was dating at that time, saw Gregorio in Argentina was in 1943, when they visited him at his Yrigoyen St. apartment: he was packing his luggage to leave for England. Twenty five years later, the Goldenbergs were in exile in Venezuela, and Gregorio visited them in Caracas. They had a millionaire friend who sent his chauffeured limousine to drive Gregorio to visit the Catholic University Andrés Bello and later to dinner at an exorbitantly luxurious mansion. When asked about the experience, Gregorio replied "*. . .too much for me. . .*." The Goldenbergs settled later in the USA, where Isabel, now 96, still lives. "We remained friends with Yoyo for life". . .she said with an emotive tone in a recent conversation (Fig. 4).

Like Gregorio, Andrés Stoppani also went to Malcolm Dixon's Department of Biochemistry in Cambridge with a British Council fellowship, partly overlapping with Gregorio's stay at that lab. Andrés Stoppani subsequently became professor of Biochemistry in Buenos Aires and Ph.D. supervisor of 1984 Argentine Nobel laureate in Medicine and Physiology César Milstein. Andrés was very close to Gregorio and was best man at Gregorio's wedding to Shirley Nixon in England. In fact, the Buenos Aires–Cambridge "connection" started in 1936, with Luis Federico Leloir conducting research under the supervision of Sir Frederick Gowland Hopkins. Ranwell Caputto, who would become a key figure in the research that led to Leloir's Nobel award in Chemistry in 1970, was another of the Argentine scientists working in Malcolm Dixon's lab at the time of Gregorio's stay in Cambridge. Ranwell traveled to the U.K. with a fellowship of the Argentine Association for the Progress of Science in 1943 (Fig. 5).

A special case among Gregorio's close companions during his student days was Carola Blitzman, currently Carola Eisenberg. She was born in 1917 (not 1923 as reported elsewhere) and formed part of the same "inner circle" of student friends. Carola told me that she had met Gregorio while queuing at the Faculty of Medicine: "I was 18 at that time. I fell in love with him. It was an adolescent, but serious love."

Fig. 4 The "old" Faculty of Medical Sciences of the University of Buenos Aires (1935), where Gregorio Weber studied medicine. The tram rails running on Avenida Córdoba can be seen. The right wing of the building was partly torn down towards the end of the 1930s, while the new (current) building was being built, being completed in 1944

In "Tributes to Gregorio Weber (1916–1997)," a collection of homages collated by the University of Cardiff which appeared on the Internet, she wrote that "he was by far the brightest of us and by far the most interested in the basic science of medicine." She and Gregorio became inseparable and spent a great deal of leisure time together. She lived with her grandmother in the peripheral Buenos Aires quarter of Mataderos whereas Gregorio lived right in the downtown area, but Carola reminisces that Gregorio would gladly take the 1-hour bus journey, being a regular guest on weekends. Carola's grandmother regularly cooked Gregorio's favorite meal: filet steak. After some months, Carola's grandmother asked whether Gregorio was her "official" boyfriend: "he is so handsome and intelligent, I am sure he is in love with you, have you considered marrying him?" Carola, a bit annoyed, blushed, and responded: "have you considered the possibility that Yoyo is in love with you and your delicious steaks?" As mentioned earlier, they shared a common passion for classical music. On one of their walking expeditions, Gregorio gave her a recording of a Sibelius concert, a present which is dear to her even now. Carola's family had a house by the sea in Mar de Ajo, on the Atlantic coast, and one summer the inner group of medical students enjoyed an unforgettable holiday there. After graduating from Medical School in Buenos Aires in 1944, Carola obtained a fellowship to go to the USA where she specialized in child psychiatry with Leo

Fig. 5 The central patio on the ground floor of the "old" Faculty of Medical Sciences building (currently Faculty of Economy). Prof. Bernardo Houssay's laboratories and the Institute of Physiology where Gregorio Weber performed his Ph.D. thesis work faced the patio with the central fountain. 2016

Kanner at John Hopkins. Kanner was the first physician to be identified as a child psychiatrist in the USA and to introduce the term "autism." Carola married Manfred Guttmacher and subsequently Leon Eisenberg. She became Dean of Students of the Massachusetts Institute of Technology (the first woman to hold that position at MIT), Dean of Student Affairs at Harvard Medical School, and cofounder of Physicians for Human Rights. Carola, Gregorio, and their respective spouses renewed contact in the USA. At the age of 98 she reaffirmed her early love for Gregorio, and at the close of a recent conversation said: ". . .the one thing I regret at this stage of my life is not to have been able to visit Yoyo when he was terminally ill."

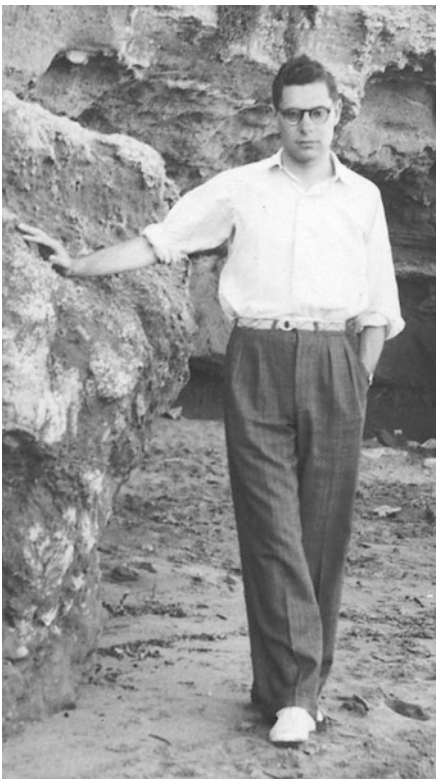

Fig. 6 Young medical student Gregorio Weber, aged 24, on holiday at the sea-side resort of Miramar, in the province of Buenos Aires, 1940

After Ana and Frida married and left the parental home and during Gregorio's time as a medical student, his cousin Nicolás Halperín moved into the family apartment for several years while studying law, sharing hours of study and leisure with Gregorio. Gregorio finished the 6-year medical career in time to graduate in 1942, completing his Ph.D. in medicine the following year. His father Leon had equipped a room for him at home with all the gadgets of the trade, from blood pressure monitor to stethoscope, but according to the family recollections the only time Gregorio ever practiced medicine was apparently when his nephew Enrique burnt his arm with boiling tea (Fig. 6).

5 Scientific Mentors and Influences During Early Research Days in Buenos Aires

Physiology, and in particular the way that Prof. Bernardo Houssay taught it at the Faculty of Medical Sciences, was Gregorio's favorite discipline during his studies at the University of Buenos Aires. Carola Blitzman reminisced that during the physiology lectures she would sit as far away as possible from Prof. Houssay to

avoid being questioned, whereas Gregorio would do the opposite and sit right at the front. When Gregorio felt the lure of basic research, it seems logical that he was attracted to Houssay, the first full-time professor of the university system in Argentina. In the 1930–1940s the Institute of Physiology was a world-class institution where physiologists from other countries were being trained, and one of the few places that cultivated state-of-the-art medically oriented research at the university, supported by the Rockefeller Foundation since 1929. It is also clear that Gregorio made the right choices – he was appointed teaching assistant at the best laboratory available and he had the best supervisor he could possibly find in the whole University of Buenos Aires. Houssay was to become the first Argentine Nobel awardee for Physiology and Medicine in 1947.

During his time at Houssay's Institute of Physiology Gregorio wanted to expand his horizons even further, particularly in physics. But the Faculty of Exact Sciences of the University of Buenos Aires did not have a critical mass of physicists; in fact, most of the Masters and Ph.D. thesis works were conducted in private or federal institutions outside the university, positioning the capital city's physical sciences behind those of La Plata (Province of Buenos Aires), where Emil H. Bose (1909–1911) and Richard Gans (1912–1925) headed the Institute of Physics with clear research aims, and Córdoba, where Gaviola set the pace from the Astronomy Observatory. Physics set off at the University of Buenos Aires with the hiring of Teófilo Isnardi, who had obtained his Ph.D. with Walter Nernst in Germany; the Institute of Physics was not founded until 1935, and the doctorate in Physics was launched in 1937 in marked contrast to Chemistry, for which a doctorate was implemented in 1897. Isnardi's chair was not only an isolated island; he was recognized as "an erudite who appeared to know everything" according to Juan J. Giambiagi, but research was clearly not a priority for him... perhaps not quite what Gregorio was looking for in a mentor.

Gregorio was well acquainted with the work of astrophysicist Ramón Enrique Gaviola in Córdoba, who had worked with Richard Gans at the University of La Plata at the time when Argentina was the only Latin American country whose scientific production in physics was quoted in the Citation Index; in fact Gaviola and Gans were the only two Argentine physicists who had "citation visibility" in Europe. In 1922 Gaviola was at the University of Berlin at the time of Max Planck, Max Born, and Albert Einstein, graduating from the University of Berlin in 1926. Gaviola constructed a phase fluorometer in 1927 [5] and had recorded not only spectra of stars but also, more closely to Gregorio's interests, was the first to measure excited state nanosecond lifetimes by phase fluorometry, with an instrument built in Pringsheim's laboratory [6]. Years later, while in Cambridge, Gregorio gave credit to Gaviola's seminal observations in one of his most famous publications on fluorescence polarization [7]. Gaviola had an immense impact on the development of science in Argentina. He was head of the Astronomy Observatory of Córdoba, founded in 1871, and introduced cosmic radiation research in Argentina. He hired scientists like the Austrian Guido Beck, who organized the so-called nucleus of theoretical physics, a group that led to the foundation of the Argentine Association of Physics in 1944. Gaviola was also a pioneer who

championed full-time research and teaching. He was succeeded by the astrophysicist Livio Gratton, Enrico Gratton's father.

Gregorio's wider interest in Science at large led him to informally train his mind in the subjects more akin to his future calling already during his medical school days. The person who played the key role in shaping Gregorio's choices was his brother-in-law Juan D'Alessio, the chemist and physicist married to his eldest sister, Ana. Juan D'Alessio was a teaching assistant at the Institute of Physics led by Isnardi and was Gregorio's coach in physics and chemistry, the two disciplines to which Gregorio was profoundly attracted and which became fundamental tools in his long research career.

6 Doctoral Thesis at the University of Buenos Aires

Gregorio wrote his first doctoral thesis work on "Viscosity anomalies of fibrinogen solutions" [8] under the formal supervision of Prof. Bernardo Houssay. The manuscript, written in impeccable Spanish, and with handwritten Greek characters in ink, is very short and concise, as was the custom for Ph.D. theses those days at the University of Buenos Aires, and focuses on a brief series of concatenated physicochemical experiments. It starts with theoretical considerations based on Newton's hypothesis on internal friction in liquids and the hydrodynamics of ideal liquids formulated one century later by Euler, Bernoulli, and others as a background for the experimental section on the thixotropy and other viscosity anomalies of fibrinogen solutions. Gregorio built an Ubbelohde-type viscometer and subsequently a Tsuda viscometer to be able to carry out his work. At the time Gregorio was reading for his thesis, the Faculty of Medical Sciences had appointed Dr. Venancio Deulofeu as professor of Biological Chemistry (1935) and Dr. Julio J. Rossignoli was in charge of Biological Physics at the Institute of Physiology. More interestingly, Dr. Dora Potick was studying the physicochemical alterations of blood serum by snake venoms. This is the closest thematic approximation to Gregorio's thesis subject. We do not know whether any of these scientists played a role in Gregorio's thesis, but they were likely to be knowledgeable in some aspects of the work. In my view Gregorio's first thesis is a cauldron in which the embryonic stages of his views on macroscopic and microscopic viscosities were concocted, and which he addressed years later after developing the appropriate fluorescence polarization tools (Figs. 6 and 7).

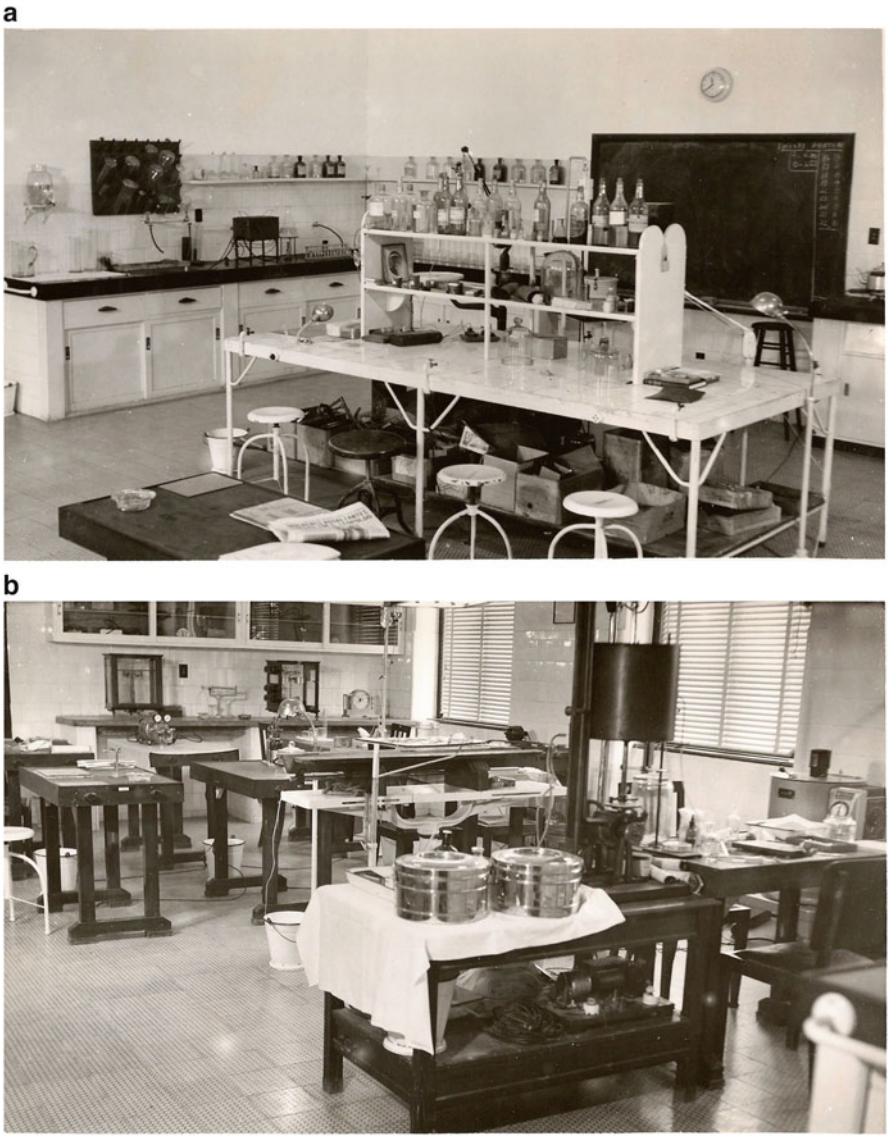

Fig. 7 (**a**–**b**). Laboratories at the Institute of Physiology, Faculty of Medical Sciences, University of Buenos Aires, where Gregorio Weber performed his experimental work on fibrinogen reading for his Ph.D. Thesis. Photographs ca. 1936

7 Second Law of Thermodynamics: Irreversible Departure from Argentina

As a background to Gregorio's medical school days a democratically elected president brought back the Radical party and a period of stability (1938–1942) to Argentina. The Rector of the University of Buenos Aires was Carlos Saavedra Lamas, a professor in international and labor law who in 1936 had been the first Latin America Nobel Prize recipient (for Peace). However, by the time Gregorio left Argentina for England in 1943, the constitutional government was unpopular and weakened; the country was profoundly divided into the supporters of the Axis powers or the Allies in World War II, the army exerting enormous pressure on the government. An interim president and a new military coup followed in rapid succession. The universities were in turmoil, becoming strongholds of resistance against the de facto rulers, and some of the most outspoken professors, Houssay included, signed a manifesto against the government. By October 1943 they had been dismissed from the University. So Gregorio must have been able to participate in a democratic vote only once in his home country, and left Argentina at the climax of disturbances within the University, amidst a chaotic situation. Just like Gregorio's science teacher at school [4], Prof. Houssay did not encourage medical graduates to engage in full-time scientific research in Argentina unless they had the private means to support themselves (see, e.g., [9]): "You're not rich are you? Because I can't offer you anything.... the paid positions I have at the Institute are all occupied and they'll never increase the number of posts." Against this backdrop it is not surprising then, that Gregorio applied for and won a British Council Fellowship which would support his second Ph.D. studies at Cambridge University. According to his classmate and friend Carola Blitzman Eisenberg when he left for the UK "...Yoyo could hardly contain his enthusiasm and excitement with his new life ahead...". Apparently his father Leon was the major force behind Gregorio's decision to travel abroad. He passionately supported his son's choice of career and told Gregorio "all I have is at your disposal to follow your dream, anywhere in the world, even if it means never seeing you again."

I will not dwell on Gregorio's stay of several years in Cambridge and Sheffield (a subject covered copiously elsewhere; the reader is referred to a delightful short paper by Brian Hartley [10] and the most read homage articles on Gregorio, by Dave Jameson [1, 4] and Chapter 1 by Jameson in this monograph) except for a brief mention of an anecdote at the commencement of his stay. Upon arriving in England Gregorio stayed a few days in London before going on to Cambridge. As was customary, he was asked to leave his passport at the hotel reception desk. When he went to retrieve it upon leaving the hotel, it couldn't be found; it had mysteriously disappeared and he had to go through painstaking red tape to get a replacement. Apparently this was not an isolated incident and it was surmised at the time (1943) that Gregorio's passport joined the many others being used to help people attempting to escape from the Holocaust.

According to his friends, Gregorio was eager to leave Argentina in search of new horizons, but his almost 3 decades in Buenos Aires had already marked him forever. By the time he left he had command of other languages besides his native Spanish, having an innate ability to rapidly expand his vocabulary and read avidly in the original idiom.[2] He carried with him his distinct, unmistakable "porteño" accent in his native Spanish (not to be confused with the "Lunfardo" underworld slang) with a remarkable richness of terms and nuances; he also carried with him years of readings of his contemporary literary geniuses, like Borges, whose poems appeared first as pleasant surprises in a local newspaper. Gregorio's departure and personal background have a parallelism with César Milstein's, who left Argentina about a decade later: the two headed to Cambridge after finishing their first thesis work at the same Faculty of Medical Sciences, and both earned a second Ph.D. at Cambridge University. Both Gregorio and César were sons of immigrants, and the two had Ukrainian ancestors. The two were born, spent their youth, and were educated and professionally trained in Argentina, but found their success as scientists abroad.

8 Family Reencounters in the Northern Hemisphere

During Gregorio's stay in England his father Leon visited him several times, and back in Buenos Aires Leon and his married daughters eagerly awaited Gregorio's letters, concerned about the austerity of war and post-war conditions. Leon would personally make regular trips to the port of Buenos Aires to ship a box addressed to Gregorio's wife, Shirley Nixon Weber, containing Argentine goodies: tinned corned beef, *dulce de leche* and a special type of soft cheese, a ritual which involved endless red tape procedures. Years later, in January 1963, Gregorio's sister Frida, Mrs Kurlat by then, organized a trip to the UK with the whole family on the vessel "HMS Arlanza" with the idea of getting to know Shirley personally. Luck would have it that by the time the family arrived in England Gregorio and family had moved to Urbana-Champaign!

In the pre-laser era, a "short" light pulse was in the order of 20–50 ns. When Gregorio's brother-in-law Juan D'Alessio was at the Atomic Energy Commission in Argentina in 1961, he worked very hard trying to produce a lamp generating pulses of shorter duration and high energy to study second-order reactions in his flash photolysis experiments. In 1963 he was invited to work at Notre Dame University in Indiana where he spent 2 years continuing his research on flash photolysis, managing to lower the duration of the pulses to 10 ns. His stay at Indiana enabled

[2] Dave Jameson described Gregorio's appreciation of the written language of Francis Perrin [4]: "…it was written in that transparent, terse style of XVIII century France, which I have tried, perhaps unsuccessfully, to imitate from then onwards." In my view, Gregorio definitely did achieve what he sought: elegance, precision and conciseness of expression in his written and oral language.

the D'Alessio family to resume the close relationship with Gregorio. Gregorio's nephew Enrique D'Alessio, a physicist, spent prolonged periods at Gregorio's apartment in Urbana. Back in Buenos Aires, Juan D'Alessio succeeded in further reducing the lamp pulses to less than 1 ns by using electrodes covered in liquid Hg which self-renewed themselves after each pulse. More than once I listened to Gregorio telling me about the splendid D'Alessio flash mercury lamp which obviously interested him as an excitation source for his polarization measurements. Pulsed lamps were subsequently superseded by high intensity laser sources with $<$0.1 ns pulses, but back in the D'Alessio lamp was one of the few instruments capable of delivering high intensity pulses with a decay time of 0.55 ns and which could be operated up to 50,000 pulses s^{-1} in the 250–600 nm range (D'Alessio et al. 1964).

9 His Long Visit in 1970: A Brief Incursion into Argentine Neuroscience

In the membrane field, the series of polarity-sensitive fluorescent probes derived from (2-(dimethylamino)-6-(acyl)naphtalene introduced by Weber in the late 1970s [11] are among the best-known and most used fluorescent compounds. When solvent polarity increases, probes of this series (Laurdan, Prodan, Acrylodan, Patman) share the property of undergoing bathochromic shifts in their fluorescence emission spectra. The basis of this phenomenon is the increase in the dipole moment in the excited state, relative to that of the molecule in the ground state. From a chemical standpoint, the members of this family of environmentally sensitive fluorescent molecules share a naphthalene structure substituted with an electron acceptor (acyl substituted carbonyl group) and donor (alkylamino group) groups.

In 1970, well before the introduction of Prodan [11] and other dansyl polarity-sensitive fluorescent probes, which were to become so useful in membrane research, Gregorio visited his alma mater, the Faculty of Medicine at the University of Buenos Aires. This visit included the Institute of Cell Biology, where I was reading for my Ph.D. under the supervision of Eduardo De Robertis. The two knew each other from medical school days. After discussing the state of affairs in the lab, Gregorio suggested the synthesis of a dansyl-choline environmentally sensitive fluorescent ligand to study the aqueous-organic solvent partition properties of hydrophobic lipoproteins being studied in De Robertis' laboratory. The probe (1-dimethylaminonaphtalene-5-sulfonamidoethyl-trimethylammonium) was synthesized in Urbana-Champaign by one of Gregorio's students, David P. Borris, and was coined "DNETMA" or simply dansyl-choline. I performed the fluorimetric measurements under Gregorio's supervision (Fig. 8).

This was my first serious lesson in fluorescence spectroscopy – directly coached by the master in the field! The ingeniously simple experimental technique designed by Gregorio involved titration experiments in a two-phase solvent system [12].

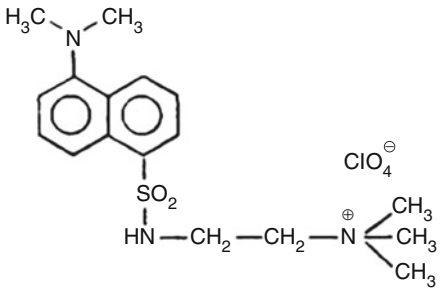

Fig. 8 Dansyl-choline (1-dimethyl aminonaphtalene 5-sulphonamido ethyl-trimethylammonium perchlorate), an environmentally sensitive fluorescent probe with cholinergic pharmacological activity, designed by Gregorio Weber in Buenos Aires [12] during his 1970 working visit. The compound was subsequently used by Changeux's group at the Pasteur Institute [15] and addition of a longer spacer arm (C6) conferred the compound agonist activity [27–29]

The lower, organic phase contained the hydrophobic lipoprotein; dansyl-choline was initially present in the upper, aqueous phase. After equilibration, the fluorescence emission in the upper aqueous phase was measured and subsequently a series of non-fluorescent acetylcholine-mimicking compounds, i.e. cholinergic ligands like acetylcholine or decamethonium were added and fluorescence intensity recorded again. Professor Weber wrote down the readings by hand as his student Pancho performed the titrations in the Amino-Bowman fluorimeter; the time gaps in between additions were filled in by subtle comments and teachings on every possible subject – what a privilege! I still keep those records. Dansyl-choline shared the ethyl-trimethylammonium end with the natural neurotransmitter, acetylcholine, exhibited a high affinity for the lipoprotein binding acetylcholine in the organic phase [13] and for horse serum cholinesterase in aqueous media [14]. The compound thus became the first fluorescent probe for the study of cholinergic macromolecules, and the introduction of a propane spacer arm having an additional carbon was adopted in a subsequent version synthesized by Jean-Pierre Changeux's group at the Pasteur Institute. This series of experiments was performed on the membrane-bound nicotinic acetylcholine receptor from *Torpedo marmorata* electric tissue by Jonathan Cohen at the Pasteur Institute in Paris [15, 16].

During this visit to Argentina Gregorio was appointed honorary President of the Albert Einstein Center for Medical Research (CIMAE), a position which he held until 1997. He used this platform to deliver several courses on fluorescence spectroscopy and protein–ligand interactions which gathered essentially all young researchers interested in these topics and became a landmark in the field. Some of the formulae written on the blackboard and the notes that Gregorio scribbled down during that period were to become part of his classic book on Protein Interactions, dedicated to "those who put doubt above belief" [17]).

I feel very privileged to have been an active player during Gregorio Weber's first and only scientific incursion in the field of fluorescence in Argentina. I couldn't have wished for a more motivating teacher to prod my mind.

10 Gregorio Weber's Influence: A Personal Experience

Gregorio had a profound influence on my scientific career in several ways. The first resulted from the somewhat serendipitous choice made by my Ph.D. supervisor, Eduardo De Robertis, to put his student – me- under Gregorio's mentoring during his prolonged 1970s visit to Buenos Aires. This guru–shishya relationship was probably the best teacher–apprentice relationship I have ever had, involving a one-on-one crash course in fluorescence techniques! A few years later, when I was a fresh postdoc working with De Robertis and waiting for a position abroad to materialize, Gregorio was again to play a crucial role in my scientific career. I had applied to the Royal Society in London and was awarded a fellowship to go to Cambridge. Enthused with the success of my application, I wrote to Gregorio telling him the good news. My letter crossed with his, written during his sabbatical leave in Europe in 1973, where he told me he had met "a young scientist who had worked with Manfred Eigen and now heads the Department of Molecular Biology at the Max-Planck Institute for Biophysical Chemistry in Göttingen." The young scientist was Tom Jovin. In his letter, Gregorio suggested that I join Tom to start a group working on membranes and receptors. I followed Gregorio's advice and within 3 months I became a member of Tom's Department.

When I wrote my Ph.D. thesis in Buenos Aires, I consulted with my supervisor, Prof. De Robertis, about possible ways to defray the cost of printing the more than 10 copies needed (this may sound ludicrous now, but in those days it was done at expensive typesetting printing houses). Without further explanation, De Robertis told me to go and see a Dr. Podolski, president of a pharmaceutical firm. Dr. Podolski complied with my request and I happily received the funds to have my thesis printed. Many years later, after Gregorio sadly passed away I was contacted by friends in Urbana-Champaign in relation to raising funds to support the Gregorio Weber Memorial Fund at the University of Illinois. At that time I was back in Argentina, working at the University in Bahía Blanca. It occurred to me to phone Dr. Podolski again. When I explained the purpose of my call, without so much as a pause, he immediately replied "yes, of course, you can come and collect a check at your earliest convenience." It was a very generous sum for local standards. It is only now, through my research on Gregorio, that I learn Dr. Podolski was the very same Miguel Podolski who was one of Gregorio's "inner circle" during his medical school years in Buenos Aires!

During my stay in Göttingen, Gregorio's influence continued. Together with Hansjörg Eibl, and inspired by Gregorio's work on pyrene butyric acid, a very long lifetime fluorescent probe (e.g., [18, 19]), we synthesized 1-pyrene butyryl-choline (PBC). This pharmacologically active fluorescent probe which, tested by Bert Sakmann on the nicotinic acetylcholine receptor at the frog neuromuscular junction, turned out to be a blocker of cholinergic neurotransmission, a work presented to PNAS by Manfred Eigen [20]. We extended the use of PBC and related compounds to the study of the high-affinity choline uptake mechanism in synaptic endings [21]. We next resorted to another of Gregorio's favorites, tryptophan fluorescence; together with Tom Jovin and Bob Bonner we successfully used the

meager intrinsic fluorescence emission of the membrane-bound nicotinic receptor to measure agonist–receptor interactions using stopped-flow techniques [22, 23]. After joining forces with Bert Sakmann and Erwin Neher as a 5-year new research group at the Max-Planck Institute in Göttingen, I resorted to intrinsic fluorescence quenching and stopped-flow rapid kinetics experiments to study the ligand-induced desensitization phenomenon [24] and with Yusuf Tan we used the pyrene butyryl-choline derivatives and other extrinsic probes as pharmacological tools interrogated with T-jump fast kinetics to learn about antagonist ligand–receptor interactions [25, 26].

11 Exploring a Possible Return

At one point Gregorio had seriously considered the possibility of returning to Argentina and made his first short exploratory visit in 1947. He must have been quite amazed at that time to see the transformation of Buenos Aires after the installation of Peron's first presidency in 1946 and the process of internal migration with people from the countryside moving to the great city, coincident with the incipient industrialization of the country. However, the situation at the university under Peron's administration was hardly propitious for a possible reinsertion into the academic arena. His former supervisor, Bernardo Houssay, who was reincorporated to the University of Buenos Aires under the general amnesty in 1945, had been ousted from the university for a second time because of his liberal political ideas, and several other scientists had gone into exile. Gregorio's sister Frida was also thrown out of the University for political reasons. This scenario must have surely impinged on Gregorio's decision not to settle in Argentina at that time.

In 1951, the National Council of Technical and Scientific Investigations (CONITYC) was founded during Perón's second presidency. Physicists like José Balseiro, Enrique Gaviola, nuclear engineer Otto Gamba and astronomer Juan Bussolini were involved. This body was dissolved in 1955 by a military regime. By the time the current Argentine Scientific and Technical Research Council (CONICET) was created in 1958 with Gregorio's Ph.D. supervisor Bernardo Houssay as its first president, Gregorio was firmly settled abroad. The relationship with his home country would flow in the opposite direction, with the recruitment in Urbana of several Argentine students over the course of the subsequent decades: Roberto Morero, Alejandro Paladini, Leonardo Erijman and myself.

12 Subsequent Short Visits to Buenos Aires

More than a decade after his first prolonged visit to Buenos Aires in 1970, Gregorio decided to buy a pied-à-terre where he could stay from time to time and perhaps encourage his daughters to spend time with the Argentine branch of the family.

He bought an apartment in Vicente López on the northern outskirts of Buenos Aires and asked me to help him choose all that was needed to furnish the place. As with most other things in life, Gregorio had a developed sense of esthetics, and fortunately we found an adequate furniture shop that had a vast collection of mid-twentieth century modern classics. Before his corneal implant Gregorio's sight had deteriorated considerably, especially when looking downwards. During one of his visits to Argentina, leaving the apartment his sister called his attention to the fact that the shoes he was wearing didn't match; Gregorio looked at them and said with his customary humor: "Oh, yes, I must have another pair like this in the closet." During the 1970s and up to the mid 1990s Gregorio visited Argentina fairly regularly, spending December/January with the D'Alessio or Kurlat families, and living alternatively at his apartment or at the sea-side resort of Punta del Este, in Uruguay, with his friend Ruth Meerapfel. Ruth was a delightful, cultivated German lady from Karlsruhe who had escaped from the Nazi regime to the Netherlands during World War II, hiding above the same premises as Anne Frank at Prinsengracht 263 in Amsterdam. She and Gregorio had developed a very close friendship. Ruth's stepdaughter is a German-Argentine film director and screenwriter, and was a member of the 1984 jury for the Berlin Film Festival, the Berlinale, and currently president of the Berlin Akademie der Künste.

Thanks to Gregorio's generosity, my daughters Alexandra and Caroline lived in his apartment during term-time when they studied at university in Buenos Aires (we were living in Bahia Blanca at this time). The only proviso was that it be available for him during his summer visits. The arrangement worked admirably and Gregorio was delighted with two young ladies looking after his place. And I of course took every possible opportunity to engage in intellectual and gastronomical experiments with him in Buenos Aires.

In 1980 Gregorio's sister Frida was diagnosed with a metastatic melanoma in her brain. Faced with this family emergency, Gregorio set off from Urbana in a rush but upon completing the first leg of his flight in Miami, he realized that his documents were not in order. His family rapidly intervened to ensure he got the required papers in Miami so he could continue his journey on to Buenos Aires without further delay. His cousin Anita told me that on other more cheerful visits to Argentina, Gregorio used to wave goodbye saying "keep away from the doctor." At the healthy age of 100 she seems to have kept strictly to this rule.

In 1987 I organized a meeting in San Martin de los Andes, a small town within the beautiful Lanin National Park against the backdrop of the foothills of the Andes, in the Patagonian province of Neuquén. Gregorio was the guest of honor and his presence was an unforgettable experience, especially for the younger generations (Fig. 9). Although he continued visiting Argentina to see his family and friends, this was one of his last scientific interventions in Argentina. His very last visit was in 1997, when already physically weak with his terminal leukemia, he came to bid farewell to his closest relatives.

Fig. 9 From *left* to *right*: Gregorio Weber at the San Martin de los Andes meeting with the author of this chapter and Drs. George Hess (Cornell University) and Julio Azcurra (Univ. of Buenos Aires). 1987

Acknowledgement My sincere gratitude to Isabel Kurlat de Zitzer and Enrique D' Alessio, Gregorio's niece and nephew, for the very enjoyable time they generously shared with me, conversing about the family links and Gregorio's background, and for providing unique photographic material. I am particularly grateful to Gregorio's 100-year-old cousin Anita Wolovick, daughter of Cecilia Gerchunoff and Miguel Wolovik, to Dr. Carola Eisenberg, currently 98, and to Isabel Fernández Vega (Mauricio Goldenberg's widow), aged 96, for sharing their first-hand life-enduring reminiscences and marvelous stories of Gregorio. I also thank Gregorio's daughter Juliet for contributing photographic material, and Dr. Antonia Stoppani, for telling me about her late husband's close contacts with Gregorio. Finally, I thank my wife, Phyllis, for critical reading of the manuscript and valuable suggestions.

References

1. Jameson DM (1998) Gregorio Weber, 1916–1997: a fluorescent lifetime. Biophys J 75 (1):419–421. doi:10.1016/s0006-3495(98)77528-9
2. Sinay J (2014) Los crímenes de Moisés Ville: una historia de gauchos y judíos.1a ed. 2a reim. - Buenos Aires, Tusquet Editores. ISBN 978-987-670-185-3. 304 pp
3. Romanos M (2003) Contribución argentina a la historiografía de la crítica del teatro español áureo Los trabajos de Frida Weber de Kurlat. I Jornadas de Historia de la Crítica en la Argentina 1:228–235
4. Jameson DM (2001) The seminal contributions of Gregorio Weber to modern fluorescence spectroscopy. In: Valeur B, Brochon J-C (eds) New trends in fluorescence spectroscopy, Springer series on fluorescence, vol 1. Springer, Berlin/Heidelberg, pp 35–58
5. Gaviola E (1927) Ein Fluorometer. Apparat zur Messung von Fluoreszenzabklingungszeiten. Z Phys 42:853–861
6. Gaviola E, Pringsheim P (1924) Über den Einfluß der Konzentration auf die Polarisation der Fluoreszenz von Farbstofflösungen. Z Phys 24:24–36
7. Weber G (1952) Polarization of the fluorescence of macromolecules. I. Theory and experimental method. Biochem J 51(2):145–155
8. Weber G (1943) Anomalías de la viscosidad de las soluciones de fibrinógeno. Tesis de Doctorado, Escuela de Medicina, Facultad de Ciencias Médicas, Universidad Nacional de Buenos Aires, pp 47
9. Pasqualini RQ (1999) En Busca de la Medicina Perdida. Editorial de Belgrano, Buenos Aires

10. Hartley B (2004) The first floor, department of biochemistry, university of cambridge (1952–58). IUBMB life 56(7):437–439. doi:10.1080/15216540412331318974
11. Weber G, Farris FJ (1979) Synthesis and spectral properties of a hydrophobic fluorescent probe: 6-propionyl-2-(dimethylamino)naphthalene. Biochemistry 18(14):3075–3078
12. Weber G, Borris DP, De Robertis E, Barrantes FJ, La Torre JL, Llorente de Carlin MC (1971) The use of a cholinergic fluorescent probe for the study of the receptor proteolipid. Mol Pharmacol 7(5):530–537
13. De Robertis E (1971) Molecular biology of synaptic receptors. Science 171(3975):963–971
14. Mayer RT, Himel CM (1972) Dynamics of fluorescent probe-cholinesterase reactions. Biochemistry 11(11):2082–2090
15. Cohen JB, Changeux JP (1973) Interaction of a fluorescent ligand with membrane-bound cholinergic receptor from *Torpedo marmorata*. Biochemistry 12(24):4855–4864
16. Cohen JB, Weber M, Changeux J-P (1974) Effects of local anesthetics and calcium on the interaction of cholinergic ligands with the nicotinic receptor protein from Torpedo marmorata. Mol Pharmacol 10:904–932
17. Weber G (1992) Protein interactions. Chapman and Hall, New York/London, p 293
18. Knopp JA, Weber G (1969) Fluorescence polarization of pyrenebutyric-bovine serum albumin and pyrenebutyric-human macroglobulin conjugates. J Biol Chem 244(23):6309–6315
19. Vaughan WM, Weber G (1970) Oxygen quenching of pyrenebutyric acid fluorescence in water. A dynamic probe of the microenvironment. Biochemistry 9(3):464–473
20. Barrantes FJ, Sakmann B, Bonner R, Eibl H, Jovin TM (1975) 1-Pyrene-butyrylcholine: a fluorescent probe for the cholinergic system. Proc Natl Acad Sci USA 72(8):3097–3101
21. Dowdall MJ, Barrantes FJ, Stender W, Jovin TM (1976) Inhibitory action of 1-pyrene butyrylcholine and related compounds on choline uptake by cholinergic nerve endings. J Neurochem 27(5):1253–1255
22. Bonner R, Barrantes FJ, Jovin TM (1976) Kinetics of agonist-induced intrinsic fluorescence changes in membrane-bound acetylcholine receptor. Nature 263:429–431
23. Barrantes FJ (1976) Intrinsic fluorescence of the membrane-bound acetylcholine receptor: its quenching by suberyldicholine. Biochem Biophys Res Commun 72(2):479–488
24. Barrantes FJ (1978) Agonist-mediated changes of the acetylcholine receptor in its membrane environment. J Mol Biol 124(1):1–26
25. Tan YP, Stender W, Harvey AL, Soria B, Barrantes FJ (1980) Interactions of fluorescent cholinergic antagonist with the membrane-bound acetylcholine receptor. Neurochem Int 2:257–267
26. Tan Y, Barrantes FJ (1980) Fast kinetics of antagonist-acetylcholine receptor interactions: a temperature-jump relaxation study. Biochem Biophys Res Commun 92(3):766–774. doi:10.1016/0006-291X(80)90769-X
27. Herz JM, Johnson DA, Taylor P (1989) Distance between the agonist and noncompetitive inhibitor sites on the nicotinic acetylcholine receptor. J Biol Chem 264:12439–12448
28. Heidmann T, Changeux J-P (1979) Fast kinetic studies on the interaction of a fluorescent agonist with the membrane-bound acetylcholine receptor from *Torpedo marmorata*. Eur J Biochem 94:255–279
29. Heidmann T, Changeux J-P (1980) Interaction of a fluorescent agonist with the membrane-bound acetylcholine receptor from *Torpedo marmorata* in the millisecond time range: resolution of an “intermediate” conformational transition and evidence for positive cooperative effects. Biochem Biophys Res Commun 97:889–896
30. Jameson DM (2016) A fluorescent lifetime: reminiscing about Gregorio Weber. Springer Ser Fluoresc. doi:10.1007/4243_2016_13

The Labyrinthine World of Gregorio Weber

Thomas M. Jovin

Abstract The trajectory of Gregorio Weber from his childhood to scientific eminence is examined in the context of the major personages and other influences that he encountered on the way. In the process, unique aspects of his personality, intellect, and philosophical outlook become apparent.

Keywords D'Alessio JT • Gaviola E • Houssay B • Weber number • Yoyo

Contents

T.M. Jovin (✉)
Laboratory of Cellular Dynamics, Max Planck Institute for Biophysical Chemistry, Göttingen, Germany
e-mail: tjovin@gwdg.de

D.M. Jameson (ed.), *Perspectives on Fluorescence: A Tribute to Gregorio Weber*,
Springer Ser Fluoresc (2016) 17: 41–56, DOI 10.1007/4243_2016_16,

1 Getting to Know Gregorio Weber

My first encounter with Gregorio Weber – admittedly indirect – was in 1947. I was 8 years old. Our family flew from Buenos Aires, Argentina, to New York City in a brand new DC4 of Pan American, a journey of almost 2 days. My father, a chemical engineer, was acquainted with a distinguished scientist on board and introduced me to him. His name was Prof. Bernardo Houssay (Fig. 1) and he was on the way to accept the 1947 Nobel Prize in Physiology or Medicine, the first such recognition of scientific excellence in Latin America. In the same year, Houssay's former assistant and protegé, Gregorio Weber (GW [1]), was awarded a PhD in Biochemistry by the faculty of Biology of the University of Cambridge, England.

2 Why This Chapter

Unlike most of the other authors in this volume, I neither studied nor worked nor published with GW, a cardinal oversight on my part. And the experience related above cannot by itself justify my contribution to a book celebrating the centennial of GW's birth. I surmise that Dave Jameson must have felt that enough GW "alumni" and even a relative+scientist (grandniece Cecilia D'Alessio) had passed through – and even survived – our lab (GW visited to make sure), such that *some* relationship of interest must have existed. The alumni were: Francisco ("Pancho") Barrantes, Rob Macgregor, Gerard Marriott, Leonardo ("Leo") Erijman (GW's last postdoc) and his scientist wife Elizabeth ("Eli") Jares-Erijman, who had not worked with GW. Eli came to my lab and Leo to that of Robert ("Bob"), Clegg, a group leader in our Department of Molecular Biology at the Max Planck Institute for Biophysical Chemistry in Göttingen. All of these individuals enriched our scientific and personal lives enormously. Perhaps as a consequence, Bob Clegg underwent a process of "retrograde transfer," at first spending a sabbatical year with GW at the University of Illinois at Urbana-Champaign, and in 1998 accepting a professorial appointment at the urging of Enrico Gratton.[2] In his omniscience Dave may have also recognized the fact that as a "fluorescence fanatic" I belong to the vast community of scientists (and others) who came under the spell of the unique individual we are honoring, and thus can serve as a "prototypic" GW admirer. I have chosen to devote my account primarily to an arbitrary selection of observations, snippets of information, and conjectures seeking to explain how it was that GW developed into the individual who so profoundly influenced our lives. The

[1] I have chosen this condensed form of reference, rather than "Weber," which somehow feels inappropriate.

[2] Eli Jares-Erijman and Bob Clegg, esteemed colleagues, died tragically from cancer in 2011 and 2012, respectively. I have written elsewhere [22] a commemoration of their persons and scientific contributions.

Fig. 1 The three individuals who provided a significant impetus to Gregorio Weber's early career decisions (see text)

treatment has a distinct Argentine bias. Most historical periods and events in GW's career are dealt with in greater detail and accuracy by the fellow authors of this volume, who had a direct, intimate association with GW in the USA and in Argentina (see the chapter of Francisco Barrantes). Dave Jameson has frequently and eloquently narrated GW's scientific legacy in written and oral form [1].

The next, as yet indirect, contact with GW was via Mike Naughton, a coauthor of my first publication in 1964. Mike, a supremely eccentric member of the Biophysics Department of Johns Hopkins Medical School, was an ex associate of Fred Sanger (Nobel Laureate × 2) at Cambridge, and Fred was a close colleague of GW in the 1940s [2]. My first face-to-face encounter with GW and some members of his group was in 1972 – finally! – at a remarkable meeting in Seattle of notables in fluorescence (Fig. 2), who were accompanied by some amateurs like me (as indicated by my position in the photo). By that time, I had been chronically infected with the fluorescence bug (see later section below) and was well aware of the legendary scientist and fellow Argentinian, GW. We hit it off, scientifically and personally.[3]

3 The Historical Brain Drain from Argentina

Let us turn back the clock, to even before 1943, the year in which GW undertook his dangerous exodus to the UK by ship. We probably would not been writing and reading this book were it not for the intervention of certain individuals at key

[3] I communicated with GW in *lunfardo*, the peculiar form of Spanish used particularly in Buenos Aires, in which the second person singular *vos* (and its associated verb forms) replaces the *tu*. It implies intimacy and equality, as opposed to normal Spanish (or English) and "the Professor," which many of GW associates seem to have utilized.

Fig. 2 Participants of the conference *Quantitative Fluorescence Techniques as Applied in Cellular Biology*, Battelle Seattle Research Center. March 27–31, 1972. Names: 1. George Guilbault; 2. Torbiörn Caspersson; 3. Rudolf Rigler; 4. Hans Neurath; 5. Bill Ware; 6. Jane Vanderkooi; 7. Juan Yguerabide; 8. Lenny Brand; 9. George Radda; 10. Gregorio Weber; 11. Ray Chen; 12. Dick Spencer; 13. George Mitchell; 14. Scott Cram; 15. Marv van Dilla; 16. Mack Fulwyler; 17. Jean LePecq; 18. Elli Kohen; 19. Bo Thorell; and 20. Tom Jovin. Spencer and Mitchell were in GW's group at the time

moments in GW's life. It is useful to first consider the circumstances in the country Argentina around the time of his birth. In 1916, the government passed from the hands of the conservatives to the liberal Radical party, initiating a period of somewhat ambiguous social reform and of economic prosperity resulting from massive agricultural exports and the neutrality of Argentina in WW I. In science

and education, the start of the century was marked by the consolidation of key developments in the previous 50 years, specifically the creation of: the Department of Exact Sciences at the University of Buenos Aires (1865); the National Academy of Sciences (1869; Charles Darwin was named a corresponding member in 1876); the Scientific Society (1872); and the Astronomical Observatory of Córdoba (1871). Much of this activity was promoted by the prescient, erudite, literary, liberal President Domingo Faustino Sarmiento. The policy was adopted of actively importing brains (professors) and academic research experience, mainly from Europe and also from the USA. Yet after 1900, there was also movement of individuals in the opposite direction, and I cite four cases involving exceptional Argentine scientists (there were more): (Guido Ramón) Enrique Gaviola (1922), Luis Federico Leloir (1936), Gregorio Weber (1943), and César Milstein (1958); the indicated dates are those of their departure from Argentina for graduate or postgraduate work abroad. I will provide further details below but first present some rather remarkable observations that bring GW's experience into perspective:

- Leloir, GW, and Milstein (the first two MDs and both at the urging of Bernardo Houssay) went to the University of Cambridge, and *all three* trained with the enzymologist Malcom Dixon.[4] Milstein received a second PhD from Cambridge, working with Fred Sanger.
- Gaviola, GW, and Milstein made fundamental, pioneering contributions to theoretical, experimental, and applied fluorescence.
- Leloir and Milstein received Nobel Prizes (1970 in Chemistry and 1984 in Physiology or Medicine, respectively). In the estimation of many (myself included), GW was also deserving of such recognition. I don't know if he was ever nominated.
- All four were in opposition to periodic oppressive governmental policies and actions in Argentina and opted for temporary or permanent exile, three of them (Gaviola, Leloir, and GW) to the USA, Milstein to England.[5]

[4] One can maintain that Malcom Dixon should have been awarded honorary Argentine citizenship for his efforts.

[5] An understanding of the circumstances that have dictated the decision of Argentine scientists to remain (or not) in the country requires a somewhat detailed account. Gaviola, as President of the Argentine Physics Society that he had created, issued a memorandum in 1946 [23] in which he anticipated that because of the postwar political and economic insecurity in Europe and the imposition (tj: *his* perception) of secrecy and censure in the USA, it would be possible to attract first rate scientists to Argentina if they would be provided with the means and the freedom for conducting research and publishing their results without restrictions. GW seems *not* to have perceived the existence of such conditions when he returned for a visit, the first in 4 years, after his PhD award in 1947; his next trip to Argentina was to be many years later. By some accounts, even his mentor Houssay, on the brink of becoming the most important scientific figure in the country, discouraged him from staying, although ambiguity exists about this issue. By 1958, Gaviola himself recognized fundamental deficiencies in the educational system and advocated the creation of private universities in response. GW was a visiting professor/lecturer in the USA in the late 1950s and early 1960s and moved permanently to Illinois in 1962. The fact is that the brain drain of exceptional scientists from Argentina continues to this day, mostly to the USA but

4 Enrique Gaviola

Enrique Gaviola is one of the most influential scientists in Argentine history (Fig. 1). He is recognized as: (1) the first argentine astrophysicist (asteroid 2504 was named after him and asteroid 5987 after Livio Gratton, Enrico Gratton's likewise distinguished astrophysicist father and Gaviola's colleague); (2) an exceptional teacher, also of the general public. He published an article, one of many, in the newspaper *La Prensa* in June, 1930, with what today could be a very topical title (in translation) "The limits of physical knowledge and human vanity. Can we expect an unlimited increase in the accuracy of our measurements with the progress of technology?"; (3) a visionary and activist of and in scientific politics; and (4) a pillar of morality and integrity, including serving as an "Oscar Schindler of scientists" during WW II. Gaviola graduated from the National University of La Plata as a surveyor (!) in 1921 but had developed an interest in mathematics and physics and was thus urged by Richard Gans (one of the "imported" German physicists) to pursue his studies in Germany. He arrived in 1922 to Göttingen, the epicenter of the quantum mechanical revolution. He took courses from the likes of Emmy Noether, James Franck, Adolf Windaus, David Hilbert, Gustav Tammann, Edmund Landau, Richard Courant, Max Born, and Robert Pohl. However, he longed for the big city and transferred to Berlin, where he studied under Albert Einstein, Lise Meitner, Peter Pringsheim, Max von Laue, and Walther Nernst. These lists include 6 Nobel Laureates, and the latter two directed Gaviola's PhD thesis (not bad for a 26-yr-old from Argentina!), awarded in 1926 *magna cum laude* by what is now the Humboldt University. The thesis, entitled (in translation) "The Fluorescence Decay of Dye Solutions," was published in the Ann. der Physik [3] and the novel lifetime apparatus, the "Fluorometer," independently in Z. der Physik [4], a less detailed publication but most often cited as the first experimental demonstration of fluorescence decay measurements *yielding correct results*. Gaviola presented data for the dependence of the lifetimes on temperature, solvent, viscosity, and concentration. He also considered the time lag or "dark-time" quandary of that time, namely the question as to whether if one illuminates a fluorescent substance with a short pulse, it remains dark for a certain finite time before "bursting" into luminosity, which then decreases exponentially. Gaviola concluded that such a dark period does not exist; we will return to this issue below. Gaviola published key papers with his mentor Peter Pringsheim (who also

---

increasingly to Europe. A few current, notable cases: Gabriela González (experimental physicist, recent co-discoverer of gravitational waves); Juan Martín Maldacena (theoretical physicist, leading string theory idealogue); and Miguel San Martín (software engineer, responsible for the descent of the rover Curiosity to the surface of Mars). Fortunately, about a decade ago the Argentine government instituted a coherent program ("Raíces," a word meaning "roots" but really the Spanish acronym for the Network of Argentine Scientists Abroad), promoting repatriation of young investigators and instituting significant improvements in scientific infrastructure and support. As a result, Argentine science in 2016 is doing relatively well, and this in spite of the endemic economic (I avoid commenting on the political) vicissitudes.

later ended up in the USA) on questions involving polarization and spent some time with J. Perrin in Paris exploring other issues.

Born and Einstein held Gaviola in great personal and scientific esteem and Einstein helped him obtain a fellowship to the USA. He is reported to have said something like "If only Argentina would have many young scientists like Gaviola. . ." Perhaps to find out, he spent a month in Argentina in 1925, giving 12 (!) conferences on his relativity theory. The subsequent development of Gaviola's extraordinary career in the USA and later back in Argentina is too extensive for further treatment here (see [5, 6]). I mention only two demonstrations of his productivity. While at Caltech, Gaviola developed the technical means for creating and testing the superior mirror surfaces required for the big reflecting telescopes at the Palomar and Wilson observatories. And although astronomy was his major scientific focus in Argentina, he also initiated in La Plata the construction of fluorescence equipment, including the first fluorimeter in Argentina (to which GW presumably had access), and the production of fluorescent materials in Buenos Aires.

5 The Gaviola–Weber Connection

Why all this attention on Gaviola in a chapter about GW? It appears (at least to me) that as an "earlier edition" he must have had an enormous influence on the scientific directions and development of GW, as well as on his philosophical views regarding the conduct of research and the manner of interaction with colleagues and students.[6] For example, one can assume that GW would have subscribed (or *did* subscribe, judging from his publications and the testimony of his associates) to the "Ten commandments about the scientific method" that Gaviola distributed to his students (my translation):

> 1. Do not steal; 2. Exercise self-criticism; 3. Neither fabricate results nor embellish them by modification of data; 4. Do not practice deception during the exposition of your postulates; 5. Do not conceal information; 6. Do not cease to investigate problems because they may antagonize figures of authority; 7. Do not resort to the invocation of authority; 8. In the execution of an experiment, seek to demonstrate the validity rather than the accuracy of a theory or of a model; 9. In the interpretation of an experimental result, do not exceed the limits of validity of the theory or model in order to achieve better agreement; 10. Do not submit a publication without having first dealt with objections raised by others and yourself.

Furthermore, it is evident from the cumulative writings by and about Houssay, Gaviola, Leloir, and GW (see [1, 2]) that they shared a set of superior human attributes: *intellectual prowess and curiosity; a strong work ethic; a sense of humanity and fair play; generosity and humility; and, by all means not least, a well-developed sense of humor*. GW had an additional, unique ability, rather useful for a research scientist. Shortly before he died, he revealed to his daughter Juliet

[6] For his outlook in 1990, see "Whither Biophysics?" [24].

that he had a perfect memory for everything he had ever read. Others with whom I have spoken appear to corroborate this claim.

6 Family Matters ("Yoyo")

One can identify multiple family and scientific interactions that shaped GW's destiny (see also the chapter of Francisco Barrantes). GW's father, Leon Weber, was an immigrant from Rumania and his mother Rosa, who died of tuberculosis when he was only 7, was a member of the extensive Gerchunoff family, one of the group of early Jewish settlers in Argentina. Her uncle, Alberto Gerchunoff, was a prominent author, columnist, socialist, anti-Nazi activist, and a progressively frustrated assimilationist. There are telling stories about GW in his youth. Within the family and to some of his acquaintances, GW had the nickname "Yoyo" [7] ("yo, yo"="me, me"), bestowed upon him by his older sister Ana Sofía because as a child he was always in the first row, demanding attention (inset, Fig. 3). In later years, GW was more relaxed (Fig. 3) as well as more circumspect in his search for recognition. Ana Sofía was a chemist – she did her thesis on the chemistry of serpents – and married to a chemist–physicist, Juan Tomás D'Alessio (Fig. 1). Both worked in the National Atomic Energy Commission (CNEA), Juan T. being involved in the earliest research with lasers in Argentina. He published interesting and still relevant papers on the production and single/dual photon detection of ns pulses [7, 8], and collaborated with GW in later years on their application in photolysis research and for fluorescence lifetime determinations. D'Alessio's cell biologist granddaughter, Cecilia D'Alessio, stresses the intellectual breadth and generosity of her grandfather. J. T. D'Alessio's son and thus nephew of GW, Enrique D'Alessio, is also a physicist who transformed an academic career (curtailed by the dictatorship instituted exactly 40 years ago) into the commercial design and production of high-end equipment for spectroscopic and automatic clinical analysis. He is very well informed about the orientation of GW's early interests and activities and relates that *it was his father and Gaviola together who prevailed on GW to study physics*.[8] GW's other sister Frida was married to Alberto Kurlat, an extroverted engineer who had a very successful career in the electric power industry and was the only relative to visit GW in England during the 1940s. Considerations regarding the immediate family were key in determining GW's ultimate career decision, i.e. the transfer to the USA in 1962. He had married Shirley Roxana Nixon, a gifted illustrator, and they had three children: Alicia, Rosalind, and Juliet. The unaccountable failure of the academic authorities in

[7] In Argentine Spanish, Yoyo is pronounced a bit like jo in "joke."

[8] In fact, J.T. D'Alessio gave GW classes in physics. Perhaps inhibited by the Cambridge Physics Department of Paul Dirac and others, GW pursued *bio*physics. He did share the view attributed to Dirac that "the laws of nature should be expressed in beautiful equations."

Fig. 3 Gregorio Weber at two stages in his life ("Yoyo," 1923; 1969)

Cambridge and then Sheffield to provide an appointment commensurate with GW's already established scientific stature served to hasten the departure of the Weber family.

7 Why Medicine

We return to the 1940s. It is not altogether obvious why GW studied medicine, although he was in good company, e.g., Luis Leloir, in taking, and probably regretting, this decision. His father Leon was certainly disappointed by the outcome, having established a fully equipped medical consultation room in his home and maintaining it for 20 years in the hope that his son would reestablish himself as a clinician in Argentina. Leloir writes in a brief autobiography [9]: "I was a bad practicing physician because I was never sure of the diagnosis or of the treatment."

GW never got that far and was not exactly affine to the medical profession in other ways.[9] Yet it is interesting to note that the trail from medicine to biophysics is one that has been traversed by many individuals, starting with the Spaniard Nicolás Monardes who in 1565 described the bluish opalescence of the water infusion from the wood of the Mexican tree *Lignum nephriticum*. Ulises Acuña identified the underlying fluorophore 434 years later as the four-ring matlaline [10]; it has a quantum yield of 1! In addition to GW, a historical list, decidedly incomplete, of "fluorescence-biophysical MDs" has other notable entries, 4 of them Nobel Laureates: Paul Ehrlich, Robert Koch, Hermann von Helmholtz, Albert Coons, Elli Kohen, Johann Ploem, Ray Chen, Lubert Stryer, Rudolf Rigler, Sam Latt, Howard Shapiro, and Jens Skou. The undeniable attraction of fluorescence as a *practical* tool in and for medicine, well recognized by GW, is exemplified by the recent contributions of Roger Tsien, a Nobel Laureate but not an MD, to fluorescence-guided surgery [11].

8 PhD Thesis and Beyond

A copy of GW's thesis "The Fluorescence of Riboflavine, Diaphorase and Related Substances" is in front of me as I compose these words. It was written on a typewriter and contains many insertions by hand.[10] GW starts by acknowledging the help of his advisor in building the necessary apparatus but then asserts that "The remainder has been solely my independent work." In the Introduction he makes rather philosophical observations: "I feel that a knowledge as deep of possible, of the physical principles concerned is indispensable. Even a close collaboration with a physicist cannot spare this task to the biochemist." There follows the frequently cited statement to the effect that the brains of a physicist and a biologist working together may come up with $2n$ ideas, few compared to the much larger $n!$ of a single brain (tj: presumably GW's) combining both sets of capabilities and knowledge.[11]

---

[9] It is said that GW had one and only patient, his nephew Enrique D'Alessio, who on one occasion suffered burns from an accident with boiling tea. GW's daughter Juliet relates: "Whenever he (GW) had to see a doctor, he was a terrible patient. Half the time he wouldn't take their advice or the medicines they prescribed." On one occasion, his primary doctor was Tamara Mitchell, wife of George Mitchell, who thus knew him well and recommended he go to a specialist for a certain condition. GW turned the prescribed treatment into a scientific experiment, treating one arm as the target and the other as the control. He was also a reluctant patient during his bout with leukemia. Juliet recalls him saying: "I know what they know and they know nothing."

[10] Richard ("Dick") Spencer, GW's graduate student who created the first cross-correlation phase fluorimeter and was later a co-founder of SLM, did the same in 1970 in a thesis of 308 pages, still a gold mine of information and formalism relevant to excited state dynamics.

[11] Considering that the human brain has ~10^{11} neurons according to current estimates, each with a $10^{4–6}$ synaptic connectivity, he was probably right. Upon reading this footnote, Enrique D'Alessio recalled that Yoyo was a master (tj: as was Dick Feynman) of order of magnitude calculations, which he made during family reunions. One Christmas, someone asked Yoyo how many neurons there were in the brain

The thesis is considered to be a milestone in biochemical fluorescence due to its novel descriptions of the spectral properties of flavins and flavoproteins, including the theory and measurement of emission polarization. However, it is also notable because it has the traces of someone who was still in the process of acquiring the rigor and exactitude that characterized GW's later work. That is, despite the prodigious memory alluded to above, GW demonstrated that he was actually *fallible* (bringing him closer to the rest of us). For example, in the Introduction, and then in thesis Chapter II, GW claims to have experimentally confirmed the existence of a dark period between excitation and emission, a phenomenon that had been postulated more than 20 years earlier, and for which he now provided a formalism based on the viscosity dependence of molecular polarization parameters. This interpretation, however, appears to conflict with the findings and conclusions Gaviola reported in his thesis and then reviewed in 1929 [12], as well as with modern concepts of excited state dynamics.[12] One should note that there were no determinations of lifetimes in the thesis of GW and he relied on the values reported by Gaviola and others, who neither anticipated nor could have resolved multicomponent emission processes. I hasten to state that these comments about the thesis are by no means intended as retrospective criticism, but rather as an indication that GW was operating as a scientific "loner" (compared to Gaviola's situation with a prestigious circle of advisors), and, in fact, continued to function as "his own best postdoc" for a number of years after his degree. Much more can be inferred from a careful inspection of the entire publication record but that is a topic in itself.[13] I restrict myself here to two instances. One is from the only book GW published: "Protein Interactions" [13], which is dedicated to "those who put doubt above belief," a statement akin to some of Gaviola's ten commandments. In the Preface, he wrote:

> At any time and in any scientific subject is comparatively easy to master the concepts that govern what is already understood and widely practiced. It is far more difficult to appreciate that simple concepts, although demonstrably valid in known cases, cannot be extended to

---

and he answered (my translation): "Very simple. If we estimate that one acquires one byte of 'knowledge' per second, in 70 years of life this would come to a number $>10^{9-10}$, and that must be the approximate number of neurons." Whatever the validity of this line of reasoning, the fact is that Yoyo long ago came up with a very respectable value, particularly if one allows, as I would hope, for thinking individuals past the age of 70.

[12] A systematic deviation of an experimental intrinsic anisotropy (r_o) from the expected value can indeed occur due to a variety of reasons (anisotropic motion, solvent relaxation, energy transfer, spectral inhomogeneity, etc.) and is still an issue being addressed from fundamental principles [25].

[13] The story is repeatedly told that the recruitment of GW to Illinois was secured at least in part, by the definition attributed to the department chairman, Irwin Gunsalus, of the *Weber Ratio* = the ratio of outstanding papers to total papers, considered to be unity in the case of GW. I propose generalizing the concept as the function (in *Mathematica* notation) WeberRatio[$n\_$, $x\_$]: = Min [200/n, x], where n is the number of publications and x is the highest value achieved by the target individual during his/her career. For GW, $n = \sim 200$ and $x = 1.0$. I would guess that GW admonished his group to "publish well but neither too little nor too much."

> all systems regardless of complexity. Physical chemistry is an area of science greatly burdened by overconfidence in the universal value of simple rules, and in applying these to the proteins I have tried to make a clear distinction between what we can and cannot take for granted.

In 1960, a remarkable symposium on "Light and Life" was held at Johns Hopkins University. The conference book [14] can be downloaded and is highly recommended. The list of participants is a who's who of physical and biological science at that time, and included Niels Bohr, who in his Introduction to the symposium made a somewhat less guarded statement than that of GW quoted above: "There appears to be no reason to expect an inherent limitation of the application of elementary physical and chemical concepts to the analysis of biological phenomena." James Frank introduced GW's presentation "The excited states of proteins." GW was asked many questions. One of them had to do with the mechanism by which he had photooxidized tryptophan, and whether he was postulating the intervention of the triplet state. GW rejoined: "No, I was postulating nothing." He was then asked about the possible existence of excited states of proteins only 1 e.v. above the ground state energy level. GW answered: "I don't know whether any experiment which I have done on fluorescence of proteins would be related to this question, to tell you the truth. I prefer not to discuss it." At age 44 but not yet securely established academically, GW was very sure of his strengths and of his limitations.

9 Weber Number

The degree of loyalty to GW's legacy expressed by his followers 19 years after his death, and well before, is unique. Like in FRET, his influence operated at a distance dictated by scientific and personal "overlaps." I propose a classification scheme, based on the publication record, which would establish quantitatively and for posterity the connectivity in the Weber scientific family. What comes to mind is a system such as that adopted for Paul Erdős, who ostensibly published more papers than any other mathematician in history. We define a Weber number (Wn) as follows: GW is assigned the number 0 and everyone else has the number $k+1$ with k the lowest Wn of any coauthor of a paper. Thus, those who have published with GW have Wn 1 and those who published with a Wn 1 coauthor have Wn 2. In the list of authors of this volume there are 8 with Wn 1 and 5 with Wn 2. This concept can be extended within the Weber family, for example, to Enrico Gratton, who exhibits a breadth, innovative capacity, and productivity close to that of GW, and deserves his own number, i.e. Wn 1 Gn 0. I hereby claim a Gn 2 but can still strive for a 1.

10 The Influence of GW on my Scientific Career

The most important lessons in life and in science tend to be simple. As an undergraduate at Caltech, I had Richard ("Dick") Feynman as an instructor in sophomore physics (electricity, optics, and magnetism). This was the only time he taught such a course (13 students) and he also served as the lab instructor. He criticized me for having too neat a lab book; he wrote in it: "you can't be writing things down as you work." I stopped using slips of paper for later transcription and the lab book became somewhat more chaotic (I still have it, including his comments). Feynman was satisfied. The take-home lesson, again reminiscent of Gaviola, was: "Record it as it is"; GW would have agreed. The pure and simple approach also guided my later efforts in "serious" fluorescence (and phosphorescence), which had their origins in the lab of Lubert Stryer and Dick Haugland at Stanford. In this case, my mentors were GW and Tomás Hirschfeld, another product of the Río de la Plata but from the other side (Uruguay). Hirschfeld was a prodigious inventor (>100 patents), scientific author (hundreds of papers and notes), experimentalist, theoretician, and entrepreneur, working in numerous areas of spectroscopy, particularly Fourier transform IR but also fluorescence applied in flow cytometry, single molecule detection, and analytical techniques. In a short, seminal paper [15] he demonstrated that the integrated photon output of a fluorophore undergoing photobleaching is independent of quantum yield. This simple, yet not altogether intuitive, observation formed the basis for the introduction by our lab (1989, 1996) of FRET imaging techniques based on donor and/or acceptor photobleaching. Hirschfeld, a gourmand, unfortunately died prematurely at age 48 but has been immortalized by a stamp issued by Uruguay (Argentina could well do the same for GW). He is also remembered for his innumerable aphorisms ("Rules of Thumb"), many, if perhaps not all, of which coincide with known GW philosophical viewpoints. The following is a small selection:

> Persistence at thinking increases average speed and decreases the instantaneous one.
> Remember all phenomena with big derivatives.
> Anything can be made smaller, never mind physics.
> Anything can be made more efficient, never mind thermodynamics.
> Everything will be more expensive, never mind common sense.
> Information theory determines physics, logic supersedes mathematics.
> If the facts don't match your intentions, look for other facts.
> If you do not ask "why this" often enough, somebody will ask "why you."

Earlier in time, the fundamental publications of GW and colleagues on fluorescence polarization had induced us to incorporate emission anisotropy (fluorescence as well as phosphorescence) into home-built cuvette and flow cytometry-sorting systems (1976), and much later (2002) for detecting rotational mobility and FRET homotransfer by phase-modulation FLIM. GW offered invaluable advice during the early developmental phase as well as at the end, when Eli Jares-Erijman and I were elaborating the simple conceptual view of a fluorophore as a photonic "enzyme," turning over input photons (the substrate) into output photons (the product) of lower

energy [16]. Determination of the "K_m" from the excitation saturation curve constitutes a measure of quantum yield and thus FRET efficiency. In this FRET imaging review (one of our better cited publications) we stated in the Acknowledgments: "They (we, the authors) are also indebted professionally and personally for the inspiration offered by the late Gregorio Weber, the acknowledged father of fluorescence in biology."

Another main GW theme, environmental sensing by small molecule probes, has been a mainstay of our research over the years. The studies have included the monitoring of amyloid protein aggregation by use of ANS and bis-ANS, both inventions of GW (in fact he gave us the bis-ANS), as well as of novel excited state intramolecular proton transfer (ESIPT) probes [17, 18], some of which are highly solvatochromic [19]. Most recently, we have focused on the development of a range of fluorescent photochromic reagents [20], intended for general use including superresolution microscopy; solvatochromism is also featured. These and the previous studies have involved very able students, postdocs, and visiting scientists, many from Argentina, and benefited greatly from the pioneering publications of GW in this area.

The most recent, current, and as yet unpublished [21], application of "Gaviola +Weber principles" in our lab has to do with the never-ending theme of lifetime determinations in solution and in imaging systems. The decay curve, the emission probability distribution function, is not really of intrinsic interest. Rather, one seeks the underlying rate constants for depopulation of the excited state(s). These we now obtain directly by measuring the lag times (equal to the lifetimes, individual or as population means) between the integrated excitation and emission signals. One avoids the conventional requirement for "delta" excitation by employing long, constant intensity pulses with which a steady-state equilibrium of the excited state is achieved. The "extended excitation FLIM" (eeFLIM) technique is simple, fast, and offers many advantages. GW would have liked it, even if it bypasses the frequency domain, as was the case in our very first FLIM experiments in 1979.

11 Concluding Remarks

There is much more we can derive from GW's intellectual output. He kept copious notes in preparation for a comprehensive book on fluorescence. Dave Jameson is the repository of this material and the scientific community can hope that such a book still comes to be, for our benefit and for the sake of posterity. And before those who knew him personally disappear from the scene, a comprehensive biography should receive high priority. Is it possible to also entice and entrust Dave Jameson with this Boswellian responsibility?

Acknowledgements During the course of preparing this chapter**,** I had the privilege and pleasure of contact with many members of the extended Weber family. They were very patient and forthcoming with abundant information, anecdotes, photos (Fig. 1, J.T. D'Alessio; Fig. 3), recommendations, and critical readings of the manuscript. My deep appreciation and gracias go to Juliet Weber, Cecilia D'Alessio, and Enrique D'Alessio. I also thank Enrico Gratton and the unflappable, infinitely patient Dave Jameson, an inexhaustible source of information of and about GW. Factual errors and errors of omission are mine alone.

References

1. Jameson D (2016) Gregorio Weber 1916–1997. http://www.lfd.uci.edu/~weber/
2. Lloyd D (2016) Tributes to Gregorio Weber (1916–1997). http://www.cf.ac.uk/biosi/staffinfo/lloyd/weber/
3. Gaviola E (1926) Die Abklingungszeiten der Fluoreszenz von Fabstofflösungen. Ann d Physik 81:681–710
4. Gaviola E (1926) Ein Fluorometer. Ein Apparat zur Messung von Fluoreszenzabklingungszeiten. Z f Physik 42:853–861
5. Bernaola OA (2001) Enrique Gaviola y el Observatorio Astronómico de Córdoba. Ediciones Saber y Tiempo, Buenos Aires, pp 562
6. Hurtado D (2007) Gaviola. El Intérprete, vol. 6. Universidad Nacional de San Martín, Provincia Buenos Aires, Argentina, pp 1–16
7. D'Alessio JT, Lanza H (1968) Discharge mechanisms in gases in the subnanosecond region. Rev Sci Instrum 39:1029–1035
8. Zampach J, D'Alessio JT, Kesque JM (1972) Medidas de tiempo de dacaimiento con dosfotomultiplicadores en condición de fotoelectrón único, CNEA-326. C. N. de E. Atómica, Buenos Aires
9. Leloir LF (1983) Far away and long ago. Annu Rev Biochem 52:1–15
10. Acuña AU, Amat-Guerri F, Morcillo P, Liras M, Rodríguez B (2009) Structure and formation of the fluorescent compound of *Lignum nephriticum*. Org Lett 11:3020–3023
11. Nguyen QT, Tsien RY (2013) Fluorescence-guided surgery with live-molecule navigation – a new cutting edge. Nat Rev Cancer 13:653–662
12. Gaviola E (1929) On time-lags in fluorescence and in the Kerr and Faraday effects. Phys Rev 33:1023–1034
13. Weber G (1992) Protein interactions. Chapman and Hall, New York, p 292
14. McElroy D, Glass B (eds) (1961) Light and life. Johns Hopkins Press, Baltimore, p 924
15. Hirschfeld T (1976) Quantum efficiency independence of the time integrated emission from a fluorescent molecule. Appl Opt 15:3135–3139
16. Jares-Erijman EA, Jovin TM (2003) FRET imaging. Nat Biotechnol 21(11):1387–1395
17. Celej MS, Jares-Erijman EA, Jovin TM (2008) Fluorescent N-arylaminonaphthalene sulfonate probes for amyloid aggregation of α-synuclein. Biophys J 94:4867–4879
18. Celej MS, Caarls W, Demchenko A, Jovin TM (2009) A triple emission fluorescent probe reveals distinctive amyloid fibrillar polymorphism of wild-type α-synuclein and its familial Parkinson's disease mutants. Biochemistry 48:7465–7472
19. Giordano L, Shvadchak VV, Fauerbach JA, Jares-Erijman EA, Jovin TM (2012) Highly solvatochromic 7-aryl-hydroxychromones. J Phys Chem Lett 3:1011–1016
20. Gillanders F, Giordano L, Diaz SA, Jovin TM, Jares-Erijman EA (2014) Photoswitchable fluorescent diheteroarylethenes: substituent effects on photochromic and solvatochromic properties. Photochem Photobiol Sci 33:603–612

21. Jovin TM, Cook NP (2016) Extended excitation FLIM (eeFLIM). Paper presented at the "International Discussion Meeting - Förster Resonance Energy Transfer in life sciences: FRET 2", Göttingen, Germany
22. Jovin TM (2013) Remembering Robert Clegg and Elizabeth Jares-Erijman and their contributions to FRET. In: Medintz IL, Hildebrandt N (eds) FRET-Förster resonance energy transfer: from theory to applications. Wiley-VCH, Weiheim, pp 9–22
23. Gaviola E (1946) Memorandum: la Argentina y la era atómica. Revista de la Unión Matemática Argentina 11:213–219
24. Weber G (1990) Whither biophysics? Annu Rev Biophys Biophys Chem 19:1–6
25. Saha S, Soni J, Chandel S, Kumar U, Ghosh N (2015) Probing intrinsic anisotropies of fluorescence: Mueller matrix approach. Biomed Opt 20:085005-085001-085007

Personal Recollections of Gregorio Weber, My Postdoc Advisor, and the Important Consequences for My Own Academic Career

Antonie J.W.G. Visser

Abstract This is a personal account of my postdoctoral research period in 1976–1977 with Professor Gregorio Weber at the University of Illinois at Urbana-Champaign (USA). For me it was a year of enlightenment that had a large impact on my own academic career. Since we worked on (high-pressure) fluorescence research on flavins and flavoproteins in Urbana, I describe in somewhat larger detail our own completed research on this topic at Wageningen University (The Netherlands). Because of increasing research interest in cellular biochemistry and biophysics we have founded the Microspectroscopy Centre in Wageningen harboring sophisticated fluorescence microscopy setups.

Keywords FCS • Flavins and flavoproteins • FLIM • Fluorescence polarization • FRET • High-pressure fluorescence • Homotransfer • Microspectroscopy • Static fluorescence quenching • Ultrafast fluorescence spectroscopy • Weber's red-edge effect

After obtaining my PhD thesis in 1975 on excited-state properties of flavins and flavoproteins at Wageningen University in The Netherlands, at that time called Agricultural University [1], my former graduate advisor Cees Veeger suggested that I perform postdoctoral research with Professor Gregorio Weber at the Department of Biochemistry of the University of Illinois at Urbana-Champaign (UIUC), USA. In the late 1950s Cees Veeger was a graduate student with Professor Bill Slater at the University of Amsterdam. During that time Cees Veeger spent several months at the Department of Biochemistry of the University of Sheffield, UK, to collaborate with Vincent Massey and Quentin Gibson on the mechanism of

A.J.W.G. Visser (✉)
Laboratory of Biochemistry, Microspectroscopy Centre, Wageningen University, P.O. Box 8128, 6700 ET Wageningen, The Netherlands
e-mail: antoniejvisser@gmail.com

D.M. Jameson (ed.), *Perspectives on Fluorescence: A Tribute to Gregorio Weber*, Springer Ser Fluoresc (2016) 17: 57–66, DOI 10.1007/4243_2016_10,

lipoamide dehydrogenase. In Sheffield, Gregorio Weber also belonged to the scientific staff and it was there that Gregorio and Cees had many interactive discussions. Although the Department of Biochemistry in Sheffield, founded by Sir Hans Krebs, was regarded as a Center of Excellence, there was a major brain drain in the early 1960s with the exodus of most of the Biochemistry faculty to various locations in the USA. While Gregorio had settled in Illinois, Vince Massey became professor at the Department of Biological Chemistry, University of Michigan, Ann Arbor and Quentin Gibson, former Department Head in Sheffield and successor of Hans Krebs, moved to the University of Pennsylvania in Philadelphia. The fact that Gregorio had pioneered flavin fluorescence research for his own PhD thesis work (1947) at the University of Cambridge (UK) [2] made my choice easier.

One year later in September 1976 my family and I arrived in Urbana. Initially, it was like a culture shock. The twin city Champaign–Urbana occurred to me as a scientific oasis in the middle of vast cornfields occupying an area almost as large as that of The Netherlands. Arriving at the beginning of the fall semester it appeared that most of the population consisted of students. We were first housed in the Illini Union in the middle of the impressively large campus, which was an adventure in itself offering a tiny sample of the American Pie. I still remember riding behind David Jameson (graduate student of Gregorio) on his motorcycle criss-crossing through the twin city to look for housing and a suitable car. We quickly succeeded in this mission.

Gregorio's laboratory was completely different from the ones I had worked in. First, Gregorio's office took a central place in the lab and was highly accessible, no barriers whatsoever. The offices of the professors in my alma mater were considerably larger and were hidden behind a secretarial wall. Gregorio used to hang up interesting New York Times articles on the walls of his office. One of those articles I remembered very well. It was about Dan Flavin, whose surname is reminiscent of the biological molecule of our common interest, but in reality was the name of an American artist specialized in light sculptures. At the very same time Bernard Valeur from Paris, France was also a postdoctoral fellow with Gregorio. David instructed both of us very well in using the different fluorescent equipment available in the Weber lab. David had acquired much expertise in fluorescence instrumentation, not only because of the vast knowledge of his thesis advisor, but also of the excellent course on "Instrumentation For Science" that was given in Urbana and published in book modules [3]. The other graduate students whom I met (John Wehrly, Fenton Williams, and Tom Li) also followed the same course. Such a course did not exist in the (bio)chemical curricula of my own universities in The Netherlands (Amsterdam and Wageningen), which explains the lack of general understanding of concepts of such equipment and instrumentation there. Both Bernard and myself were attracted very much by the ultra-sensitive, steady-state fluorescence polarization instrument using photon counting detection [4]. Bernard and Gregorio used this instrument for their seminal paper on excitation wavelength-dependent fluorescence polarization of indole and tryptophan in cryogenic solutions [5]. My own research assignment was on the application of high pressure on two flavinyl tryptophan methyl esters, separated by three or five methylene links and on

four flavodoxins from different bacterial sources, which are small electron-transferring proteins.

Successful collaboration was with graduate student Tom Li and Chemical Engineering Professor Harry Drickamer. The papers arising from that work had been accepted for publication even before I left Urbana, because Gregorio had such an efficient way of writing papers and of handling reviewer's comments during the peer review process [6, 7]. With five methylene links rotation around the C–C bonds permits almost unrestricted approach of the flavin and indole rings, while with the three-methylene separation this approach was restricted. This was illustrated by the much larger change in the standard volume on the formation of the internal complex of five-methylene separation model. In the case of flavodoxins, the pressure-induced changes were not completely reversible at high pH, but the reversibility greatly improved at lower pH. Volume changes between a "native" protein at atmospheric pressure and a "denatured" protein at high pressure (8–11 kbar) were calculated from the spectral data. The volume changes were small, on the order of 0.25% of the molar volume. It was a real joy to discuss the research results with Gregorio, because he directed me on the right track and could distinguish main points from minor ones. What I further recollect from that year in Urbana were the open discussions with other scientists working there, just having left or about to arrive: Bill Mantulin, Enrico Gratton, Joe Lakowicz, Tom Baldwin, Robert Gennis, Dick Spencer, George Mitchell, Alejandro Paladini, and others. Dick Spencer and George Mitchell had just started the SLM Instruments company specialized in fluorescence equipment. I also remember lively joint scientific meetings together with the Department of Physics in Monticello, IL. In summary, spending 1 year in Gregorio Weber's lab was for me a year of enlightenment.

I will now highlight some aspects of my own career after returning to the Department of Biochemistry of Wageningen University emphasizing research on flavins and flavoproteins with my own group. I wish to mention two persons who were important: my colleagues Arie van Hoek and Franz Müller. Inspired by my stay in Gregorio Weber's lab, I wanted to set up a state-of-the-art facility for steady-state and time-resolved fluorescence spectroscopy, not only to study flavins and flavoproteins, but also to investigate other biomolecular systems. Together with Arie van Hoek, an electro-optical engineer by training and nicknamed "laser wizard," we succeeded in establishing this facility. This was by no means easy especially in the first decade after my return. First of all, despite our close collaboration we belonged to different departments implying a generic unwillingness to collaborate with each other. Each department formed its own fiefdom with different priorities and interests (and noticeable at the financial level). Owing to successful grant applications, suitable housing, economic maintenance of expensive lasers, elimination of many artifacts involved in time-correlated single photon counting (TCSPC), proper use of the machine shop, and development of efficient data collection and analysis software, we were able to set up a sensitive polarized time-resolved fluorescence system that attracted many researchers within and outside The Netherlands to visit us for experiments. This resulted in a continuous stream of publications starting about 1979. In that period Franz Müller could be

considered as the main flavin chemistry expert in The Netherlands (and perhaps among one of them internationally). He was a magician in synthesis of flavin model compounds. Franz synthesized the flavinyl tryptophan methyl esters mentioned above. Already during my undergraduate years we had had a very fruitful collaboration over about 15 years. Franz synthesized many other model flavin compounds such as lumiflavin equipped with a long aliphatic alkyl chain that could be incorporated in crystalline *n*-decane for high-resolution fluorescence spectroscopy at 4.2 K [8]. Roelof Platenkamp, first author in [8], used this collaborative work for his own PhD thesis work at the University of Leiden, The Netherlands (PhD in 1981). Franz also synthesized monomeric and dimeric model flavins to corroborate the electronic energy transfer between the two flavin prosthetic groups (FMN and FAD) in NADPH-cytochrome P-450 reductase [9]. These monomeric and dimeric flavin model compounds can be immobilized in poly(methyl methacrylate), machined, and polished to fully transparent "cuvettes" or cylinders. First author Philippe Bastiaens in [9], in the framework of his own MSc project, spent time in Gregorio Weber's lab to measure the excitation dependent steady-state fluorescence polarization spectra of both enzyme and dimeric flavins on the sensitive fluorescence polarization instrument [4]. The flavin fluorescence quantum yield of the enzyme is extremely small and therefore the sensitive equipment was required to obtain reliable results. On the basis of the great similarities of both sets of fluorescence anisotropy data, electronic energy transfer (homotransfer) occurs both in the biflavinyl models and in the native reductase.

In Fig. 1 I have redrawn part of the anisotropy data set consisting of N^3-methyllumiflavin and one of the biflavinyl compounds to illustrate one important effect, namely the failure of homotransfer among identical aromatic molecules that frequently takes place upon excitation at the red edge of the absorption band of the first electronic transition. This phenomenon was (of course) first observed by Gregorio Weber in concentrated cryogenic solutions of aromatic fluorescent molecules [10].

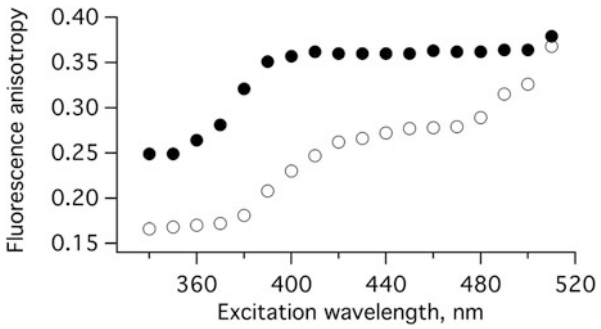

Fig. 1 Steady-state fluorescence anisotropy of N^3-methyllumiflavin (*filled circle*) and the biflavinyl compound (N^{10},$N^{10'}$-hexamethylenebis-(3,7,8-trimethylisoalloxazine)) (*open circle*) in poly(methyl methacrylate) as function of the excitation wavelength. This figure is redrawn from [9]

My own remembrance of the period 1979–1989 in Wageningen brings mixed thoughts. Because of all successful collaborations our fluorescence facility developed a much better reputation outside Wageningen than within our own departments. There arose some intra-departmental rivalry and criticism, which required Arie and me to develop "thick skins" in order for us to improve our facility, but Franz decided to leave the department because of these unworkable conditions. He took up a job in a pharmaceutical company in his home country Switzerland.

Philippe Bastiaens was my first graduate student working on flavoproteins (PhD in 1992), followed by Rik Leenders (PhD in 1993) and Petra van den Berg (PhD in 2002). Philippe worked on the time-resolved fluorescence properties of FAD in lipoamide dehydrogenase and glutathione reductase [11, 12]. Lipoamide dehydrogenase was formerly known as Straub diaphorase, which also constituted part of Gregorio's own thesis work. Vince Massey, then still working in Sheffield, discovered that Straub diaphorase is in fact lipoamide dehydrogenase (earlier also named (dihydro)lipoyl dehydrogenase) and that it functions as a critical component in the 2-ketoglutarate dehydrogenase complex [13, 14]. Philippe discovered, among other things, that the two FAD molecules in dimeric lipoamide dehydrogenase (100 kDa molecular weight) exhibit homotransfer resulting in time-resolved depolarization of the fluorescence even in cryogenic aqueous solution at 203 K [11]. The experimental fluorescence anisotropy decay of lipoamide dehydrogenase can be analyzed using the maximum entropy method (MEM) leading to two main correlation time distributions centered at around 8 ns due to homotransfer and another one that appeared as a constant term due to very slow rotation. When the MEM distribution of correlation times of lipoamide dehydrogenase at 20°C is integrated [12], one obtains a steady-state anisotropy $<r> = 0.289$. Looking on p. 111 of the PhD thesis of Gregorio Weber the degree of fluorescence polarization (p) of Straub diaphorase is equal to 0.387. By using $<r> = 2p/(3-p)$ this gives $<r> = 0.296$, which is amazingly similar! One should realize that before 1947 only the eye functioned as the fluorescence detector, whereas in the early 1990s the fluorometer contained the most sensitive microchannel plate photomultiplier. Gregorio assumed that the depolarization was solely due to rotation of a protein of 70 kDa molecular weight, but now we know that the depolarization is also due to homotransfer. One of the published chapters of Philippe's PhD thesis also contained beautiful work on spectral relaxation spectroscopy of lipoamide dehydrogenase, since it is a relatively strongly fluorescent flavoprotein ($Q = 0.1$) [15]. The maximal attainable information from the fluorescence spectrum of a flavoprotein under different experimental conditions was thus obtained.

Rik Leenders studied time-resolved fluorescence properties of flavodoxins, which are small electron-transfer proteins and characterized by strongly quenched FMN fluorescence (static quenching). All flavodoxins have in the FMN binding site multiple aromatic amino acids such as tryptophan and tyrosine flanking the isoalloxazine of FMN. It was suggested that photoinduced electron transfer from the electron-rich aromatic side chain of tryptophan or tyrosine to the light-excited isoalloxazine was responsible for this ultrarapid quenching process [16, 17]. Rik was one of the first researchers who made a comparison between experimental

fluorescence properties and dynamical structural properties obtained from molecular dynamics simulations [18]. These simulations have been carried out in collaboration with Professors Herman Berendsen (University of Groningen, The Netherlands) and Wilfred van Gunsteren (ETH Zürich, Switzerland). Although the simulation time was only about 0.5 ns, Rik could only achieve this on the Dutch national supercomputer facility during the Christmas holidays of 1992, when he was almost the lone user. One should realize that this period is about half way on the timescale of Moore's law (the observation that the transistor density in an integrated circuit is doubled approximately every 2 years) (http://en.wikipedia.org/wiki/Moore%27s_law). Nowadays it is possible to cover a 30-ns simulation time in a time of 0.5 ns two decades ago for a protein of the same size [19]. One of the published chapters of Rik's thesis also showed an illustrative comparison between the steady-state fluorescence anisotropy of flavin derivatives from time-resolved fluorescence anisotropy obtained in our lab [20] and the steady-state fluorescence polarization of Gregorio Weber [21]. The latter fluorescence polarization data were published in the proceedings of the very first Flavins and Flavoproteins Symposium, which was organized by Bill Slater with the aid of Cees Veeger in Amsterdam in 1965. There is excellent agreement between both data sets.

During the period 1994–1999 Petra van den Berg performed research on flavoenzymes with time-resolved flavin fluorescence spectroscopy. Within the framework of her research project Petra has travelled to various places in Europe and The Netherlands to receive training, performing experiments, and receiving first-hand information from the experts in the fields of flavoenzymes, fluorescence correlation spectroscopy, and molecular dynamics simulations on proteins. She had successfully applied for European and national travel grants. Petra investigated first the mechanism of quenching of FAD fluorescence in *Escherichia coli* glutathione reductase (GR) in large detail [22]. This was a follow-up study of that of Philippe Bastiaens (and colleagues), who studied the enzyme isolated from human erythrocytes [12]. In the crystal structure of the *E. coli* GR, tyrosine 177 blocks the access to the NADPH binding site. During catalysis, this tyrosine is thought to move away from the flavin. The fluorescence decay of the wild-type GR is highly heterogeneous with a predominant lifetime of 7 ps that accounts for ~90% of the fluorescence decay and could be attributed to quenching by Y177, because of the absence of the 7-ps component in the mutant enzymes Y177F and Y177G. Based on the temperature invariance for this lifetime, and the very high quenching rate, electron transfer from Y177 to the light-excited isoalloxazine part of FAD is proposed as the mechanism of flavin fluorescence quenching. Contrary to the mutant enzymes, wild-type GR shows a rapid fluorescence depolarization. This depolarization process is likely to originate from a transient charge transfer interaction between Y177 and the light-excited FAD [22, 23]. Petra spent some time at the Biochemistry Department of the University of Cambridge (UK) under the guidance of Professor Richard Perham (who sadly passed away in February 2015) for collaboration on *E. coli* glutathione reductase. What a coincidence that she probably worked in the same Biochemistry laboratories as Gregorio Weber! Right in that same period Petra met Professor Charles Williams (University of Michigan), who spent a sabbatical

leave in Cambridge. Charles also knew Gregorio, since he was a postdoc with Vince Massey in Sheffield in 1961 and had a bench space next to the lab of Gregorio. Petra and Charles planned to collaborate on time-resolved fluorescence of thioredoxin reductase (TrxR), which belongs to the same flavoenzyme family as lipoamide dehydrogenase and glutathione reductase. This collaboration turned out to be very successful, because a joint paper was published [24]. In this elaborate study the most sophisticated ultrafast fluorescence equipment was used to characterize the time-resolved flavin fluorescence properties of both wild-type and mutant TrxR under various conditions of substrate analog binding, temperature and addition of co-solvent glycerol [24]. Petra van den Berg spent also time with Professors Rudolf Rigler and Jerker Widengren at the Karolinska Institute in Stockholm, Sweden to investigate the application of fluorescence correlation spectroscopy (FCS) on FMN, FAD, and lipoamide dehydrogenase in aqueous buffer. It was found that all flavin systems did exhibit unwanted photochemistry at increasing laser light intensity that resulted in increasing build-up of non-fluorescent molecules [25]. Finally, in collaboration with Professors Herman Berendsen and Alan Mark and graduate student Anton Feenstra at the University of Groningen, Petra carried out molecular dynamics simulations of FAD in different "open" starting structures to investigate the coplanar stacking of the isoalloxazine and the adenine ring systems of FAD and to relate these results to the fluorescence quenching of stacked FAD, which exhibited a dominant 7-ps lifetime after analysis of time-resolved fluorescence with the TCSPC setup [26]. Simulation times of up to 8 ns showed that transitions from "open" to "closed" conformations occurred within the lifetime of the flavin excited state (4.7 ns), the characteristic closing time depended on the exact starting conformation, which was obtained from the crystal structure of different flavoproteins. Hydrogen bond formation of the side-chains connecting both ring systems created a highly cooperative network facilitating stacking interactions. Of course, Gregorio Weber first reported the remarkably low fluorescence of FAD with respect to free riboflavin more than half a century ago [27]. An intramolecular ground-state complex between the isoalloxazine ring and the adenine part of FAD was proposed to prevail in aqueous solution resulting in the formation of a non-fluorescent complex (this is the basis of static fluorescence quenching). Now we know that the fluorescence quenching in FAD is most likely through a mechanism of photo-induced electron transfer from ground-state adenine to excited isoalloxazine. In stacked conformations of FAD fluorescence is quenched instantaneously explaining the ultrashort 7-ps lifetime component.

Because a lifetime of 7 ps is close to the detection limit of the TCSPC setup it was desirable that the experiments should be repeated with the fluorescence upconversion technique, which has much better time resolution in the sub-picosecond range. Owing to a JSPS fellowship I was able to carry out these experiments in the Institute of Laser Technology, Osaka, Japan together with Professors Fumio Tanaka and Noboru Mataga and with staff members of the institute. Fumio Tanaka was, by the way, also a postdoctoral research associate with Gregorio Weber and involved in a pressure study of FAD [28]. Using the fluorescence upconversion technique applied to examine the ultrafast fluorescence

decay of FAD at different emission wavelengths a 9-ps component, which must be the same as the 7-ps lifetime obtained with TCSPC, was attributed to the intramolecular complex between isoalloxazine and adenine, whereas the nanosecond decay was due to the unstacked form of FAD [29].

The time-resolved fluorescence facility was not only used for flavin research, but also for many other research projects. Let me summarize a few of them. First, I had (and still have) a very successful, long-standing collaboration with Professor John Lee of the University of Georgia, USA. As far as I remember we were the first to detect the interaction between an antenna protein and the bacterial luciferase by using time-resolved fluorescence anisotropy [30]. I also had a very fruitful collaboration with Professor Karel Wirtz of the University of Utrecht, The Netherlands, in the field of lipid–protein interaction, because that collaboration elicited our common interest in signal transduction research eventually leading to monitoring biochemistry in the living cell. Eward Pap prepared his PhD thesis (1994) around this topic. Eward synthesized fluorescent second messenger phospholipids equipped with pyrene-containing fatty acids and studied the interaction with protein kinase C, which is a serine/threonine-specific kinase that is a crucial factor in transmembrane cellular signaling [31, 32].

The latter results make it understandable that the time-resolved fluorescence facility should be extended with advanced microscopy setups. In their postdoctoral periods in my group Philippe Bastiaens, Dorus Gadella, Eward Pap, and Nina Visser (yes, my wife) initially paved the way. In the period 1990–2000 grants for research and investment were obtained to create the necessary infrastructure. One granting source I wish to mention in particular: Mibiton (Material Infrastructure Biotechnology Netherlands), which was founded to stimulate the use of innovative equipment and facilities in the field of the life sciences. A Mibiton investment grant (in 1995) enabled us to start the Microspectroscopy Centre as an innovative Dutch life sciences facility, which, most importantly, operates independently from university departments. Several persons played a crucial role in the realization of the Microspectroscopy Centre: Hans Tanke (University of Leiden), Colja Laane (then Biochemistry Department Head at Wageningen University), Ton Bisseling (Department of Molecular Biology, Wageningen University), and Hans Grande (then investment manager of the Mibiton foundation). Tom Jovin (Max Planck Institute for Biophysical Chemistry, Göttingen, Germany) must also be acknowledged for long-standing collaboration and indispensable advice on all aspects of cellular biophysics. Hans Grande and I were colleagues at the Biochemistry Department of Wageningen University in the early 1970s. We gave lectures in quantum mechanics and molecular spectroscopy for students in the newly created curriculum Molecular Sciences until the new Chair Molecular Physics was created. After creation of the Microspectroscopy Centre microscopic fluorescence research started to flourish. We have set up facilities for fluorescence fluctuation spectroscopy (FFS) and fluorescence lifetime imaging microscopy (FLIM). Mark Hink (PhD in 2002) and Ruchira Engel (PhD in 2005) developed themselves as experts in FFS applied to cellular systems during their graduate work. Similarly, Jan Willem Borst (PhD in 2006) and Sergey Laptenok (PhD in 2009) were experts in FLIM applied to cellular

biochemistry and biophysics. One of the activities of the Microspectroscopy Centre was (and still is) to organize FEBS (Federation of European Biochemical Societies) courses on microspectroscopy at a frequency of once in two years. These FEBS courses attracted many European students and were unanimously rated as excellent. After obligatory retirements of Arie van Hoek and myself, the Microspectroscopy Centre is now run by Herbert van Amerongen (my successor), Jan Willem Borst, and Arjen Bader (successor of Arie van Hoek).

An important lesson of Gregorio Weber is that scientists should put doubt above belief. Without any doubt I believe that my career would not have developed so positively without the mentorship of Gregorio Weber.

References

1. Visser AJWG (1975) The investigation of interactions in the excited state of flavins using time-resolved spectroscopy. PhD thesis, Agricultural University, Wageningen
2. Weber G (1947) Fluorescence of riboflavin, diaphorase and related substances. PhD thesis, St John's College, University of Cambridge
3. Malmstadt HV, Enke CG (1973) Instrumentation for scientists series. W.A. Benjamin, Menlo Park
4. Jameson DM, Weber G, Spencer RD, Mitchell G (1978) Fluorescence polarization: measurements with a photon-counting photometer. Rev Sci Instrum 49:510–514
5. Valeur B, Weber G (1977) Resolution of the fluorescence excitation spectrum of indole into the ^1L_a and ^1L_b excitation bands. Photochem Photobiol 25:441–444
6. Visser AJ, Li TM, Drickamer HG, Weber G (1977) Volume changes in the formation of internal complexes of flavinyltryptophan peptides. Biochemistry 16:4883–4886
7. Visser AJ, Li TM, Drickamer HG, Weber G (1977) Effect of pressure upon the fluorescence of various flavodoxins. Biochemistry 16:4879–4882
8. Platenkamp RJ, van Osnabrugge HD, Visser AJ (1980) High-resolution fluorescence and excitation spectroscopy of N_3-undecyllumiflavin in *n*-decane. Chem Phys Lett 72:104–111
9. Bastiaens PI, Bonants PJ, Müller F, Visser AJ (1989) Time-resolved fluorescence spectroscopy of NADPH-cytochrome P-450 reductase: demonstration of energy transfer between the two prosthetic groups. Biochemistry 28:8416–8425
10. Weber G, Shinitzky M (1970) Failure of energy transfer between identical aromatic molecules on excitation at the long wave edge of the absorption spectrum. Proc Natl Acad Sci U S A 65:823–830
11. Bastiaens PI, van Hoek A, Benen JA, Brochon JC, Visser AJ (1992) Conformational dynamics and intersubunit energy transfer in wild-type and mutant lipoamide dehydrogenase from *Azotobacter vinelandii*. A multidimensional time-resolved polarized fluorescence study. Biophys J 63:839–853
12. Bastiaens PI, van Hoek A, Wolkers WF, Brochon JC, Visser AJ (1992) Comparison of the dynamic structures of lipoamide dehydrogenase and glutathione reductase by time-resolved polarized flavin fluorescence. Biochemistry 31:7050–7060
13. Massey V (1960) The identity of diaphorase and lipoyl dehydrogenase. Biochim Biophys Acta 37:314–322
14. Massey V (1960) The composition of the ketoglutarate dehydrogenase complex. Biochim Biophys Acta 38:447–460
15. Bastiaens PI, van Hoek A, van Berkel WJ, de Kok A, Visser AJ (1992) Molecular relaxation spectroscopy of flavin adenine dinucleotide in wild type and mutant lipoamide dehydrogenase from *Azotobacter vinelandii*. Biochemistry 31:7061–7068

16. Visser AJ, van Hoek A, Kulinski T, Le Gall J (1987) Time-resolved fluorescence studies of flavodoxin. Demonstration of picosecond fluorescence lifetimes of FMN in *Desulfovibrio* flavodoxins. FEBS Lett 224:406–410
17. Leenders R, van Hoek A, van Iersel M, Veeger C, Visser AJ (1993) Flavin dynamics in oxidized *Clostridium beijerinckii* flavodoxin as assessed by time-resolved polarized fluorescence. Eur J Biochem 218:977–984
18. Leenders R, van Gunsteren WF, Berendsen HJ, Visser AJ (1994) Molecular dynamics simulations of oxidized and reduced *Clostridium beijerinckii* flavodoxin. Biophys J 66:634–645
19. Nunthaboot N, Tanaka F, Kokpol S, Visser NV, van Amerongen H, Visser AJ (2014) Molecular dynamics simulation of energy migration between tryptophan residues in apoflavodoxin. RSC Adv 4:31443
20. Leenders R, Bastiaens PI, Lunsche R, van Hoek A, Visser AJ (1990) Rotational resolution of methyl-group substitution and anisotropic rotation of flavins as revealed by picosecond fluorescence depolarization. Chem Phys Lett 165:315–322
21. Weber G (1966) Intramolecular complexes of flavins. In: Slater EC (ed) Flavins and flavoproteins. Elsevier, Amsterdam
22. van den Berg PA, van Hoek A, Walentas CD, Perham RN, Visser AJ (1998) Flavin fluorescence dynamics and photoinduced electron transfer in *Escherichia coli* glutathione reductase. Biophys J 74:2046–2058
23. van den Berg PA, van Hoek A, Visser AJ (2004) Evidence for a novel mechanism of time-resolved flavin fluorescence depolarization in glutathione reductase. Biophys J 87:2577–2586
24. van den Berg PA, Mulrooney SB, Gobets B, van Stokkum IH, van Hoek A, Williams CH Jr, Visser AJ (2001) Exploring the conformational equilibrium of *E. coli* thioredoxin reductase: characterization of two catalytically important states by ultrafast flavin fluorescence spectroscopy. Protein Sci 10:2037–2049
25. van den Berg PA, Widengren J, Hink MA, Rigler R, Visser AJ (2001) Fluorescence correlation spectroscopy of flavins and flavoenzymes: photochemical and photophysical aspects. Spectrochim Acta A Mol Biomol Spectrosc 57:2135–2144
26. van den Berg PA, Feenstra KA, Mark AE, Berendsen HJ, Visser AJ (2002) Dynamic conformations of flavin adenine dinucleotide: simulated molecular dynamics of the flavin cofactor related to the time-resolved fluorescence characteristics. J Phys Chem B 106:8858–8869
27. Weber G (1950) Fluorescence of riboflavin and flavin-adenine dinucleotide. Biochem J 47:114–121
28. Weber G, Tanaka F, Okamoto BY, Drickamer HG (1974) The effect of pressure on the molecular complex of isoalloxazine and adenine. Proc Natl Acad Sci U S A 71:12641266
29. Chosrowjan H, Taniguchi S, Mataga N, Tanaka F, Visser AJ (2003) The stacked flavin adenine dinucleotide conformation in water is fluorescent on picosecond timescale. Chem Phys Lett 378:354–358
30. Visser AJ, Lee J (1982) Association between lumazine protein and bacterial luciferase: direct demonstration from the decay of the lumazine emission anisotropy. Biochemistry 21:2218–2226
31. Pap EH, Bastiaens PI, Borst JW, van den Berg PA, van Hoek A, Snoek GT, Wirtz KW, Visser AJ (1993) Quantitation of the interaction of protein kinase C with diacylglycerol and phosphoinositides by time-resolved detection of resonance energy transfer. Biochemistry 32:13310–13317
32. Pap EH, van den Berg PA, Borst JW, Visser AJ (1995) The interaction between protein kinase C and lipid cofactors studied by simultaneous observation of lipid and protein fluorescence. J Biol Chem 270:1254–1260

Measurements of Fluorescence Decay Time by the Frequency Domain Method

Enrico Gratton

Abstract Among the many contributions of Gregorio Weber to science and technology, the development of frequency domain technology in his lab in 1969 has caused a deep controversy, dividing scientists that will refuse using anything but the frequency domain approach to measure the fluorescence decay from the other camp that simply refuses anything but the time-correlated single photon counting (TCSPC) approach. Although at the time of the major contribution of Gregorio Weber and Richard Spencer in 1969, the TCSPC method was not yet invented, the basic controversy "frequency domain vs time domain" in the field continues today. We have made progress both in the scientific understanding and in describing the technical differences between the two approaches; still it is interesting how scientists continue to be divided. As for many of the contributions of Gregorio Weber that stirred controversy, I would like to mention a common theme of my conversations with Dr. Weber about refusing to follow a "god' and about the independence of the scientific thinking from "common beliefs" that ultimately slows scientific progress. In this chapter I would like to describe the scientific progress brought about by Weber's ideas in this specific "technological" area that should be judged by "pure" scientific analysis rather than by beliefs.

Keywords FLIMbox • Frequency domain • Gregorio Weber • Lifetime decay • Multifrequency • Parallel fluorometer

E. Gratton (✉)
Laboratory for Fluorescence Dynamics, Department of Biomedical Engineering, University of California, Irvine, CL, USA
e-mail: egratton22@gmail.com

D.M. Jameson (ed.), *Perspectives on Fluorescence: A Tribute to Gregorio Weber*,
Springer Ser Fluoresc (2016) 17: 67–80, DOI 10.1007/4243_2016_15,

Contents

1 Time and Frequency Domain

Much has been said about measuring fluorescence lifetime decay in the time or in the frequency domain [1]. A common misconception is that the time-correlated single photon counting method (TCSPC) used in the time domain is more accurate and has better time resolution than the frequency domain approach [2]. From the statistics point of view the uncertainty of the TCSPC measurement depends on the number of photons collected which is considered the ultimate error possible. Also the dark noise, which are photons detected but not correlated with the decay, are minimal in TCSPC. However, the total number of photons collected in the TCSPC is not maximal. The TCSPC technique based on the TAC (time to amplitude converter) approach has a relatively large dead time and poor duty cycle which depends on the method used to measure the delay between the laser and the detection of a photon. Furthermore, when used in conjunction with high repetition rate lasers, which is the norm today, the entire laser period cannot be measured unless the duty cycle is reduced.

In the classical analog approach to frequency domain methods, the modulated detector photocurrent is directly used without the need of a discriminator, avoiding dead time and possibly detecting all photons including the dark counts from thermal emission of the dynodes [3]. In the classical frequency domain approach the detection and data processing are done in the analog mode. At a late stage the signal is converted in digital form after filtering for the desired light modulation frequency. Although it has been shown that the uncertainty in lifetime determination in the frequency domain method is also limited by the number of photons collected [4], a common criticism of the frequency domain method is that the system operates at a single frequency and it cannot resolve very short lifetimes. Another criticism is that the duty cycle is 50% or lower due to the modulation of the gain of the detector. A typical use of the frequency domain method is for cases where the photon flux is very high; a regime that the time domain method cannot keep up.

Clearly, both the TCSPC method and the traditional frequency domain method are far from being “ideal” and there is ample room for improvement in both camps.

From the mathematical point of view, the time domain or the frequency domain analyses of periodic signals are equivalent, being related by the Fourier transform. Therefore the differences between the two methods are a consequence of the way data are collected and processed rather than due to any profound reason. In this chapter we discuss the photon counting parallel frequency domain method, an evolution of Weber's original idea. This method has been previously proposed but never described in detail in the context of parallel frequency acquisition [5]. It is based on the "FLIMbox" approach which is an electronic circuit for producing the "frequency representation" of the fluorescence decay. Here we discuss the common features and the difference between the FLIMbox approach and the common TCSPC method. Importantly, in the FLIMbox method, a set of modulation frequencies are measured in parallel with a duty cycle of 100%.

One application we have in mind for this technique is fluorescence lifetime imaging microscopy (FLIM). This is a particularly demanding application since very few photons are collected at each pixel (typically less than 1,000) but a few bright pixels can have very large instantaneous counting rate. For this application the duty cycle of data acquisition must be as large as possible and the dead time for the detection of the photons emitted should be minimal to avoid saturation of the electronics at the bright pixels. Another application is for the collection of lifetime data at high speed as in stop flow experiments. In both applications we need to distinguish several molecular species at each spatial or temporal location.

In the following I will present a personal view of the evolution in frequency domain phase fluorometry up to today's most current instruments starting with the state of the field when I joined Gregorio Weber's lab during my first visit in April–June, 1974.

2 The Frequency Domain Method

In retrospect, major technical developments in light sources and detectors found in current fluorometers were just starting at that time and fast repetition pulsed laser sources became available only after many more years. Perhaps more importantly, the focus in the field was in using the intrinsic fluorescence of proteins and several dyes available in the 1970s that were absorbing in the ultraviolet-blue region of the spectrum. Nanosecond pulsed lasers were not available in the protein absorption region and the nitrogen laser emitting at 337 nm was too slow and not far enough in the UV for protein work. The available light sources were nanosecond low pressure gas discharge sources or modulated high pressure arc lamps. Weber's lab in the 1970s was one of the places where great developments in fluorescence were occurring in all areas, instrumentation for steady state and time resolved fluorescence, landmark work for the development of methods for the measurement and application of fluorescence anisotropy, synthesis of novel fluorescence probes, and applications of fluorescence in many areas of biophysics, biochemistry, and biology. In Fig. 1 we reproduce the basic design of the optics and electronics of Spencer and Weber's cross-correlation frequency domain fluorometer [4].

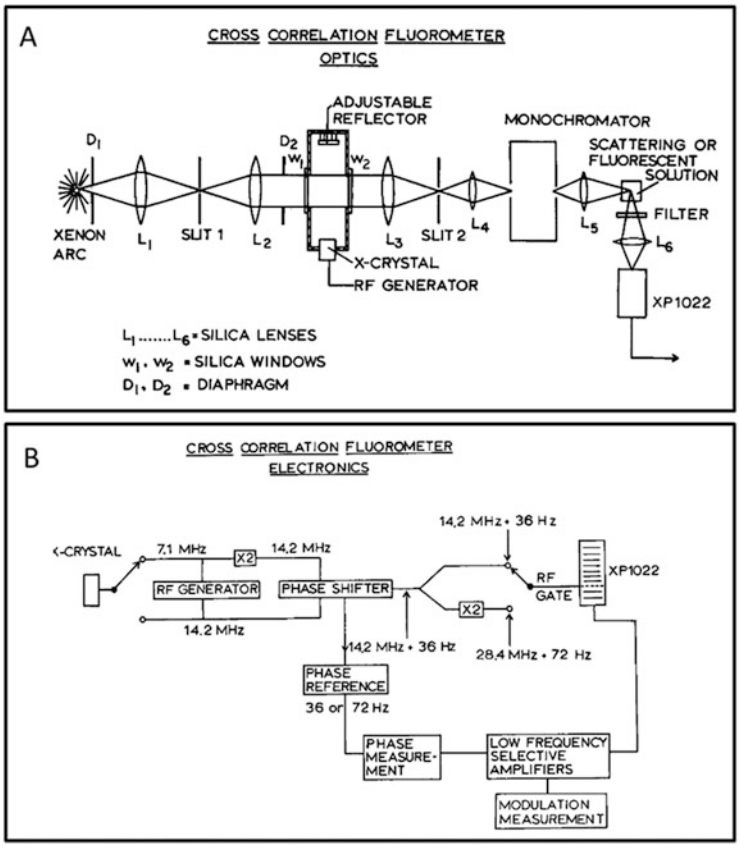

Fig. 1 Schematic of the original Spencer and Weber cross-correlation frequency domain fluorometer. (**a**) Schematic of the optical diagram. A high pressure xenon arc lamp is modulated by an ultrasonic Debye–Sears tank at high frequency generated by the X-crystal. The amplitude modulated light intensity is used to excite a fluorescence sample. (**b**) The X-crystal generator is shifted in frequency by the phase shifter and this shifted frequency is used to modulate the gain of the photomultiplier tube XP1022

During these years the idea of building a multifrequency phase fluorometer was a major discussion at the lab since in this type of future instrument the decay could be measured at many modulation frequencies. If available this instrument would advance the great innovation in the field at that time that was the frequency domain instrument invented in Weber's lab designed to modulate incoherent light sources at fixed frequencies, for example, at 14 and 28 MHz [4]. Of course, there were many predecessors of fluorometers using high frequency modulated light but one crucial innovation in Weber's work was the "cross-correlation" method first introduced in the Spencer and Weber instrument in which detection of the phase shift and of the modulation ratio was performed using the heterodyning or cross-correlation principle [4]. In this implementation of the technique, the detector gain was modulated

at a frequency which is slightly different from the frequency used to modulate the light source. Because of the detector gain modulation, this approach provided a maximum duty cycle of 50%. The gain modulation produces a difference frequency which is filtered and digitized for accurate phase and modulation determination. Using the heterodyning technique, phase shifts measurements as small as 0.1° were achieved [4]. For the purpose of comparing the phase histogram to the time bin histogram of the TCSPC, we note that 0.1° (which is the typical error in the phase value) in a period of 33 ns (30 MHz) corresponds to a time uncertainty of about 10 ps ($\delta\tau = \delta\phi/(2\pi f)$). Even for modern standards, the uncertainty obtained by frequency domain methods is remarkable since single exponential decay times of the order of one nanosecond could be measured with a precision of 10ps. However, one limitation of these early instruments was that complex exponential decays could not be resolved using only one or two light modulation frequencies. This explains the interest in developing the frequency domain technique but for multiple modulation frequencies.

The modulation frequency of the excitation light must be in a range that matches the rate of decay of the excited state [3, 6, 7]. For example, if the lifetime of the excited state is about 1ns, then the modulation frequency that has the highest sensitivity to changes around $\tau = 1$ ns must be in the range of 160 MHz:

$$f = \frac{1}{2\pi\tau} \approx 160\text{MHz}$$

Since it is technically difficult to measure the phase and modulation at very high frequencies and also the distortion of the waveform will render methods based on zero-crossing triggers subject to artifacts, the high frequency, at which the measurement is performed, is down converted to a very low frequency δf, generally on the order of 100–1,000 Hz where the signal is filtered and the phase and modulation of the emission with respect to the excitation is measured. The low frequency δf is called the heterodyning (or cross-correlation) frequency. The implementation of the cross-correlation method is achieved by generating two frequencies, one used for the modulation of the intensity of the light source at a frequency f and a second frequency at $f + \delta f$ used to modulate the gain of the detector where δf is in the 10–1,000 Hz range [4]. The detector in this case acts as a mixer by multiplying the signals at these two frequencies. The two signals are the modulated light impinging on the detector and the voltage used to modulate the gain of the detector. The output current of the detector is proportional to the light intensity times the gain of the detector. The product of two frequencies gives the sum and the difference of these frequencies. The sum is at very high frequency and it can be filtered from the difference δf using low pass frequency filters. Only the difference frequency is used.

For these early instruments, multifrequency referred to the possibility to sweep the frequency over a relatively large frequency range. True multifrequency was introduced later based on the principle of two locked frequency synthesizers [6] as shown in Fig. 2 where the light source was an argon ion laser.

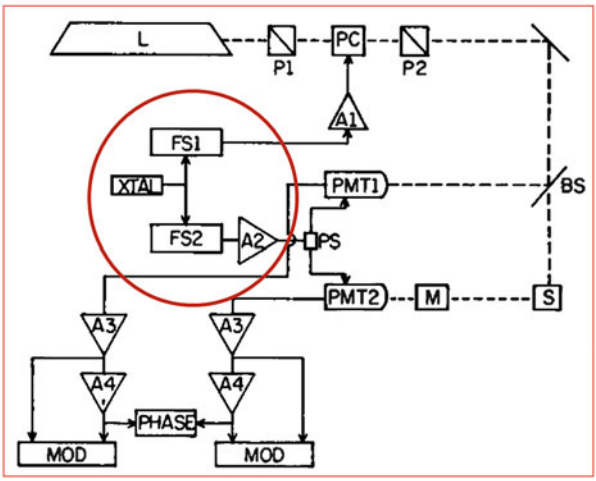

Fig. 2 Schematic and electronics of the Gratton–Limkeman multifrequency domain fluorometer. The *red circle* shows the two frequency-synthesizers FS1and FS2 that are phase locked to the same crystal. Similar to the Spencer and Weber design, the frequencyFS1 is used to modulate the light using a wide band Pockels cell and the frequency FS2 is used to modulated the gain of the PMT1 detectors

This technology is still used in commercial instruments. In the first multifrequency phase and modulation fluorometer [8], two phase-locked synthesizers generated the frequency f and $f + \delta f$. This approach provided a continuous range of modulation frequencies, limited only by the time response of the source or the detector. In this type of instrument, the operator selects the modulation frequencies generally in the range from 1 to 300 MHz and their number. The phase shift and the demodulation are measured for each frequency in a sequential fashion. An example of one of these commercial instruments is shown in Fig. 3 where the light source is a high pressure arc lamp emitting in the entire spectrum from 200 nm to above 800 nm.

A problem with these early instruments was that the zero-crossing detector used for the measurement of the phase was affected by the harmonic content of the low frequency signal. It was soon realized that the best measurement of the phase and modulation could be achieved if the signal at the heterodyning frequency was filtered from higher harmonics using a Fourier transform method. This method analyzes the harmonic content of the signal in separate orthogonal harmonics and required digitization of the low frequency signal [9]. The approach of analyzing the signal in Fourier components is still used today in most frequency domain instruments.

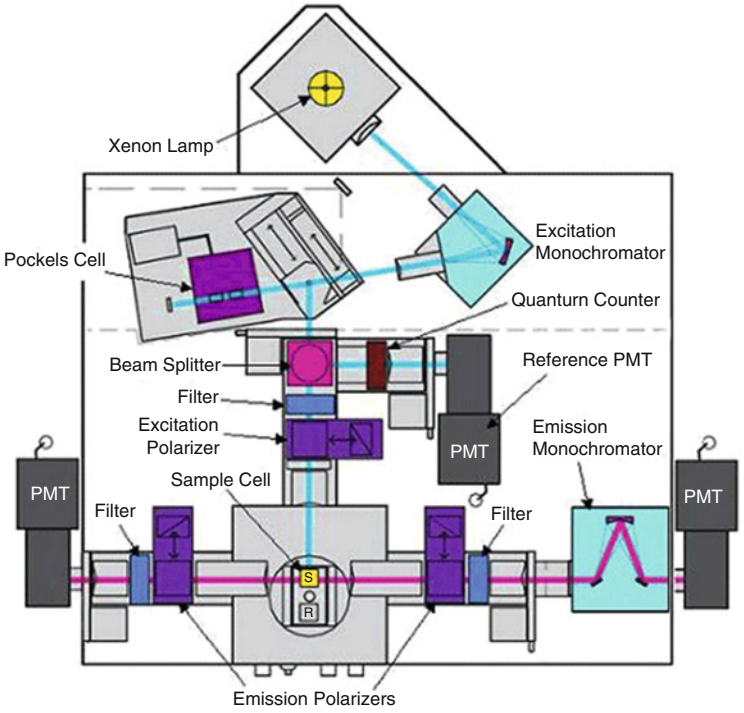

Fig. 3 Schematics of optics of the K1 multifrequency phase fluorometer built by ISS (Champaign, IL) circa 1987. A Pockels cell modulates the intensity from a high pressure xenon arc lamp. The gain of the 3 PMTs in this schematic are modulated at a slightly different frequency from the frequency used to modulate the intensity of the arc lamp

3 Pulsed Sources

However, another idea was discussed in Weber's lab at that time based on the availability of a new kind of light source: synchrotron radiation. Few synchrotrons were available in the 1980s but their characteristic time structure as well as their wavelength range was quite appealing for UV time resolved spectroscopy. The light emitted when the electrons circulating in a storage ring are deflected by a magnetic field is under the form of pulses at a relatively high repetition rate, which depends on the diameter of the storage ring and of the radiofrequency of operation used to accelerate the electrons. In an early design available at the time in Weber's lab (the Spencer design) the synchrotron radiation was used as a continuous light source to be modulated externally with a similar light modulator used in the original 2-frequency fluorometer in Weber's lab. Because of the experience in cross-correlation that we had acquired during these years we realized that we could cross-correlate directly with the pulsed light emitted at the synchrotron with our detection system and that no external modulators were required. The idea of using

the harmonic content of the synchrotron radiation was also discussed in a paper with Ricardo Lopez Delgado [10], but the synchronization with the radiofrequency of the synchrotron was our original idea. Based on the synchronization idea, we built the first multifrequency phase fluorometer that utilized a fast repetition pulsed source, rather than sweeping the frequency at discrete values [11]. At this point, the way was paved for the future developments of the parallel phase fluorometer that makes use of the harmonic content of fast repetition lasers sources, in which all harmonic frequencies are collected and analyzed at the same time [12]. Still today, the synchronization with the source pulse train is the technique used with pulsed lasers including for the development of FLIM with multiphoton excitation. It is notable that in this paper of 1984 [11], we discussed how to transform the analog acquisition in the instrument used at the synchrotron with a photon counting acquisition, a development that had to wait for about 20 years to be fully realized.

4 The Parallel Fluorometer Principle

As we described in the previous section, the conversion from the high frequency of the source repetition to the low frequency of the measurement is produced by the heterodyning process in which the output current of the detector which is at the frequency of light modulation is mixed (multiplied) by a slightly different frequency. If instead of using a sinusoidal signal to modulate the gain of the detector we use a signal which contains many harmonics, the multiplication generates not one, but a spectrum of harmonics that is the replica of the spectrum at high frequency.

In 1989 a "parallel multifrequency" fluorometer instrument was described by Feddersen et al. [9]. In this instrument, the excitation light is pulsed and the detector gain is modulated by a narrow pulse rather than by a sinusoidal signal. It was soon realized that although all harmonic frequencies were measured in parallel, the mixing scheme obtained by modulating the gain of the detector in the parallel multifrequency instrument was very ineffective. In fact, the operation of "pulsing" the detector gain is equivalent to turning the detector "on" for a very brief period, resulting in substantial decrease of the detector duty cycle. Feddersen et al. discussed this limitation [9] and they suggested keeping the detector "on" for 1/16 of the source period, providing about 16 frequencies in parallel. It was demonstrated that this is the optimal duty cycle that maximizes the speed of data acquisition and minimizes losses arising from turning "on" and 'off" the detector [9]. This scheme has been used ever since in the so-called parallel frequency domain lifetime instruments. Table 1 shows the evolution of various frequency domain phase fluorometers developed in my lab.

In the "original" parallel fluorometer system described in 1989 by Feddersen et al. [9] the advantages of multifrequency acquisition were discussed vis-a-vis the reduction of the duty cycle needed in the analog system to achieve acquisition of several harmonic frequencies simultaneously. In the original parallel acquisition

Table 1 Parallel frequency domain history

Parallel fluorometer (1986)	Digital mixing (2000)	First FLIMBox (2007)	Parallel-FLIMBox (2009)
Analog mixing with pulsed external generator. Mixing using the detector gain	Digital mixing with external square wave generator. Detector gain not modulated	Digital mixing. Internal generator modulate signal after detector @48 MHz	Digital mixing. Internal generator produce pulsed modulating signal @10, 20 MHz
Duty cycle depends on harmonics. 6% for $n = 16$	Duty cycle is 50%	Duty cycle is 100%	Duty cycle is 100%
Parallel frequency domain lifetime instruments	FCS. System not ready to implement parallel acquisition	FLIM. System not ready to implement parallel acquisition	Parallel digital frequency domain for cuvette, FLIM, and FCS
One input channel	One input channel	Two input channel	Up to four input channel
Average acquisition time takes several minutes			Average acquisition time takes seconds
		Frame synchronization and saturation problems. Limited number of windows, design instable	Flexible synchronization. Saturation control. Eight and 16 windows available. Stable design

system, it was discussed that a reduction of duty cycle to about 6.25% was giving optimal performance. Several commercial systems were produced to achieve the parallel frequency acquisition in which the duty cycle was sacrificed at the expense of the harmonic content. With the invention of the FLIMbox approach this limitation was removed since the FLIMbox has 100% duty cycle.

5 Photon Histograms

From the point of view of the construction of the decay histogram, the TCSPC and the FLIMbox essentially do the "same thing" but with some notable technical differences. In the TCSPC the time axis is divided in "time bins" typically 1024 time channels or more. If the total time range is 12.5 ns (for a laser operating at 80 MHz repetition rate), each channel width (in time) assuming that we collect 256 time bins is about 49ps. In FLIM microscopy, due to the limited number of photons collected per pixel, the number of channels is generally reduced to 256 or 128 since the total counts per pixels is no more than 1,000 counts (Fig. 4).

The "same" concept of dividing the photons time of arrival in bins is also used in the FLIMbox, where the laser repetition period is divided in 256 phase intervals, but synchronized with the period of the laser (Fig. 5). For a laser operating at 80 MHz,

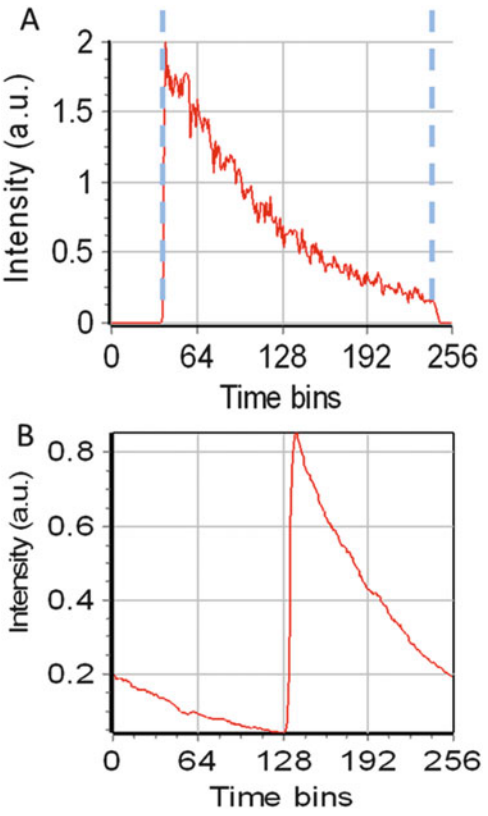

Fig. 4 Demonstration of the useful range of the Becker and Hickl 830 card. (**a**) For a 80 MHz repetition frequency laser using 50 ns total range at a TAC gain of 4 the total range is 12.5 ns. However the useful range is from channel 50 to 250 out of 256 (78%), and the time record is incomplete since the entire period of the laser is not used. (**b**) Using a TAC gain of 2 the total range is 25 ns of which a portion of 12.5 ns could be extracted. In this case the effective useful range is 50% but the record is complete since we cover an entire laser period

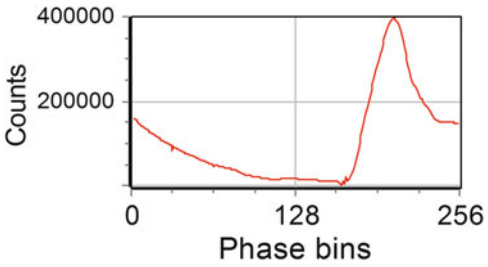

Fig. 5 The photon counting phase histogram produced by the FLIMbox. In this example, the laser repetition period is 12.5 ns. This interval is divided into 256 bins. The entire laser period is collected at 100% duty cycle

dividing the period in 256 parts results in a time bin of 48.9 ps or, referring to the period of 360°, each phase bin is 1.4°.

So the technical difference with respect to the TCSPC time domain approach is that the FLIMbox approach uses always 256 phase bins, it covers the entire laser repetition period and the bins size and phase are synchronized with the laser. In the TCSPC, generally the time range is set to be a part of the period, the size of the bin is dependent on an internal clock independent of the laser period and the phase of the bin sequence is synchronized with the laser by the start–stop clock of the Time

to Amplitude Converter (TAC) converter. In the frequency domain method, the phase bin size (in terms of time) is directly derived from the rep rate of the laser so that the time calibration depends on the laser repetition frequency.

Of course, if the laser repetition rate becomes much slower, the number of phase bins could be increased in the FLIMbox circuit. In a few words, the "basic" difference between the FLIMbox and the TCSPC is the way the time bins are generated. In the FLIMbox, the time bins are derived by division of the laser repetition period. In the TCSPC the time bins are produced independently of the laser rep rate as they are determined by sampling a linear ramp using the TAC principle. This lack of synchronization with the laser rep rate results in several problems when high rep rate lasers are used, which is today the rule for FLIM.

5.1 Dead Time

The dead time of the FLIMbox technique is due to the discriminator rather than the internal FLIMbox circuit. The discriminator dead time used in this work is about 7 ns. The FLIMbox has two totally independent inputs so that two channels can be used simultaneously without loss of photons. The TCSPC dead time depends on the recovery time of the TAC. According to manufactures' specifications, both PicoQuant and B&H quote figures in the order of 100–120 ns dead time, depending on the model of their data acquisition card. At high counting rates, this large dead time can strongly affect the linearity of the data collection in terms of time and intensity linearity.

5.2 Duty Cycle

This is an important difference between the FLIMbox frequency domain approach and the TCSPC method. The FLIMbox is always active, so that photons are collected irrespective of their time of arrival. In the TCSPC the time axis is limited to a percentage of the total period of the laser pulse. For example, if the laser repeats at 12.5 ns (typical of the Ti:Sa laser at 80 MHz) the usable range is generally on the order of 10 ns only (about 80% of the total range) as shown in Fig. 4a. However, in the tail of the distribution at longer delay times some photons are lost. To fix this problem, the TAC range could be set to collect data at twice the laser period, so that the total TAC range is 25 ns and is at least one complete period of the laser (Fig. 4b). In this case the losses are in terms of photons falling outside the range of the measurement and they can be substantial since part of the lost range occurs at times when the photon flux is large. If the losses are minimized using the 12.5 ns range (in this example), evidently the entire decay range is not available. The fitting routines will only use a smaller range with consequences about the accuracy of fitting longer lifetime components which contribute more in the lost region. Also,

since the entire period is not available, the phasor transformation cannot be done correctly, unless some assumptions are introduced about the behavior of the decay in the region that is not collected. If data are collected on a longer period (for example, 25 ns and only 12.5 ns are used for analysis) the duty cycle is only 50% (instead of 80%). However, the advantage of reducing the duty cycle is that an entire period is available; the phasor transformation can be used without assumptions about the missing parts and longer lifetime components could be properly analyzed.

Based on the dead time and duty cycle considerations, it appears that with the FLIMbox approach the frequency domain method is more effective than the TCSPC.

5.3 Time Resolution

As mentioned in the introduction, a common belief is that the TCSPC has better time resolution than the frequency domain approach. If time resolution refers to the pulse-to-pulse separation, this is true since the TCSPC uses a very small bin time. However, in the case of a "lifetime," which is an exponential process, photons are necessarily spread among bins. In this case the time resolution depends primarily on the number of photons collected in the decay curve. The FLIMbox is very efficient and maximizes the photons collected.

6 Photon Counting Multifrequency Parallel Fluorometer

The FLIMbox concept is now at the second generation stage due to the availability of high frequency digital electronics in new FPGA chips as well as the availability of programming languages for the FPGA that makes the code developed for a given chip, transportable to a next generation chip. We show in Fig. 6 a comparison of the bandwidth available in a current chip (FPGA Spartan 6, Xilinx) compared to the original FLIMB box chip (Spartan 3, Xilinx).

The first zeros of the original FLIMbox acquisition algorithm were at 160 MHz, 320 Mhz, repeating each even harmonics. Since the amplitude of these frequencies is zero, they are removed from the analysis. Figure 6 (green lines) shows that there are at least 20–30 harmonics that can be collected using the new generation FPGA. The high frequency limit is actually given by the lifetime of the probe. Fluorescein at basic pH has a lifetime of 4.04 ns. The absolute modulation of this sample is about 3% at 200 MHz.

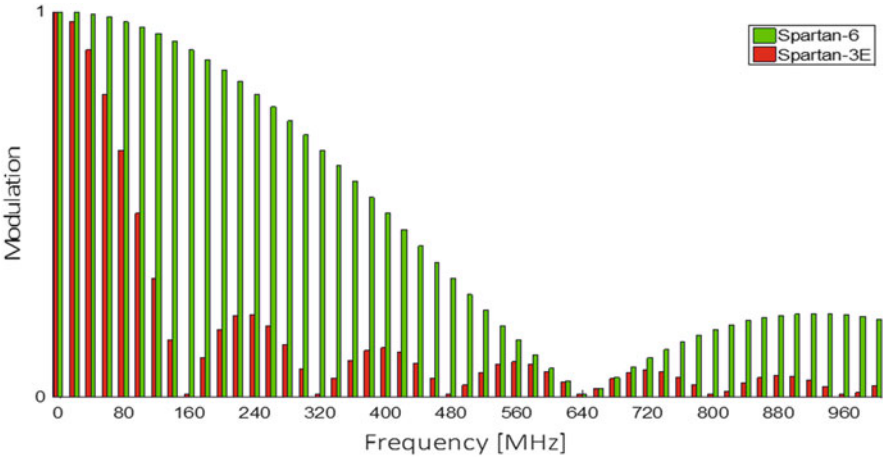

Fig. 6 Harmonic content of the original FLIMbox based on the Spart3 chip (in *red*) and of the new generation FLIMbox based on the Spartn6 chip. The new generation FLIMbox has a very good modulation (about 30%) in the GHz region

7 Conclusions

With the advent of the very inexpensive digital electronics available in current FPGA chips, a new technology is now available for the measurement of fluorescence lifetime decays at high speed and in many channels simultaneously. Since the frequency of operation of the FPGA chip is continuously increasing, it is possible that this technology one day will be used for all time domain or frequency domain instruments. Clearly, using this technology, the time and frequency domain is a distinction that is not needed any more. This result was anticipated in many of the discussions I had with Gregorio Weber starting in 1974 and continued while Dr Weber was alive.

The maximum frequency obtained in the FLIMbox is now limited to about 1GHz by the particular chip and technology we are using (Spartan 6, XILINX). However, faster and large chips are already in the market. It is the moment to further develop the digital technology so that the user can just choose which representation of the decay is preferable. At the inner core of the technology there should be no differences. The representation the user wants to see is determined by a click in the software.

The FLIMbox design can be synchronized with lasers that are intrinsically modulated or it can generate a frequency to amplitude modulate a laser diode or LED. In the most current implementation it provides up to 16 independent input channels, it has a saturation feedback control to avoid any time information loss, and it is only limited by the number of photons collected rather than by the sampling window implementation scheme.

This new design, in summary, is very stable, has very low power requirements, has high frequency capability and higher precision, and allows the multi exponential analysis to be performed on almost every photon detection based acquisition system (imaging microscopy, FLIM, FCS, multifrequency fluorometer, and tissue imaging).

Acknowledgments Part of the work described in this chapter was supported by the following grants NIH P41-GM103540 and NIH P50-GM076516

References

1. Gratton E, Breusegem S, Sutin J, Ruan Q, Barry N (2003) Fluorescence lifetime imaging for the two-photon microscope: time-domain and frequency-domain methods. J Biomed Opt 8 (3):381–390
2. Becker W, Bergmann A, Hink MA, König K, Benndorf K, Biskup C (2004) Fluorescence lifetime imaging by time-correlated single-photon counting. Microsc Res Tech 63(1):58–66
3. Gratton E, Jameson DM, Hall RD (1984) Multifrequency phase and modulation fluorometry. Ann Rev Biophys Bioeng 13:105–124
4. Spencer RD, Weber G (1969) Measurements of subnanosecond fluorescence lifetimes with a cross-correlation phase fluorometer. Ann NY Acad Sci 158:361–376
5. Colyer RA, Lee C, Gratton E (2008) A novel fluorescence lifetime imaging system that optimizes photon efficiency. Microsc Res Tech 71(3):201–213
6. Jameson DM, Gratton E (1983) Analysis of heterogeneous emissions by multifrequency phase and modulation fluorometry. In: Eastwood D (ed) New directions in molecular luminescence. ASTM-STP 822, American Society of Testing and Materials. pp 67–81
7. Lakowicz JR, Gratton E, Cherek H, Maliwal BP, Laczko G (1984) Determination of time-resolved fluorescence emission spectra and anisotropies of a fluorophore-protein complex using frequency-domain phase-modulation fluorometry. J Biol Chem 259(17):10967–10972
8. Gratton E, Limkeman M (1983) A continuously variable frequency cross-correlation phase fluorometer with picosecond resolution. Biophys J 44(3):315–324
9. Feddersen BA, Piston DW, Gratton E (1989) Digital parallel acquisition in frequency domain fluorimetry. Rev Sci Instrum 60(9):2929–2936
10. Gratton E, Delgado RL (1979) Use of synchrotron radiation for the measurement of fluorescence lifetimes with subpicosecond resolution. Rev Sci Instrum 50(6):789
11. Gratton E, Jameson DM, Rosato N, Weber G (1984) Multifrequency cross-correlation phase fluorometer using synchrotron radiation. Rev Sci Instrum 55(4):486–494
12. Alcala RJ, Gratton E, Jameson DM (1985) A multifrequency phase fluorometer using the harmonic content of a mode-locked laser. Anal Instrum 14:225–250

Ultra-Fast Fluorescence Anisotropy Decay of *N*-Acetyl-L-Tryptophanamide Reports on the Apparent Microscopic Viscosity of Aqueous Solutions of Guanidine Hydrochloride

Antonie J.W.G. Visser, Nina V. Visser, Arie van Hoek, and Herbert van Amerongen

Abstract The very fast fluorescence anisotropy decay of *N*-acetyl-L-tryptophanamide (NATA) in aqueous solutions has been measured with sub-picosecond laser excitation and detection with time-correlated single photon counting. By using global analysis of both parallel and perpendicular polarized fluorescence intensity decays involving deconvolution, the rotational correlation times of NATA in the tens of picosecond range are accurately recovered. Since rotational correlation times are directly proportional to viscosity, we have used these correlation times to derive the (relative) microscopic viscosity of increasing concentrations of guanidine hydrochloride (GuHCl) in buffered water. GuHCl is a well-known chaotropic agent of protein denaturation. We give a step-by-step description how to obtain the final results. Subsequently, we compare the obtained microscopic viscosities with macroscopic viscosity data reported half a century ago using capillary viscosimeters. From the results it is clear that GuHCl, present in molar concentration, associates with NATA making the apparent molecular volume larger.

Keywords Fluorescence anisotropy • Fluorescence lifetime • Fluorescence polarization • Global analysis • Microscopic and macroscopic viscosity • Protein denaturant • Time-correlated single photon counting • Tryptophan fluorescence

A.J.W.G. Visser (✉)
Laboratory of Biochemistry, Microspectroscopy Centre, Wageningen University, P.O. Box 8128, 6700 ET Wageningen, The Netherlands
e-mail: antoniejvisser@gmail.com

N.V. Visser, A. van Hoek, and H. van Amerongen
Laboratory of Biophysics, Microspectroscopy Centre, Wageningen University, P.O. Box 8128, 6700 ET Wageningen, The Netherlands

D.M. Jameson (ed.), *Perspectives on Fluorescence: A Tribute to Gregorio Weber*,
Springer Ser Fluoresc (2016) 17: 81–94, DOI 10.1007/4243_2016_11,

Contents

1 Introduction

Gregorio Weber played a pioneering role in developing protein fluorescence in all its modern facets. In 1957 Gregorio Weber and his co-worker John Teale published the first corrected emission and excitation spectra of the aromatic amino acids: phenylalanine, tyrosine, and tryptophan [1]. A few years later Weber published fluorescence polarization as function of excitation wavelength (polarization spectrum) of tyrosine, tryptophan, and related compounds (phenol and indole) in cryogenic solutions [2] and of the same amino acid residues in proteins at both ambient and low temperature [3]. From measurements in more concentrated solutions of the individual compounds and mixtures a distinct depolarization was observed, which could be ascribed to electronic energy transfer between the same molecules (homotransfer) or between different molecules (heterotransfer) [2]. Similar depolarization processes in proteins indicate, depending on the particular protein, the occurrence of homotransfer between tyrosine or tryptophan residues or heterotransfer from tyrosine to tryptophan residues [3]. Many researchers now refer to Förster Resonance Energy Transfer or FRET for this process instead of electronic energy transfer. In 1977 Bernard Valeur and Gregorio Weber published polarization spectra of indole and tryptophan in cryogenic solutions to spectrally resolve the ^1L_a and ^1L_b electronic transitions, which are close in energy [4]. The ^1L_a transition is in most cases the emitting state and it can be selectively excited without much interference of the ^1L_b transition when excitation wavelengths are >300 nm. Already in the final chapter of Gregorio Weber's PhD thesis (published in 1947) it was shown that fluorescence polarization can be used to determine the internal viscosity (or microscopic viscosity) of gels. When the molecular dimension of the

fluorescent molecule (the solute) is large as compared to the one of solvent molecules, the microscopic viscosity, which determines the resistance (or friction) to rotational diffusion, is the same as that determined from the resistance of the solvent to flow (or macroscopic viscosity). When the molecular dimensions of solute and solvent are similar, microscopic and macroscopic viscosities may differ markedly. The actual (first) publication on viscosity measurements with fluorescence polarization in gel systems such as micelles appeared much later [5].

In this chapter we report on ultra-fast fluorescence anisotropy decay of the well-known tryptophan (Trp) analogue *N*-acetyl-L-tryptophanamide (NATA) in aqueous solutions of increasing concentrations of the protein denaturant guanidine hydrochloride (GuHCl). Previously, we have used GuHCl to investigate denaturant-induced (un)folding of apoflavodoxin from *Azotobacter vinelandii* with polarized time-resolved fluorescence methods [6, 7]. Using picosecond-resolved fluorescence anisotropy of wild-type apoflavodoxin containing three tryptophan residues and of mutant proteins lacking one or two Trps, it has been demonstrated that photo-excited tryptophan residues of apoflavodoxin exchange energy through a FRET mechanism [7]. Energy transfer from Trp167 to Trp128, residues that are 6.8 Å apart, leads to a rapid decay of the experimental anisotropy signal with a unidirectional 50-ps transfer correlation time [7]. FRET between the other Trp-Trp couples turned out to be much slower or even absent. The short rotational correlation time of NATA in aqueous solutions, obtainable from analysis of time-resolved fluorescence anisotropy, will be a challenging test case to recover ultra-fast depolarization processes of the type described in [7]. The protocol how to obtain these correlation times, which are even shorter than the FWHM of the impulse response function, is the subject of this chapter. In addition, the results will show that aqueous GuHCl solutions cannot be considered as a homogeneous solvent, since the denaturant exhibits molecular interaction with NATA that lasts much longer than the fluorescence lifetime.

2 Experimental Section

2.1 Materials and Solutions

Scintillation grade *p*-terphenyl and *N*-acetyl-L-tryptophanamide were purchased from BDH and Sigma, respectively. Spectroscopically pure cyclohexane and spectrophotometric grade carbon tetrachloride (CCl_4) were purchased from Merck and Janssen Chimica, respectively. 1 μM of *p*-terphenyl in cyclohexane/CCl_4 (50/50 v/v) has been used as a reference compound [8]. Aqueous solutions of different concentrations of guanidine chloride (GuHCl) in 100 nM potassium pyrophosphate buffer (pH 6.0) were prepared as previously described [7]. The final concentration of NATA amounted to 4.4 μM. The temperature of all experiments was 25°C.

2.2 Measurement Setup

Time-resolved fluorescence measurements were performed using mode-locked continuous wave lasers for excitation and the time-correlated single photon counting (TCSPC) technique for detection as described elsewhere [9]. We will summarize the main elements of the setup. For elaborate functional details and manufacturers of the different parts, we refer to the previous publication [9]. The pump laser was a CW diode-pumped, frequency-doubled Nd:YVO_4 laser and the mode-locked laser was a titanium: sapphire laser (in fs mode) tuned to 900 nm. At the output of the titanium: sapphire laser a pulse picker was placed, decreasing the repetition rate of excitation pulses to 3.8×10^6 pulses per second (3.8 MHz). The output of the pulse picker was directed towards a frequency tripler. For excitation a maximum pulse energy of sub-pJ was used, the wavelength was 300 nm and the pulse duration about 0.2 ps. An excitation wavelength of 300 nm was chosen because then the highest initial anisotropy was obtained by selective excitation in the ^1L_a transition of the indole ring [4]. The samples were in 1.5 mL and 10-mm light path fused silica cuvettes in a temperature controlled sample holder, which was placed in a housing also containing the main detection optics. Extreme care was taken to avoid artifacts from depolarization effects. At the front of the sample housing a Glan-laser polarizer was mounted, optimizing the already vertical polarization of the input light beam. The fluorescence was collected at an angle of 90° with respect to the direction of the exciting light beam. Both the sample and the photomultiplier detector were placed a single fast lens (uncoated fused silica, F/3.0), a Schott UV-DIL 348.8 nm ($\Delta\lambda = 5.4$ nm) interference filter, a rotatable sheet type polarizer (Polaroid type HNP'B suitable for ultraviolet radiation), and a second single fast lens (uncoated fused silica, F/3.0) focusing the fluorescence on the photomultiplier cathode. The polarizer sheet was in a dc motor driven ball-bearing holder with mechanical stops, allowing computer-controlled rotation (0.2 s) to parallel and perpendicular polarized detection of emission. The polarizers were carefully aligned and the performance of the setup finally checked by measuring suitable reference samples [10]. Detection electronics were TCSPC modules detailed in [9]. A microchannel plate photomultiplier was used for the detection of the fluorescence photons. The single photon responses of this photomultiplier were processed as previously described and finally collected in 4096 channels of a multichannel analyzer. The channel time spacing was 5.0 ps. By reducing the energy of the excitation pulses with neutral density filters, the rate of fluorescence photons was decreased to less than 30,000 per second (≈1% of 3.8 MHz), to prevent pile-up distortion. For the deconvolution procedure, the dynamic instrumental response function was determined using a freshly made solution of *p*-terphenyl in a mixture of 50/50 (v/v) cyclohexane and CCl_4 [8]. One complete measurement consisted of the recording of three cycles of the parallel (10 s) and perpendicularly (10 s) polarized fluorescence of the reference compound, ten cycles of parallel (10 s) and perpendicularly (10 s) polarized fluorescence of the sample, and two cycles of polarized background emission of the buffer (with increasing amounts of GuHCl) measured under the same conditions as the sample and again the reference compound.

2.3 Data Analysis

Time-resolved polarized fluorescence data analysis was essentially as described by Borst and co-workers [9]. Global fitting of parallel and perpendicular polarized fluorescence intensity decays was performed using the "TRFA Data Processing Package" of the Scientific Software Technologies Center (www.sstcenter.com; Belarusian State University, Minsk, Belarus) [11]. For the deconvolution procedure, the dynamic instrumental response function was determined using a freshly made solution of *p*-terphenyl in cyclohexane/CCl_4 (50/50 v/v). Fluorescence lifetime analysis of NATA required a minimum model of a one-component model for good fitting. However, we will compare also a two-component model. After optimization of amplitudes and lifetimes of the total fluorescence, the time-dependent fluorescence anisotropy $r(t)$ is calculated from the parallel and perpendicular intensity components in which the initial anisotropy at zero time, $r(0)$, and the rotational correlation time, ϕ, are the fitting parameters. Global analysis was performed by simultaneous fitting of parallel and perpendicular polarized fluorescence intensity decays and linking the common correlation time ϕ and initial anisotropy $r(0)$. In addition, a rigorous error analysis at the 67% confidence level was applied to the optimized rotational correlation time.

3 Results

3.1 Searching for the Optimum Fluorescence Lifetime of the Reference Compound

In Ref. [12] a method is described to fit the fluorescence lifetime of the reference compound *p*-terphenyl in ethanol together with the fluorescence of NATA in water in the fluorescence decay analysis. This resulted in excellent fits giving a lifetime value of 1.07 ns for *p*-terphenyl in ethanol, which is insensitive to temperature between 4 and 30°C. In contrast, the fluorescence lifetime of NATA in water is sensitive to temperature giving values of 3.98 ns at 4°C, 3.01 ns at 20°C, and 2.48 ns at 30°C. For the fluorescence decay of *p*-terphenyl in cyclohexane, which is dynamically quenched by CCl_4, a similar procedure of using fluorescence lifetimes of quenched and unquenched *p*-terphenyl in cyclohexane as fitting parameters worked well leading to a fluorescence lifetime of 0.94 ns for *p*-terphenyl in cyclohexane and of 12 ps for *p*-terphenyl in cyclohexane/CCl_4 (50/50 v/v) at 20°C [8]. In this work we used a similar procedure by performing a single-component fluorescence decay analysis of NATA in water (pH 6.0) with *p*-terphenyl in cyclohexane/CCl_4 (50/50 v/v) as a reference compound at 25°C. When we systematically varied the fluorescence lifetime of the reference compound (τ_{ref}), performed the decay analysis, and listed the value of the fitting criterion χ^2, a minimum χ^2 is reached for $\tau_{ref} = 14$ ps (results not shown). It did not matter whether we took the fluorescence lifetime of NATA (2.72 ns) as fixed or free parameter in the analysis.

3.2 Total Fluorescence Decay Analysis of NATA in Aqueous Buffer

The fluorescence decay analysis of NATA in aqueous buffer is presented in Fig. 1. Three curves are presented in the upper panel as detailed in the legend of Fig. 1. At first sight a single lifetime component of 2.72 ns appears to be sufficient to describe the fluorescence decay of NATA, since there is no difference between both black

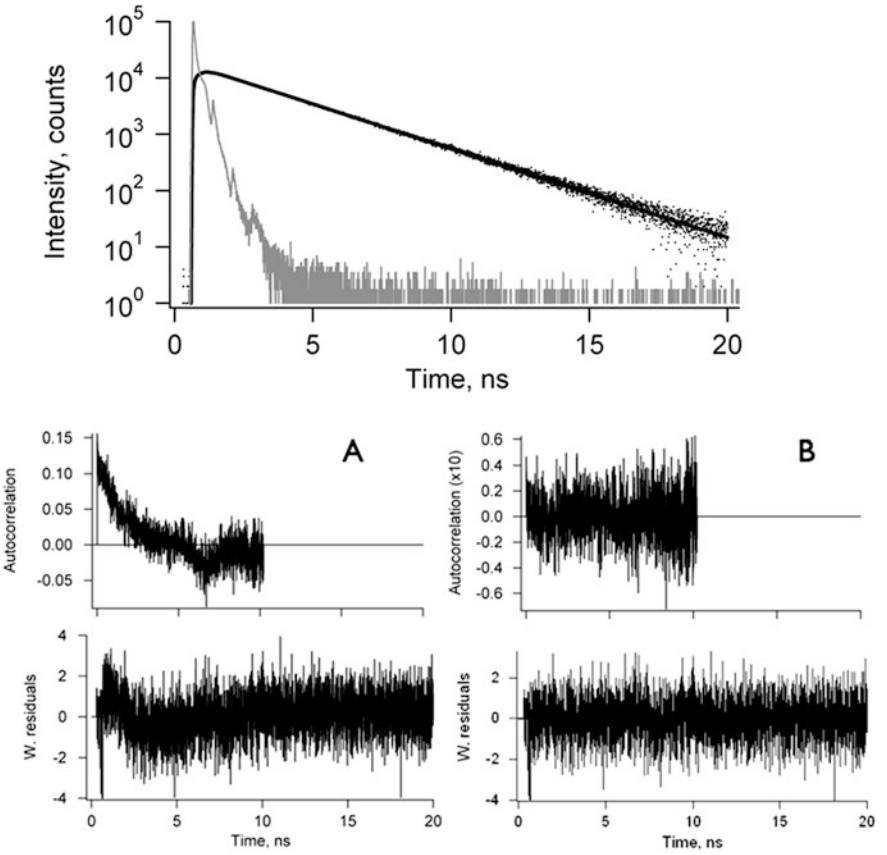

Fig. 1 *Top panel*. Fluorescence decay analysis of NATA in aqueous buffer. The figure shows the experimental fluorescence decay (*black dots*) and the fitted curve (*black solid line*) on a semi-logarithmic scale. In *grey* is the instrumental response function taken from a *p*-terphenyl cyclohexane/CCl_4 (50/50 v/v) solution. Fitting was accomplished over the complete rise and decay curve. The recovered fluorescence lifetime was 2.72 ns and the reduced χ^2 (i.e., fitting criterion) amounted to 1.17. *Lower panel*. Comparison between fits of one-exponential component (**a**) and of two-exponential components (**b**) applied to the same data. The first point in the autocorrelation function should always start with one, but it is suppressed for clarity. For the two-exponential fit the recovered fluorescence lifetimes were $\tau_1 = 1.3$ ns ($\alpha_1 = 0.07$) and $\tau_2 = 2.77$ ns ($\alpha_2 = 0.93$) and the reduced χ^2 amounted to 1.04. Note that in **b** the autocorrelation function is multiplied by 10

curves (dots and line) and the reduced χ^2 is equal to 1.17, which is sufficiently low. However, when other fitting criteria are presented, such as the presentation of weighted residuals and the autocorrelation of the weighted residuals (Fig. 1), the conclusion of a single fluorescence lifetime is not a firm one. The autocorrelation function of the residuals is a very good indicator of the goodness of a fit. This function clearly indicates that NATA fluorescence decay is not for 100% single exponential (Fig. 1, panel a), but a second, shorter component (~1.3 ns) of small amplitude (~7%) is needed to make both residuals and autocorrelation functions randomly fluctuate around zero (Fig. 1, panel b). We will address this apparent non-exponential behavior of the fluorescence decay of NATA in the discussion section.

3.3 Fluorescence Anisotropy Decay Analysis of NATA in Aqueous Buffer

The rotational correlation time of NATA in aqueous buffer will be extremely fast in the range of tens of picoseconds. It is therefore a large challenge to accurately determine these rotational correlation times from analysis of the fluorescence anisotropy decay. The complexity of the analysis is illustrated in four panels of Fig. 2. In Fig. 2a the normalized time traces of reference response curve, total fluorescence, and the experimental anisotropy recovered after deconvolution are shown. The reference response curve has a full width at half the maximum intensity (FWHM) of 80 ps, which is the same as the FWHM of the instrumental response function (IRF, results not shown) measured with TCSPC. The pure anisotropy after deconvolution shows a decay within the reference response curve. In addition, the fluorescence of NATA still has to be built up because of the finite width of the IRF.

Despite the ultra-short rotational correlation time of NATA in water, global analysis of the individual polarized fluorescence intensity components is advantageous as illustrated in Fig. 2b. Parallel and perpendicular polarized fluorescence curves are fitted very well over the whole rise and decay curves of NATA fluorescence. At this stage it is important to note that we used the best fitted total fluorescence decay profiles, since this will lead to the lowest total reduced χ^2. In this case the two-exponential fit of the total fluorescence decay is merely used as a mathematical function to optimally emulate the total fluorescence decay of NATA.

Rather than presenting the whole analyzed anisotropy curve between 0 and 20 ns, it is much more illustrative to present the most relevant part of the curve (see line markers at two time points in Fig. 2c). The experimental anisotropy points at the left side of the shortest time point become unstable, as the fluorescence intensity approaches zero. However, the fitted anisotropy points show a much clearer behavior (Fig. 2d), which makes the choice of the first point of presentation much easier. It corresponds to the time point where the maximum is reached. In Fig. 2c the left marker is placed at time $t = 0.625$ ns. The right marker at longer time

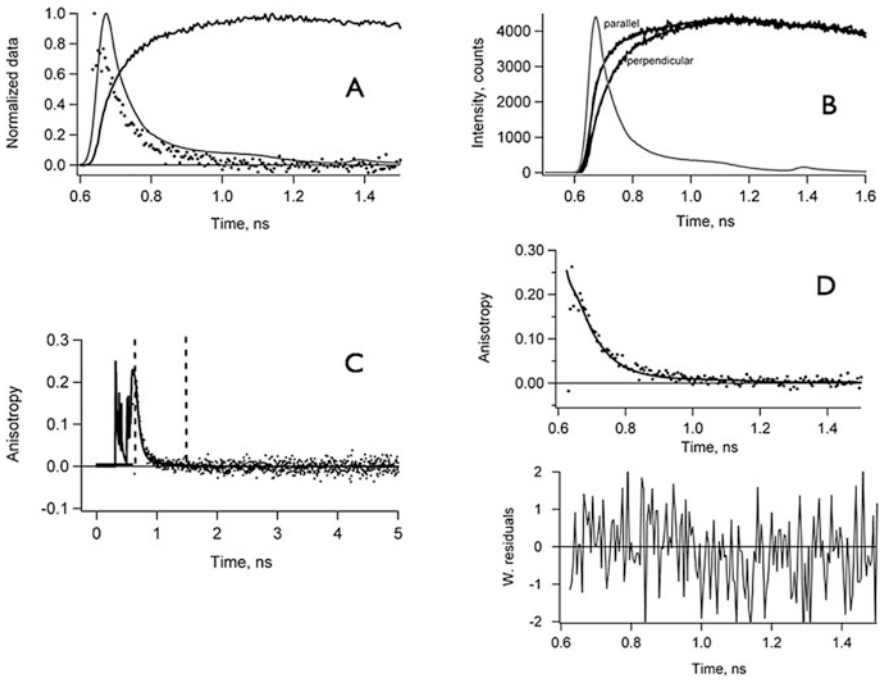

Fig. 2 Fluorescence anisotropy decay analysis of NATA in aqueous buffer. (**a**) Normalized curves on an expanded time scale to illustrate the time limits. Shown are the total fluorescence (*solid black line*), the anisotropy decay *after deconvolution* (*black points*), and the reference response curve (*grey*; 80 ps FWHM). (**b**) Global analysis of parallel and perpendicular polarized fluorescence. The experimental (noisy traces) and calculated curves (*solid lines*) are presented in *black* and the reference response curve is shown in *grey*. Analysis took place over the whole decay curves, but only the initial part is shown. Note that both polarized curves become indistinguishable after 1.2 ns. The reduced χ^2-values are for the parallel component 1.145 and for the perpendicular component 1.077. (**c**) Snapshot of the first 5 ns (out of 20 ns) of the observed (*dots*) and fitted (*line*) anisotropies and the borders within to present analysis details in panel **d**. (**d**) Deconvoluted fluorescence anisotropy decay of NATA in aqueous buffer. In the top panel the experimental (*points*) and the fitted data (*solid line*) are shown. In the lower panel the weighted residuals between experimental and fitted curves are presented. The recovered rotational correlation time $\phi = 43$ ps between 38 ps (lower bound confidence limit) and 48 ps (upper bound confidence limit). The initial anisotropy $r(0) = 0.261$

is placed rather arbitrarily, namely, where the anisotropy is completely decayed to zero. It is placed at $t = 1.5$ ns. In Fig. 2d a snapshot of anisotropy decay analysis corresponding to the two time markers is presented. The fit of experimental data points (175 channels) with an exponential function with single rotational correlation time $\phi = 43$ ps is nearly perfect as judged from the randomly distributed weighted residuals. The initial anisotropy $r(0) = 0.261$.

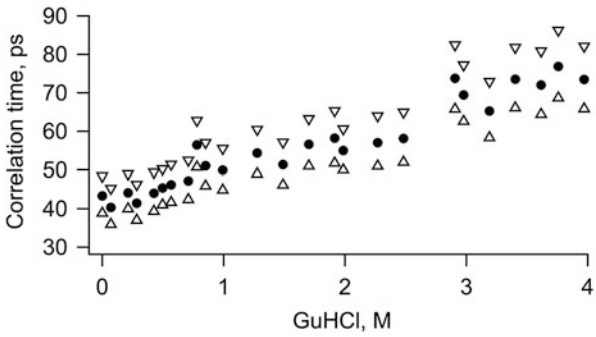

Fig. 3 Rotational correlation times (in picoseconds) of NATA in aqueous buffer versus the molar concentration of guanidine hydrochloride (GuHCl). Shown are the recovered correlation times (*closed circles*) and the upper (*open inverted triangle*) and lower (*open triangle*) confidence limits at the 67% level

3.4 Fluorescence Anisotropy Decay Analysis of NATA in Aqueous Buffer Containing GuHCl

The rotational correlation times of NATA in aqueous buffer containing increasing GuHCl concentrations are obtained after a similar analysis procedure described in the previous section. A bi-exponential fluorescence decay is assumed. The long fluorescence lifetime was pretty constant, namely 2.71 ± 0.06 ns, which is the same value as obtained for a one-exponential decay analysis. The other fluorescence lifetime component, which is present in small percentage, did not have a fixed value. The obtained overall χ^2 value amounted to 1.13 ± 0.03. Rotational correlation times are presented in Fig. 3. Upper and lower confidence limits at the 67% level are also presented in the same graph. It can be clearly seen that in most cases the upper confidence limit is larger than the lower one, which is due to the rigorous error analysis not giving Gaussian standard errors. The initial anisotropies are averaged yielding $r(0) = 0.251 \pm 0.019$. The correlation times become longer at higher GuHCl concentrations.

3.5 Relative Increase of Viscosity at Increasing GuHCl Concentration

The well-known Stokes-Einstein equation for spherical molecules gives the rotational diffusion coefficient D_r according to:

$$D_r = \frac{k_B T}{6\eta V_h} = \frac{k_B T}{8\pi\eta r_h^3} \tag{1}$$

where k_B is the Boltzmann constant, T is the absolute temperature, η is the viscosity of the medium, V_h is the hydrodynamic volume, and r_h is the hydrodynamic radius of the sphere. The rotational correlation time ϕ is equal to:

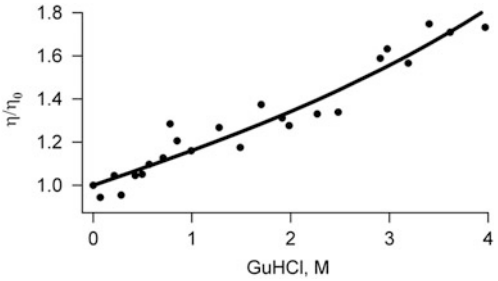

Fig. 4 Relative viscosity values (η/η_0) of NATA in aqueous buffer versus the molar concentration of guanidine hydrochloride (GuHCl). The experimental data are obtained by dividing the rotational correlation times of NATA by the one at [GuHCl] = 0 M, which corresponds to η_0. The solid line is a polynomial fit to the data points: $\eta/\eta_0 = 1 + 0.1571*x + 0.019*x^2 + 0.0025*x^3$, where x is [GuHCl]. Nonlinear least-squares curve fitting was accomplished with the Microsoft Excel Solver. In the fitting procedure the data points were weighted by 1/(standard error)^2

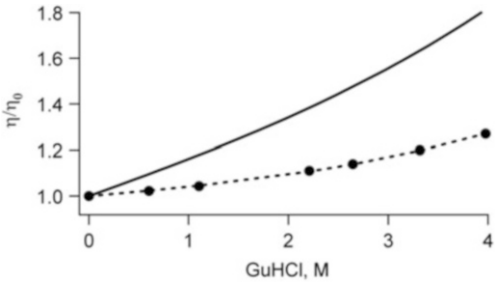

Fig. 5 Comparison of relative viscosities of aqueous solutions of guanidine hydrochloride obtained by us (*solid line*, see Fig. 4) and by Kawahara and Tanford [13] (*closed circles*). The experimental data of Kawahara and Tanford were fitted to a polynomial function (*dashed curve*) to the data points between 1 and 6 M GuHCl: $\eta/\eta_0 = 1 + 0.0385*x + 0.0009*x^2 + 0.0016*x^3$, where x is [GuHCl]. Fitting was accomplished as described in the legend of Fig. 4 with equal weighting factors

$$\phi = \frac{1}{6D_r} = \frac{\eta V_h}{k_B T} \tag{2}$$

The hydrodynamic volume of NATA is not necessarily that of a sphere, but is, in first approximation, assumed to be the same in all experiments. Therefore the rotational correlation time would be directly proportional to the viscosity η.

When all rotational correlations are divided by the one obtained in the absence of GuHCl, the relative viscosities are obtained and plotted in Fig. 4. The TRFA Data Processing Package does not only provide confidence limits of the parameters after a rigorous error analysis, but also standard errors. The standard errors can be used as weighting factors in a nonlinear fitting procedure to fit a polynomial function through the data points (solid line in Fig. 4; see corresponding legend).

Macroscopic viscosities of aqueous solutions of GuHCl at 25°C were determined using capillary viscosimeters about half a century ago [13]. These values are plotted together in Fig. 5 with the microscopic viscosities, as obtained in Fig. 4. We

will discuss the relative large differences between relative macroscopic and microscopic viscosities in the discussion section.

4 Discussion

4.1 Is NATA a Single Fluorescence Lifetime Standard?

Szabo and Rayner observed that the fluorescence decay of tryptophan in aqueous solution (at 20°C and pH 7) exhibits two lifetime components of 3.1 and 0.5 ns with fluorescence maxima at 350 and 335 nm, respectively [14]. The authors assigned the different lifetimes to different rotamers of the alanyl side chain of tryptophan. Three predominant rotameric structures exist for tryptophan. The heterogeneity of the tryptophan environment was corroborated by hybrid quantum mechanical and molecular mechanical simulations of both wavelengths and lifetimes for rotamers of tryptophan in different cyclic hexapeptides [15]. The latter simulations indeed reveal that rotamers having blue-shifted emission possess shorter average fluorescence lifetimes than those having red-shifted emission. The different fluorescence lifetimes of rotameric states of tryptophan reflect differences in rates of photo-induced electron transfer from indole to the alanyl part.

NATA in water at 20°C is considered to have a mono-exponential fluorescence decay, which fluorescence lifetime amounts to 3.1 ± 0.1 ns [10]. However, if we look at the autocorrelation function of the weighted residuals in Fig. 1, there is not a perfect match with one lifetime, while the match is nearly perfect with two lifetime components of 1.3 ns (7%) and 2.77 ns (93%). Similar observations are reported by Rolinski and co-workers, who found that the fluorescence decay of NATA could not be fitted to one- or two-exponential functions because of unacceptably high χ^2 values [16]. Instead, the latter authors find a reasonable fit from a maximum entropy method using gamma function distributions peaking at $\tau_F = 3.0$ ns with ~0.5-ns FWHM at 23°C. The distributions are attributed to a single rotamer. For NATA the distribution is broad with τ_F strongly dependent on temperature. Each distribution also shows a distribution of much smaller amplitude with a peak between 1 and 1.5 ns, which was tentatively interpreted as a much less populated rotamer involved in more efficient photo-induced electron transfer from indole to the amide group [16]. This smaller distribution may have the same origin as the second lifetime of 1.3 ns found in our work.

Recent near microsecond molecular dynamics simulations of NATA in water indicate that there is a mixture of rotamers that interchange on a time scale similar to the excited state lifetime leading to a single exponential decay [17]. In these simulations two rotameric species are assumed, one in which the energy gap between the charge transfer state and emitting ^1L_a state is far apart (F state) for effective quenching and one in which the energy gap is close (C state) resulting in strong fluorescence quenching by electron transfer to the amide.

4.2 Microscopic and Macroscopic Viscosities

The relative microscopic and macroscopic viscosities of aqueous solutions of guanidine hydrochloride, plotted in Fig. 5, become increasingly different at higher concentration of GuHCl. At 4 M GuHCl the relative microscopic viscosity is 1.81, which is significantly larger than the relative macroscopic viscosity of 1.27. The ratio of these numbers is 1.42. A very likely explanation is that the apparent hydrodynamic volume V_h in Eq. (1) becomes larger. This can be caused by association of GuHCl molecules to NATA, for example, by hydrogen bonding facilitated by water molecules. When this hydrogen-bonding interaction persists much longer than the fluorescence lifetime of NATA, then the rotation of NATA will be slower, since GuHCl molecules are dragged along, thus making the effective size of NATA larger. When it is assumed that in first approximation the relative increase in V_h is proportional to the relative increase of molecular weights, then a simple calculation shows that $(MW_{NATA}+MW_{GuHCl})/MW_{NATA} = (245.28 + 95.53)/245.28 = 1.39$, which is very close to the above-mentioned ratio of 1.42 suggesting that a 1:1 complex is formed. The equilibrium dissociation constant of this weak complex would be in the order of a few molar of GuHCl. We can conclude that aqueous solutions of the strong chaotropic agent GuHCl cannot be considered as a homogeneous solvent such as glycerol/water mixtures.

How can we prove that GuHCl associates with NATA? Microsecond molecular dynamics simulations as described above for NATA in water [17] may provide the answer. In this case analysis of molecular dynamics trajectories of NATA (in the excited singlet state) in a water box with an excess of GuHCl molecules might indicate the presence of these long lasting hydrogen-bonding networks.

5 Conclusions

Comparison of macroscopic and microscopic viscosities shows an antagonistic effect. In contrast to most other observations, the microscopic viscosity, measured via time-resolved fluorescence depolarization of NATA, is larger than the macroscopic one, measured with capillary viscosimeters without NATA. This apparent discrepancy must be ascribed to formation of a weak complex between NATA and GuHCl making the apparent hydrodynamic volume larger. Finally, one may wonder whether steady-state fluorescence anisotropy, $\langle r \rangle$, will yield the same conclusive results. For calculation of $\langle r \rangle$ the following relationship is used:

$$\langle r \rangle = r(0)\frac{\phi}{\tau_F + \phi} \tag{3}$$

with all parameters already defined. With $r(0) = 0.251$ and $\tau_F = 2.71$ ns we find $\langle r \rangle = 0.004$ for $\phi = 0.043$ ns (0 M GuHCl) and $\langle r \rangle = 0.007$ for $\phi = 0.073$ ns (4 M

GuHCl). In other words, one should measure the steady-state fluorescence anisotropy with a precision better than 0.001 to obtain the same results. Therefore, the time-resolved fluorescence anisotropy experiment offers a much larger dynamic range than its steady-state counterpart.

Acknowledgments NVV was supported by The Netherlands Organization for Scientific Research.

References

1. Teale FWJ, Weber G (1957) Ultraviolet fluorescence of the aromatic amino acids. Biochem J 65:476–482
2. Weber G (1960) Fluorescence polarization spectrum and electronic energy transfer in tyrosine, tryptophan and related compounds. Biochem J 75:335–345
3. Weber G (1960) Fluorescence polarization spectrum and electronic energy transfer in proteins. Biochem J 75:345–352
4. Valeur B, Weber G (1977) Resolution of the fluorescence excitation spectrum of indole into the ^1L_a and ^1L_b excitation bands. Photochem Photobiol 25:441–444
5. Shinitzky M, Dianoux AC, Gitler C, Weber G (1971) Microviscosity and order in the hydrocarbon region of micelles and membranes determined with fluorescent probes. I. Synthetic micelles. Biochemistry 10:2106–2113
6. Laptenok SP, Visser NV, Engel R, Westphal AH, van Hoek A, van Mierlo CP, van Stokkum IH, van Amerongen H, Visser AJ (2011) A general approach for detecting folding intermediates from steady-state and time-resolved fluorescence of single-tryptophan-containing proteins. Biochemistry 50:3441–3450
7. Visser NV, Westphal AH, van Hoek A, van Mierlo CP, Visser AJ, van Amerongen H (2008) Tryptophan-tryptophan energy migration as a tool to follow apoflavodoxin folding. Biophys J 95:2462–2469
8. Visser NV, Visser AJ, Konc T, Kroh P, van Hoek A (1994) New reference compound with single, ultrashort lifetime for time-resolved tryptophan fluorescence experiments. Proc SPIE 2137:618–626
9. Borst JW, Hink MA, van Hoek A, Visser AJ (2005) Effects of refractive index and viscosity on fluorescence and anisotropy decays of enhanced cyan and yellow fluorescent proteins. J Fluoresc 15:153–160
10. Boens N, Qin W, Basaric N, Hofkens J, Ameloot M, Pouget J, Lefevre JP, Valeur B, Gratton E, vandeVen M, Silva ND Jr, Engelborghs Y, Willaert K, Sillen A, Rumbles G, Phillips D, Visser AJ, van Hoek A, Lakowicz JR, Malak H, Gryczynski I, Szabo AG, Krajcarski DT, Tamai N, Miura A (2007) Fluorescence lifetime standards for time and frequency domain fluorescence spectroscopy. Anal Chem 79:2137–2149
11. Digris AV, Novikov EG, Skakun VV, Apanasovich VV (2014) Global analysis of time-resolved fluorescence data. Methods Mol Biol 1076:257–277
12. Vos K, van Hoek A, Visser AJ (1987) Application of a reference convolution method to tryptophan fluorescence in proteins. A refined description of rotational dynamics. Eur J Biochem 165:55–63
13. Kawahara K, Tanford C (1966) Viscosity and density of aqueous solutions of urea and guanidine hydrochloride. J Biol Chem 241:3228–3232
14. Szabo AG, Rayner DM (1980) Fluorescence decay of tryptophan conformers in aqueous solution. J Am Chem Soc 102:554–563

15. Pan CP, Muino PL, Barkley MD, Callis PR (2011) Correlation of tryptophan fluorescence spectral shifts and lifetimes arising directly from heterogeneous environment. J Phys Chem B 115:3245–3253
16. Rolinski OJ, Scobie K, Birch DJS (2009) Protein fluorescence decay: a gamma function description of thermally induced interconversion of amino acid rotamers. Phys Rev E 79:050901
17. Callis PR, Tusell JR (2014) MD+QM correlations with tryptophan fluorescence spectral shifts and lifetimes. Methods Mol Biol 1076:171–214

Weber's Red-Edge Effect that Changed the Paradigm in Photophysics and Photochemistry

Alexander P. Demchenko

> *Another area in which the interpretation of the data of fluorescence in terms of molecular properties is lacking is that of the red-edge effects . . . . Investigation of this spectral region is often important in biological samples because it offers the best possibilities of detecting compositional heterogeneities.*
>
> G. Weber (1997) *Methods Enzymol*. 278, 13.

Abstract Weber's red-edge effect is formulated as follows: "In rigid and highly viscous environments the excited-state energy transfer producing depolarization of fluorescence emission in concentrated dye solutions stops to be observed when fluorescence is excited at the red (long wavelength) edge of absorption spectrum." After its discovery, it led to finding of a number of new wavelength-selective effects in spectral shifts, quenching, anisotropy and lifetimes, and also in different excited-state reactions forming a new vision of structural disorder and molecular dynamics in condensed media. These effects were consistently explained based on a new paradigm that accounts for statistical distribution of fluorescence emitters on their interaction energy with the environment leading to static or dynamic inhomogeneous broadening of spectra and to directional excited-state energy homo-transfer. These phenomena can be modulated by the energy of the excitation quanta. Their description, optimal conditions for their observation, information that they carry, and overview of their different applications are the subject of this chapter.

Keywords Anisotropy-based assays • Fluorescence polarization • Gregorio Weber • Inhomogeneous broadening • Red edge • Solvation dynamics

A.P. Demchenko (✉)
Palladin Institute of Biochemistry, Kiev 01030, Ukraine
e-mail: alexdem@ukr.net

D.M. Jameson (ed.), *Perspectives on Fluorescence: A Tribute to Gregorio Weber*,
Springer Ser Fluoresc (2016) 17: 95–142, DOI 10.1007/4243_2016_14,

Contents

1 Historical Introduction

The story of this unusual phenomenon started in 1960 with the observation made by Gregorio Weber [1] studying concentrated solutions of tyrosine, tryptophan, and their analogs. He demonstrated an almost complete loss of depolarization of fluorescence emission existing both at room temperatures and on deep freezing at special excitation conditions. These conditions were the solid fluorophore environments (glass-forming solvents at low temperatures) and the shift of excitation at the red edge of absorption band (Fig. 1). In 1969 Weber reported that this effect can be observed for the already popular dye 1,8-ANS (1-anilino-8-naphthalene sulphonate) that was previously introduced by him as the fluorescent polarity-sensitive probe. It was observed not only in supercooled solvent glasses but also at room temperatures on binding to protein serum albumin [2]. These findings led to understanding on the generality of the observed effect.

The results of systematic studies of fluorescence polarization as a function of excitation wavelength appeared in 1970 [3]. The experiments were performed in conditions that excluded fluorophore rotation as the mechanism of depolarization, so that in highly concentrated solutions it should be due to the excited-state energy *homo*-transfer (the transfer between the same molecules). Migrating between differently located and oriented fluorophores, the emitted light loses its initial polarization. What was surprising, is that in solid solvent glasses the depolarization of

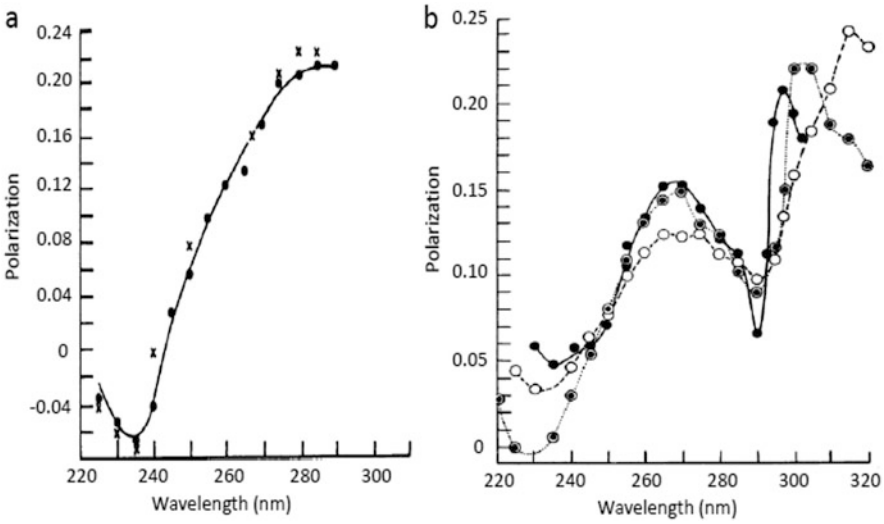

Fig. 1 Excitation polarization spectra of concentrated solutions of tyrosine, tryptophan, and their analogs [1]. (**a**) Cresol (x) and tyrosine (•), (**b**) indole (•), *N*-methylindole (o), and tryptophan (©). In propylene glycol at −70°C. Concentrations 0.2–0.5 mM

fluorescence emission drops at the red edge of excitation band. In these conditions the polarization almost reached the values observed for highly diluted systems.

Special care was taken for excluding trivial reabsorption, optical artifacts, fluorescent contaminants, and evident aggregation as a possible cause of this phenomenon, but the effect existed. Moreover, the new effect was observed in dye dimers, polymers, and on their incorporation into micelles. The statement was made that "The failure of depolarization upon excitation at the long wave edge of the absorption spectrum was found to be a completely general phenomenon without a single exception among the aromatics investigated."

By the time of Weber's discovery the excited-state energy homo-transfer (*homo*-EET) had become a well-studied phenomenon. Being described for the first time by Gaviola and Pringsheim in 1924 for concentrated solutions of dyes dissolved in glycerol [4], in the middle of last century this phenomenon has attracted attention of different scientists, and Gregorio Weber was among them. Following Förster [5] and Vavilov [6] that treated the excitation energy transfer between the same molecules (*homo*-EET) as the resonance coupling between two oscillators, he derived an equation relating the fluorophore concentration in solution with the transfer efficiency [7]. Other researchers used this dependence for calculating molecular distances involved in the energy transfer process. These results were consistent and well understood. The dramatic situation with the discovery of red-edge effect was such that it could not be explained based on existing concepts.

In his classical paper [3] Weber tried to fit this new effect on the basis of the paradigm dominating at that time. A paradigm dominated in photophysics up to 1970 was based on two empirical principles that were considered fundamental

[8, 9]. One of them is the Vavilov's law stating an independence of emission energy on excitation energy within the absorption band or, in other words, an independence of fluorescence quantum yield on excitation wavelength [10, 11]. The other called the Kasha's rule [12] states that the emission spectrum occupies the same position on energy scale irrespective of the wavelength of excitation so that the emission always proceeds from the lowest electronic and vibrational state of the same multiplicity. Being formulated in terms of Vavilov law and Kasha rule [9], it was inherently assumed that all fluorophore molecules in their studied ensemble were identical, so that the fast relaxational processes occurring on their electronic excitation always drive the system to the same lowest in energy excited state, from which the emission occurs (see, e.g., [13]). Based on this paradigm, the position of fluorescence emission spectra, quantum yield of this emission, and reactivity in excited-state processes including the energy *homo*-transfer should not depend on the excitation wavelength. Therefore the only possibility to explain the new phenomenon within that paradigm was to suggest that the excited state generated by excitation at the edge of the absorption band differs from the excited state achieved on excitation over the bulk of absorption. If it is so and since vibrational relaxation to the lowest excited state is an ultrafast process, then there must be at least two distinct lowest energy excited electronic states. The state excited by the quanta of lowest energy must have the lowest energy transfer probability.

The arguments that Weber presented for that were based on observations of wavelength-dependent differences in some fluorescence characteristics, such as quantum yield, lifetime, and sensitivity to collisional quenchers, which was also unusual. An obvious weak point in this interpretation was the generality of the red-edge effect. It was hard to assume that undetected electronic states that can be revealed only on excitation at low energies really exist in the cases of all studied aromatic compounds and of their associates. It became evident that here a new feature in photophysics was discovered that required a new paradigm for its explanation.

The new paradigm came with new discoveries. Two laboratories, of Bill Galley [14] in Canada and of Anatoliy Rubinov [15] in Belarus being a part of USSR, have reported on discovery of a new red-edge effect – the bathochromic shift of fluorescence spectra at the red-edge excitations. Both of these groups stated that the spectra of individual fluorophores in solutions shift differently because of differences in their intermolecular interactions with their environment. They form distributions on these interactions resulting in inhomogeneous broadening of spectra. Within such distribution, the photoselection of the fluorophores, the interactions of which with their environment deviates from their mean values, can be provided on the low-energy slope of excitation band (red edge). These photoselected fluorophores exhibit the wavelength-shifted emission. Of course, the molecular mobility in such systems should be slower than the excited-state lifetime, otherwise the local environments will be mixed and the effect has to disappear.

I can witness that the pathways to these findings by these two groups were really independent. At the time of cold war, such high barriers existed between Soviet and

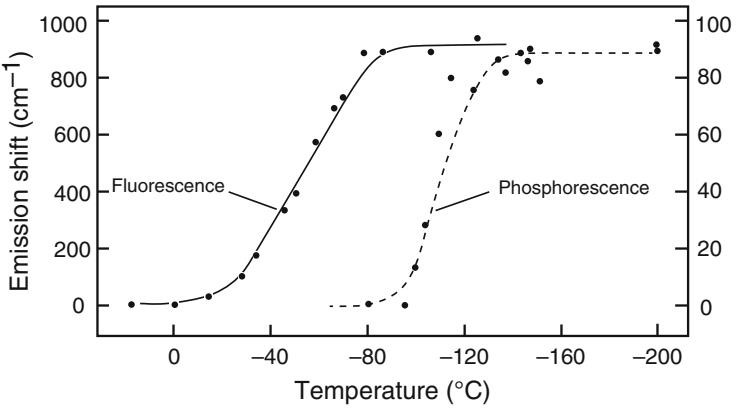

Fig. 2 Plot of the excitation-wavelength dependence for the indole (10^{-3} M) fluorescence and phosphorescence spectra versus the temperature of the 4:1 glycerol–water medium. Fluorescence and phosphorescence shifts were measured as the average of the red edge (295 nm excitation) and blue edge (280 nm excitation) differences between the recorded spectra [14]

Western science that the exchange of information could be retarded for years. The Canadian group made an important observation that in the sequence of aromatic molecules with different polarities the emission band position dependence on exciting wavelength was the most prominent for the polar ones (indole, tryptophan, 13-naphthol, 9-aminoacridine cation, and proflavin), whereas small or even undetectable shifts were observed for nonpolar aromatic hydrocarbons, such as anthracene, perlyene, and naphthalene. Dependence on the solvent was also remarkable, the effect decreased as one passes from polar to nonpolar vitrified media. These results are quite understandable since the noncovalent dipole–dipole interactions between polar molecules provide the strong contributions to dielectric solvation.

The experiments of the Canadian group allowed providing direct connection between observation of red-edge effect and the dynamics of solvent molecules. They discovered the edge-excitation shifts not only for fluorescence but also for phosphorescence for the same dyes (Fig. 2). Studying the temperature dependences, they observed disappearance of red-edge effect on transition from cryogenic to room temperatures. For phosphorescence this transition was found to occur at much lower temperatures than for fluorescence, which correlated with much longer lifetimes providing larger time window for dynamic processes in the solvent.

The interpretation of these data was based on the following assumptions: (1) the electronic energies of chromophores in solution are a function of geometry-dependent solute–solvent interactions, (2) at any time instant there is an ensemble of interactions that gives rise to a distribution of electronic energies in the sample, and (3) the interactions of a solute molecule with its solvent environment, which rapidly fluctuate with time in fluid solution, become static if the system becomes rigid on a time scale of emission. The most essential conclusion from these data was that the dependence on the excitation wavelength of the emission spectra of polar

aromatic molecules in rigid, polar solutions is a very general phenomenon and that its occurrence depends on both the excited-state lifetime of the chromophore and the degree of rigidity of the medium [16].

The conclusions made by Rubinov's group [15] were quite similar. They observed the excitation-wavelength-dependent shifts of fluorescence spectra for different dyes in solvent glasses and reported on "bathochromic luminescence" as a new phenomenon of general significance. These results were confirmed in another laboratory of the same institution [17]. Weber's effect of repolarization of emission in concentrated solid dye solutions at the red edge has also found its confirmation and a new interpretation based on inhomogeneous broadening was given [18]. It was then quite logical to look for the site-photoselection of emission quanta, and this effect was found at the "blue edge" of fluorescence bands [19].

New groups of researchers were attracted by these interesting phenomena, and original results on their correlation with solute–solvent molecular relaxations were confirmed in temperature-dependent studies [20]. The understanding that the excitation energy-dependent spectral shifts and the time-dependent spectral shifts have to be based on the same mechanism stimulated the time-resolved studies. Then it was found that in the systems performing solvent relaxations during the excited-state lifetime collisional or light-induced fluorescence quenching increases the red-edge effects and the motions of time-resolved spectra depend on excitation wavelength [21, 22]. This dependence was specific: the motions of spectra disappear at the red edge, and on shifting the excitation wavelength further to the far anti-Stokes region they can even proceed with the increase of excited-state energy [21]. This phenomenon was called "up-relaxation." Instead of releasing the energy to the environment, it required absorbing the energy for achieving the relaxed state, providing the local cooling.

Among new site-selective effects that have been observed in time domain, one was quite unexpected but confirming the general concept. It was the rotation of fluorescent dye induced by excitation light and detected by time-resolved anisotropy [23]. It can be observed when the dye molecule is smaller than surrounding molecules, and the electric field formed by their dielectric environment activates the motion to equilibrium of the dye itself. Such situations can appear for the dyes incorporated into biomembrane [24].

Since in essence of Weber's red-edge effect is the failure of excited-state energy transfer, it was of particular interest to observe it in connection with directed EET in solid environments. As a result of inhomogeneous broadening due to non-identical dye environments in their concentrated solutions the dyes do not simply exchange of their energies. The energy flows directly from the species displaying short-wavelength absorption and emission to those exhibiting long-wavelength absorption and emission, as a result of which the spectra move to longer wavelengths as a function of time [25]. This fact stimulated modeling the assembly of pigments in the natural systems of photosynthesis [26]. Since EET stops at the red edge, such motions of spectra discontinue also.

With these developments it became clear that all the effects observed on variation of excitation and emission wavelengths should originate not from the

violation of fundamental principles, but from their operation in specific conditions, when the ensemble of excited molecules is distributed on interaction energy with molecules in their surrounding. To explain them, a physical theory and modeling started to play an increasingly important role. First of such models was developed by Gregorio Weber [27]. His analysis was based on a simple model considering the interaction of physical dipole (the dipole with distributed charge) with solvent dipoles when these interactions conformed to the Langevin distribution. Mazurenko [28] developed a quasi-thermodynamic method for the description of stochastic solvation of molecules in solutions. Gorbatsevich et al. [29] calculated the distribution function on the frequency of electronic transition in polar solvent using the Monte-Carlo technique. As a result of both experimental and theoretical studies the concept was developed on the exclusive role in all these phenomena of *inhomogeneous broadening* of spectra that arises from solute-solvent distribution in excitation energy. This broadening allows for providing site-photoselection by excitation and emission quanta with well-defined energies deviating from their average values. The observed deviating properties can be compared with their mean values.

With such a wealth of new knowledge on the dependence of new effects on structure and dynamics it was quite natural to start addressing the reverse problem – to gain the information on structure, dynamics, and interactions in unknown or poorly characterized systems on molecular level. The present author was the first who initiated such applications. The first objects were the protein molecules possessing tryptophan as an intrinsic probe [30]. The results obtained were summarized in the monograph of the author [31]. The application of fluorescence probes was also quite successful [30]. All these results allowed demonstrating that proteins in solutions on the time scale of nanoseconds behave as nanoscopic solids with the dynamics slower by several orders of magnitude than the surrounding solvent. In lipid analogs of biomembranes the probe depth dependence of the lipid segment dynamics was characterized [32]. Quantitative measure of dipole relaxation rate was introduced [33]. Many new applications came after demonstrating the great power of the approach and they were the subject of numerous reviews [34–37] some of them with particular focus of studying proteins [38–42], biomembranes [39, 43], ionic liquids [44], etc.

Thus, the major idea, which is behind different approaches used in site-photoselection spectroscopy, is the selection and observation of a small part of the fluorophore population together with studying the whole population that is responsible for an inhomogeneously broadened spectrum. The great number of recently published articles indicates that the field is blooming, and many more advancements are to be expected.

2 Modern Interpretation of Red-Edge Effects and of Related Phenomena

Operating with excitation light of definite energy and polarization one can excite exclusively those dye molecules, the energy and orientation of electronic transition of which match these excitation parameters. Thus, if a dye is excited by polarized light, its emission will be also highly polarized. Depolarization occurs only when the time correlation of these selectively excited species is lost due to their rotation or participation in some photophysical process, such as excitation energy transfer. Similarly, photoselection can be provided by variation of excitation energy. The dye molecule can absorb only the light quanta that correspond to its electronic transition energy. Being selected from the whole ensemble by the energy of electronic transition, this sub-ensemble can possess diverging features observed in fluorescence emission and also, as we will see below (Sect. 3), in photochemical reactivity. These basic considerations allow to explain consistently a group of phenomena that are known under a common name "Red-Edge effects." The optimal conditions in which these phenomena are observed are now well understood [35, 45]. The dye should be solvatofluorochromic, that is, its fluorescence spectra should respond to the changes in interaction energy with its environment by significant shifts. In the case of recording the steady-state spectra the dye environment should be relatively polar but rigid or highly viscous, so that the relaxation times of its dipoles, τ_R, should be comparable or longer than the fluorescence lifetime τ_F. When time-resolved recording is applied, the relaxations should proceed slower or be on the same scale as the time scale of emission. Thus, these effects are coupled with molecular dynamics in condensed media and allow distinguishing and characterizing rigid, viscous, and highly mobile media.

2.1 Inhomogeneous Broadening and the Principle of Photoselection

When organic dyes are studied in any liquid or solid media their electronic absorption and fluorescence emission spectra do not represent a sequence of sharp lines corresponding to electronic-vibrational transitions. They usually display broadbands with vibrational structure smoothened or even entirely lost, so that cooling to cryogenic temperatures does not result in improvement of structural resolution. This means that in addition to common strongly temperature-dependent homogeneous broadening (which is mainly due to electron–lattice and electron–vibrational interactions), in the systems with molecular disorder there exists the so-called inhomogeneous broadening of the spectra [45]. The latter originates from non-equivalence of dye solute environments (sub-states) that results in the distribution on solute–solvent interaction energies. All types of intramolecular and intermolecular relaxations may contribute to the energy difference between the

maxima of the absorption and emission spectra, the so-called Stokes shift. The contribution of dielectric relaxations is often the strongest, and the site-photoselection effects can be observed if they are frozen or not complete. As a result, for every species the electronic transition energies become distributed on the scale of energy and their superposition forms an inhomogeneously broadened contour. Each sub-state in this ensemble can possess a sharp maximum, but when their contributions are added, the broad-band absorption and emission in its spectrum are observed. This is the *inhomogeneous broadening* of spectra.

The extent of this broadening is determined by the energies of intermolecular interactions, which exhibit statistical variation in the ensemble. The estimated by Weber [27] distributions of ground-state energies were 200 cm^{-1}. The width of inhomogeneous broadening function $\Delta\nu$ depends on the polarity of the solvent (the number and the magnitudes of solvent dipoles) and, most importantly, on the change of fluorophore dipole moment on excitation, $\Delta\mu$ [45]. For its estimation one can use an expression obtained in the Onsager sphere approximation:

$$\Delta\nu = A\Delta\mu a^{-3/2}(kT)^{1/2}, \tag{1}$$

where

$$A = (2/h)\,[(\varepsilon - 1)/(2\varepsilon + 1)]^{1/2}. \tag{2}$$

Here ε is the dielectric constant of the medium, and a is the Onsager sphere radius. According to these estimates for 3-aminophthalimide in ethanol, $\Delta\nu$ at 20°C ranges from 400 to 500 cm^{-1}, and it decreases to 300–400 cm^{-1} at the freezing point of solution. For the same dye in toluene these values are 250–300 and 200–250 cm^{-1} correspondingly. In contrast, for low-polar dye coronene in toluene $\Delta\nu$ is 25–30 cm^{-1} only [45]. The solvent–solute hydrogen bonding may provide additional increase of the width of the distribution [46].

These values are in reasonable agreement with experimental data obtained in cryogenic site-selective experiments. However, they show that in organized environments such as protein molecules the distribution can be dramatically narrower [47], which is the result of smaller variation in the ensemble of fluorophores of electric field effects between structurally identical highly ordered protein molecules. The proteins with different structure exhibit different $\Delta\nu$ values. Thus, for Mg-myoglobin it is around 100 cm^{-1}, while for peroxydase it is much narrower, 40 cm^{-1}. Upon denaturation of Zn-cytochrome c, when the porphyrin changes its environment from being inside the protein globule to become exposed to a polar solvent, $\Delta\nu$ changes from 65 to 360 cm^{-1} [48]. The transformation of the resonance Raman excitation profiles for the π–π* Soret band of native heme proteins provides an estimate of 100–200 cm^{-1} [49].

In molecular spectroscopy it is a common way to present the electronic transitions generating absorption and emission spectra as the two-dimensional functions of vibrational and solvation coordinates. Meantime the main difference between

these coordinates is the quantized origin of vibrational modes, achieved in a very fast Franck–Condon process. According to Kasha rule, they relax rapidly to the lowest energy level of the first excited state [50]. In contrast, solvation modes are intrinsically over-damped. This allows treating solvation coordinate as a classical coordinate with continuous availability of electronic states. Thus, in molecular ensemble at any finite temperature a Boltzmann distribution in population of different solvent configurations is responsible for the inhomogeneous broadening in the steady-state spectra [51]. Such broadening arises from the solute–solvent distribution in excitation energy that reflects the distribution in energy of dye interactions with its dielectric environment. The stronger will be these interactions, the broader the distribution. Thus, the contour of absorption band must contain valuable information on the extent of molecular disorder.

In condensed medium such distributions should always exist at the time of excitation. But its display in a variety of spectroscopic phenomena depends on how fast are the transitions between the species forming this ensemble of states. Depending on these conditions, the broadening of spectra can be either static or dynamic [45]. The signatures of static broadening are observed in rigid environments, when the dynamics described in terms of dipolar relaxation times τ_R is slower than the rate of emission. The broadening is dynamic if the motions in the dye environment occur simultaneously or faster than the emission, so that the correlation time τ_c or more frequently used relaxation time τ_R, $\tau_R \leq \tau_F$. The static effect that is integrated over the time of emission depends upon the time window. In viscous media (when $\tau_R \approx \tau_F$) not only the freezing (increasing τ_R) but also the fluorescence quenching (reduction of τ_F) may cause the appearance of red-edge effects. Thus, the inhomogeneous broadening effects contain the information about the dynamic properties of condensed systems, and the rate of fluorescence emission provides the necessary time scale for these observations. The scheme presented below shows the correlation between different mechanisms of spectral broadening.

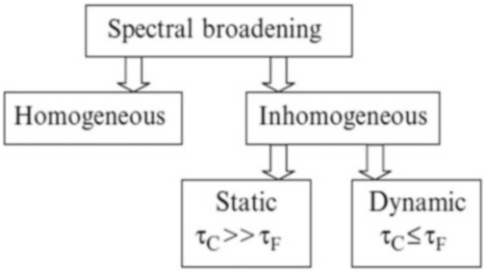

Thus, being the major factor that produces broadening of the spectra, inhomogeneous broadening originates from non-equivalence of dye environments in an ensemble of otherwise identical molecules resulting in the distribution in solute–solvent interaction energies [45]. In fact, every molecule is under the influence of different forces produced by configuration of surrounding molecules. Therefore the dye species become distributed on their electronic transition energy and their superposition forms inhomogeneously broadened contour. Excitation at the band

edge selects a part of this distribution, the spectroscopic properties of which can be quite different from their mean values. At the long-wavelength edge of the absorption band only those species are excited, for which the excitation energy with the environment is the strongest, their excited-state energy level occupies the lowest position, and for them the emission spectrum becomes shifted to longer wavelengths.

One of the major goals in cryogenic site-selective spectroscopy (at liquid helium temperatures) is the dramatic improvement of spectral resolution by suppressing the homogeneous broadening [51–53]. This goal is not achievable at ambient temperatures because of unavoidable existence of a broad homogeneous component [45, 54]. Therefore the possibility of photoselection within the ensemble remains only from the side of low energies of absorption band (red excitation edge) and from the side of high energy in emission (blue emission edge). The essence of such

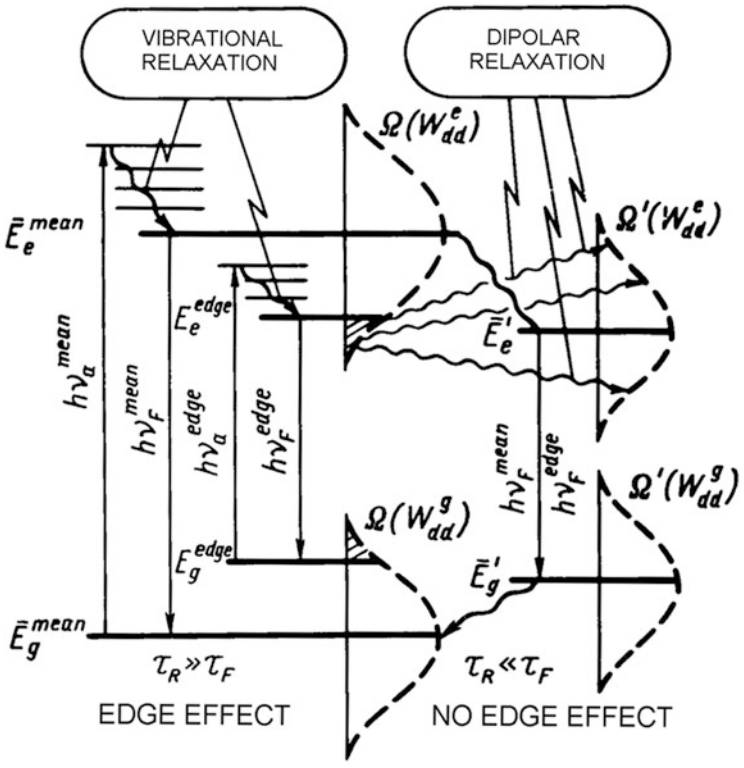

Fig. 3 Energy diagram of S_0 and S_1 electronic states, which takes into account the relaxation phenomena [30, 55]. Vibrational relaxation is shown for the S_1 state only. Dipolar (dielectric) relaxation is described as the evolution of the excited-state distribution and a temporal loss of photoselection between different energy dipole-orientational states excited at the "red edge" (see text)

photoselection can be explained based on the energy diagram presented in Fig. 3, see also [35].

Absorption spectra reflect the transitions from the ground-state energy levels E_g to excited-state levels E_e (upward arrows). Their contour is formed by 0-0 transition plus transitions to different vibrational levels of the excited state of molecule, while fluorescence emission (downward arrows) is formed by 0-0 transitions and transitions from the lowest level of excited state (achieved by vibrational relaxation) to different vibrational sub-levels of the ground state. In condensed media the energy of any ground or excited state is modified by dipolar interaction energy with the environment, W_{dd}, to a different extent for every member of molecular ensemble. This is shown by the distributions along the scale of energy – $\Omega(W_{dd})$. Since the fluorophore dipole moments μ differ in the ground and excited states, we have to observe two types of distributions – $\Omega(W_{dd}^{g})$ for the ground state and $\Omega(W_{dd}^{e})$ for the excited state. The absorption of a light quantum with sufficiently high energy corresponding to mean of the distribution ($h\nu_{a}^{mean} \geq E_{e}^{mean} - E_{g}^{mean}$) causes excitation of fluorescence of all possible solute–solvent configurations that differ in interaction energy. The common case is the excitation at the band maximum, which corresponds to the center of excited-state distribution, and emission proceeding from the center of this distribution.

Now we consider the case when we excite the system with the quanta of energy that are so low that they cannot excite even the 0-0 transition for all members of the ensemble – $h\nu_{a}^{edge}$ (at the "red" edge). Then only the fluorophores constituting a part of the distribution will be selectively excited. It will be those species that interact most strongly with the environment in the excited state (and form the lower part of the distribution $\Omega(W_{dd}^{e})$) and the least strongly in the ground state (and constitute an upper part in the distribution $\Omega(W_{dd}^{g})$), see Fig. 3. If the fluorophore–environment interactions remain unchanged during the time of emission (no dielectric relaxations in the medium), then the emission energies of these fluorophores ($h\nu_{F}^{edge}$) will be also lower than for the mean of the distribution ($h\nu_{F}^{mean}$). As a result, the emission spectra will be shifted towards longer wavelengths, compared to that excited at the band maximum. Often the vibrational structure is not resolved in absorption spectra. Since it propagates from 0-0 band to higher energies, the photoselection within its $\Omega(W_{dd}^{g})$ distribution (or within the distribution of most active long-wavelength vibronic band) is possible at its red edge only. So if we decrease substantially the energy of excitation quanta (shift the excitation to red edge on the wavelength scale), then this energy will become so small that it will not be able to excite all the species in dye ensemble but only those which can interact with the environment in the excited state much stronger than the average and which possess their individual excited-state levels shifted down along the energy scale, achieving photoselection in excitation energy. When excited, these selected species will emit fluorescence differently than that of the mean of the distribution. Their emission spectra will be shifted in the direction of low energies to longer wavelengths. This is the site-selective in excitation red-edge effect that is the most popular in many applications.

Thus, electronic transitions occur between ground and excited states of dyes participating in distributions on interaction energy with the environment existing both in the ground and excited states. These interactions involve molecular dipoles and the distributions of these dipolar interactions with the environment can be different. The stronger interactions always result in a broader distribution on the energy of these interactions. Typically for solvatochromic dyes the dipole moment is small in the ground state and it increases substantially in the excited state enhancing the broad distribution. Then the ground state can be approximated by a single energy level and the excited state as the state exhibiting a broad distribution on dye–environment interaction energy. In the other limiting case, when the chromophore dipole moment is high in the ground state but decreases substantially in the excited state, the ground state should exhibit a broad distribution and the excited state can be represented by a single energy level. Then by variation of the energy of the light quanta we can produce photoselection within the ground-state distribution. So if we decrease the energy of excited light quanta, these quanta will be absorbed mostly by species, the ground-state energy of which is higher than the mean (they interact weaker with the environment than the average species in the distribution), so that the separation of energy between ground and excited states for them is smaller than the mean. The energy of emitted quanta will also be small, and we will have the same red-edge effect – the shift of fluorescence spectra to longer wavelengths. In a more general case when the dye dipole moments are relatively high both in the ground and excited states and the distributions of interaction energies are broad but due to redistribution of electronic density in the excited state the dipole moment changes its orientation. Here the weakest ground-state interactions may become the strongest in the excited state and the shift to the red excitation edge will select from the whole ensemble the chromophore molecules that interact weaker in the ground state (upper part of the distribution) but stronger in the excited state (the lower part of its distribution). This will result in the long-wavelength shifting red-edge effect.

It is known that the most precise information about solute–matrix interactions can be obtained by site-selection spectroscopy at cryogenic conditions (5 K or less). Here the zero-phonon lines were spectrally distinguished and analyzed by probing of inhomogeneously broadened zero-phonon line performed by spectrally very narrow laser beam [56]. These methods got the names of *energy-selection* spectroscopy, such as *hole-burning* in absorbance [57] and *line-narrowing* in fluorescence [55], see [56] for recent review. They were designed to circumvent the problem of large inhomogeneous line width existing in common condensed media by selecting a narrow package of molecules absorbing light around a certain frequency within the inhomogeneous band via a narrow bandwidth laser excitation. By applying this technique, a strong variation of the electron–phonon coupling strength on excitation wavelength through the inhomogenously broadened absorption origin band was demonstrated [51]. Ultrafast dynamic hole-burning and hole-filling have been realized [58]. Though technically complicated, these methods have found different applications in chemistry and biology [59]. Meantime, featuring a highly improved resolution of spectra they are limited to cryogenic

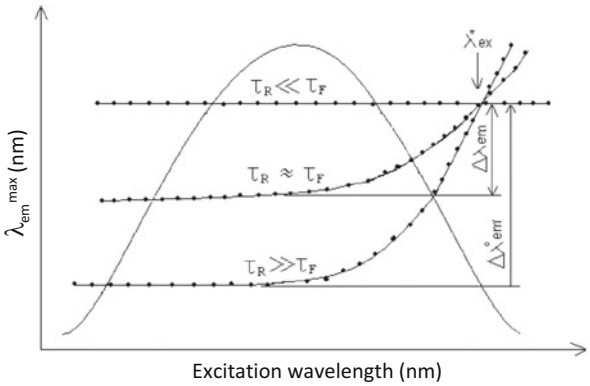

Fig. 4 Dependencies of positions of fluorescence band maxima, λ_{em}^{max} , on excitation wavelength, λ_{ex}, for different correlations between the dipole relaxation time, τ_R, and fluorescence lifetime, τ_F. When the relaxations are slow, the fluorescence band occupies extreme short-wavelength position and the red-edge effect is the most significant, and when they are faster than the emission rate, the spectrum is located at long wavelengths and the red-edge effect is absent. The excitation spectrum, $F(\lambda_{ex})$, is also presented schematically. $\Delta\lambda^0_{em}$ and $\Delta\lambda_{em}$ are the magnitudes of red-edge effect, and λ^*_{ex} is the isorelaxation point (the excitation wavelength at which the position of fluorescence band does not depend on relaxations) [60]

temperatures or ultra-short observation times, so that all the dynamic information on solute–solvent interactions is lost. And attractive feature of red-edge effects is that here observations are not limited to any temperature ranges and the information on molecular motions can be obtained.

Thus, the widely explored red-edge effect is the long-wavelength shift of fluorescence spectra at the red excitation edge. Exciting by monochromatic light and shifting the wavelength from of the band maximum further and further to the red edge, a smaller and smaller number of dye molecules are excited with correspondent reduction of light emission intensity. Out of total population of dyes those sub-populations are photoselected, which happen to have their light absorption energies fitting to the decreased energy of illuminating light and their emissive properties differ from the mean values more and more significantly. The experiment on shifting the excitation wavelength stops when the emission intensity becomes very low and the spectrum becomes indistinguishable from the background. This dependence becomes steep without reaching any limit at the far red edge (Fig. 4). Sometimes one can even reach the anti-Stokes region, where the excitation wavelength, λ_{ex}, becomes longer than the position of the maximum of fluorescence spectrum, λ_{em}^{max}, excited at the band maximum, λ_{ex}^{max}. In this far edge region the shift of emission spectrum approaches in value the shift of excitation wavelength. Such typical dependence of λ_{em}^{max} on λ_{ex} is observed only at the red edge, and no such dependence is detected at the excitation band maximum and shorter wavelengths.

2.2 Connection with Molecular Relaxations

In order to understand this connection, a short excursion to fluorescence spectroscopy of molecular relaxation is needed (Fig. 5). The energies of both ground and excited states are always influenced by intermolecular interactions: the stronger are the interactions the lower is the correspondent level on an energy scale. On excitation, the electronic distribution in dye molecule changes, so change the interactions with the surrounding. If they are stronger in the ground state, then on their increase the difference in energy between the states increases. It can be the opposite: increase of interactions in the excited state. Thus, the spectra can move to either direction. The rigid medium conditions are those, in which the interactions are strong but at the absence of solvent mobility they are not at equilibrium with excited dye molecule. Such dependence is typical for every system with static ($\tau_R >> \tau_F$) or slow dynamic ($\tau_R \geq \tau_F$) inhomogeneous broadening. With an increase of relaxation rate the fluorescence spectra at the main-band excitation shift in time to longer wavelengths (the common relaxational shift of spectra) [61]. In liquid medium the fast mobility allows achieving the relaxed state during fluorescence lifetime [62]. Since the extent of this shift depends on solvent polarity, the dyes with most pronounced shift are used as polarity-sensitive probes.

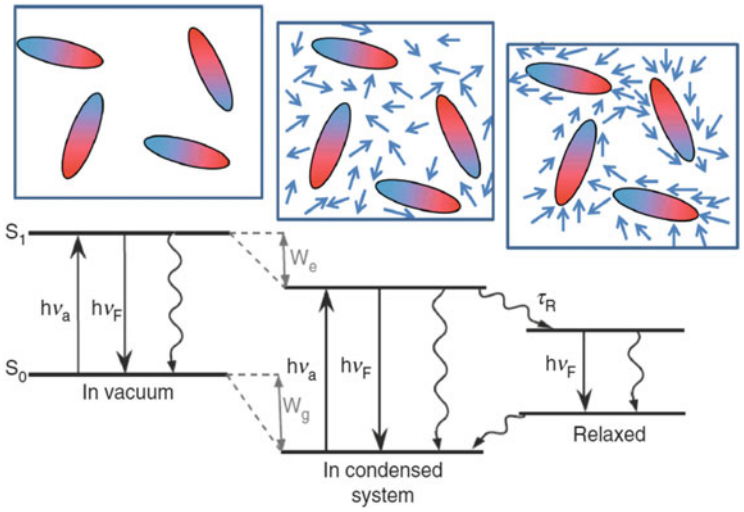

Fig. 5 Simplified Jablonski diagram of ground S_0 and excited S_1 energy levels and transitions between them. *Vertical upward arrow* shows the excitation and *downward arrows* show emissive (straight) and non-emissive transitions to the ground state. In condensed media, the energies of ground and excited states are decreased due to electronic interactions with the environment by solvation energies W_g and W_e correspondingly. In addition, in polar media there occurs an establishment of equilibrium in interactions of dye and surrounding dipoles (dipolar relaxation). As a result, the energy gap between S_0 and S_1 states decreases and the spectra shift to longer wavelengths

Thus, the time window for observing this relaxation is determined by the rate of fluorescence emission. Depending on molecular mobility in the medium the process of attaining a new equilibrium (relaxation) may be faster, slower, or occur simultaneously with the emission decay. In the case if it occurs simultaneously with the decay, complex emission-wavelength dependence should be observed for the decay kinetics, and the spectra should move as a function of time in the direction of lower energies.

If N_0 molecules are excited at an instant $t = 0$, the number dN of emitted quanta within a time interval dt and a frequency range dv can be determined from the formula:

$$dN = N_0 Q_F I(v,t)\, dv dt, \tag{3}$$

where Q_F is the quantum yield of emission and

$$I(v,t) = (1/\tau_F)\, I(v-\xi)\exp(-t/\tau_F). \tag{4}$$

The latter function determines the number of quanta emitted per unit time within a unit frequency interval. At a fixed time it can be regarded as an "instantaneous" emission spectrum, while at a fixed frequency v it represents a law of emission decay. ξ is the maximum or, more precisely, the center of gravity of the spectrum (in cm^{-1}). It was shown [63] that within the Debye model of relaxation (single relaxation time τ_R) the position of the spectrum ξ has to change exponentially with time:

$$\xi(t) = \xi_{t\to\infty} + (\xi_{t=0} - \xi_{t\to\infty}) \exp(-t/\tau_R). \tag{5}$$

Since the relaxation is the time-dependent loss of correlation between initial site distribution and the distribution at time t, a time-dependent correlation function $C(t)$ for $\xi = \xi(t)$ can be used for describing the process of relaxation:

$$C(t) = [\xi(t) - \xi_{t\to\infty}]/(\xi_{t=0} - \xi_{t\to\infty}). \tag{6}$$

It normalizes the spectral shifts to unity and allows comparison of the effects produced by different dyes. Such motions of spectra to longer wavelengths as a function of time are observed in experiment [64]. By assuming τ_F to be unchanged in relaxation process the following expression can be obtained for the behavior of the steady-state spectra:

$$(\xi_{St} - \xi_{t\to\infty})/(\xi_{t=0} - \xi_{t\to\infty}) = \tau_R/(\tau_R + \tau_F). \tag{7}$$

Here ξ_{St} is the position of steady-state spectrum. The limiting values of $\xi_{t\to\infty}$ and $\xi_{t=0}$ and the variations of temperature are usually applied. The limit of slow relaxations $\xi_{t=0}$ should be achieved at low temperatures (when $\tau_R >> \tau_F$) and the limit of fast relaxations $\xi_{t\to\infty}$ – at high temperatures (when $\tau_R << \tau_F$).

It is hard to reach these conditions in real systems, especially in biophysical applications. Whereas reducing the temperature with maintenance of observed structure is frequently possible, subjecting to high temperatures often cannot be tolerated. Therefore in our earlier works [33, 35] we suggested an extension of this approach by incorporating the information obtained in the study of red-edge effect. When the relaxation is complete, it produces a new dynamic distribution of sites that becomes uncorrelated with initial distribution. Due to molecular motions, the excitation energies fluctuate in time causing redistribution within this ensemble, "mixing" different environments. Being selected at any wavelength, the sub-population of dyes is rapidly mixed within the whole population, so that the spectra become λ_{ex}-independent and the red-edge effect has to vanish. If we assume that τ_R and τ_F at the red-edge excitation do not differ from their mean values, we obtain a very simple relation that allows us to obtain dynamic information from the steady-state spectra. By re-writing Eq. (7) for the mean and for the edge excitations and taking into account that when the relaxation is complete, $\xi_{t\to\infty}^{\text{mean}} = \xi_{t\to\infty}^{\text{edge}}$, we obtain

$$\xi - \xi^{\text{edge}} = \left(\xi_{t=0} - \xi_{t=0}{}^{\text{edge}}\right)\tau_R/(\tau_R + \tau_F). \tag{8}$$

Equation (8) uses only the data on steady-state spectra and allows us to analyze the red-edge-excitation shifts of fluorescence maxima. ξ values on wavenumber scale can be easily transformed into wavelength λ values, $\xi(\text{cm}^{-1}) = 10^7/\lambda(\text{nm})$ and the positions of wavelength maxima, $\lambda_{em}^{\max}$, can be used. Thus, dynamic information about molecular relaxations can be obtained in simple steady-state measurements using τ_F as a time marker and analyzing the red-edge effects.

As a result of relaxation, two processes occur simultaneously: the shift of spectra to longer wavelengths and the decrease of excitation-wavelength dependence (see Fig. 4). In the dependence of the positions of fluorescence band maxima on λ_{ex} there is one characteristic point, λ_{ex}^*, in which the energy of electronic transition corresponds to that of the relaxed state. At $\lambda_{ex} > \lambda_{ex}^*$ the relaxation occurs with the decrease of energy, and the spectra have to move in time to longer wavelengths, while at $\lambda_{ex} > \lambda_{ex}^*$ the relaxation results in increase in energy and in order to achieve the equilibrium the spectra move to shorter wavelengths (up-relaxation [21, 54]). We call λ_{ex}^* an *isorelaxation point*. Its presence allows us to introduce the quantitative characteristics of red-edge effect as the shift of fluorescence spectrum $\lambda_{em}^{\max}(\text{mean}) - \lambda_{em}^{\max}(\text{edge})$ on variation of λ_{ex} from that at excitation band maximum $\lambda_{ex}^{\text{mean}}$ to λ_{ex}^*. The relaxational shift of emission spectra can be observed at any λ_{ex} beside λ_{ex}^*. Thus, the inhomogeneous broadening effects contain information about the dynamic properties of condensed systems, and the rate of fluorescence emission provides the necessary time scale for the observations of red-edge effect [35].

One of the most intriguing properties of structurally disordered materials (liquid or solid) is the huge dispersion of structural relaxation rates [65, 66], therefore a simple model operating with single τ_R and τ_F values may not be applicable in all cases. However, being conceptually correct, it helps us to understand the basis of

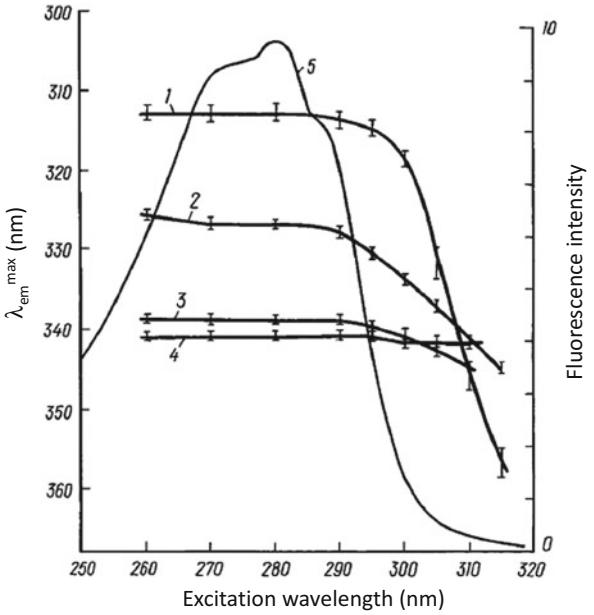

Fig. 6 Dependence of the maximum of fluorescence spectrum of tryptophan in glycerol on excitation wavelength at different temperatures: −196°C (1), −14°C (2); 20°C (3) and 50°C (4). Curve 5 is the excitation spectrum. The strong temperature dependence of spectra is observed at any wavelength beside the range 307–308 nm at the red edge [33]

studied phenomena and the interpretation of many experimental data on quantitative level is quite satisfactory. One such result was was obtained for tryptophan, the major fluorescence emitter in proteins (Fig. 6). For tryptophan in glycerol in the lowest range of temperatures the fluorescence spectrum at the main-band excitation is the most significantly shifted to shorter wavelengths, and the red-edge effect is dramatic. On increase of temperature the spectrum at the main-band excitation shifts to longer wavelengths, and the red-edge effect decreases. At high temperatures, when the solvent becomes low-viscous, it becomes undetected. We observe, however, that all the curves λ_{em}^{max} as a function of λ_{ex} cross at the same point at about 307 nm.

2.3 Observations with Time Resolution

The new view on inhomogeneous distributions of light emitters in molecular ensembles required re-interpretation of many time-resolved spectroscopic data. Unlike radioactive isotope decay, which is strictly single-exponential, the fluorescence decays often display non-exponential, distributed character. The difference is that the nuclear processes responsible for radioactive decay do not depend on intermolecular interactions, but such dependence exists for light emitting dye molecules. Being in variable environments, the dyes may emit light with different rates, leading to non-exponentiality and site-selectivity on the population level. The

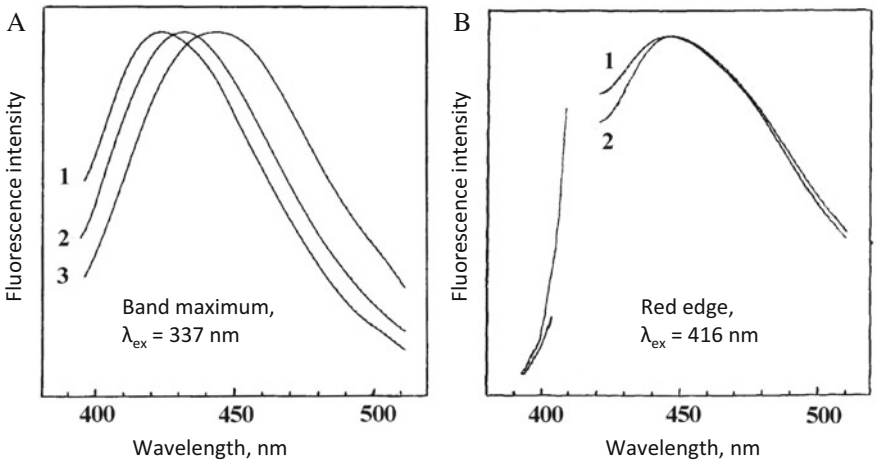

Fig. 7 Instantaneous fluorescence spectra of *1*-phenylnaphthylamine in glycerol at 22°C for various excitation wavelengths: (**a**). Band maximum, $\lambda_{ex} = 337$ nm, registration time $t_{reg} = 2$ ns (1), 3 ns (2), 14 ns (3); (**b**) Red edge, $\lambda_{ex} = 416$ nm, $t_{reg} = 2$ ns (1), 8 ns (2) [69]

spectral kinetics originated by dielectric relaxations and photochemical reactivity develops on this background.

Commonly, the spectroscopic observations of dielectric (dipolar) relaxation are provided by excitation at the band maximum and recording the shifts of emission spectra to longer wavelengths as a function of time [67]. As a result, when observed at the blue edge, the emission decay contains short-decaying positive component(s) due to fast temporal decrease of a number of emitters possessing higher energies. When observed at the red emission edge the decay contains a negative component due to increase with time of the number of excited-state species emitting at low energies. The major features of this process can be adequately described based on the Bakhshiev–Mazurenko model of dipolar relaxations [62, 63] that uses Eqs. (3–5). Such picture is often obscured by non-exponential decay functions recorded at different emission wavelengths that are used for constructing the time-resolved spectra. Moreover, apparent motions of spectra in time that derive from wavelength-dependent decay rates have been described that originate not from molecular relaxation but from heterogeneity of fluorescence emission [68].

The red-edge effects introduce a new dimension into this picture and allows probing the redistribution on emission energy as a function of time between the sites in an ensemble [21]. They allow decreasing or even eliminating this type of heterogeneity. Moreover, these studies bring in new concept of relaxation, which is the reorganization in ensemble of distributed states on the achievement of excited-state equilibrium [45]. In the conditions at which the major part of the excited dye population on achieving the equilibrium demonstrates the motion of spectra to longer wavelengths, the spectra of the sub-population selected at the red edge do not move [69], Fig. 7. This is because those species are photoselected, the interactions of which with the environment are close to the relaxed state. When the dye is

excited by energy lower than that of the relaxed state, the spectra move to opposite direction, to higher energies (up-relaxation) [21].

The changes at the red edge of time-dependent evolution of spectra can be observed in different ways. In the conditions of observing the time-dependent spectral shifts the time-resolved emission decays change dramatically at the red-edge excitation: its short components at the blue and red slopes of emission spectrum that reflect the relaxation, disappear [70]. The emission kinetics excited at the red edge becomes uni-modal and almost single-exponential. The evolution of fluorescence bandwidth in time-resolved spectra is much more pronounced at the red-edge than at the main-band excitation. The spectra are initially more narrow (since a part of the distribution is selected) and are broadened in the course of relaxation due to redistribution to a broader number of different sites. If fluorescence is selectively excited by a narrow-band pulse, then a time-dependent broadening (spectral diffusion) is observed [71], and due to temporal depopulation of 'selected' fluorophores, a selective decrease of τ_F is observed at the frequency of excitation [72]. Site-photoselection at the red edge results in disappearance of these effects.

Thus, the time-resolved fluorescence methods can be easily extended to experiments with site-selective excitation. These results allowed achieving better understanding the molecular relaxation phenomena. Relaxation can be viewed as not only the decrease in time of the energy of the average (or most probable) species of molecular ensemble but also reorganization in this ensemble, the loss of time correlation and site-selected species as a function of time.

2.4 Diversity of Wavelength-Selective Effects

Since in absorption spectra the band corresponding to the 0-0 electronic transition is observed at the lowest energies (longest wavelengths), and the vibrational structure (often not observable) propagates in the direction of higher energies, the best site-selectivity can be achieved at the low-energy slope of absorption spectra, the "red edge." In some organic dyes the 0-0 absorbance is weak and other Franck–Condon active vibronic bands can participate in this site-selectivity. In the cases when vibrational structure is relatively well resolved, the site-photoselection to some extent can be achieved at the red edge of every electron-vibrational band [73]. This depends on fluorophore structure and, together with fluorophore–environment interaction, determines the dynamic range of observed effects.

With these facts in mind let us summarize all the possibilities in observing the site-selective effects manipulating with excitation and emission wavelengths. Excitation proceeds from thermally relaxed ground state to different unrelaxed vibrational modes of excited state. Vibrational relaxation and thermalization on intramolecular and intermolecular level occur much faster than the emission [74] and the red-edge effects should be observed only if dielectric relaxations in intermolecular interactions proceed slower or in comparable rate with the emission.

If these rates are comparable, then the red-edge effects will depend on the following factors:

- Variation of temperature. Both τ_R and τ_F depend on temperature, so the correlation between them, $\tau_R/(\tau_R + \tau_F)$, expressed by Eq. (6), should be temperature-dependent. Usually the relaxation rate increases with temperature faster than the emission rate. In some cases structural changes in the system with the change of τ_R can be detected, but there may be the cases when the relaxation rates change without conformational change [75].
- The effects of fluorescence quenchers. The result of collisional quenching is the change of fluorescence lifetime τ_F that shortens the time window for relaxations and increases the red-edge effects [45].
- The time-resolved observations. The spectra move to longer wavelengths as a result of dielectric relaxation with the decrease of energy (the common case). They stop to move if by shifting the wavelength the isorelaxation point is achieved, and they start to move to shorter wavelengths at the far red edge, when the relaxed state is of higher energy (the case of "up-relaxation") [21]. Instead of heat release as a result of relaxation, a local cooling in the dye environment can be detected [76].

Photoselection can be observed also in emission spectra. The emissive electronic transitions extend from vibrationally relaxed excited state to different vibrational sub-levels of the ground state, so the vibrational progression extends from the 0-0 band located at higher energies in the direction of lower energies, to longer wavelengths. Emission proceeds to different vibronic high energy ground-state levels, which makes impossible the photoselection by collecting the low-energy emission quanta. Therefore excitation spectra measured by setting the emission wavelength longer than the band maximum will be always emission-wavelength-independent. The site-photoselection by probing the emission wavelengths is possible only from the side of high energies of emitted quanta, when the selected species possess the ground-state solvation (stabilization) energies higher than the mean, while their excited state should be less stabilized than for the average of the ensemble. This situation can be realized only at the blue (short-wavelength) edge of emission band. As a result, the excitation spectrum will gradually shift to the blue at the "blue edge" of emission band, i.e., at the high energy side of 0-0 transition [19]. Thus, in emission spectrum the site-selectivity leads to another site-selective effect – the dependence of excitation spectra on emission wavelength. Similarly to the other red-edge effects, this effect disappears as a result of relaxation.

Figure 8 illustrates the correlation of motions of excitation and emission spectra: red-edge effect by photoselecting the excitation and blue edge effect by photoselecting the emission wavelengths. The shift of excitation spectra to the blue is observed when fluorescence emission is collected at wavelengths shorter than fluorescence band maximum. The dependence of excitation spectra on emission wavelength appears if we collect the emitted quanta that possess higher energies than the mean, since they correspond to lower part of the distribution in the ground state and higher part of the distribution in the excited state. As a result,

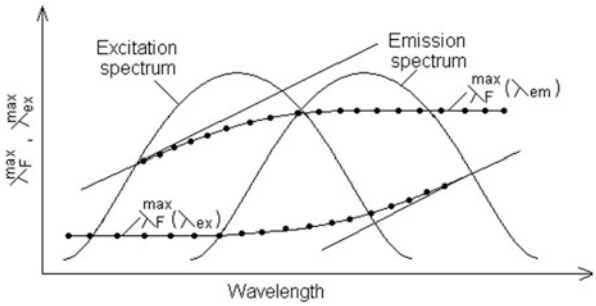

Fig. 8 Typical dependences of positions of fluorescence band maxima on excitation wavelength, $\lambda_F^{max}(\lambda_{ex})$, and positions of excitation band maxima, $\lambda_{em}^{max}(\lambda_{em})$, on emission wavelength for the case of inhomogeneous broadening of spectra [60]

the excitation spectrum will shift to the blue. This dependence increases with the further shift to the blue edge, and no saturation point is observed.

Light has a selective power to excite exclusively those dyes, the properties of which match the energy and polarization of their electronic transitions. Thus, if the dye excitation is produced by polarized light, its emission will be also highly polarized. Depolarization occurs only when the time correlation in the excited state is lost due to the dye rotation or its participation in some photophysical process, such as excitation energy transfer [77]. Often the decay of time-resolved anisotropy, $r(t)$, is non-exponential due to asymmetry of dye molecule and anisotropy of its interactions. Also, since in the course of relaxation τ_F becomes shorter at the blue and longer at the red slopes of emission spectrum, a higher value of anisotropy is observed in the blue and lower in the red parts of the spectrum [78]. Such effects are produced due to variation of time window, in which fluorophore rotations are observed. Excitation at the red edge suppresses the relaxational shift of spectra and makes the emission decay more homogeneous [79, 80].

The spectral and temporal inhomogeneity of emission probed by the dependence on excitation and emission wavelengths may produce additional influence on $r(t)$, even without EET in dilute solutions. Because of release of excessive vibrational and intermolecular energy, the local heating can occur [79, 80]. This effect is called a "*light-induced rotation*," it is suppressed when λ_{ex} is shifted far to the red edge where $\lambda_{ex} > \lambda_{ex}^{*}$ (λ_{ex}^{*} is the *isorelaxation point*, explained in Fig. 4), since in this case we excite the solutes with the strongest intermolecular energy in the excited state [80]. The local heating depends on the excess of configurational energy of selectively excited solvates and leads to specific dependencies of the kinetics of radiation anisotropy on the exciting light frequency and the frequency at which the emission is recorded [23]. It is clearly observed for fluorescence probes in biomembranes [24].

There is one more possibility of introducing time domain into spectrally selective molecular relaxation technique. It is the transient hole-burning spectroscopy [51, 81, 82]. Unlike persistent hole-burning [55–57] this method does not require cryogenic temperatures. By exciting the probe molecule with pulses shorter than the solvation time but longer than the dephasing time, a subset of the ground-state population is excited only and it can be recorded in a picosecond transient

absorption spectrum. This subset corresponds to probe molecules experiencing similar interactions with the solvent. The rate of this broadening (hole-filling) is attributed to solvent dielectric relaxation kinetics resulting in a time-dependent disappearance of "selected" species. Thus, even at room temperature a transient spectrum initially shows a slightly sharp hole around the exciting energy, resulting in the time-dependent broadening of its shape.

Though in the background of this technique is a different methodology (the selection is produced within the ground-state distribution and the relaxation occurs within the ensemble of ground-state species), it has important common features with the time-dependent red-edge effects:

- photoselection is produced within inhomogeneously broadened absorption band,
- relaxation is observed as a time-dependent disappearance of "selected" species,
- the time window for the observation of relaxation process is determined by the excited-state lifetimes. Usually it is the picosecond–nanosecond time range, but by populating the triplet state the time window can be extended to milliseconds.

3 Red-Edge Effects in Photochemical Transformations

Based on the interpretation presented above, of spectral broadening and molecular relaxations in solutions, it can be expected that any excited-state reaction, the rate of which depends on the energy and dynamics of weak noncovalent interactions with the environment will be modulated by site-selection effects. It is known that solvent-reorganizational coordinate is important for many excited-state reactions [83, 84], but not for all of them. There are reactions that are uncoupled with dipolar relaxations and that can occur on ultra-short time scale even at extremely low temperatures (for instance, intramolecular proton tunneling [85] and non-adiabatic electron transfer [86]). At the other extreme are slow reactions that occur in solution after attaining dielectric equilibrium, for instance, the reactions of diffusional bimolecular quenching. But there are many examples of those reactions that are coupled with these relaxations, and the study of this coupling may be used as an important clue for elucidating their mechanisms [87]. In unrelaxed states the distribution of excited-state species on their interaction energies with the environment may result in distributed reaction kinetics [88]. It was shown that the part of this distribution that interacts stronger with the environment may exhibit an extreme increase in reactivity in intramolecular electron transfer reaction and a decreased reactivity in proton transfer and energy transfer reactions [89, 90]. Site-photoselective spectroscopy allows not only to characterize the selective photochemical reactivity but also to provide the means to model the reactions occurring in the ground states, especially those of them which possess low intrinsic activational barriers and depend on dynamics in the environment. Those are many biocatalytic reactions.

3.1 Photoinduced Electron Transfer

The solvent effects influence the excited-state photoinduced electron transfer (PET) if the transition from the initial "locally excited" (LE) state to charge-transfer (CT) state is adiabatic, i.e. occurs in the conditions of strong electronic coupling between two states and proceeds continually along the reaction coordinate on a common adiabatic potential energy surface [84]. Quite often the PET reactions result in quenching, which complicates the observation of red-edge effects [91]. Bianthryl is a bright exception, in which PET reaction is intramolecular leading to brightly fluorescent product. It is an anthracene dimer demonstrating the excited-state electron switching between monomers in liquid polar media, and this reaction does not proceed if the solution is frozen.

This reaction in bianthryl was studied by variation of excitation wavelength (Fig. 9). It was found that PET, which requires dielectric relaxation and commonly does not occur in vitrified polar solutions, is dramatically facilitated when photoselection was provided at the red edge of excitation band [90].

The temperature range of disappearance of such red-edge effect correlates strongly with the solvent mobility. It occurs in the range of nanosecond dielectric relaxations in the solvent [89]. This connection with the solvent mobility is clearly demonstrated when the temperature dependences of spectral shift of LE band, the change of the band width, and the extent of PET reaction expressed as the relative ratio of LE and CT band intensities are displayed in the same plot (Fig. 10).

The results obtained demonstrate the possibility of photoselection in the rigid environment of species, for which the solute–solvent configurations are close to the "relaxed" state. Because of that the solvent-reorganization barrier does not exist and the PET reaction proceeds easily. An attractive idea can be suggested to make

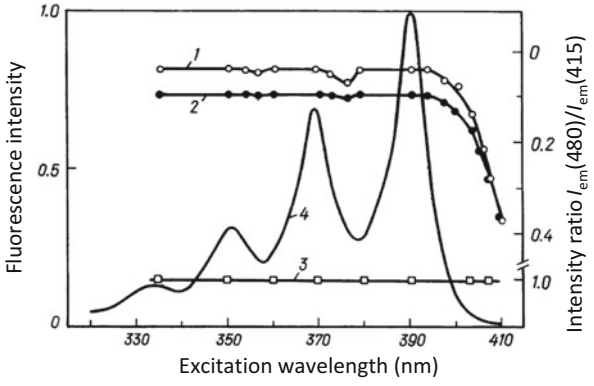

Fig. 9 Influence of the excitation wavelength on fluorescence spectra of bianthryl in propylene glycol [90]. $I_{em}(480)/I_{em}(415)$ is the ratio of intensities at emission wavelengths 480 and 415 nm that reflects the relative contribution of CT and LE forms. The temperatures were −100°C (1), −53°C (2), and 18°C (3). Curve 4 and the *left scale* represent the excitation spectra at −53°C at emission velengths 395, 415, 445, and 480 nm, which are superimposed

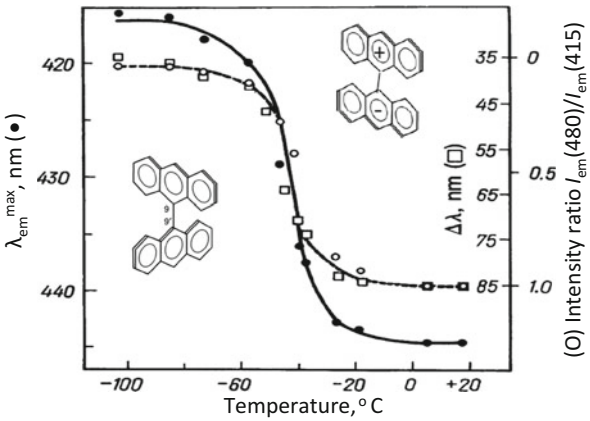

Fig. 10 Temperature dependences of the bianthryl spectroscopic parameters in propylene glycol [90]. λ_{em}^{max} is the position of fluorescence maxima at excitation wavelength 403 nm and $\Delta\lambda$ is the half-maximum bandwidth of the spectrum, excitation wavelength 365 nm. The red-edge effect is displayed as the intensity ratio at two emission wavelengths, $I_{em}(480)/I_{em}(415)$, the same parameter as in Fig. 9

organic solid-state optoelectronic devices switchable just by the energy of excitation light.

3.2 *Intramolecular Charge Transfer and Excited-State Isomerizations*

Electronic excitations may lead to intramolecular charge transfer (ICT) reactions that involve redistribution of electronic charge within the same molecule. These effects are typical for fluorophores that contain electron donor and electron acceptor groups incorporated into aromatic heterocycles. The intramolecular electronic charge redistribution is coupled with electronic and nuclear polarization of the medium resulting in dielectric relaxations. If the relaxations do not occur in rigid environments, the static distribution of sub-states may result in different ICT reactivity and the site-selective excitation may allow observing the switching of emission between initially locally excited (LE) and ICT forms. Dynamic solvent effects are observed when this reaction is adiabatic, i.e., occurs in the conditions of strong electronic coupling between two states and proceeds continually along the reaction coordinate on a common adiabatic potential energy surface [84]. Of special interest are the cases, in which the reactant and product forms are represented by separate emission bands. For the fluorescent dye Laurdan, popular in many applications, two fluorescence bands with maxima at 425 and 500 nm are observed in cooled glycerol [92]. Remarkably, together with redistribution of intensities between two bands, only the long-wavelength CT band shifts dramatically on transition of excitation energy to the red edge.

Charge redistribution is often coupled with rotations of molecular fragments. A number of fluorophore molecules that exhibit intramolecular flexibility and are planar in the ground state can rotate in the excited state to a perpendicular

conformation (which can be energetically more favorable in polar environments). The reaction is easily observable when both forms are present in the emission and are represented by separate maxima. In these cases the fluorescence spectrum is usually shifted to longer wavelengths. Classical in this respect is *N*,*N*′-dimethylaminobenzonitrile (DMABN), for which the twisted intramolecular charge-transfer (TICT) state can be achieved even in rigid polymeric matrices. It was shown [93] that in polar polyvinyl alcohol (PVA) glass the contribution of the TICT form being small at the main-band excitation increases dramatically when fluorescence is excited at the red edge. Meantime, a strong deformation of an excitation spectrum as a function of emission wavelength indicated the significant site distribution within the ground-state species.

The barrierless stochastic staircase model of Bagchi was used for interpretation. Within this model, the long-wavelength excitation selects in the initial population the species that are closer on reaction coordinate to the region where the reaction occurs [94]. In related experiments on 1,4-diphenyl-1,3-butadiene the red-edge selective excited-state production of s-*cis* rotamers has been demonstrated [95]. Switching between LE and ICT emissions can be achieved with the shift of excitation wavelength in argon matrix for pyrrolyl benzonitrile [96]. These and other related experiments suggest that site-photoselection in excited state isomerizations coupled with ICT occur in the excited state, although their pre-existence in the ground state as minor forms is not excluded.

For organic dyes exhibiting intrinsic flexibility the possibility to form the distribution of sub-states due to formation of population of rotamers and the existence of variable free volumes in solid matrix was pointed out by different authors [97]. The cases are known, in which two rotamers are present in the ground state but only one of them is present in emission spectra at long-wave excitation, demonstrating the red-edge effect [98]. Recent experiments with DMABN point to this possibility. The red-edge effects reveal itself in the dependence of ratio LE to CT fluorescence bands on the wavelengths of excitation [99]. These features can be observed even in a liquid solvent acetonitrile within quite broad temperature interval from 0°C to 80°C [100], which may be connected both with slow interconversion between these sub-states and very short lifetimes narrowing the time window for observation.

Thus, the red-edge effects are important tools to study the excited-state dynamics and its coupling with the motions in reactant environment for ICT reactions and when these reactions are coupled with conformational changes. However, one has to keep in mind the possibility of selecting within the species already existing in the ground state. Photoselection in the latter case is quite different from that on existence of classical red-edge effect. This issue will be discussed in Sect. 5.

3.3 *Excited-State Intramolecular Proton Transfer*

Excited-state intramolecular proton transfer (ESIPT) reactions demonstrate very strong wavelength shifts and a great variety of rates, starting from ultrafast proton tunneling [101] to that coupled with solvation dynamics [92] and proceed under either thermodynamic or kinetic control [102]. In 3-hydroxyflavone (3HF) derivatives all these different conditions and mechanisms of photo-transformations can be realized. The initially excited LE and reaction product proton transfer (PT) excited-state forms are dramatically separated in emission energy. In 3HF derivatives possessing strong excited-state dipole moments, both spectral position of LE form and interplay of two forms in fluorescence spectrum depend strongly on solvent polarity [103, 104].

The site-selectivity of this reaction was first demonstrated in the complex of 4′-(diethylamino)-3-hydroxyflavone with the protein (serum albumin) [88]. It was found that while both LE and PT forms are present at the main-band excitation, the excitation at the red-edge results in elimination of the PT band from the spectrum (Fig. 11).

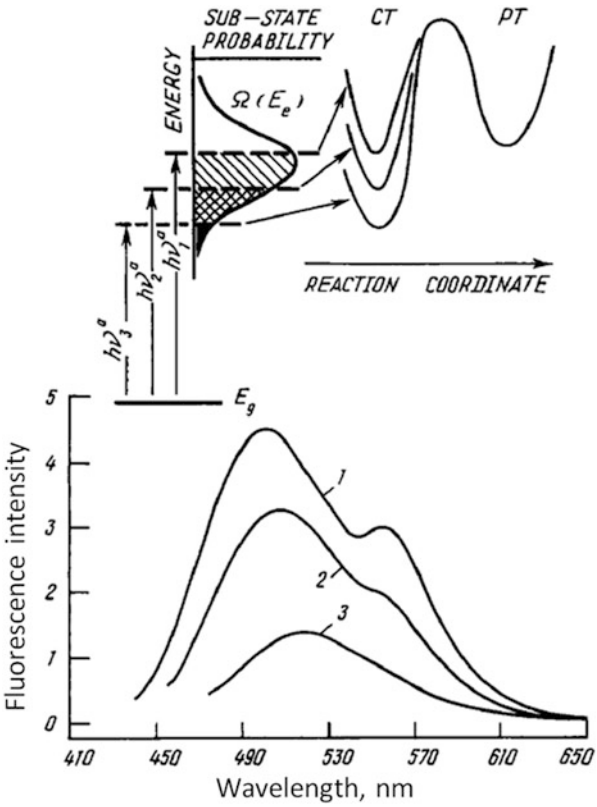

Fig. 11 The scheme illustrating the appearance of red-edge effect in ESIPT reaction of 3HF derivatives (above) and experimental data on the disappearance of PT band (below) [83]. The notations in scheme are those as in Fig. 3. The site-photoselection of polar and highly solvated species in the LE state suppresses the PT reaction. The results on 3HF derivative demonstrate the spectral shift of LE band and disappearance of PT band in emission on shifting the excitation from 420 nm (1) to 440 nm (2) and further to 460 nm (3)

The scheme presented in Fig. 11 (above) illustrates the mechanism of site-photoselection modulating the PT reaction yield. The excitation results in the appearance of highly polar dipolar LE state that, interacting with the environment, generates an ensemble of sub-states of different energies. The reaction proceeds with the activation barrier to a low-polar PT state, in which the distribution in interaction energy with the environment is minimal. Since the reaction rate is much faster than any orientational relaxation of the environment dipoles, the distribution in LE state persists on the scale of reaction. The species on the lowest edge of this distribution need to overcome much higher activation energy, than in the middle of distribution, and for them the ESIPT reaction is suppressed.

Serum albumin was selected in our initial studies because this protein has a function to bind and transport in the blood of different substances with low solubility in water and its binding sites are well characterized. The high-affinity binding of 3HF derivatives to particular protein site was demonstrated [105]. The local environment formed by the binding site is rigid, so the distribution is maintained during the lifetime of LE state. The studies in polymer films, phospholipid membranes, and in complexes with proteins allow characterizing the static and dynamic disorder in these systems. This effect is easily observed as an excitation wavelength-dependent dramatic change of the emission band profile resulting in dramatic change of color [106].

The same effect of retardation of ESIPT reaction at the red-edge excitation is observed in viscous solvent triacetin [107], in ionic liquids [107, 108] and erythrocyte membranes [109]. Recently Tomin [110] demonstrated that it can be manifested even in liquid solvents due to strong shortening of excited-state lifetime. Thus, in the case of ESIPT reaction in excited-state dipolar 3-hydroxyflavones the site-photoselection at the red excitation edge results in stabilization of initially excited LE state and to disappearance of reaction product proton transfer band. This example of the red-edge effect in ESIPT reaction is a demonstration, how the coupling of site-photoselection with excited-state reaction can provide a significant amplification of spectroscopic signatures of molecular disorder.

Concluding this section, we derive that the red-edge effects have become the important tools for studying the mechanisms of different excited-state reactions, for which the solvent-reorganizational coordinate is important. They allow studying the coupling of these reactions with dielectric relaxations in the reaction site environments and the involvement of inhomogeneous reaction kinetics. These observations demonstrate how the coupling of site-photoselection with excited-state reaction can provide a significant amplification of spectroscopic signatures of molecular disorder. Strong site-selectivity is observed for different low-barrier excited-state reactions in the conditions of slow mobility in the environment of the excited reactant species. Some of them are very useful practically for characterization of the dynamic properties in particular systems and predicting their behavior in chemical and biochemical reactivity [83]. Because elementary rates in these reactions are also site-selective, their inhomogeneous kinetics should also be observed. Wavelength-selective reactivity was found in photochemistry for charge-recombination reactions [111]. In analogy, this type of reaction kinetics

was suggested for biocatalytic reactions [83, 88]. Recently such reaction behavior was found in single-molecular studies [112].

4 Directional Excited-State Energy Transfer and Red-Edge Effects

The discovered by Weber [1–3] red-edge effect of failure of energy homo-transfer between the dyes in highly concentrated solutions in rigid and highly viscous media (see Fig. 1) can be naturally explained by site-photoselection within the inhomogeneously contour of absorption band. Here the same molecules serve the role of both donors and acceptors. However, they are distributed being located in different environments and because of that their absorption and emission spectra are not identical. The species from upper part of the distribution (Fig. 3) can transfer their energy to another species on the same or lower energy level. In contrast, the species from the lower part of the distribution (their effective concentration is low) can transfer their energy only to other species of the lower part of this distribution. Because of low concentration of these selected species, such transfer is a low probable event. Thus, due to the presence of inhomogeneous broadening, the excited-state energy transfer between chemically identical molecules is not random, it is directed from those members of the ensemble which emit at shorter wavelengths to those which absorb at longer wavelengths [18].

As a result of this *directed transfer* the fluorescence spectra in concentrated dye solutions in rigid and highly viscous environments are shifted to longer wavelengths. This shift can be observed as a function of time [25], even if the environment is completely immobile. Such transfer stops at the red edge just because of low probability of site-photoselected species.

There is also an emission analog of this effect: in concentrated solid dye solutions the energy homo-transfer fails to occur at the short-wavelength edge of emission band [113, 114]. In this case the emission of the dyes serving as EET acceptors and emitting at lower energies is not recorded, and the emission of donors remains at high energies and is highly polarized. In this case also the failure of energy transfer occurs in rigid and highly viscous solutions or very short observation times in liquid solvents and can be recorded as highly polarized emission.

Figure 12 serves as illustration of the mechanism of failure of excited-state energy transfer leading to observed Weber red-edge effect.

4.1 Spectral Dependence of Emission Polarization

Fluorescence polarization technique is one of the most popular and informative tools in the studies of molecular structure and dynamics [77, 116] and the Weber's

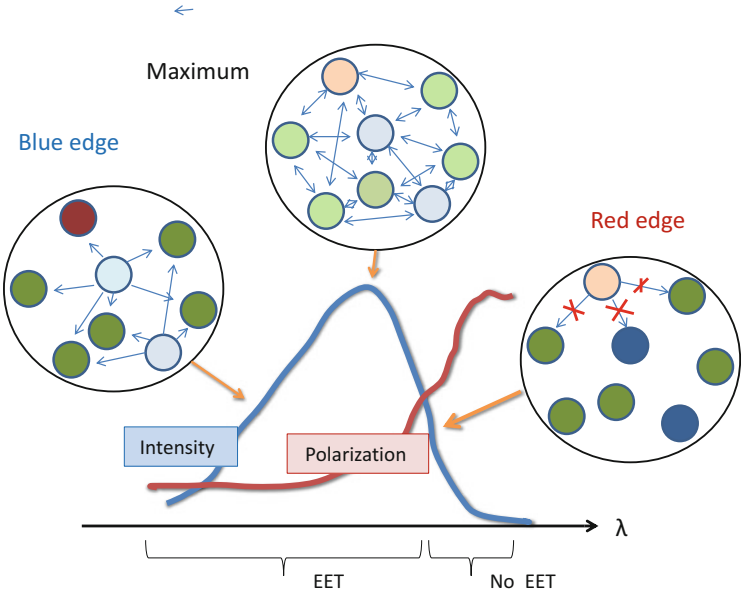

Fig. 12 The scheme explaining the red-edge effect as the site-photoselection within the population of fluorescence emitters and the disappearance of EET leading to increase of polarization at the red edge of excitation spectrum [115]. The system composed of similar molecules located within the distances of efficient homo-EET is shown. At shorter wavelengths (case a) and band maximum (case b) the emitters exhibiting different interactions with the environment (marked with different colors) have equal probability to absorb light and transfer the excitation energy to its neighbors, which dramatically depolarizes the emission. At long-wavelength edge (case c) the species absorbing and emitting the low-energy quanta are excited only. They do not exhibit EET and emit independently, so their emission is highly polarized

red-edge effect opens new dimension in these studies. One of the most important practical applications is to discriminate two generally occurring effects leading to fluorescence depolarization: excitation energy transfer and fluorophore rotations. Rotational depolarization of fluorescence commonly occurs as a diffusional motion in structurally relaxed environments, and the depolarized emission should not depend on the excitation or emission energy. On contrary, the energy transfer efficiency depends on the correspondence of excited-state energies of donor and acceptor and is influenced by photoselection. Therefore the red-edge effect allows introducing the reference point at which this process fails to occur providing the means to detect and characterize EET. In view that in homo-transfer systems the spectral changes may not be significant, emission anisotropy is probably the most convenient method for such analysis.

This tool is the most frequently used in protein and biomembrane studies. Thus, for the measurements of polarization of the protein Trp fluorescence the excitations at 295 and 310 nm (near the red edge) were chosen [117]. Rotational diffusion leads to depolarization of the emission excited at either 295 or 310 nm, but homo-transfer

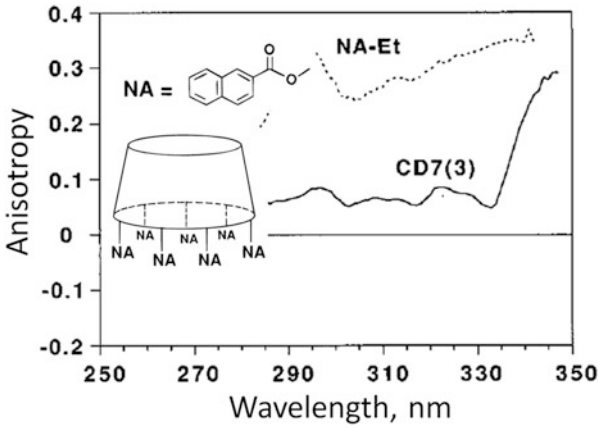

Fig. 13 Chemical structure and excitation polarization spectra (observation wavelength: 380 nm) of the multichromophoric cyclodextrin CD7(3) in comparison with the model chromophore NA-Et (ethyl naphthoate) in a mixture of ethanol and methanol (9:1 v/v) at 110 K [119]

only contributes to depolarization upon excitation at 295 nm. Hence, the 310/295 polarization ratio gives an indication of Trp–Trp energy transfer.

This effect of wavelength shifting opens the ways of manipulating with emission anisotropy by creating or avoiding the EET conditions. It has got interesting application in fluorescence polarization microscopy for detecting the interactions between the molecules within the living cells [118]. In biomolecular studies, homo-EET allows single labeling in contrast to more difficult double labeling that is normally used for observing proximity effects in hetero-EET systems.

The study of the effect of excitation wavelength on energy switching among the dyes located in well-defined positions in supramolecular structures is of both theoretical and practical value since it allows evaluating the extent of molecular order in the studied systems. As an example, β-cyclodextrin with appended seven 2-naphthoyloxy dyes, CD7(6), was synthesized [119, 120], see Fig. 13. Because the rotational motions of the dyes are frozen in the rigid glass, the depolarization effect observed with CD7(6) as compared with free dye NAEt (which displays strongly polarized emission over the whole long-wavelength part of the spectrum) is attributed solely to energy transfer between the appended dyes. It was found that despite the attachment to rigid structures they have their emission transition moments oriented variably from that of the directly excited one. When increasing the excitation wavelength beyond 335 nm, the emission anisotropy drastically increases, thus indicating a gradual decrease in energy transfer efficiency, so that at the extreme red edge (~350 nm) there is a complete lack of energy transfer (the Weber red-edge effect).

4.2 Shifts in Emission Spectra

Whereas the increase of the degree of polarization of light emission known as the Weber red-edge effect is the most convenient for observation, the spectroscopic

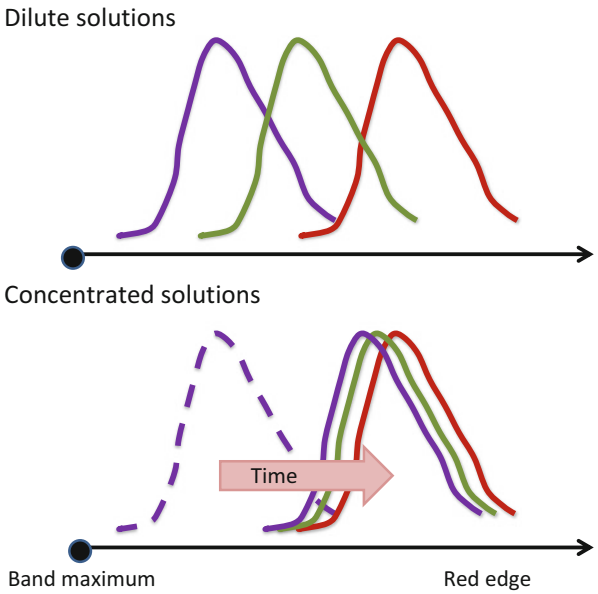

Fig. 14 Illustration of typical transformations of fluorescence spectra on transition to the red excitation edge in rigid environments for dilute solutions (no EET) and concentrated solutions (efficient EET at the main-band excitation). In dilute solutions the spectral shift is maximal. In contrast, in concentrated solutions because of EET the steady-state spectra are already shifted (and this shift can be observed as a function of time from initial position shown as a *dashed line*). Because of that the shift on transition to the red edge is much smaller leading to the same spectral position as in dilute solutions

changes are no less spectaculous and important. Since both donors and acceptors in homo-EET are chemically identical molecules located in the same medium, their excited-state distributions (see Fig. 3) are identical, so that each donor can serve as acceptor and the reverse. However, as a result of this transfer directed from those members of the ensemble that emit at shorter wavelengths to those that absorb at longer wavelengths, in rigid and highly viscous environments the fluorescence spectra are shifted to longer wavelengths [18].

Directed transfer can be easily observed in rigid media by comparing the spectra at the main-band excitation for concentrated and dilute dye solutions (Fig. 14). Due to transfer from "blue" to "red" emitters occurring in time, the fluorescence spectra are already shifted at the main-band excitation. The transfer from the main-band excitation to the red excitation edge results in two effects operating in opposite directions. One is the failure of transfer that increases the population of short-wavelength emitting donors and the other is the red-edge photoselection of low-energy emitters within the population. As a result, the observed shift will be much smaller. Finally, in the case of absence of aggregation in concentrated solutions the spectra recorded in the red-edge wavelength range should occupy the same positions as in the absence of energy homo-transfer.

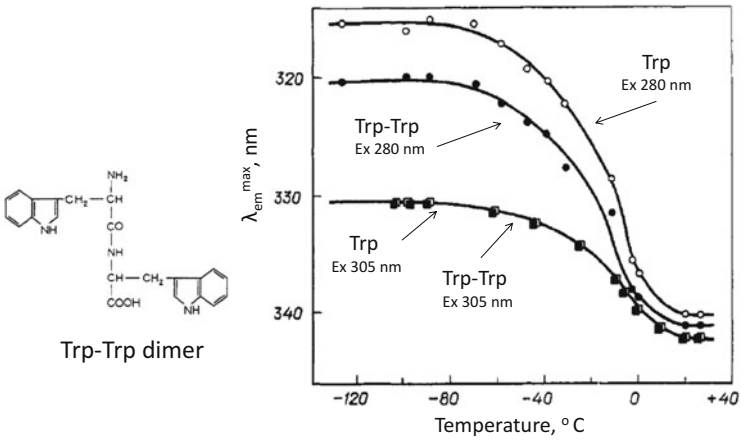

Fig. 15 Temperature dependence in the positions of fluorescence band maxima of tryptophan monomer (Trp) and the dimer (Trp–Trp) in glycerol on excitation wavelength at the band maxima (280 nm) and red edge (305 nm) [89]

Such wavelength-dependent behavior of steady-state spectra is characteristic for all systems exhibiting homo-EET. As an example, the results of studies of tryptophan dimer Trp–Trp [89] are presented (Fig. 15). At the main-band excitation 280 nm the spectrum of Trp occupies the short-wavelength position and is dramatically shifted on the shift of excitation wavelength to the red edge (305 nm). For Trp–Trp dimer, due to homo-EET the spectrum is shifted already and therefore the shift on the change of excitation wavelength is much smaller. Essentially, the spectral positions of Trp and Trp–Trp at 305 nm excitation superpose.

Interesting result is observed when the temperature is increased over the solvent relaxation range (see Fig. 15). Excitation wavelength stops to be a tool for site-photoselection and EET becomes no longer directed. We observe that the failure of directed transfer correlates with temperature-dependent activation of relaxational dynamics in the solvent. Therefore in liquid environment the spectra of Trp and Trp–Trp are nearly identical and excitation-wavelength independent.

4.3 The Effects Observed in Time Domain

Excitation energy homo-transfer proceeds in time on the scale of picoseconds–nanoseconds that is available to time-resolved fluorescence technique. In solid environments, when both dielectric relaxations and dye rotational motions are retarded, it can be detected both by the temporal loss of anisotropy and by the shifts of fluorescence emission bands. As a result of this directed transfer the fluorescence spectra in concentrated dye solutions in rigid and highly viscous environments are shifted as a function of time to longer wavelengths [22, 25, 45].

The time-resolved technique makes possible to visualize the dynamics of the process and measure the required kinetic parameters. The higher the dye molecule concentration, the faster is the energy transfer.

Transition to the red edge of excitation suppresses the transfer and modifies dramatically the emission decay by decreasing its emission-wavelength dependence (see Fig. 15), which allows introducing an important "no-transfer" reference limit. At these wavelengths the fluorophores emit individually, their emission spectra are similar to that observed at low concentrations and the decay kinetics simplified.

4.4 Light Harvesting and Its Modulation at the Red Edge

Directed excitation energy hopping between chromophores is a fundamental process occurring in the antennae pigments of photosynthetic units. The studies of photosynthetic antenna pigments in solutions [26] suggested the directed energy transfer to be an important mechanism of light-harvesting of solar energy in photosynthesis. Here the idea is to accommodate the pigments in high density to provide optimal collection of sunlight. The energy migrating between them with gradual decrease become assembled at the site with the lowest energy where it will be transferred to the electron-generating site. It was shown that in isolated core complexes, the polarization of the emission increases smoothly as a function of the excitation wavelength, starting from the center of absorption band, whereas in membranes the increase is abrupt and occurs in the extreme red edge [121]. These facts demonstrating the Weber red-edge effect suggest the possibility of modulation in the system of natural pigments its efficiency by the energy of absorbed light.

In analogy with natural systems of photosynthesis the idea on energy collection and migration was implemented into artificial antenna-based photomolecular devices, such as artificial solar concentrators [122]. Different molecular ensembles and nanostructures were designed for that [123, 124]. An example of directed transfer in polymer films and of its absence for single molecules can be the result on poly(3-hexylthiophene) [125]. Essentially, in these systems just due to inhomogeneous broadening and site-photoselection effects the on–off switching of light harvesting can be achieved just by shifting the excitation energy.

5 Red-Edge Effects and Ground-State Heterogeneity

Excitation-wavelength guided site-selectivity can be achieved not only within inhomogeneous broadening profile of absorption band, which is in the background of red-edge effects. It can be observed in different structurally heterogeneous systems, since also different types of impurities as well as ground-state heterogeneity in dye state (ionization, charge-transfer complexes, and H-bonding) may be in

the origin of photoselection by shifting the wavelength. Operating on the atomic scale of distances, the positional heterogeneity can arise from imprecise location and orientation of the dye, e.g. its distribution between the sites of different polarities or at the surface of molecule or nanoparticle. Apparent spectral broadening can be the result of all these factors, and this could result in preferable excitation of one of the species with respect to others, resulting in shifted fluorescence spectrum.

Thus there can exist the effects of ground-state heterogeneity that are usually discrete in nature and bring new site-photoselection effects that overlap those resulting from common inhomogeneous broadening. Many such cases were reported. For instance, two polypyridyl ruthenium complexes possessing an extended conjugation and strongly coupled electronic states had strong excitation dependent emission behaviors caused by mixing of different electronic states [126]. Two or more conformers having different geometry existing in ground-state equilibrium and absorbing light at different wavelengths may display variations in positions of their emission bands [127]. In our work [128] we tried to introduce the criteria that distinguish the effects of inhomogeneous broadening and those that originate from positional (ground-state) heterogeneity.

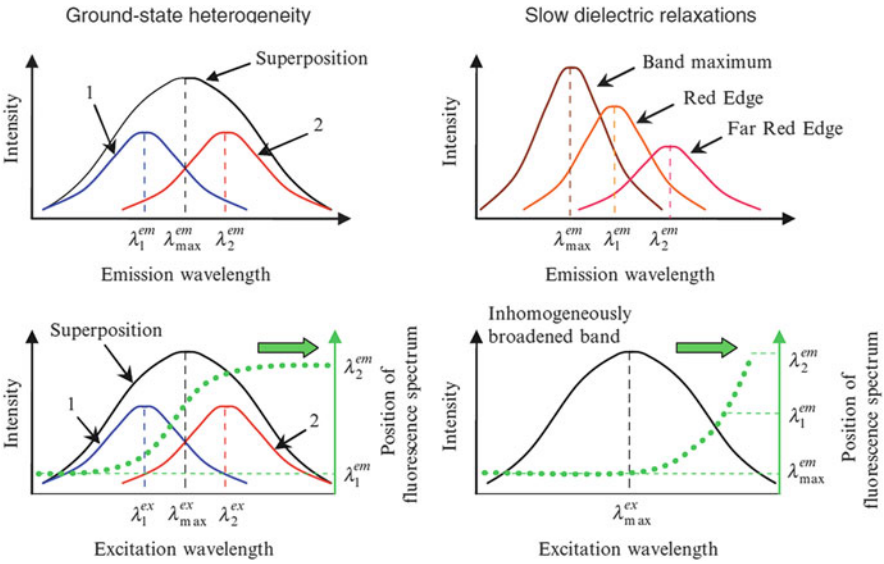

Fig. 16 Schematic representation of spectroscopic effects of (**a**) ground-state heterogeneity and (**b**) slow dielectric relaxations leading to red-edge effects [128]. In the case (a) variation of excitation wavelength leads to photoselection between the species possessing difference in excitation spectra, so that the dye excited at shorter wavelengths (λ_1^{ex}) exhibits blue emission at λ_1^{em} and, correspondingly, excited at λ_2^{ex} exhibits red-shifted emission at λ_2^{em}. The shifting of excitation wavelength leads to change of relative contributions of two emissions. In the case (b) there is a single ground-state form but the shift of excitation wavelength from band maximum, λ_{max}^{ex}, to the red edge of excitation leads to progressive shift of emission spectra (two of them, λ_1^{em} and λ_2^{em} are shown) to longer wavelengths

The distinction between the cases of inhomogeneous broadening and ground-state heterogeneity can be observed when the excitation-wavelength dependencies of fluorescence spectra are analyzed on a broad scale (Fig. 16). The red-edge effects demonstrate a very characteristic shape with the absence of the shifts of fluorescence spectra as a function of excitation wavelength at the maxima and short-wavelength wing of excitation bands but an unlimited increase of effect at the red excitation edge [30, 31, 35]. In contrast, the ground-state heterogeneity comes from superposition of absorption (excitation) spectra of the dyes present in different forms or residing in different locations. Because the quantum yield, anisotropy, and lifetime of a dye in these forms or locations can differ, the shapes of measured excitation-wavelength dependences as a general case is variable, even sigmoid [129].

The measurements of the shifts in excitation spectra and their polarization as a function of excitation wavelength may also serve as a good criterion [98]. Such effect was demonstrated in 6-methoxyquinoline in different polymer matrices [130]. Excitation-wavelength dependence of the dual emission and the fluorescence decays show a non-exponential behavior throughout the emission profile. The results are interpreted in terms of two groups (normal and charge transfer species) of ground-state conformers that are inhomogeneously distributed and assume different geometries in the polymer matrices.

Sometimes it is hard to distinguish the ground-state heterogeneity, especially in the case of excited-state reactions. The fluorescence of dimethylaminobenzonitrile (DMABN) and similar molecules in polymer glass consists of two bands due to formation of twisted intramolecular charge-transfer (TICT) state, as in polar fluid solvents. The TICT band in emission being small at the mainband excitation increases dramatically when fluorescence is excited at the red edge. Meantime, a strong deformation of an excitation spectrum as a function of emission wavelength indicated the significant site distribution of the ground-state species [93]. Describing site-selectivity in the redistribution of intensities of these fluorescence bands, Tomin [100] explained it by the presence of rotational isomers. They may possess different orientations of the dimethylamino group with respect to the plane of the benzonitrile residue and display the TICT reaction with different rates.

Important criterion for distinguishing the red-edge effects can be based on time-resolved data. Commonly the inhomogeneous broadening leads to non-exponential fluorescence decays that can extend over several orders of magnitude. Approximating of such inhomogeneous (in other terms, polychromatic or dispersive) kinetics by two or more exponential functions usually do not fit the experimental data. It can be provided using Kohlrausch "stretched exponential" function [131]. The decay $N(t)$ of initial number N_o of reactant molecules can be described as follows:

$$N(t) = N_o \exp\left[-(t/\tau)^{\beta}\right],\ 0 < \beta < 1. \tag{9}$$

Here β describes the deviation from the first-order kinetics and τ characterizes the time scale of the reaction [131–133]. Generally, a smaller value of β corresponds to a wider distribution of lifetimes, suggesting a more disordered system. At the site-photoselective excitations due to decrease of the distribution width the fluorescence decays should become closer to exponential.

The red-edge effects depend strongly on the properties of a fluorophore. The dyes with low dependence for absorption spectra on solvent polarity and a very strong such dependence for emission spectra could be ideal for this application. They demonstrate a strong increase of the dipole moment in the excited state and exhibit a broad excited-state distribution on interaction energies. These features will determine their properties in spectral, anisotropy, and time domains. Good in this respect is tryptophan, which is the constituent of many proteins, and therefore we observe many applications of this method in protein research [31, 35]. Regarding different fluorescence dyes used for probing, the situation is variable. For instance, Nile Red, with its strong dependence on the environment polarity variation of both excitation and emission spectra, can display both the red-edge effects and the ground-state heterogeneity [134], and the analysis of these effects is complicated by the strong variation of its lifetime.

Fluorescent nanoparticles and composites are the structures that may be heterogeneous in size and composition by their origin. If the positions of their excitation and emission bands are size-dependent, the site-photoselection effects can be observed in their mixtures [135]. By combining semiconductor quantum dots of different sizes the effect of directed energy transfer can be achieved [136]. Carbon dots may demonstrate strong excitation-wavelength dependence of emission spectra [137] and single-molecular studies demonstrated that this is the result of structural heterogeneity [138]. Therefore the reported "giant red-edge effect" observed in graphene oxide nanoparticles [139] is probably the sole result of their structural heterogeneity.

6 Connection with the Studies of Single Molecules

It is common for us to assume that molecules of the same chemical composition must have identical properties. In reality though, every molecule in a condensed medium is different. Unlike an ideal crystal, where only vibrational motions are allowed, real condensed matter systems display much greater possibilities for intermolecular configurations resulting in structural, energetic, and dynamic molecular disorders. This results in a variety of new properties: broadening or even disappearance of first-order phase transitions in macromolecules [140], non-exponential kinetics of photophysical and photochemical reactions [141], non-Arrhenius-type activated processes [142], and others. Therefore it is extremely important to characterize molecular disorder in both conceptual and quantitative terms. Heterogeneity arising on the level of weak, in physical terms, intermolecular interactions with the local dye environment and their fluctuations on a time scale

may result in broad variation of photophysical properties and of photochemical reactivity, which can be studied by fluorescence techniques. As we discussed above, the power of red-edge effects in these studies is their ability to compare the static and dynamic spectroscopic information of the whole ensemble of innumerable number of molecules with its sub-ensemble of energy-selected species.

Further decrease of this ensemble leads us to a single molecular level. These studies required introduction of new methods enabling to achieve the absolute limit of sensitivity in fluorescence spectroscopy [143, 144]. Observing a single molecule removes the usual ensemble-averaged picture and allows obtaining the most valuable information on the intensity, excitation and emission spectra, polarization, fluorescence decay rate of chosen individual molecules and of their chemical and photochemical reactivity in comparison to average molecules in ensemble of presumably identical species [145]. Selection of individual molecules from the ensemble can be achieved by ultimate dilution of dye solutions, illumination of ultra-small sample volumes, and application of confocal or two-photon microscopy [146]. On a single molecular level the spectral shifts and intensity fluctuations can be revealed even if they are present as rare events allowing the exploration of hidden heterogeneity in complex condensed phases [147].

The single-molecule detection allows providing a conceptually important move from ensemble analysis to individual event analysis. Individual molecules can be fitted to statistical ensemble. The more informative histograms based on single-molecular studies can be recorded, in which the responses from the members of molecular ensemble are seen as distinct events [148].

In studies of single molecules the concept on broad distribution of solvation energies in ensembles of fluorophore molecules in condensed media has got final confirmation. It has become evident that the red-edge effects do not break the Kasha rule. The Kasha rule must be applied not to whole ensemble but to individual emitters forming their inhomogeneously broadened ensemble.

Thus, the role of red-edge effects in photophysical studies of dyes in condensed phase in comparison with common spectroscopic experiments and investigations of single molecules can be summarized as follows (see Fig. 17):

- The standard spectroscopic measurements yield the information on ensemble of emitters. Those are the average values of studied parameters for a large number of molecules. These studies remain to be of great value, since in real systems the physical behavior and chemical reactivity is the property of whole molecular ensembles.
- The red-edge effects allow the observations of inhomogeneous broadening and molecular dynamics based on comparison in behavior of molecular ensemble and its sub-ensemble. They have become “classical,” playing their important role as a part of standard spectroscopic techniques.
- The level of single molecules allows studying the fluctuations and statistical distributions, and an inhomogeneous contour of the ensemble of molecules can be built from these individual contributions. By removing completely the ensemble averaging, the distribution of every measured parameter can be

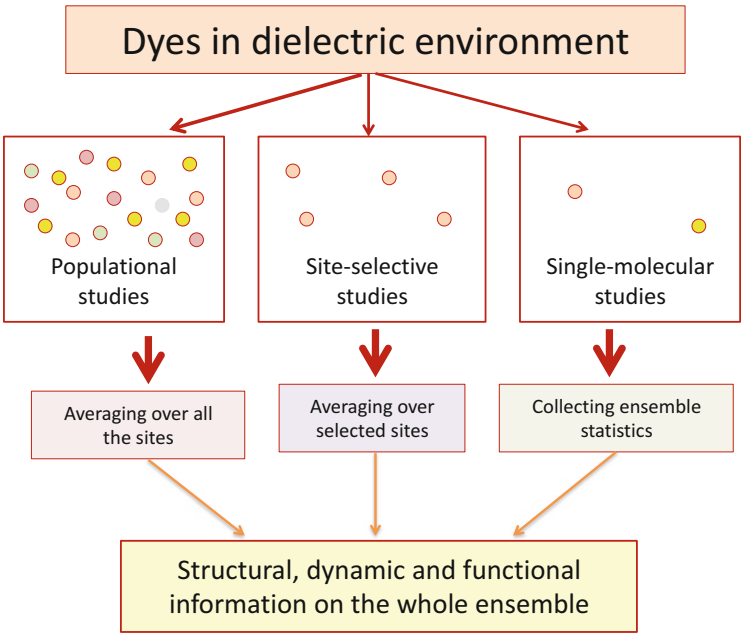

Fig. 17 Illustration of comparative information that can be obtained in populational research in condensed phase, explorations of red-edge effects in site-selective studies and the reconstructing of molecular ensemble properties from single molecular data. In populational studies the properties of individual molecules or their sub-ensembles are not resolved. At the red edge the site-selective studies of specific sequence of states are possible. In single molecular research the members of the ensemble are studied one by one. They can be identical chemical species, which differ in interactions with the environment, and an inhomogeneous contour of the ensemble of molecules can be built up from their individual contributions

obtained and a frequency histogram of the actual distribution of values can be constructed. Such distributions contains more information than the average value alone [149].

7 Perspective

The observation and analysis of red-edge effects introduced by Gregorio Weber has developed into a powerful methodology for studying molecular disorder and its coupling with molecular dynamics. With years of exploration, variation of excitation wavelength has become an important spectroscopic tool generating informative response in all optical parameters: spectral shifts, quenching, anisotropy, and lifetimes. This methodology is simple in application; it can easily complement other fluorescence spectroscopic methods in studying microscopically heterogeneous systems of different kind, including biological macromolecules in solutions

and complex nanoscale systems. New areas of research were opened for rapid development.

The red-edge effects gave rise to a new understanding of spectroscopy of organic molecules in condensed phase. They showed that variation in solute–solvent local interactions is a significant source of the broadening in the absorption and emission spectra. Even in a structurally homogeneous phase, solute molecules can occupy a broad population of solvation sites differing in interaction with the environment and generating an array of electronic transition energies. It is their summation that comprises the absorption or emission spectra. Selective excitation of some members of this population enables them to be studied and treated selectively, so that comparison with the results obtained for the whole population gives new knowledge. This field of research can be called the site-selective spectroscopy of organic molecules.

In molecular dynamics of condensed matter a new very productive concept was introduced: the light absorption and emission spectra being formed by inhomogeneous ensemble of molecules reflect the stochastic dynamics of their formation and re-arrangement in time. Therefore the possibility appears to extract dynamic information by comparing the data of spectroscopic, time-resolved and anisotropy studies obtained for the whole ensemble on comparison with its selected part. From the above discussion it is clearly seen that the relaxation in molecular ensembles not only changes the average energy of excited fluorophores (commonly, it decreases). It is also the loss of "molecular memory", so the process in time develops from correlated to uncorrelated behavior.

In photochemical reaction dynamics, a direct connection was established of the reaction yield and rate with the interaction of reaction site with its environment and dynamics of this environment. Site-selective photochemistry is demonstrated for all types of these reactions: isomerizations, intramolecular charge transfer, electron and proton transfer. Studies of solvation dynamics are very important for a detailed understanding of chemical reaction dynamics, catalysis and biocatalysis in solutions. Many chemical reactions proceed with significant intramolecular charge redistribution, and when they occur in condensed media they may exhibit site-selective inhomogeneous behavior.

In designing new nanoscale and molecular devices, scientists are often interested in assembling fluorophores to their high density. Here these species can exchange the interaction energies due to mechanism of non-radiative energy transfer. Different compositions can be designed to modulate such transfer, including light harvesting and wavelength conversion, and the possibility to suppress such transfer at the red excitation edge can be used for such modulation.

Finally, we observe how the unusual phenomenon became classical with extremely broad range of applications. We came to recognition that molecular disorder is not a complication in spectroscopic studies if we know how to extract extremely important information regarding the behavior of condensed matter on molecular scale and on the scale of intermolecular interactions. This information is especially valuable if the observed systems are microscopically heterogeneous and exhibit hierarchical dynamic features.

References

1. Weber G (1960) Fluorescence-polarization spectrum and electronic-energy transfer in tyrosine, tryptophan and related compounds. Biochem J 75(2):335
2. Anderson SR, Weber G (1969) Fluorescence polarization of the complexes of 1-anilino-8-naphthalenesulfonate with bovine serum albumin. Evidence for preferential orientation of the ligand. Biochemistry 8(1):371–377
3. Weber G, Shinitzky M (1970) Failure of energy transfer between identical aromatic molecules on excitation at the long wave edge of the absorption spectrum. Proc Natl Acad Sci USA 65(4):823–830
4. Gaviola E, Pringsheim P (1924) Über den Einfluß der Konzentration auf die Polarisation der Fluoreszenz von Farbstofflösungen. Z Physik 24:24–36
5. Förster T (1948) Zwischenmolekulare energiewanderung und fluoreszenz. Ann Physik 437 (1-2):55–75
6. Vavilov VI, Galanin MD (1949) Emission and absorption of light in the system of inductively coupled molecules. Dokl Akad Nauk USSR 67:811–818
7. Weber G (1954) Dependence of the polarization of the fluorescence on the concentration. Trans Faraday Soc 50:552–555
8. Terenin AN (1967) Photonics of dye molecules. Nauka, Leningrad
9. Birks JB (1975) Organic molecular photophysics. Wiley, New York
10. Turro NJ (1991) Modern molecular photochemistry. University Science Books, Sausalito, CA
11. Turro NJ, Ramamurthy V, Scaiano JC (2009) Principles of molecular photochemistry: an introduction. University Science Books, Sausalito, CA
12. Kasha M (1950) Characterization of electronic transitions in complex molecules. Disc Faraday Soc 9:14–19
13. Lamola AA, Turro NJ (1969) Energy transfer and organic photochemistry, vol 14. Interscience Publishers, New York
14. Galley WC, Purkey RM (1970) Role of heterogeneity of the solvation site in electronic spectra in solution. Proc Natl Acad Sci USA 67(3):1116–1121
15. Rubinov A, Tomin V (1970) Bathochromic luminescence in solutions of organic dyes at low temperatures. Opt Spektrosk USSR 29(6):578
16. Milton JG, Purkey RM, Galley WC (1978) Kinetics of solvent reorientation in hydroxylated solvents from exciting-wavelength dependence of chromophore emission-spectra. J Chem Phys 68(12):5396–5404
17. Rudik K, Pikulik L (1971) Effect of exciting light on fluorescence spectra of phthalimide solutions. Opt Spektrosk USSR 30(2):147
18. Gulis I, Komyak A (1977) Peculiarities of inductive-resonance energy transfer in the conditions of organic molecule electronic levels inhomogeneous broadening. J Appl Spectrosc 27 (5):841–845
19. Pavlovich V (1976) Dependence of the spectra of excitation of dipole molecule solutions on the recording wavelength. J Appl Spectrosc 25(3):1141–1147
20. Azumi T, Itoh KI, Shiraishi H (1976) Shift of emission band upon the excitation at the long wavelength absorption edge. III. Temperature dependence of the shift and correlation with the time dependent spectral shift. J Chem Phys 65(7):2550–2555
21. Nemkovich N, Matseyko V, Tomin V (1980) Intermolecular up-relaxation in phthalimide solutions at excitation by frequency tuned dye laser. Opt Spektrosk USSR 49(2):274–283
22. Rubinov AN, Tomin VI, Bushuk BA (1982) Kinetic spectroscopy of orientational states of solvated dye molecules in polar solutions. J Luminescence 26:377–391
23. Gakamsky D, Nemkovich N, Rubinov A (1992) Wavelength-dependent rotation of dye molecules in a polar solution. J Fluorescence 2(2):81–92
24. Nemkovich N, Rubinov A (1995) Spectral inhomogeneity and wavelength-dependent rotation of probe molecules in membranes. J Fluorescence 5(3):285–294

25. Nemkovich N, Rubinov A, Tomin V (1981) Kinetics of luminescence spectra of rigid dye solutions due to directed electronic energy transfer. J Luminescence 23(3):349–361
26. Rubinov A, Zen'kevich E, Nemkovich N, Tomin V (1982) Directed energy transfer due to orientational broadening of energy levels in photosynthetic pigment solutions. J Luminescence 26(4):367–376
27. Macgregor RB, Weber G (1981) Fluorophores in polar media: spectral effects of the Langevin distribution of electrostatic interactions. Ann N Y Acad Sci 366(1):140–154
28. Mazurenko YT (1983) Statistics of solvation and solvatochromy. Opt Spektrosk USSR 55 (3):471–478
29. Gorbatsevich S, Gulis I, Komyak A (1982) Molecular distribution function over the 0-0 transition frequencies in polar solutions. J Appl Spectrosc 36(3):332–337
30. Demchenko AP (1982) On the nanosecond mobility in proteins. Edge excitation fluorescence red shift of protein-bound 2-(p-toluidinylnaphthalene)-6-sulfonate. Biophys Chem 15:101–109
31. Demchenko AP (1986) Ultraviolet spectroscopy of proteins. Springer Verlag, Berlin-Heidelberg-New York
32. Demchenko AP, Shcherbatska NV (1985) Nanosecond dynamics of charged fluorescent probes at the polar interface of a membrane phospholipid bilayer. Biophys Chem 22:131–143
33. Demchenko AP, Ladokhin AS (1988) Red-Edge-Excitation Fluorescence Spectroscopy of Indole and Tryptophan. Eur Biophys J 15(6):369–379
34. Demchenko AP (1991) Fluorescence and dynamics in proteins. In: Lakowicz JR (ed) Topics in fluorescence spectroscopy, vol 3. Plenum, New York, pp 61–111
35. Demchenko AP (2002) The red-edge effects: 30 years of exploration. Luminescence 17 (1):19–42
36. Mulkherjee S, Chattopadhyay A (1995) Wavelength-selective fluorescence as a novel tool to study organization and dynamics in complex biological systems. J Fluorescence 5:237–246
37. Chattopadhyay A, Haldar S (2014) Dynamic insight into protein structure using red edge excitation shift. Ac Chem Res 47(1):12–19
38. Demchenko AP (1986) Fluorescence analysis of protein dynamics. Essays Biochem 22:120–157
39. Lakowicz JR (2000) On spectral relaxation in proteins. Photochem Photobiol 72:421–437
40. Haldar S, Chaudhuri A, Chattopadhyay A (2011) Organization and dynamics of membrane probes and proteins utilizing the red edge excitation shift. J Phys Chem B 115:5693–5706
41. Raghuraman H, Kelkar DA, Chattopadhyay A (2005) Novel insights into protein structure and dynamics utilizing the red edge excitation shift approach. In: Reviews in fluorescence 2005. Springer, New York, pp 199–222
42. Chattopadhyay A, Haldar S (2013) Dynamic insight into protein structure utilizing red edge excitation shift. Acc Chem Res 47(1):12–19
43. Chattopadhyay A (2003) Exploring membrane organization and dynamics by the wavelength-selective fluorescence approach. Chem Phys Lipids 122(1-2):3–17
44. Hu Z, Margulis CJ (2007) Room-temperature ionic liquids: slow dynamics, viscosity, and the red edge effect. Acc Chem Res 40(11):1097–1105
45. Nemkovich NA, Rubinov AN, Tomin VI (1991) Inhomogeneous broadening of electronic spectra of dye molecules in solutions. In: Lakowicz JR (ed) Topics in fluorescence spectroscopy, vol 2. Plenum, New York, pp 367–428
46. Bushuk B, Rubinov A, Stupak A (1987) Inhomogeneous broadening of spectra of dye solutions due to intermolecular hydrogen bonding. J Appl Spectrosc 47(6):1251–1254
47. Gafert J, Friedrich J, Vanderkooi JM, Fidy J (1995) Structural changes and internal fields in proteins: a hole-burning Stark effect study of horseradish peroxidase. J Phys Chem 99 (15):5223–5227
48. Logovinsky V, Kaposi A, Vanderkooi J (1993) Native and denatured Zn cytochrome c studied by fluorescence line narrowing spectroscopy. Biochim Biophys Acta 1161 (2):149–160

49. Schomacker K, Champion P (1986) Investigations of spectral broadening mechanisms in biomolecules: cytochrome-c. J Chem Phys 84(10):5314–5325
50. Klán P, Wirz J (2009) Photochemistry of organic compounds: from concepts to practice. Wiley, New York
51. Rätsep M, Pajusalu M, Freiberg A (2009) Wavelength-dependent electron–phonon coupling in impurity glasses. Chem Phys Lett 479(1):140–143
52. Jankowiak R, Reppert M, Zazubovich V, Pieper Jr, Reinot T (2011) Site selective and single complex laser-based spectroscopies: a window on excited state electronic structure, excitation energy transfer, and electron–phonon coupling of selected photosynthetic complexes. Chem Rev 111(8):4546–4598
53. Reppert M, Naibo V, Jankowiak R (2010) Accurate modeling of fluorescence line narrowing difference spectra: Direct measurement of the single-site fluorescence spectrum. J Chem Phys 133(1):014506
54. Tomin V, Rubinov A (1981) Spectroscopy of inhomogeneous configurational broadening in dye solutions. J Appl Spectrosc 35(2):855–865
55. Personov R, Al'Shits E, Bykovskaya L-A (1972) The effect of fine structure appearance in laser-excited fluorescence spectra of organic compounds in solid solutions. Optics Communs 6(2):169–173
56. Wagie HE, Geissinger P (2012) Hole-burning spectroscopy as a probe of nano-environments and processes in biomolecules: a review. Appl Spectrosc 66(6):609–627
57. Rebane L, Gorokhovskii A, Kikas J (1982) Low-temperature spectroscopy of organic molecules in solids by photochemical hole burning. Appl Phys B 29(4):235–250
58. Murakami H, Kinoshita S, Hirata Y, Okada T, Mataga N (1992) Transient hole-burning and time-resolved fluorescence spectra of dye molecules in solution: Evidence for ground-state relaxation and hole-filling effect. J Chem Phys 97(11):7881–7888
59. Jankowiak R, Hayes J, Small G (1993) Spectral hole-burning spectroscopy in amorphous molecular solids and proteins. Chem Rev 93(4):1471–1502
60. Demchenko AP (2008) Site-selective red-edge effects. Chapter 4. In: Methods in enzymology, vol 450. Academic, New York, pp 59–78
61. Ware WR, Lee SK, Brant GJ, Chow PP (1971) Nanosecond time-resolved emission spectroscopy: spectral shifts due to solvent-excited solute relaxation. J Chem Phys 54 (11):4729–4737
62. Bakhshiev NG, Mazurenko YT, Piterskaya IV (1966) On the emission decay in various regions of molecule luminescence spectra in viscous solutions. Opt Spektrosk USSR 21 (5):550–554
63. Mazurenko YT, Bakhshiev NG (1970) The influence of orientational dipolar relaxation on spectral, temporal and polarization properties of luminescence in solutions. Opt Spektrosk USSR 28:905–913
64. Brand L, Gohlike JR (1971) Nanosecond time-resolved fluorescence of a protein-dye complex BSA+TNS. J Biol Chem 246:2317–2324
65. Yang M, Richert R (2001) Observation of heterogeneity in the nanosecond dynamics of a liquid. J Chem Phys 115(6):2676–2680
66. Richert R (2002) Heterogeneous dynamics in liquids: fluctuations in space and time. J Phys Condensed Matter 14(23):R703
67. Maroncelli M (1993) The dynamics of solvation in polar liquids. J Mol Liquids 57:1–37
68. Fee RS, Milsom JA, Maroncelli M (1991) Inhomogeneous decay kinetics and apparent solvent relaxation at low temperatures. J Phys Chem 95(13):5170–5181
69. Nemkovich N, Rubinov A (1996) Spectral and spatial heterogeneity of fluorescent probes in membranes. J Appl Spectrosc 63(4):522–529
70. Vincent M, Gallay J, Demchenko AP (1995) Solvent relaxation around the excited state of indole: analysis of fluorescence lifetime distributions and time-dependent spectral shifts. J Phys Chem 99:34931–34941

71. Richert R (2001) Spectral diffusion in liquids with fluctuating solvent responses: dynamical heterogeneity and rate exchange. J Chem Phys 115(3):1429–1434
72. Lëvshin L, Struganova I, Toleutaev B (1988) Dynamics of inhomogeneous broadening of fluorescence spectra of dye solutions. J Appl Spectrosc 49(1):695–699
73. Voropay E, Koyava V, Saechnikov V, Sarjevsky A (1980) Some effects in inhomogeneous level broadening at excitation energy transfer conditions. J Appl Spectrosc 32:457–463
74. Kovalenko S, Schanz R, Hennig H, Ernsting N (2001) Cooling dynamics of an optically excited molecular probe in solution from femtosecond broadband transient absorption spectroscopy. J Chem Phys 115(7):3256–3273
75. Demchenko AP, Ladokhin AS (1988) Temperature-dependent shift of fluorescence spectra without conformational changes in protein; studies of dipole relaxation in the melittin molecule. Biochim Biophys Acta 955(3):352–360
76. Clark J, Miller P, Rumbles G (1998) Red edge photophysics of ethanolic rhodamine 101 and the observation of laser cooling in the condensed phase. J Phys Chem A 102(24):4428–4437
77. Jameson DM, Ross JA (2010) Fluorescence polarization/anisotropy in diagnostics and imaging. Chem Rev 110(5):2685–2708
78. Mazurenko YT, Bakhshiev N, Piterskaya I (1968) Spectral dependence of the degree of rotational depolarization of the fluorescence of complex molecules in viscous solutions. Opt Spektrosk USSR 25:46
79. Gakamsky DM, Goldin AA, Petrov EP, Rubinov AN (1992) Fluorescence decay time distribution for polar dye solutions with time-dependent fluorescent shift. Biophys Chem 44(1):47–60
80. Gakamskii D, Nemkovich N, Rubinov A (1991) Molecular relaxation and rotation of dye molecules in polar solvents (A review). J Applied Spectrosc 54(2):99–111
81. Kinoshita S, Itoh H, Murakami H, Miyasaka H, Okada T, Mataga N (1990) Solvent relaxation effect on transient hole-burning spectra of organic dyes. Chem Phys Lett 166(2):123–127
82. Huang J, Ridsdale A, Wang J, Friedman JM (1997) Kinetic hole burning, hole filling, and conformational relaxation in heme proteins: direct evidence for the functional significance of a hierarchy of dynamical processes. Biochemistry 36(47):14353–14365
83. Demchenko AP (1994) Protein fluorescence, dynamics and function: exploration of analogy between electronically excited and biocatalytic transition states. Biochim Biophys Acta 1209:149–164
84. Maroncelli M, McInnis J, Fleming GR (1989) Polar solvent dynamics and electron transfer reactions. Science 243:1674–1681
85. Bader AN, Pivovarenko VG, Demchenko AP, Ariese F, Gooijer C (2004) Influence of redistribution of electron density on the excited state and ground state proton transfer rates of 3-hydroxyflavone and its derivatives studied by Spol'skii spectroscopy. J Phys Chem B 108(29):10589–10595
86. Marcus R, Sutin N (1985) Electron transfer in chemistry and biology. Biochim Biophys Acta 811:265–322
87. Demchenko AP, Tang K-C, Chou P-T (2013) Excited-state proton coupled charge transfer modulated by molecular structure and media polarization. Chem Soc Rev 42(3):1379–1408
88. Demchenko AP (1992) Does biocatalysis involve inhomogeneous kinetics? FEBS Lett 310 (3):211–215
89. Demchenko AP, Sytnik AI (1991) Site-selectivity in excited-state reactions in solutions. J Phys Chem 95:10518–10524
90. Demchenko AP, Sytnik AI (1991) Solvent reorganizational red-edge effect in intramolecular electron transfer. Proc Natl Acad Sci USA 88(20):9311–9314
91. Letrun R, Vauthey E (2014) Excitation wavelength dependence of the dynamics of bimolecular photoinduced electron transfer reactions. J Phys Chem Lett 5(10):1685–1690
92. Tomin V, Heldt J (2003) The red-edge effects in Laurdan solutions. Z Naturforschung A 58 (2–3):109–117

93. Al-Hassan KA, Rettig W (1986) Free volume sensing fluorescent probes. Chem Phys Lett 126(3–4):273–279
94. Braun D, Rettig W (1997) Excitation energy dependence of the kinetics of charge-transfer formation. Chem Phys Lett 268(1–2):110–116
95. Wallace-Williams SE, Møller S, Goldbeck RA, Hanson KM, Lewis JW, Lee WA, Kliger DS (1993) Excited-state s-cis rotamers produced by extreme red edge excitation of all-trans-1, 4-diphenyl-1, 3-butadiene. J Phys Chem 97(38):9587–9592
96. Schweke D, Baumgarten H, Haas Y, Rettig W, Dick B (2005) Charge-transfer-type fluorescence of 4-(1 H-Pyrrol-1-yl) benzonitrile (PBN) and *N*-phenylpyrrole (PP) in cryogenic matrixes: evidence for direct excitation of the CT band. J Phys Chem A 109(4):576–585
97. Al-Hassan KA (1988) Edge-excitation red shift of the fluorescence of flexible solute molecules in a poly (methyl methacrylate) polymer matrix. J Polym Sci B Polym Phys 26 (8):1727–1733
98. Józefowicz M, Heldt JR, Bajorek A, Pączkowski J (2008) Red-edge and inhomogeneous broadening effects of the electronic spectra of ethyl 5-(4-aminophenyl)-3-amino-2, 4-dicyanobenzoate. J Photochem Photobiol A: Chem 196(1):38–43
99. Tomin V, Hubisz K (2006) Instantaneous emission spectra and molecular rotation of n-dimethylaminobenzonitrile fluorescing in the long-wavelength spectral range. Opt Spektrosk USSR 100(1):65–74
100. Tomin V, Wlodarkiewicz A (2013) The influence of temperature on red-edge excitation effects in liquid solutions of N,N′-dimethylaminobenzonitrile. Opt Spektrosk USSR 115 (1):86–93
101. Bader AN, Pivovarenko VG, Demchenko AP, Ariese F, Gooijer C (2004) Excited state and ground state proton transfer rates of 3-hydroxyflavone and its derivatives studied by Shpol'skii spectroscopy: the influence of redistribution of electron density. J Phys Chem B 108(29):10589–10595
102. Tomin VI, Demchenko AP, Chou P-T (2015) Thermodynamic vs. kinetic control of excited-state proton transfer reactions. J Photochem Photobiol C: Photochem Rev 22:1–18
103. Klymchenko AS, Demchenko AP (2003) Multiparametric probing of intermolecular interactions with fluorescent dye exhibiting excited state intramolecular proton transfer. Phys Chem Chem Phys 5(3):461–468
104. Ghosh D, Batuta S, Das S, Begum NA, Mandal D (2015) Proton transfer dynamics of 4′-N, N-dimethylamino-3-hydroxyflavone observed in hydrogen-bonding solvents and aqueous micelles. J Phys Chem B 119(17):5650–5661
105. Ercelen S, Klymchenko AS, Demchenko AP (2003) Novel two-color fluorescence probe with extreme specificity to bovine serum albumin. FEBS Lett 538(1):25–28
106. Demchenko AP, Ercelen S, Klymchenko AS (2002) Site-selective red-edge spectroscopy of disordered materials and microheterogeneous systems: polymers, phospholipid membranes and proteins. SPIE Int Soc Optics Photonics 4938. doi:10.1117/12.486641
107. Suda K, Terazima M, Kimura Y (2012) Excitation wavelength dependence of photo-induced intramolecular proton transfer reaction of 4′-N, N-diethylamino-3-hydroxyflavone in various liquids. Chem Phys Lett 531:70–74
108. Suda K, Terazima M, Sato H, Kimura Y (2013) Excitation wavelength dependence of excited state intramolecular proton transfer reaction of 4′-N,N-diethylamino-3-hydroxyflavone in room temperature ionic liquids studied by optical Kerr gate fluorescence measurement. J Phys Chem B 117(41):12567–12582
109. Nemkovich N, Kruchenok J, Rubinov A, Pivovarenko V, Baumann W (2001) Site selectivity in excited-state intramolecular proton transfer in flavonols. J Photochem Photobiol A Chem 139(1):53–62
110. Tomin V, Jaworski R (2013) Modulation of the proton transfer rate by excitation photons. Opt Spektrosk USSR 114(5):729–736

111. Nicolet O, Banerji N, Pages S, Vauthey E (2005) Effect of the excitation wavelength on the ultrafast charge recombination dynamics of donor-acceptor complexes in polar solvents. J Phys Chem A 109(37):8236–8245
112. Engelkamp H, Hatzakis NS, Hofkens J, De Schryver FC, Nolte R, Rowan AE (2006) Do enzymes sleep and work? Chem Communs 9:935
113. Koyava V, Popechits V (1979) Directed energy transfer in solid polar dye mixtures. J Appl Spectrosc 31(6):1484–1488
114. Koyava V, Popechits V, Sarzhevskii A (1980) Concentration depolarization of fluorescence in systems with nonuniformly broadened electronic levels. J Appl Spectrosc 32(6):597–602
115. Demchenko AP (2013) Nanoparticles and nanocomposites for fluorescence sensing and imaging. Meth Appl Fluorescence 1(2):022001
116. Jameson DM, Croney JC (2003) Fluorescence polarization: past, present and future. Comb Chem High Throughput Screen 6(3):167–176
117. Moens PD, Helms MK, Jameson DM (2004) Detection of tryptophan to tryptophan energy transfer in proteins. Protein J 23(1):79–83
118. Squire A, Verveer PJ, Rocks O, Bastiaens PI (2004) Red-edge anisotropy microscopy enables dynamic imaging of homo-FRET between green fluorescent proteins in cells. J Struct Biol 147(1):62–69
119. Berberan-Santos MN, Pouget J, Valeur B, Canceill J, Jullien L, Lehn JM (1993) Multichromophoric cyclodextrins. 2. Inhomogeneous spectral broadening and directed energy hopping. J Phys Chem 97(44):11376–11379
120. Berberan-Santos MN, Canceill J, Gratton E, Jullien L, Lehn J-M, So P, Sutin J, Valeur B (1996) Multichromophoric cyclodextrins. 3. Investigation of dynamics of energy hopping by frequency-domain fluorometry. J Phys Chem 100(1):15–20
121. Monshouwer R, Visschers RW, van Mourik F, Freiberg A, van Grondelle R (1995) Low-temperature absorption and site-selected fluorescence of the light-harvesting antenna of *Rhodopseudomonas viridis*. Evidence for heterogeneity. Biochim Biophys Acta 1229 (3):373–380
122. Harriman A (2015) Artificial light-harvesting arrays for solar energy conversion. Chem Communs 51(59):11745–11756
123. Andrews DL (2008) Energy harvesting: a review of the interplay between structure and mechanism. J Nanophotonics 2(1):022502–022525
124. Joly D, Delgado JL, Atienza C, Martın N (2015) Light-harvesting materials for organic electronics. Photonics Nanophotonic Struct Mat 2:311
125. Thiessen A, Vogelsang J, Adachi T, Steiner F, Bout DV, Lupton JM (2013) Unraveling the chromophoric disorder of poly (3-hexylthiophene). Proc Natl Acad Sci USA 110(38):E3550–E3556
126. Xiao L, Xu Y, Yan M, Galipeau D, Peng X, Yan X (2010) Excitation-dependent fluorescence of triphenylamine-substituted tridentate pyridyl ruthenium complexes. J Phys Chem A 114 (34):9090–9097
127. Józefowicz M, Heldt JR (2011) Excitation-wavelength dependent fluorescence of ethyl 5-(4-aminophenyl)-3-amino-2, 4-dicyanobenzoate. J Fluorescence 21(1):239–245
128. Demchenko AP, Yesylevskyy SO (2011) Interfacial behavior of fluorescent dyes. In: Advanced fluorescence reporters in chemistry and biology III. Springer, Heidelberg, pp 3–62
129. Sharma VK, Sahare PD, Rastogi RC, Ghoshal SK, Mohan D (2003) Excited state characteristics of acridine dyes: acriflavine and acridine orange. Spectrochim Acta A 59(8):1799–1804
130. Mehata M, Joshi H, Tripathi H (2001) Edge excitation red shift and charge transfer study of 6-methoxyquinoline in polymer matrices. J Luminescence 93(4):275–280
131. Valeur B, Berberan-Santos MN (2012) Molecular fluorescence: principles and applications. Wiley, New York
132. Berberan-Santos M, Bodunov E, Valeur B (2005) Mathematical functions for the analysis of luminescence decays with underlying distributions 1. Kohlrausch decay function (stretched exponential). Chem Phys 315(1):171–182

133. Edholm O, Blomberg C (2000) Stretched exponentials and barrier distributions. Chem Phys 252(1-2):221–225
134. Datta A, Mandal D, Pal SK, Bhattacharyya K (1997) Intramolecular charge transfer processes in confined systems. Nile Red in reverse micelles. J Phys Chem B 101:10221–10225
135. Tintu R, Nampoori V, Radhakrishnan P, Unnikrishnan N, Thomas S (2012) Cluster size and excitation wavelength dependent photoluminescence behavior of nano colloidal Ge-Se-Sb-Ga chalcogenide glass solutions. J Optoelectronics Adv Mat 14(11):918
136. Kawazoe T, Kobayashi K, Ohtsu M (2005) Optical nanofountain: a biomimetic device that concentrates optical energy in a nanometric region. Appl Phys Lett 86(10):103102
137. Demchenko AP, Dekaliuk MO (2013) Novel fluorescent carbonic nanomaterials for sensing and imaging. Meth Appl Fluorescence 1(4):042001
138. Ghosh S, Chizhik AM, Karedla N, Dekaliuk MO, Gregor I, Schuhmann H, Seibt M, Bodensiek K, Schaap IA, Schulz O (2014) Photoluminescence of carbon nanodots: dipole emission centers and electron–phonon coupling. Nano Lett 14(10):5656–5661
139. Cushing SK, Li M, Huang F, Wu N (2013) Origin of strong excitation wavelength dependent fluorescence of graphene oxide. ACS Nano 8(1):1002–1013
140. Scharnagl C, Reif M, Friedrich J (2005) Stability of proteins: temperature, pressure and the role of the solvent. Biochim Biophys Acta 1749(2):187–213
141. Richert R, Elschner A, Bassler H (1986) Experimental-study of nonexponential relaxation processes in random organic-solids. Z Phys Chem Neue Folge 149:63–75
142. Demchenko A (1997) Breaks in Arrhenius plots for enzyme reactions: the switches between different protein dynamics regimes? Comments Mol Cell Biophys 9:87–112
143. Moerner W, Kador L (1989) Optical detection and spectroscopy of single molecules in a solid. Phys Rev Lett 62(21):2535
144. Ambrose W, Moerner W (1991) Fluorescence spectroscopy and spectral diffusion of single impurity molecules in a crystal. Nature 349:225–227
145. Moerner WE (2007) New directions in single-molecule imaging and analysis. Proc Natl Acad Sci USA 104(31):12596–12602
146. Tinnefeld P, Herten D-P, Sauer M (2001) Photophysical dynamics of single molecules studied by spectrally-resolved fluorescence lifetime imaging microscopy (SFLIM). J Phys Chem A 105(34):7989–8003
147. Xie XS, Trautman JK (1998) Optical studies of single molecules at room temperature. Ann Rev Phys Chem 49(1):441–480
148. Deniz AA, Mukhopadhyay S, Lemke EA (2008) Single-molecule biophysics: at the interface of biology, physics and chemistry. J Royal Soc Interface 5(18):15–45
149. Hohlbein J, Gryte K, Heilemann M, Kapanidis AN (2010) Surfing on a new wave of single-molecule fluorescence methods. Phys Biol 7(3):031001

Imaging Lifetimes

Richard N. Day

Abstract This chapter discusses the critical contributions of Gregorio Weber to the development of techniques to measure fluorescence lifetimes. The fluorescence lifetime is the average time required for a population of fluorophores in the excited state to decay to the ground state. Events in a fluorophore's environment that influence the excited state can alter the lifetime, and this is measured using fluorescence lifetime imaging microscopy (FLIM). This chapter describes the application of FLIM to quantify Förster resonance energy transfer (FRET) between labeled proteins inside living cells. FRET is a non-radiative pathway through which a donor fluorophore in the excited state transfers energy to nearby acceptor molecules. The transfer of energy reduces the donor's fluorescence lifetime, and this can be quantified by FLIM. Since energy transfer occurs through near-field electromagnetic interactions, it can only occur over a distance of 80 angstroms or less. Thus, FRET microscopy has become a valuable tool for investigating biochemical networks inside living cells. In this regard, Gregorio Weber recognized the importance of measuring the biological and physical properties of proteins as integrated systems. Here, proteins labeled with the genetically encoded fluorescent proteins (FPs) are used to demonstrate how FRET-FLIM enables robust and sensitive measurements of protein interactions inside living cells.

Keywords FLIM • Fluorescence • Fluorescent proteins • FRET • Lifetime • Protein interactions

R.N. Day (✉)
Department of Cellular and Integrative Physiology, Indiana University School of Medicine, 635 Barnhill Dr., MS 333, Indianapolis, IN 46202, USA
e-mail: rnday@iupui.edu

D.M. Jameson (ed.), *Perspectives on Fluorescence: A Tribute to Gregorio Weber*,
Springer Ser Fluoresc (2016) 17: 143–162, DOI 10.1007/4243_2016_1,

Contents

1 Introduction

We have long viewed the emission of light from objects in nature with wonder. One of the earliest accounts to capture our fascination with luminescence in nature is Pliny the Elder's description of the glow of jellyfish in the Bay of Naples written in the first century AD [1]. Eighteen centuries later, Thomas Lamb Phipson wrote extensively about the occurrence of spontaneous light in nature, and observed that: "A flame is always a flame, light is everywhere light; but it remains necessary to ascertain *how this light is produced* in different circumstances" [*his emphasis*, 2]. This is a central tenet for those who devote their life's work to studying and harnessing the character of light. This chapter is dedicated not only to the pioneering work of Gregorio Weber, but to the other luminaries in the field as well, because it is from their shoulders that we see further.

This chapter discusses the application of fluorescence lifetime imaging microscopy (FLIM) to the measurement of protein interactions inside living cells. As we shall see, the development of this approach is due in large part to the work of Gregorio Weber. More recently, the broader application of FLIM to studies in living cells has been driven by improvements in the photophysical qualities of the genetically encoded fluorescent proteins (FPs) [3]. The improved FPs are especially useful for Förster resonance energy transfer (FRET) microscopy – a method that provides the nanometer-scale measurements necessary to detect protein interactions in living cells. Here, I describe why FLIM is an especially sensitive approach for measuring FRET between cellular proteins labeled with FPs. The critical considerations for FRET-FLIM measurements in living cells will be demonstrated using simplified theoretical frameworks, as well as experimental results. The reader can then explore these topics in more depth in the references to gain an appreciation for the history and application of FRET by FLIM. Readers interested in detailed

information are directed to a several excellent reviews and books that cover these topics [3–6].

1.1 A Brief History of Lifetime Measurements

Phipson and his contemporaries devoted considerable effort to the classification of luminous objects in nature [2]. They distinguished fluorescent substances, which appear to stop emitting light immediately upon removal of the excitation source, from phosphorescent materials that have a lasting glow. Intrigued by the *lifetime* of phosphorescence – the interval of time between the end of excitation and the extinction of light emission – they began to develop techniques to accurately measure it. In the middle of the nineteenth century, Alexandre-Edmond Becquerel built a phosphoroscope that briefly exposed a phosphorescent material to sunlight, and then measured the resulting emission of light through holes in a rotating disc. The intensity of the emission could be measured for different rotation speeds, providing the first rigorous measurements of phosphorescence lifetimes on the scale of milliseconds [7]. Becquerel used his measurements to determine that the extinction of phosphorescence occurs as an exponential decay over time [5–7].

By the turn of the twentieth century, Nichols and Merritt were using a Lummer and Brodhun photometer to standardize their measurements of phosphorescence. They demonstrated that the decay of phosphorescence remained constant for a particular material, even with very short duration, intense excitations [8]. Then, in the early 1920s Robert Wood illuminated a heated vapor of mercury inside a condenser tube and measured the ensuing fluorescence. He demonstrated that the emission of light was displaced in the moving vapor relative to the excitation spot. By measuring the velocity of the vapor, he determined that there was a dark period following the excitation that lasted about a microsecond [9]. Two years later Phillip Gottling used an improved version of Wood's approach to determine that the dark period following the excitation of rhodamine was twenty nanoseconds. He proposed that the "exciting energy was imprisoned for a short but definite and measurable interval of time" within the fluorescent molecule [10]. His ideas fit well with the model of the atom developed by Niels Bohr [11]. The Bohr model describes how the absorption of energy causes electrons to move from inner to outer stable orbits, with their return to the original orbit being coupled to the emission of quanta of light.

Both Wood and Gottling based their methods on earlier work of Abraham and Lemoine [12] and Lord Rayleigh [13]. They used a Kerr cell (an electro-optical shutter) to achieve very fast light pulses with high temporal precision. In 1926, Enrique Gaviola, a gifted physicist from Argentina working in Germany, developed the first phase *fluorometer*, an instrument designed specifically for lifetime measurements. Gaviola used two Kerr cells to achieve precise control over the excitation light, and the improved sensitivity of his fluorometer permitted the first accurate measurements of nanosecond lifetime decays [14]. This also allowed

Gaviola to show that a fluorophore's environment could influence its lifetime. This meant that the lifetime of a fluorophore could be used as a *molecular stopwatch* to measure events in the probe's environment on the timescales of nanoseconds. It is this property that is exploited by the technique of FLIM.

2 Taking the Measure of FRET

It is from these foundations that we understand that when a fluorophore absorbs energy it is driven into an excited state that persists for a brief time. The molecule then transitions back to the lower energy ground state by one of several possible pathways. Some of the pathways for de-excitation to the ground state are illustrated in the simplified Perrin–Jabłoński plot in Fig. 1. The pathways include internal conversion (*ic*), decay by fluorescence (k_f), quenching (loss of excitation energy without the emission of light, k_{nf}), or intersystem crossing (*isc*) to the triplet state followed by decay by phosphorescence (k_{pf}). The average time required for a population of fluorophores in the excited state to decay to the ground state is called the *fluorescence lifetime*, which, as Becquerel observed, is described by the exponential function (Fig. 1):

$$I(t) = I_0 e^{-t/\tau} \tag{1}$$

where $I(t)$ is the fluorescence impulse response at time t, I_0 is the initial intensity after the excitation pulse, and τ is the fluorescence lifetime.

The fluorescence lifetime is an *intrinsic property* of a fluorophore. Because the measurements of lifetimes are made in the time domain, they are unaffected by variations in probe concentration or by changes in the excitation intensity. But, as Gaviola observed, the fluorescence lifetime can reflect events in the probe

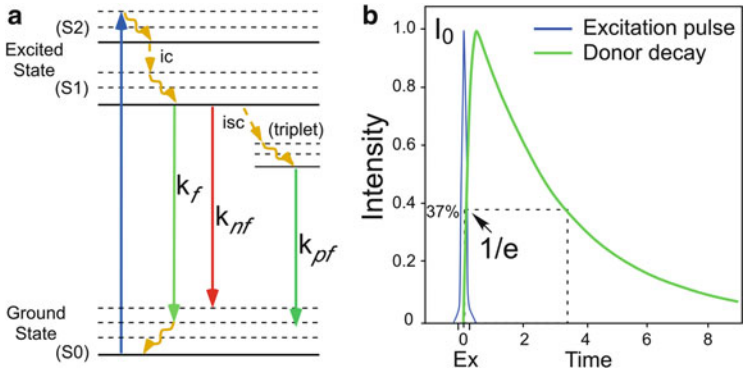

Fig. 1 (**a**) A simplified Perrin–Jabłoński plot illustrating the decay from the excited state to the ground state by radiative (k_f, k_{pf}) and non-radiative (k_{nf}) pathways. (**b**) The exponential decay of fluorescence from a population of molecules illuminated by a brief excitation pulse

environment that can compete in the deactivation from the excited state (Fig. 1). Therefore, the *measured* fluorescence lifetime (τ_f) will represent the combination of the radiative (k_f) and non-radiative (k_{nf}) decay rates that contribute to the transition from the excited state:

$$\tau_f = \frac{1}{k_f + k_{nf}} \tag{2}$$

As we shall see, FRET is a non-radiative quenching pathway by which a fluorophore in the excited state (*the donor*) can transition to the ground state by transferring energy to another nearby molecule (*the acceptor*) [15, 16]. This depletes the donor's excited-state energy, which quenches its emission and reduces its fluorescence lifetime. The change in the donor lifetime that occurs because of energy transfer can be quantified by FLIM.

2.1 A Brief History of FRET

Another of Gaviola's seminal contributions was his observation that the polarized emission from fluorescent dyes in solution decreases rapidly at concentrations above about three millimolars, while the intensity continues to increase with concentration [17, *reviewed in* 18]. In 1927, Jean-Baptiste Perrin proposed that the decreased polarization occurred because molecules in the excited state behave as oscillating dipoles that generate electric fields. He reasoned that the electric field of an excited donor molecule could allow energy to be transferred to other nearby acceptor molecules, resulting in depolarized emission (called *sensitized emission*) [19]. He presumed there was *exact resonance* between the molecules, but this was a misguided view that led him to propose that energy could be transferred over distances greater than the wavelength of the emitted light (>500 nm). Fortunately, Perrin's son Francis began work in his father's laboratory, and recognized that molecular collisions with the solvent would broaden the absorption and emission spectra of the fluorophores. This would decrease the probability of dipole–dipole interactions and reduce the distances over which energy could be transferred [20].

In 1943, Gregorio Weber, another talented Argentinean scientist, began his graduate studies with Malcolm Dixon, a well-known enzymologist at King's College in Cambridge. Since his thesis work would involve studies of the naturally fluorescent flavin and flavoprotein systems, Dixon suggested that he read the pioneering work of Francis Perrin on fluorescence depolarization [21]. Being fluent in French from his secondary education in Argentina, Weber understood not only the scientific content, but also appreciated the literary quality and clarity of thought in Perrin's work [22]. So, it was the earlier work of Perrin and Gaviola that set the stage for Gregorio Weber to make many critical contributions to modern fluorescence spectroscopy.

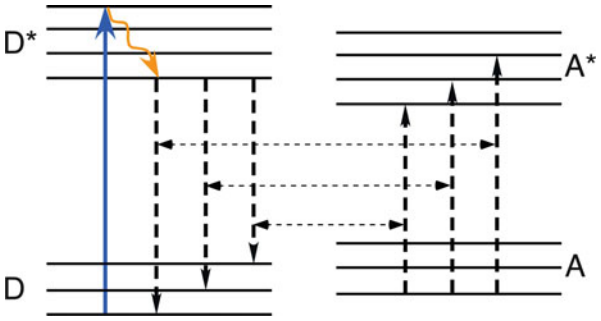

Fig. 2 A simplified FRET energy diagram showing the coupled transitions between the excited-state donor (D*) and an acceptor (A) molecule when they are in resonance

About this same time, Theodor Förster was applying the new quantum theory of the electronic structure of molecules to the problem of energy transfer during photosynthesis [18]. Förster also studied Perrin's work and he understood that energy transfer depends on the *spectral overlap integral* between the emission spectrum of the donor and the absorption spectrum of the acceptor [23]. He realized that the overlap determined the *probability* that the frequency-dependent oscillators will be in resonance. When resonance occurs, the energy difference for the deactivation of the donor will match the absorption transition of a nearby acceptor, allowing the efficient transfer of energy (Fig. 2). From this, Förster derived the expression describing how the efficiency of energy transfer (E_{FRET}) varies as the inverse of the sixth power of the separation distance (r):

$$E_{\mathrm{FRET}} = \frac{R_0^6}{\left(R_0^6 + r^6\right)} \tag{3}$$

R_0 is the *Förster distance* – the separation distance where energy transfer and donor emission occur with an equal probability. Förster's 1946 paper [*translated in* 23] provides a complete framework for understanding all FRET applications, and this is why we call it "Förster" resonance energy transfer [*reviewed in* 18].

After his graduate studies at Cambridge, Gregorio Weber moved to the University of Sheffield where he began characterizing the excitation polarization spectra of the aromatic amino acids in proteins. He realized the importance of Förster's work, as well as that of Arnold and Oppenheimer [24] that elaborated on Förster's studies of energy transfer during photosynthesis. The Professor (the appellation Weber favored) recognized that Förster's quantitative approach to energy transfer could be applied to the intermolecular transfer of energy among the aromatic amino acids. His work, published in 1960, was the first to demonstrate that electronic energy transfer between phenol and indole groups could be used to determine the distance between the molecules in proteins [25, 26].

2.2 FRET Microscopy

Since FRET occurs through near-field dipole interactions, the transfer of energy between donor and acceptor probes commonly used in biological studies ($R_0 \sim 50$ Å) is limited to separation distances less than about 80 Å (*see* Eq. 3). Thus, microscopy methods that can measure FRET have become valuable tools for investigating biochemical networks inside living cells. In 1976, Fernandez and Berlin were the first to demonstrate that a microscope capable of detecting FRET could be used to measure temporal variations in the distribution of labeled receptors on the surface of cells [27]. However, it was not until the early 1990s that progress in both microscope and detector technology enabled the development of FRET *imaging* techniques. In 1991, the laboratories of Roger Tsien and Susan Taylor developed a FRET-based *biosensor* to detect the activation of cyclic adenosine monophosphate (cAMP)-dependent protein kinase A (PKA) in living cells. They used ratio imaging of single living cells to measure the loss of the FRET signal that occurred when cAMP bound to PKA, causing the labeled subunits of the kinase to dissociate [28]. Then, in 1995 Thomas Jovin's group pioneered the use of FLIM to measure the FRET that occurred upon ligand binding to labeled epidermal growth factor receptors on the surface of single cells [29]. Since then, many different FRET microscopy approaches have been developed that are broadly subdivided into methods that detect either the sensitized emission from the acceptor or the effect of energy transfer on the donor [30].

2.3 Spectral Bleedthrough

Förster recognized that the efficient transfer of energy requires a strong overlap between the emission spectrum of the donor and absorption spectrum of the acceptor (Fig. 3). This, however, leads to significant background fluorescence, called spectral bleedthrough (SBT) that is detected in the FRET channel (donor excitation, acceptor emission; *see* Fig. 3). The SBT background originates from the direct excitation of the acceptor at donor excitation wavelengths (arrow, Fig. 3), as well as the bleedthrough of the donor emission into the FRET channel (hatching, Fig. 3). Therefore, the accurate measurement of FRET from the signal in the acceptor channel requires that you first remove the SBT background [30]. In contrast, the signal in the donor channel is not contaminated by SBT (Fig. 3). Thus, measurements of the effect of energy transfer on the donor signal do not require corrections and can be the most accurate way to quantify FRET. This is what FLIM does.

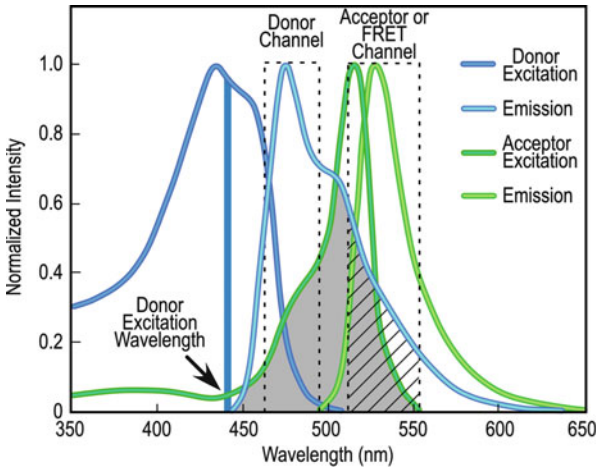

Fig. 3 The spectral overlap between donor and acceptor fluorophores that is required for FRET. The excitation and emission spectra for a *cyan* (donor) and *yellow* FP (acceptor) are shown, with the overlap between the donor emission and acceptor excitation spectra indicated by *shading*. The *dashed boxes* indicate typical detection channels for the donor and acceptor or FRET emission signals. The *arrow* indicates the direct acceptor excitation at the donor excitation wavelength, and the hatching shows the donor spectral bleedthrough into the acceptor (FRET) channel

3 Using Frequency Domain FLIM to Quantify Lifetimes

In 1962, Gregorio Weber moved to the University of Illinois at Urbana-Champaign where he set about improving the design for the phase fluorometer originally developed by Gaviola [17, 31]. The phase fluorometer uses a light source that is modulated at high radio frequencies to excite the probes. Since the excitation source is modulated, the emission from the fluorophores will also be modulated. Because of the persistence of the excited state, however, there is a *phase delay* (Φ) and a change in the *modulation* (M) of the emission signal relative to the corresponding excitation waveform (Fig. 4). The fluorescence lifetime (τ) can be determined *directly* from the Φ ($\tau_{(p)}$) and the M ($\tau_{(m)}$) of the emission signal for each excitation frequency:

$$\tau_{(p)} = \tan \Phi \text{ and } \tau_{(m)} = \sqrt{\frac{1}{M^2} - 1} \tag{4}$$

The phase fluorometer that Weber developed added a second, variable low frequency component to the main frequency to permit cross-correlation [31]. This improved the accuracy and reduced the noise when compared to measurements using only one frequency. His design, commercialized by Richard Spencer, David Laker, and George Mitchell (all had worked in Weber's laboratory and together formed the company SLM), became the first widely used phase fluorometer (the

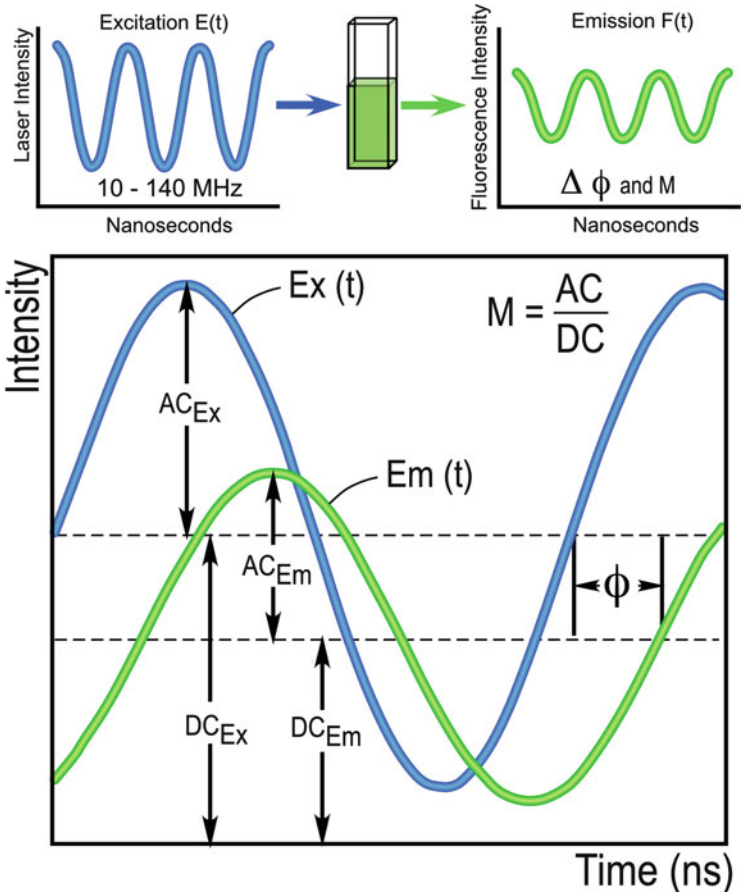

Fig. 4 Frequency domain FLIM measures the phase delay (Φ) and the change in the modulation (M) of the emission signal (Em) relative to the corresponding excitation waveform (Ex). The fluorescence lifetime can be determined from both the phase delay (Φ) and the change in modulation (M) of the emission signal for each excitation frequency

SLM 4800 series) [22]. In 1981, Weber developed an algorithm that allowed him to resolve the distinct lifetimes for two non-interacting fluorophores in solution, as well as their corresponding fractions [32]. However, more than two modulation frequencies are needed to resolve the component lifetimes that result from multi-exponential decays. In 1983, Enrico Gratton developed a multi-frequency phase fluorometer that operated over the range of 1–160 MHz [33]. Jameson and Gratton then developed their nonlinear least-squared approach to analyze the data and applied *phasor plots*, described below, to visualize complex lifetime decays [34].

3.1 Phasor Plots

The phasor plot is a simple geometric representation of the frequency characteristics of the signals resulting from repetitive excitations [34, 35; *reviewed in* 36]. Weber's algorithm [32] describes the Φ and the M of an emission signal as the Fourier transform components G and S of the fluorescence impulse response $I(t)$:

$$G = M \cos \Phi \text{ and } S = M \sin \Phi \quad (5)$$

The phasor plot maps the frequency characteristics from each image pixel to the G and S coordinates using *vectors* with angles specified by the Φ and lengths determined by M (*see* Fig. 5). For fluorophores with single-component decays, the relationship $M = \cos \Phi$ describes a vector with an endpoint falling somewhere on a *universal semicircle*, irrespective of the modulation frequency or lifetime. The distribution of lifetimes for a species with a short lifetime will fall to the right on the semicircle, while those with longer lifetimes will move to the left along the semicircle. Most importantly, phasor plots allow you to directly visualize complex lifetime decays without the need for any a priori knowledge of the system [34–38].

Here, frequency domain FLIM is used to measure the lifetimes for Coumarin 6 dissolved in ethanol and HPTS (8-hydroxypyrene-1,3,6-trisulfonic acid) dissolved in phosphate buffer (pH 7.8). The dyes are added to separate chambers on a coverglass, and confocal images are acquired using a 440 nm diode laser that is modulated at a fundamental frequency of 10 MHz, with 13 additional sinusoidal harmonic frequencies (20–140 MHz). The Φ and the M of the emission signals for both Coumarin 6 and HPTS are measured at each frequency, and the results are

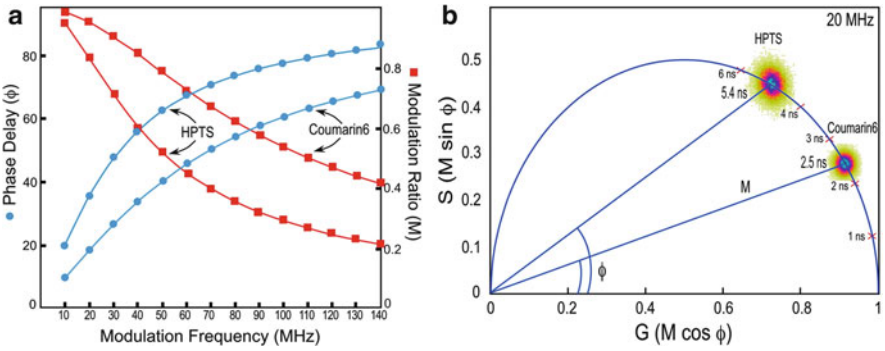

Fig. 5 (**a**) The multi-frequency response curves for Coumarin 6 and HPTS showing the phase delay (Φ) and the modulation ratio (M) measured at 14 different frequencies. (**b**) A composite phasor plot showing the distributions of the fluorescence lifetimes for Coumarin 6 and HPTS measured at 20 MHz. For Coumarin 6, the centroid of the distribution falls on the universal semicircle, indicating a single exponential lifetime of 2.5 ns. For HPTS, the distribution for the longer lifetime probe is shifted to the left along the semicircle. The centroid of the distribution falls on the semicircle, indicating a single exponential lifetime of 5.4 ns

represented by *multi-frequency response curves* (Fig. 5a). The fitting of the data demonstrates that the decays for both dyes are best characterized as single exponential. The distributions of lifetimes for both dyes measured at a single frequency (here, 20 MHz) are then represented on a composite phasor plot (Fig. 5b). The lifetime distribution for Coumarin 6 falls on the universal semicircle, indicating a single-component decay with an average lifetime of 2.5 ns (Fig. 5b). The lifetime distribution for HPTS, by contrast, is shifted to the left along semicircle relative to Coumarin 6 reflecting its longer lifetime. Again, the distribution falls on the semicircle, indicating a single-component lifetime of 5.4 ns (Fig. 5b).

3.2 Measuring FRET by FLIM

FLIM can be used to quantify the change in the donor lifetime that occurs as the result of FRET. Because the lifetime is determined from the donor signal, SBT corrections are unnecessary (*see* Fig. 3), making FLIM one of the most accurate ways to quantify FRET. The rate of energy transfer (k_T) is related to the donor lifetime (τ_D) by

$$k_T = \left(\frac{1}{\tau_D}\right)\left(\frac{R_0}{r}\right)^6 \tag{6}$$

where R_0 is the Förster distance for the fluorophore pair [39]. This relationship shows that the rate of energy transfer will equal the decay rate ($1/\tau_D$) when the separation distance (r) equals the R_0. The FRET efficiency (E_{FRET}) can therefore be determined from the change in the donor lifetime (τ_D) in the presence of an acceptor (τ_{DA}) as

$$E_{FRET} = 1 - \left(\frac{\tau_{DA}}{\tau_D}\right) \tag{7}$$

4 Using the Fluorescent Proteins (FPs) for FRET Measurements in Living Cells

The cloning of the green fluorescent protein (GFP) from the jellyfish *Aequorea victoria*, and its subsequent production in an astonishing array of organisms have revolutionized studies of cellular physiology [3]. Because the FPs are genetically encoded, they can be used to label any protein that can be produced in living cells or organisms. This has enabled new strategies to study the behavior of proteins in their natural physiological environment – something that Gregorio Weber would have

greatly appreciated. The sequence encoding the *Aequorea* GFP has been extensively engineered to yield new FPs that emit in the blue to yellow range of the visible spectrum. Additionally, many similar FPs that emit across the visible spectrum have been isolated from other marine species. The method of *directed evolution* through random and targeted mutagenesis has been applied with great effect to the FPs, generating many different monomeric (m) FPs with dramatically improved spectral and photophysical attributes [3].

For example, efforts to improve the photophysical characteristics of the enhanced cyan FP (ECFP) yielded a brighter variant called mCerulean [40]. However, mCerulean still has problems associated with photostability [41, 42], and photoswitching behavior [42, 43]. To address these shortcomings, mutagenesis was used to substitute residues that influence the planarity of the chromophore, yielding new cyan FPs called mCerulean3 [43] and mTurquoise [44]. The newer cyan FPs are brighter and more photostable than mCerulean and, notably for the FLIM measurements described below, have single-component fluorescence lifetimes [38]. Similarly, the earliest form of the enhanced yellow FP (EYFP) had deficiencies that were also addressed by directed mutagenesis. The resulting proteins, mVenus [45] and mCitrine [46] are significant improvements over EYFP and have proven to be excellent acceptors for FRET applications. These newer generation cyan and yellow FPs share the spectral overlap required for efficient energy transfer (*see* Fig. 3), and the improved photophysical characteristics make them most useful for the measurement of FRET by FLIM [38].

4.1 Validating the Measurement of FRET by FLIM

Genetically encoded *FRET standards* have been developed as a straightforward approach to verify measurements made by FRET microscopy. The original FRET standards are fusion proteins that consist of mCerulean (the donor) coupled to mVenus (the acceptor) through linkers of varying length [47, 48]. To improve the utility of the FRET standards for FLIM, we replaced mCerulean with mTurquoise, because of its single-component lifetime [38]. When making FLIM measurements in living cells it is important to recognize that the environment will always cause some quenching of the fluorophores. Therefore, it is *critical* to determine the donor lifetime (τ_D) in the same cellular environment from which FRET will be measured. For the FRET standards (as well as the similarly designed *biosensor probes*), this can be achieved by mutating the acceptor FP. For example, converting the chromophore tyrosine of mVenus to cysteine (mVenusY67C) generates a non-fluorescent protein called Amber, which folds correctly but cannot act as a FRET acceptor [48]. The mTurquoise–Amber fusion protein produced in living cells provides an accurate measurement of τ_D within the subcellular environment.

Here, living cells expressing FRET standard proteins consisting of mTurquoise coupled to mVenus through linkers with length varying between 5 and 46 amino acids (aa) are used to demonstrate FRET-FLIM measurements. Representative

results for the donor-alone standard mTurquoise-5aa-Amber (T5A), a high E_{FRET} standard mTurquoise-5aa-Venus (T5V), and a low E_{FRET} standard mTurquoise-46aa-Venus (T46V) are compared using a composite phasor plot (Fig. 6). The average lifetime for the donor-alone standard (T5A) was 3.84 ns (Table 1), and its lifetime distribution falls on the semicircle, indicating a single-component decay (Fig. 6b). In striking contrast the lifetime distribution for the high-FRET standard T5V is shifted to the right on the phasor plot relative to T5A, indicating its shorter (quenched) lifetime (Fig. 6b). The lifetime distribution for the low FRET standard, T46V, falls between that for T5A and T5V on the phasor plot (Fig. 6b).

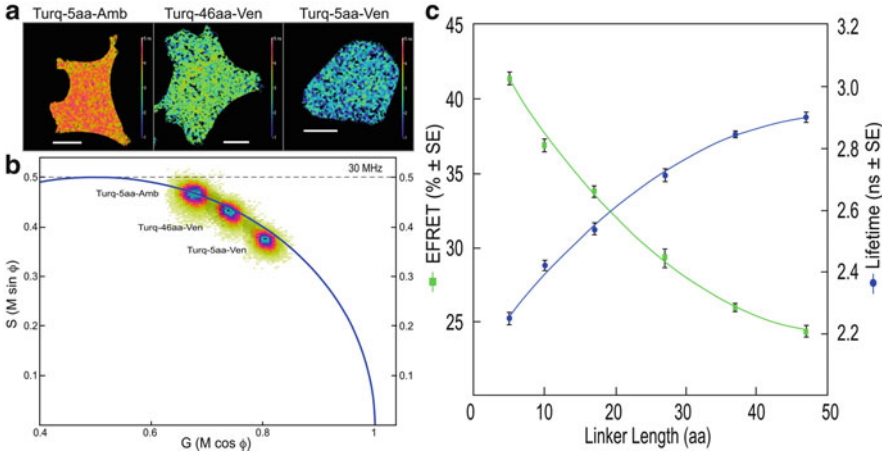

Fig. 6 The FLIM analysis of the FRET standards produced in living cells. (**a**) The lifetime maps showing the distribution of lifetimes in living cells expressing Turquoise-5aa-Amber (unquenched donor), Turquoise-46aa-Venus, or Turquoise-5aa-Venus (the calibration bars are 10 μm). (**b**) The phasor plot analysis measured at 30 MHz for the cells shown in panel (**a**). (**c**) The lifetimes and FRET efficiencies determined from regions of interest in multiple cells expressing each of the different FRET standards (*see* text and Table 1)

Table 1 FLIM analysis of FRET standards

FRET standard[a]	2-Component lifetime (fraction)	Tau[b] (±SEM)	χ^{2c}	E_{FRET}[d]
Turquoise-5aa-Amber	3.84 (0.99)	3.84 ± 0.01	8.8	NA
Turquoise-5aa-Venus	3.29 (0.66) 1.43 (0.34)	2.25 ± 0.02	1.4	41.4 ± 0.4
Turquoise-10aa-Venus	3.34 (0.69) 1.48 (0.31)	2.42 ± 0.01	1.3	36.9 ± 0.4
Turquoise-17aa-Venus	3.44 (0.67) 1.58 (0.33)	2.54 ± 0.01	1.2	33.8 ± 0.3
Turquoise-27aa-Venus	4.03 (0.49) 2.05 (0.51)	2.71 ± 0.02	1.9	29.3 ± 0.6
Turquoise-36aa-Venus	2.61 (0.81) 4.39 (0.19)	2.85 ± 0.01	2.6	25.9 ± 0.2
Turquoise-46aa-Venus	2.84 (0.78) 5.32 (0.22)	2.90 ± 0.01	2.3	24.3 ± 0.3

[a]Produced in living cells and measured at 37°, 5% CO_2; $n = 15$ or more
[b]Tau is the average intensity weighted lifetime for Turquoise-5 aa-Amber. The average amplitude-weighted lifetime is used for all others
[c]Average Chi-square value from n measurements using 12 frequencies (10–120 MHz)
[d]Determined by $E_{FRET} = 1 - (\tau_{DA}/\tau_D)$, where τ_D is the lifetime of Turquoise-5aa-Amber (3.84 ns)

The lifetime distributions for both the low and high E_{FRET} standards also fall inside the semicircle, which indicates the presence of more than one lifetime component [36]. The reason these linked FRET probes have multi-component lifetimes is that the FPs rotate slowly relative to their fluorescence lifetime. Therefore, there can be little averaging of the dipole orientations during the excited state, which leads to a distribution of orientations and thus FRET efficiencies [49]. When determining FRET efficiency from multi-exponential lifetimes the amplitude-weighted lifetime is used [39]. The amplitude-weighted lifetime for T5V is 2.25 ns, which corresponds to an average E_{FRET} of 41%, whereas the 2.90 ns lifetime for T46V equates to an average E_{FRET} of 24% (Table 1). The results in Fig. 6c and Table 1 show the remarkably tight relationship between the donor lifetime (and therefore E_{FRET}) and the length of the intervening linker for the series of standards with progressively longer linkers. The linkers in our FRET standards are rich in glycine, which provides flexibility, and serine and threonine, which provide conformational stability. The shape of the curve in Fig. 6c reflects the flexibility of the longer linkers. Together, these results show that the frequency domain FLIM approach is an extremely sensitive and accurate method for quantifying FRET measurements.

4.2 *Measuring Protein Interactions in Their Natural Environment*

Gregorio Weber was a pioneer in studies of protein dynamics, and much of his career was dedicated to understanding how proteins interact, culminating in 1992 with the publication of his book *Protein Interactions* [50]. The Professor recognized that proteins are the "site of *lively* spontaneous dynamics" induced by changes in their environment, behaving as "kicking and screaming stochastic molecules" in solution [50, 51]. He anticipated that future knowledge relating protein function to structural dynamics would need to come from studies of "proteins as integrated systems possessing certain biological and physical properties" [50].

Here, FRET-FLIM is used to measure the interactions that occur between the basic-leucine zipper (BZip) domain of the transcription factor C/EBPα and the heterochromatin protein 1 alpha (HP1α) in the nuclei of living cells. In earlier studies, we demonstrated that HP1α and C/EBPα interact, but only when the proteins are bound to heterochromatin [38, 52]. For these intermolecular FRET measurements the lifetime for the C/EBPα BZip domain labeled with mTurquoise (donor alone) was measured in regions of heterochromatin (typically 5–10 ROI per cell nucleus) for ten different cells, yielding an average donor lifetime (τ_D) of 3.89 ns. Intensity images and lifetime measurements were then acquired from cells co-producing the mTurquoise-BZip domain, and HP1α labeled with Venus (Fig. 7a). As a control for potential non-specific interactions, measurements were

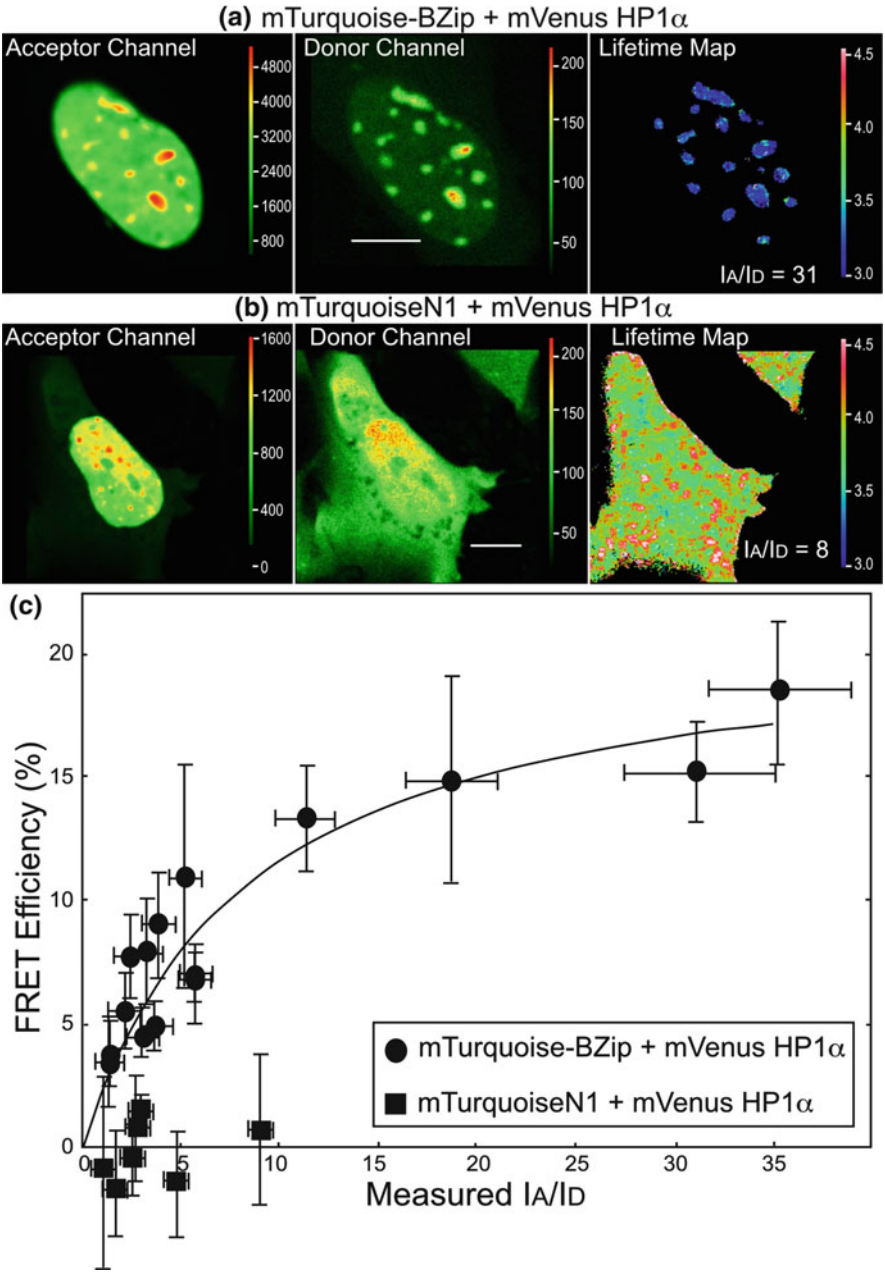

Fig. 7 The quantification of FRET occurring between the C/EBPα BZip domain and HP1α in the nuclei of living cells. (**a**) The intensity images acquired of the nucleus of a cell expressing both the mTurquoise-BZip domain (donor channel; the calibration bars are 10 μm) and mVenus-HP1α (acceptor channel), and the corresponding lifetime map with the acceptor to the donor (I_A/I_D) ratio indicated. (**b**) The intensity images acquired of a cell expressing both the mTurquoiseN1 (localized throughout the cytoplasm and nucleus; the donor channel) and mVenus-HP1α (nuclear; the acceptor channel), and the corresponding lifetime map with the I_A/I_D ratio indicated. (**c**) FLIM

also made from cells producing the mTurquoiseN1 protein (localized in both cytoplasm and nucleus) and Venus-HP1α (nuclear, see Fig. 7b). The lifetime map in Fig. 7b demonstrates the quenched lifetimes of the Turquoise-BZip domain co-expressed with the Venus-labeled HP1α, indicated by cooler colors on the look-up table. In contrast, the lifetime of the TurquoiseN1 protein was unchanged when co-expressed with Venus-HP1α (Fig. 7b). To characterize the interaction between mTurquoise-BZip domain proteins and Venus-HP1α the E_{FRET} was determined from lifetime measurements of 15 cells co-producing the proteins at different acceptor to donor (I_A/I_D) ratios (Fig. 7c). The results show the dependence of E_{FRET} between BZip domain and HP1α in regions of heterochromatin on the I_A/I_D ratio, indicating the fluorophores labeling the proteins are in close proximity (Fig. 7c). In contrast, there was no change in the lifetime of mTurquoiseN1 with increasing Venus-HP1α.

5 Concluding Remarks

Gregorio Weber understood the importance of studying proteins as integrated systems. In this regard, labeling proteins in their natural environment with the genetically encoded FPs has enabled new strategies to investigate the function and dynamics of proteins in their natural environment [3]. The combination of the FPs and lifetime imaging described here provides a sensitive method to quantify FRET, allowing changes in protein conformation (e.g., biosensor probe activities) or protein interactions (intermolecular FRET) to be monitored inside living cells and organisms. A general limitation to the FRET-FLIM approach is the necessity of producing the proteins of interest labeled with the FPs inside living cells. This can lead to artifacts associated with overexpression that could potentially interfere with cellular processes. Therefore, any approach that involves the expression of exogenous proteins requires careful control experiments to verify protein function and behavior. Significantly, FLIM is not limited to the detection of exogenously labeled proteins, and is being used in novel ways to monitor intrinsic auto-fluorescence signals from living cells. Phasor plots of cellular auto-fluorescence, for example, have been used to generate "fingerprints" that identify the unique metabolic states of cells in different stages of differentiation or of cancer cells [53, 54]. Most notably, the measurements obtained from proteins in their natural environment inside living cells provide the most physiologically relevant information about protein behavior currently available.

Fig. 7 (continued) was used to measure the donor lifetime in multiple ROI for each cell, and the FRET efficiency (%) was determined for each ROI using Eq. (7). Each point represents the average E_{FRET} (±SD) and the average I_A/I_D (±SD) for multiple ROI in individual cells expressing the indicated donor- and acceptor-labeled proteins [Reprinted from 38]

Acknowledgements This chapter is dedicated in memory of Dr. Robert (Bob) M. Clegg, a colleague of Gregorio Weber at the University of Illinois at Urbana-Champaign. In 2011, Bob presented a lecture entitled "History of trials, blunders, tribulations and finally success in the dark ages of fluorescence lifetime measurements" that contained many historical insights referenced here. The author thanks Drs. Yuansheng Sun and Shih-Chu (Jeff) Liao (ISS Inc., Champaign, IL) for their advice and technical help with FLIM, Michael Davidson (FSU) for providing plasmids encoding the FPs, and Dr. Jing Qi for excellent laboratory support.

References

1. Pliny, Bostock J, Riley HT (1855) The natural history of Pliny, Book XXXII. Remedies derived from aquatic animals. Chapter 52—Other aquatic productions. Adarca or Calamochnos: three remedies. Reeds: eight remedies. The ink of the sæpia. Gaius Plinius Secundus (Pliny the Elder). AD77. Bohn's classical library. H.G. Bohn, London
2. Phipson TL (1862) Phosphorescence, or, the emission of light by minerals, plants, and animals. L. Reeve, London
3. Day RN, Davidson MW (2014) The fluorescent protein revolution. Series in cellular and clinical imaging. Taylor & Francis, Boca Raton
4. Periasamy A, Clegg RM (2010) FLIM microscopy in biology and medicine. CRC Press, Boca Raton
5. Elson DS, Marcu L, French PMW (2014) Fluorescence lifetime spectroscopy and imaging. Principles and applications in biomedical diagnostics. CRC Press, Taylor & Francis Group, Boca Raton
6. Berezin MY, Achilefu S (2010) Fluorescence lifetime measurements and biological imaging. Chem Rev 110(5):2641–2684
7. Becquerel AE (1867) La Lumière, ses cause et ses effets, tome 1: sources de lumière. Didot, Paris
8. Nichols EL, Merritt E (1912) Studies in luminescence. The Carnegie Institution of Washington, Publication 152. Gibson Brothers Press, Washington
9. Wood RW (1921) The time interval between absorption and emission of light in fluorescence. Proc R Soc London Ser A 99(700):362–371
10. Gottling PF (1923) The determination of the time between excitation and emission for certain fluorescent solids. Phys Rev 22:566–573
11. Bohr N (1913) On the constitution of atoms and molecules. Philos Mag Ser 6 26:1–25
12. Abraham H, Lemoine J (1899) Disparition instantanée du phénomène de Kerr. Comptes rendus hebdomadaines des seances de academic des sciences. Sci Nat 129:206–208
13. Rayleigh L (1904) On the measurement of certain very short intervals of time. Nature 69 (1798):560–561
14. Gaviola E (1926) The time decay of the fluorescence of dye solutions. Ann Phys (Leipzig) 81:681–710
15. Förster T (1965) Delocalized excitation and excitation transfer. In: Sinanoglu O (ed) Modern quantum chemistry. Academic, New York, pp 93–137
16. Stryer L (1978) Fluorescence energy transfer as a spectroscopic ruler. Annu Rev Biochem 47:819–846
17. Gaviola E (1926) Die Abklingungszetem der Fluoreszenz. Ann Phys 386(23):681–710
18. Clegg RM (2006) The history of FRET. In: Geddes CD, Lakowicz JR (eds) Reviews in fluorescence. Springer Science+Business Media Inc., New York, pp 1–145
19. Perrin J (1927) Fluorescence et induction moleculaire par resonance. CR Hebd Seances Acad Sci 184:1097–1100

20. Perrin F (1932) Théorie quantique des transferts ďactivation entre molécules de méme espèce. Cas des solutions fluorescentes. Ann Chim Phys 17:283–314
21. Perrin F (1926) Polarisation de la lumière de fluorescence. Vie moyenne des molécules dans l'état excité. J Phys 7:390–401
22. Jameson DM (2001) The seminal contributions of Gregorio weber to modern fluorescence spectroscopy. In: Valeur B, Brochon J-C (eds) New trends in fluorescence spectroscopy. Springer, Berlin, pp 35–58
23. Förster T (2012) Energy migration and fluorescence. 1946. J Biomed Opt 17(1):011002
24. Arnold W, Oppenheimer JR (1950) Internal conversion in the photosynthetic mechanism of blue-green algae. J Gen Physiol 33:423–435
25. Weber G (1960) Fluorescence-polarization spectrum and electronic-energy transfer in tyrosine, tryptophan, and related compounds. Biochem J 75:335–345
26. Weber G (1960) Fluorescence-polarization spectrum and electronic-energy transfer in proteins. Biochem J 75:345–352
27. Fernandez SM, Berlin RD (1976) Cell surface distribution of lectin receptors determined by resonance energy transfer. Nature 264(5585):411–415
28. Adams SR, Harootunian AT, Buechler YJ, Taylor SS, Tsien RY (1991) Fluorescence ratio imaging of cyclic AMP in single cells. Nature 349(6311):694–697
29. Gadella TW Jr, Jovin TM (1995) Oligomerization of epidermal growth factor receptors on A431 cells studied by time-resolved fluorescence imaging microscopy. A stereochemical model for tyrosine kinase receptor activation. J Cell Biol 129(6):1543–1558
30. Periasamy A, Day RN (2005) Molecular imaging: FRET microscopy and spectroscopy. The American physiological society methods in physiology series. Oxford University Press, New York
31. Spencer RD, Weber G (1969) Measurements of subnanosecond fluorescence lifetimes with a cross-correlation phase fluorometer. Ann N Y Acad Sci 158:361–376
32. Weber G (1981) Resolution of the fluorescence lifetimes in a heterogeneous system by phase and modulation measurements. J Phys Chem 85:949–953
33. Gratton E, Limkeman M (1983) A continuously variable frequency cross-correlation phase fluorometer with picosecond resolution. Biophys J 44(3):315–324
34. Jameson DM, Gratton E, Hall RD (1984) The measurement and analysis of heterogeneous emissions by multifrequency phase and modulation fluorometry. Appl Spectrosc Rev 20 (1):55–106
35. Redford GI, Clegg RM (2005) Polar plot representation for frequency-domain analysis of fluorescence lifetimes. J Fluoresc 15(5):805–815
36. Eichorst JP, Wen Teng K, Clegg RM (2014) Polar plot representation of time-resolved fluorescence. Methods Mol Biol 1076:97–112
37. Hinde E, Digman MA, Welch C, Hahn KM, Gratton E (2012) Biosensor Forster resonance energy transfer detection by the phasor approach to fluorescence lifetime imaging microscopy. Microsc Res Tech 75(3):271–281
38. Day RN (2014) Measuring protein interactions using Forster resonance energy transfer and fluorescence lifetime imaging microscopy. Methods 66:200–207
39. Lakowicz JR (2006) Principles of fluorescence spectroscopy, 3rd edn. Springer, New York
40. Rizzo MA, Springer GH, Granada B, Piston DW (2004) An improved cyan fluorescent protein variant useful for FRET. Nat Biotechnol 22(4):445–449
41. Shaner NC, Steinbach PA, Tsien RY (2005) A guide to choosing fluorescent proteins. Nat Methods 2(12):905–909
42. Shaner NC, Lin MZ, McKeown MR, Steinbach PA, Hazelwood KL, Davidson MW, Tsien RY (2008) Improving the photostability of bright monomeric orange and red fluorescent proteins. Nat Methods 5(6):545–551
43. Markwardt ML, Kremers GJ, Kraft CA, Ray K, Cranfill PJ, Wilson KA, Day RN, Wachter RM, Davidson MW, Rizzo MA (2011) An improved cerulean fluorescent protein with enhanced brightness and reduced reversible photoswitching. PLoS One 6(3), e17896

44. Goedhart J, van Weeren L, Hink MA, Vischer NO, Jalink K, Gadella TW Jr (2010) Bright cyan fluorescent protein variants identified by fluorescence lifetime screening. Nat Methods 7 (2):137–139
45. Nagai T, Ibata K, Park ES, Kubota M, Mikoshiba K, Miyawaki A (2002) A variant of yellow fluorescent protein with fast and efficient maturation for cell-biological applications. Nat Biotechnol 20(1):87–90
46. Griesbeck O, Baird GS, Campbell RE, Zacharias DA, Tsien RY (2001) Reducing the environmental sensitivity of yellow fluorescent protein. Mechanism and applications. J Biol Chem 276(31):29188–29194
47. Thaler C, Koushik SV, Blank PS, Vogel SS (2005) Quantitative multiphoton spectral imaging and its use for measuring resonance energy transfer. Biophys J 89(4):2736–2749
48. Koushik SV, Chen H, Thaler C, Puhl HL 3rd, Vogel SS (2006) Cerulean, Venus, and Venus Y67C FRET reference standards. Biophys J 91(12):L99–L101
49. Vogel SS, Nguyen TA, van der Meer BW, Blank PS (2012) The impact of heterogeneity and dark acceptor states on FRET: implications for using fluorescent protein donors and acceptors. PLoS One 7(11), e49593
50. Weber G (1992) Protein interactions. Chapman and Hall, New York
51. Weber G (1975) Energetics of ligand binding to proteins. Adv Protein Chem 29:1–83
52. Siegel AP, Hays NM, Day RN (2013) Unraveling transcription factor interactions with heterochromatin protein 1 using fluorescence lifetime imaging microscopy and fluorescence correlation spectroscopy. J Biomed Opt 18(2):25002
53. Stringari C, Cinquin A, Cinquin O, Digman MA, Donovan PJ, Gratton E (2011) Phasor approach to fluorescence lifetime microscopy distinguishes different metabolic states of germ cells in a live tissue. Proc Natl Acad Sci U S A 108(33):13582–13587
54. Wright BK, Andrews LM, Markham J, Jones MR, Stringari C, Digman MA, Gratton E (2012) NADH distribution in live progenitor stem cells by phasor-fluorescence lifetime image microscopy. Biophys J 103(1):L7–9

The Impact of Laser Evolution on Modern Fluorescence Spectroscopy

Jianhua Xu and Jay R. Knutson

Abstract The judicious use of traditional spectroscopy light sources throughout the postwar era led to the foundations of fluorescence spectroscopy, both theoretically and experimentally. Those principles provided many tools for understanding the structure and dynamics of macromolecules, cells, and even tissues. In the last four decades those tools have been supplemented and sometimes extended by the availability of novel light sources, advanced electronics, and burgeoning computing power. This chapter will chronicle the former – the impact of four decades of laser evolution upon biological fluorescence spectroscopy and microscopy. It is necessarily focused on only the systems that were most popular and influential (many other sources were of great value) and (for space concerns) it also summarizes only a few of the many linked technological advances.

Keywords Femtosecond • Laser • Picosecond • Tunable • Ultrafast

Contents

J. Xu
LMB, NHLBI, NIH, Bldg. 10 Rm. 5D-14 NIH, Bethesda, MD 20892-1412, USA

J.R. Knutson (✉)
Optical Spectroscopy Section, LMB, NHLBI, NIH, Bldg. 10 Rm. 5D-14 NIH, Bethesda, MD 20892-1412, USA
e-mail: knutsonj@helix.nih.gov

D.M. Jameson (ed.), *Perspectives on Fluorescence: A Tribute to Gregorio Weber*, Springer Ser Fluoresc (2016) 17: 163–178, DOI 10.1007/4243_2016_21,

1 Comparing Lasers to Other Light Sources

In order to understand the impact of lasers, it is necessary to understand their advantages over the traditional sources of light for fluorescence spectroscopy. Laser light is generated by stimulated emission within a resonating structure, and this can imbue the emitted light with many unique features.

1.1 Brightness

When lasers first became known in the popular press, the catchphrase that drew the greatest attention was that in the laboratory, with large and complex equipment, it was now possible to generate light "brighter than the surface of the sun" [1]. Replacing the popular term "brightness" with the term "luminance" (i.e., candela/m^2), one finds the sun has about 1.6×10^9 cd/m^2 of (human eye-weighted) "brightness" and an "illuminance" of ~100 klux. Using the peak of green sensitivity, it takes only about 1.5 mW/m^2 to make one lux – or 0.15 mW/cm^2 to make one klux = 10^3 lux. To make the solar equivalent of 10^5 lux, one requires only 15 mW/cm^2. Common laser pointers purchased by children now create 3 mm spots that exceed this, even with the safety limits holding them below 3 mW.

In spectroscopy, the power in **watts** (radiometric rather than eye-centric units) is the key; lasers *with tens to hundreds of watts* of average power are now available to the researcher. To compare, arc lamp sources typically deliver hundreds of microwatts when collimated and filtered down into few-nm bandwidths. We will discuss the time structure of the power below.

1.2 Spectral Purity

Before lasers, the purity of excitation light could be achieved by either (1) selecting a gas arc lamp whose weak emission was dominated by atomic transitions (and broadened at minimum by the Maxwell–Boltzmann velocities therein), or (2) spectral filtering of broader and brighter sources, e.g., the xenon arc lamp. In biological fluorescence, the Xe (or Xe/Hg) arc lamp, passed through one or two stage monochromators, has been the workhorse since WWII. Transmitted power is often

directly proportional to spectral width in such a system, demanding compromise. One percent of bandwidth was typical in common steady state fluorophotometry use.

Lasers, in contrast, have intrinsic linewidths determined by the gain media (sometimes using the narrow atomic transitions mentioned above) reduced by the internal frequency selecting elements of the cavity. Tuning elements can be traversed hundreds of times by the recirculating photons, each pass sharpening the spectrum. A wide variety of internal elements are available. Most lasers used by the biophysicist are broad (i.e., 0.5% bandwidth) simply because we seldom need better. In other fields requiring long coherence lengths, locking to atomic vapor standards, etc., the combination of high quality factor resonators, grazing incidence grating feedback, passive elements like Fabry–Perot etalons, and active cavity length feedback quite easily provides ppb purity.

1.3 Collimation

Spectral sources for spectroscopy other than lasers carried simple optical properties. The arc or filament or spark had a particular size and radiance, and only lens and aperture formulas would determine the power you could focus – if the elements were perfect. Short paths were mandatory, since the size (and therefore cost and complexity) of the optics grew with length to maintain efficiency.

Lasers, on the other hand, were limited only by the geometric quality of the resonator and the formulae for light propagation. Fifty some years ago, the accomplishment of a laser creating kilometer sized spots on the moon was touted. Meter accuracy is now standard. More practically, a modern laser source can traverse multiple optical elements in the spectroscopy or microscopy laboratory, yet focus with nanometric accuracy.

1.4 Spectral Versatility

This has always been the place where one could say “Advantage: Xenon.” The initial offerings for lasers in the laboratory were sparse, and frequency conversion became a priority. Lasers were used to pump other lasers having gain in desired regions, most notably dye lasers. In the NIR, a paucity of dyes was answered by cryogenic color center lasers for a time. Once the visible/NIR dye emissions were available, a few percent of their output could be produced in the UV via SHG (Second Harmonic Generation – the nonlinear response certain non-centrosymmetric crystals provided for intense focused visible light).

[Aside: What is SHG?]: The intense electric fields of focused laser light cause electrons in a transparent crystal to oscillate with the lightwave; in some crystals the springlike Coulomb forces holding the electrons in place are asymmetric and nonuniform with power applied. This causes the electrons to not only oscillate in the original direction (e.g., vertically) but also, by tracing double figure-eights, horizontally. Oscillating electrons create light; in this case, at half the wavelength/twice the frequency.

2 Laser Sources for Fluorometry

Four or more decades ago, the lasers that became widely available in the fluorescence community were based on either noble gas discharge (e.g., Ar+ or Kr+) within ceramic capillaries or on the popular Nd+/glass or YAG transition found near 1.06 u. The former offered a variety of lines spaced in the visible, with weaker emissions in the UV and NIR. Some of the visible lines (e.g., 514 nm) could be *modelocked* and this provided the short-pulse excitation appropriate for TCSPC and other pulse fluorometric methods (Fig. 1).

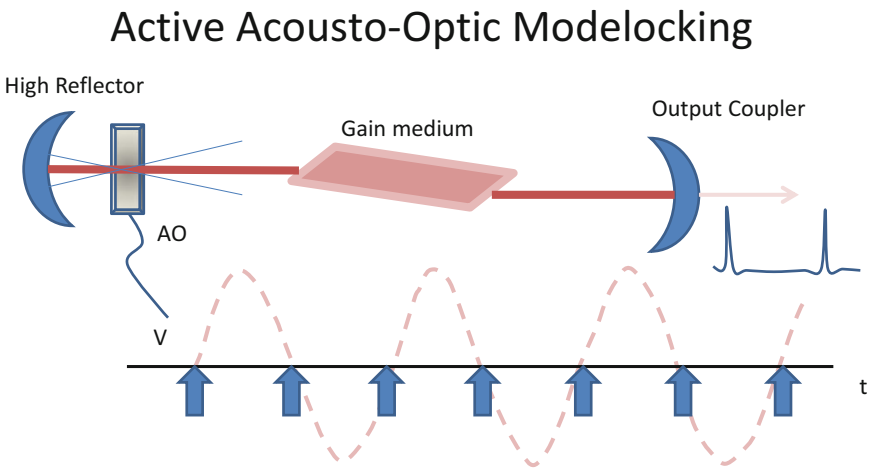

Fig. 1 The resonant crystal is driven with a sinusoidal voltage pattern to diffract the intracavity beam. *Arrows* indicate times when rear mirror reflectivity is optimal; pulses recirculating to match these times will be amplified and shortened while mistimed light is diffracted out of the cavity path

[Aside: What is modelocking?]: Light in a laser cavity makes round trips at the repetition rate (typically twice the cavity length divided by the speed of light) and, during each pass, the photons grab followers in the gain medium and lose some to either imperfect optics or optics meant to leak ("output coupler"). This is a random process unless the loss or gain can be modulated at the repetition rate. If the net gain peaks at the same time in a pass each time, only photons in that brief interval will survive/grow through many round trips; the pulse evolves to be shorter to select the best gain moments.

Of course, gas laser beams could also be directly modulated with Pockel's cells at hundreds of MHz, and these lines therefore fueled the rapid growth of multifrequency phase fluorometry in the early 1980s [cf. 2]. The HeCd laser became a popular source near 325 nm in the first "Greg200" series of commercial instruments for this purpose. If the Ar+ or Kr+ cavity was locked with acousto-optic modulators to yield ca. 100 ps pulses, this generated intrinsic modulation at multiples of the lock frequency. More important, the modelocked gas laser beams were useful to ***synchronously*** pump dye lasers sharing the cavity length of the pump, providing tunable emission over significant (~50 nm) ranges and a reliable source for SHG beams in the near UV. The acousto-optic active modelocker was popular; alternatively, the gas cavities could be modelocked by the saturable transient absorbance of the dye stream itself to create sub-ps dye pulses [3].

[Aside: What is a saturable absorber?]: Einstein derived the equations for saturating a two level optical transition to solve theoretical questions about black body radiation in the early days of quantum physics. Essentially, a pot of colored molecules can become transparent – albeit briefly – if intense light drives almost all of them to their upper (sometimes fluorescent) state. If the saturable transient absorber is inside a laser cavity, this transient transparency will occur at the round trip rate of intense pulses and act to modelock them (ibid.)] . . .

In contrast to gas lasers with many visible lines, Nd+ provided only narrow 1 u output, but often with sufficient intensity to yield watt-level harmonics at 532, 355, and 266 nm. The most popular lasers in this Nd+ gain medium (popular even now) were flashlamp (more recently diode) pumped and Q-switched to yield pulses in the 2 J range at ~10 Hz repetition rate. They could also be passively modelocked and/or amplified, and they had both average and peak powers appropriate for Raman conversion in suitable gases. These versatile and robust workhorses were used in various forms across ultrafast fluorescence, e.g., to do the earliest fluorescent upconversion [4], practical transient absorbance [5], and myriad other applications. For biophysical time and phase-resolved fluorometry, however, the 10-30Hz repetition rate of these systems was a major limitation. Too much power was being

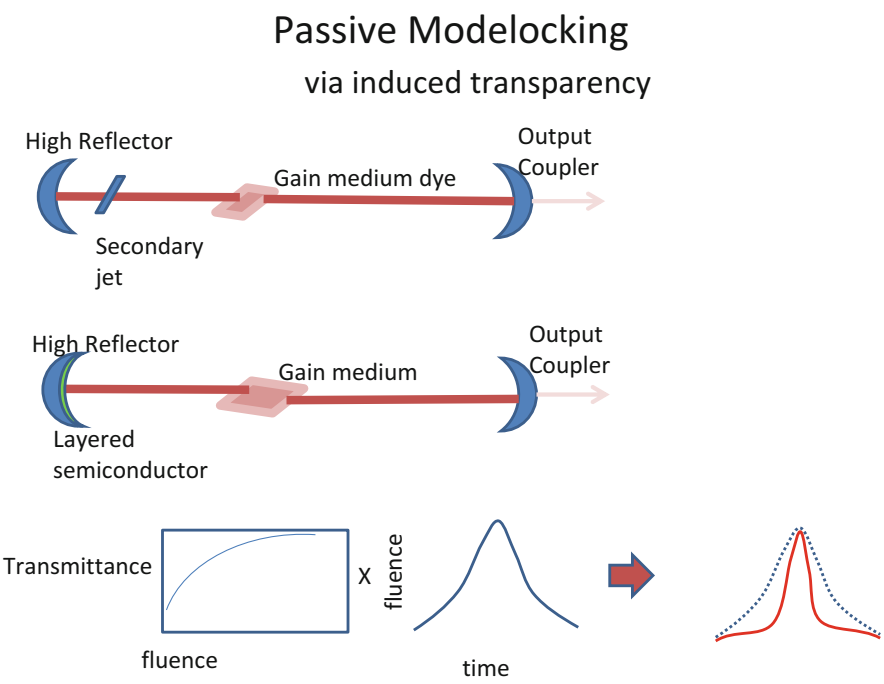

Fig. 2 Passive modelocking occurs when high peak power pulses induce transparency in a cavity element, improving net gain at peak times–while lower powers at other times experience more loss

applied to biological samples with a tiny duty cycle. In Time-Correlated Single Photon Counting (TCSPC), the pileup phenomenon [6] limited counting to a few Hz in such systems (impractical for biological samples) and the timing of the pulses was not reliable enough for phase fluorometry. The Streak Camera approach was successful for high yielding samples that could tolerate the concentrated flux [7]. In the UV, a lesser but important role was played by the sub-100 Hz N2 gas laser that emitted ns pulses upon spark-gap discharge, centered near 337 nm. These inexpensive lasers could even be home built with inexpensive components (e.g., hacksaw blades: [8]) and they were used to pump simple cuvette – based dye lasers for ~100 ps pulses [9, 10] (Fig. 2).

All of these low repetition rate systems had high peak powers and low duty cycles, making them stars in chemistry but less popular in biophysical fluorescence; we will skip them in the remainder of this chapter.

The actively mode-locked Ar+ (or Kr+) laser, synchronously pumping a tunable dye laser (e.g., Rh6G or DCM in Ethylene Glycol/Propylene Carbonate viscous carrier jets) solved many of these problems. At first, the full repetition rate of such lasers was employed [2, 11, 12] but the appearance in the commercial market of acousto-optic cavity dumping for synchronous dye cavities in the early 1980s both increased the power per pulse and reduced repetition rates to near-ideal values for

each of those methods (~4 MHz). For phase fluorometry, the realization (gleaned from synchrotron bunch removal) that imperfect pulse switching was not troublesome [13, 14] made this particularly useful.

[Aside: What is Cavity Dumping?]: If instead of constant (typically 10%) loss to output coupling, one had a laser cavity bounded by high reflectors, internal powers built to ~100× greater peaks. A transparent element in this cavity could either switch the polarization (electrooptic "Pockels" cell) or direction (acousto-optic transient grating "Bragg" cell) during a pass to switch the pulse out of the cavity. Several gain passes later, the cavity that was "dumped" would recover full power.

Soon thereafter (mid-1980s), the Continuous Wave pumping of a modelocked Nd + YAG (or YLF) gain cavity with AO modelocking and external SHG yielded more powerful (>1 W) 53 u green pump sources at 76 or 80 MHz producing ~80 ps pulses for synchronous dye pumping. These robust synch-pumped dye systems drove much of the TCSPC and Phase fluorometric research community [cf. 15] – for almost 15 years until the arrival of Ti:Sapphire. In that decade plus, the stability and pulsewidth of such YAG/dye systems improved, partly because the Semiconductor Saturable Absorber Modelocking (SESAM) method of [16] was adapted to 1.05 u, making them produce sub 10 ps pulses rather than AO modelocked ~100 ps trains (e.g., "Vanguard" from S/P, Oscillator from Lightwave). Synchronous pumping improved, yielding sub-ps "femtosecond" dye performance (rather than original ~5 ps dye pulses from 100 ps synch pumps – although we note those 5 ps visible pulses were sometimes fiber-stretched and compressed. Alternatively, the intense 1 um pulses could themselves be stretched and compressed to a few ps before pumping the dye (e.g., "S/P 3800"). Secondary jets within the dye laser cavity could also (via transient absorbance "trimming") shorten pulse durations (e.g., in "Coherent 702") or transient absorbers could be mixed into the primary dye stream (e.g., "Kiton Red" or "DQOCI" in S/P 3500). It is important to remember that much of the early work in two-photon fluorometry for eventual multiphoton microscopy came from these ~700 fs visible and NIR dye systems [17] (Fig. 3).

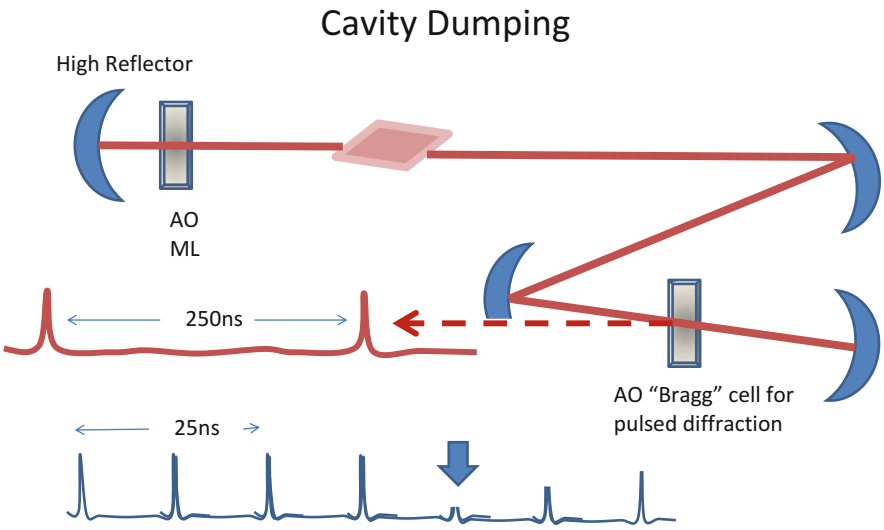

Fig. 3 Cavity dumping (shown here using Acousto-Optic deflection) extracts the full intracavity power of the recirculating pulse. The cavity recovers full power a few round-trips later

Ti:Sapphire is a gain medium that cannot be synch-pumped like dye, as it integrates input over many nanoseconds, but has a tremendously wide (670–1070 nm) gain envelope supporting modelocking and ultrafast pulse generation. The dispersion control methods learned in the fs dye lasers mentioned above to achieve shorter pulses were instrumental in developing the prism or chirped mirror compensation schemes for the dispersion of the gain medium in Ti:Sapphire. At first, Ti+ systems were pumped with CW Ar+ lasers; later, CW internally doubled Nd + YLF lasers were developed with much more stability, power, compact form factor, and efficiency. With the advent of Ti:Sapphire, suddenly the investigator's pulsewidth regime dropped routinely below 200 fs, with some 50 fs versions. For picosecond performance, Ti:sapphire was AO modelocked, but for fs performance the nonlinear properties of the gain rod directly provided a better "Kerr Lens Modelocking" mechanism, yielding routine sub-200 fs performance (Fig. 4).

[Aside: KLM?]: Crystalline glasses experiencing high power Gaussian illumination with polarized light can slightly change their index of refraction (the Kerr effect) in one direction. The sapphire rod/disk hosting the Ti+ gain then becomes a slightly cylindrical lens. Unlike nuisance thermal lensing, this lensing can help select short pulses – a slit in the cavity passes Kerr-lensed photons while rejecting lower power symmetric gain mode photons. After many passes, the edge-trimming feedback is strong enough to generate pulses close to being limited only by the uncertainty principle $\Delta E^* \Delta t >$ Planck's constant ("transform limited pulses").

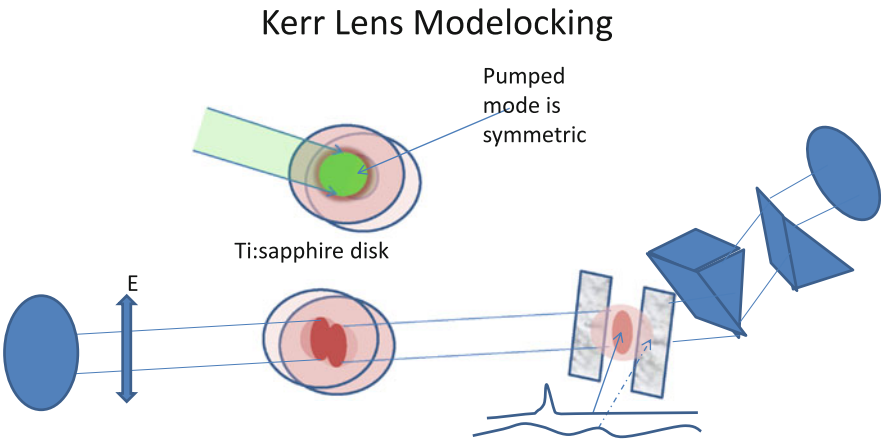

Fig. 4 Polarized intense light induces weak cylinder lensing within gain region; the original symmetric mode is disfavored by the blockage from a slit and this encourages pulse evolution toward higher field strength, less slit-attenuated (i.e., shorter) pulses

Although the very broad gain envelope provided a practical SHG source occurring above 350 nm, this temporarily left a gap for tryptophan spectroscopy enthusiasts, since 295 nm could only be achieved by THG (trebling) 885 nm, leaving little power from oscillators after pulse rate reduction ("picking" via external Bragg cell) . . . until cavity dumping of the oscillator followed by THG again made deep UV a routinely accessible region (e.g., Coherent "Pulse Switch").

2.1 Parametric Gain Lasers

The last decade has witnessed the rise of lasers that employ a very strong femtosecond laser (either Ti:Sapphire or 1-micron sources using Nd+ or Yb+ in disks or fibers) to drive nonlinear processes yielding very widely tunable, powerful femtosecond sources. The "femtosecond Xe arc" is still elusive, but the goal is coming within reach.

Parametric Gain is the ability of electrons in nonsymmetric crystals to invert processes like the SHG explained above. Basically, a strong pump beam generates two ***lower*** *frequency beams ("signal" and "idler") whose frequencies sum to that of the pump beam. If the ~1 u pump is strong, they each can subsequently be doubled to yield tunable UV or visible beams.*

The efficient use of Parametric Gain to build either high power, low repetition rate sources (OPA = Optical Parametric Amplifier) or synchronous high repetition rate versions (Synchronously Pumped/Optical) Parametric Oscillator systems is now widespread.

The low rep rate OPA opens new avenues into deep UV spectroscopy of, e.g., Tryptophan dynamics within proteins and the solvation processes that Trp can monitor [18, 19]. To date, the studies of Trp done to reveal ultrafast protein dynamics have stayed mostly near 295 nm (trebled Ti or doubled OPA sources) [20–23].

Importantly, the upconversion process also allowed us to directly confirm some predictions of Professor Weber that were made during times when nanosecond pulse fluorometry sources (and comparable 30 MHz phase fluorometry) were state-of-the art. Most notably:

1. For initial anisotropy ("r_0") of planar fluorophores (in predictions made by extrapolation from viscous media) – that initial anisotropy would be determined by transition strengths and small librations, not cooling of excess energy from S2 vs. S1 [24]. Subpicosecond upconversion [20] and MD simulation confirmed this [25, 26].
2. For solvent relaxation and heterogeneity of Trp: Prediction was that both solvation- and excitation-dependent heterogeneity would persist on several timescales [27]. This was confirmed with subpicosecond upconversion and 5F-Trp incorporation for monellin, where both processes exist in a 20 ps timeframe [28]

These were all done with limited high power tunability – for Trp excited only near 295 nm.

Doubled OPAs available now, however, have full UV tunability appropriate for testing the importance of Phe->Trp or Tyr->Trp FRET, separating in vs. out-of-plane Trp anisotropy, and selectively exciting 5F- or 5OH-Trp proteins in a milieu. Thus the Parametric Oscillator offers new windows (via upconversion) into protein dynamics that need to be explored, esp., if we wish to explore the red- and blue-edge effects posited by Prof. Weber in early water response to excitation.

For Microscopy and other lower-peak-power visible demands, the Synchronously Pumped Parametric Oscillator (SPPO) has been more used. In SPPOs at first, the short (~120 fs) pulses of Ti:Sapphire (i.e., "Opal" from S/P, "MIRA-OPO" from Coherent, and others) were preferred for higher peak powers compared to ca. 0.7 ps pulses available from 1 um pumps; lately, however, the 1 um sources are generating widths nearer 200 fs, yielding SPPOs with dual outputs useful for not only fluorometric work but also SFG, 4 WM and esp. CARS spectroscopies (systems like S/P "Insight").

2.2 "White Light" Lasers

High peak power pump pulses, esp. when confined to the small cross section of a nanometrically structured optical fiber, can elicit not only Stokes and AntiStokes Raman lines [Emission energies −/+ a vibrational quantum for a host atom] but also a cascade of multiple such scatterings at different energies and orders, yielding a broad continuum of emission at the fiber end [29]. This initially weak curiosity has evolved and been engineered to yield commercial laser sources with ca. 10 MHz repetition, 250 fs width, and considerable power across the near UV and visible (i.e., 0.2 mW/nm bandwidth) [30].

2.3 The Impact of These Laser Technology Advances: Most Visible Areas They Enabled

1. Fast, multidimensional fluorescence spectroscopy (1–100 ns regime):
   The modelocked synchronously pumped dye laser led a revolution in cuvette-based fluorescence studies, rapidly advancing the range of achievable targets and speed of data collection in both time and phase domains [1, 13–15, 31].
2. Ultrafast spectroscopy below 100 ps
   The power and sub-ps duration of amplified Ti:Sapphire pulses permitted us and others to study the ps relaxation of water in and around proteins along with ultrafast quenching events "QSSQ, QuasiStatic Self Quenching" previously unseen, lending insight into the dynamics of proteins and their slaving to solvent motion [18–22, 32, 33].
3. Multiphoton microscopy and sectioning
   The realization that a high NA (numerical aperture) objective could focus Near Infrared ("NIR") laser pulses in the microscope to achieve 2 or more photon excitation of fluorescence came about initially with fs synch-pumped dye lasers (above), but the field grew rapidly once it was realized that the KLM-modelocked Ti:sapphire laser would robustly provide tunability appropriate to almost all of the dyes and fluorescent proteins used in the microscopy community [34, 35]. This was aided by 2 p selection rules that gave large cross sections at wavelengths other than twice the 1 p absorbance peaks.
   The automatic generation of z-sectioning in these microscopes made the more demanding detection of confocal microscopy moot, as "non-descanned" detectors obtained more light unsullied by "out-of-focus" contributions. This was further extended by total emission detection [36, 37] and [38] schemes that recover all of the multiphoton-generated emission, even in thick samples [39].
   More recently, the Ti:Sapphire laser, sometimes accompanied with an OPA, has virtually become a "black box" (turnkey) source of multiphoton excitation in the microscope; all functions (Diode pump, doubled YLF CW pump laser, Ti: sapphire, dispersion compensation) come in single automated boxes (e.g., S/P

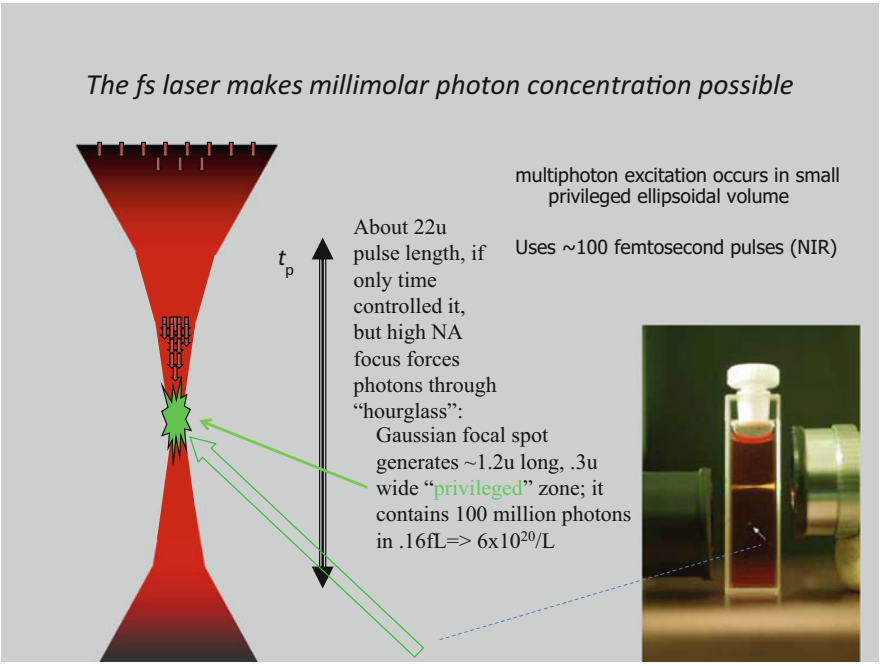

Fig. 5 The two (or more) photon excitation of fluorophores occurs in a tiny (fL) volume where one can imagine mM photon concentration occurs (if that is easier to understand than field strengths). The tiny privileged volume permits automatic Z sectioning, non-descanned (e.g., "TED") detection, and fluctuation spectroscopy

"Mai-tai-Deepsee" or Coherent "Chameleon"). Multiphoton microscopy is a routine accessory unlike the exotic spectroscopic phenomenon it started as (Fig. 5).

4. Multiphoton Correlation Spectroscopy within cells
   The "privileged zone" of multiphoton excitation is typically 0.3 u wide and 0.9 u tall with ellipsoidal shape and near Gaussian profile; this creates an ideal locus for studying the diffusion of fluorescently tagged molecules [40]. Whether raster scanned, held at a point, or orbited [41], this excitation zone reveals unprecedented detail about macromolecular movement within living cells. Importantly, the multiphoton focus can simultaneously excite several different species (again, multiphoton selection rules fortuitously leading to broad cross sections), so *cross-correlation* provides direct evidence of macromolecules not only occupying the same volume ("colocalization"), but also cotransportation. (If traditional microscopy colocalization tells you two molecules live in the same city, cross-correlation tells you they hold hands – or, at minimum, they ride the same bus). This has led us, for example, to studies of binding between hormone effectors and receptors [42] and HIV *nef* acting as a cell surface clearing agent, furthering the immune avoidance of that virus [43].

5. Superresolution Microscopy
   The Nobel prize of 2 years ago in Chemistry was shared by two different methods, both laser dependent. In one, an ultraviolet laser (~405 nm) activated random photoactivatable fluorescent proteins in an image, and they were interrogated over and over with a blue laser so each one would provide a Gaussian spot (width of the point spread function, but accurately centered) before photobleaching. The central points catalogued, a new activation + readout would occur on a new ensemble of points. This pointillist approach eventually yields ~30 nm resolution. The second approach used the realtime coincidence of two beams: one with normal Gaussian shape, the other a donut (Bessel) beam. The first beam populates the upper state for dyes within the spot, and the second stimulates the emission of the dyes in a spatially selective manner. This Stimulated Emission Depletion leaves only survivors in the center of the donut hole for subsequent detection. It typically yields 50 nm resolution but can be driven down to dye dimensions with high power. The former method requires only AO gated CW lasers, but the latter (STED) benefitted enormously from the availability of the Ti:Sapphire pumped, doubled OPO [44]. We have developed schemes to enhance the STED dyes' propensity to deplete via conjugation with depletion-assisting antennae [45].
6. Stimulated Emission, Resonant label free, and related Raman Microscopies
   The availability of reliable Ti:sapphire lasers with stable ps pulses and the ability to synchronize that cavity to another with ~0.3 ps accuracy (e.g., Coherent "Synchrolock-AP" or S/P "lok-to-clok" devices) enabled the transition of Coherent AntiStokes Raman Spectroscopy (CARS) from the gas phase to liquid state microscopy [46]. For abundant species, (typically >50 uM), this provided true chemical selectivity in the cell with submicron mapping accuracy. More recently, the picosecond Nd + laser driving an OPO has become the most popular turnkey system for CARS [47].
   More recently, it was realized that the broad frequency content of the fs lasers and OPOs on the market could be tamed and synchronized to pump the ca. 15 cm-1 wide transitions of many bonds, using a "spectral focusing" approach to chirp both pump and stokes pulses so the difference frequency was preserved throughout a pulse [48]. We have recently adapted the "Insight" series from S/P for this task, smoothly alternating imaging between the narrow vibrational bands of lipids and the broad bands of water and D_2O. SPPOs driven by stable, powerful disk lasers [49] also enable SRS [50] and related microscopies.
   The rise of Raman microscopy using stimulated processes and mixing, in our partisan fluorescence context, proves the adage "one person's artifact is another's grant proposal."

2.4 Closing Perspective

The coevolution of lasers and our applications in the world of spectrophotofluorometry has been remarkable. It is fair to expect the imminent availability of lasers with not only all of the spectral and temporal structure we have desired over the years, but also the power and synchrony with accompanying pulses at *different* colors. While STED already used this synchrony for spatially selective depletion (and CARS for chemical selection), our own use of transient absorbance FRET in the STAQ mechanism [45] is likely to be a harbinger of a much larger class of multiquantum events fluorescence aficionados will engineer to expand the use of fluorescent probes. We should soon be able to use new multicolor laser systems to switch time, polarization, spatial and spectral encoding of fluorophores as we choose.

This manipulation of, e.g., "already excited" fluorophores will expose new phenomena in biomolecules and add new specificity in imaging. Meeting the need for such multibeam experiments will motivate the laser engineers, and the happy coevolution should continue.

Acknowledgements First, thanks to both Professor Weber and David Jameson for encouragement during difficult early career "barrier crossings"; Second, thanks to the many unnamed colleagues who discussed laser features with us. Finally, absolutely no endorsement by the US Government of any particular laser or laser firm is implied.

References

1. Beechem JM (1992) Multiemission wavelength picosecond time-resolved fluorescence decay data obtained on the millisecond time scale: application to protein: DNA interactions and protein-folding reactions. Proceedings of SPIE, the international society for optical engineering. ISSN: 0277–786X; pp 676–680, doi:10.1117/12.58264.
2. Gratton E, Limkeman M (1983) A continuously variable frequency cross-correlation phase fluorometer with picosecond resolution. Biophys J 44(3):315–324
3. Wang YL, Bourkoff E (1988) Passive modelocking of the Ar+ laser. Appl Opt 27(13):2655
4. Halliday L, Topp M (1977) Picosecond luminescence detection using type-2 phasematched frequency-conversion. Chem Phys Lett 46:8
5. Lapidus LJ, Eaton WA, Hofrichter J (2000) Measuring the rate of intramolecular contact formation in polypeptides. Proc Natl Acad Sci 97(13):7220
6. Selinger BK (1983) The pileup problem. In: Cundall RB, Dale RE (eds) Time resolved fluorescence spectroscopy in biochemistry and biology. Plenum, New York
7. Lin S, Knox RS (1988) Time resolution of a short-wavelength chloroplast fluorescence component at low temperature. J Lumin 40:209–210
8. Stong CL (1974) Scientific American; ISSN: 0036–8733; Vol. 230(3); pp 110–115, doi: 10.1038/scientificamerican0374-110
9. Fox RF, James GE, Roy R (1984) Laser with a fluctuating pump: intensity correlations of a dye laser. Phys Rev Lett 52(20):1778–1781
10. Liesegang GW, Smith PD (1982) Vidicon characteristics under continuous and pulsed illumination. Appl Opt 21(8):1437–1444

11. Maroncelli M, Fleming GR (1987) Picosecond solvation dynamics of coumarin 153: the importance of molecular aspects of solvation. J Chem Phys 86(11):6221–6239
12. Rayner DM, Krajcarski DT, Szabo AG (1978) Excited state acid–base equilibrium of tyrosine. Can J Chem 56(9):1238–1245
13. Gratton E, Jameson DM, Hall RD (1984) Multifrequency phase and modulation fluorometry. Annu Rev Biophys Bioeng 13(1):105–124
14. Gratton E, Jameson D, Rosato N, Weber G (1984) Multifrequency cross-correlation phase fluorometer using synchrotron radiation. Rev Sci Instrum 55:486
15. Royer CA (1992) Investigation of the structural determinants of the intrinsic fluorescence emission of the trp repressor using single tryptophan mutants. Biophys J 63(3):741–750
16. Keller U, Weingarten KJ, Kartner FX, Kopf D, Braun B, Jung ID, Fluck R, Honninger C, Matuschek N, der Au JA (1996) Semiconductor saturable absorber mirrors (SESAM's) for femtosecond to nanosecond pulse generation in solid-state lasers. IEEE J Sel Top Quantum Electron 2(3):435–453
17. Denk W, Piston DW, Webb WW (1995) Two-photon molecular excitation in laser-scanning microscopy. In: Pawley JB (ed) Handbook of biological confocal microscopy. Springer, Boston, pp 445–458
18. Lu W, Kim J, Qiu W, Zhong D (2004) Femtosecond studies of tryptophan solvation: correlation function and water dynamics at lipid surfaces. Chem Phys Lett 388(1–3):120–126
19. Zhang L, Kao Y-T, Qiu W, Wang L, Zhong D (2006) Femtosecond studies of tryptophan fluorescence dynamics in proteins: local solvation and electronic quenching. J Phys Chem B 110(37):18097–18103
20. Xu J, Chen J, Toptygin D, Tcherkasskaya O, Callis P, King J, Brand L, Knutson JR (2009) Femtosecond fluorescence spectra of tryptophan in human γ-crystallin mutants: site-dependent ultrafast quenching. J Am Chem Soc 131(46):16751–16757
21. Xu J, Knutson JR (2008) Ultrafast fluorescence spectroscopy via upconversion: applications to biophysics. In: Brand L, Johnson ML (eds) Methods in enzymology, vol 450. Academic Press, St. Louis, pp 159–183
22. Xu J, Toptygin D, Graver KJ, Albertini RA, Savtchenko RS, Meadow ND, Roseman S, Callis PR, Brand L, Knutson JR (2006) Ultrafast fluorescence dynamics of tryptophan in the proteins monellin and IIAGlc. J Am Chem Soc 128(4):1214–1221
23. Xu J, Shen X, Knutson JR (2003) Femtosecond upconversion study of the rotations of perylene and tetracene in hexadecane. J Phys Chem A 107:8383
24. Mantulin WW, Weber G (1977) Rotational anisotropy and solvent–fluorophore bonds: an investigation by differential polarized phase fluorometry. J Chem Phys 66(9):4092–4099
25. Rosales T, Xu J, Wu X, Hodoscek M, Callis P, Brooks BR, Knutson JR (2008) Molecular dynamics simulations of perylene and tetracene librations: comparison with femtosecond upconversion data. J Phys Chem A 112(25):5593–5597
26. Xu J, Shen X, Knutson JR (2003) Femtosecond upconversion study of the rotations of perylene and tetracene in hexadecane. J Phys Chem A 107:8383
27. Weber G (1983) Old and new developments in fluorescence spectroscopy. In: Cundall RB, Dale RE (eds) Time resolved fluorescence spectroscopy in biochemistry and biology. Plenum, New York
28. Xu J, Chen B, Callis P, Muiño PL, Rozeboom H, Broos J, Toptygin D, Brand L, Knutson JR (2015) Picosecond fluorescence dynamics of tryptophan and 5-fluorotryptophan in monellin: slow water-protein relaxation unmasked. J Phys Chem B 119(11):4230–4239
29. Kafka JD, Watts ML, Peterse JW (1992) Quantum Electron 28(10):2151
30. Fenske R, Näther DU, Goossens M, Smith SD (2006) New light sources for time correlated single photon counting in commercially available spectrometers/Edinburgh Instruments 25 October 2006/Vol 6372, 63720H/Proc. SPIE
31. Jay R Knutson (1988) Fluorescence Detection: Schemes To Combine Speed, Sensitivity And Spatial Resolution. In: Joseph R. Lakowicz (ed), Proc. SPIE 0909, Time-Resolved Laser

Spectroscopy in Biochemistry; doi:10.1117/12.945368; Published in SPIE Proceedings Vol. 0909
32. Shen X, Knutson JR (2001) Subpicosecond fluorescence spectra of tryptophan in water. J Phys Chem B 105(26):6260–6265
33. Xu J, Knutson JR (2009) Quasi-static self-quenching of Trp-X and X-Trp dipeptides in water: ultrafast fluorescence decay. J Phys Chem B 113(35):12084–12089
34. Denk W, Strickler JH, Webb WW (1990) Two-photon laser scanning fluorescence microscopy. Science 248(4951):73–76
35. Piston DW, Masters BR, Webb WW (1995) Three-dimensionally resolved NAD(P)H cellular metabolic redox imaging of the in situ cornea with two-photon excitation laser scanning microscopy. J Microsc 178(1):20–27
36. Combs CA, Smirnov A, Chess D, McGavern DB, Schroeder JL, Riley J, Kang SS, Lugar-Hammer M, Gandjbakhche A, Knutson JR (2011) Optimizing multiphoton fluorescence microscopy light collection from living tissue by noncontact total emission detection (epiTED). J Microsc 241(2):153–161
37. Combs CA, Smirnov AV, Riley JD, Gandjbakhche AH, Knutson JR, Balaban RS (2007) Optimization of multiphoton excitation microscopy by total emission detection using a parabolic light reflector. J Microsc 228(3):330–337
38. Gratton E, vande Ven MJ (1995) Laser sources for confocal microscopy. In: Pawley JB (ed) Handbook of biological confocal microscopy. Springer, Boston, pp 69–97
39. Gratton E, Barry NP, Beretta S, Celli A (2001) Multiphoton fluorescence microscopy. Methods 25(1):103–110
40. Berland KM, So PT, Gratton E (1995) Two-photon fluorescence correlation spectroscopy: method and application to the intracellular environment. Biophys J 68(2):694–701
41. Schwille P, Haupts U, Maiti S, Webb WW (1999) Molecular dynamics in living cells observed by fluorescence correlation spectroscopy with one- and two-photon excitation. Biophys J 77 (4):2251–2265
42. Docquier A, Garcia A, Savatier J, Boulahtouf A, Bonnet S, Bellet V, Busson M, Margeat E, Jalaguier S, Royer C, Balaguer P, Cavaillès V (2013) Negative regulation of estrogen signaling by ERβ and RIP140 in ovarian cancer cells. Mol Endocrinol 27(9):1429–1441
43. Yi L, Rosales T, Rose JJ, Chaudhury B, Knutson JR, Venkatesan S (2010) HIV-1 Nef binds a subpopulation of MHC-I throughout its trafficking itinerary and down-regulates MHC-I by perturbing both anterograde and retrograde trafficking. J Biol Chem 285(40):30884–30905
44. Hell SW, Bahlmann K, Schrader M, Soini A, Malak HM, Gryczynski I, Lakowicz JR (1996) Three-photon excitation in fluorescence microscopy. J Biomed Opt 1(1):71–74
45. Rosales T, Sackett D, Xu J, Shi ZD, Xu B, LI H, Kaur G, Frohart E, Shenoy N, Cheal S, Dulcey A, HU Y, Li C, Lane K, Griffiths G, Knutson JR (2015) STAQ: a route toward low power, multicolor nanoscopy. Microsc Res Tech 78:1–13
46. Zumbusch A, Holtom GR, Xie XS (1999) Three-dimensional vibrational imaging by coherent anti-stokes Raman scattering. Phys Rev Lett 82(20):4142–4145
47. Cheng, Ji-Xin; Xie, Xiaoliang Sunney; Coherent Raman Scattering Microscopy. 05/2012; CRC Press; ISBN:1-4398-6765-8, 978-1-4398-6765-5
48. Rocha-Mendoza I, Langbein W, Watson P, Borri P (2009) Differential coherent anti-Stokes Raman scattering microscopy with linearly chirped femtosecond laser pulses. Opt Lett 34 (15):2258–2260
49. Kong L, Ji M, Holtom GR, Fu D, Freudiger CW, Xie XS (2013) Multicolor stimulated Raman scattering microscopy with a rapidly tunable optical parametric oscillator. Opt Lett 38(2):145–147
50. Fu D, Holtom G, Freudiger C, Zhang X, Xie XS (2013) Hyperspectral imaging with stimulated Raman scattering by chirped femtosecond lasers. J Phys Chem B 117(16):4634–4640

Effects of Sterol Mole Fraction on Membrane Lateral Organization: Linking Fluorescence Signals to Sterol Superlattices

Parkson Lee-Gau Chong

Abstract Research highlights cited here illustrate some unconventional usage of fluorescent probes in biophysical studies on sterol superlattices in model membranes. The use of small sterol mole fraction increments over a wide range correctly delineates the global trend as well as the fine details of the effects of sterol content on membrane properties. An alternating variation of fluorescence signals and membrane properties with sterol content, with maxima or minima appeared at critical sterol mole fractions, was observed in many different membrane systems and can be explained by the sterol superlattice model. This model has been progressing over the last two decades. The current model links sterol superlattice formation with condensed complex formation, gives a deeper understanding of the liquid-ordered phase, and reveals two concentration-induced sharp phase transitions immediately below and above a critical sterol mole fraction for maximal superlattice formation. The density and size of membrane rafts isolated from model membranes as detergent resistant membrane fragments show characteristics typical for sterol superlattices, which suggests that membrane rafts and sterol superlattices are closely related. The concept of sterol superlattice formation can be used to optimize liposomal drug formulations and develop a method for a facile screening of lipid-soluble antioxidants for potency and toxicity.

Keywords Cholesterol • Fluorescent probes • Liposomes • Membrane lateral organization • Sterol superlattices

P.L.-G. Chong (✉)
Department of Medical Genetics and Molecular Biochemistry, Lewis Katz School of Medicine at Temple University, Philadelphia, PA 19140, USA
e-mail: pchong02@temple.edu

D.M. Jameson (ed.), *Perspectives on Fluorescence: A Tribute to Gregorio Weber*,
Springer Ser Fluoresc (2016) 17: 179–196, DOI 10.1007/4243_2016_8,

Contents

1 "Being Interested in It"

On a day in early September of 1977, I met with Professor Gregorio Weber in his Roger Adam's fourth floor office to seek his advice on how to select a permanent mentor for my Ph.D. thesis work in the Biochemistry Department at the University of Illinois, Champaign-Urbana. I asked him, "Professor, do you think a good background in electronics, physics, organic chemistry, and mathematics is required for a biochemistry student working in your laboratory?" This question came to my mind because I saw some of his papers full of equations, and I noticed that his students worked on a wide range of topics including instrumentation design, photophysics theories, and probe synthesis. Professor Weber answered my question with a smile. "You know, only one thing is important in research. That is – 'being interested in it'."

In February of 1978, I joined Professor Weber's laboratory. After joining his laboratory, Professor Weber asked me to synthesize a diketone derivative of PHADAN (6-phenylacetyl-2-dimethylaminonaphthalene) that would be an arginine-specific, environmentally sensitive fluorescent probe (Fig. 1). I found that selenium dioxide (SeO_2) in dioxane could be used to convert PHADAN to diketone PHADAN (DKPHADAN). However, I did not continue to pursue this study and never really made use of DKPHADAN for arginine research partly because the DKPHADAN that I synthesized was not water soluble and partly because I was attracted to an even more interesting project.

One day Professor Weber walked into the laboratory and asked if anybody wanted to do high pressure studies on membranes. The subject I was really "interested in" was membranes; so, by taking Professor Weber's sage advice early on, I volunteered to do it. It led to my thesis entitled Pressure Effects on Liposomes, Biological Membranes and Membrane-bound Proteins. Professor

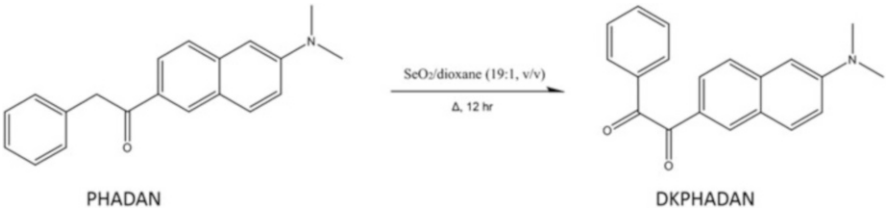

Fig. 1 The reaction used to synthesize diketone PHADAN (DKPHADAN) from PHADAN. DKPHADAN has an extinction coefficient = 14143 M^{-1} cm^{-1} (in ethanol at 360 nm)

Weber gave me tremendous freedom to do research in his laboratory. For the work on membranes at high pressures, I was indebted to several wonderful colleagues and collaborators including Alex Paladini, Andy Cossins, David Jameson, George Fortes, Robert Macgregor, and of course, to Professor Weber, particularly through his many inspirations for both work and personal life. For work, he often mentioned the importance of concentration, which was manifested in his own work on oligomeric protein dissociation and was influential to my later research on sterol superlattices. In the following, I will provide highlights from the research work on sterol superlattices and use those to illustrate some unconventional usage of fluorescent probes in biophysical studies of membranes and discuss the rather surprising results and their implications.

2 Use of Fluorescent Probes as a Membrane Component to Study Sterol Lateral Organization in Lipid Membranes

Extrinsic fluorescent probes such as 1,6-diphenyl-1,3,5-hexatriene (DPH) and 6-lauroyl-2-(dimethylamino)naphthalene (Laurdan) have been used extensively to explore membrane properties. Most extrinsic membrane probes are bulky compared to their naturally occurring lipid counterparts. The bulkiness causes lipid bilayer perturbations when probes are incorporated into the membrane [1]. Conventionally, the probe-to-lipid molar ratio is kept at or below 1/500 in order to minimize membrane perturbation and yet gain sufficient fluorescence signals for detection. Even with such a low molar ratio, fluorescence signals may be complicated by probe aggregation-induced self-quenching [2]. The selections of probes and probe-to-lipid molar ratios become even more critical when probes are not used to explore the bulk membrane properties, but rather to delineate the structure–activity relationship of a particular lipid such as cholesterol.

Cholesterol is an etiological factor of many diseases such as coronary heart disease, diabetes, Alzheimer's disease, and high blood pressure. On the other hand, cholesterol is required for normal body functions. Cholesterol is a precursor of steroid hormones and bile salts, a major component in cell membranes and myelin

sheath, and a regulator of membrane activities. In the last 40 years or so, through the use of many biophysical and biochemical techniques, a great deal of information about cholesterol and its derivatives in model membranes have been revealed. However, how cholesterol is organized in the plane of the membrane at the molecular level, which is one of the most fundamentally important issues in this field, still requires more studies.

In the last two decades, our group, among many others, have used fluorescence methodologies to address this issue. Cholesterol is non-fluorescent. To study cholesterol lateral organization, we chose to use the naturally occurring fluorescent cholesterol analog dehydroergosterol (DHE, ergosta-$\Delta^{5,7,9(11),22}$-tetraen-3β-ol) as our probe and at the same time as a component of the membrane. This strategy is of critical importance for studies of membrane sterol lateral organization. First, not all cholesterol derivatives act like cholesterol. DHE, cholesta-$\Delta^{5,7,9(11)}$-trien-3β-ol, and (22*E*,20*S*)-3β-hydroxy-23-(9-anthryl)-24-norchola-5,22-diene are among a handful of fluorescent cholesterol analogs that are both structurally and functionally closely resembling cholesterol [3, 4]. The use of DHE minimizes perturbations in membrane lateral organization. Second, since DHE is also used as a component of the membrane, DHE membrane content can be varied over a wide range (0–66 mol %) [5] in order to detect any peculiar membrane behaviors at specific mole fractions. This approach is very different from the conventional use of a membrane probe that is typically maintained at 0.2 mol% (1/500 molar ratio) or below, as mentioned earlier.

3 Fascinating Details Revealed When Using Small Sterol Increments Over a Wide Mole Fraction Range

Conventionally, physical properties in sterol/phospholipid mixtures were examined using large sterol mole fraction increments such as 5–10 mol%. It was not until 1994 when the first fluorescence data on DHE/1,2-dimyristoyl-*sn*-glycero-3-phosphocholine (DMPC) mixtures with small sterol mole fraction increments (~0.3 mol%) over a wide range (1–55 mol%) were published [6]. In that study, we found that the plot of the normalized DHE fluorescence intensity versus the mole fraction of DHE exhibited a number of intensity drops, referred to as DHE dips. DHE dips occur at particular sterol mole fractions (C_r) such as 20.0, 25.0, 33.3, 40.0, and 50.0 mol%, predicted by the theory of sterol superlattice formation [6, 7]. DHE dips were also observed in the mixtures of DHE, cholesterol, and phospholipids whenever the total sterol mole fraction, irrespective of the DHE content, was at C_r, indicating that the DHE dips reflect genuine sterol behaviors in membranes, not a fluorescent artifact due to the use of high DHE mole fractions [8]. In addition to DHE fluorescence intensity, DHE fluorescence lifetimes and anisotropy showed a similar alternating variation with sterol mole fraction [8].

Although non-sterol membrane probes such as DPH and Laurdan were subsequently employed to show similar fluorescence signal maxima or minima at C_r in a

variety of sterol/phospholipid two-component and multi-component mixtures (reviewed in [9, 10]), the DHE data offer more direct evidence for membrane sterol regular distribution as the data came from sterols directly. Another point is that DHE/DMPC is a true two-component system, whereas DPH/cholesterol/DMPC or Laurdan/cholesterol/DMPC is not. In terms of studying membrane lateral organization, the fluorescence data obtained from DHE/phosphatidylcholine (PC) can be interpreted in a more straightforward manner than those from non-sterol probes in PC bilayers. However, the extrinsic probes such as DPH and Laurdan have higher quantum yields than DHE, and the fluorescence signals obtained from DPH and Laurdan are still valuable as their signal maxima (or minima) match with the C_r values predicted by the sterol superlattice theory [11–13]. The alternating variation of membrane properties with sterol content was detected not only by fluorescence measurements, but also by infrared spectroscopy [14], surface plasmon resonance [15], computer simulations [16, 17], as well as non-fluorescence based enzyme assays [18, 19].

The necessity of using small sterol increments in membrane studies is illustrated in the plot of Laurdan's generalized polarization (GP_{ex}) versus cholesterol content in 1-palmitoyl-2-oleoyl-*sn*-glycerol-phosphocholine (POPC) bilayers [13] (Fig. 2). When using small cholesterol increments such as 0.3 mol% (left-top panel in Fig. 2), an alternating variation in GP_{ex} is clearly observable and the GP_{ex} dips appear at C_r. When the same data are replotted using 11 mol% increment

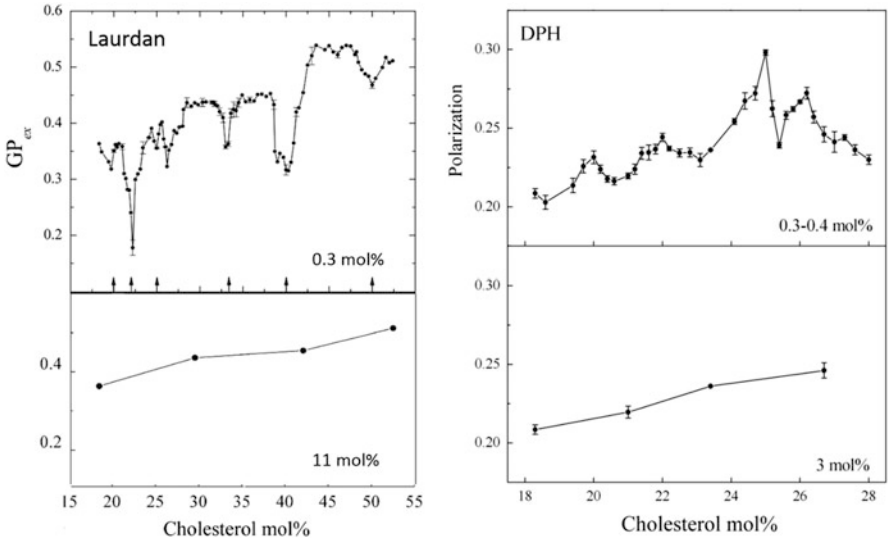

Fig. 2 (*left-top & right-top*) Laurdan's GP_{ex} and DPH steady-state fluorescence polarization, respectively, as a function of cholesterol content in POPC large unilamellar vesicles using 0.3–0.4 mol% sterol increments. *Vertical bars*: standard deviations ($n = 3$). (*left-bottom & right-bottom*) The data in the top panels are replotted using a larger sterol mole fraction increment (e.g., >3 mol%). [POPC] = 40–60 μM. Vesicle diameter = ~160–180 nm. $T = 24°C$. *Arrows* indicate the theoretically predicted C_r values. Data were taken from [13]

(left-bottom, Fig. 2), one could draw a wrong conclusion that GP_{ex} increases monotonically with increasing cholesterol content. The same message can be drawn from the plot of DPH steady-state polarization versus cholesterol content in POPC liposomes (right, Fig. 2). Figure 2 clearly demonstrates that the use of reasonably small sterol mole fraction increments over a wide range is necessary in order to correctly delineate the global trend as well as the fine details of the effects of sterol content on membrane properties. When using a large mole fraction increment, the actual sterol dependence of spectral or membrane properties eludes detection, or the result leads to an erroneous conclusion.

These studies clearly demonstrated that fluorescent probe studies of model membranes are not as simple as previously thought. Sterol content is extremely important in membrane structure and function, and it affects membrane probe signals in a complicated but predictable manner. A minute change in sterol content could have a profound or little effect on membrane properties or membrane probe signals, depending on the original sterol content in the membrane. If the original sterol mole fraction is near C_r, membrane structure and activity as well as the fluorescence signals are sensitive to minute changes in sterol content. If the original sterol mole fraction is in the middle between two adjacent C_rs, membrane properties and the fluorescence signals of membrane probes are relatively less sensitive to sterol content variations. This principle should apply to both cuvette fluorescence studies of model membranes and fluorescence microscopy studies of giant unilamellar vesicles (GUVs). Although small sterol mole fraction increments over a wide range have not been employed to fully test the above principle on GUVs, a dramatic change in lateral patterns has been visualized by fluorescence microscopy at a sterol mole fraction close to C_r [20].

While DHE dips have been known for more than 20 years, many researchers have not yet taken this finding into consideration when studying membranes containing sterols. This hesitation is largely due to the fact that obtaining experimental results showing an alternating variation in spectroscopic or membrane properties with sterol content and displaying a biphasic change at C_r is not a trivial matter. This type of experiment is extremely tedious as it needs a number of liposome samples due to the use of small sterol content increments (~0.3–0.4 mol %) over a wide mole fraction range (18–52 mol%). In addition, all the samples must be under tight thermal history control, the mole fraction must be accurately determined, sterol must be purified by HPLC or recrystallized prior to use, and care must be taken to avoid sterol auto-oxidation. Moreover, sufficient incubation and multiple heating/cooling cycles on samples are essential [6, 13, 15]. A longer incubation time is needed for liposomes at high lipid concentrations [13, 15], which suggests that it is more difficult to observe a biphasic change in membrane properties at C_r when using less sensitive techniques such as NMR. Exactly how we achieved highly accurately determined sterol mole fractions has been described in [21]. The critical factors that are required in order to make vesicles for superlattice studies are specified in [13]. By following these procedures and precautions, one should be able to produce a biphasic change in membrane properties at C_r.

4 Progressing the Sterol Superlattice Model

4.1 The Original Model

The alternating variation of the fluorescence signals and membrane properties with sterol content can be explained by the sterol superlattice model [6, 10]. The model states that, in fluid sterol-containing lipid membranes, there is a tendency for sterol to be regularly distributed into superlattices and that regularly distributed sterol superlattices (shaded areas in rectangle-like objects in Fig. 3) and irregularly distributed lipid areas (blank areas) always coexist, with the ratio of irregular to regular regions (R; solid line in the bottom diagram of Fig. 3) reaching a local

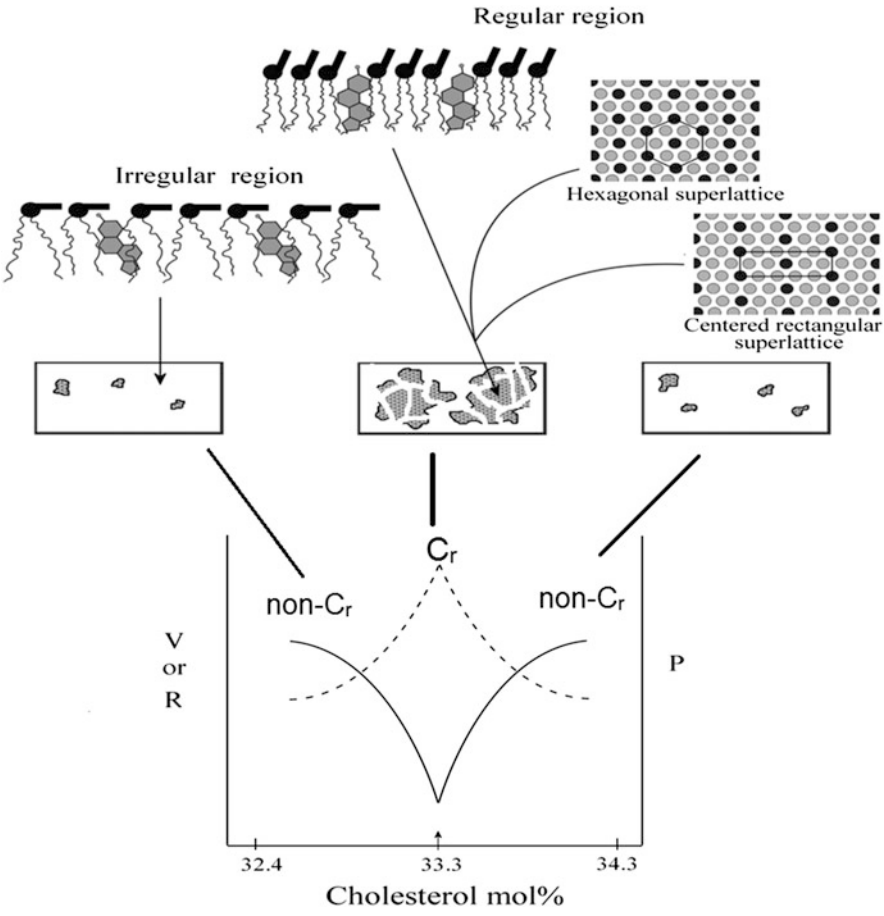

Fig. 3 Schematic description of the original sterol superlattice model. R (*solid line*): ratio of irregular to regular regions; V (*solid line*): membrane free volume for probe rotation; and P (*dashed line*): perimeter of the regular regions. Modified from [13]

minimum at critical sterol mole fractions (C_r). The C_r values can be calculated from the superlattice theories [6, 11, 22]. In the regular regions, cholesterol molecules (dark circles, Fig. 3) are distributed into either hexagonal or centered rectangular superlattices. Superlattices require stringent lateral geometric arrangements, therefore, possessing little free volume. Since the extent of superlattice reaches a local maximum at C_r, membrane free volume for probe rotation (V; solid line in the bottom diagram of Fig. 3) exhibits a local minimum at C_r (Fig. 3). The shape and size of the regular distribution fluctuate with time [23], and lipids inside and outside the regular regions undergo constant exchanges [24]. The perimeter (P; dashed line in Fig. 3) of the regular regions increases abruptly when approaching C_r, which causes a large increase in the interfacial area between the regular and irregular regions, making more sterol molecules exposed to the aqueous phase at C_r than at non-C_r [13]. The diagram in the bottom of Fig. 3 illustrates the membrane properties in the vicinity of $C_r = 33.3$ mol%. Since there are several C_r values in the range 18–52 mol%, there is an alternating variation of membrane properties with sterol content over a wide range.

Not the entire membrane surface is covered by superlattices [6]. This concept was first realized in the study of superlattices in 1-palmitoyl-2-(10-pyrenyl) decanoyl-*sn*-glycerol-3-phosphatidylcholine (Pyr-PC)/DMPC mixtures [25]. It was found that the excimer (E)-to-monomer (M) intensity ratio of pyrene fluorescence drops (E/M dips) abruptly at critical Pyr-PC mole fractions predicted for maximal superlattice formation due to maximal separation of pyrene-labeled acyl chains, but does not go to zero due to the coexistence of regular and irregular regions [25, 26]. The presence of irregular regions at C_r was thought to come from impurity, thermal fluctuations, membrane defects, or local changes in membrane curvature [6, 25]. The coexistence of regular and irregular regions was subsequently revealed by Monte Carlo simulations [24]. Furthermore, based on the fluorescence data of nystatin partitioning into membranes, the area covered by sterol superlattices (A_{reg}) was calculated to be ~71–89% (not 100%) at C_r; and, A_{reg} dropped abruptly when the sterol mole fractions were slightly (e.g., ~1 mol%) deviated from C_r [18, 27].

4.2 The Relationship Between Sterol Superlattices and Condensed Complexes

Sterol/phospholipid mixtures have also been described as condensed complexes between sterol (C) and phospholipid (P) [28]. The critical sterol mole fractions theoretically predicted for maximal superlattice formation coincide with the relative stoichiometries due to C–P complex formation. The condensed complex model has other features similar to those proposed in the sterol superlattice model. Both models contend that stability is greater and molecular order is higher at critical sterol mole fractions. Because of these similarities, it has been speculated that

condensed complexes and superlattices may share the same physical origin and may just occur at different times [13].

4.3 The Sludge-Like Sterol Superlattice Model

In 2012, my longtime collaborator István Sugár proposed a statistical mechanical model [29] which described a new theory of sterol superlattice formation and presented calculations that also led to a biphasic change in A_{reg} at C_r. The calculations showed that A_{reg} is significantly below 100% at all the critical mole fractions for superlattice formation without assuming the presence of impurity and local changes in membrane curvature. In this new model (Fig. 4), a cholesterol-containing membrane is considered as a sludge-like mixture of fluid phase and aggregates of rigid clusters. A rigid cluster is formed by a cholesterol molecule with phospholipid molecules condensed to the cholesterol. The composition of a rigid cluster agrees with a measured critical mole fraction, C_r, with $C_r = (1 + M/2)^{-1}$ where M is the number of acyl chains condensed to the cholesterol molecule. Rigid clusters of similar size tend to form aggregates. Within each aggregate of closely packed rigid clusters the cholesterol molecules are regularly distributed into superlattices. In the fluid phase, both cholesterol and phospholipid molecules are

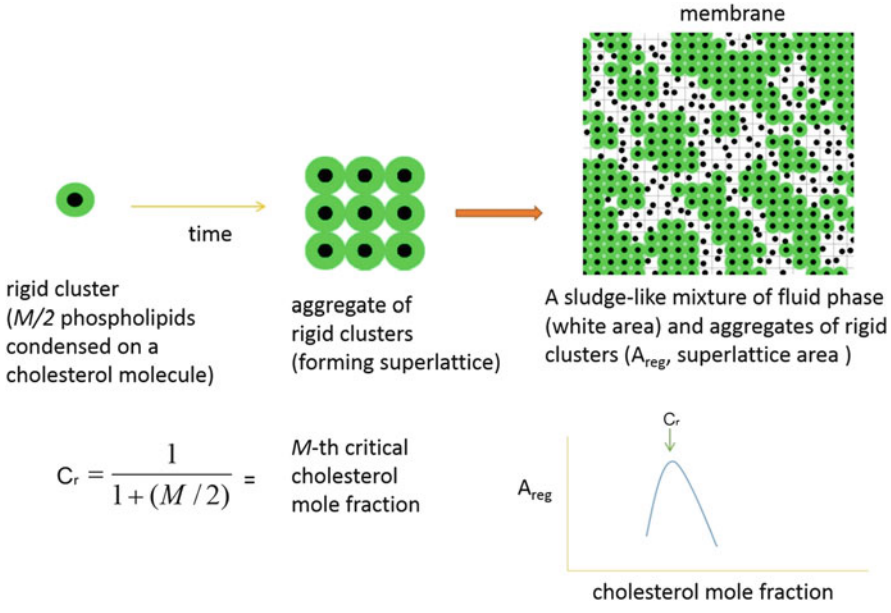

Fig. 4 Schematic description of the sludge-like sterol superlattice model. *Black circles*: cholesterol molecules. *Green areas*: phospholipid molecules that are condensed to the cholesterol molecules. Modified from [29]

able to diffuse laterally, similar to liquid disordered phase. Since the cooperativity energy of aggregation of rigid clusters (w) is small, about 300 cal/mol, which is less than the thermal energy unit, kT [29], there are numerous aggregates with a broad size distribution [30]. This explains why the perimeter (P) of the regular region reaches a local maximum at C_r (Fig. 3). The sludge-like sterol superlattice model explains how cholesterol superlattices and cholesterol/phospholipid condensed complexes are interrelated. The sludge-like sterol superlattice model [29] is able to predict more critical mole fractions (e.g., 28.6 mol%) than the original sterol superlattice model.

5 Gaining a Deeper Understanding of the Liquid-Ordered (or LG_I) Phase and Revealing Concentration-Induced Phase Transitions

We have previously pointed out [29] that two phase diagrams have been frequently cited for cholesterol/PC mixtures. The first phase diagram proposes (e.g., [31]) that, near the transition temperature of the PC component, three phases exist: liquid disordered phase (l_d) at $\leq$8 mol% cholesterol; liquid-ordered phase (l_o) at $\geq$25 mol % cholesterol; and the phase coexistence region at intermediate mole fractions. The second phase diagram (e.g., [32]) proposes that, near the transition temperature of the PC component, the system is in fluid phase up to ~8 mol% and then as the cholesterol content increases from 8 to 66 mol%, the fluid phase gradually converts to l_o phase (also called LG_I region, i.e., liquid-gel type phase), without a phase boundary at 25 mol%. These phase diagrams build on studies using large cholesterol increments (e.g., >3 mol%).

When using small sterol mole fraction increments (~0.3 mol%), it was found that membrane properties of sterol/PC mixtures vary with sterol content in an alternating manner, following the physical principles of sterol superlattice formation, as mentioned earlier. These new data [6, 10, 33] are still compatible with the idea of liquid-ordered phase. According to the sludge-like superlattice model [29], the LG_I region (including the liquid-ordered phase) is considered to be a mixture of fluid phase (irregular regions) and aggregated rigid clusters (regular regions). This characterization of the LG_I region is consistent with the experimental data obtained from DSC, NMR, and other techniques. For example, the presence of condensed complexes and the aggregation of clusters increase the acyl chain order. The rigid clusters decrease the membrane lateral compressibility. The microscopic size of the aggregates of the rigid clusters in coexistence with fluid phase keeps the membrane in a mechanically fluid state. As such, the concept of sterol superlattice formation is not against liquid-ordered phase; actually, the sterol superlattice formation gives a deeper understanding of the liquid-ordered (or LG_I) phase (see Fig. 4 in [29]).

More intriguingly, the alternating biphasic change in A_{reg} with sterol content [18, 27, 29] suggests that, within the LG_I region (including the l_o phase), multiple

concentration-induced phase transitions may exist. Indeed, based on the sludge-like superlattice model, Sugar et al. used statistical thermodynamics calculations to reveal that there are a series of first- or second-order cholesterol mole fraction-induced phase transitions in cholesterol/PC mixtures, which are strongly dependent upon lateral interaction energies [34]. Very small changes (e.g., 0.8%) in the lateral interaction energy, which can be triggered by physical or chemical perturbations, may result in considerable changes in the phase properties of the cholesterol/PC mixtures.

For example, a steep change in A_{reg} occurs at the sterol mole fraction 0.213 (Fig. 5), which is slightly lower than $C_r = 0.222$. This transition represents a phase change from fluid to superlattice. At the sterol mole fraction 0.232, which is slightly higher than $C_r = 0.222$, there is another steep change in A_{reg} (Fig. 5). This transition is from superlattice to fluid phase. Note that at $C_r = 0.222$, A_{reg} reaches a local maximum; however, the first-order phase transition occurs slightly below and slightly above the C_r, not at the C_r. This kind of sharp concentration-induced phase transitions in the vicinity of C_r is not limited to $C_r = 0.222$; they may also occur near other C_rs over a wide range of sterol mole fractions, depending on the lateral interaction energy. These findings suggest that the phase behaviors of cholesterol/PC mixtures are much more complicated than previously thought. The lipid composition-induced phase transitions as specified in this study should have far more important biological implications than temperature- or pressure-induced phase transitions. This is the case because temperature and pressure in cell membranes are largely invariant under physiological conditions whereas the lipid composition can vary significantly in accordance with metabolic and dietary changes.

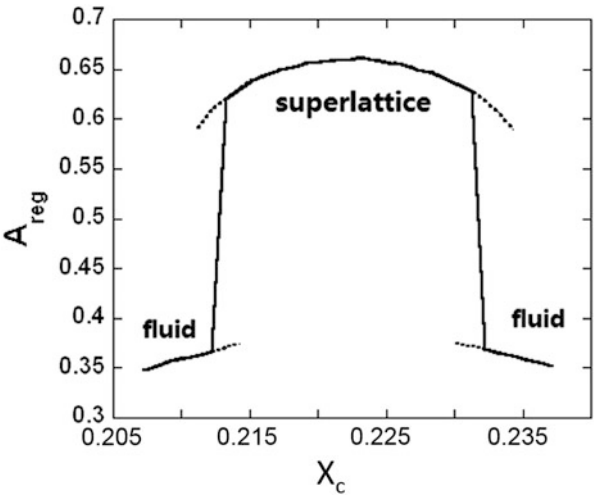

Fig. 5 Regular area fraction A_{reg} is plotted against cholesterol mole fraction X_c in the vicinity of $C_r = 0.222$. Modified from [34]

6 Linking Sterol Superlattices to Membrane Rafts

Cell membrane microdomains that are rich in cholesterol, sphingolipids, saturated phosphatidylcholines, and certain proteins are termed membrane rafts [35]. Membrane rafts play important roles in cellular activities such as endocytosis, exocytosis, intracellular lipid/protein trafficking, signal transduction, virus binding, cell polarization, and activities of surface acting enzymes and membrane-bound proteins.

We had reasons to suspect that sterol superlattices might be associated with the physical origin of membrane rafts. Firstly, membrane rafts are always accompanied by non-raft regions in cells; similarly, in liposomes, regular regions always coexist with irregular regions. Secondly, raft lipids possess higher molecular order than non-raft lipids [36]; similarly, lipids in sterol superlattices are more ordered than those in irregular regions [12, 13]. Thirdly, membrane rafts are highly dynamic [37]. Similarly, computer simulations showed that the shape and size of the superlattices fluctuate with time [23], and lipids inside and outside the superlattice regions undergo constant exchanges [24]. Fourthly, the physical origin of membrane rafts cannot be just the liquid-ordered phase of membrane lipids because the large liquid-ordered domains found in model membranes cannot be detected in cell plasma membranes [37]. As discussed earlier, the liquid-ordered phase actually contains both regular and irregular regions. The regular regions are not a single large domain. Monte Carlo simulations and statistical mechanical calculations showed that the regular regions, particularly, at C_r, exist as many small superlattice islands [24, 34]. Taken together, it may well be that these superlattice islands are closely related to membrane rafts. The presence of many small superlattice islands could explain why membrane rafts are small (50–200 nm) in cells as revealed by microscopy techniques [37, 38].

Su-in Yoon, my former graduate student, did a series of experiments to test if sterol superlattices are related to membrane rafts [39]. She prepared unilamellar vesicles (~530 nm in diameter) composed of POPC, porcine brain sphingomyelins (pSPM), ganglioside GM1, and cholesterol and varied the cholesterol content with 0.5 mol% increments. All the samples in the same set were treated with 0.18% Triton X-100 on ice for 30 min. The membranes in each sample were then layered on a continuous sucrose density gradient tube. Isopycnic ultracentrifugation (Beckman L7, SW41 rotor) was carried out at 40,000 rpm (200,000 × g) for 16 h at 4°C. The typical result is schematically presented in Fig. 6. The milky bands (Fig. 6) are membrane rafts (detergent resistant membrane fragments) because similar bands obtained from mammalian cell membranes by the same experimental protocols were proven to have the highest cholesterol content relative to phospholipids [40].

It is interesting to find that the membrane raft density in the sucrose density gradient tube varies with the cholesterol mole fraction of the original liposomes (before the Triton X-100 treatment) in a biphasic manner, showing a maximum at C_r (Fig. 6). This result is consistent with the sterol superlattice model, which states that the lipids in superlattice regions are more tightly packed than those in irregular regions. It is also interesting to observe that the size of the particles in the milky band varies with the cholesterol content of the original liposomal membrane,

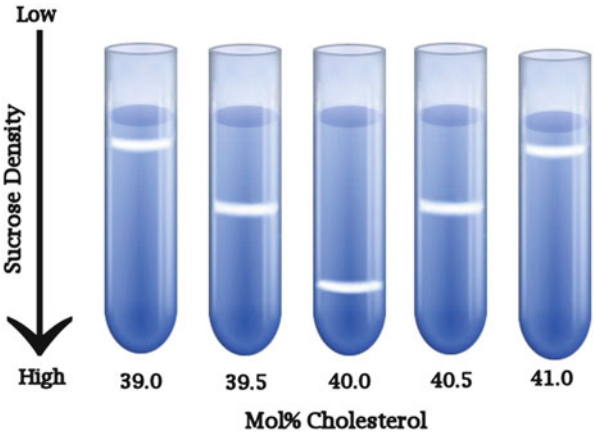

Fig. 6 Effect of cholesterol content on the density of membrane rafts (milky bands) isolated from POPC/pSPM/GM1/cholesterol large unilamellar vesicles. GM1 content was fixed at 1 mol%. Molar ratio of POPC-to-pSPM = 1. The sucrose density increases from 5 to 45% in the centrifuge tube. In this sample set, 40.0 mol% is the only C_r. Derived from [39]

showing a local minimum at C_r. For example, the average size of the particles in the milky band was 219 nm for liposomes at 39.0 mol% cholesterol, 215 nm at 39.5 mol %, 211 nm at 40.0 mol%, 227 nm at 40.5 mol%, and 233 nm at 41.0 mol% [39]. The particle size of the milky bands isolated from this model membrane system is in the same range as those previously reported for membrane rafts observed from cell studies (50–200 nm) [37, 38]. The observation that the particle size in the milky band at C_r is significantly lower than those at nearby non-C_rs agrees with the statistical mechanical calculations in that sterol superlattices at C_r exist as many small islands, rather than a single big domain [34].

In short, these data demonstrated that the density and size of membrane rafts isolated from model membranes as detergent resistant membrane fragments show characteristics typical for sterol superlattices, which suggests that membrane rafts and sterol superlattices may be closely related.

7 Applications Based on the Concept of Sterol Superlattice Formation

Liposomes have been used in many applications. Since sterol-containing liposomes have high thermodynamic tendency to form sterol superlattices, the concept of sterol superlattice formation can be used to optimize current liposomal applications or develop new applications. Here are two examples.

7.1 Optimization of Liposomal Drug Formulation

The concept of sterol superlattice formation can be taken into consideration when designing liposomal drugs. Liposomal drugs are a useful alternative to conventional

drugs and hold great promise for targeted delivery in the treatment of many diseases, particularly, cancers. Most of the liposomal drugs on the market or under clinical trials include cholesterol as a membrane stabilizing agent. Previous studies have demonstrated that the amount of cholesterol in liposomal drugs is important (e.g., [41]). However, these studies used large cholesterol increments (10–30 mol%); as a result, the genuine cholesterol dependence of liposomal drug activity could elude detection.

Indeed, when using small sterol mole fraction increments, we were able to demonstrate that cholesterol content can actually modulate the release and cytotoxicity of liposomal combretastatin A4 disodium phosphate (CA4P), a fluorescent antivascular drug, in a predictable manner [42]. We found that both the rate of the CA4P release from the interior aqueous compartment of the liposomes to the bulk aqueous phase (Fig. 7a) and the extent of the drug's cytotoxicity against MCF-7

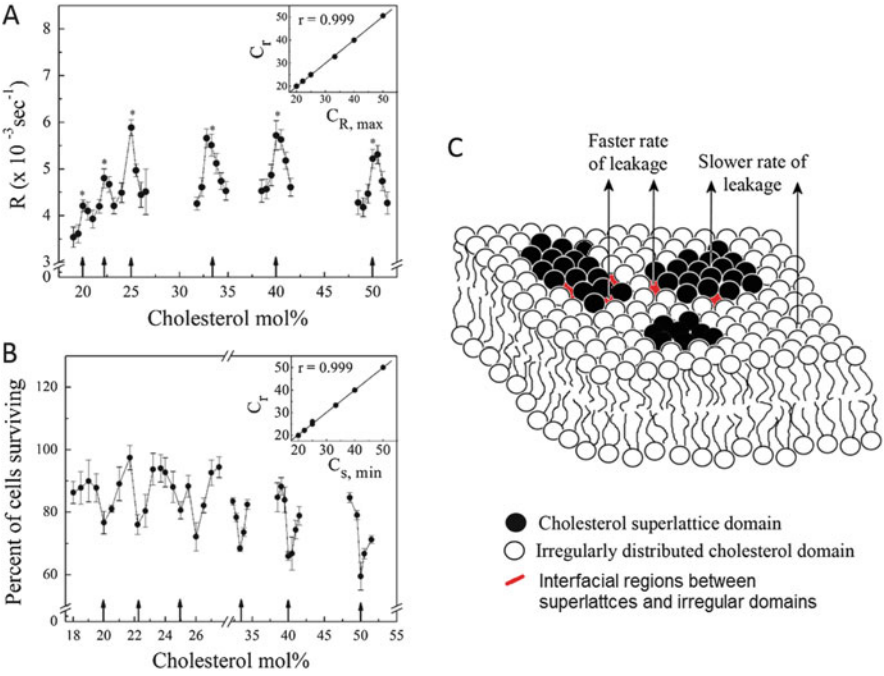

Fig. 7 (**a**) Effect of cholesterol content on the initial rate (R) of CA4P release from cholesterol/POPC liposomes at 24°C. *Vertical bars*: standard deviations ($n \geq 3$). *Inset*: correlation between C_r and the observed critical sterol mole fractions for maximal R, $C_{R,max}$. (**b**) Effect of liposomal cholesterol content on the number of MCF-7 cells surviving in the microplate wells after a 90-min incubation with liposomal CA4P. *Error bars*: standard deviations of the cell numbers counted ($n = 6$). *Inset*: correlation between C_r and the observed critical cholesterol mole fractions for minimal cell survival ($C_{s,min}$). r is the correlation coefficient. (**c**) The interfacial areas (*red*) between superlattice and non-superlattice domains are more defective, possessing more void space and volume fluctuations. Hence, the spontaneous release of CA4P through the interfacial regions is faster than through other regions of the membranes. Modified from [42]

breast cancer cells (Fig. 7b) undergo a biphasic variation, as large as 50%, with liposomal cholesterol content at C_r. At C_r, CA4P can be released from the liposomes more readily than at non-C_r, probably due to the increased domain boundaries between superlattice and non-superlattice regions (Fig. 7c), which consequently results in increased cytotoxicity. The idea that the increased domain boundaries at C_r would facilitate the escape of molecules from membranes (Fig. 7c) was further supported by the data of DHE transfer from liposomes to methyl-β-cyclodextrin [42]. These results together demonstrated that the functional importance of sterol superlattice formation in liposomes can be manifested in targeted cells and that the extent of cholesterol superlattice can control the release of entrapped molecules in liposomal membranes.

7.2 *Assay for Antioxidant Potency and Adverse Effect*

The concept of sterol superlattice has also been used to develop a fluorescence assay to monitor the potency and possible adverse effect of lipid-soluble antioxidants [43]. Reactive oxygen species (ROS) play a major role in the initiation of inflammation and pathophysiological changes associated with conditions such as Alzheimer's disease, cancer, and coronary heart disease. Oxidative damage of membrane lipids by ROS should in theory be reduced or prevented by the use of lipid-soluble antioxidants (e.g., vitamin E). However, many studies have shown that these substances can be ineffective or even harmful (e.g., [44]). Thus, there is a need for a method of a facile, quantitative screening of antioxidants for potency and toxicity.

Since lipid-soluble antioxidants reside in the membrane, we tackled this problem by considering antioxidant–membrane interactions. Our method involves contacts of antioxidants with model membrane systems, which comprise a sterol superlattice formation capable of generating a detectable fluorescence signal from the membrane sterol DHE. A pro-oxidant can oxidize DHE, therefore diminishing its fluorescence intensity. An antioxidant reduces sterol oxidation, thus slowing down the decrease in DHE fluorescence engendered by the pro-oxidant, which provides information on the potency of the antioxidant. The potential toxicity of an antioxidant, on the other hand, can be assessed by measuring its ability to abolish or attenuate sterol superlattice formation. We have used the depth of the DHE dips to monitor the extent of sterol superlattice formation [10, 43, 45]. The threshold antioxidant concentration (C_{th}) to abolish the DHE dips can be determined. The C_{th} value varies with each antioxidant; thus, this method could be employed to assess and rank the potential adverse effects of many different lipid-soluble antioxidants. When a compound has a high tendency to disrupt sterol superlattice structure, the compound will have a low C_{th} value and is likely to impair the membrane and cell functions. Using this method, one can do the first-line screening of lipid-soluble antioxidants that are potent but not harmful.

8 Concluding Remarks

Before I graduated, I asked Professor Weber's opinion about what to do with my postdoctoral training. I was debating whether I should continue membrane biophysics studies or change gears to work on more popular subjects such as molecular biology. Professor Weber's reply was straightforward: "The molecular biology field is already crowded. Why not continue to do what you are doing since you are leading in this area (fluorescence studies on membranes at high pressure)?" The inspiration I received was "pursuing what is new, not what is popular." When I first saw the results of DHE dips and E/M dips, I knew we had opened a new avenue to understanding membrane lateral organization. We started with very simple but very tedious fluorescence intensity measurements. The key is to vary membrane sterol content with small increments over a wide range, while considering all the possible chemical and physical controlling factors that might affect membrane lateral organization. This reminds me of Professor Weber's saying "the simpler the better" at a lab meeting to a couple of renowned visiting scientists who just talked about the complicated cellular events they studied. Even as simple as cholesterol/PC mixtures are, it took us more than 20 years to explore this subject to the extent described in this chapter.

Acknowledgment I thank AHA, DOD, ACS, NSF, and ARO for supporting the superlattice project and all the students, postdoctoral fellows, and collaborators involved, with special thanks to István Sugár, Su-In Yoon, and Berenice Venegas for re-using their data in this chapter.

References

1. Chong PLG, Capes S, Wong PT (1989) Effects of hydrostatic pressure on the location of PRODAN in lipid bilayers: a FT-IR study. Biochemistry 28:8358–8363
2. Khan TK, Chong PLG (2000) Studies of archaebacterial bipolar tetraether liposomes by perylene fluorescence. Biophys J 78:1390–1399
3. Schroeder F (1984) Fluorescent sterols: probe molecules of membrane structure and function. Prog Lipid Res 23:97–113
4. Grechishnikova IV, Bergstrom F, Johansson LBA, Brown RE, Molotkovsky JG (1999) New fluorescent cholesterol analogs as membrane probes. Biochim Biophys Acta 1420:189–202
5. Huang J, Buboltz JT, Feigenson GW (1999) Maximum solubility of cholesterol in phosphatidylcholine and phosphatidylethanolamine bilayers. Biochim Biophys Acta 1417:89–100
6. Chong PLG (1994) Evidence for regular distribution of sterols in liquid crystalline phosphatidylcholine bilayers. Proc Natl Acad Sci U S A 91:10069–10073
7. Somerharju P, Virtanen JA, Cheng KH, Hermansson M (2009) The superlattice model of lateral organization of membranes and its implications on membrane lipid homeostasis. Biochim Biophys Acta 1788:12–23
8. Liu F, Sugar IP, Chong PLG (1997) Cholesterol and ergosterol superlattices in three-component liquid crystalline lipid bilayers as revealed by dehydroergosterol fluorescence. Biophys J 72:2243–2254
9. Chong PLG, Olsher M (2004) Fluorescence studies of the existence and functional importance of regular distributions in liposomal membranes. Soft Mater 2:85–108

10. Chong PLG, Zhu W, Venegas B (2009) On the lateral structure of model membranes containing cholesterol. Biochim Biophys Acta 1788:2–11
11. Virtanen JA, Ruonala M, Vauhkonen M, Somerharju P (1995) Lateral organization of liquid-crystalline cholesterol-dimyristoylphosphatidylcholine bilayers: evidence for domains with hexagonal and centered rectangular cholesterol superlattices. Biochemistry 34:11568–11581
12. Chong PLG, Liu F, Wang MM, Truong K, Sugar IP, Brown RE (1996) Fluorescence evidence for cholesterol regular distribution in phosphatidylcholine and in sphingomyelin lipid bilayers. J Fluoresc 6:221–230
13. Venegas B, Sugar IP, Chong PLG (2007) Critical factors for detection of biphasic changes in membrane properties at specific sterol mole fractions for maximal superlattice formation. J Phys Chem B 111:5180–5192
14. Cannon B, Heath G, Huang J, Somerharju P, Virtanen JA, Cheng KH (2003) Time-resolved fluorescence and Fourier transform infrared spectroscopic investigations of lateral packing defects and superlattice domains in compositionally uniform cholesterol/phosphatidylcholine bilayers. Biophys J 84:3777–3791
15. Melzak KA, Melzak SA, Gizeli E, Toca-Herrera JL (2012) Cholesterol organization in phosphatidylcholine liposomes: a surface plasmon resonance study. Materials 5:2306–2325
16. Huang J (2002) Exploration of molecular interactions in cholesterol superlattices: effect of multibody interactions. Biophys J 83:1014–1025
17. Helrich CS, Schmucker JA, Woodbury DJ (2006) Evidence that nystatin channels form at the boundaries, not the interiors of lipid domains. Biophys J 91:1116–1127
18. Wang MM, Olsher M, Sugar IP, Chong PLG (2004) Cholesterol superlattice modulates the activity of cholesterol oxidase in lipid membranes. Biochemistry 43:2159–2166
19. Ali MR, Cheng KH, Huang J (2007) Assess the nature of cholesterol-lipid interactions through the chemical potential of cholesterol in phosphatidylcholine bilayers. Proc Natl Acad Sci U S A 104:5372–5377
20. Fidorra M, Duelund L, Leidy C, Simonsen AC, Bagatolli LA (2006) Absence of fluid-ordered/fluid-disordered phase coexistence in ceramide/POPC mixtures containing cholesterol. Biophys J 90:4437–4451
21. Chong PLG, Venegas B, Olsher M (2007) Fluorescence detection of signs of sterol superlattice formation in lipid membranes. Methods Mol Biol 400:159–170
22. Virtanen JA, Somerharju P, Kinnunen PKJ (1988) Prediction of patterns for the regular distribution of soluted guest molecules in liquid crystalline phospholipid membranes. J Mol Electron 4:233–236
23. Parker A, Miles K, Cheng KH, Huang J (2004) Lateral distribution of cholesterol in dioleoylphosphatidylcholine lipid bilayers: cholesterol-phospholipid interactions at high cholesterol limit. Biophys J 86:1532–1544
24. Sugar IP, Tang D, Chong PLG (1994) Monte Carlo simulation of lateral distribution of molecules in a two-component lipid membrane. J Phys Chem 98:7201–7210
25. Tang D, Chong PLG (1992) E/M dips. Evidence for lipids regularly distributed into hexagonal super-lattices in pyrene-PC/DMPC binary mixtures at specific concentrations. Biophys J 63:903–910
26. Somerharju PJ, Virtanen JA, Eklund KK, Vainio P, Kinnunen PKJ (1985) 1-Palmitoyl-2-pyrenedecanoyl glycerophospholipids as membrane probes: evidence for regular distribution in liquid-crystalline phosphatidylcholine bilayers. Biochemistry 24:2773–2781
27. Wang MM, Sugar IP, Chong PLG (1998) Role of the sterol superlattice in the partitioning of the antifungal drug nystatin into lipid membranes. Biochemistry 37:11797–11805
28. McConnell HM, Radhakrishnan A (2003) Condensed complexes of cholesterol and phospholipids. Biochim Biophys Acta 1610:159–173
29. Sugar IP, Chong PLG (2012) A statistical mechanical model of cholesterol/phospholipid mixtures: linking condensed complexes, superlattices, and the phase diagram. J Am Chem Soc 134:1164–1171

30. Sugar IP (2008) On the inner structure and topology of clusters in two-component lipid bilayers. Comparison of monomer and dimer Ising models. J Phys Chem B 112:11631–11642
31. Ipsen JH, Karlstrom G, Mouritsen OG, Wennerstrom H, Zuckermann MJ (1987) Phase equilibria in the phosphatidylcholine-cholesterol system. Biochim Biophys Acta 905:162–172
32. Huang TH, Lee CWB, Das Gupta SK, Blume A, Griffin RG (1993) A ^{13}C and ^{2}H nuclear magnetic resonance study of phosphatidylcholine/cholesterol interactions: characterization of liquid-gel phases. Biochemistry 32:13277–13287
33. Virtanen JA, Somerharju P (1999) Cholesterol superlattice model is compatible with the calorimetric behavior of cholesterol/phosphatidylcholine bilayers. J Phys Chem B 103:10289–10293
34. Sugar IP, Simon I, Chong PLG (2013) Series of concentration induced phase transitions in cholesterol/phosphatidylcholine mixtures. Biophys J 104:2448–2455
35. Simons K, Ikonen E (1997) Functional rafts in cell membranes. Nature 387:569–572
36. Xu X, London E (2000) The effect of sterol structure on membrane lipid domains reveals how cholesterol can induce lipid domain formation. Biochemistry 39:843–849
37. Kusumi A, Koyama-Honda I, Suzuki K (2004) Molecular dynamics and interactions for creation of stimulation-induced stabilized rafts from small unstable steady-state rafts. Traffic 5:213–230
38. Dietrich C, Yang B, Fujiwara T, Kusumi A, Jacobson K (2002) Relationship of lipid rafts to transient confinement zones detected by single particle tracking. Biophys J 82:274–284
39. Yoon SI (2007) Effect of cholesterol content on lipid microdomains in model membranes and cells. PhD Thesis, Temple University School of Medicine
40. Xu W, Yoon SI, Huang P, Wang Y, Chen C, Chong PLG, Liu-Chen LY (2006) Localization of the kappa opioid receptor in lipid rafts. J Pharmacol Exp Ther 317:1295–1306
41. Nallamothu R, Wood GC, Kiani MF, Moore BM, Horton FP, Thoma LA (2006) A targeted liposome delivery system for combretastatin A4: formulation optimization through drug loading and in vitro release studies. J Pharm Sci Technol 60:144–155
42. Venegas B, Zhu W, Haloupek NB, Lee J, Zellhart E, Sugar IP, Kiani M, Chong PLG (2012) Cholesterol superlattice modulates combretastatin A4 disodium phosphate (CA4P) release from liposomes and CA4P cytotoxicity on mammary cancer cells. Biophys J 102:2086–2094
43. Olsher M, Chong PLG (2008) Sterol superlattice affects antioxidant potency and can be used to assess adverse effects of antioxidants. Anal Biochem 382:1–8
44. Sesso HD (2006) Carotenoids and cardiovascular disease: what research gaps remain? Curr Opin Lipidol 17:11–16
45. Chong PLG, Olsher M (2007) Fluorometric assay for detection of sterol oxidation in liposomal membranes. Methods Mol Biol 400:145–158

The Use of 6-Acyl-2-(Dimethylamino) Naphthalenes as Relaxation Probes of Biological Environments

Luis A. Bagatolli and Roberto P. Stock

Abstract As Gregorio Weber anticipated in his seminal 1979 article, 6-acyl-2-(dimethylamino)naphthalene probes became excellent tools to study nanosecond relaxation processes of biological systems. Examples are the use of PRODAN (or DANCA) to study relaxation of specific protein matrixes, or LAURDAN (as well as PRODAN) extensively used to study the extent of water dipolar relaxation processes in biological membranes. In this chapter a novel application for this family of molecules is presented and discussed. Specifically, we show how these fluorescent probes can be used to monitor intracellular water dipolar relaxation in living cells displaying oscillatory metabolism. Our experimental results show a strong coupling between metabolism and intracellular water dynamics, challenging the view that water in the interior of cells exists mostly as a medium whose global properties are comparable to the properties of dilute solutions. The observed results can be very well interpreted in light of the association-induction hypothesis postulated by Gilbert Ling in 1962.

Keywords ATP • Fluorescent probes • Glycolysis • Molecular crowding • Oscillatory metabolism • Water dipolar relaxation

Contents

L.A. Bagatolli (✉) and R.P. Stock (✉)
Membrane Biophysics and Biophotonics Group/MEMPHYS – Center for Biomembrane Physics, Department of Biochemistry and Molecular Biology, University of Southern Denmark, Campusvej 55, DK-5230 Odense, Denmark
e-mail: bagatolli@bmb.sdu.dk; rpstepoz@gmail.com

D.M. Jameson (ed.), *Perspectives on Fluorescence: A Tribute to Gregorio Weber*, Springer Ser Fluoresc (2016) 17: 197–216, DOI 10.1007/4243_2016_7,

Abbreviations

ACDAN	6-Acetyl-2-dimethylamine-naphthalene
DAN	2-(Dimethylamino)-6-acylnaphtalenes
GP	Generalized Polarization function
LAURDAN	6-Dodecanoyl-2-dimethylamine-naphthalene
PRODAN	6-Propionyl-2-dimethylamine-naphthalene

1 A Relevant Contribution from Gregorio Weber: The 2-(Dimethylamino)-6-Acylnaphtalenes Family

The displacement of the fluorescence spectrum to longer wavelengths (red shift) with increasing polarity of solvents has been the object of both theory and experiment since the 1950s. This type of red shift is largely dependent upon a large increase in the molecule's dipole moment in the fluorescent state over that of the ground state [1] and particular substituted aromatic molecules can satisfy this condition. Among his many seminal contributions to biological fluorescence in 1979 Gregorio Weber introduced a family of environmentally sensitive dyes based on a naphthalene structure substituted with electron donor (alkylamino group) and acceptor (acyl substituted carbonyl) groups in position 2 and 6, respectively [1]. This structure possesses a maximum distance between the electron donor and acceptor groups, resulting in a lowest excited state with an important charge transfer character. In his influential publication, Weber presented a general method for the synthesis of 2-(dimethylamino)-6-acylnaphtalenes, i.e., 6-propionyl (PRODAN), 6-acetyl (ACDAN), and 6-lauroyl (LAURDAN), together with a careful study of the response of PRODAN's absorption and fluorescence properties to solvents of different polarity. In this description the dipole interaction theory of Lippert [2] was considered and generalized to the other synthesized naphthalene derivatives [1]. For example, a 130 nm red shift (one of the largest reported to date) was described for PRODAN's emission maximum from cyclohexane to water with an important change in the magnitude of its transition dipole. Additionally, a significantly (larger) Stoke's shift was reported in solvents that can form hydrogen bonds (i.e., that can act as proton donors) with respect to aprotic solvents [1]. Later

on, further studies of PRODAN's response to solvent polarity were conducted in Weber's laboratory, where the Langevin distribution of electrostatic interactions was considered [3]. It is very important to remark that Weber's contribution went well beyond the rational design of environmentally sensitive fluorescent molecules and the characterization of their response in solvents with different polarity. An essential idea was the application of this knowledge to the study of biological material. More precisely, in 1979 Weber presented a study of the interaction of PRODAN with bovine serum albumin, proposing the use of this 2-(dimethylamino)-6-acylnaphtalene derivative as "*a relaxation probe of various biological environments*" [1].

In a later work, Weber exploited the nanosecond relaxation phenomenon in a protein matrix (addressed earlier in his laboratory [4]) to determine the polarity of the myoglobin haem pocket [5]. Specifically, Weber designed and used another 2,6 substituted naphthalene derivative, i.e., 6′-(*N*,*N*-dimethyl)amino-2-naphtophyl-4-trans-cyclohexanoic acid (DANCA) [5], a probe with greater affinity than PRODAN for apomyoglobin. In a similar way, Prendergast et al. synthesized 6-Acryloyl-2-dimethylaminonaphthalene (Acrylodan), a 6,2 substituted naphthalene derivative that selectively labels thiol moieties in proteins [6]. In the Prendergast et al. paper, the usefulness of Acrylodan in the study of "hydrophobic" domains, conformational changes, and dipolar relaxation processes in proteins was demonstrated by measurements of fluorescence spectra and lifetimes of a mercaptoethanol adduct in different solvents and of adducts of this agent with parvalbumin, troponin C, papain, and carbonic anhydrase [6].

In those early years the interest in environmental relaxation processes in biological systems was not restricted only to proteins. Similar ideas were applied as well to explore relaxation in membranes (i.e., model membranes but also biological membranes) using different 2-(dimethylamino)-6-acylnaphtalene derivatives introduced by Weber, such as LAURDAN, PRODAN, ACDAN [7–9], and 6-palmitoyl-2-[[(2-trimethylammonium)ethyl]methyl]amino] naphthalene (PATMAN), the last one introduced by Lakowicz et al. in 1983 [10, 11]. Other related derivatives had been also synthesized in Weber's group, i.e., 2-diisopropylamino-6-lauroylnaphthalene (LAURISAN), 2-methoxy-6-lauroylnapthalene (LAURMEN), and 2-hydroxy-6-lauroylnapthalene (LAURNA), and further characterized by Parasassi et al. [8]. Very recently, a new 2,6 naphthalene derivative has been introduced 6-dodecanoyl-2-[*N*-methyl-*N*-(carboxymethyl)amino]naphthalene (C-LAURDAN), to explore membranes mainly using fluorescence microscopy [12, 13].

The theme of this chapter is to discuss novel results recently obtained in our laboratory using some members of the 2-(dimethylamino)-6-acylnaphtalene family (called here DAN probes). Specifically, we discuss a new strategy that uses ACDAN, PRODAN, and LAURDAN (Fig. 1) to monitor the dynamics of intracellular water in cells displaying metabolic oscillations [14]. Because of their different partition properties and shared response to solvent dipolar relaxation, these DAN probes were chosen as sensors to monitor heterogeneities in the collective dynamics of the most abundant intracellular dipoles, namely water molecules. In this work we

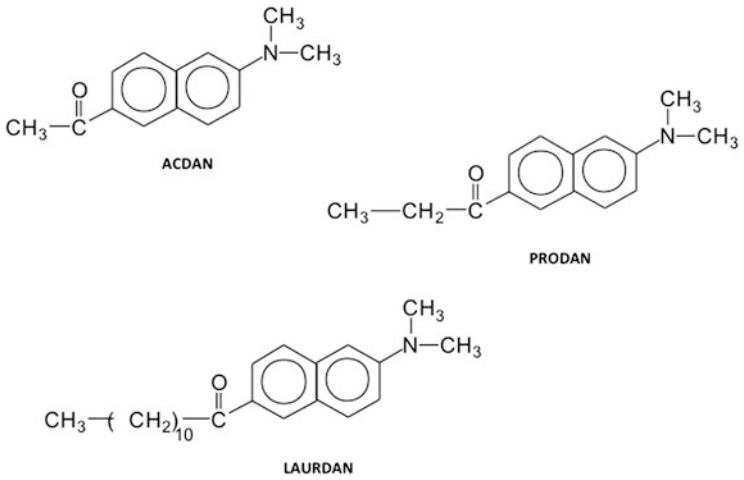

Fig. 1 Chemical structures of different 2,6 substituted naphthalene derivatives

took advantage of the oscillatory behavior of glycolysis in yeast cells to add a temporal dimension (phase and period) that would allow us to establish correlations between the fluorescence dynamics of the probes and metabolism. Before discussing this new material a brief review of important features of these probes will be presented in the two following sections.

2 A Model for DAN Relaxation in Biological Environments

A model to explain the fluorescence response of DAN probes in biological environments was proposed for LAURDAN and PRODAN inserted in lipid bilayers. Once these probes are incorporated in glycerophospholipid membranes an emission red shift of ~50 nm is observed when the membrane undergoes a solid-ordered (s_o) to liquid-disordered (l_d) phase transition [15–17]. Since changes in the "static" dielectric constant between the two membrane phase states are not sufficient to explain the observed fluorescence emission shift, a model to interpret these changes was originally provided by Parasassi et al. [17]. These authors anticipated that the nanosecond relaxation process observed in the l_d phase [15, 16, 18] is caused by the presence of water molecules with restricted mobility in the region where the probe is located (near the glycerol backbone of the glycerophospholipids) [17, 19, 20]. Part of probe's excited state energy is utilized for the reorientation of the water dipoles diminishing the singlet excited state (S_1) energy (see Fig. 2) and so shifting the emission spectrum of the probe to longer wavelengths. Notice that the emission shift is accompanied by a decrease in the lifetime of the probe and, consequently, in its quantum yield. Importantly, the relaxation caused by these water molecules is different to the water molecules existing in bulk phase that have

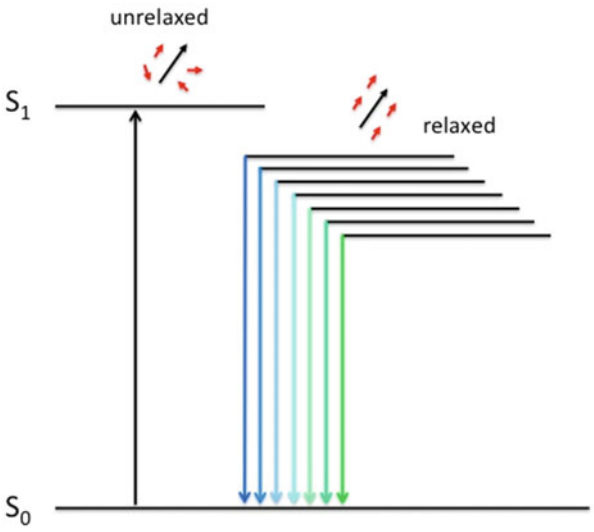

Fig. 2 Schematics of the ground (S_0) and excited state (S_1) energy levels in the presence of the solvent dipolar relaxation. S_1 decreases in energy as solvent dipolar relaxation proceeds

an orientational relaxation time below one picosecond [17]. Relaxation times have been measured for the l_d and s_o phases using an expression equivalent to the classical Perrin equation for the generalized polarization function (GP, for details see below, Sect. 3), assuming a two-state process [18]. These values were reported to be 2.5×10^9 s^{-1} and 4×10^7 s^{-1} for the l_d and s_o phases, respectively.

There is considerable experimental evidence that supports the idea that the particular dynamics of structured water molecules in the vicinity of the probe are the cause of the observed emission shift in membranes undergoing a phase transition [8, 21]. For example, experiments in membranes composed of DMPC in D_2O show slower relaxation dynamics at and above the phase transition, although the main phase transition temperature is the same with respect to that observed for the same lipid membranes in H_2O [8]. This important observation, which cannot be the consequence of a chemical reaction because the transition involves no compositional changes, points that the greater mass of the ensemble of (membrane-associated) D_2O molecules reorienting (sensed by LAURDAN) as the supramolecular structure changes is enough to slow down the transition.

A very useful parameter to monitor transitions between these unrelaxed and relaxed states was introduced by Enrico Gratton and his group of collaborators in 1990 [16]. This parameter, called the generalized polarization, has become very popular to study membrane and will be briefly discussed in the next section.

3 The Generalized Polarization Function

The generalized polarization (GP) function was defined to exploit a simple steady state parameter (the probe's emission spectra) to study structural and dynamical processes in model and biological membranes. Specifically, the GP function was introduced to quantitatively determine the relative amounts and temporal fluctuations of two distinct lipid phases when they coexist in a model membrane (for comprehensive reviews see [7, 8, 21]). This function was originally defined as

$$\mathrm{GP} = \frac{I_\mathrm{B} - I_\mathrm{R}}{I_\mathrm{B} + I_\mathrm{R}} \tag{1}$$

where I_B and I_R are the measured fluorescence intensities under conditions in which wavelength (or a band of wavelengths) B (for blue shifted) and R (for red shifted) are both observed using a given excitation wavelength. Being a weighted difference, the values of the GP must fall within -1 and 1; the lower this value the greater the extent of bathochromic shift in the fluorescence emission spectrum. This definition is formally identical to the classical definition of fluorescence polarization, in which B and R represent two orthogonal orientations of the observation polarizers in the fluorometer. The advantage of the GP function for the analysis of the spectral properties of the DAN probes is derived from the well-known properties of the classical polarization function, which contains information on the interconversion between two different "states" of the emitting dipole of the fluorophore. In the original studies, the LAURDAN GP was shown to distinguish between the extent of water relaxation in a phospholipid membrane, which is very low in a solid-ordered (gel) phase with respect to a liquid-disordered phase [7, 8, 21]; importantly, it was possible to distinguish fluctuations in the GP values *only* when the two lipid phases coexist. In general terms the states B and R will, respectively, correspond to unrelaxed and relaxed environments sensed by the probes. In the particular case of yeast cells displaying oscillating glycolysis that will be addressed in the remaining sections of this chapter, a generalization of the use of the GP function is applied, i.e., we explore fluctuations in water relaxation throughout the cell rather than in just membrane-associated water.

4 Glycolytic Oscillation in Yeast and the State of Intracellular Water in the Cell

The oscillatory behavior of many biological processes has been studied for decades. Examples include slow genetic oscillations of circadian rhythms [22], periodic pattern formation in embryogenesis [23], oscillating cytoskeletal structure in mechano-sensitive hair bundles in the auditory system, and, at the single cell level, the oscillations of Min gene products in *Escherichia coli* that dynamically

determine the site of cell division, among others [24]. The oscillatory nature of glycolysis in *Saccharomyces cerevisiae* becomes apparent when unmasked by inhibition of respiration. As cells utilize glucose supplied in the medium, glycolysis products accumulate and disappear following a well-known waveform. Oscillations can be measured in real time following the intrinsic fluorescence of reduced nicotine adenine dinucleotide, NADH [25, 26]. However, oscillations of other intracellular glycolytic intermediates [27], CO_2 [28], mitochondrial potential, ATP, and intracellular pH [29] have been observed, suggesting the existence of underlying coupling mechanisms. Glycolytic oscillations are a property of single cells [26] but, at high cellular density, they become macroscopic since cells are quickly and robustly synchronized via diffusing metabolites. As described previously in the literature, these oscillations are induced by synchronizing the cells by starvation, followed by addition of cyanide (or argon), which inhibits the respiratory chain, and glucose (which provides the substrate for continued glycolysis); for details see [14].

Attempts to understand oscillating glycolysis have generally taken the form of models of a few to tens of enzymatic reactions and some rate-controlling steps (e.g., phosphofructokinase). However, a more recent and kinetically equivalent proposal of control of oscillations by sugar transport has established that the origin of oscillations is diffuse and not governed by a single reaction, whether chemical transformation or sugar transport [30]. All models have in common that they are premised on mass action kinetics. In other words, they rely on the assumption that the intracellular milieu is, at a relevant scale, a homogeneous environment where diffusing chemical species, consumed and produced by enzymes at particular rates (with requisite delays, [31]), are responsible for the periodic accumulation and disappearance of measured metabolites.

This view of the intracellular environment as a nanoscale replica of dilute systems, however, is probably missing crucial information [32, 33]. It does not consider the peculiar physicochemical properties of the intracellular aqueous phase, treating it as a featureless isotropic environment in which chemical species move and react. This view has an honorable history going back to van't Hoff's insight that solutes could, in dilute conditions, be treated with formalisms successfully applied to gases. A view that incorporates the altered colligative properties of the intracellular aqueous milieu would, however, provide a more comprehensive picture [32]. Considering what is now known of the behavior of hydrogel materials [34], coherent macroscopic behavior in cells or sets of cells (physiology) can be conceived as the result of dynamical coupling of mechanochemical (i.e., viscoelastic) properties of the medium to chemical transformations (metabolism).

Water constitutes the most abundant component of the cell. Its unusual properties as a polar solvent have been recognized as part and parcel of life processes [35]. While van't Hoff's insight has proven invaluable, it reaches its limit of usefulness when water itself is strongly impacted by solutes (that is, deviates from tractable ideality). Furthermore, water in the cell is not just a medium where reactions occur but an active participant, e.g., many cellular reactions are condensations that produce water, or hydrolytic ones, that consume it. It has been long

known that the cellular environment is highly crowded with very little water exhibiting the properties of dilute solutions (for example, transverse relaxation times in muscle, [36]). Even in simple model systems, NMR studies of interfacial water indicate that its properties are quite dissimilar to dilute systems (see [37]). Many cellular processes, such as secretion and endocytosis, have been productively modeled by responsive hydrogels [38]. An explicit treatment of the dynamics of intracellular water should, therefore, provide elements for a more detailed structural, mechanistic, and dynamical understanding of the coherence of cellular behavior, that is, the coupling between chemical and mechanical levels of description [39]. For such a treatment to be feasible, however, time resolved information on intracellular water behavior is essential.

5 Response of the DAN Probes in Resting and Oscillating Yeast Cells

The idea of transitions between unrelaxed and relaxed environments, which are included in the model presented in Sect. 2 for membranes, can be extended to other systems such as the cell cytoplasm. Thus, we extended the notion to use ACDAN, PRODAN, and LAURDAN to study cell-wide intracellular water dynamics [14]. These DAN probes constitute a series in which the fluorescent group is coupled to progressively longer hydrophobic chains (see Fig. 1), thus exhibiting different affinities for hydrophobic/hydrophilic environments [9]. The shortest of these (C_2, ACDAN) is essentially insensitive to membrane-associated water dynamics since it partitions to hydrophilic environments. The next (C_3, PRODAN) partitions to both membranes and surrounding water. The most hydrophobic probe contains a lauroyl chain (C_{12}, LAURDAN), which in principle places it squarely within bilayers as its solubility in water is negligible. Thus the partition properties of these different molecules allow the exploration of a broad range of intracellular environments, which is important to establish whether the measured responses constitute a global cellular phenomenon [14]. Results observed in resting cells, which relate the spatial distribution of the probe with their fluorescence emission response, demonstrated a heterogeneous environment in terms of the extent of intracellular water dipolar relaxation across the cell cytoplasm. Interestingly, the three probes show two discernible populations with maxima in the green (G, $\approx$490 nm) and blue (B, $\approx$440 nm). An example is depicted in Fig. 3 for ACDAN (observed both in the fluorometer and the fluorescence microscope) where the fluorescence intensity ratio between these two bands (G/B) decreases in the order ACDAN>PRODAN>LAURDAN following the affinity of the probes for hydrophilic environments (ACDAN is the most water soluble). In any case, the spatial distribution of LAURDAN is not far from that observed with the other two probes, although its overall fluorescence emission band is narrower [14]. Moreover and very important, the fluorescence emission spectra of the DAN probes are far from

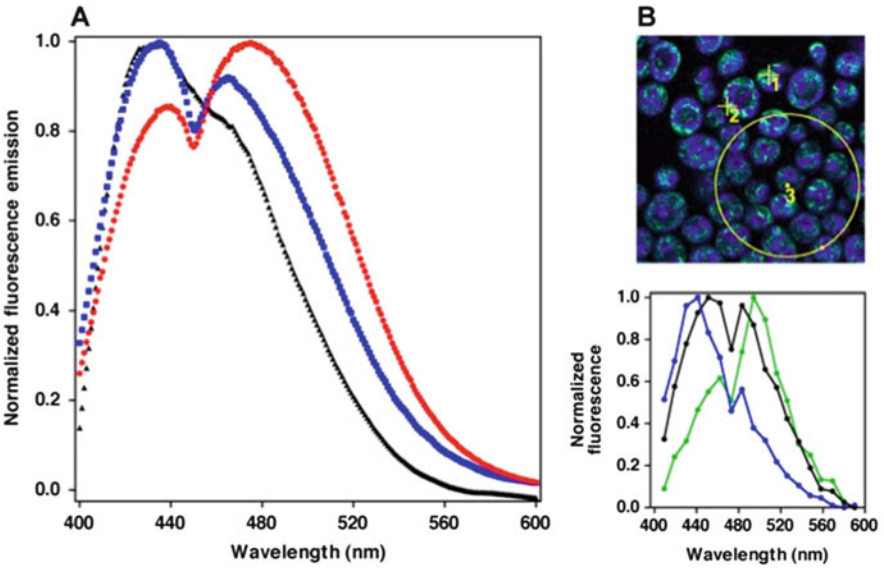

Fig. 3 Fluorescence response of DAN probes in resting cells. Panel (**a**) Emission spectra of cells labeled with ACDAN (*red*), PRODAN (*blue*), and LAURDAN (*black*) measured in the fluorometer. Panel (**b**) Spectral image of cells labeled with ACDAN (*top*) with spectra (*bottom*) of selected regions of interest: single B region (*blue*, ROI 1), single G region (*green*, ROI 2), and the overall spectrum (*black*, large circle defines ROI 3). Spectral resolution in the microscope is lower than in the spectrofluorometer. Image size is 15×15 μm. The spectral images of PRODAN and LAURDAN are not shown (the reader can find this information in Ref. [14])

what is expected from liquid water (where the emission maximum is located around 520 nm). In light of these results the application of the model discussed in Sect. 2 is justified by the observation that the DAN probes detect two main fluorescence contributions, which we assigned to correspond to unrelaxed and relaxed states of the probe, Fig. 3.

The most conspicuous observation arose when yeast labeled with the DAN probes exhibits glycolytic oscillations. This has been observed both using cuvette fluorescence spectroscopy measurements and fluorescence microscopy [14]. As shown in Fig. 4 the fluorescence intensity of these reporters fluctuates at the same frequency to that measured for NADH and ATP. This phenomenon, which is emission wavelength independent, is also reflected in oscillations measured in the GP function (Fig. 4c). Following the model presented in Sect. 2, oscillations of the GP function in the cell yielding the measured changes in the intensity of emission (quantum yield) of the probes at any given wavelength can be explained only if solvent relaxation is the dominant mechanism. Importantly, spatially resolved information obtained from fluorescence microscopy experiments show that oscillations of both NADH concentration and the DAN probes span all measured size scales, as established by multiphoton excitation microscopy in progressively

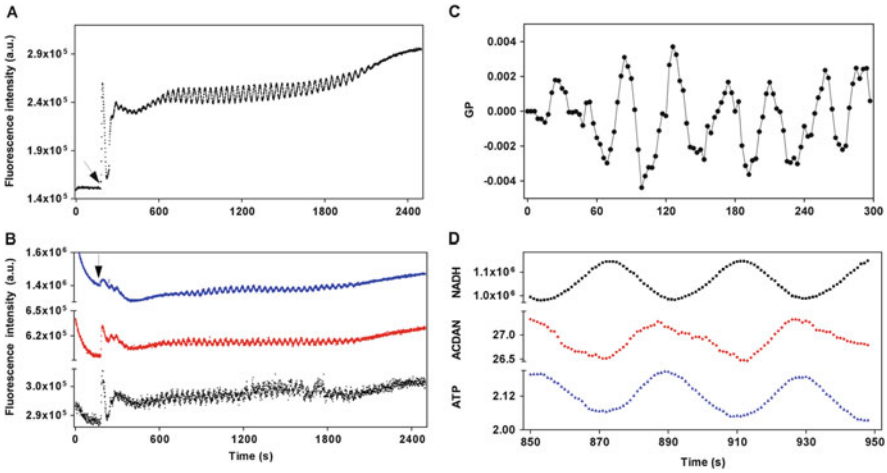

Fig. 4 Oscillatory behavior of glycolysis and DAN probes in the fluorometer. Panel (**a**) Oscillations of NADH. Panel (**b**) Oscillations of ACDAN (*red*), PRODAN (*blue*), and LAURDAN (*black*). Panel (**c**) Oscillations in the Generalized Polarization (GP) function (for ACDAN). Panel (**d**) Phase relationships: ACDAN and NADH are expressed as fluorescence intensity, ATP is plotted in concentration units (mM). The *arrows* in panels (**a**), (**b**), and (**c**) indicate the time of addition of 30 mM glucose followed by 5 mM KCN

smaller regions of interest (ROIs), ranging from many cells to a single intracellular pixel (see Fig. 5 for a representative example) [14].

Control experiments were performed to confirm whether the oscillations observed for DAN probes have a different origin to those included in the above-mentioned model. For example, similar experiments using ANS – which specifically interacts with membranes and proteins and shows negligible fluorescence emission when dissolved in liquid water [40] – show a total lack of oscillatory behavior, arguing against oscillations originating in interactions not mediated by water [14]. Additionally, iodoacetate (a blocker of glycolysis) causes a correlated disappearance of all oscillations (NADH, ATP, and DAN probes) and, as ATP is depleted, a bathochromic spectral response of the probes is observed. *All these observations indicate that water properties are coupled with the metabolic process that generates ATP in the intracellular environment*. It is important to note that ATP/ADP by themselves in a crowded solution do not affect ACDAN fluorescence [14], suggesting that it is the cellular environment that is responsible for the oscillatory behavior of the probe.

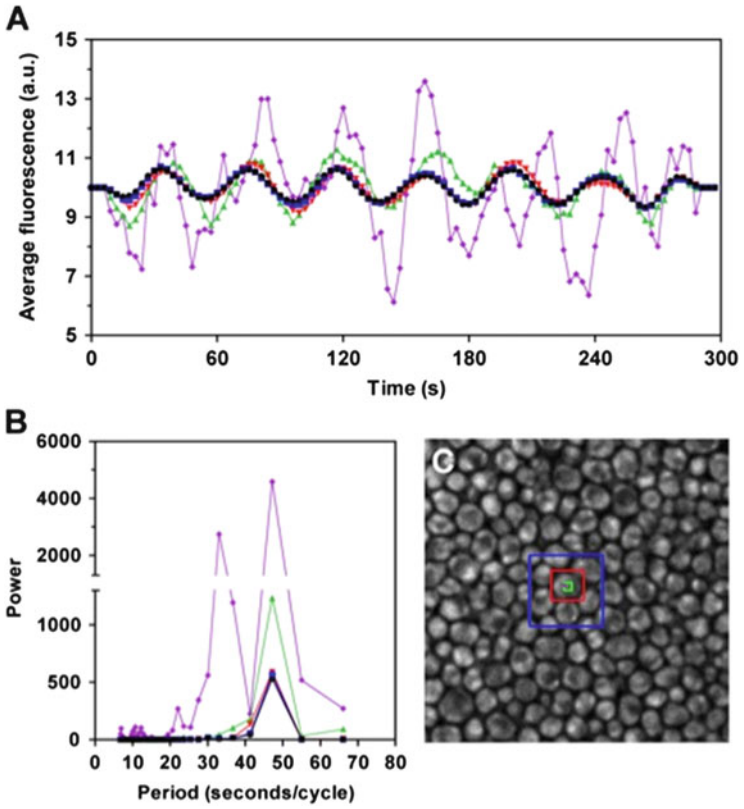

Fig. 5 NADH oscillations in the microscope. Panel (**a**) Running average of NADH oscillations at different scales. *Black*, whole image; *Blue*, 7 cells; *Red*, 1 cell; *Green*, 7×7 intracellular pixels; and *Purple*, single pixel. Panel (**b**) Power analysis of oscillations in each region. Panel (**c**) Picture of NADH fluorescence (438 ± 12 nm) with color-coded regions of interest. Pixel size is 0.1 μm, image corresponds to a field of 25.6×25.6 μm

6 Experiments with D_2O

Pure water relaxes at an extremely fast rate [41], in picoseconds, yielding the observed ACDAN (or PRODAN) fluorescence emission maximum at 520 nm. Compared to water, D_2O is denser, has higher freezing and boiling temperatures, and is more viscous. However, ACDAN and PRODAN in pure H_2O and D_2O display exactly the same emission peak (Fig. 6). In other words, *in bulk* (i.e., when dipoles reorient much faster than the excited state lifetime) the DAN probes are "blind" to any differences between normal and "heavy" water: both solvents draw the maximum possible energy from the excited state of the probes. However, when yeast cells are suspended in increasing concentrations of D_2O (10, 20, and 50% v/v) and the oscillations of NADH, ACDAN, and PRODAN are measured, there is a significant decrease in their oscillation frequency (Fig. 7a), which is

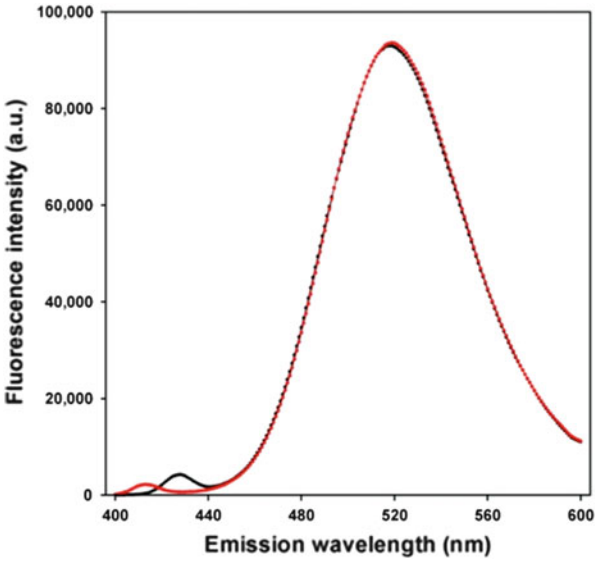

Fig. 6 Fluorescence of ACDAN in solvents. Raw fluorescence emission spectra of 5 μM ACDAN in pure H_2O (*black*) and pure D_2O (*red*). The lower peak at shorter wavelengths corresponds to the Raman effect of the solvent. The same behavior was observed for PRODAN

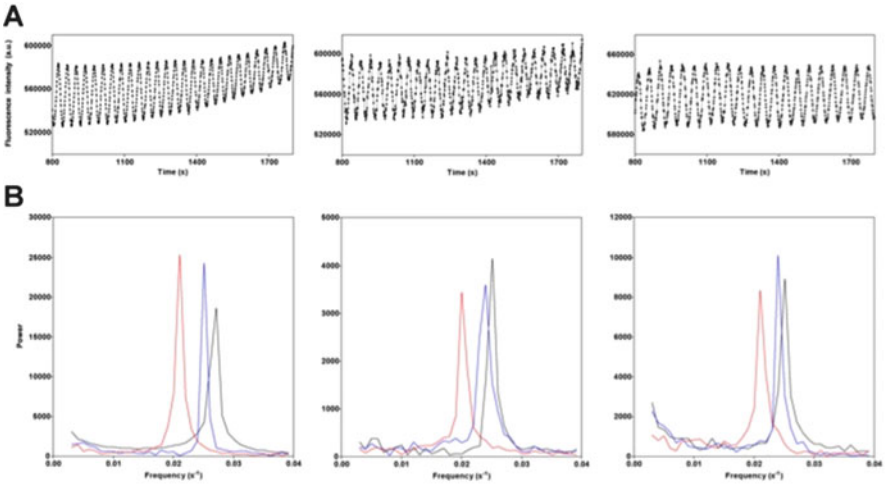

Fig. 7 The effect of D_2O on NADH, ACDAN, and PRODAN oscillations. (**a**) The *top panels* show NADH oscillations in the presence of no D_2O, 10% D_2O, and 50% D_2O (from *left* to *right*). (**b**) The *bottom panels* show the power spectra of the oscillations of NADH, ACDAN, and PRODAN with increasing concentrations of D_2O (*black* 0%, *blue* 10%, and *red* 50%)

apparent in the power spectrum representation (Fig. 7b). It is important to notice that in resting cells, 50% D_2O does not alter the emission spectrum of any of the DAN probes [14], consequently, the effect observed in Fig. 7 is on the temporality of the oscillations, not on the probes.

Heavy water has many biological effects [42]. Its impact on cytoskeletal dynamics is well documented although quantitative explanations are still under investigation [43]. The lower frequency of glycolytic oscillations in the presence of D_2O might be conceived as a consequence of the fact that deuterated compounds are chemically more stable and that the rates of reactions involving deuterated bonds can be slower. However, while this would be an apparently straightforward explanation for the *chemical transformations* very much in the spirit of van't Hoff, it fails to explain why the oscillations of the DAN probes occur at all, and why they remain synchronous with the slowed down ATP oscillations. It is important to stress that it is the *frequency* of all oscillations that is affected by D_2O, not the response of the probes [14].

We propose that a more comprehensive explanation requires consideration of the well-known fact that the presence of deuterium affects the rates of reactions even if deuterated bonds are not themselves involved (cf. membrane phase transitions mentioned in Sect. 2). This effect is termed the secondary isotope effect [42]; with deuterated water in the medium, it seems reasonable to conclude that the entire nanoenvironment where oscillating glycolysis occurs involves some degree of structure that is *dynamically* affected by the addition of a small amount of extra mass per molecule in the most abundant class of molecules [14]. These results also sustain the exquisite sensitivity of these probes to detect changes due to solvent dipolar relaxation in biological systems.

7 A Challenge for the Classical View Describing the Intracellular Environment

Our current framework of understanding of cellular processes relies on the premise that the cell cytosol is, at the relevant scale, like the dilute aqueous solutions in which we study biochemical processes in vitro. If this were true, partially water-soluble probes like ACDAN and PRODAN, sensitive to dipolar relaxation dynamics, would not be expected to sense significant changes in the intracellular medium at this scale. In our view, the properties of the oscillations of the DAN probes are more consistent with the intracellular environment behaving as a responsive hydrogel, a view with very strong experimental support [34]. The study of hydrogels has traditionally relied on classical physicochemical measurements of equilibrium properties of the medium affected by crowding such as vapor pressure, swelling, and shrinking. The results presented along this chapter *provide robust direct spatial and temporal evidence of the intracellular aqueous phase as a medium exhibiting fast and coherent coupling of an intensive* (*scale-invariant*) *cellular property* (*i.e.*,

intracellular water relaxation) *with a central metabolic process* [14]. This conclusion challenges the use of the concept of "normal" diffusion, a corollary of van't Hoff's theory of ideal solutions, to explain and build models of integrated cellular behavior. The coupling, at multiple scales, of water dynamics to ATP levels during glycolytic oscillations may offer a more complete perspective of the category of phenomena generally described as anomalous diffusion. In fact, the very term "anomalous diffusion" is an acknowledgement that the environment inhabited by intracellular molecules of interest – in this case a key product of glycolysis whose concentration oscillates – cannot be accurately described in terms of concepts derived from the chemistry of dilute solutions, or diffusion in terms of a straightforward application of the Stokes–Einstein relationship.

Considering that polymerization/depolymerization of cytoskeletal structures is strongly dependent on ATP and ATPase activity [43–45], it is reasonable to suppose that ATP acts on the overall state of the cytoskeleton and that this impacts dipolar relaxation of the aqueous phase, possibly due to changes in viscoelastic properties. As metabolism oscillates so do interfacial water dynamics; as D_2O makes the system "heavier," all oscillations are synchronously slowed down. The chemistry and physics of the system are thus bidirectionally coupled. Solvent (water) motion has been shown to govern an important part of the energy landscape occupied by proteins, affecting catalysis [46, 47] and folding [48]. The observations reported in this chapter provide a robust biological system for theoretical development and experimental testing of Erwin Schrodinger's insight that life depends on the maintenance of a low entropy state [49, 50]. The cytosol as a hydrogel, with most of its water dynamically coupled to central metabolic processes, may provide the substrate where an entropic level of understanding of key processes of life can be found [51].

But is there any useful model that can help us to explain this phenomenon?

8 Coupling Between Intracellular Water Dynamics and Metabolism: A Call for Models

In 1861 Max Schultze, professor of Botany in Bonn, pronounced his protoplasmic doctrine, according to which a living cell is a membrane-less lump of protoplasm containing a nucleus. The view was supported by Thomas Huxley, the once opponent of the concept of protoplasm, who then stated that protoplasm constitutes the physical basis of life. Without going into excessive historical detail, this view known as protoplasmatic theory evolved along the years developing a strong foundation in the physicochemical properties of colloidal systems, i.e., building on the observations that the behavior of most solutes inside cells does not necessarily resemble their behavior in dilute solutions. In this model cells are conceived as colloidal systems that dynamically respond to fluctuations, either by dampening them or by amplifying them cooperatively. Therefore their properties are

considered as emergent properties of organized supramolecular systems. Importantly and different from the membrane theory which assumes intracellular water to exist in the liquid state, the cellular interior accommodates solutes based on adsorption sites and solubility properties of its colloidal water and it is kept organized by central metabolism in a low entropy state, which becomes responsive to environmental factors in very defined ways. Although important contributors to these ideas during the twentieth century were Dmitrii Nasonov and Afanasy S. Troshin (among others), the most complete version of this theory was provided in 1962 by Gilbert N. Ling, who called it the *Association-Induction* (*A-I*) *hypothesis* [49]. Ling's A-I hypothesis strongly challenges the modern mainstream consensus model of cellular membranes based on the fluid-mosaic model that envisions a lipid bilayer separating the inside from the outside of cells with associated ion channels, pumps, and transporters giving rise to the permeability processes of cells. In addition, Ling's A-I hypothesis is not giving any relevant role to lipids or to their supramolecular structures, emphasizing that interactions among proteins, water, salts, and relevant metabolites are the dominant parameters for cellular functioning. A brief description is provided below. For detailed (and updated) sources describing these concepts see references [52, 53]. In particular, reference [52] introduces an interesting idea to explain the macroscopic physical properties of the cell cytoplasm, i.e., a basic structural unit composed of proteins, water, ATP, and ions he termed the nano-protoplasm.

8.1 The Association-Induction Hypothesis

If water in the cell is comparable to dilute solutions, then all phenomena central to cell physiology, that is, integrated and coherent cellular behavior, will be the result of the properties of the membranes separating the various dilute aqueous compartments within the cell, and between the cell and the extracellular milieu. Three related phenomena that conform the core of cell physiology, namely solute distributions, electric potentials, and volume regulation, are today understood to map to the particular constitutions and activities of interfaces (membranes) between compartments. Marginal importance – if any – is accorded to the bulk properties of the aqueous media on either side of the borders. In other words, intensive (i.e., scale-invariant) properties of the compartments are not considered to be of relevance as the activities that define the compartments lie at their boundaries; their compositions and dynamics are the result of what their boundaries contain and, consequently, what they allow through or remove.

Gilbert Ling, following Troshin's Sorption Theory [54], developed a comprehensive statistical mechanical treatment of the behavior of solutes, both ionic and non-ionic, in the context of complex polyelectrolytes, as well as the response of the polymers themselves to the solutes. Both the theoretical developments and his careful experimentation were published in numerous articles and integrated in his monumental, and barely known, *A physical theory of the living state*: *The*

Association-Induction hypothesis [49]. Although his conclusions are far reaching and difficult to summarize fairly, it would be fair to state that he provides the first integrated description of the coupling between high molecular weight polymers (mostly proteins), small solutes (metabolites and ions), and the mechanical properties of the aqueous environment both at equilibrium (the "resting state" of cells) and during cellular responses to stimuli (cellular action). Although Ling concentrated mostly on the physiology of muscle contraction and neural transmission, his theoretical framework extends well beyond and generalizes to all physiological phenomena [52, 53]. It provides thorough interpretations of all three physiological phenomena mentioned above, and a context for the observations we report in our study of metabolic oscillations and water dipolar relaxation.

In the A-I hypothesis, the influence of polymers and solutes on the integrated properties of the water-protein-metabolite system is a central feature of the structural and dynamic properties of cellular behavior. The products of central metabolic processes modulate the bulk properties of cells and cellular compartments, which in turn govern the interchange of ionic species (Na^+, K^+, and others) and metabolites based on differential adsorption and solubility in the crowded water phase. Specifically, Ling proposed that fluctuations in the activity of metabolites (e.g., ATP) during an active metabolic process, through association with – an inductive effect on – alter the conformational states of fibrillar proteins (e.g., those that participate in the cytoskeleton). This association-induction effect modulates the binding affinity of these ions for proteins, changing also the structure of intracellular water (described by the polarized-oriented multilayer theory of cell water [52]) and, therefore, the partition coefficients of numerous molecular actors. In the current dominant view of the cell the conceptual model is the semipermeable membrane that divides two mostly aqueous phases (compartments) and, consequently, its key concepts for interpretation of cell structure and behavior are permeability and transport. In the A-I view, however, a more accurate model is the ion-exchange resin (i.e., the structured polyelectrolyte or fixed-charge system) and the tools for interpretation of physiological data are adsorption and partition coefficients [49, 53]. In more current terminology we could call the latter systems responsive hydrogels, capable of responding to fluctuations in their environments with many of the non-linear properties of living systems.

9 Concluding Remarks

Considering our results with the exquisitely sensitive DAN probes, we find ourselves in a situation where the dipolar relaxation phenomena as reported by the DAN fluorophores reveal coupling between (bio)chemical oscillations and some property of the major aqueous component of the cell. In the A-I hypothesis, ATP plays a critical role by keeping the cell at a low entropy state. The oscillations of water relaxation and their tight temporal coupling to the oscillating process (glycolysis) that cyclically produces and consumes ATP are a very suggestive indicator

of the power of the A-I interpretation of physiological processes. This coupling is difficult to explain in light of the canonical cell model, where water is considered a passive liquid medium.

As an author put it, "It needs, perhaps, a certain intellectual effort to accept that (...) highly specific and regularly localised events (...) can be generated by interactions of vaguely spread, almost or completely constant parameters with some quite degenerate, occasionally localised dynamical perturbations, rather than by strictly specific and precisely located events" [55].

The A-I hypothesis provides a rigorous body of theory and a wealth of experimental data to couple the chemical (metabolic transformations) and physical (mechanical cellular responses), as well as tools for the interpretation of much of the most recent research on cellular physiology, unavailable at the time of Schrödinger and Ling. Considering what we now know about polymer physical chemistry and excitability, and the tools we now possess to explore the behavior of living systems non-invasively and in multiple spatial and temporal scales, it may be high time to rethink the standard models that guide our thinking and interpretation of physiology using the A-I framework as a starting point.

A Note from the First Author

The first author of this paper was extremely privileged to meet Gregorio Weber for first time during his PhD studies in Argentina, specifically at the meeting of the Argentinian Biophysical Society that took place in the beautiful hills of Villa Giardino, province of Córdoba in November of 1994:

> My PhD advisor requested help to pick up Gregorio Weber at a Hotel in the city of Córdoba and drive him to Villa Giardino. I obviously pushed very hard to (successfully) get that duty; being a young student it was a moment of great excitement to have the chance to meet "the professor". I will never forget the enthusiasm and expectations I had. Biological fluorescence was one of my favorite topics, which largely influenced on my decision to pursue a PhD in biophysics at the University of Córdoba in Argentina. I had everything planned, I had at least 1 h of travel from Córdoba to Villa Giardino, so I prepared many questions based on my study of his seminal papers on fluorescence. My plan however was not accomplished at all and I ended up hearing an amazing history of Gregorio as a young boy, travelling in a train through the Córdoba hills for vacations. With his wording he had the ability to transform the beautiful landscape around us into a 1920s postcard scene. Notwithstanding a fruitful discussion in my poster, during that meeting he also gave me advice that influenced enormously my scientific career: to join Enrico Gratton's group as a post-doc. Another relevant lesson from the professor came later in that meeting, when he gave an hour-long closing talk on fluorescence using only one overhead! Needless to say, one of the most interesting and inspiring talks I have ever attended in my entire professional career.

Acknowledgements This work is supported by a grant from the Danish Research Council (FNU, 12-124751 0602-02507B).

References

1. Weber G, Farris FJ (1979) Synthesis and spectral properties of a hydrophobic fluorescent probe: 6-propionyl-2-(dimethylamino)naphthalene. Biochemistry 18(14):3075–3078
2. Lippert E (1957) Spektroskopische Bestimmung des Dipolmomentes aromatischer Verbindungen im ersten angeregten Singulettzustand. Z Elektrochem 61:962–975
3. Macgregor RB, Weber G (1981) Fluorophores in polar media: spectral effects of the Langevin distribution of electrostatic interactions. Ann NY Acad Sci 366:140–154
4. Lakowicz JR, Weber G (1973) Quenching of protein fluorescence by oxygen. Detection of structural fluctuations in proteins on the nanosecond time scale. Biochemistry 12 (21):4171–4179
5. Macgregor RB, Weber G (1986) Estimation of the polarity of the protein interior by optical spectroscopy. Nature 319(6048):70–73
6. Prendergast FG, Meyer M, Carlson GL, Iida S, Potter JD (1983) Synthesis, spectral properties, and use of 6-acryloyl-2-dimethylaminonaphthalene (Acrylodan). A thiol-selective, polarity-sensitive fluorescent probe. J Biol Chem 258(12):7541–7544
7. Parasassi T, Gratton E (1995) Membrane lipid domains and dynamics as detected by LAURDAN fluorescence. J Fluoresc 5(1):59–69
8. Parasassi T, Krasnowska EK, Bagatolli L, Gratton E (1998) LAURDAN and PRODAN as polarity-sensitive fluorescent membrane probes. J Fluoresc 8(4):365–373
9. Zeng J, Chong PL (1995) Effect of ethanol-induced lipid interdigitation on the membrane solubility of Prodan, Acdan, and Laurdan. Biophys J 68(2):567–573
10. Lakowicz JR, Bevan DR, Maliwal BP, Cherek H, Balter A (1983) Synthesis and characterization of a fluorescence probe of the phase transition and dynamic properties of membranes. Biochemistry 22:5714–5722
11. Jurkiewicz P, Sykora J, Olzynska A, Humpolickova J, Hof M (2005) Solvent relaxation in phospholipid bilayers: principles and recent applications. J Fluoresc 15(6):883–894
12. Kim HM et al (2007) A two-photon fluorescent probe for lipid raft imaging: C-laurdan. Chembiochem 8(5):553–559
13. Dodes Traian MM, Gonzalez Flecha L, Levi V (2012) Imaging lipid lateral organization in membranes with C-laurdan in a confocal microscope. J Lipid Res 53(3):609–616
14. Thoke HS et al (2015) Tight coupling of metabolic oscillations and intracellular water dynamics in saccharomyces cerevisiae. PLoS One 10(2), e0117308
15. Parasassi T, Conti F, Gratton E (1986) Time-resolved fluorescence emission spectra of laurdan in phospholipid vesicles by multifrequency phase and modulation fluorometry. Cell Mol Biol 32(1):103–108
16. Parasassi T, De Stasio G, d'Ubaldo A, Gratton E (1990) Phase fluctuation in phospholipid membranes revealed by laurdan fluorescence. Biophys J 57(6):1179–1186
17. Parasassi T, De Stasio G, Ravagnan G, Rusch RM, Gratton E (1991) Quantitation of lipid phases in phospholipid vesicles by the generalized polarization of laurdan fluorescence. Biophys J 60(1):179–189
18. Parasassi T, Gratton E (1992) Packing of phospholipid vesicles studied by oxygen quenching of laurdan fluorescence. J Fluoresc 2(3):167–174
19. Antollini SS, Barrantes FJ (1998) Disclosure of discrete sites for phospholipid and sterols at the protein-lipid interface in native acetylcholine receptor-rich membrane. Biochemistry 37 (47):16653–16662
20. Jurkiewicz P, Olzynska A, Langner M, Hof M (2006) Headgroup hydration and mobility of DOTAP/DOPC bilayers: a fluorescence solvent relaxation study. Langmuir 22(21):8741–8749
21. Bagatolli LA (2013) LAURDAN fluorescence properties in membranes: a journey from the fluorometer to the microscope. In: Mely Y, Duportail G (eds) Fluorescent methods to study biological membranes, Springer series on fluorescence, vol 13. Springer, Heidelberg

22. Roenneberg T, Dragovic Z, Merrow M (2005) Demasking biological oscillators: properties and principles of entrainment exemplified by the Neurospora circadian clock. Proc Natl Acad Sci U S A 102(21):7742–7747
23. Jaeger J, Goodwin BC (2001) A cellular oscillator model for periodic pattern formation. J Theor Biol 213(2):171–181
24. Kruse K, Julicher F (2005) Oscillations in cell biology. Curr Opin Cell Biol 17(1):20–26
25. Goldbeter A (1996) Biochemical oscillations and cellular rhythms: the molecular basis of periodic and chaotic behaviour. Cambridge University Press, Cambridge
26. Richard P (2003) The rhythm of yeast. FEMS Microbiol Rev 27(4):547–557
27. Richard P, Teusink B, Hemker MB, Van Dam K, Westerhoff HV (1996) Sustained oscillations in free-energy state and hexose phosphates in yeast. Yeast 12(8):731–740
28. Poulsen AK, Lauritsen FR, Olsen LF (2004) Sustained glycolytic oscillations–no need for cyanide. FEMS Microbiol Lett 236(2):261–266
29. Olsen LF, Andersen AZ, Lunding A, Brasen JC, Poulsen AK (2009) Regulation of glycolytic oscillations by mitochondrial and plasma membrane H+-ATPases. Biophys J 96(9):3850–3861
30. Reijenga KA et al (2001) Control of glycolytic dynamics by hexose transport in Saccharomyces cerevisiae. Biophys J 80(2):626–634
31. Novak B, Tyson JJ (2008) Design principles of biochemical oscillators. Nat Rev Mol Cell Biol 9(12):981–991
32. Clegg JS (1984) Properties and metabolism of the aqueous cytoplasm and its boundaries. Am J Physiol 246(2 Pt 2):R133–R151
33. Luby-Phelps K (2000) Cytoarchitecture and physical properties of cytoplasm: volume, viscosity, diffusion, intracellular surface area. Int Rev Cytol 192:189–221
34. Fels J, Orlov SN, Grygorczyk R (2009) The hydrogel nature of mammalian cytoplasm contributes to osmosensing and extracellular pH sensing. Biophys J 96(10):4276–4285
35. Spitzer J (2011) From water and ions to crowded biomacromolecules: in vivo structuring of a prokaryotic cell. Microbiol Mol Biol Rev 75(3):491–506, second page of table of contents
36. Hazlewood CF, Chang DC, Nichols BL, Woessner DE (1974) Nuclear magnetic resonance transverse relaxation times of water protons in skeletal muscle. Biophys J 14(8):583–606
37. Yoo H, Paranji R, Pollack GH (2011) Impact of hydrophilic surfaces on interfacial water dynamics probed with NMR spectroscopy. J Phys Chem Lett 2(6):532–536
38. Kiser PF, Wilson G, Needham D (1998) A synthetic mimic of the secretory granule for drug delivery. Nature 394(6692):459–462
39. Fenimore PW, Frauenfelder H, McMahon BH, Young RD (2004) Bulk-solvent and hydration-shell fluctuations, similar to alpha- and beta-fluctuations in glasses, control protein motions and functions. Proc Natl Acad Sci U S A 101(40):14408–14413
40. Slavik J (1982) Anilinonaphthalene sulfonate as a probe of membrane composition and function. Biochim Biophys Acta 694:1–25
41. Zasetsky AY (2011) Dielectric relaxation in liquid water: two fractions or two dynamics? Phys Rev Lett 107(11):117601
42. Thomson JF (1963) Biological effects of deuterium. Pergamon, Oxford
43. Leterrier JF (2001) Water and the cytoskeleton. Cell Mol Biol 47(5):901–923
44. Korn ED, Carlier MF, Pantaloni D (1987) Actin polymerization and ATP hydrolysis. Science 238(4827):638–644
45. Stark BC, Wen KK, Allingham JS, Rubenstein PA, Lord M (2011) Functional adaptation between yeast actin and its cognate myosin motors. J Biol Chem 286(35):30384–30392
46. Frauenfelder H, Fenimore PW, Young RD (2007) Protein dynamics and function: insights from the energy landscape and solvent slaving. IUBMB Life 59(8–9):506–512
47. Frauenfelder H (2008) What determines the speed limit on enzyme catalysis? Nat Chem Biol 4 (1):21–22
48. Frauenfelder H, Fenimore PW, Chen G, McMahon BH (2006) Protein folding is slaved to solvent motions. Proc Natl Acad Sci U S A 103(42):15469–15472

49. Ling GN (1962) A physical theory of the living state: the association-induction hypothesis. Blaisdell, New York
50. Schrödinger E (1944) What is life? The physical aspect of the living cell. Cambridge University Press, Cambridge
51. Young RD, Fenimore PW (2011) Coupling of protein and environment fluctuations. Biochim Biophys Acta 1814(8):916–921
52. Ling G (2007) Nano-protoplasm: the ultimate unit of life. Physiol Chem Phys Med NMR 39 (2):111–234
53. Ling G (1984) In search of the physical basis of life. Plenum, New York
54. Troshin AS (1966) Problems of cell permeability. Pergamon, Oxford
55. Beloussov LV (1989) Dynamical levels in developing systems. In: Goodwin B, Sibatani A, Webster G (eds) Dynamic structures in biology. Edinburgh University Press, Edinburgh

Continuing Inspiration: Gregorio Weber's Influence on Understanding the Basis of Allosteric Regulation of Enzymes

Gregory D. Reinhart

Abstract In addition to his pioneering work utilizing quantitative fluorescence techniques to study biological macromolecules and assemblies, Gregorio Weber contributed substantially to our understanding of the thermodynamic relationships between different ligand-binding equilibria and subunit association equilibria in proteins. These ideas have proven to be very valuable in clarifying the basis for allosteric modification of enzyme behavior when allosteric ligands act predominantly to modify the affinity of an enzyme's substrate. Dr. Weber's influence, both scientific and personal, on the author's efforts to understand the allosteric behavior of prokaryotic and eukaryotic phosphofructokinase (PFK) in particular is described. These observations not only serve to illuminate the regulatory properties of this important enzyme, but they also, in turn, serve to illustrate the validity of the principles that Weber originally described. Not surprisingly fluorescence techniques have played important roles in elucidating many of these insights.

Keywords Allosteric regulation • Coupling free energy • Entropy domination • Fluorescence polarization • Phosphofructokinase

Contents

G.D. Reinhart (✉)
Department of Biochemistry and Biophysics, Texas A&M University and Texas A&M AgriLife Research, College Station, TX 77843-2128, USA
e-mail: gdr@tamu.edu

D.M. Jameson (ed.), *Perspectives on Fluorescence: A Tribute to Gregorio Weber*, Springer Ser Fluoresc (2016) 17: 217–234, DOI 10.1007/4243_2016_20,

1 Early Years

On paper, at least that which contains my CV, my connection with Gregorio Weber seems tenuous as my only formal relationship with him stems from the single year I spent in his lab as an undergraduate researcher my senior year from 1972 to 1973. However, the impact of my association with "the Professor" could not have been more profound or formative for my eventual career. This dichotomy is made all the more ironic when I reflect on my utter intimidation at the time that caused me to adopt a primarily observational role in the lab while meekly pursuing my own experiments. Never before had I been exposed to so many homemade precision scientific instruments and, more importantly, so many individuals engaged in such high-level scientific discourse. And I must confess, it took me a while to get used to the accent. . .

My project was to synthesize a fluorescent probe, chrysenebutyric acid, that could be used in a manner similar to pyrenebutyric that Weber and Knopp [1, 2] had recently put forth as a long-lifetime probe suitable for studying very large proteins. Chrysenebutyric acid was expected to have a shorter, but still relatively long, lifetime that could be used for studying somewhat smaller proteins.

Eventually I succeeded with the synthesis and therefore needed to venture into the realm of fluorescence characterization using the aforementioned homebuilt instruments. Fortunately (for me anyway) Dave Jameson, then a second year graduate student in the lab, took me under his wing at that point, and through his efforts I was able to utilize most of the various spectrometers, spectrofluorometers, and fluorometers in the lab. I remember in particular collecting the fluorescence polarization data, that were eventually to appear as Figure 11 in my undergraduate thesis, with a sample of chrysenebutyric acid in propylene glycol at –55°C on the T-format polarization instrument designed and built by Weber and Bablouzian some years before [3]. What made this experiment particularly memorable was that Dave and I collected the data in the wee hours of a Saturday night/Sunday morning – thus defining "nerd-like" behavior long before the term was in common use. The most lasting benefit of this exercise for me, though, was the concomitant discussions with Dave, and subsequently Dr. Weber, about the meaning and significance of fluorescence polarization.

Fast forward to the latter part of my graduate career that I spent, largely at Dr. Weber's recommendation, at the University of Wisconsin in the laboratory of Dr. Henry Lardy. Unbeknownst to me, a postdoc had begun lobbying for the lab to acquire a research-grade spectrofluorometer better than the old Aminco-Bowman that was then ubiquitous in non-fluorescence-centric research labs such as ours. Dr. Lardy had delegated the task of new instrument acquisition to a research scientist, Fritz Stratman, in the lab (it was a big lab), and one day Fritz came up to me and asked if I knew anything about the company "SLM" that was headquartered in Urbana and the instrument they had just put on the market – a state-of-the-art photon-counting spectrofluorometer. After quickly connecting a couple of dots in my mind, I replied: "Not specifically, but if the 'S' stands for

Spenser and the 'M' for Mitchell, I'm sure it's a good instrument." Dick Spenser and George Mitchell had been postdocs in Weber's lab when I was there, and Dick and Dave had been working on applying the then new technology of photon-counting detection to a scanning spectrofluorometer, the end result of which had just been described [4]. (Dick Spenser had previously developed the first 2-frequency phase/modulation fluorometer as a graduate student [5]. I had used prototypes of each of these instruments to characterize the chrysenebutyric acid I synthesized, along with the polarization instrument built by Weber and Bablouzian.) My surmise proved to be correct (the 'L' stood for Dave Laker – the talented machinist in the Departmental machine shop who actually fabricated much of the hardware for Weber's instruments whom I had not met as an undergraduate), and we soon acquired one of the early SLM Model 8000 photon-counting spectrofluorometers.

Over the next few months my project in Lardy's lab was increasingly focused on understanding the tendency of liver phosphofructokinase (PFK) to self-associate to extremely large aggregates. Liver PFK was (and is) thought to be an important component to the regulation of blood sugar homeostasis in mammals [6, 7]. I was beginning to suspect that the self-association behavior might play a significant role in PFK's physiological regulation. I recalled somewhat vaguely the technique of fluorescence polarization that I had been introduced to in Weber's lab and thought it might be useful in following this self-association reaction. Also, the postdoc who had pushed to acquire our SLM instrument had moved on so the instrument, along with its nice set of Glan-Thompson polarizers, was sitting there "begging" for me to take advantage. So I made a "cold" call to Dave Jameson (still in Weber's lab) roughly 4-years after our late-night experiments to inquire (1) whether labeling PFK with a commercially available reactive pyrene probe would be straightforward; and (2) whether embarking on such an effort would likely be a scientific excursion of no more than 6 months since I was already feeling pressures to bring my Ph.D. research to a culmination. Dave immediately invited me to come down to Urbana for a couple of weeks during which time he was convinced that we would not only label the enzyme but also make the majority of the critical measurements I was interested in. Suffice it to say, my trip down to Urbana initiated a 2-year investigation, involving several trips to Urbana, which completely changed the nature of my Ph.D. dissertation.

During that first visit my old feelings of intimidation came back, exacerbated by my uncertainty as to whether Dr. Weber would even remember this former undergraduate who had made a point of being as inconspicuous as possible. My concern was not alleviated when, in the first conversation Dave and I had with Weber, which Dave has recently recounted in his book [8], Dr. Weber indicated that "of course" the commercially available pyrene probe we were using would have a short lifetime, rather than the long lifetime I had expected, because there was a carbonyl conjugated to the pyrene ring system. That night, the three of us went out to eat and while we were in the car, I thanked Dr. Weber for allowing me to try to get this project started by working once again in his lab, and that I had been worried that he might not remember me or my previous time in the lab. Dr. Weber once again chose the perfect words to address my concerns both spoken and unspoken at the time – he

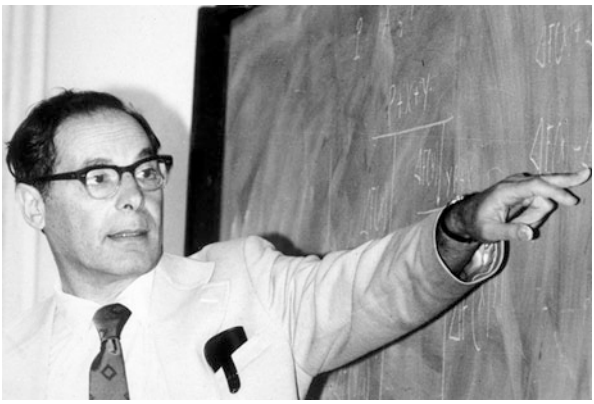

Fig. 1 Gregorio Weber illustrating the idea behind coupling free energies circa 1970. Photo courtesy of Dave Jameson

said: "Yes Greg, once you are in the lab you are always a member of the family." I immediately felt at ease, and over the next 20 years Dr. Weber became one of my two closest scientific mentors (Dr. Lardy, of course, being the other).

It was during this re-association with Dr. Weber and his lab toward the end of my graduate training in Wisconsin that I became aware of the papers that Dr. Weber had written in the early to mid-1970s regarding ligand binding to proteins and the thermodynamic constraints that must occur when multiple ligands bind to the same protein [9–11]. Indeed, Weber always looked upon fluorescence techniques as tools that he implemented to gain greater insight into biological macromolecules and assemblies. In particular he focused much of his early attention on proteins and protein-ligand interactions. (Once when I was still an undergraduate in his lab, Weber entered the lab from his nearby office to excitedly announce to all who quickly assembled that he thought he "finally understood BSA." Only later did I connect the "dots" that he was working on the ligand-binding papers [10, 11] at the time (Fig. 1).)

A simple linkage argument, as framed by Weber, was soon to take center stage as the foundational principle upon which the central thesis of my Ph.D. research rested. My overall objective had been to understand the molecular basis by which the hormone glucagon effected an inhibition of the glycolytic enzyme PFK in rat liver, concomitant with glucagon's well-known stimulation of hepatic gluconeogenesis. However, when I isolated the enzyme, it was already completely inhibited when assessed with physiological concentrations of substrates and allosteric regulators [12]. My problem, therefore, morphed into trying to understand how PFK was active in the first place before I felt it was reasonable to address the glucagon-dependent inhibition mechanism.

The various allosteric activators and inhibitors of PFK share a common feature – they act by modifying the apparent binding affinity the enzyme displays for its substrate, fructose 6-phosphate (Fru-6-P). The activation I was seeking, therefore, was one that substantially improved the apparent binding affinity of Fru-6-P, particularly in the face of an ever-present, and surprisingly constant concentration of, MgATP – both the co-substrate for the enzyme and more importantly under

physiological concentrations, an important allosteric inhibitor. At the average intracellular concentration of MgATP (~3 mM), the apparent affinity for Fru-6-P is in the mM range while the physiological concentration of Fru-6-P is roughly only 10 μM [12].

It soon became apparent when working with the enzyme isolated from rat livers that it had a strong tendency to self-associate to very large species that remained active. Analogous species had been observed previously to be formed by the much more studied PFK from rabbit muscle [13–15], but rat liver PFK tended to form these high molecular weight forms at much lower protein concentrations [16]. The smallest active form of mammalian PFK is a homotetramer comprised of subunits with molecular weights of approximately 80,000 (i.e., tetramer M_r equal to 320,000). Yet the high molecular weight self-association represented an association of these tetramers – my early estimates based on ultracentrifugation behavior were that species comprised of about 12 tetramers (molecular weight equal to 3.8 million) were being formed. It was to study this self-association that sent me back to Weber's lab with the intent to label PFK with pyrene to allow the monitoring of the extent of association using fluorescence polarization.

Once this assay was in place (using a more appropriate derivative of pyrene), it quickly became apparent that the high molecular weight self-association was dramatically influenced by ligand binding [16, 17]. The ligands with the most pronounced effects were MgATP and Fru-6-P. When observed at an enzyme concentration comparable to that which exists in the cell, MgATP favored the formation of the tetrameric form of the enzyme while Fru-6-P promoted the self-association of the tetramers to the high molecular weight form(s). Weber, of course, had also considered the coupling of ligand binding to self-association, what he termed "micro- and macro-associations," respectively, in his ligand-binding papers of the early 1970s (Fig. 2) [10, 11]. This coupling dictates a simple prediction: If a ligand promotes oligomerization, then the oligomer itself must have a higher affinity for that ligand. Since Fru-6-P promoted the formation of the high molecular weight species, I concluded that those species must exhibit a higher affinity for Fru-6-P than the tetramer.

We observed these effects at a physiological enzyme concentration that was 2 orders of magnitude higher than the enzyme concentration that was normally employed when studying enzyme kinetics. We concluded, as had those working with the rabbit muscle enzyme, that PFK was largely, if not completely, tetrameric at that dilution. Therefore, the self-association likely to occur at the physiological PFK concentration, particularly given the other features of the cellular milieu, would promote the binding of Fru-6-P beyond what was evident during in vitro kinetic assessment. Lardy and I proposed that the self-association of the tetramers represented the activation mechanism I had been looking for [17]. Weber's ligand-binding analyses, and the utility of fluorescence polarization measurements, were the key to this proposal.

As luck (and the insights of other researchers) would have it, about a year after my thesis defense, several labs nearly simultaneously discovered the metabolite, fructose 2,6-bisphosphate, and found that it was a profound activator of PFK [18–22].

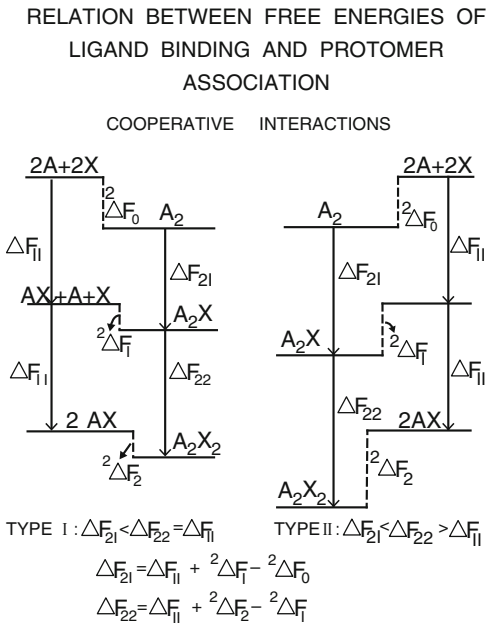

Fig. 2 Free energy diagram from [10] with which Weber illustrates the relationship between cooperative ligand binding and protomer–protomer interactions

Moreover its synthesis and degradation proved to be manipulated by glucagon in a manner that was consistent with the proposed stimulation of gluconeogenesis through the inhibition of PFK [23, 24]. This more dramatic discovery overshadowed our proposal, although subsequently I examined the effect of Fru-2,6-BP on the self-association properties of PFK and concluded that they may still play a role in fully rationalizing the apparent activity of PFK in vivo even in the presence of the activator Fru-2,6-BP [25].

2 Ligand Binding and Allosteric Regulation of Enzymes

Weber's ligand-binding papers had a far more profound impact on my ensuing career as an independent investigator. After some reflection, I felt that the Professor's papers on ligand binding provided a better basis for analyzing allosteric behavior of enzymes than the alternative models then generally employed. So I set about first casting the basic thermodynamic ideas that Weber discussed into terms that I hoped would be more familiar to enzymologists, employing a variation of the notation proposed by Cleland and widely used by the enzymology community [26, 27]. A key point was to direct attention to the determination of the coupling parameter, which I called "Q."

This analysis, as it relates to an allosteric enzyme, begins with the single-substrate, single-modifier enzyme mechanism depicted in Scheme 1:

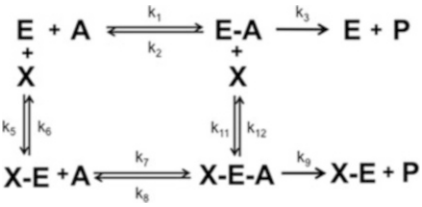

Scheme 1 Single substrate- single modifier enzyme mechanism to which Weber's linkage analysis can be applied

where A is substrate, P is product, X is allosteric ligand, E is free enzyme, XE is enzyme with allosteric ligand bound, EA is enzyme with substrate bound, XEA is the ternary complex with enzyme with both substrate and allosteric ligand bound, K_a^0 is equal to the Michaelis Constant in the absence of allosteric ligand, K_a^∞ is equal to the Michaelis Constant in the saturating presence of X, K_{ix}^0 is equal to the dissociation constant of X in the absence of substrate, and K_{ix}^∞ is the dissociation constant of X when substrate is saturating. Even a mechanism as simple as this one yields a complex rate equation if only steady state is presumed [28]. However, it is common to presume that the rapid-equilibrium assumption is valid, i.e., that the enzyme-substrate complexes are more likely to dissociate reforming free substrate than to proceed on to form product. This assumption is usually valid for allosteric enzymes, which often have fairly low turnover numbers, and it has been found experimentally to be valid for Fru-6-P binding to PFK [29]. Under conditions of rapid-equilibrium, the rate equation for Scheme 1 is given by:

$$v = \frac{V^0[A] + V^0QW[A]}{K_{ia}^0K_{ix}^0 + K_{ia}^0[X] + K_{ix}^0[A] + Q[A][X]} \tag{1}$$

where V^0 equals the maximal velocity in the absence of X, K_{ia}^0 equals the dissociation constant for A in the absence of X (which in turn equals K_a^0 under conditions of rapid-equilibrium). The parameters W and Q are defined by the following two equations:

$$W = \frac{V^\infty}{V^0} \tag{2}$$

$$Q = \frac{K_{ia}^0}{K_{ia}^\infty} = \frac{K_{ix}^0}{K_{ix}^\infty} \tag{3}$$

where V^∞ equals the maximal velocity when X is saturating, K_{ia}^∞ equals the dissociation constant for substrate when X is saturating, and K_{ix}^∞ equals the dissociation constant for X when substrate is saturating. W and Q quantitatively describe the nature and magnitude of the allosteric effect on turnover and substrate affinity, respectively, with values greater than one signifying activation and values less than one signifying inhibition. Q defines the effects of PEP and MgADP on PFK since these ligands almost exclusively modulate the affinity PFK displays for its substrate, fructose-6-phosphate. Q is also related to the coupling free energy, or

free energy of interaction, between the substrate ligand and the allosteric ligand, ΔG_{ax}, as defined by Weber [9–11], as follows:

$$\Delta G_{ax} = -RT\ln(Q_{ax}) \tag{4}$$

where R is the gas constant, T is temperature in Kelvin, and the subscripts denote the coupled ligands. Expressing the action of an allosteric ligand in terms of coupling free energy presents two practical advantages: the sign of ΔG_{ax} gives the nature of the allosteric effect (positive sign → inhibition, negative sign → activation), and the energetic effects of activation and inhibition are expressed with equal dynamic range.

Determining the coupling between a substrate and an allosteric ligand is straightforward – one simply performs a substrate titration to yield a saturation curve from which an apparent K_a can be determined. This basic experiment is then repeated at varying concentrations of allosteric ligand. The values of K_a as a function of allosteric ligand concentration can then be fit to the functional dependence suggested by Eq. (1), which is given by:

$$K_a = K_{ia}^0\left(\frac{K_{ix}^0 + [X]}{K_{ix}^0 + Q_{ax}[X]}\right) \tag{5}$$

We have found it useful to construct a plot of log (K_a) vs. log [X] to visualize the trend of K_a transitioning from the limiting value at low [X] (K_{ia}^0) to the limiting value at high [X] (K_{ia}^∞) from which the value of log (Q_{ax}) can be estimated. The concepts were useful, and could be applied straightforwardly, even on complex, oligomeric, highly cooperative enzymes, such as rat liver PFK, by focusing on the behavior of the half-saturation value, $K_{1/2}$, which is functionally equivalent to K_a, rather than on the more complex saturation behavior of substrate, and fitting the data to Eq. (5). We demonstrated straightforward utilization of these concepts in the characterization of the pH dependence of the allosteric inhibition of PFK by ATP [30], and subsequently the effects of Fru-2,6-BP [31].

Central to Weber's point in his papers was that, because the binding energy of a small ligand is derived from multiple interactions each contributing a small amount, it would be unreasonable that the consequences of binding a ligand on the subsequent binding of another ligand at a distant site would be anything other than a fraction of the binding energy, i.e., roughly 1–2 kcal/mole for a single ligand. This magnitude predicted that, even in the case of an inhibitory allosteric ligand, the effects of that ligand should saturate – a consequence of forming the ternary complex with both substrate and inhibitor bound simultaneously to the protein. Although in principal the apparent coupling observed in an oligomeric protein could increase with the number of interacting sites, we were gratified to observe, initially with rat liver PFK and eventually with several other enzymes including at

the time mitochondrial isocitrate dehydrogenase (ICDH), that such saturation could be demonstrated – allowing the coupling to be quantified in most cases.

The quantification of the coupling parameter, therefore, provides an unambiguous characterization of both the nature of an allosteric effect. It also allowed for the separation of these issues from the binding affinity of the allosteric ligand, something that becomes conflated when one presumes the nature of the allosteric effect is somehow predetermined by a pre-existing conformational state to which functional attributes are ascribed and the ligand need only bind to that form. This then (and I fear still) prevailing view only leaves the respective binding affinities as the basis of comparison of one inhibitor to another, while clearly the coupling free energy framework allows different ligands to exhibit different efficacies regardless of how their binding affinities compare. Indeed, we have over the ensuing several years made note of several situations where a ligand binds less tightly than its counterpart but actually inhibits more strongly once bound [29, 32].

3 Protein Dynamics and Allosterism

In a classic case of doing the right experiment for the wrong reason, I began to consider how the coupling free energy might vary with temperature. Drawing an analogy to membranes, I wondered whether a temperature might be reached at which the internal organization of the protein's folded structure might become disorganized – akin to the phase transition in membranes. Although even I didn't expect such a dramatic change, I wondered whether any discontinuity might be observed in the coupling free energy as a function of temperature. The coupling free energy, after all, was a direct measure of "communication" between two sites on a protein and, particularly if those sites were on opposite sides of the protein, it should be sensitive to any sudden change that might occur. When we proceeded to analyze coupling free energies as a function of temperature, we didn't observe the expected discontinuities, but upon reflection we felt that we had observed something possibly more significant.

The coupling free energy describing the inhibition of Fru-6-P binding to rat liver PFK by MgATP, as well as coupling free energy describing the activation by ADP of isocitrate binding to beef heart mitochondrial ICDH, instead of exhibiting discontinuities, demonstrated a continuous trend that was quite linear when subjected to a van't Hoff analysis (Fig. 3) [33]. As Weber had shown, the coupling free energy can be considered to be the standard free energy associated with the disproportionation equilibrium:

Scheme 2 Disproportion equilibrium for which the standard free energy is equal to the coupling free energy between A and X

$$EA + XE \rightleftharpoons XEA + E$$

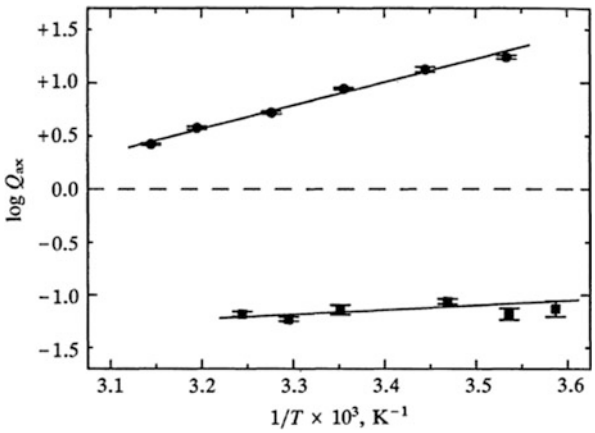

Fig. 3 Variation with reciprocal temperature of the logarithm of the coupling between isocitrate and ADP binding to isocitrate dehydrogenase (*top panel*) and between Fru-6-P and MgADP binding to rat liver PFK (*bottom panel*). The coupling free energy is negative for the data in the *top panel* and positive for the *bottom panel*. Yet the positive slope of both lines indicates that the coupling enthalpy is negative for both cases. In PFK, therefore, the positive coupling free energy must be the result of a negative TΔS component that is larger in absolute value than the absolute value of the coupling enthalpy. The significance is discussed in the text. Figure from [33]

Consequently the temperature dependence of the equilibrium constant giving rise to coupling free energy, which we found to be linear when plotted as the logarithm versus reciprocal temperature, can be interpreted in terms of the underlying ΔH and ΔS components that give rise to the coupling free energy. Not surprisingly for both cases, the sign of ΔH and ΔS was the same indicating a substantial degree of compensation when the individual values of ΔH and TΔS are compared to the value of ΔG. The coupling free energy for the activation by ADP of ICDH, which has a negative value by definition according to the sign conventions used by Weber [10, 11] and adopted by us [26], was derived from a negative value of the coupling enthalpy that dominated the contribution of the negative value of TΔS (i.e., ΔH had a greater absolute value than TΔS). This result taken in isolation was not that surprising given a "conformation-centric" view of the structural basis for ligand binding. What was surprising was that the coupling exhibited for the MgATP inhibition of rat liver PFK was entropy dominated, meaning that the positive sign of the coupling free energy was derived from ΔH and TΔS terms that also were negative, just as they had been for ICDH, but unlike that case, for the MgATP–Fru-6-P coupling in PFK the absolute value of TΔS was bigger than that for ΔH giving rise to the positive value for ΔG. We termed this "entropy-dominated coupling" because it was the entropy term that established the sign, and hence the nature, of the allosteric effect. A corollary to this observation was that the sign of the coupling enthalpy was the opposite that for ΔG. Hence, for MgATP inhibition of rat liver PFK, ΔH was negative and thereby actually favoring activation rather than the inhibition that is observed.

Of course, I discussed our observations with Dr. Weber on many occasions, often in his apartment over meals of "microwave pasta" – the result of a process he developed involving a layering of Saran Wrap over the uncooked pasta in water, with only a corner folded back for venting, and then running the microwave a precise amount of time. He delighted in describing this procedure to the uninitiated because it yielded perfect "al dente" pasta every time.

The fact that entropy change could be the dominant, and directing, component of the allosteric effect begged the question of what was causing the entropy change, particularly in the "entropy-dominated" situations. Given that the entropy change pertains to the disproportionation coupling reaction (Scheme 2), it is notable that free ligand is absent from this reaction. Consequently the large hydration changes expected when ligand binding occurs should not be a factor when considering the molecular basis for allosteric coupling. Certainly the possibility exists that the different protein-ligand complexes on each side of the equilibrium have different extents of hydration, but since the filled and unoccupied binding sites are balanced, the likelihood of this mechanism being dominant would seem to be minimized. Instead, the possibility that changes in conformational entropy may be the dominant mechanism at play seemed compelling. To the extent that this occurs, it suggests that conformational changes that might be evident in X-ray crystal structures of various ligated species would not reveal the true conflict that causes an inhibitor to actually antagonize the binding of substrate ligand (and vice versa). Instead, the dynamics of the structure might contain the actual basis for the inhibition. Moreover, since the coupling enthalpy actually favors activation, the crystal structures actually might contain features that would directly mislead one from understanding the basis of inhibition per se.

The other striking feature of our temperature results was that the trend was in fact quite continuous – indeed essentially linear in a van't Hoff presentation. Although our original data for ICDH and rat liver PFK exhibited positive slopes in the van't Hoff plots, we have since observed negative slopes as well for other systems. But in almost all cases, linearity is observed over at least a 30° span around 25°C. Since a coupling free energy equal to 0 is indicative of no allosteric effect, with positive signs indicating inhibition and negative values activation, we predicted that it might be possible for temperature alone to cause the sign of the coupling free energy to transition from positive to negative (or vice versa) – hence leading to a temperature-induced inversion of the allosteric effect. Subsequently we published several examples of just this type of cross-over of allosteric effect by modifying only temperature [34, 35].

Of course virtually all of these ideas were explored and matured in my conversations with Dr. Weber over the course of several visits. Ultimately we published our findings in a PNAS paper that was communicated by Dr. Weber [33] in 1989. And I was particularly honored when he chose to include our result and conjectures in his seminal book on "Protein Interactions" published in 1992 [36]. The notion that the transmission of allosteric influence might have an entropic, and hence dynamic, origin was also gaining credence with other investigators [37].

4 Deflating the Two-State Premise

Concomitant with the prediction and the demonstrations of saturation of the allosteric affect, necessary to quantify the coupling free energy, was the obvious incompatibility of these observations with the notion that allosteric enzymes consist of only two conformational states that exclusively bind either substrate or allosteric inhibitor exclusively. Despite Dr. Weber's eloquent arguments against this simplistic notion as being not just inadequate, but fundamentally misleading with respect to the true nature of proteins and their interactions with other proteins and small molecular weight ligands, the idea, probably because of its simplicity and its appeal to "intuitive common sense," continued to (and does to this day) dominate both the rhetoric and the thinking about the basis of regulation exhibited by allosteric enzymes. After being emboldened to seek evidence for the role of dynamics in allosteric transmission, we switched much of our attention from rat liver PFK to PFK from prokaryotes, notably *E. coli* and *B. stearothermophilus*. These enzymes have several advantages for this objective, being much smaller (subunit molecular weight 34,000), extremely stable obligate homotetramers with no propensity to self-associate further, and much simpler allosteric properties derived from a single allosteric site per subunit to which either the inhibitor phospho(*enol*)pyruvate (PEP) or the activator ADP can bind. But most compelling for our purposes was that both *E. coli* PFK and *B. stearothermophilus* PFK contain only a single tryptophan per subunit. At the time (early 1990s) the fluorescence of many single tryptophan proteins had been characterized using time-resolved techniques in an effort to understand the nature of the internal dynamical properties of proteins. We hoped to utilize similar approaches to examine the relationship between dynamics and allosteric functionality. Eventually this effort would take advantage of the power of site-directed mutagenesis to manipulate the tryptophan position in an effort to sample a wider range of interior environments, but initially we settled for examining the tryptophan in the native position of *E. coli* PFK. Of course our first experiments involved steady state fluorescence measurements.

Since *E. coli* PFK could bind either an inhibitor or an activator, and the actions of these ligands seemed to exclusively influence the binding of the substrate, Fru-6-P, the allosteric properties had been viewed as providing a nice example of a straightforward R-T system in which the inhibited form of the enzyme bound the inhibitor PEP well and the substrate Fru-6-P poorly, while the active form of the enzyme bound Fru-6-P and ADP well and PEP poorly. Not only had the kinetic behavior of the enzyme been characterized in this fashion [38], but the previous work on the intrinsic tryptophan fluorescence seemed to support this idea as well [39]. Both ADP and Fru-6-P cause the intrinsic fluorescence of *E. coli* PFK to diminish to nearly the same level whereas PEP binding causes the intrinsic fluorescence to increase to a small extent. These observations, together with the positive cooperativity the kinetics display with respect to Fru-6-P titrations in the absence of either allosteric ligand, reinforced the notion that apo enzyme exists in a

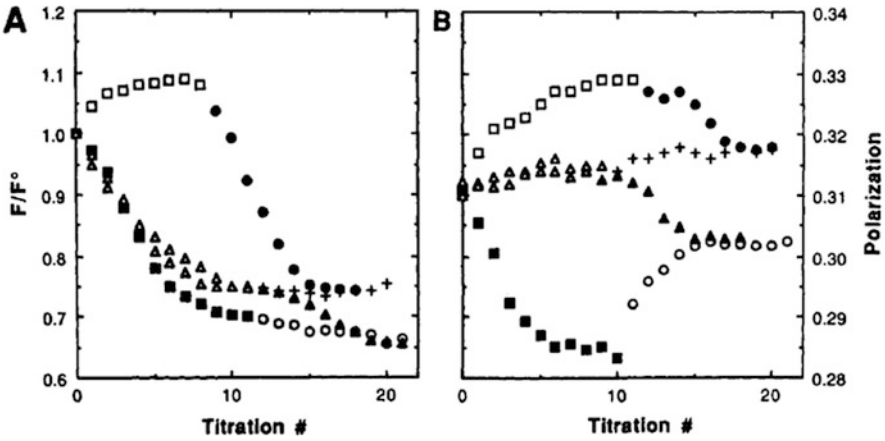

Fig. 4 Response of intrinsic tryptophan fluorescence emission (**A**) and polarization (**B**) to titration of successive equal quantities of ligand to *E. coli* PFK. Either Fru-6-P (*closed squares*), MgADP (*open triangles*), or MgATP (*open squares*) was added to free enzyme. Subsequently MgADP was added after Fru-6-P (*open circles*), Fru-6-P was added after MgADP (*closed triangles*), or MgATP was added after MgADP (*plus sign*). Note how different the responses are to the binding of Fru-6-P and MgADP when polarization is monitored in contrast to the similar response of the emission. Figure from [40]

form very similar to the "T" form adopted when PEP binds and that either Fru-6-P or ADP can upon binding induce the "R" form.

We took another look at these results and largely confirmed the effects of these two ligands on quantum yield [40, 41]. The intrinsic fluorescence of the single tryptophan substantially decreased when either Fru-6-P or ADP bound (Fig. 4), and the fluorescence increased to a small but significant extent when PEP bound (Fig. 5). Although we were able to detect a slightly different extent of decrease in quantum yield with ADP binding compared to Fru-6-P binding, that difference was small relative to the overall decrease. Additionally, when Fru-6-P was titrated after PEP saturation, to form the ternary complex, the fluorescence intensity diminished to what was arguably a value comparable to the Fru-6-P binary complex alone. These results were generally consistent with previous observations and in general support of a 2-state model.

A very different picture emerged, however, when we looked at the steady state polarization of the tryptophan fluorescence in response to ligand binding. Fru-6-P binding caused a decrease in fluorescence polarization, but ADP did not, clearly demonstrating that Fru-6-P and ADP do not form the same "R" state when assessed in this manner. In addition, when Fru-6-P and ADP both bind simultaneously, the fluorescence polarization of the tryptophan clearly adopts a unique value quite distinct from either of the Fru-6-P or ADP binary complexes.

In contrast to the quantum yield changes, PEP binding caused a decrease in the fluorescence polarization, although to a somewhat lesser extent than did Fru-6-P. The ternary complex formed when Fru-6-P and PEP bind simultaneously exhibits a

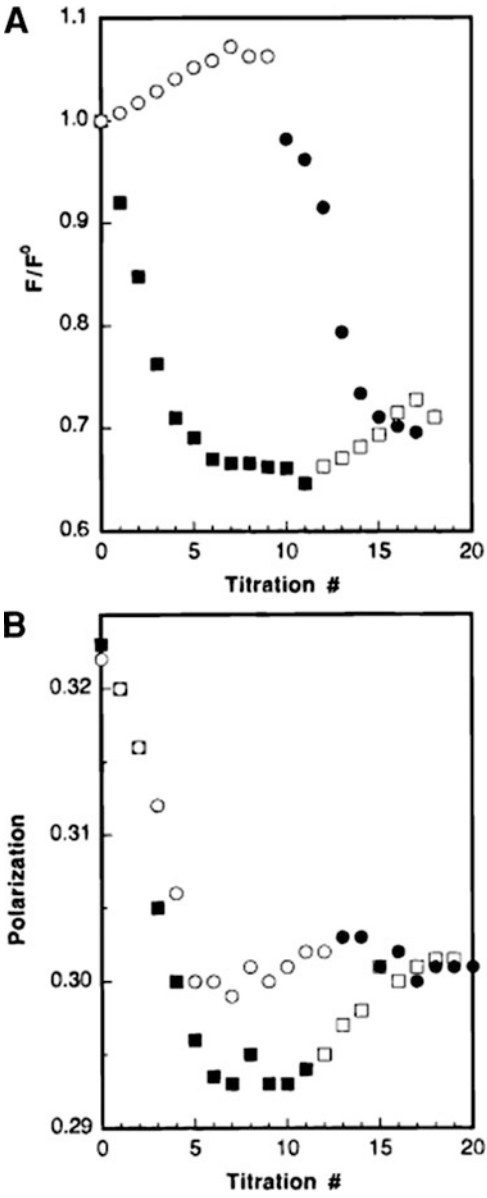

Fig. 5 Response of intrinsic tryptophan fluorescence emission (**A**) and polarization (**B**) to titration of successive equal quantities of ligand to *E. coli* PFK. Either Fru-6-P (*closed squares*) or PEP (*open circles*) was added to free enzyme. Subsequently either PEP was added to enzyme saturated with Fru-6-P (*open squares*) or Fru-6-P was added to enzyme saturated with PEP (*closed circles*). Figure from [41]

quantum yield comparable to the Fru-6-P bound form but a fluorescence polarization value comparable to the PEP binary complex. Clearly, when the intrinsic fluorescence of the native tryptophan is thoroughly assessed, one cannot escape the conclusion that Fru-6-P, ADP, and PEP each form binary complexes with unique conformational properties and that the ternary complexes formed by the

binding of any two of these ligands (except ADP and PEP which cannot bind simultaneously) produce unique conformations as well.

Moreover, given that the overall size and shape of *E. coli* PFK do not change upon ligand binding, these results directly suggested that the internal dynamics of the protein, at least in the vicinity of the lone tryptophan per subunit, must be perturbed by ligand binding. We proceeded to examine, via the time-resolved fluorescence properties of this tryptophan, how the motion of this tryptophan changed with ligand binding [41, 42]. In general the data suggested that the amplitude of motion, rather than the rate of motion per se, was perturbed, increasing most notably when the substrate Fru-6-P bound. Thus this prediction made from the temperature dependence data Weber and I had discussed several years previously, also seemed to be born out, although relating the motion changes to a measurable thermodynamic parameter cannot be expected without greater sampling of the overall protein structure.

5 Summary

In the years since these first observations, we have gone on to dissect the coupling relationships in the homotetramer of prokaryotic PFK, study the dynamical properties of allosteric enzymes as they relate to allosteric functionality using an expanding array of techniques including recently NMR, and the implications of ligand-induced quaternary changes as they may relate to enzyme regulatory behavior, using techniques such as fluorescence correlation spectroscopy. In all of these efforts we have been, and continue to be, inspired by Gregorio Weber – by his scientific insights and achievements as well as his approach to science. I am exceedingly grateful that in the beginning he accepted this reserved undergraduate into his research "family." I am proud to say that in the end he was my mentor and friend.

References

1. Knopp J, Weber G (1967) Fluorescence depolarization measurements on pyrene butyric-bovine serum albumin conjugates. J Biol Chem 242(6):1353–1359
2. Knopp JA, Weber G (1969) Fluorescence polarization of pyrenebutyric-bovine serum albumin and pyrenebutyric-human macroglobulin conjugates. J Biol Chem 244(23):6309–6315
3. Weber G, Bablouzian B (1966) Construction and performance of a fluorescence polarization spectrophotometer. J Biol Chem 241(11):2558–2561
4. Jameson DM, Spencer RD, Weber G (1976) Construction and performance of a scanning, photon-counting spectrofluorometer. Rev Sci Instrum 47(9):1034–1038
5. Spencer RD, Weber G (1969) Measurements of subnanosecond fluorescence lifetimes with a cross-correlation phase fluorometer. Ann N Y Acad Sci 158(1):361–376

6. Clark MG, Kneer NM, Bosch AL, Lardy HA (1974) The fructose 1,6-diphosphatase-phosphofructokinase substrate cycle. A site of regulation of hepatic gluconeogenesis by glucagon. J Biol Chem 249(18):5695–5703
7. Clark MG, Bloxham DP, Holland PC, Lardy HA (1974) Estimation of the fructose 1,6-diphosphatase-phosphofructokinase substrate cycle and its relationship to gluconeogenesis in rat liver in vivo. J Biol Chem 249(1):279–290
8. Jameson DM (2014) Introduction to fluorescence. CRC/Taylor and Francis, New York
9. Weber G (1970) Binding of small ligands by proteins. Hormonal steroids. In: Proceedings of the Third International Congress, Hamburg, September 1970, pp 58–65
10. Weber G (1972) Ligand binding and internal equilibiums in proteins. Biochemistry 11 (5):864–878
11. Weber G (1975) Energetics of ligand binding to proteins. Adv Protein Chem 29:1–83
12. Reinhart GD, Lardy HA (1980) Rat liver phosphofructokinase: kinetic activity under near-physiological conditions. Biochemistry 19(7):1477–1484
13. Aaronson RP, Frieden C (1972) Rabbit muscle phosphofructokinase: studies on the polymerization. The behavior of the enzyme at pH 8, pH 6, and intermediate pH values. J Biol Chem 247(23):7502–7509
14. Pavelich MJ, Hammes GG (1973) Aggregation of rabbit muscle phosphofructokinase. Biochemistry 12(7):1408–1414
15. Lad PM, Hill DE, Hammes GG (1973) Influence of allosteric ligands on the activity and aggregation of rabbit muscle phosphofructokinase. Biochemistry 12(22):4303–4309
16. Reinhart GD, Lardy HA (1980) Rat liver phosphofructokinase: use of fluorescence polarization to study aggregation at low protein concentration. Biochemistry 19(7):1484–1490
17. Reinhart GD, Lardy HA (1980) Rat liver phosphofructokinase: kinetic and physiological ramifications of the aggregation behavior. Biochemistry 19(7):1491–1495
18. Furuya E, Uyeda K (1980) An activation factor of liver phosphofructokinase. Proc Natl Acad Sci U S A 77(10):5861–5864
19. Furuya E, Uyeda K (1980) Regulation of phosphofructokinase by a new mechanism. An activation factor binding to phosphorylated enzyme. J Biol Chem 255(24):11656–11659
20. Claus TH, Schlumpf J, Pilkis J, Johnson RA, Pilkis SJ (1981) Evidence for a new activator of rat liver phosphofructokinase. Biochem Biophys Res Commun 98(2):359–366
21. Pilkis SJ, El-Maghrabi MR, Pilkis J, Claus TH, Cumming DA (1981) Fructose 2,6-bisphosphate. A new activator of phosphofructokinase. J Biol Chem 256(7):3171–3174
22. Van Schaftingen E, Jett MF, Hue L, Hers HG (1981) Control of liver 6-phosphofructokinase by fructose 2,6-bisphosphate and other effectors. Proc Natl Acad Sci U S A 78(6):3483–3486
23. Richards CS, Uyeda K (1980) Changes in the concentration of activation factor for phosphofructokinase in hepatocytes in response to glucose and glucagon. Biochem Biophys Res Commun 97(4):1535–1540
24. Hue L, Blackmore PF, Exton JH (1981) Fructose 2,6-bisphosphate. Hormonal regulation and mechanism of its formation in liver. J Biol Chem 256(17):8900–8903
25. Reinhart GD (1983) Influence of fructose 2,6-bisphosphate on the aggregation properties of rat liver phosphofructokinase. J Biol Chem 258(18):10827–10830
26. Reinhart GD (1983) The determination of thermodynamic allosteric parameters of an enzyme undergoing steady-state turnover. Arch Biochem Biophys 224(1):389–401
27. Cleland WW (1963) The kinetics of enzyme-catalyzed reactions with two or more substrates or products. I. Nomenclature and rate equations. Biochim Biophys Acta 67:104–137
28. Frieden C (1964) treatment of enzyme kinetic data. I. The effect of modifiers on the kinetic parameters of single substrate enzymes. J Biol Chem 239:3522–3531
29. Tlapak-Simmons VL, Reinhart GD (1994) Comparison of the inhibition by phospho(enol) pyruvate and phosphoglycolate of phosphofructokinase from B. stearothermophilus. Arch Biochem Biophys 308(1):226–230
30. Reinhart GD (1985) Influence of pH on the regulatory kinetics of rat liver phosphofructokinase: a thermodynamic linked-function analysis. Biochemistry 24(25):7166–7172

31. Reinhart GD, Hartleip SB (1986) Relationship between fructose 2,6-bisphosphate activation and MgATP inhibition of rat liver phosphofructokinase at high pH. Kinetic evidence for individual binding sites linked by finite couplings. Biochemistry 25(23):7308–7313
32. McGresham MS, Lovingshimer M, Reinhart GD (2014) Allosteric regulation in phosphofructokinase from the extreme thermophile Thermus thermophilus. Biochemistry 53(1):270–278. doi:10.1021/bi401402j
33. Reinhart GD, Hartleip SB, Symcox MM (1989) Role of coupling entropy in establishing the nature and magnitude of allosteric response. Proc Natl Acad Sci U S A 86(11):4032–4036
34. Braxton BL, Tlapak-Simmons VL, Reinhart GD (1994) Temperature-induced inversion of allosteric phenomena. J Biol Chem 269(1):47–50
35. Tlapak-Simmons VL, Reinhart GD (1998) Obfuscation of allosteric structure-function relationships by enthalpy- entropy compensation. Biophys J 75(2):1010–1015
36. Weber G (1992) Protein interactions. Chapman and Hall, New York
37. Cooper A, Dryden DTF (1984) Allostery without conformational change – a plausible model. Eur Biophys J 11:103–109
38. Blangy D, Buc H, Monod J (1968) Kinetics of the allosteric interactions of phosphofructokinase from Escherichia coli. J Mol Biol 31(1):13–35
39. Deville-Bonne D, Garel JR (1992) A conformational transition involved in antagonistic substrate binding to the allosteric phosphofructokinase from Escherichia coli. Biochemistry 31(6):1695–1700
40. Johnson JL, Reinhart GD (1994) Influence of MgADP on phosphofructokinase from Escherichia coli. Elucidation of coupling interactions with both substrates. Biochemistry 33 (9):2635–2643
41. Johnson JL, Reinhart GD (1997) Failure of a two-state model to describe the influence of phospho(enol)pyruvate on phosphofructokinase from Escherichia coli. Biochemistry 36 (42):12814–12822
42. Johnson JL, Reinhart GD (1994) Influence of substrates and MgADP on the time-resolved intrinsic fluorescence of phosphofructokinase from Escherichia coli. Correlation of tryptophan dynamics to coupling entropy. Biochemistry 33(9):2644–2650

Using Fluorescence to Characterize the Role of Protein Oligomerization in the Regulation of Gene Expression

Catherine A. Royer

Abstract Gregorio Weber's legacy, in addition to seminal contributions in the application of fluorescence to the study of biological molecules, includes, as well, a profound understanding of how protein–protein interactions are intimately coupled to their interactions with ligands. Such energetic and structural coupling implies that protein sequences have evolved such that these interactions are finely tuned to the physiological habitat and state of the organisms in which these proteins function. The work of my group, in collaboration with a number of biologists and biochemists over the years, has sought to discover how protein–protein interactions, both homologous oligomerization and heterologous complex formation, are implicated in the regulation of gene expression. Herein are given several examples of how fluorescence can be applied to characterize the molecular and energetic basis for the role of protein interactions in the regulation of gene expression. Described are several fluorescence approaches, some quite basic and others more complex, how they were applied to specific gene expression regulatory systems both in vitro and in vivo, and what information could be extracted from the results. Apparent from these few examples is the central role played by protein–protein interactions in these regulatory mechanisms, and how any model for regulatory mechanisms must take into account these higher order protein interactions.

Keywords Allostery • Free energy coupling • Oligomerization • Transcription • Translation

C.A. Royer (✉)
Department of Biological Sciences, Rensselaer Polytechnic Institute, Troy, NY, USA
e-mail: royerc@rpi.edu

D.M. Jameson (ed.), *Perspectives on Fluorescence: A Tribute to Gregorio Weber*,
Springer Ser Fluoresc (2016) 17: 235–254, DOI 10.1007/4243_2016_12,

Contents

1 Introduction

In addition to Gregorio Weber's seminal contributions to the field of biological fluorescence, his work in the area of protein interactions, cooperativity, and allostery remains a major legacy in biochemistry [1]. Given his dual expertise in fluorescence and bio-molecular interactions, it is not surprising that he was able to make great progress in both fields simultaneously. Since Weber's early work on the polarization of fluorescent dyes bound to proteins [2, 3], fluorescence emerged and has remained one of the best methods for quantitative measurements of protein interactions. The widespread use of fluorescence in modern quantitative biology stems from several major advantages over alternative methods, advantages that Gregorio Weber recognized, developed and exploited over his illustrious career. One major advantage of fluorescence is its high sensitivity, which allows for equilibrium measurements of very high affinities between biomolecules. Indeed, with the development of instrumentation capable of single molecule detection, fluorescence has replaced most detection methods based on radioactivity. Another advantage of fluorescence for measuring protein interactions is the fact that binding is determined at equilibrium with no need to separate bound from free species. In addition, given its high sensitivity, fluorescence can be measured very quickly, allowing highly quantitative characterization of the kinetics of protein interactions, extending down to the microsecond range, which is useful for monitoring the intramolecular protein interactions implicated in fast protein folding (e.g., [4, 5]). Fluorescence detection is easily coupled to instrumentation for perturbing equilibria such as stopped flow or titration devices and microfluidic systems, as well as temperature and pressure perturbation. Indeed, Weber pioneered the use of fluorescence coupled to pressure perturbation to monitor protein interactions, both intra- and inter-molecular [6].

Weber used the many fluorescence approaches he developed to probe a number of different types of protein interactions. These include ligand binding (cooperative and antagonistic) [7–14], homologous and heterologous protein subunit interactions [15–25], and the coupling between the two [1, 26]. These studies highlighted the

energetic subtlety of the protein and ligand concentration dependencies of important regulatory circuits. I was a graduate student in Gregorio Weber's group in the early 1980s at the time he was working on the subject of free energy couplings between ligand binding and protein oligomerization. During that period, Brian Matthews visited the University of Illinois and gave a seminar presenting the first 3-D structure of a transcriptional repressor, the *lambda* Cro Repressor dimer [27], which is necessary to induce the lytic cycle of *lambda* phage infection. It binds to two operator regions in the phage DNA in competition with the *cI* repressor, which is required to maintain the lysogenic state. Each of the operator regions contains three binding sites for the repressor dimers, which exhibit different affinities for the different target sites in the operators. Together these two repressors control the switch between lysogenic and lytic phases of infection [28, 29]. Inspired by Brian Matthews' beautiful dimeric structure, the complexity of this apparently finely tuned biological switch and Weber's work on free energy couplings between subunit oligomerization and target binding, I asked if and how protein subunit interactions might be coupled to operator DNA binding in such cases. Indeed, work in the group of Gary Ackers [30–34] and later Don Senear [35, 36] revealed the quantitatively exquisite control at work in *lambda* switch, and the complex oligomerization equilibria involved. In collaboration with Kathleen Matthews we carried out a study of the role of subunit interactions in the mechanism of *lac* repressor function, a major subject of her research group [37–41]. This set me on the path of over thirty years of work using fluorescence approaches to characterize the energetics and structure–function relationships for protein systems implicated in the regulation of gene expression. In this chapter, I will review the major applications of these techniques by my group, highlighting what sort of information they have provided concerning the systems under study.

2 The *Lac* Repressor

I began to work on the *lac* repressor system in collaboration with Kathleen Matthews at Rice University, although less was known from a structural point of view at the time [42, 43] than for the *cI*/*cro* system. The *lac* repressor is predominantly tetrameric. Each monomer is made up of a ligand binding domain, to which the inducer galactose binds in a deep cleft, a linker region and a DNA binding domain. The DNA binding domain forms a helix-turn-helix motif that presents the recognition helix to a half operator site. LacI binds to three operator regions separated by a long intervening loops. Each site can be bound with high affinity by a dimer of the repressor with one DBD interacting in each of two half-sites. High affinity operator interactions are observed for the unliganded protein, and inducer binding (the synthetic inducer iso-propyl-thio-galactoside or IPTG is typically used in vitro) leads to a decrease in affinity for the operator by about five orders of magnitude, depending upon the salt concentration used in the measurements [44].

We used a combination of pressure and tryptophan or dansyl fluorescence polarization and tryptophan emission energy to measure the tetramer–dimer

dissociation and to probe the effect of IPTG binding on this equilibrium [45, 46]. We found that the tetramer–dimer dissociation constant was 14 nM at 21°C and that addition of IPTG stabilized the tetramer against dissociation by a factor of 4 at that temperature. We also found that pressure dissociated the IPTG, with a rather large volume change, ~−70 ml/mol. In addition to revealing a free energy coupling between ligand binding and subunit interactions which could be important in controlling DNA looping upon induction, determination of the affinity between LacI dimers has become somewhat useful in recent years, as the stochastic modeling of transcriptional control by *lac* and other repressors requires knowledge of these constants.

3 The *Trp* Repressor: Affinity and Cooperativity

I became interested in another bacterial transcription factor, the *trp* repressor (TrpR), because its function was more akin to a rheostat than the toggle switch of the *lac* repressor. *Trp* repressor represses transcription of genes in *E. coli* involved in the biosynthesis of tryptophan [47–49]. It also represses its own transcription [50]. Its affinity for the three (*trp*, *aroh*, and *trpR*) operator sites is controlled by the co-repressor, tryptophan, such that when tryptophan is plentiful, it binds to TrpR, increasing its affinity for the operator sites and shutting down transcription of the tryptophan biosynthesis genes. However, since it also shuts down its own transcription at the *trpR* site, this decreases gradually the repressor concentration, leading to a gradual relief of repression that is accentuated if, in addition, tryptophan levels drop.

Typically at that time, protein–DNA interaction affinities were measured using either nitrocellulose filter binding assays or electrophoretic mobility shift assays (EMSA), both relying on radiolabeled oligonucleotides. Neither of these techniques is an equilibrium technique, since they involve separation of the free from bound species. Moreover, it is difficult to implement studies of the effects of solution conditions or temperature because the conditions for the function of the assays themselves are rather stringent. Trained by Gregorio, it occurred to me that a fluorescence anisotropy-based assay would provide an attractive alternative to these techniques. The sensitivity could be nearly as good as the radioactive assays and the measurement is made in solution at equilibrium, with no need to separate the bound from the free species. In previous studies by us and others using dyes of rather low quantum yield and wavelength, high affinity interactions could not be measured [51–53]. To overcome this limitation, we chose to use an oligonucleotide labeled at the 5′ end via phosphoramidite chemistry with fluorescein via a six carbon linker. We chose fluorescein as a dye because it was the most sensitive at the time. At neutral pH, the quantum yield was sufficiently high and the wavelength sufficiently removed from UV contaminants, that we could detect quite well, with some modifications to the instrument, 200 pM concentrations of fluorescein. At the time it had become possible to purchase custom labeled oligonucleotides from Promega Corporation (Madison, WI), as such labeling was being explored for use

in new fluorescence-based sequencing approaches that are the norm today. Using a solution containing 200 pM of this 5′ fluorescein labeled double-stranded 25mer oligonucleotide containing the sequence of the trp operator, also in collaboration with Kathleen Matthews, we carried out measurements of protein–DNA interactions based on anisotropy [54]. We found that TrpR bound to its operator cooperatively, and analyzed the binding with a model of coupled monomer–dimer and dimer DNA binding, which yielded dissociation constants of 4 and 0.1 nM, respectively. We were also able to directly measure the effect of tryptophan on the interaction (Fig. 1).

The thermodynamic binding model used to fit the data in Fig. 1 was based on the crystal structure of the *trp* repressor bound to a target oligonucleotide, the first repressor-operator co-complex ever published [55]. It revealed a dimer of the repressor with the recognition helix of the helix-turn-helix motif interacting with at CTAG palindromic sequence. However, the actual stoichiometry of binding and the true recognition sequence came into question. Uncertainty concerning stoichiometry and target sequence is rather typical in the case of protein–DNA interactions. Using a variety of techniques, fluorescence anisotropy, but also analytical ultracentrifugation, we and our collaborators had demonstrated that the repressor itself, in solution formed higher order oligomers that could be disrupted by the addition of the co-repressor, tryptophan or salt [51, 56]. Jannette Carey and colleagues published a crystal structure of an oligomeric form of *trp* repressor bound to a target sequence in which an alternative recognition mode was evident via a GNACT palindrome [57]. We went on to use fluorescence anisotropy, fitting the high affinity binding event as a cooperative dimer–tetramer equilibrium and demonstrated that the stoichiometry and affinity of the *trp* repressor-operator interactions depended on the length and sequence of the target oligonucleotide, with the different natural targets exhibiting different stoichiometry and cooperativity [58, 59].

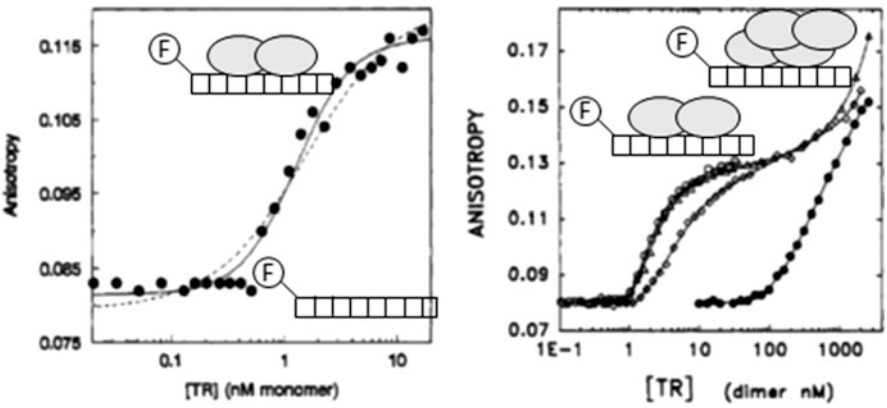

Fig. 1 Anisotropy titration of 5′ fluorescein labeled 25mer oligonucleotide bearing the trp operator sequence at 21°C pH 7.6 10 mM phosphate buffer with purified trp repressor. (*Left*) 300 pM 25mer; (*Right*) 30 nM 25mer with 0 (*closed circles*), 0.04 (*open diamonds*), 0.4 (*open triangles*), and 4.0 (*open circles*) mM L-tryptophan. Figures reworked from [54]

We also examined the effect of super-repressor mutations on DNA binding [60]. Using a variety of fluorescence techniques and isothermal titration calorimetry we demonstrated that the super-repressor phenotype of the AV77 super-repressor discovered by Yanofsky and coworkers [61] was due to the fact that the free WT protein is partially unfolded in the DNA binding domain and that substitution of alanine by valine at the N-cap position of the recognition helix stabilized it in its folded form such that the binding of tryptophan, which also stabilizes the recognition helix, had little further effect in the super-repressor mutant [62]. It has recently come to my attention (Harish Subramanian and Jannette Carey, personal communication) that the TrpR DBD is not unfolded in absence of tryptophan, but in equilibrium between multiple conformations. In addition to a large number of studies by the Yanofsky, Carey, Sigler, Hurlburt, Matthews, Jardetsky, and other groups that will not be covered here, this ensemble of fluorescence studies on a transcriptional regulator, augmented by crystallography, calorimetry, analytical ultracentrifugation, and circular dichroism, allowed a highly quantitative and thorough characterization of the molecular mechanisms and thermodynamics in this highly complex regulatory system involving coupled folding, oligomerization, ligand binding, and DNA target recognition, all exquisitely tuned to achieve the appropriate level of tryptophan synthesis and energy usage for *E. coli* under varying nutrient conditions.

4 Nuclear Receptor Ligand Modulated Heterologous Protein Interactions

Nuclear receptors (NR) comprise a large family of ligand modulated transcription factors responsible for many important aspects of differentiation, growth, and homeostasis in metazoans [63]. There are two major subfamilies of NRs, the homo-dimeric NRs, which include the hormone receptors, estrogen receptors (ER), glucocorticoid receptors (GR), and androgen receptors (AR), and which bind to palindromic DNA target sites and the hetero-dimeric NRs, such as the retinoid receptors, RXR/RAR, thyroid hormone receptors, TR, peroxisome proliferator receptors, PPARs, etc., which bind to direct repeats. The NRs harbor structurally homologous C-terminal ligand binding domains, generally endowed with a ligand-dependent activation domain in the C-terminal helix, a DNA binding domain, and a highly variable N-terminal domain that can also exhibit activation functions. NRs interact with ligands (agonists, antagonists, partial agonists, and inverse agonists), which are generally hydrophobic in nature, although some NRs are thought to respond to gases such as NO via a bound heme moiety. Ligand binding modulates NR interactions with co-repressors and coactivators of transcription, which themselves exhibit chromatin remodeling activity and recruit other transcription factors. The stoichiometries, affinities, and cooperativity of the multiple linked interactions implicated in NR function are finely tuned to the proper level of control of these important physiological functions. Indeed, NRs represent

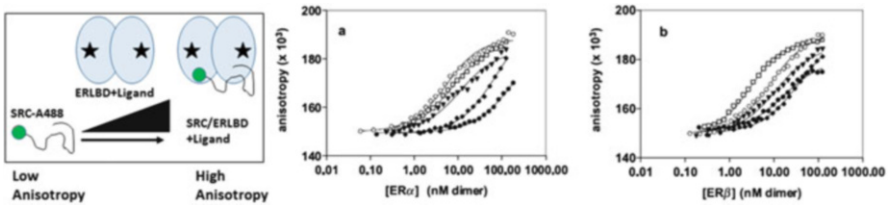

Fig. 2 Titrations of 2 nM Alexa488 labeled 26 kDa fragment of the SRC-1 NR coactivator with either ERα or ERβ in presence of saturating concentrations of agonist ligands, estradiol (*open circles*), genistein (*open squares*), estrone (*closed circles*), estriol (*triangles*), and ethylene estradiol (*diamonds*)

an important class of targets for development of therapeutic agents, many of which have long been on the market, for the treatment of human disease states including many forms of cancer, heart disease, diabetes, and inflammation. Not surprisingly, the literature on NR structure function relationships is vast, and will not be reviewed here. However, few groups have been interested in deciphering the complex energetic relationships between ligand binding, both homologous and heterologous protein interactions and nucleic acid interactions. One exception is the work of David Bain's group [64, 65]. For our part, often in collaboration with the structural group of William Bourguet, we have used fluorescence anisotropy to investigate ligand-dependent NR-DNA interactions [66–69] and NR-coregulator interactions [70–75].

We were the first to use anisotropy to investigate the impact of different types of ligands on NR interactions with fluorescently labeled peptides derived from co-activators (Fig. 2) [73]. We found differential effects of ligands for recruitment of the SRC-1 coactivator to two different subtypes of ER. Such differences can have significant impact on tissue specific therapeutic effects, since the ER subtypes are differentially expressed in different tissues. Indeed, this anisotropy assay for the effect of ligands on NR coregulator interactions has become a common practice in the pharmaceutical industries drug development programs targeting NRs. Following Schwabe and co-workers [76], we also used C-terminal labeling of the activation helix 12 on RAR to investigate by time-resolved anisotropy, the effects of ligation and peptide binding on the dynamics of this all important helix [71]. More recently, we have used FCS to measure the ER-Tif2 coactivator interaction K_d as a function of ligand in live Cos7 cells, using transient transfection of cerulean and mCherry fusions of the two proteins [77].

5 Translational Control of Ribosomal Protein Production: L20 – Stoichiometry

As noted above, ascertaining the stoichiometry of protein–nucleic acid complexes under physiologically significant conditions of concentration, temperature, salt, etc., is often rather challenging. A lack of clarity as to the stoichiometry of the

large ribosomal protein, L20, from *E. coli* and other bacterial species with a long and complex translational operator on its messenger RNA illustrates the issue [78–82]. The translational operator RNA sequence comprises hundreds of base pairs and forms a required long-range pseudoknot that is recognized by L20 and which overlaps the Shine-Dalgarno sequence of the mRNA. Another similar site also exists within this operator, and both sites mimic the site recognized by L20 in the 16S ribosomal RNA. Both sites are required for translational control in vivo. Anisotropy assays had indicated that perhaps the stoichiometry might not be 2:1, at least under the conditions of titrations. In this case we used fluorescence correlation spectroscopy (FCS) and fluorescence cross-correlation spectroscopy (FCCS), to ascertain whether two molecules of L20 could bind to the operator RNA. FCS first proposed by Magde et al. [83] uses the fluctuations in fluorescence intensity in a small confocal observation (or in our case 2-photon excitation) volume to characterize the concentration and diffusion properties of the molecules. If one uses molecules labeled with different colors in two different detection channels it is possible to deduce whether the two molecules form a complex. For a review of FCS and FCCS, see [84].

We labeled separately two solutions of a C-terminal construct of L20 known to be sufficient for translational control in vivo, with a green and red fluorescent dye (Alexa 488 and Atto647N) on the N-terminus of the protein via succinimidyl ester chemistry. First, we carried out FCS experiments observing only the fluorescence from the Alexa488 (green) labeled L20 (Fig. 3, left). Upon addition of the operator RNA at a concentration tenfold the K_d [85] determined by anisotropy, the correlation profile shifted to longer lag times, indicating binding of the protein to the RNA (which was large, 660 base pairs). Then, still observing in the green channel, we added the red (Atto647N) labeled L20. If two or more molecules of L20 could bind to the RNA, then we would have expected (under the equimolar conditions used) that the curve would remain at the same lag time, since the L20 C-terminal

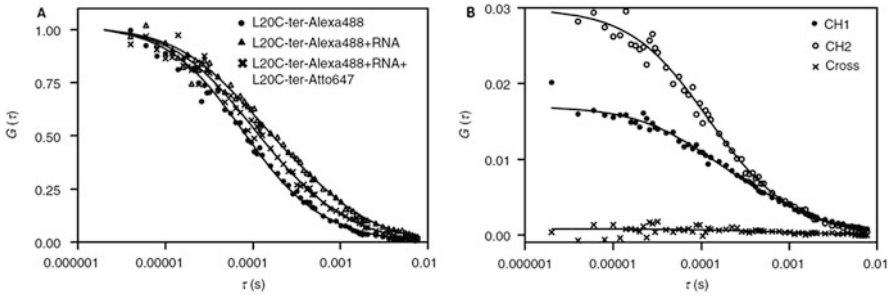

Fig. 3 Stoichiometry of the L20-operator RNA complex investigated by fluorescence correlation spectroscopy. (*Left*) 150 nM L20-Alexa488 (*circles*), plus 150 nM operator RNA (*triangles*), and 150 nM L20-Alexa488, plus 150 nM operator RNA, plus 150 nM L20-Atto647N (*crosses*); (*Right*) 150 nM L20-Alexa488, plus 150 nM operator RNA plus 150 nM L20-Atto647N – Alexa488 channel (*closed circles*), Atto647N channel (*open circles*), cross-correlation (*crosses*). Figures reworked from [85]

construct is only 6 kDa, and would not be expected to make a significant difference to the diffusion time of the already large complex of the operator RNA bound by the green labeled L20. Instead, the curve was shifted back to faster diffusion times, indicating that the green L20 was competed off of the operator RNA by the red L20. To further demonstrate that two L20 proteins could not bind simultaneously to the operator RNA, we carried out cross-correlation measurements. Here we added equimolar amounts of L20 green and L20 red, with the RNA at a concentration tenfold above the K_d [85]. If more than one L20 molecule could interact simultaneously with the RNA, then we would have expected to see some cross-correlation signal. Instead, absolutely no cross-correlation amplitude was observed (Fig. 3, right), indicating that the stoichiometry of the L20/operator RNA complex was 1:1, despite the existence of two possible sites. Further studies indicated anti-cooperative allosteric interaction between the two putative binding sites on the operator RNA [85].

6 Control of the Switch Between Glycolysis and Gluconeogenesis in *B. subtilis*

In collaboration with Nathalie Declerck and Stephane Aymerich, we set out to use fluorescence approaches in the characterization of the molecular mechanisms of transcriptional regulators involved in the control of the central carbon metabolism in the soil bacterium, *Bacillus subtilis*. The switch between glycolysis and gluconeogenesis in *B. subtilis* is controlled at the level of the transformation of glyceraldehyde phosphate to 1,3-diphosphoglycerate (Fig. 4) [86–88]. The reaction in the glycolysis direction is catalyzed by the GapA enzyme, while the reverse reaction, unlike in *E. coli*, requires a second enzyme, GapB. Expression of GapA is controlled at the transcriptional level by the central glycolytic genes repressor or CggR. CggR is induced by fructose bis-phosphate (FBP) a product of glucose degradation. Expression of the GapB enzyme is very strongly catabolite repressed when cells are grown on a glycolytic carbon source by the control catabolite protein of gluconeogenic genes (CcpN). The mode of induction of CcpN upon a nutrient shift to gluconeogenic carbon sources, such as malate, is not known, but genetic evidence suggests that the co-transcribed YqfL protein is implicated [88].

6.1 In Vitro Biophysical Studies

The groups of Declerck and Aymerich had investigated in detail the structural and in vivo functional properties of this genetic metabolic switch. Our collaboration with these groups involved applying a variety of fluorescence approaches, coupled with other biophysical methodologies, to characterize the energetic couplings

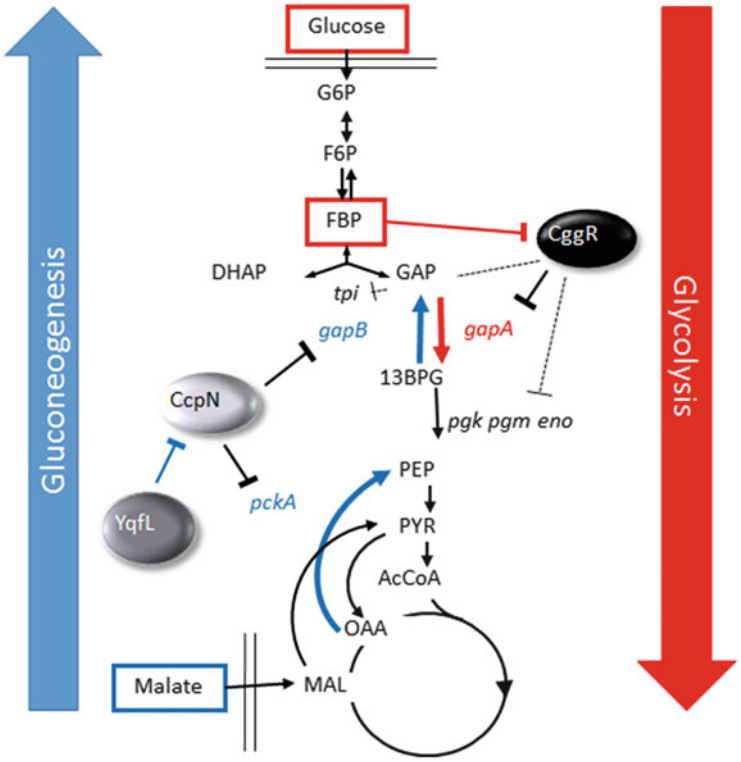

Fig. 4 Schematic diagram of the switch between glycolysis and gluconeogenesis in *B. subtilis*. In *blue*, operative interactions under gluconeogenesis and in *red* operative interactions under glycolysis. Repressor proteins and co-regulators are shown as *black* and *grey* ellipses

implicated in their function. In the case of CcpN, the repressor that strongly downregulates the *gapB* and *pckA* promoters on glucose, we showed by FCCS, using DNA oligonucleotides labeled with a red dye and the CcpN protein labeled with a green dye (Fig. 5) that the stoichiometry of binding was different on oligonucleotides bearing the proposed sequence recognition motifs for these two operator sites [89]. Plotting the ratio of the cross-correlation amplitude to that of the amplitude of the fluctuations in the green channel (that of the protein, tenfold more concentrated than the red-labeled target DNA oligonucleotides) provides a direct measure of binding, and the value of this ratio at the plateau of the binding curve depends upon the stoichiometry of the complex. Indeed it can be seen directly from the Go_x/Go_G ratios in Fig. 5, that the stoichiometry of one complex is approximately twice that of the other. Correcting for labeling ratios and CcpN oligomerization, we deduced stoichiometries of dimer and tetramer, respectively, for the *gapB* and *pckA* target oligonucleotides. Later it was shown that the target sequence for the *gapB* oligonucleotide was not complete, and that the protein bound as a tetramer to the full-length *gapB* target as well.

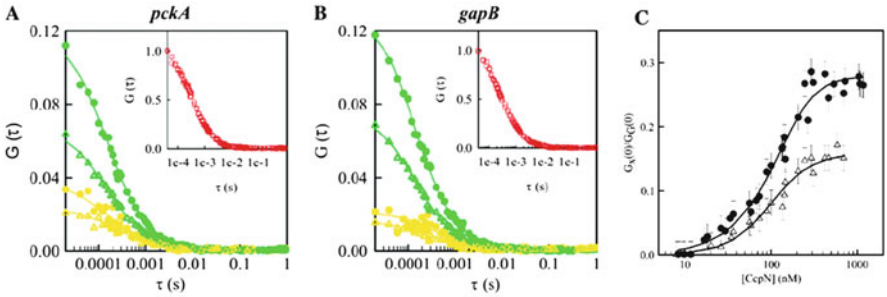

Fig. 5 FCCS measurements of CcpN interaction with target oligonucleotides bearing recognitions sequences for the operators present in the *pckA* and *gapB* promoters. *Red curves* are the FCS profiles for the oligonucleotides labeled with the red dye, Atto-647N. *Green curves* are the FCS profiles for the CcpN protein labeled with fluorescein. The FCCS (cross-correlation) profiles are shown in *yellow*. (**a**) CcpN interactions with the *pckA* oligonucleotide. (**b**) CcpN interactions with the *gapB* oligonucleotide. (**c**) Go_x/Go_G ratio for the pckA and gapB targets as a function of CcpN concentration

Co-variance analysis was used in the case of the CggR protein to investigate the coupled effects of ligand binding and oligomerization in the control of its operator interactions. CggR represses transcription of the *gapA* operon when the bacteria are grown on gluconeogenic carbon sources, such as malate (see schematic in Fig. 4). In addition to the genes coding for the glycolytic enzymes, the first gene in the *gapA* operon is that encoding CggR itself, such that this system includes an autorepression loop. CggR is induced (i.e., dissociates from the operator) when the bacteria sense glucose in the environment. It had been thought that the inducer was FBP. Our work using fluorescence and other biophysical approaches confirmed this hypothesis and demonstrated that FBP played a structural role as well, with two binding sites per CggR monomer. The high affinity site was the structural stabilization site, while the low affinity site was responsible for allosteric induction of CggR [90]. In a classical Weber free energy coupling analogy, using fluorescence anisotropy and analytical ultracentrifugation, we showed how inducer binding was allosterically coupled to cooperative DNA binding by CggR [91].

A model based on these data by which FBP binding leads to CggR tetramer dissociation, and hence decreased affinity and cooperativity in operator binding was confirmed using a combination of FCCS, non-covalent mass spectrometry, and small angle X-ray scattering [92]. The effect of FBP on dimerization is most clearly shown in the FCCS profiles in Fig. 6. Two double-stranded DNA oligonucleotides containing CggR half-sites (able to bind one CggR dimer) were labeled with a red and a green dye, respectively, on the 5′-end of the sense and anti-sense strand. When annealed with their complementary unlabeled strand and mixed in absence of CggR, no interaction between the two double-stranded oligonucleotides is observed, as expected (Fig. 6a). When the two labeled complementary oligonucleotides are annealed, cross-correlation is observed (Fig. 6b). The cross-correlation amplitude is not 100% due to imperfect labeling ratios of the oligonucleotides. If

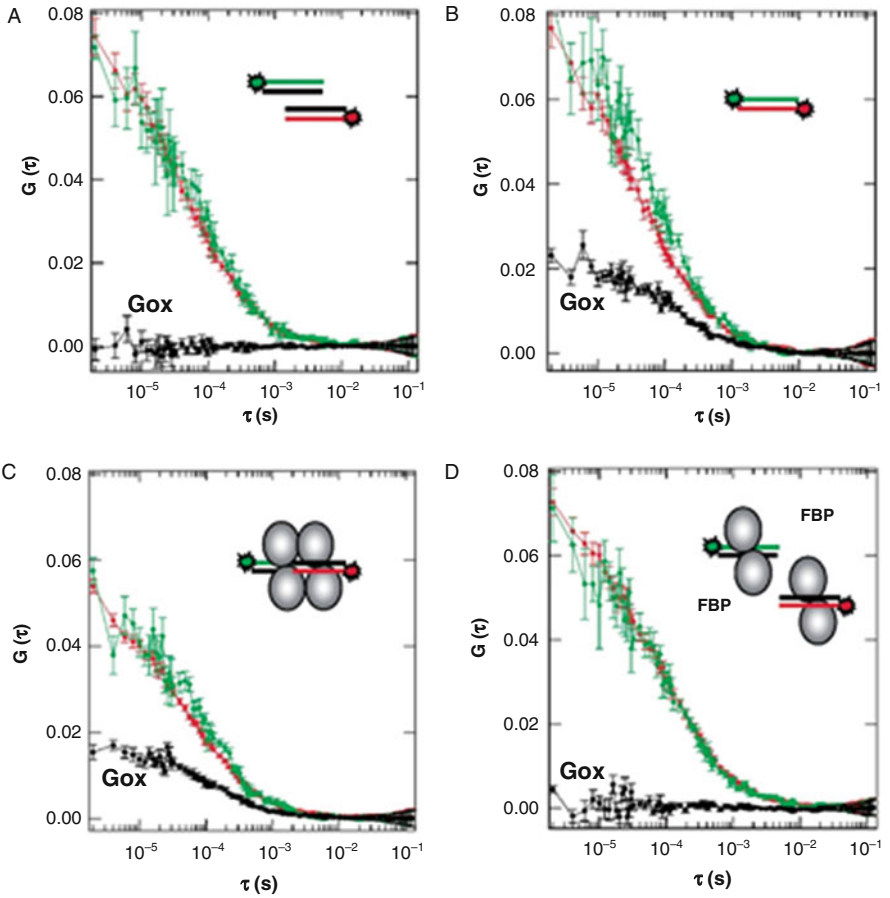

Fig. 6 FCCS measurements of CggR interaction with target oligonucleotides bearing recognitions sequences for half-site operators. (**a**) Two singly labeled double-stranded oligonucleotides labeled, respectively, on the 5′-end of the sense strand for one with fluorescein and the 5′-end of the anti-sense strand for the other with Atto 647N. *Green* and *red curves* are FCS profiles for the *red* and *green* labeled oligonucleotides as depicted in the schematics. *Black curves* are cross-correlation profiles between the *red* and the *green* detected fluorescence. CggR protein is depicted as *grey* ellipses. (**a**) 60 nM each of separately labeled *green* and *red* double-stranded oligonucleotides with the CggR half-sites. (**b**) 60 nM doubly labeled double-stranded oligonucleotide with the CggR half-site. (**c**) 60 nM each of the two separately labeled double-stranded oligonucleotides in presence of saturating CggR protein. (**d**) 60 nM each of the two separately labeled double-stranded oligonucleotides in presence of saturating CggR protein (300 nM in monomer units) and 0.5 mM FBP

the two separately labeled double-stranded oligonucleotides are mixed with the CggR protein in absence of FBP, cross-correlation is observed (Fig. 6c), and the amplitude under these concentrations conditions is maximal, with respect to that observed for the doubly labeled double-stranded oligonucleotide in Fig. 6b. This

indicates that the CggR tetramer can non-covalently cross-link the two oligonucleotides into a single complex. However, this interaction is abolished when FBP is added (Fig. 6d), although mass spectrometry and fluorescence anisotropy demonstrated that the protein is still bound to DNA under these conditions. However, the CggR is dimeric in presence of FBP and can no longer cross-link the two oligonucleotides.

6.2 *In Vivo Fluctuation Microscopy*

The above in vitro biophysical studies on the CcpN/CggR control of the switch between glycolysis and gluconeogenesis provided models for how the proteins functioned in vivo. In the case of the CcpN protein, we hypothesized a "hold back" mechanism, by which the CcpN protein bound to the operator overlapping the *gapB* and *pckA* promoters, would interact directly with the RNA polymerase, preventing transcription initiation. In the case of the CggR repressor a "road-block" model proposed that CggR bound to the operator, downstream of the start site of the *gapA* promoter and blocked transcription elongation by RNA polymerase. We sought to verify these proposed models in vivo using an advanced microscopy technique based on fluorescence fluctuations introduced by Digman and Gratton in 2008 and called scanning Number and Brightness [93]. In scanning Number and Brightness, two-photon in our case, a field of view is imaged using rapid scanning of the excitation laser via galvanometric mirrors, such that the dwell-time at each pixel is shorter than the diffusion time (i.e., that one is sampling at a rate near the top of the FCS curves shown in Figs. 5 and 6, for example). Multiple (50–100) raster scans of the field of view (FOV) are carried out, such that at each pixel, one has 50–100 values for the fluorescence intensity. If the fluorescent molecules have diffused in the time between imaging of the same pixel (about 2–3 s for the frame time), then the fluorescence intensity values incorporate fluctuations due to diffusion. The average and variance of these values at each pixel can be used in a moment analysis to calculate the number of fluorescent molecules in the excitation volume at each pixel, and their molecular brightness. These values must be corrected for shot noise and where possible background auto-fluorescence contributions.

We adapted the two-photon scanning N&B approach to determine the level of gene expression from bacterial GFP promoter fusions [94]. Given the low photon statistics and small size of the bacteria, pixel averaging strategies were implemented in order to obtain robust values for single cell GFP concentrations. We then used this approach to measure and model stochastic expression form the *gapA* and *gapB* GFP promoter fusions in the natural chromosomal locus of *B. subtilis* grown on glycolytic (glucose) and gluconeogenic (malate) carbon sources (Fig. 7). This approach, which yields absolute protein concentrations for single cells, allows for stochastic modeling and absolute determination of the biological noise parameters (Fig. 8). Extremely strong catabolite repression with low noise for the CcpN repressor, and high noise repression for CggR support the

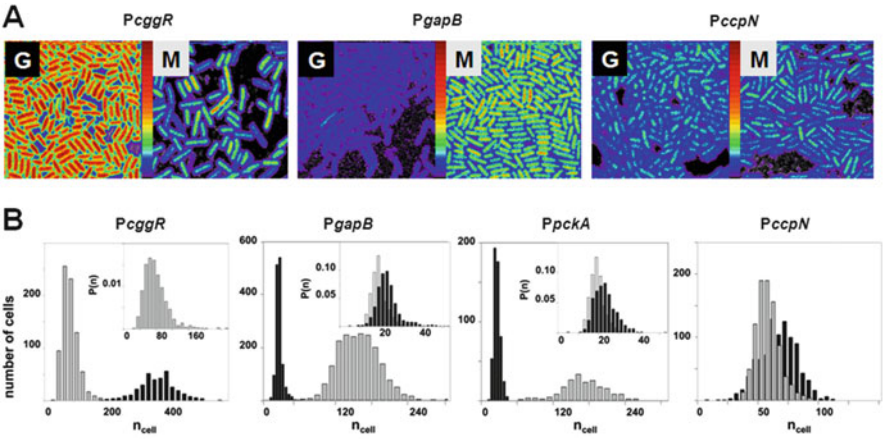

Fig. 7 Scanning 2-photon N&B measurements on *B. subtilis* live cells expressing GFP from promoter fusions of the *gapA*, *gapB*, *pckA*, and *pccpN* promoters. (**a**) Images of bacteria on pads in presence of G, glucose or M, malate for the *gapA*, *gapB*, and *pccpN* promoters as labeled. (**b**) Histograms of the number of GFP molecules in the excitation volume from the quantification of multiple FOV for the *gapA*, *gapB*, *pckA*, and *pccpN* promoters in presence of glucose (*black*) or malate (*grey*)

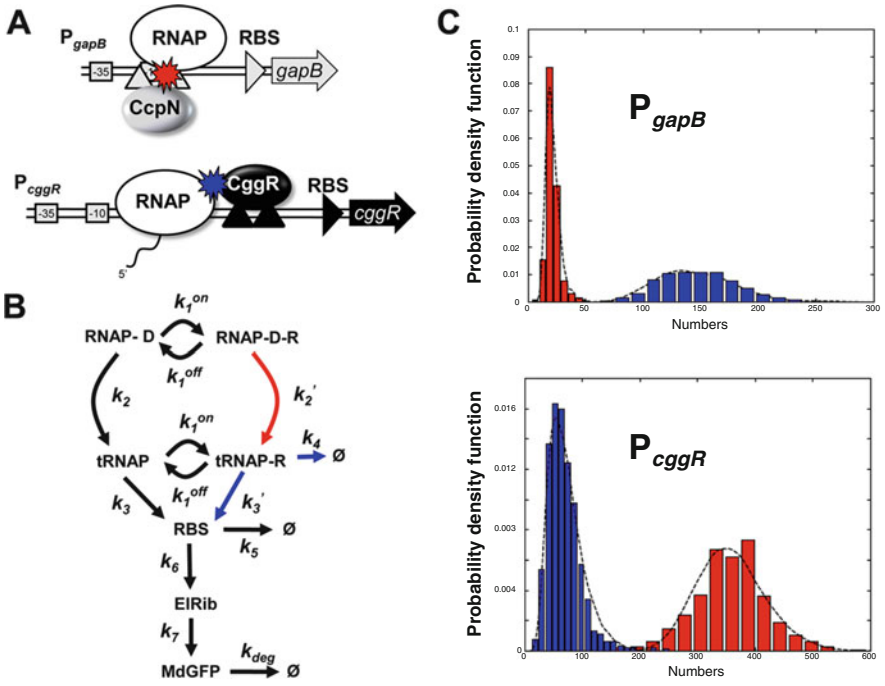

Fig. 8 Stochastic modeling based on the scanning 2-photon N&B measurements on *B. subtilis* live cells expressing GFP from promoter fusions of the *gapA*, *gapB*, *pckA*, and *pccpN* promoters. (**a**) The "hold back" and "road block" models for CcpN and CggR repression, respectively. (**b**) Stochastic model for repression. (**c**) Fits of the experimental distributions for GFP expression on glucose (*red*) and malate (*blue*) to the model in (**b**) for *pccpN* and *pcggR* promoters as labeled

"hold back" and "road block" mechanisms for CcpN and CggR, respectively. Stochastic modeling of the gapA/gapB promoter system under different nutrients yielded rate constants that were entirely consistent with the biophysical models.

7 Conclusions

The above set of examples serves to illustrate how multiple fluorescence approaches can be used both in vitro and in vivo to reveal the very subtle mechanisms underlying the regulation of gene expression. These examples are by no means exhaustive, and our group as well as many others has applied such approaches to multiple protein systems involved in gene regulation. What is clear from these examples is the central role of protein oligomerization interactions, both homologous and heterologous, in the fine tuning of gene expression levels. This key role of protein interactions is a lesson learned from Gregorio Weber, whose insight continues to inspire all of the work of my group. Protein stoichiometry is often missing in the models proposed for biological regulation of gene expression, as well as many other important physiological processes. The work we have carried out over the years, some of which is presented here, underscores that quantitative determination of the coupling between protein–protein interactions and transcriptional regulation is absolutely required for the understanding of these systems, and eventually, the intelligent modulation of their activity in the context of therapeutic strategies to combat disease.

References

1. Weber G (1972) Ligand binding and internal equilibria in proteins. Biochemistry 11:864–878
2. Weber G (1952) Polarization of the fluorescence of macromolecules. I. Theory and experimental method. Biochem J 51:145–155
3. Weber G (1952) Polarization of the fluorescence of macromolecules. II. Fluorescent conjugates of ovalbumin and bovine serum albumin. Biochem J 51:155–167
4. Dumont C, Emilsson T, Gruebele M (2009) Reaching the protein folding speed limit with large, sub-microsecond pressure jumps. Nat Methods 6:515–519
5. Zhu L, Ghosh K, King M, Cellmer T, Bakajin O, Lapidus LJ (2011) Evidence of multiple folding pathways for the villin headpiece subdomain. J Phys Chem B 115:12632–12637
6. Weber G, Drickamer HG (1983) The effect of high pressure upon proteins and other biomolecules. Q Rev Biophys 16:89–112
7. Anderson SR, Weber G (1969) Fluorescence polarization of the complexes of 1-anilino-8-naphthalenesulfonate with bovine serum albumin. Evidence for preferential orientation of the ligand. Biochemistry 8:371–377
8. Weber G (1974) Addition of chemical and osmotic energies by ligand-protein interactions. Ann N Y Acad Sci 227:486–496
9. Weber G (1972) Addition of chemical and osmotic free energies through negative interaction of protein-bound ligands. Proc Natl Acad Sci U S A 69:3000–3003
10. Weber G (1982) Asymmetric ligand binding by haemoglobin. Nature 300:603–607

11. Daniel E, Weber G (1966) Cooperative effects in binding by bovine serum albumin. I. The binding of 1-anilino-8-naphthalenesulfonate. Fluorimetric titrations. Biochemistry 5:1893–1900
12. Weber G, Daniel E (1966) Cooperative effects in binding by bovine serum albumin. II. The binding of 1-anilino-8-naphthalenesulfonate. Polarization of the ligand fluorescence and quenching of the protein fluorescence. Biochemistry 5:1900–1907
13. Kolb DA, Weber G (1975) Cooperativity of binding of anilinonaphthalene sulfonate to serum albumin induced by a second ligand. Biochemistry 14:4476–4481
14. Weber G (1975) Energetics of ligand binding to proteins. Adv Protein Chem 29:1–83
15. Brewer JM, Weber G (1968) The reversible dissociation of yeast enolase. Proc Natl Acad Sci U S A 59:216–223
16. Erijman L, Weber G (1991) Oligomeric protein associations: transition from stochastic to deterministic equilibrium. Biochemistry 30:1595–1599
17. Erijman L, Lorimer GH, Weber G (1993) Reversible dissociation and conformational stability of dimeric ribulose bisphosphate carboxylase. Biochemistry 32:5187–5195
18. Foguel D, Weber G (1995) Pressure-induced dissociation and denaturation of allophycocyanin at subzero temperatures. J Biol Chem 270:28759–28766
19. King L, Weber G (1986) Conformational drift of dissociated lactate dehydrogenases. Biochemistry 25:3632–3637
20. Paladini AA Jr, Weber G (1981) Pressure-induced reversible dissociation of enolase. Biochemistry 20:2587–2593
21. Pin S, Royer CA, Gratton E, Alpert B, Weber G (1990) Subunit interactions in hemoglobin probed by fluorescence and high-pressure techniques. Biochemistry 29:9194–9202
22. Rawitch AB, Weber G (1972) The reversible association of lysozyme and thyroglobulin. Cooperative binding by near-neighbor interactions. J Biol Chem 247:680–685
23. Ruan K, Weber G (1988) Dissociation of yeast hexokinase by hydrostatic pressure. Biochemistry 27:3295–3301
24. Silva JL, Miles EW, Weber G (1986) Pressure dissociation and conformational drift of the beta dimer of tryptophan synthase. Biochemistry 25:5780–5786
25. Xu G, Weber G (1982) Dynamics and time-averaged chemical potential of proteins: importance in oligomer association. Proc Natl Acad Sci U S A 79:5268–5271
26. Weber G (1984) Order of free energy couplings between ligand binding and protein subunit association in hemoglobin. Proc Natl Acad Sci U S A 81:7098–7102
27. Anderson WF, Ohlendorf DH, Takeda Y, Matthews BW (1981) Structure of the cro repressor from bacteriophage lambda and its interaction with DNA. Nature 290:754–758
28. Reichardt LF (1975) Control of bacteriophage lambda repressor synthesis after phage infection: the role of the N, cII, cIII and cro products. J Mol Biol 93:267–288
29. Reichardt LF (1975) Control of bacteriophage lambda repressor synthesis: regulation of the maintenance pathway of the cro and cI products. J Mol Biol 93:289–309
30. Ackers GK, Johnson AD, Shea MA (1982) Quantitative model for gene regulation by lambda phage repressor. Proc Natl Acad Sci U S A 79:1129–1133
31. Darling PJ, Holt JM, Ackers GK (2000) Coupled energetics of lambda cro repressor self-assembly and site-specific DNA operator binding I: analysis of cro dimerization from nanomolar to micromolar concentrations. Biochemistry 39:11500–11507
32. Darling PJ, Holt JM, Ackers GK (2000) Coupled energetics of lambda cro repressor self-assembly and site-specific DNA operator binding II: cooperative interactions of cro dimers. J Mol Biol 302:625–638
33. Johnson AD, Poteete AR, Lauer G, Sauer RT, Ackers GK, Ptashne M (1981) Lambda repressor and cro—components of an efficient molecular switch. Nature 294:217–223
34. Shea MA, Ackers GK (1985) The OR control system of bacteriophage lambda. A physical-chemical model for gene regulation. J Mol Biol 181:211–230

35. Senear DF, Laue TM, Ross JB, Waxman E, Eaton S, Rusinova E (1993) The primary self-assembly reaction of bacteriophage lambda cI repressor dimers is to octamer. Biochemistry 32:6179–6189
36. Senear DF, Ross JB, Laue TM (1998) Analysis of protein and DNA-mediated contributions to cooperative assembly of protein-DNA complexes. Methods 16:3–20
37. Dunaway M, Manly SP, Matthews KS (1980) Model for lactose repressor protein and its interaction with ligands. Proc Natl Acad Sci U S A 77:7181–7185
38. Dunaway M, Matthews KS (1980) Hybrid tetramers of native and core lactose repressor protein. Assessment of operator and nonspecific DNA binding parameters and their relationship. J Biol Chem 255:10120–10127
39. Dunaway M, Olson JS, Rosenberg JM, Kallai OB, Dickerson RE, Matthews KS (1980) Kinetic studies of inducer binding to lac repressor.operator complex. J Biol Chem 255:10115–10119
40. Friedman BE, Olson JS, Matthews KS (1977) Interaction of lac repressor with inducer, kinetic and equilibrium measurements. J Mol Biol 111:27–39
41. Swint-Kruse L, Matthews KS (2009) Allostery in the LacI/GalR family: variations on a theme. Curr Opin Microbiol 12:129–137
42. Matthews HR, Thielmann HW, Matthews KS, Jardetzky O (1973) NMR studies of the binding of an inducer and an anti-inducer to the lac repressor. Ann N Y Acad Sci 222:226–229
43. Matthews KS, Wade-Jardetzky NG, Graber M, Conover WW, Jardetzky O (1977) High resolution 1H NMR of a selectively deuterated analogs of the lac repressor. Biochim Biophys Acta 490:534–538
44. Mossing MC, Record MT Jr (1985) Thermodynamic origins of specificity in the lac repressor-operator interaction. Adaptability in the recognition of mutant operator sites. J Mol Biol 186:295–305
45. Royer CA, Weber G, Daly TJ, Matthews KS (1986) Dissociation of the lactose repressor protein tetramer using high hydrostatic pressure. Biochemistry 25:8308–8315
46. Royer CA, Chakerian AE, Matthews KS (1990) Macromolecular binding equilibria in the lac repressor system: studies using high-pressure fluorescence spectroscopy. Biochemistry 29:4959–4966
47. Gunsalus RP, Yanofsky C (1980) Nucleotide sequence and expression of *Escherichia coli* trpR, the structural gene for the trp aporepressor. Proc Natl Acad Sci U S A 77:7117–7121
48. Klig LS, Carey J, Yanofsky C (1988) Trp repressor interactions with the trp aroH and trpR operators. Comparison of repressor binding in vitro and repression in vivo. J Mol Biol 202:769–777
49. Rose JK, Yanofsky C (1974) Interaction of the operator of the tryptophan operon with repressor. Proc Natl Acad Sci U S A 71:3134–3138
50. Kelley RL, Yanofsky C (1982) Trp aporepressor production is controlled by autogenous regulation and inefficient translation. Proc Natl Acad Sci U S A 79:3120–3124
51. Fernando T, Royer C (1992) Role of protein–protein interactions in the regulation of transcription by trp repressor investigated by fluorescence spectroscopy. Biochemistry 31:3429–3441
52. Guest CR, Hochstrasser RA, Dupuy CG, Allen DJ, Benkovic SJ, Millar DP (1991) Interaction of DNA with the Klenow fragment of DNA polymerase I studied by time-resolved fluorescence spectroscopy. Biochemistry 30:8759–8770
53. Heyduk T, Lee JC (1990) Application of fluorescence energy transfer and polarization to monitor *Escherichia coli* cAMP receptor protein and lac promoter interaction. Proc Natl Acad Sci U S A 87:1744–1748
54. LeTilly V, Royer CA (1993) Fluorescence anisotropy assays implicate protein–protein interactions in regulating trp repressor DNA binding. Biochemistry 32:7753–7758
55. Otwinowski Z, Schevitz RW, Zhang RG, Lawson CL, Joachimiak A, Marmorstein RQ, Luisi BF, Sigler PB (1988) Crystal structure of trp repressor/operator complex at atomic resolution. Nature 335:321–329

56. Martin KS, Royer CA, Howard KP, Carey J, Liu YC, Matthews K, Heyduk E, Lee JC (1994) Electrostatic forces contribute to interactions between trp repressor dimers. Biophys J 66:1167–1173
57. Carey J, Combatti N, Lewis DE, Lawson CL (1993) Cocrystals of *Escherichia coli* trp repressor bound to an alternative operator DNA sequence. J Mol Biol 234:496–498
58. Grillo AO, Brown MP, Royer CA (1999) Probing the physical basis for trp repressor-operator recognition. J Mol Biol 287:539–554
59. Reedstrom RJ, Brown MP, Grillo A, Roen D, Royer CA (1997) Affinity and specificity of trp repressor-DNA interactions studied with fluorescent oligonucleotides. J Mol Biol 273:572–585
60. Grillo AO, Royer CA (2000) The basis for the super-repressor phenotypes of the AV77 and EK18 mutants of trp repressor. J Mol Biol 295:17–28
61. Kelley RL, Yanofsky C (1985) Mutational studies with the trp repressor of *Escherichia coli* support the helix-turn-helix model of repressor recognition of operator DNA. Proc Natl Acad Sci U S A 82:483–487
62. Reedstrom RJ, Royer CA (1995) Evidence for coupling of folding and function in trp repressor: physical characterization of the superrepressor mutant AV77. J Mol Biol 253:266–276
63. Billas I, Moras D (2013) Allosteric controls of nuclear receptor function in the regulation of transcription. J Mol Biol 425:2317–2329
64. Bain DL, Heneghan AF, Connaghan-Jones KD, Miura MT (2007) Nuclear receptor structure: implications for function. Annu Rev Physiol 69:201–220
65. Connaghan-Jones KD, Bain DL (2009) Using thermodynamics to understand progesterone receptor function: method and theory. Methods Enzymol 455:41–70
66. Boyer M, Poujol N, Margeat E, Royer CA (2000) Quantitative characterization of the interaction between purified human estrogen receptor alpha and DNA using fluorescence anisotropy. Nucleic Acids Res 28:2494–2502
67. Ozers MS, Hill JJ, Ervin K, Wood JR, Nardulli AM, Royer CA, Gorski J (1997) Equilibrium binding of estrogen receptor with DNA using fluorescence anisotropy. J Biol Chem 272:30405–30411
68. Poujol N, Margeat E, Baud S, Royer CA (2003) RAR antagonists diminish the level of DNA binding by the RAR/RXR heterodimer. Biochemistry 42:4918–4925
69. Szatkowski OM, Hill JJ, Ervin K, Royer CA, Gorski J (2001) The dissociation rate of estrogen receptor alpha from the consensus estrogen response element. Mol Cell Endocrinol 175:101–109
70. Bourdoncle A, Labesse G, Margueron R, Castet A, Cavailles V, Royer CA (2005) The nuclear receptor coactivator PGC-1alpha exhibits modes of interaction with the estrogen receptor distinct from those of SRC-1. J Mol Biol 347:921–934
71. le MA, Teyssier C, Erb C, Grimaldi M, Alvarez S, de Lera AR, Balaguer P, Gronemeyer H, Royer CA, Germain P, Bourguet W (2010) A unique secondary-structure switch controls constitutive gene repression by retinoic acid receptor. Nat Struct Mol Biol 17:801–807
72. Margeat E, Poujol N, Boulahtouf A, Chen Y, Muller JD, Gratton E, Cavailles V, Royer CA (2001) The human estrogen receptor alpha dimer binds a single SRC-1 coactivator molecule with an affinity dictated by agonist structure. J Mol Biol 306:433–442
73. Margeat E, Bourdoncle A, Margueron R, Poujol N, Cavailles V, Royer C (2003) Ligands differentially modulate the protein interactions of the human estrogen receptors alpha and beta. J Mol Biol 326:77–92
74. Nahoum V, Perez E, Germain P, Rodriguez-Barrios F, Manzo F, Kammerer S, Lemaire G, Hirsch O, Royer CA, Gronemeyer H, de Lera AR, Bourguet W (2007) Modulators of the structural dynamics of the retinoid X receptor to reveal receptor function. Proc Natl Acad Sci U S A 104:17323–17328
75. Pogenberg V, Guichou JF, Vivat-Hannah V, Kammerer S, Perez E, Germain P, de Lera AR, Gronemeyer H, Royer CA, Bourguet W (2005) Characterization of the interaction between

retinoic acid receptor/retinoid X receptor (RAR/RXR) heterodimers and transcriptional coactivators through structural and fluorescence anisotropy studies. J Biol Chem 280:1625–1633
76. Kallenberger BC, Love JD, Chatterjee VK, Schwabe JW (2003) A dynamic mechanism of nuclear receptor activation and its perturbation in a human disease. Nat Struct Biol 10:136–140
77. Savatier J, Jalaguier S, Ferguson ML, Cavailles V, Royer CA (2010) Estrogen receptor interactions and dynamics monitored in live cells by fluorescence cross-correlation spectroscopy. Biochemistry 49:772–781
78. Chiaruttini C, Milet M, Springer M (1996) A long-range RNA-RNA interaction forms a pseudoknot required for translational control of the IF3-L35-L20 ribosomal protein operon in *Escherichia coli*. EMBO J 15:4402–4413
79. Chiaruttini C, Milet M, de SM, Springer M (1996) Translational coupling in the *Escherichia coli* operon encoding translation initiation factor IF3 and ribosomal proteins L20 and L35. Biochimie 78:555–567
80. Guillier M, Allemand F, Raibaud S, Dardel F, Springer M, Chiaruttini C (2002) Translational feedback regulation of the gene for L35 in *Escherichia coli* requires binding of ribosomal protein L20 to two sites in its leader mRNA: a possible case of ribosomal RNA-messenger RNA molecular mimicry. RNA 8:878–889
81. Guillier M, Allemand F, Dardel F, Royer CA, Springer M, Chiaruttini C (2005) Double molecular mimicry in *Escherichia coli*: binding of ribosomal protein L20 to its two sites in mRNA is similar to its binding to 23S rRNA. Mol Microbiol 56:1441–1456
82. Raibaud S, Lebars I, Guillier M, Chiaruttini C, Bontems F, Rak A, Garber M, Allemand F, Springer M, Dardel F (2002) NMR structure of bacterial ribosomal protein l20: implications for ribosome assembly and translational control. J Mol Biol 323:143–151
83. Magde D, Elson EL, Webb WW (1974) Fluorescence correlation spectroscopy. II. An experimental realization. Biopolymers 13:29–61
84. Bacia K, Haustein E, Schwille P (2014) Fluorescence correlation spectroscopy: principles and applications. Cold Spring Harb Protoc 2014:709–725
85. Allemand F, Haentjens J, Chiaruttini C, Royer C, Springer M (2007) *Escherichia coli* ribosomal protein L20 binds as a single monomer to its own mRNA bearing two potential binding sites. Nucleic Acids Res 35:3016–3031
86. Doan T, Aymerich S (2003) Regulation of the central glycolytic genes in *Bacillus subtilis*: binding of the repressor CggR to its single DNA target sequence is modulated by fructose-1,6-bisphosphate. Mol Microbiol 47:1709–1721
87. Fillinger S, Boschi-Muller S, Azza S, Dervyn E, Branlant G, Aymerich S (2000) Two glyceraldehyde-3-phosphate dehydrogenases with opposite physiological roles in a nonphotosynthetic bacterium. J Biol Chem 275:14031–14037
88. Servant P, Le CD, Aymerich S (2005) CcpN (YqzB), a novel regulator for CcpA-independent catabolite repression of *Bacillus subtilis* gluconeogenic genes. Mol Microbiol 55:1435–1451
89. Zorrilla S, Ortega A, Chaix D, Alfonso C, Rivas G, Aymerich S, Lillo MP, Declerck N, Royer CA (2008) Characterization of the control catabolite protein of gluconeogenic genes repressor by fluorescence cross-correlation spectroscopy and other biophysical approaches. Biophys J 95:4403–4415
90. Zorrilla S, Chaix D, Ortega A, Alfonso C, Doan T, Margeat E, Rivas G, Aymerich S, Declerck N, Royer CA (2007) Fructose-1,6-bisphosphate acts both as an inducer and as a structural cofactor of the central glycolytic genes repressor (CggR). Biochemistry 46:14996–15008
91. Zorrilla S, Doan T, Alfonso C, Margeat E, Ortega A, Rivas G, Aymerich S, Royer CA, Declerck N (2007) Inducer-modulated cooperative binding of the tetrameric CggR repressor to operator DNA. Biophys J 92:3215–3227
92. Chaix D, Ferguson ML, Atmanene C, Van DA, Sanglier-Cianferani S, Royer CA, Declerck N (2010) Physical basis of the inducer-dependent cooperativity of the central glycolytic genes repressor/DNA complex. Nucleic Acids Res 38:5944–5957

93. Digman MA, Dalal R, Horwitz AF, Gratton E (2008) Mapping the number of molecules and brightness in the laser scanning microscope. Biophys J 94:2320–2332
94. Ferguson ML, Le CD, Jules M, Aymerich S, Declerck N, Royer CA (2011) Absolute quantification of gene expression in individual bacterial cells using two-photon fluctuation microscopy. Anal Biochem 419:250–259

Light Initiated Protein Relaxation

Ludwig Brand

Abstract Absorption of light by solvatochromic dyes including tryptophan leads to formation of an excited state with a change in the magnitude and/or direction of its permanent electric dipole moment. The excited state can interact with surrounding atoms with formation of a relaxed state. The kinetics of this process can be measured by time/energy-resolved fluorescence spectroscopy. Time-dependent spectral shifts (time-resolved emission spectra) provide information about protein relaxation. Ground-state heterogeneity, two-state excited-state reactions, and dielectric relaxation all give rise to time-dependent spectral shifts. Ways to tell these processes apart are discussed. Examples are presented which illustrate how rates and extent of spectral shifts can differentiate between ordered and disordered parts of a protein molecule. Rates of spectral shifts can be related to nanosecond motions of specific protein residues.

Keywords DAS • FSS • Nanosecond time-resolved fluorescence • Protein fluorescence • Protein relaxation • Pseudo-TDFFS • Solvent relaxation • TDFFS • TDSS • Time-dependent spectral shifts • Time-resolved emission spectra • TRES • Tryptophan fluorescence

Contents

L. Brand (✉)
Biology Department, Johns Hopkins University, Baltimore, MD, USA
e-mail: Ludwig.Brand@jhu.edu

D.M. Jameson (ed.), *Perspectives on Fluorescence: A Tribute to Gregorio Weber*,
Springer Ser Fluoresc (2016) 17: 255–270, DOI 10.1007/4243_2016_18,

1 Introduction

I first met Gregorio Weber in 1960 while I was a postdoctoral at Brandeis University. I knew of him previously, since I had reviewed his classical papers on fluorescence polarization for our research group while I was a graduate student. At Brandeis, we became good friends immediately and I visited him in Sheffield, England, on my way to a second postdoctoral at the Weizmann Institute in Israel. He showed me his fluorescence polarization instrument which worked with visual detection (no electronic photodetection). Of relevance to this chapter, he handed me a small vial with 1,8-ANS (1-anilinonaphthalene-8-sulfonate) and showed me that its fluorescence color depended on solvent polarity. By the time I returned to the USA, he had moved to Urbana, Illinois. We saw each other frequently in Baltimore and in Urbana and at meetings all over the world. He was a friend who influenced every aspect of my work.

In his classical contribution to the McCollum-Pratt Symposium on Light and Life [1], Weber discussed the effect of solvent environment on the fluorescence of substituted naphthalenes and on the amino acid, tryptophan. He emphasized the importance of dielectric effects on the fluorescence of proteins. He was asked to summarize the material in his contribution. He replied, "There are numerous ways in which the properties of the excited state can be utilized to study points of ignorance of the structure and function of protein molecules." This statement also summarizes the spirit of the present chapter.

The functions of proteins including enzyme catalysis, control, and signaling require flexibility of the protein. Individual atoms must be able to move over a wide range of time. This review summarizes the way in which the fluorescence emission of extrinsic and intrinsic dyes in proteins is sensitive to elemental motions of atoms.

There is an extensive literature describing an empirical relation between the fluorescence maximum of dyes and the solvent environment [2–4]. The basic idea is that the dipole moment of "solvatochromic" fluorophores is greater in the excited state than in the ground state. In the excited state, solvent reorientation takes place, decreasing the energy between the ground state and the excited state and leading to a red shift in the fluorescence emission. The Lippert equation applies to dyes in liquid solution and gives reasonable predictions for the effect of solvent polarity on the emission spectra.

$$\overline{\nu}_{\mathrm{A}} - \overline{\nu}_{\mathrm{F}} = \frac{2}{hc}\left(\frac{\varepsilon - 1}{2\varepsilon + 1} - \frac{n^2 - 1}{2n^2 + 1}\right)\frac{(\mu_{\mathrm{E}} - \mu_{\mathrm{G}})^2}{a^3} + \text{Const.} \qquad (1)$$

$\overline{\nu}_{\mathrm{A}}$, $\overline{\nu}_{\mathrm{F}}$ the wave number of absorption and fluorescence. h is Planck's constant, c is the speed of light, and ε is the dielectric constant. n is the refractive index, μ_{E}, μ_{G} are the dipole moments of the excited state and the ground state. a is the radius of the cavity in which the fluorophore exists.

Relations of this type do a reasonable job of predicting the effect of solvent polarity on fluorescence emission in liquid, homogeneous solvents (but not all).

They are of more limited value for fluorophores in proteins. Proteins represent a heterogeneous and constrained environment. Moreover, the concept of "dielectric constant" in the protein matrix, although much used, is difficult to define.

This chapter summarizes ways in which fluorescence decay studies can add to our understanding of dielectric effects on fluorophores in proteins. When fluorescence decay measurements are done as a function of emission wavelength a data matrix of fluorescence as a function of time and energy is obtained. This can be visualized as time-resolved emission spectra (TRES) and decay-associated spectra (DAS). The latter are the pre-exponential terms as a function of energy. Examination of this data makes it possible to better understand the environment of the fluorophore including dielectric relaxation. In proteins, a lengthening of decay time with increasing wavelength and concomitant red shift in the TRES with time is frequently observed. What is the origin of these effects and what can one learn about proteins?

2 Heterogeneity

The first and simplest explanation is a mixture of two or more fluorophores with different decay times and different emission spectra. In this situation a change in the shape of the emission spectra with time is expected. A good example is horse liver alcohol dehydrogenase [5, 6]. This enzyme is a dimer with identical subunits each of which has two tryptophan residues in different positions (Trp 314 and Trp 15). Quenching studies allowed the resolution of the different emission spectra of the two tryptophan residues. The decay times corresponding to different emission spectra can also be assigned with the aid of cofactor binding studies. The time-resolved fluorescence is described by Eq. (2).

$$f(\lambda, t) = \alpha_1(\lambda)e^{-t/\tau_1} + \alpha_2(\lambda)e^{-t/\tau_2} \tag{2}$$

This is a simple sum of two exponentials. The decay times correspond to the two tryptophans and the alphas to the relative intensity of each as a function of wavelength.

The TRES represent a heterogeneous mixture of the spectra of the two tryptophan residues, which are resolved with the aid of Eq. (2). It should be noted that there is no negative amplitude here. Since these decay curves (as a function of emission wavelength) are related to each other according to Eq. (2), it is advantageous to analyze them simultaneously by a procedure known as "global analysis" [7]. The spectra of the mixture of two compounds with similar decay times could be resolved with the use of global analysis. Global analysis methods were not available at the time that the heterogeneity of the two tryptophans in alcohol dehydrogenase was resolved. It is likely that with the newer instrumentation together with the global analysis procedures now available, it should be possible not only to resolve

the spectra of the two tryptophans in alcohol dehydrogenase, but also to observe relaxation processes (see below) around one or both fluorophores.

3 Two-State Excited-State Interactions

A second situation that can lead to increasing decay time with increasing wavelength, together with time-dependent spectral shifts, is a two-state excited-state reaction. An example is the excited-state ionization of 2-naphthol. This occurs because there is a dramatic decrease in the excited-state pK_a, as compared to the ground-state pK_a. In the case of this excited-state reaction, the decay at the red side of the spectrum is associated with the fluorescence of naphtholate and has a negative amplitude (rise time). Naphtholate is formed in the excited state. It starts out at zero and shows an initial rise in intensity (negative amplitude) followed by a decay. The shape of the time-resolved emission spectrum changes with time. At early times the emission spectrum looks like naphthol. At intermediate times it reflects a mixture of naphthol and naphtholate and is thus broadened. Finally, at late times the spectra are due mainly to naphtholate emission.

The fluorescence for a two-state excited-state reaction is described by a double exponential at all wavelengths. In the wavelength region where naphthol emits

$$F(t) = \alpha_1 e^{-t/\tau_1} + \alpha_2 e^{-t/\tau_2} \tag{3a}$$

In the wavelength region where naphtholate emits

$$F(t) = \beta e^{-t/\tau_1} - \beta e^{-t/\tau_2} \tag{3b}$$

important features are that the decay times, τ_1 and τ_2, are identical whether looking at naphthol or naphtholate emission. The two pre-exponential terms β for the fluorescence of naphtholate are equal in magnitude but opposite in sign. This is the case for any two-state excited-state reaction. It is of interest to point out that the two decay constants are associated with the system rather than with the individual species, naphthol or naphtholate.

4 Dielectric Relaxation

Finally, we come to dielectric relaxation in proteins. The model in this case is that the fluorophore is homogeneous in the ground state. It is excited with an increase (and change in orientation) in dipole moment, and then undergoes a smooth interaction with solvent (or other atoms) to a relaxed state of lower energy.

Two fluorescence probes will be discussed. First the *N*-aryl-aminonaphthalene sulfonates (ANS and TNS) and then tryptophan. Anilino naphthalene sulfonate (ANS) and toluidino naphthalene sulfonate (TNS) have very low fluorescence in aqueous buffers. They bind to some proteins, in some cases, at active site regions [8–11].

The basic observations are as follows: ANS exhibits intense fluorescence in liquid organic solvents but the emission spectra do not shift with time (on the nanosecond time scale). Nanosecond time-resolved spectral shifts are observed when ANS is dissolved in viscous polar solvents such as glycerol [12]. In contrast to ground-state heterogeneity or to two-state excited-state interactions, the spectral shape does not change. Decay curves at the red edge of the spectra show a negative amplitude (rise time) indicative of an excited-state reaction. This can be attributed to excited-state solvent relaxation. An important finding is that similar time-resolved spectral shifts are observed when ANS is bound to serum albumin and to apomyoglobin. As is the case with ANS in glycerol, negative amplitudes are observed for decay in the red region of the spectra and the emission spectra do not change their shape as a function of time.

In the case of ANS bound to some proteins little or no negative amplitude is observed. Is there relaxation occurring on the protein in this case? What does the lack of negative amplitude imply? If there is relaxation, what is relaxing. Bakhshiev et al. [13] expressed the non-exponential decay as a function of emission wavelength, in terms of a damping function that is continuously shifting in time from the initially formed Frank–Condon state.

$$I(\overline{\nu}, t) = i(t)\rho(\overline{\nu} - \xi(t)) \tag{4}$$

$i(t)$ is a damping term. $\rho(\overline{\nu} - \xi(t))$ is the intensity distribution in the spectrum shifted in energy by the amount $\xi(t)$ *at time t*.

Separation of TRES into a damping function and a shifting function is useful in that it allows simulation of decay curves for a system of this type [14, 15]. The relation between the spectral width, the extent- and rate- of the shift and the relation between the damping function and the shifting function determine whether a negative amplitude in the red region of the time-resolved spectra will be observable or it will be masked. Observation of a rise time or negative amplitude can be taken as evidence for an excited-state interaction. Absence of a negative amplitude cannot be taken as evidence for lack of an excited-state interaction.

The wavelength- and time-resolved spectroscopy of 2-anilinonaphthalene has been studied in cyclohexane with addition of small amounts of the polar solute, ethanol, in pure ethanol, in pure cyclohexane, and in glycerol [15]. The excited-state solvation behavior can vary, depending on the relation between the fluorescence decay times and the rates of the excited-state reactions. In pure ethanol, solvation is fast compared to the decay time and mono-exponential decay is observed on the nanosecond time scale. In pure cyclohexane mono-exponential decay is observed since there is no polar solvent. In cyclohexane containing 0.1 M ethanol, two-state excited-state behavior is found (similar to the kinetics observed

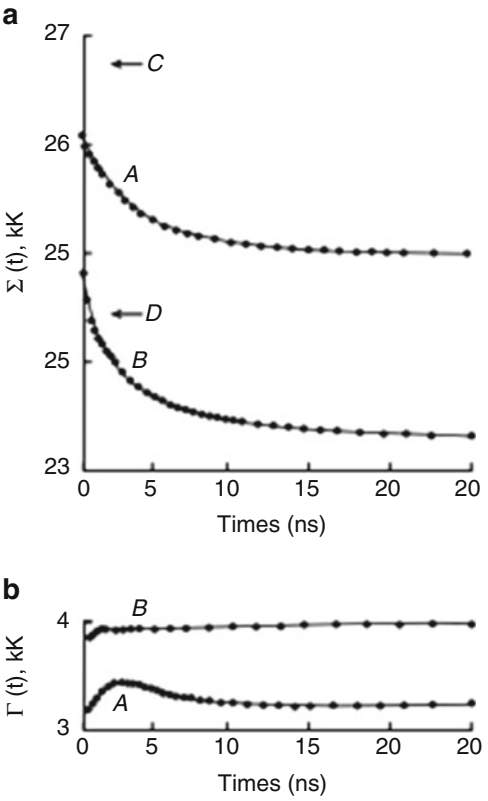

Fig. 1 Time-resolved emission maxima (**a**) and bandwidths (**b**) of 2-anilinonaphthalene (2-AN). (*A*) In 0.1 M ethanol, cyclohexane: (*B*) in glycerol. The *arrows* indicate the steady-state emission maxima of 2-AN in pure cyclohexane (*C*) and pure ethanol (*D*) [15]

in the case of excited-state proton transfer). There is a change in bandwidth with time. In glycerol (a viscous, polar solvent) a smooth time-resolved spectral shift is observed (similar to that found with ANS bound to proteins). An important feature is that the bandwidth of the time-dependent spectral shift does not change in glycerol but does change for the case of the two-state excited-state reaction. These findings are summarized in Fig. 1 which shows the time-resolved spectral shifts and half bandwidths for 2-anilinonaphthalene in glycerol and in cyclohexane with 0.1 M ethanol. The minimal change in band shape is similar to what is seen with ANS or TNS bound to proteins.

Weber and Laurence [10] reported that 1,8-ANS (1-anilinonaphthalene-6-sulfonate) bound to serum albumin with strong blue fluorescence, in contrast to the very weak green fluorescence seen in aqueous buffers. Later studies by Stryer [9] showed that this dye adsorbed at the heme binding site of apohemoglobin. The complex between a similar dye, 2,6-TNS (2-p-toluidinonaphthalene-6-sulfonate) showed time-resolved spectral shifts on the nanosecond time scale [16].

As is shown in Fig. 2, the decay becomes longer at the red edge of the spectrum but without a rise (negative amplitude). Does this mean that there is no excited-state relaxation? No it does not. As discussed above, the Bakshiev formulation can be

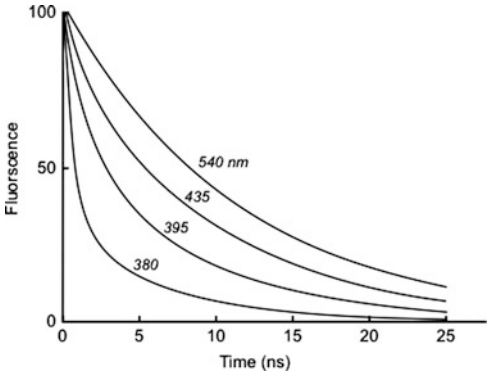

Fig. 2 The normalized decay at four wavelengths for the 2,6 p-TNS apomyoglobin complex at 4°C [16]

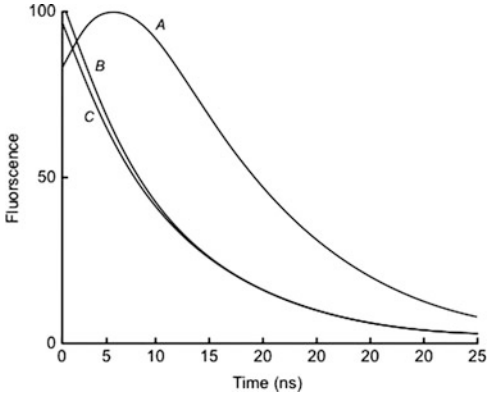

Fig. 3 Simulated decay curves based on the Bakhshiev formulation of solvent relaxation. Curve A, tau relaxation equals tau fluorescence, tau relaxation = 0.01 tau fluorescence and curve C, tau relaxation = 100 tau fluorescence. Tau fluorescence = 10 ns [16]

utilized to simulate this situation. As is shown in Fig. 3, adjustment of the relation of the damping and shifting rates can lead to masking of the negative amplitude. The TNS-apomyoglobin time-resolved spectral data is consistent with solvent relaxation.

As is indicated above, a negative amplitude at the red edge is direct evidence for an excited-state reaction but its absence does not mitigate against it.

Time-resolved fluorescence of indole and of tryptophan in proteins:

A major interest of Gregorio Weber throughout his career was the fluorescence of proteins, in particular the emission of tryptophan. The time- and wavelength-resolved fluorescence of indole (the parent chromophore) has been studied in glycerol [17]. The results are consistent with a homogeneous electrostatic relaxation model. The decay over the spectral region of emission can be fit by a sum of four exponential terms using "global analysis," with the four decay constants independent of emission wavelength. The pre-exponential factor, DAS, spectra are shown in Fig. 4.

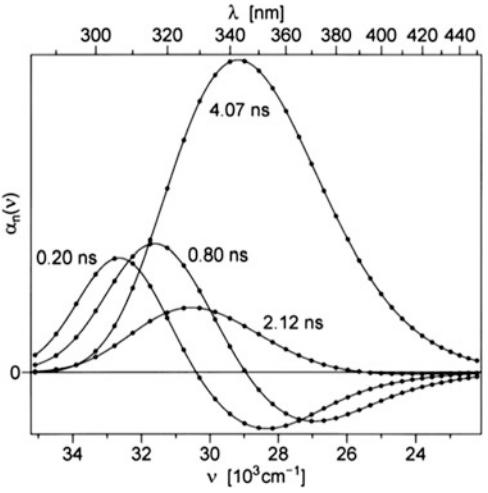

Fig. 4 Pre-exponential spectra (DAS) for indole in glycerol at 20°C [17]

Three of the four pre-exponential spectra, DAS, are negative at long wavelengths. The DAS representation is helpful for visualizing negative amplitudes. Figure 5 shows the peak normalized TRES indicating no change in shape as a function of time.

The decay of the excited indole population is essentially exponential. The decay of the intensity at individual wavelengths is *not* exponential, due to the shifting function, discussed above. These results provide a baseline for understanding the time-resolved fluorescence spectra of tryptophan in proteins [18–20].

Homogeneous spectrally and time-resolved emission from two single tryptophan mutants of the protein IIA^{Glc} was studied using the monophoton counting method. IIA^{Glc} is a phospho-carrier protein of the bacterial phosphoenolpyruvate: glycose phosphotransferase (PTS) pathway responsible for some bacterial sugar transport. The native IIA^{Glc} has neither tryptophan nor tyrosine and the two mutant forms investigated had only a single tryptophan each. The protein IIA^{Glc} has a well-defined structure as determined by NMR and X-ray diffraction. It consists of a rigid globule of residues 19–168 and a flexible tail of the first 18 residues. In the mutant form, E21W, a tryptophan residue was inserted into the globular part of the protein. In the mutant form, F3W, a tryptophan residue was inserted into the flexible tail. Time-resolved fluorescence spectra were obtained. As discussed above, by the shape conservation criterion, dielectric relaxation was homogeneous for both mutant forms. The dielectric responses of the tryptophan regions in both mutant forms cover a wide range of relaxation rates. In F3W the dielectric relaxation is practically complete within 3 ns while in E21W the relaxation is not even complete within 20 ns. The difference in relaxation rates between the solid globule and the flexible tail suggests that dielectric relaxation kinetics, as measured by time-resolved fluorescence spectroscopy, is a useful tool for studying and quantifying differences between structured and unstructured proteins or structured and flexible regions within one protein.

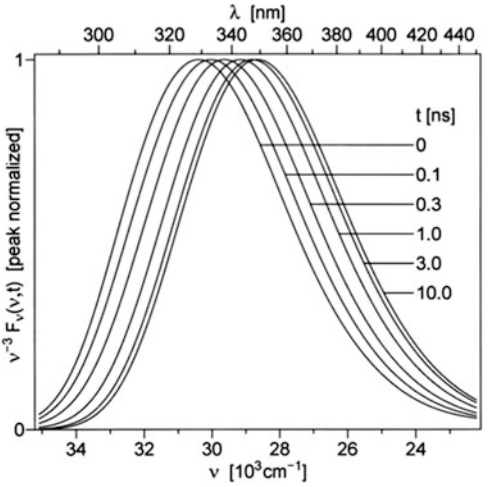

Fig. 5 Instantaneous peak normalized emission spectra, at the times indicated, for indole in glycerol [17]

It is clear that dielectric relaxation observed with proteins will depend on the environment of the chromophore, the structural characteristics of the protein and also on the chromophore itself. To gain a better understanding of this, the nanosecond relaxation dynamics of tryptophan and the related 5-fluorotryptophan was studied in the protein GB1 [19, 21]. This is the B1 immunoglobulin binding domain of streptococcal protein G. This protein has high thermal stability (melting at 87°C.). The protein contains a single tryptophan residue which is easily replaced by 5-fluorotryptophan. The dielectric relaxation of the protein matrix has been studied using aladan [22], a synthetic amino acid incorporated in GB1 at the location of the tryptophan residue and other regions. TRES for tryptophan were obtained over a wide wavelength range and analyzed by the method of global analysis. The pre-exponential spectra (DAS) are shown for Tryptophan GB1 and 5-fluorotryptophan GB1 in Fig. 6.

Four exponential terms are required to fit the data. Negative amplitudes are found for tryptophan and also for 5-fluorotryptophan. The shape of the time-resolved spectra (TRES) remained unchanged with time, consistent with the notion of excited-state dielectric relaxation. The spectrally and time-resolved fluorescence shows that the amplitude but not the rate of the time-dependent red shift depends on whether the reporter is tryptophan or 5-fluorotryptophan. This suggested that the dynamics of the dielectric relaxation depends on the protein matrix. The dynamics of relaxation is faster for GB1 than for the IIA^{Glc} protein discussed above.

Nilsson and Halle [23, 24] and Toptygin [20] used molecular dynamics simulations to determine the origin of the time-dependent spectral shifts in the single tryptophan GB1 protein. The data simulation of the total nanosecond and picosecond time-dependent spectral shift was separated into components due to protein, solvent, and the fluorophore. The results are shown in Figs. 7 and 8.

The rate of the spectral shifts shown in Figs. 7 and 8 can be resolved into five exponential terms (36.1 fs, 384 fs, 5.63 ps, 131 ps, and 2.58 ns). The **amplitudes** of

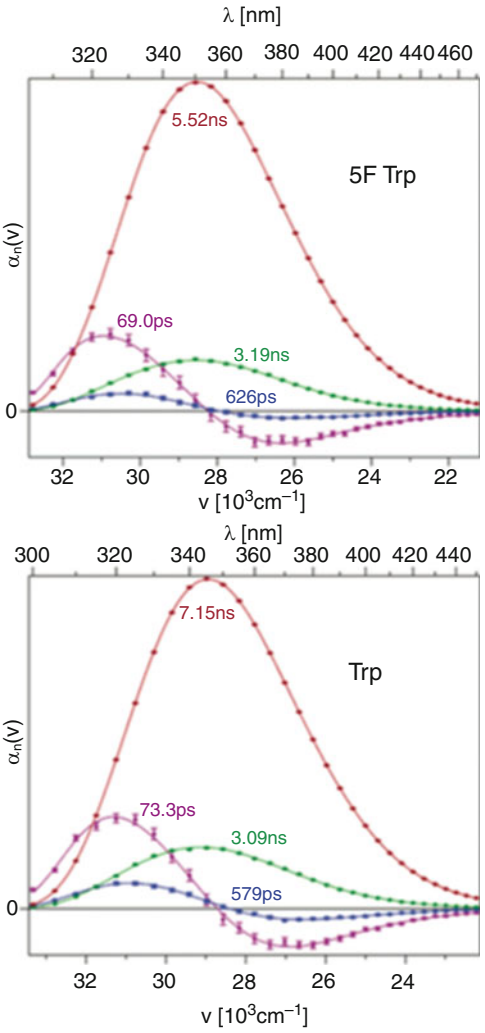

Fig. 6 The best global fit pre-exponential spectra (DAS) for tryptophan and 5-fluoro tryptophan GBO [19]

these exponential terms are shown in Fig. 9. Each term shows the contribution due to protein, solvent, and fluorophore. A substantial portion of the spectral shift occurs on a time scale too rapid to be measured on a single photon counting decay instrument.

The very fast 36.1 fs component accounts for the largest part of the total spectral shift. 59% of this relaxation component is due to solvent and 41% is due to motions of protein atoms. The second fast component, 384 fs, is essentially due to solvent. An intermediate component 5.63 ps is due to solvent motions. A second to slowest component, 131 ps has contributions due to solvent and protein atoms. The slowest component, 2.58 ns, has both solvent and protein contributions. The negative amplitude of the water component can be explained by a dielectric model suggested

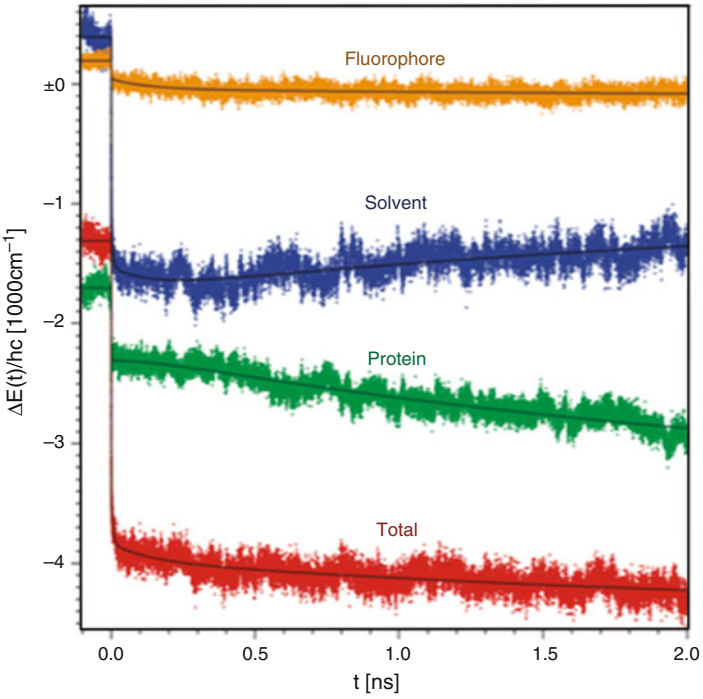

Fig. 7 Time-dependent spectral shifts calculated with molecular dynamics simulations. The total spectral shift is separated into that due to protein, solvent, and fluorophore [20]

by Halle and Nilsson [24]. The apparent slow water component is a secondary effect due to relaxation induced by the slow motions of protein atoms.

The wealth of detail about atomic motions as revealed by time/emission-resolved fluorescence in combination with molecular dynamic simulations is illustrated in Fig. 10, which illustrates the time-dependent evolution of glutamate-42 side-chain rotamers within two nanoseconds following excitation of the tryptophan of GB1.

This is just to illustrate the detail of information that is available from the simulation of spectral shifts following excitation of tryptophan in a protein. A protein contribution on this time scale can be attributed to specific motions of glutamate 42 (adjacent to the tryptophan residue).

This short review began with observations made in the 1950–1960 era by Weber and others which indicated that the fluorescence color of dyes such as naphthalene derivatives and tryptophan depended on solvent polarity. The fluorescence is red shifted in polar solvents and blue shifted in non-polar solvents. In proteins, these fluorophores tend to behave as in a non-polar environment. Of course proteins are heterogeneous and cannot be considered to be liquid, so the comparison of the fluorescence behavior of chromophores in liquid solvents to their behavior in proteins is a little like comparing apples to oranges. We have tried to review

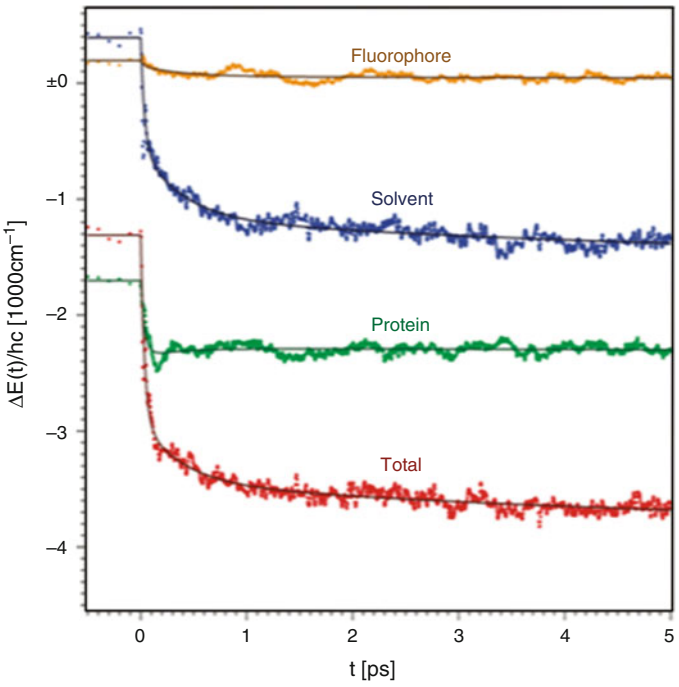

Fig. 8 Expanded time scale [20]

some studies that show what can be learned from nanosecond time-resolved fluorescence decay studies about interactions of the excited states of tryptophan and naphthalene dyes.

The ability to measure fluorescence lifetimes and the evolution of fluorescence emission spectra during the emission decay has enhanced our understanding of dielectric interactions in proteins. What about the question of heterogeneity versus generalized dielectric interactions? If dielectric interactions are very fast compared to the measured decay time, they will appear as heterogeneity. For example, the two tryptophans in horse liver alcohol dehydrogenase appear as heterogeneous. Dielectric relaxation may be taking place but on a time too rapid to measure with the instrumentation and procedures for data analysis available at the time that work was done. Heterogeneity can dominate spectral behavior, if it persists during the fluorophore lifetime. What about the "negative amplitude" and the question of relaxation? If you see it, that proves that an excited-state process is involved. In many situations the negative amplitude may be masked, depending on the amount and rates of shift and the rates of decay.

For this reason, lack of a negative amplitude in the decay of tryptophan in proteins cannot be taken as evidence for lack of an excited-state relaxation process. Another lesson to be learned from the molecular dynamics simulations is that relaxation measured with a typical nanosecond decay instrument will only reveal

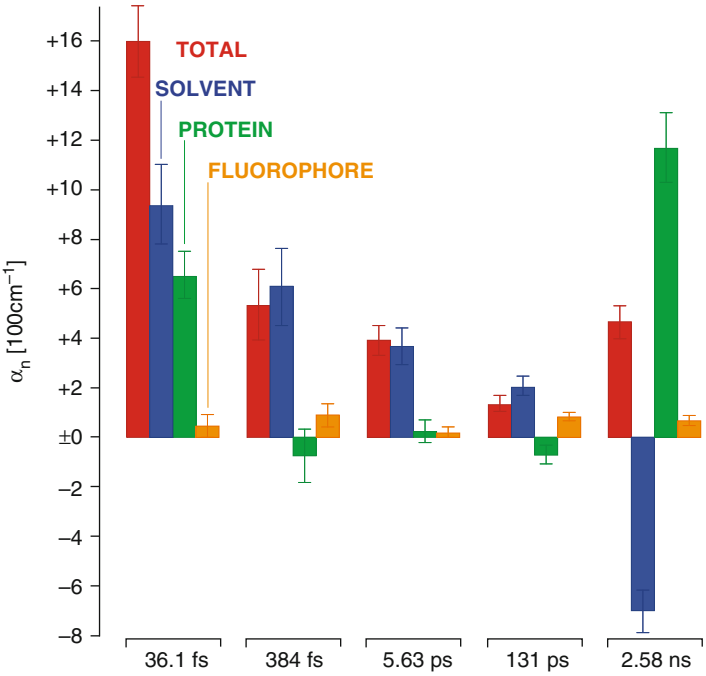

Fig. 9 Histogram of the amplitudes corresponding to the five exponentials recovered from the analysis of the time-dependent spectral shifts obtained from the simulations [20]

a small time window of the total relaxation processes occurring around tryptophan residues in proteins. In particular dielectric relaxation processes due to solvent take place on a very rapid time scale.

Time-resolved spectral shifts on the nanosecond time scale reflect motions of charged residues on a protein such as glutamate, lysine, and imidazole. Rearrangements of ionized residues in proteins are of importance to protein functions such as catalysis. Since tryptophan can be moved to various sites in a protein, time-resolved spectral shifts with tryptophan provide an important tool for better understanding the kinetics of these motions under different conditions.

Time-resolved fluorescence spectra observed with proteins are limited on the short side by the time resolution of the available instrumentation and on the long side by the lifetime of the fluorophore. Thus spectroscopic experimental data is available over a limited time window. Tryptophan is an excellent probe to use to study proteins. It can readily be removed or inserted into regions of interest in proteins. Furthermore, the photophysics of tryptophan is well understood [25, 26] allowing intelligent interpretation of spectroscopic measurements.

There continue to be significant advances in procedures for data analysis, allowing the processing of large data sets and testing complex photo-physical mechanisms against experimental results. For example, ground-state heterogeneity can be differentiated from dielectric reaction relaxation. The ability to simulate the

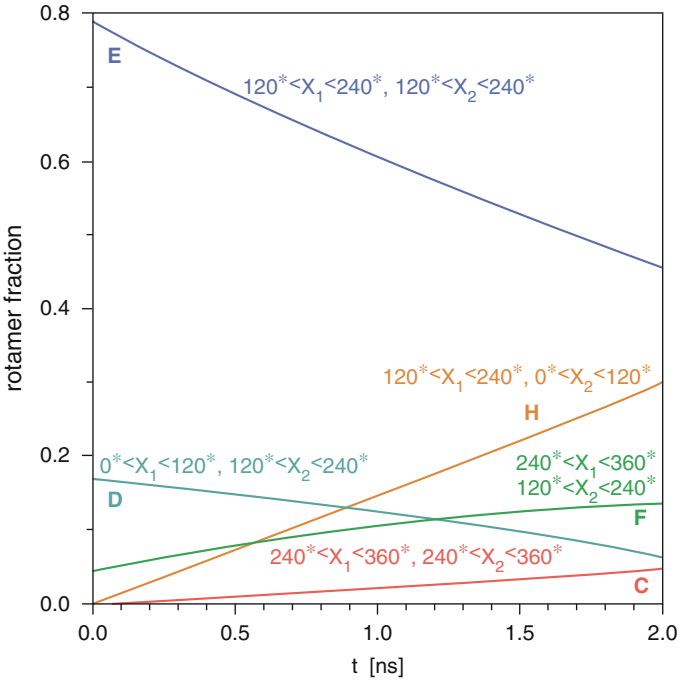

Fig. 10 Dynamics of the Glu-42 side chain, rotamer populations following excitation of the tryptophan. Rotamer E is the most populated rotamer at any time during the simulation. It decreases with time, following excitation of the tryptophan. The fraction of some of the other rotamer populations with time is also shown [20]

extent and rates of fluorescence spectral shifts of tryptophan in proteins with the aid of molecular dynamics calculations represents an important advance. Significant advances in computing power and force fields will facilitate the resolution of spectral shifts due to solvent and motions of charges related to motions of specific protein atoms. The combination of time- and energy-resolved fluorescence data with molecular dynamics simulations will make it possible to understand details of atomic motion in proteins under a variety of experimental conditions.

This chapter summarized some of the recent experiments with *N*-aryl-aminonaphthalene sulfonates and with tryptophan in proteins. There is now a large literature in this area of research and no attempt was made to be all inclusive.

It will be of interest to extend time-resolved emission spectral shift studies to coenzymes such as NADH, flavines, and pyridoxal. It is also of interest that so many enzymes have an aromatic amino acid at the active site or utilize a cofactor with aromatic character such as NADH. It will be important to further explore the excited states of these chromophores.

The experimental methods and procedures for data analysis to obtain time-dependent spectral shifts of tryptophan fluorescence in proteins have been reviewed by Toptygin [24]. Molecular dynamics simulation of tryptophan fluorescence

spectral shifts in proteins have been reviewed by Toptygin [26], and the reader is referred to these papers for details of the approaches alluded to in the present review.

References

1. Weber G (1961) Excited states of proteins. In: McElroy WD, Glass B (eds) Light and life. Johns Hopkins Press, Baltimore, pp 82–105
2. Mataga N, Kaifu Y, Koizumi M (1956) Solvent effects upon fluorescence spectra and the dipole moments of excited molecules. Bull Chem Soc Jpn 29:465–470
3. Bakhshiev NG (1961) Universal molecular interactions and their effect on the position of the electronic spectra of molecules in component solutions. I. Theory (Liquid solutions). Opt Spectrosc 10:379–384
4. von Lippert E (1957) Spectroskopische bistimmung des dipolmomentes aromatischer verbndungen im ersten angeregten singulet tzustant. Z Electrochem 61:962–975
5. Ross JBA, Schmidt CJ, Brand L (1981) Time resolved fluorescence of the two tryptophans in horse liver alcohol dehydrogenase. Biochemistry 20:4369–4377
6. Knutson JR, Walbridge DG, Brand L (1982) Decay-associated fluorescence spectra. Biochemistry 21:4671–4679
7. Knutson JR, Beechem JM, Brand L (1983) Simultaneous analysis of multiple fluorescence decay curves: a global approach. Chem Phys Lett 102:501–506
8. Daniel E, Weber G (1966) Cooperative effects in binding by bovine serum albumin. I. The binding of 1-anilino-8-naphthalenesufonate. Biochemistry 5:1893–1900
9. Stryer L (1965) The interaction of a naphthalene dye with apomyoglobin and apohemoglobin: a fluorescent probe of non-polar binding sites. J Mol Biol 13:482–495
10. Weber G, Laurence DJR (1954) Fluorescent indicators of adsorption in aqueous solution and on the solid phase. Biochem J 56:xxxi
11. Edelman GM, McClure WO (1968) Fluorescence probes and the conformation of proteins. Acc Chem Res 1:65
12. Brand L, Gohlke JR (1971) Nanosecond time-resolved fluorescence spectra of a protein-dye complex. J Biol Chem 24:2317–2324
13. Bakhshiev NG, Mazurenko Yu. T, Piterskayer VI (1966) Luminescence decay in different portions of the luminescence spectrum of molecules in viscous solution. Opt Spectrosc 21:307–309
14. DeToma RP, Easter JH, Brand L (1976) Dynamic interactions of fluorescence probes with the solvent environment. J Am Chem Soc 98:6001–6007
15. DeToma RP, Brand L (1977) Excited-state solvation dynamics of 2-anilinonaphthalene. Chem Phys Lett 47:231–236
16. Gafni A, DeToma RP, Manrow RE, Brand L (1977) Nanosecond decay studies of a fluorescence probe bound to apomyoglobin. Biophys J 17:155–168
17. Toptygin D, Brand L (2000) Spectrally- and time-resolved fluorescence emission of indole during solvent relaxation: a quantitative model. Chem Phys Lett 322:496–502
18. Toptygin D, Savtchenko RS, Meadow ND, Brand L (2001) Homogeneous. J Phys Chem B 105:2043–2055
19. Toptygin D, Gronenborn AM, Brand L (2006) Nanosecond relaxation dynamics of protein GB1, by the time-dependent red shift in the fluorescence of tryptophan and 5-fluorotryptophan. J Phys Chem B 110:26292–26302
20. Toptygin D, Woolf TB, Brand L (2010) Picosecond protein dynamics: the origin of the time-dependent spectral shift in the fluorescence of the single trp in the protein GB1. J Phys Chem B 114:11323–11337

21. Tcherkasskaya O, Knutson JR, Bowley SA, Frank MA, Gronenborn A (2000) Nanosecond dynamics of the single tryptophan reveals multi-state equilibrium unfolding of protein GB1. Biochemistry 39:11216–11226
22. Cohen BE, McAnaney TB, Park ES, Jan YN, Boxer SC, Jan LY (2002) Probing protein electrostatics with a synthetic fluorescent amino acid. Science 396:1700–1703
23. Nilsson L, Halle B (2005) Molecular origin of time-dependent spectral shifts in proteins. Proc Natl Acad Sci U S A 102:13867–13872
24. Halle B, Nilsson L (2009) Does the dynamic shift report on slow protein hydration dynamics? J Phys Chem B Lett 113:8210–8213
25. Toptygin D (2014) Analysis of time-dependent red shifts in fluorescence emission from tryptophan residues in proteins (Ch 9). In: Engelborghs Y, Visser AJWG (eds) Fluorescence spectroscopy and microscopy: methods and protocols. Springer Science, pp 215–255
26. Toptygin D (2016) Time-dependent spectral shifts spectral shifts in tryptophan fluorescence: bridging experiments with molecular dynamics simulations (Ch 2). In: Geddes CD (ed) Reviews in fluorescence. Springer, pp 29–69

Synthetic and Genetically Encoded Fluorescence Probes for Quantitative Analysis of Protein Hydrodynamics

Gerard Marriott

Abstract The fluorescence polarization technique that Prof. Weber developed at Cambridge University between the late 1940s and early 1950s has had a tremendous impact on our understanding of the structure and dynamics of macromolecules and in the analysis of proteins interactions and detection of target proteins in biologically complex samples. His decision to develop dimethylaminonaphthalene sulfonyl chloride (Dansyl-Cl) as the first probe for fluorescence polarization studies was brilliant, as its long fluorescence lifetime and well-defined dipole are ideally suited to study protein conjugates as large as 100 kDa. Indeed, after almost 70 years, the Dansyl group is still the probe of choice for in vitro applications of fluorescence polarization. Unfortunately, Dansyl is not very suitable for related studies in living cells, primarily because it requires excitation in the near ultraviolet, while the in vivo labeling of a target protein with Dansyl group is challenging. We have developed a new class of genetically encoded fluorescent protein that may help to overcome these limitations. The lumazine-binding protein (LUMP) harbors a fluorescent probe with a cerulean-colored emission that like Dansyl has a long excited state lifetime (14 ns). Moreover, LUMP has a smaller mass than GFP that allows us to genetically append capture sequences as large as 20 kDa and still generate a fusion protein with sufficient dynamic range in the fluorescence polarization value to quantify the amounts of the free and target-bound states in an equilibrium. In this article, I will compare and contrast key features of Dansyl and LUMP as probes for fluorescence polarization studies and discuss the potential of using LUMP and related encoded proteins to advance the application of fluorescence polarization to analyze target proteins and protein interactions in living cells.

G. Marriott (✉)
Department of Bioengineering, University of California-Berkeley, Berkeley, CA, USA

Lawrence Berkeley National Laboratory, Berkeley, CA, USA
e-mail: marriott1@berkeley.edu

D.M. Jameson (ed.), *Perspectives on Fluorescence: A Tribute to Gregorio Weber*,
Springer Ser Fluoresc (2016) 17: 271–286, DOI 10.1007/4243_2016_17,

Keywords Dansyl chloride • Fluorescence polarization • Lumazine-binding protein

Contents

One of the highlights of my undergraduate experience in the department of biochemistry at Birmingham University (UK) was the final year research project. I was particularly interested in pursuing the project that was offered by Prof. John Teale who had developed a number of thiol-reactive fluorescent dyes that he wanted to use to prepare fluorescent protein conjugates. Recognizing my strong interest in fluorescence, Prof. Teale suggested that I should read papers on fluorescence spectroscopy, including a paper on thiol-reactive fluorophores published by Gregorio Weber [1]. A year after graduating from Birmingham, I applied to PhD programs in the USA – after discussing my choices with Prof. Teale, I decided to go to Urbana where I was lucky enough to end up working in Prof. Weber's laboratory [2]. I remember soon after joining the group, I had a conversation with Prof. Weber about some of the physical biochemistry courses I had taken at Birmingham with Prof. John Teale – on mentioning Teale's name, he told me about Teale's dry humor – the only story I remember was the time when they were in line at the canteen in the Scala Theatre at Sheffield University waiting for the invariable Friday lunch offering of fish and chips, when Teale told Weber "you know Gregorio, ever since I arrived at Sheffield I have become a cod-fearing man."

I learned a lot of new techniques in the Weber lab, including projects that involved the chemical synthesis of fluorescent probes and site-specific labeling of proteins with reactive fluorescent probes and their applications to study protein dynamics. This early chemical synthesis experience had a great impact on my later research program that over time has led to the development of a wide variety of sensor molecules, including thiol-reactive probes that we have used for quantitative analysis of proteins and their complexes over multiple scales of time and distance [2–5]. I thought I would use the invitation to contribute to this dedicated volume to Gregorio Weber to compare and contrast the properties and performances of synthetic and genetically encoded fluorescent probes for fluorescence polarization-based analysis of macromolecules. The history of this probe development for polarization studies began with 1,8-Dansyl-chloride (Fig. 1a), a probe that

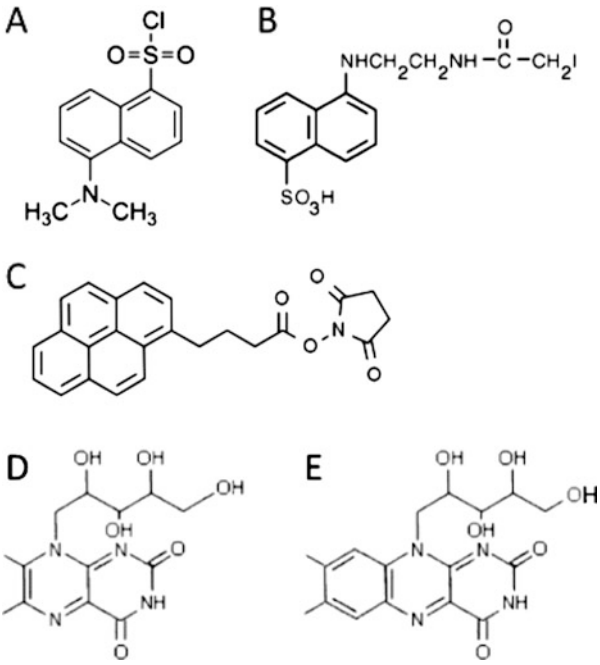

Fig. 1 Molecular structures of probes discussed in this article. (**A**) 1,8-Dimethylamino-8-naphthalenesulfonylchloride (Dansyl chloride). (**B**) *N*-(Iodoacetylaminoethyl)-8-naphthylamine-L-sulfonic acid (1,8-IAEDANS). (**C**) 1-Pyrenebutyric acid *N*-hydroxysuccinimide ester. (**D**) Ribityl-lumazine. (**E**) Flavin mononucleotide

Weber designed and synthesized at Cambridge in the latter part of the 1940s. This probe was introduced in the second of his 1952 papers in the *Biochemical Journal* on the theory and practice of fluorescence polarization [6, 7]. Weber relayed to me the difficulties he had in preparing Dansyl chloride that were finally overcome in a beautifully simple and high-yield reaction that I repeated in my first chemical synthesis in the Weber lab. The reactive sulfonyl chloride of 1,8-dimethylaminonaphthalene sulfonic acid was prepared by grinding solid forms of 1,8-Dansyl sulfonic acid, a light brown flaky material, with phosphorous pentachloride using a mortar and pestle for 15 min. The final step involved solubilizing the liquefied reaction mix in a small volume of acetone, which was poured slowly over a beaker of ice cubes – the product precipitates on the ice as a yellow-colored mass – the yellow precipitate has a mesmerizing brilliance and unique hue.

Dansyl chloride has been used as a label for many other applications in biology and chemistry, including the first fluorescence-based method for protein sequencing. In his recollections of life on the first floor of the MRC building in Cambridge, Brian Hartley described two important discoveries he made using the Dansyl chloride probe he received from Gregorio Weber [8]. The first discovery with

Vince Massey was to show Dansyl chloride reacted quickly with the active site serine (Ser-65) in chymotrypsin, which resulted in an orange fluorescent conjugate that was one of the first examples of fluorescent active site titrant [9]. The second application was in protein sequencing [10], where the Dansyl chloride was reacted with the α-amino acid residue in a peptide – the peptide was hydrolyzed and the mixture of amino acids applied to one side of a 2-sided polyamide sheet. The other side of the polyamide sheet was spotted with a solution containing all 20-Dansylated amino acids that were separated using a 2D-chromatographic separation technique [10]. The position of the N-terminal fluorescent amino acid from the peptide was compared to the positions of the 20 known amino acid derivatives of Dansyl that had been separated on the reverse side of the side of the plate. The identity of the N-terminal residue in the peptide was revealed by the overlap of fluorescent spots on each side of the plate.

In this article I will compare and contrast small-molecule synthetic probes and genetically encoded fluorescent proteins as probes for fluorescence polarization measurements. Attention is focused on the properties of 1,8-Dansyl, the prototypical small-molecule probe for fluorescence polarization [7, 11], which is compared and contrasted with genetically encoded fluorescent proteins including GFP and lumazine-binding proteins [12].

1 Design of Small-Molecule Fluorescent Sensors for Target Proteins

Fluorescent sensors including those incorporating 1,8-Dansyl [7] have been widely used to determine the size and shape of macromolecules, to detect target proteins, and to study protein interactions in complex samples [1, 2, 7, 11]. For these latter applications, the fluorescent sensor should exhibit marked differences in one or more properties of the emission between the free and target-bound states. Better still is if these differences are based on an absolute parameter of the fluorescence emission, which we consider as the quantum yield of fluorescence, the lifetime of the excited state, the energy of the emission, or the polarization of the fluorescence. Other absolute measures include changes in the rate of an excited state reaction, including those associated with FRET, excimer formation, and deprotonation. Dansyl probes are highly valued for fluorescence-based investigations of protein interactions. Protein complexation will often result in appreciable changes of the quantum yield, lifetime, and the energy of the emission. This feature arises in part because of the long fluorescence lifetime of 1,8-Dansyl (13–16 ns) [7], which makes it sensitive to dynamic events in its immediate environment, including quenching by nearby residues, while its excited state dipole is sensitive to both general and specific solvent effects [13]. Interestingly, 2,5-Dansyl has a fluorescence lifetime of ~32 ns, which should make it even more sensitive to dynamic quenching events [14].

2 Fluorescence Sensors of Protein Hydrodynamics

Weber developed the theory and experimental technique that relates values of the polarization of the fluorescence to the size and shape of the molecule [6, 7]. Moreover, the increase in the fluorescence polarization value of a sensor on complex formation with a larger target molecule can be predicted accurately using the Perrin–Weber equation [6, 12], a feature that simplifies the design of new FA sensors, especially when compared to that for a FRET-based sensor [13, 14]. Determinations of the fluorescence anisotropy value of appropriately labeled ligands or proteins have been widely used to quantify target proteins or protein interactions [15] – this popularity is a consequence of several factors that include the ability to record accurate measurements of the FA value using steady-state instrumentation under "no-wash" conditions. Before we consider the suitability of small-molecule and genetically encoded fluorescent proteins as probes for fluorescence polarization studies, it may be useful to review some of the essential relationships that relate the fluorescence polarization value to the size (and/or shape) of a probe-labeled protein [6, 7]. I will start by replacing the term fluorescence polarization with *fluorescence anisotropy* (FA), as the latter is easier to manipulate mathematically. FA values are computed using Eq. (1) from measurements of the polarized components of fluorescence emission of the sensor (I_{para} and I_{perp}) in response to vertically polarized excitation of a solution composed of mixtures of the free and target-bound states of the sensor [2]:

$$\text{FA} = I_{\text{para}} - I_{\text{perp}}/\left(I_{\text{para}} + 2I_{\text{perp}}\right) \tag{1}$$

The FA value increases in the sensor-target complex because of its larger volume and slower rate of tumbling in solution [6, 15]. This is shown schematically in Fig. 2. The Perrin–Weber equation [3, 4] expressed in terms of FA values is

$$r_0/r = (1 + \tau_{\text{f}}/\tau_{\text{c}}) \tag{2}$$

where r is the measured FA value and r_0 is the limiting FA value, which depends on molecular properties of the probe molecule and the angle between the absorption and emission transition dipole moments. This limiting value is usually recorded from a dilute solution of the probe in a viscous solvent such as glycerol at $-20°\text{C}$. The excited state lifetime is given by τ_{f}, while τ_{c} is the rotational correlation time, which is the time it takes for a sphere to rotate through 1 radian [12] (Fig. 2) – the rotational correlation time is related to the hydrodynamic volume V according to Eq. (3) [6, 7]:

$$\tau_c = \eta V/RT \tag{3}$$

where η is the solvent viscosity and T is the temperature in Kelvin. Equations (2) and (3) show that a suitable probe or protein conjugate for FA-based analysis of a

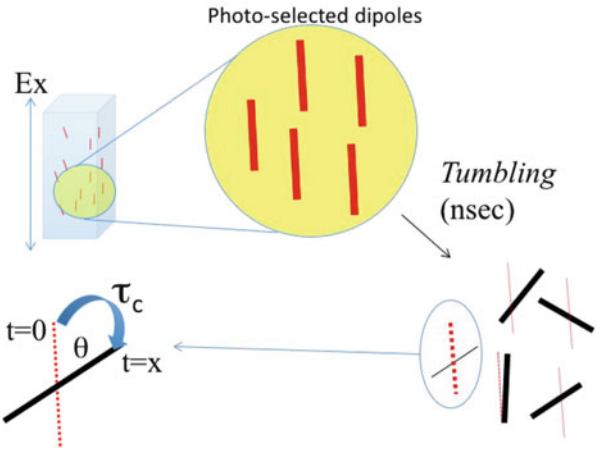

Fig. 2 Schematic representation of the photo selection of fluorescent probes using polarized excitation of the sample, and subsequent tumbling and reorientation of dipoles. *Lower left* shows the change in the average orientations of a dipole at the instant of excitation and after the decay

target protein would have a small molecular volume and a τ_f/τ_c ratio of unity or less. τ_c can also be related to the mass of a spherical protein according to $\tau_c = \eta$ MW $(\nu + h)/RT$, where $R = 8.314 \times 10^7$ erg.mol^{-1} K^{-1}, η is the viscosity, MW is the molecular weight of the spherical protein, ν is the partial specific volume of 0.74, and h is the degree of hydration 0.3 ml H_2O/g protein. We will now consider the suitability of some small-molecule fluorescent probes and larger genetically encoded fluorescent proteins.

3 Small-Molecule Probes for FA-Based Measurements

1,8-Dansyl is well suited for fluorescence polarization studies when used as a fluorescent analogue of a ligand for a target protein or when conjugated chemically to a sensor protein [7]. In particular, 1,8-Dansyl has one of the longest lifetimes (~13 ns) of any small-molecule fluorescent probe, and the direction of the dipole in the molecule is well defined and leads to a relatively uniform anisotropy value at red side of the S_0–S_1 excitation band (340–350 nm). Another useful feature of Dansyl chloride results from the coupling of the sulfonyl chloride to the ε-amino group on a lysine residue, which produces a short and rigid link that allows the probe to report primarily on the hydrodynamics of the protein molecule [7]. On the other hand, fluorophores having longer and flexible links to the protein allow the probe to experience a range of local and rapid motions that contribute in a complex manner to the depolarization.

The nonlinear relationship between the calculated FA value and the molecular volume (and mass) for fluorescently labeled spherical proteins is revealed by fitting equations (2) and (3) for different fluorescent lifetime values (Fig. 3). The plots clearly reveal the nonlinear relationship between FA and molecular weight. The relationship between the predicted FA value and the mass of a spherical protein

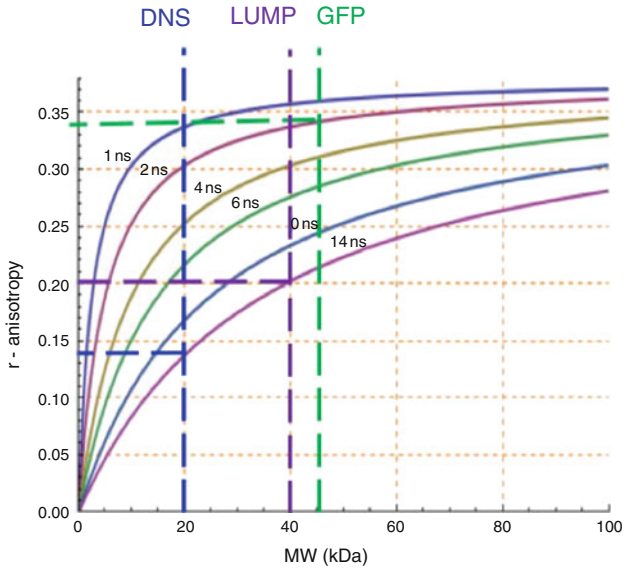

$$r_0 / r = (1 + \tau_f / \tau_c)$$

$$\tau_c = \frac{\eta V}{RT} \qquad \tau_c = \frac{\eta \ MW \ (\upsilon + h)}{RT}$$

Fig. 3 Simulations of the dependence of FA value for a spherical protein on its mass for different values of the excited state lifetime of the probe

conjugated with 1,8-Dansyl is shown in Fig. 3. In particular, the FA curve for a 20 kDa protein chemically coupled to a single 1,8-Dansyl probe is considered, which is easily achieved by treating proteins with a single cysteine residue with the thiol-reactive probe IAEDANS [1] (Fig. 1b). Using a fluorescence lifetime for the Dansyl of 14 ns, one can calculate the FA for a spherical 20 kDa Dansyl conjugate as 0.140 (blue dotted line in Fig. 3). The range of FA values between the free and bound states of this conjugate sensor (0.140 ± 0.001 to the limiting anisotropy of ~0.325 [1]) would allow one to conduct accurate FA-based binding studies with target proteins larger than 80 kDa (Fig. 3). In his classic 1952 *Biochemical Journal* paper, Weber exploited the FA-properties of 1,8-Dansyl to study the hydrodynamic properties of native and denatured ovalbumin and BSA (35 kDa and 68 kDa) [7]. In addition to providing Dansyl chloride to Hartley, Weber also collaborated with Kenneth Bailey, who with his student T.C. Tsao and G.S. Adair described fluorescence polarization studies on Dansyl-tropomyosin that were performed by Prof. Weber [16]. They reported the tropomyosin molecule has two rotational diffusion constants (ρ) where $\rho = 3\tau_c$ of 6.3×10^6 s^{-1} (159 ns) and 1.9×10^8 s^{-1} (5.3 ns) that correspond to rotations about the short axis and long axis of the molecule, respectively. Separately Tsao acknowledged Prof. Weber in two 1953 studies for his

unfailing help in the application of fluorescence polarization to study the size of subunits in myosin [17] and actin [18]. In both studies, he prepared Dansyl conjugates of each protein and used the Perrin plot to determine the size of the subunits. While he was successful in assigning correct molecular weights to the heavy and light subunits of myosin [17], his calculation of the mass of the spherical actin monomer was somewhat high at 70 kDa [18].

It is quite remarkable that in the almost 70 years since Prof. Weber introduced the 1,8-Dansyl probe [7], it is still one of the most suitable probes for FA-based analysis of proteins and their complexes. While pyrene (Fig. 1c) and related symmetrical polyaromatic hydrocarbons can boast even longer excited state lifetimes, they have low limiting anisotropy values, with excitation anisotropy spectra that are often characterized by sharp changes in the anisotropy value [19].

4 Genetically Encoded Fluorescent Proteins for FA-Based Measurements

Unfortunately, 1,8-Dansyl is not a very useful probe for FA-based analysis of proteins in living cells. This limitation arises from the low molar extinction coefficients of Dansyl conjugates, which are on the order of 4–6,000 M^{-1} cm^{-1} [7] compared to >100,000 M^{-1} cm^{-1} for probes optimized for imaging single molecules [20]. Moreover, excitation of the Dansyl group requires near ultraviolet light (<350 nm), which may result in photocytotoxicity, while also exciting natural fluorescent molecules in cells, including free and protein-bound NADH and flavin mononucleotide. Perhaps the biggest drawback in using small-molecule fluorophores as probes for FA-based analysis of protein interactions in living cells are the difficulties associated with probe delivery and chemical coupling to a target protein in the cytoplasm. It is for this reason perhaps that most studies described to probe protein interactions in living cells use genetically encoded fluorescent proteins with excitation spectra in the visible region of the electromagnetic spectrum. However, GFP-like fluorescent proteins are unsuitable for FA-based imaging of target proteins in living cells for reasons given in the following section.

In spite of the dearth of suitable probes, fluorescence anisotropy holds great promise as a technique to image and quantify specific proteins and their interactions in living cells [11, 15, 21–23]. Unfortunately, the large mass and short lifetime of GFP and related proteins make them unsuitable as probes for FA-based determinations of target proteins. This limitation may be best appreciated with reference to the simulations shown in Fig. 3. This time the predicted FA values for a 20 kDa capture appended to GFP (~30 kDa) is considered. With a mass of ~50 kDa and a fluorescent lifetime of ~2 ns, the predicted steady-state FA value of the free fusion protein in buffer at 20°C is already 0.340, which agrees almost exactly with the experimentally determined FA value for GFP [24]. The small dynamic range in FA

values for this fusion protein (0.340–0.390) coupled with the nonlinear response of FA value with mass in this plateau region would make it difficult to record accurately a change in the FA value of GFP in complexes with larger proteins.

5 New Genetically Encoded Proteins for FA-Based Analysis of Proteins

The lumazine-binding protein (LUMP) from *Photobacterium leiognathi* is a 20 kDa polypeptide composed of two structurally homologous spherical domains (α and β), with the α-subunit binding 6,7-dimethyl-8-(1′-D-ribityl) lumazine (ribityl-lumazine; Figs. 1d and 4) close to its surface with a dissociation constant of 16 nM at 20°C [25–27]. Ribityl-lumazine is synthesized within bacteria and most nonmammalian cells – when these cells are transfected with a gene encoding the α-subunit of LUMP, they produce large amounts of the fluorescent LUMP (Fig. 5a). The absorption spectrum of the lowest energy (S_0–S_1) transition of purified LUMP is similar to CFP and has a maximum at 420 nm (23,810 cm^{-1}) and a full width half maximum of 3,468 cm^{-1}. LUMP functions as a FRET acceptor in complexes with marine bacterial luciferases, and it is consequently highly optimized as a FRET acceptor probe, shifting the color of the bioluminescence to a cerulean color (Fig. 5a, b) [12, 25, 26]. This optimization also includes respectable fluorescence quantum yield ($\Phi_f = 0.55$) and, most importantly, one of the longest excited state lifetimes of any natural fluorescent proteins [12, 26].

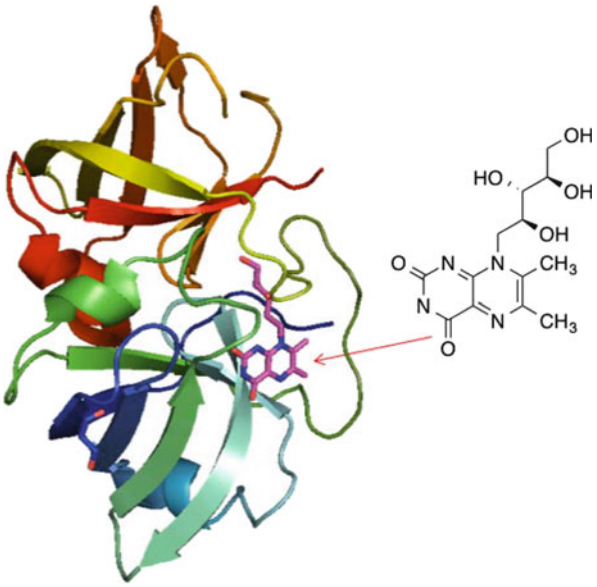

Fig. 4 High-resolution structure of LUMP showing the surface location of the bound ribityl-lumazine probe [25]

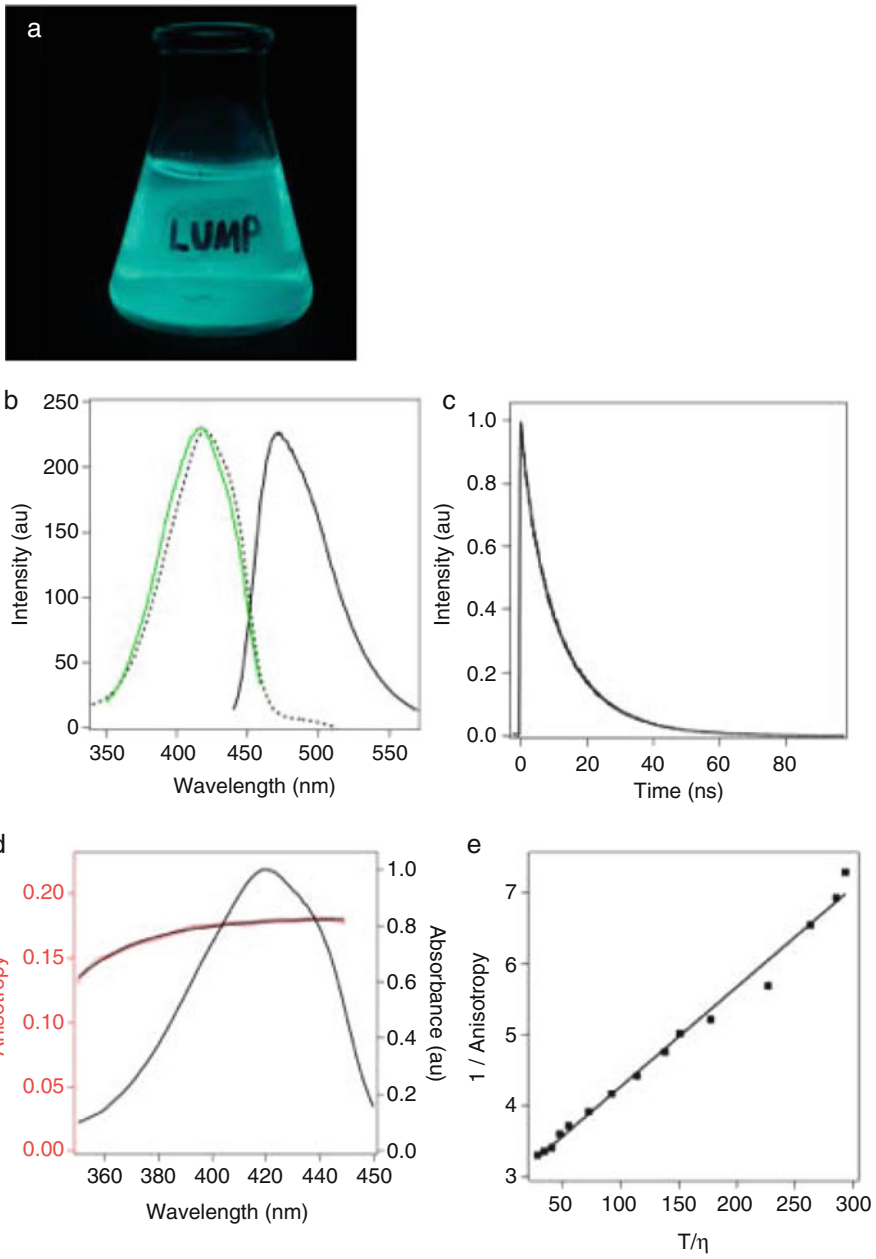

Fig. 5 Characterization of LUMP. (**a**) Photograph recorded on an iPhone showing the cerulean-colored emission from LUMP in a culture of *E. coli*. (**b**) Peak-normalized absorption (*dashed*), excitation spectrum (*green*) with emission at 470 nm, and emission spectrum of LUMP measured in aqueous buffer. (**c**) Time-resolved fluorescence intensity decay of LUMP in aqueous buffer. (**d**) Excitation anisotropy scan with fluorescence emission at 470 nm superimposed on absorbance scan of LUMP. (**e**) Perrin–Weber plot of inverse anisotropy versus T/η where η is the viscosity in centipoise (cP) in a water/sucrose solution

The FA excitation spectrum of purified LUMP (20 kDa) in a viscous medium (75% sucrose) shows a fairly uniform S_0–S_1 transition that extends from 380 nm to 480 nm, with a limiting FA value of 0.350 (Fig. 5c). The limiting FA value of LUMP increases to 0.360 when measured at an even higher viscosity [26]. The theoretical maximum FA value of 0.400 is not attained for ribityl-lumazine bound to LUMP presumably because the absorption and emission dipoles are not colinear [25]. The Perrin–Weber plot for LUMP shows a linear plot from which the fluorescence lifetime is calculated as 13.25 ns (Fig. 5d), which is similar to that measured using fluorescence lifetime imaging microscopy (13.6 ns; FLIM; Fig. 5e) [12]. The predicted FA value of LUMP at 20°C is computed using Eq. (2) as 0.133 ($\tau_f = 13.6$ ns, $r_0 = 0.360$ [26]) and assumes $\tau_c = 8.0$ ns, which is based on the assumption that τ_c increases by 1 ns for every 2.5 kDa increase in mass. The experimentally determined FA value of LUMP is 0.166 ± 0.002, suggesting that the protein molecule is not strictly spherical. The change in FA values between free LUMP at 1 cP (0.166) and its limiting FA value (0.360) is the largest recorded difference in FA values for a genetically encoded fluorescent protein – the corresponding change for GFP would be ~0.050 [24].

The simulations in Fig. 3 illustrate why LUMP and its fusion proteins are suitable probes for FA-based analysis of target proteins [12]. Referring to the purple-colored trace, the predicted FA value for fusion protein composed of LUMP fusion and a 20 kDa capture proteins (40 kDa in total) is ~0.195, which is close to the mid-range of FA values for LUMP – this value could in principle increase to the limiting FA value of 0.360 in complexes with very large proteins. For example, the FA value of this sensor would increase to 0.281 on binding to an 80 kDa target protein and reach 90% of the limiting FA on binding to a 325 kDa protein ($\tau_c = 140$ ns).

6 FA-Based Protein Sensors of GTP-Bound Cdc42

A LUMP-based FA sensor for GTP-bound Cdc42 was developed by appending the 32 amino acid GTPase-binding domain (GBD) from kinase ACK1 (human activated Cdc42 kinase 1: residues 448–489) [12] to the N-terminus of LUMP via a flexible six-amino acid linker (GSGSAS; Fig. 6a). LUMP-GBD (25 kDa) binds to Cdc42 specifically with a K_d of 23 nM [26]. The FA value of unbound LUMP-GBD is 0.176 ± 0.004 and increases to 0.207 ± 0.002 ($\Delta \sim 18\%$) when bound in a stoichiometric complex with GTP-Cdc42. The FA values for the free and bound states of this LUMP sensor agree with those calculated from the Perrin–Weber equation. Thus, using τ_f as 13.6 ns, and a limiting FA of 0.360, the free and bound forms of the FA sensor (with masses of 25 kDa and 47 kDa) with calculated τ_c values of 10 ns and 19 ns, respectively, would result in calculated FA values of 0.155 and 0.212. Once again these values indicate that the LUMP-GBD molecule is not strictly spherical. Regardless the sensor allows one to conduct accurate titrations of a fixed concentration of LUMP-GBD with increasing amounts of GTP-bound

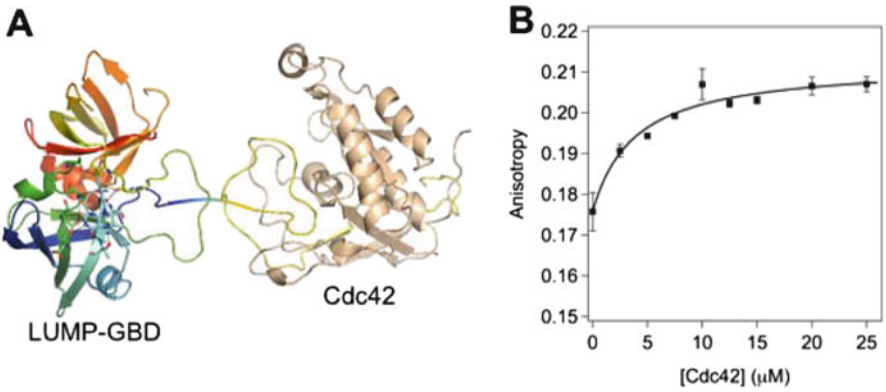

Fig. 6 Fluorescence anisotropy-based binding study of LUMP-GBD to Cdc42. (**a**) Cartoon of crystal structures of LUMP and GBD-Cdc42. (**b**) Fluorescence anisotropy plot of GBD-LUMP versus titrated equivalents of Cdc42 in 20 mM HEPES, pH 7.9, 150 mM NaCl, 2 mM GTP at 20°C

Cdc42 (Fig. 6b), with saturation occurring at equimolar concentrations of Cdc42 and GBD-LUMP (10 μM).

7 Microscope-Based FA Imaging of LUMP Fusion Proteins

Having demonstrated the suitability of LUMP and its fusion proteins as genetically encoded FA sensors of target proteins, we subsequently showed that FA measurements on the same fusion proteins can be carried out using a slightly modified confocal fluorescence microscope (Zeiss 700). In particular, microscope-based imaging of the polarized fluorescence emission of LUMP was used to compute FA images to quantify the distribution of free and bound populations of a LUMP sensor in a sample [28]. A confocal fluorescence microscope was modified to incorporate two film polarizers that were placed in the emission path [12]. The intensity image of LUMP emission shows that the probe is largely localized to the outer surface of the 80 μm NTA-agarose beads, where it presumably binds to the surface coupled NTA. The polarized images of the emission of LUMP in the sample were first registered and then analyzed using Eq. (1) to generate steady-state-polarized emission images of His-tagged LUMP (23 kDa) in a field of nitrilotriacetic acid (NTA)-functionalized agarose beads. The FA values of His-tagged LUMP at the surface of the bead cluster are around 0.310 (Fig. 7b), which is within 14% of the limiting FA value. This result suggests that LUMP molecules are almost completely immobilized when bound to NTA-beads.

An FA image of His-tagged LUMP in solution with agarose beads lacking the NTA-group shows a uniform FA value of 0.185, which corresponds to the unbound LUMP probe. This study highlights an important benefit of using FA images to map the distributions of different molecular forms of the LUMP probe. In particular,

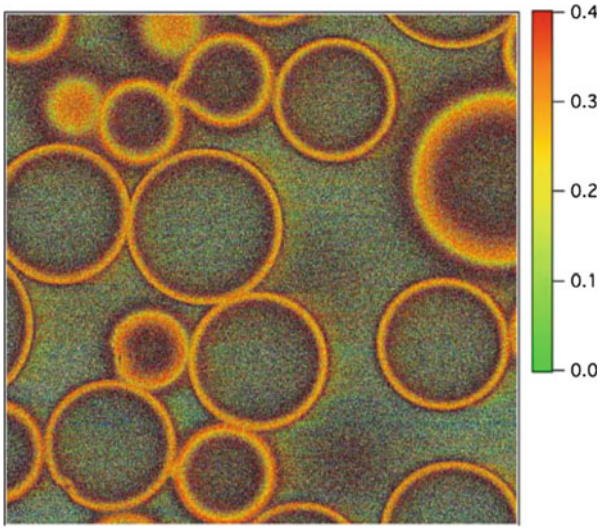

Fig. 7 Fluorescence anisotropy image of His-tagged LUMP on Ni-NTA-agarose beads with an average FA value on the beads of 0.310

since FA values are additive, we can estimate the fraction of LUMP molecules that are free or that interact transiently with the agarose bead in the FA image. Thus, fractional contributions of each species to the total intensity can be calculated according to the relationship ($r_{\text{measured}} = r_1 f_1 + r_2 f_2$), where r_1 is the FA value of LUMP that is transiently immobilized of fractional intensity f_1, r_2 is the FA value of unbound LUMP within the bead of fractional intensity f_2, and $f_1 + f_2 = 1$. This feature of FA imaging is useful as it can be used to quantify the fractions of two populations of the probe in a sample, whereas the intensity image would indicate the presence of a single and uniform population of LUMP molecules. In this particular study, the FA value of His-tagged LUMP outside of the bead is 0.185 (Fig. 7b). The latter value arises from a mixture of free LUMP (0.185) and LUMP molecules that bind transiently and nonspecifically to the bead (0.310) – an FA value that is obtained from a study of NTA-agarose beads. Using the relationships above, the percentages of free and transiently bound LUMP within agarose beads are calculated as 76% and 24%, respectively.

8 Concluding Remarks

To date it has not been possible to use FA methods to quantify target proteins or their complexes in living cells. This limitation arises because small-molecule fluorophores with long-lived excited states are generally unsuitable for studies in living cells, owing to their requirements for UV excitation and associated phototoxicity and the considerable challenge of directing these probes to target proteins in the cell. Genetically encoded fluorescent proteins offer a chance to overcome these limitations, but their large mass and short lifetimes would severely limit the

dynamic range of FA values between the free and bound states of the probe. Interestingly, FA-based measurements of homo-FRET can be used to map changes in the distributions of GFP-fusions with proteins that exist in monomeric or dimeric states [23]. LUMP and related proteins that bind tightly to flavin mononucleotide (Fig. 1e) and combine long-lived excited states with smaller mass than GFP hold great promise in advancing the FA approach to the study of protein complexes in living cells. These imaging studies can be conducted on most commercial confocal fluorescence microscopes with minor modifications. The FA imaging studies on LUMP conducted by our group were carried out using low numerical aperture (NA) objectives that do not result in a "high-NA effect." In any case, our studies have shown that any high-NA effect within polarized images of fluorescence recorded with high-NA objectives can be corrected for quite easily and used to generate high-resolution FA images of a labeled sample [29].

LUMP is unique among genetically encoded fluorescent proteins in being sensitive changes in protein hydrodynamics and molecular volume. While Dansyl has been a popular probe for FA-based determinations of target proteins in vitro, we believe that LUMP, with its similar fluorescence lifetime, holds even greater promise for quantitative FA analysis of target proteins both in vitro and in vivo. This advantage derives in part from the more favorable excitation condition for LUMP compared to Dansyl. Moreover, the quality of a specific FA sensor can be greatly enhanced by encoding large capture sequences onto the C-terminus of LUMP. In principle it should be possible to generate a library of LUMP-based FA sensors with each member harboring a common LUMP probe and a sequence unique to each protein in an organism. LUMP and related genetically encoded FA sensors [12] also offer an attractive alternative to genetically encoded FRET-based sensors for high-throughput screening, quantitative imaging, and analysis of target molecules in biological systems. FA sensors are far easier to design compared to FRET fusion proteins, as they are composed of a single fluorescent probe linked to a specific capture sequence. Moreover, since FA values are additive, and given the large differences in FA values between the free and target-bound states of LUMP-based FA sensors, one can read out the amounts of the free and bound states of a sensor at any pixel in an FA image.

Acknowledgments The work was supported by grants awarded to GM including NIH R21CA191067-01. I would like to thank Prof. Yuling Yan for his help in editing the manuscript and Dr. Alexander Hoepker for his valuable discussions on fluorescence.

References

1. Hudson EN, Weber G (1973) Synthesis and characterization of two fluorescent sulfhydryl reagents. Biochemistry 12(21):4154–4161
2. Jameson DM (2001) The seminal contributions of Gregorio Weber to modern fluorescence spectroscopy, New trends in fluorescence spectroscopy. Springer, Heidelberg, pp 35–58

3. Marriott G, Zechel K, Jovin TM (1988) Spectroscopic and functional characterization of an environmentally sensitive fluorescent actin conjugate. Biochemistry 27(17):6214–6220
4. Sakata T, Yan Y, Marriott G (2005) Family of site-selective molecular optical switches. J Org Chem 70(6):2009–2013
5. Marriott G, Jovin TM, Yan-Marriott Y (1994) Synthesis and spectroscopic characterization of 1-bromo-(4-bromoacetyl) naphthalene. A thiol-reactive phosphorescent probe. Anal Chem 66 (9):1490–1494
6. Weber G (1952) Polarization of the fluorescence of macromolecules. I. Theory and experimental method. Biochem J 51(2):145
7. Weber G (1952) Polarization of the fluorescence of macromolecules. II. Fluorescent conjugates of ovalbumin and bovine serum albumin. Biochem J 51(2):155
8. Hartley B (2004) The First Floor, Department of Biochemistry, University of Cambridge (1952–58). IUBMB Life 56(7):437–439
9. Richmond V, Hartley BS (1959) A two-dimensional system for the separation of amino acids and peptides on paper. Nature 184:1869–1870
10. Hartley BS, Massey V (1956) The active centre of chymotrypsin: I. Labelling with a fluorescent dye. Biochim Biophys Acta 21(1):58–70
11. Jameson DM, Ross JA (2010) Fluorescence polarization/anisotropy in diagnostics and imaging. Chem Rev 110(5):2685–2708
12. Hoepker AC, Wang A, Le Marois A, Suhling K, Yan Y, Marriott G (2015) Genetically encoded sensors of protein hydrodynamics and molecular proximity. Proc Natl Acad Sci 112 (20):E2569–E2574
13. Chen RF (1967) Fluorescence of dansyl amino acids in organic solvents and protein solutions. Arch Biochem Biophys 120(3):609–620
14. Herron JN, Voss EW (1981) Characterization of fluorescent 2-dimethylaminonaphthalene-5-sulfonyl-immunoglobulin G conjugates for application in fluorescence polarization studies. J Biochem Biophys Methods 5(1):1–17
15. Hoepker A, Yan Y, Marriott G (2015) Genetically-encoded sensors of protein hydrodynamics. Oncotarget 6(19):16808
16. Tsao TC, Bailey K (1953) Aspects of polymerization in proteins of the muscle fibril. Discuss Faraday Soc 13:145–151
17. Tsao TC (1953) Fragmentation of the myosin molecule. Biochim Biophys Acta 11:368–382
18. Tsao TC (1953) The molecular dimensions and the monomer-dimer transformation of actin. Biochim Biophys Acta 11:227–235
19. Knopp J, Weber G (1967) Fluorescence depolarization measurements on pyrene butyric-bovine serum albumin conjugates. J Biol Chem 242(6):1353–1354
20. Shaner NC, Steinbach PA, Tsien RY (2005) A guide to choosing fluorescent proteins. Nat Methods 2(12):905–909
21. Suhling K, Siegel J, Lanigan PM, Lévêque-Fort S, Webb SE, Phillips D, Davis DM, French PM (2004) Time-resolved fluorescence anisotropy imaging applied to live cells. Opt Lett 29 (6):584–586
22. Yan Y, Marriott G (2003) Analysis of protein interactions using fluorescence technologies. Curr Opin Chem Biol 7(5):635–640
23. Gautier I, Tramier M, Durieux C, Coppey J, Pansu RB, Nicolas J-C, Kemnitz K, Coppey-Moisan M (2001) Homo-FRET microscopy in living cells to measure monomer-dimer transition of GFP-tagged proteins. Biophys J 80(6):3000–3008
24. Volkmer A, Subramaniam V, Birch DJS, Jovin TM (2000) One- and two-photon excited fluorescence lifetimes and anisotropy decays of green fluorescent proteins. Biophys J 78:1589–1598
25. Chatwell Y et al (2008) Structure of lumazine protein, an optical transponder of luminescent bacteria. J Mol Biol 382:44–55
26. Lee J, O'Kane DJ, Visser AJWG (1985) Spectral properties and function of two lumazine proteins from photobacterium. Biochemistry 24:1476–1483

27. Sato Y et al (2010) Crystal structures of the lumazine protein from Photobacterium kishitanii in complexes with the authentic chromophore, 6,7-dimethyl- 8-(1'-D-ribityl) lumazine, and its analogues, riboflavin and flavin mononucleotide, at high resolution. J Bacteriol 192:127–133
28. Mott HR et al (1999) Structure of the small G protein Cdc42 bound to the GTPase-binding domain of ACK. Nature 399:384–388
29. Yan Y, Marriott G (2003) Fluorescence resonance energy transfer imaging microscopy and fluorescence polarization imaging microscopy. Methods Enzymol 360:561–580

Spatiotemporal Fluorescence Correlation Spectroscopy of Inert Tracers: A Journey Within Cells, One Molecule at a Time

Francesco Cardarelli and Enrico Gratton

Abstract The fundamental unit of biology is unarguably the cell. Thus, as we move forward in our understanding of the processes occurring in the cell, it is crucial to reflect on how much of the cell biophysics remains unexplained or unknown. A ubiquitous observation in cell biology is that the translational motion of molecules within the intracellular environment is strongly suppressed as compared to that in dilute solutions. By contrast, molecular rotation is not affected by the same environment, indicating that the close proximity of the molecule must be aqueous. Theoretical models provide explanations for this apparent discrepancy pointing to the presence of macromolecular intracellular crowding, but with expectations that depend on the nanoscale organization assigned to crowding agents. A satisfactory experimental discrimination between possible scenarios has remained elusive due to the lack of techniques to explore molecular diffusion at the appropriate spatiotemporal scale in the 3D-intracellular environment. Here we discuss our recent experimental evidences for molecular diffusion in crowded biological media. By using monomeric GFP as a fluorescent tracer, and spatiotemporal fluorescence correlation spectroscopy (FCS) as main analytical tool, we reconstruct an imaginary journey, one molecule at a time, across intracellular compartments, such as cytoplasm and nucleoplasm, as well as within subcellular dynamic nanostructures, such as the nuclear pore complex. Results in cells are complemented by in vitro experiments where a variety of model systems mimic physiological crowding conditions. During this journey, Gregorio Weber intuitions on the nature of the cell protoplasm (see below) and on the intrinsic link between

F. Cardarelli (✉)
Center for Nanotechnology Innovation @NEST, Istituto Italiano di Tecnologia, Piazza San Silvestro 12, 56127 Pisa, Italy
e-mail: francesco.cardarelli@iit.it

E. Gratton
Laboratory for Fluorescence Dynamics, Department of Biomedical Engineering, University of California, Irvine, CA 92697, USA

D.M. Jameson (ed.), *Perspectives on Fluorescence: A Tribute to Gregorio Weber*,
Springer Ser Fluoresc (2016) 17: 287–310, DOI 10.1007/4243_2016_6,

the *spatial* and *temporal* scales of diffusion processes both inspired our measurements and guided data interpretation. We do believe that the experimental observations on molecular diffusion collected in the interior of cells might influence the way biochemical reactions take place, with possible significant contributions to our understanding of crucial, still obscure phenomena, e.g., the biological benefit of anomalous transport, the regulation of protein folding/unfolding, intracellular signaling, target-search processes, and bimolecular reactions kinetics.

Keywords Chromatin • Diffusion • Fluorescence correlation spectroscopy • GFP • Gregorio Weber • Live cell • Nuclear pore complex

Contents

> There are these two young fish swimming along, and they happen to meet an older fish swimming the other way, who nods at them and says, "Morning, boys, how's the water?" And the two young fish swim on for a bit, and then eventually one of them looks over at the other and goes, "What the hell is water?"—(David Foster Wallace, This is water, 2009)

> Both the microscopic and macroscopic viscosity of the protoplasm are of importance; the first in relation to diffusion processes and the second in relation to the organization of the cells—(Gregorio Weber, PhD Thesis)

We often mark the progress in human science and knowledge by improvements in imaging, i.e., improvements in our ability to look at the world. The very first Nobel Prize (in physics, 1901) was an imaging prize, awarded to Wilhelm Rontgen for his discovery of X-rays and their astonishing ability to allow the noninvasive viewing of the human skeleton. Over the years several other imaging techniques and their developers have been honored by the Nobel Foundation, up to the last Nobel Prize in Chemistry, jointly awarded to E. Betzig, S.W. Hell, and W.E. Moerner "*for the development of super-resolved fluorescence microscopy*," i.e., for pushing the potentialities of optical microscopy to the nanolevel. The underlying principle is that "*the more we can see*, *the more we can investigate*," as reminded us by another Nobel laureate, Martin Chalfie, during his dissertation on the discovery of the green fluorescent protein (GFP) in 2008 [1]. Unfortunately, this is not always a successful process. The immediate point of the fish story reported above, in fact, is that the most obvious, ubiquitous, and important realities are often the ones that are the hardest to see and, consequently, to understand. This reasoning

applies even to the fundamental unit of biology, the cell. The biochemistry of life is orchestrated by the concerted action of molecules at the subcellular level but the imaging and analytical tools currently at our disposal to investigate such fundamental processes in live samples are not always entirely adequate, i.e., they afford a valuable description of the process, but they do not lead to a satisfactory comprehension of it. In this picture, current efforts in the development of advanced biophysical tools are tentatively filling the gap between "biology" and "physics." For instance, one of the natural, yet almost inaccessible, conditions of living matter is that of nanoscopic molecules (proteins, ions, nucleic acids, etc.) rapidly moving within the intracellular milieu. Here, molecules are part of a complex 3D environment that we typically depict as made of *water* together with a mixture of both diffusing/colliding crowding agents and almost immobile structures/compartments. Well, the presence of *water* as part of the intracellular milieu is among the most obvious facts in cell biology but, as the fish story teaches us, surprisingly one of the hardest to see! Just at the turn of the millennium, a bunch of pioneering scientific contributions was able to highlight such a crucial paradox. In fact, it was demonstrated that small inert molecules exert rotational diffusion within live cells almost as they would do in dilute solutions, i.e., water [2, 3]. By contrast, however, their translational diffusion is invariably suppressed compared to that in dilute solutions, thus suggesting an increased (apparent) viscosity of the intracellular milieu as compared to water [2, 3]. A satisfactory explanation of this (apparent) discrepancy remains an open challenge of current research in cell biology. The intense efforts made by the scientific community in the last decade pointed out that the entire field is experiencing a kind of "technical impasse." In fact, several theoretical models do provide explanations for suppressed translational motion, pointing to the presence of macromolecular intracellular crowding (for an exhaustive review see Ref. [4]). However, their predictions drastically depend on the nanoscale organization assumed for crowding agents. On the other hand, experimental discrimination between existing theories in the actual intracellular environment remains elusive owing to the lack of techniques capable of probing macromolecular crowding at the required spatiotemporal scale. We approached this complex area as a team of physicists, chemists, and biologists motivated by our interest on the regulation of molecular diffusion within cells. Along this way, Gregorio Weber's intuition on the nature of the cellular protoplasm, reported in a brief (but enlightening) note in the last chapter of his PhD thesis, besides being truly inspirational, represented for us a constant reminder not to forget that what we are going to see within cells inevitably depends on the characteristic spatial and temporal scales of our investigations. Also, we kept clear in mind Weber's intuition that proteins must be dynamic in nature in order to properly exert their complex function within cells, in contrast to views of the time describing proteins as rigid/static building blocks, or "rocks" (as from X-ray crystallography studies). Our imaginary journey within cells is conducted by using the Green Fluorescent Protein (GFP) as a model of inert, nanoscopic probe of the intracellular environment. Results are collected into three separate sections, encompassing what we observed in the cell cytoplasm, cell

nucleus, and across the tiny channel that puts them into communication, the nuclear pore complex (NPC).

1 GFP Diffusion Within the Cell Cytoplasm

Historically, as mentioned above, credit must be given to the pioneering works by Alan Verkman and collaborators on the diffusion of GFP in the cytoplasm and nucleus of live cells [2, 3]. The main purpose of their studies was to evaluate the suitability of GFP as a probe for rapid solute diffusion in living cells and to measure the apparent viscosity of cell cytoplasm/nucleoplasm from the rates of GFP rotational and translational diffusion. Of note, in the cell cytoplasm, they found a GFP rotational correlation time (measured through anisotropy decay) of about 36 ns, only 1.5-fold slower than that in non-viscous saline solution. There was no evidence for GFP binding to intracellular structures, which would slow apparent GFP rotation. The rapid GFP rotational rate in cytoplasm was deemed consistent with the notion that particle rotation is relatively unhindered when particle size is smaller than the characteristic spacing between obstacles. The rotational data per se would suggest an intracellular viscosity close to that of water. By contrast, however, this picture was not confirmed when GFP translational motion was probed. By using fluorescence recovery after photobleaching (FRAP), Verkman and co-workers found that GFP translational diffusion in cytosol is reduced by 3.2-fold compared to that in water, a behavior similar to that found for dextrans of comparable size. Also, the further slowing of GFP translation in shrunken cells and the acceleration of GFP translation in swollen cells were interpreted as consistent with the barrier properties of intracellular obstacles [2, 3]. The apparent discrepancy between rotational and translational data must be linked to the different temporal and spatial scales probed in the two approaches. Anisotropy decay measurements, in fact, probe the nanoscale (both in terms of time and space), while FRAP-based assays, although potentially fast in terms of temporal resolution, are inherently limited in spatial resolution by the detection spot of the confocal microscope and therefore yield an average over the details of molecular diffusion below 200 nm in radial and 600 nm in axial distance [5, 6]. Of note, Single Particle Tracking (SPT) methods can in principle provide an answer below the diffraction limit but tracking small molecules in 3D is technically challenged by their rapid diffusion [7]. On the other hand, classical single-point Fluorescence Correlation Spectroscopy (spFCS) [8] measurements are again spatially limited by the detection spot of the confocal microscope. Several variants of FCS have been proposed to overcome these limitations. For instance, it was demonstrated that molecular diffusion laws can be recovered by fluctuation analysis at various spatial scales by increasing the laser spot size [9–11]. Based on this approach, however, only inferences can be drawn about molecular dynamic behavior below the diffraction limit. A new avenue was opened by spatially modulating the fluorescence emission with stimulated emission depletion (STED) methods [12]. This technology, in fact, allows the direct

observation of biological phenomena with sub-diffraction spatial resolution and with the high temporal resolution needed to track molecules in a 3D environment. STED-based lateral resolutions of ~40 nm allowed probing the nanoscale spatiotemporal dynamics of lipids and proteins in live cell membranes [13, 14]. Although theoretically attainable, however, effective STED-based nanoscopy of biomolecules in the 3D intracellular environment has yet to be tested by experiments. Finally, it is worth mentioning that Shusterman et al. [15] derived an expression of the single-point FCS correlation function that is directly related to the molecular Mean Squared Displacement (MSD). Based on this, the MSD of DNA polymers in a homogeneous solution has been successfully measured well below the diffraction limit. Yet, in a heterogeneous environment such as the intracellular medium, *spatial* sampling is indispensable in addition to *temporal* sampling in order to understand if the diffusion properties measured locally are representative of the whole environment [16]. Motivated by this lack of experimental/analytical strategies, we developed a straightforward implementation of fluorescence fluctuation analysis at variable timescales to probe the average diffusion properties of protein-sized molecules in the 3D cellular environment with an unprecedented temporal resolution and with no a priori assumptions on their diffusion properties (Fig. 1) [17]. We started from multiple scan-speed image correlation spectroscopy (msICS) of fluorescence fluctuations [18]. However, instead of using the different pixel-dwell/line-scan times to generate a temporal autocorrelation function for every pixel shift, we extract the characteristic molecular mean square displacement for each scan speed (hereafter named *i*MSD). Each scan speed is used as a filter to select the characteristic temporal scale of molecular displacements that significantly contributes to the measured correlation function (Fig. 1a). This approach covers a hitherto unexplored dynamic range, as determined by available pixel-dwell times, from 0.5 μs to several milliseconds, giving access to average molecular displacements much smaller than the diffraction limit and thus partially filling the gap in spatiotemporal resolution between rotational and translational approaches. As a consequence, at high scan speed, the particle image is only slightly deformed by the scan process, i.e., it almost coincides with the autocorrelation of the instrumental point spread function (PSF) (Fig. 1b). On the contrary, for decreasing scanning speeds the apparent particle image is deformed due to molecular movement (Fig. 1b), i.e., the spatial correlation function becomes much larger than the PSF. We use a Gaussian interpolation of experimental correlation functions to obtain an estimate of the width of the particle-displacements distribution (Equation in Fig. 1b). This allows retrieving the particle mean square displacement directly from the raster-scan images (Fig. 1c). Following the obvious preliminary controls on solutions (Fig. 1d), we investigated the motion of monomeric GFP transiently transfected into living cells under physiological conditions (Fig. 2). To start, we targeted arbitrary μm-sized areas in the cell cytoplasm and performed sequential raster scans at tunable timescales, as previously described. GFP average displacements at different timescales are reported (black dots in Fig. 2) and compared to those in solution (dashed green line). Remarkably, the hitherto unexplored timescale below 2×10^{-5} s reveals the unobstructed motion of GFP at the nanoscale in the

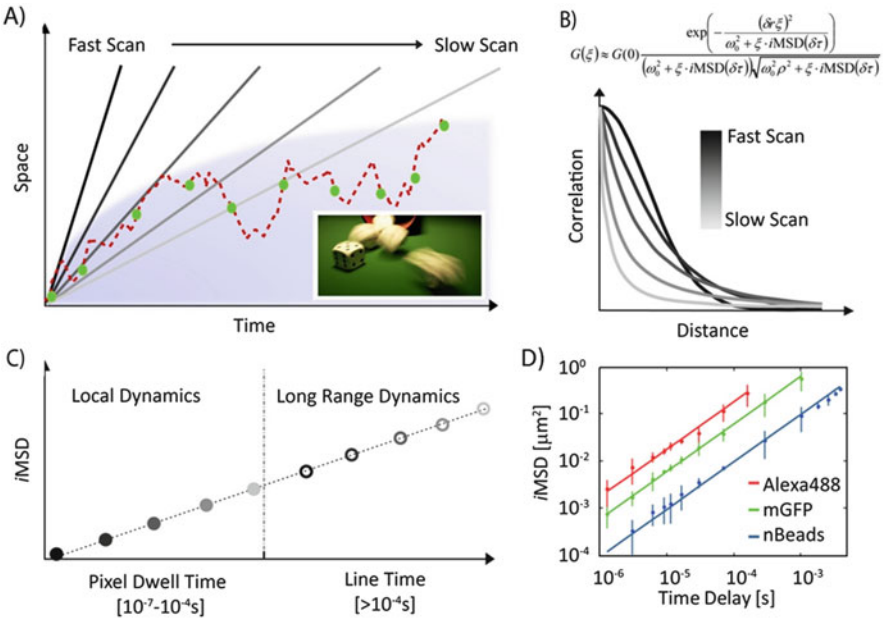

Fig. 1 *i*MSD analysis of GFP motion in 3D by raster-scan imaging at tunable timescales. (**a**) Pictured experiment: "fluorescent" molecules freely diffuse distributing in space and time. Scanning the samples with decreasing speed allows measuring the average particle displacements over a wide spatiotemporal scale. *Inset*: the "image" of the particle that can be retrieved is reminiscent of what happens by eye if we look at objects moving at different speeds. (**b**) When the scanning is faster than the particle dynamics the particle image corresponds to the auto-convolution of the instrumental point spread function, that is well approximated by a Gaussian profile. On the other hand, when scanning speed decreases, the particle starts to move significantly, i.e., the correlation function squeezes in space becoming much larger than the PSF. The Equation reported describes this deformation effect as a function of the particle average displacement, and allows recovering the *i*MSD as a function of time delay. (**c**) Schematic representation of the *i*MSD for a molecule diffusing in 3D. Each point is retrieved from the analysis of an image series recorded at a certain speed. (**d**) Experimental *i*MSD values at the different timescales for differently sized molecules in dilute solution at 37°C. Monomeric GFP ($N = 7$ measurements, *green dots*) shows a linear behavior in time, as expected for Brownian motion: fit by a free-diffusion model (Eq. 13 in Supporting Information) yields $D_w = 134 \pm 4$ μm^2/s ($H_r = 2.5$ nm); Alexa488 ($D_w = 428 \pm 15$ μm^2/s, $H_r = 0.75$ nm, $N = 7$ measurements; *red dots*) and 30 nm-diameter fluorescent beads ($D_w = 22 \pm 0.5$ μm^2/s, $H_r = 15$ nm, $N = 7$ measurements; *blue dots*) are acquired under the same conditions

cytoplasm of a living cell (blue square in Fig. 2). In detail, *i*MSD values in the range from 25 to 100 nm match those measured in dilute solutions on the same timescale. This accordance suggests that 3D Brownian motion of an inert globular protein is possible on this spatiotemporal scale in the cell cytoplasm. Fit to the free-diffusion model for $t < 2 \times 10^{-5}$ s yields a GFP diffusion coefficient in cell (D_0) of 126 ± 3 μm^2/s at 37°C, thus implying that cytoplasmic viscosity at this scale (hereafter referred to as "*nano*viscosity" to recall Weber's "*micro*viscosity") is

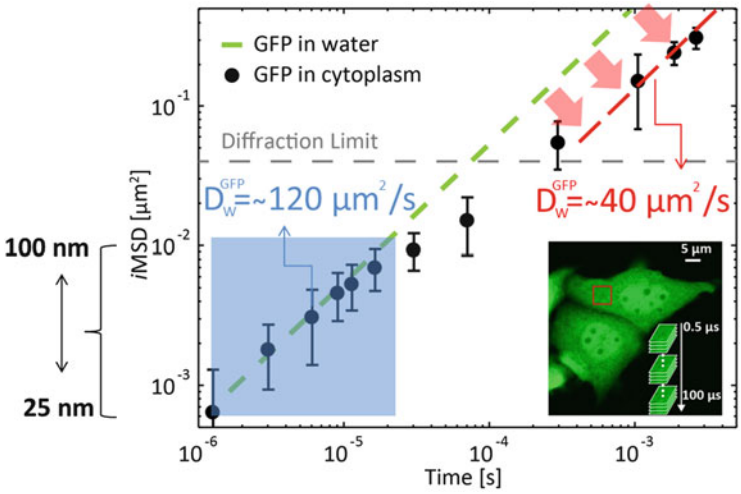

Fig. 2 *i*MSD analysis of GFP diffusing in the cell cytoplasm. *Inset*: GFP is transiently transfected into living CHO cells and analyzed under physiological conditions. Arbitrary μm-sized areas in the cell cytoplasm are imaged sequentially at tunable timescales. The complete *i*MSD of GFP in cytoplasm is reported, as average of $N = 3$ experiments, $n = 24$ cells (*black dots*), and compared to the *i*MSD in solution (*dashed green line*). The local dynamics can be well described by free diffusion ($D_0 = 126 \pm 3$ μm^2/s, $\chi^2 = 0.42$, $p < 0.01$). However, this dynamics is not representative for the whole *i*MSD ($\chi^2 \gg 25$, $p > 0.995$). In fact, three different diffusive regimes can be easily described in the cell cytoplasm: free diffusion at a timescale from 1×10^{-6} to 10^{-5} s, subdiffusion with $\alpha = 0.5 \pm 0.2$ at an intermediate scale (10^{-5}-to-10^{-4} s), and reduced (but again free) diffusion above 10^{-4} s ($D_{inf} = 37 \pm 2$ μm^2/s)

almost equal to that of dilute solutions, and also matching for the first time what concluded from local measurements of protein rotation by time-resolved fluorescence anisotropy [2, 3]. On the other hand, the *i*MSD plot above 2×10^{-5} s shows a clear deviation from the Brownian regime. This deviation implies reduced protein translational motion, again matching what is typically reported in the literature thus far on similar timescales [4]. Well above the diffraction limit we observe an almost threefold suppressed (long-range) GFP motion as compared to dilute solutions (red arrows in Fig. 2), perfectly in keeping with Verkman's observations by FRAP [3, 19]. This in turn confirms the usual appearance of an apparent increased viscosity in the cytoplasm (hereafter referred to as "*micro*viscosity," which recalls Weber's "*macro*viscosity") compared to the dilute solution, but limits its significance to length scales above at least 100 nm. It is worth noting that the overall phenomenology observed here in the cell cytoplasm was already predicted in silico by Saxton M.J. for the diffusion of a particle in presence of obstacles [20] and experimentally described for lipids and proteins diffusing on the plasma membrane [21–23]. In particular, we argue that the characteristic crossover spatial scale between unobstructed and suppressed motion in the cell interior (~100 nm) is almost coincident to the typical length of cytoskeleton-induced protein confinement

measured on the plasma membrane (~150 nm for Transferrin Receptor, TfR [22, 24]), in turn suggesting a possible universal spatial scale at which cells regulate dynamic processes. The observation of unobstructed Brownian-like motion in the cell cytoplasm prompted us to propose a model in which the movement of GFP is regulated by the excluded-volume effect of immobile structures, rather than by freely diffusing solutes. To verify this hypothesis, we measured GFP motion in two model systems that mimic the macromolecular crowding effects of homogeneously diffusing solutes and of excluded volume (Fig. 3). The former system was implemented with a crowded aqueous solution of bovine serum albumin (Fig. 3a). The *i*MSD plot unequivocally depicts GFP hindered motion over the entire spatiotemporal scale observed, with a mobility that decreases with increasing BSA volume fraction (up to 20%) but does not depend on the timescale of the measurement, in keeping with recent quasi-elastic neutron backscattering measurements [25]. For the excluded-volume case, the model system consisted of nanostructured polymeric beads (Fig. 3b). Here GFP molecules move in a heterogeneous environment where crowding is represented by the excluded-volume effect imposed by the bead structural organization (Fig. 3b, inset). Notably, the *i*MSD plot in this case shows GFP short-range unobstructed motion as in dilute solution (i.e., Brownian), followed by suppressed motion at later times (Fig. 3b), in analogy to what we observed in cells. In the polymeric beads samples the observed phenomenology must be interpreted as the effect of immobile structures acting as barriers to molecular motion. In this regard, it is worth mentioning that Novak et al. demonstrated by simulations that cytoskeleton filaments are unlikely to constitute diffusion barriers sufficient to suppress diffusion of molecules in the cytoplasm (they would need to fill ~90% of space!) while, by contrast, internal membranes (e.g., the ER sheets, mitochondria, vesicles, Golgi apparatus, etc.) appear to be a more likely candidates [26]. In keeping with this idea, selective disruption of the microtubules network by treatment with 10 μM nocodazole did not significantly alter GFP behavior in the cytoplasm (data not shown, see Ref. [17] for more details).

2 Probing Intracellular Structural Heterogeneity: Is the Cell Nucleus Nanostructure Different from That of Cytoplasm?

The dominant mode of motion of inert molecules throughout the nucleus is, as a matter of fact, diffusion. How this motion is directed and regulated, however, has several significant physiological implications. To start, in analogy with the cytoplasm, we used GFP as an inert tracer and spatiotemporal fluorescence correlation spectroscopy at tunable timescales as a means to derive diffusion parameters (Fig. 4). Quite surprisingly, the *i*MSD values measured within intranuclear environment yielded a very different trend with respect to the cytoplasm. In particular,

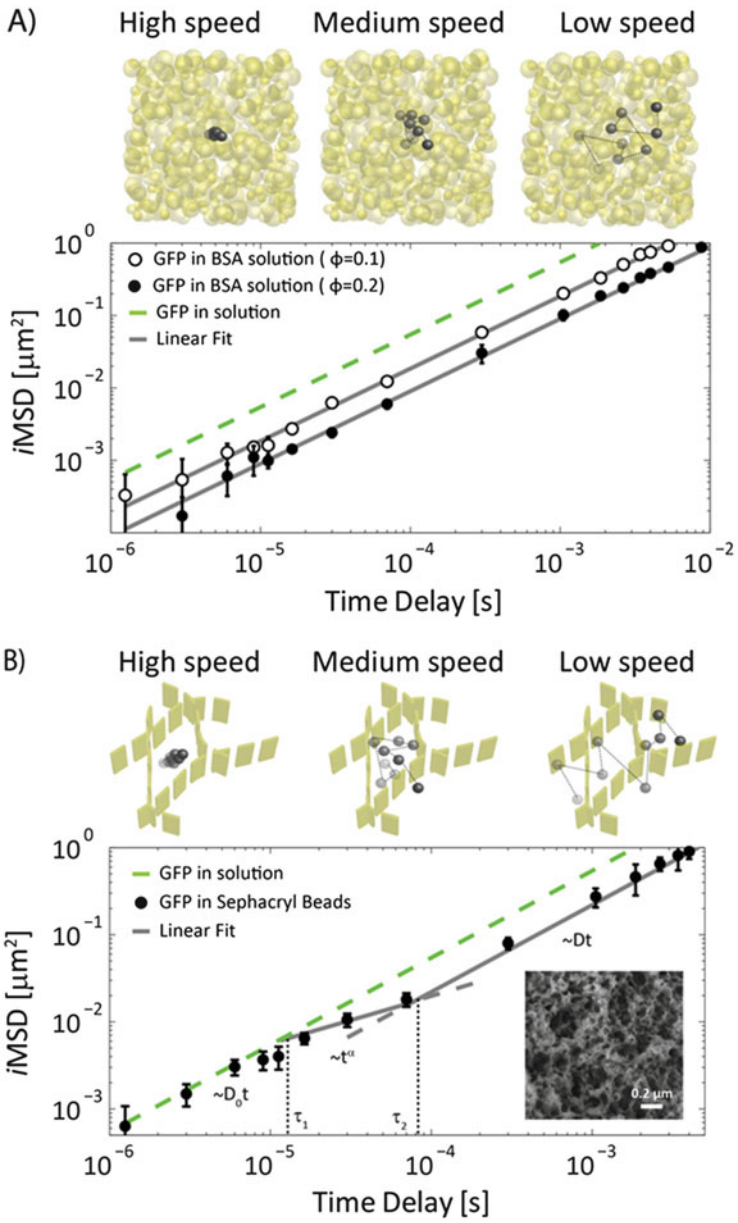

Fig. 3 *In cuvette* validation of the protein dynamics model. (**a**) *Upper panel*: pictured GFP dynamics in the presence of colliding crowders. *Lower panel*: experimental *i*MSD of GFP diffusing in BSA solution with different excluded volumes (φ). For both tested excluded volumes the *i*MSD is not distinguishable from free diffusion. Also, molecular diffusivity decreases at increasing excluded volumes (e.g., for $\varphi = 0.1$, $D = 46 \pm 2$ μm^2/s, for $\varphi = 0.2$, $D = 24 \pm 2$ μm^2/s). (**b**) *Upper panel*: pictured GFP dynamics in the presence of spatially organized obstacles. Fast scanning allows measuring GFP dynamics in the free space between obstacles. Decreasing the

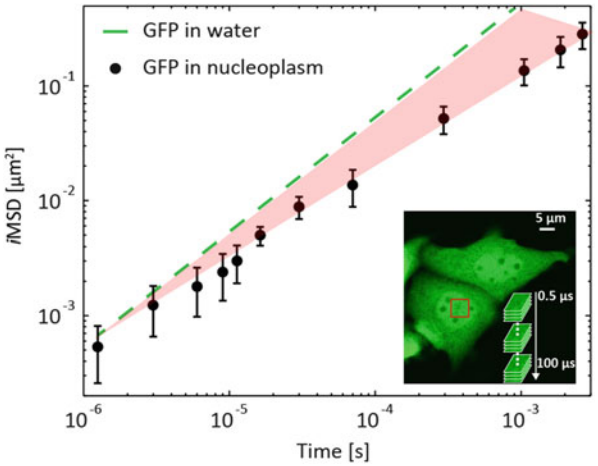

Fig. 4 *i*MSD analysis of GFP diffusing in the cell nucleus. GFP is transiently transfected into living CHO cells and analyzed under physiological conditions (*inset*). Arbitrary μm-sized areas in the cell nucleus are imaged sequentially at tunable timescales. The *i*MSD values at the different timescales in the nucleoplasm are reported in a double-logarithmic representation, as average of $N = 3$ experiments, $n = 22$ cells (*black dots*), and compared to the *i*MSD in solution (*dashed line*, taken from Fig. 1). The GFP motion in this compartment is never coincident with that in dilute solution. Conversely, it is suppressed over the entire spatiotemporal scale observed. Also, no clear crossover spatial scale is visible over time

GFP intranuclear motion is never coincident with that in a dilute solution, and no clear crossover timescale is visible throughout the considered spatiotemporal scale. This in turn suggests that excluded-volume effects on protein motion weight much less in the nucleoplasm (i.e., a structurally different compartment, for instance, devoid of membranes) than in the cytoplasm, in keeping with previous reports [27]. The persistence of "anomalous" GFP intranuclear diffusion up to the microsecond timescale does not directly contradict rotational diffusion data and concomitantly well agrees with the GFP reduced translational motion typically observed by diffraction-limited measurements (e.g., single-point FCS or FRAP) [2, 3, 28]. At the same time, the virtual absence of GFP unobstructed Brownian motion up to the

Fig. 3 (continued) scanning speed allows measuring the effect of boundaries on GFP dynamics. *Lower panel*: the complete *i*MSD of GFP in Sephacryl beads is reported, as average of $N = 5$ beads (*black dots*), and compared to the *i*MSD in solution outside the beads (*dashed green line*). The local dynamics can be well described by free diffusion ($D_0 = 110 \pm 5$ μm^2/s, $\chi^2 = 0.8$, $p < 0.025$). However, this dynamics is not representative for the whole *i*MSD ($\chi^2 > 25$, $p > 0.995$). Analogously to cells, three different diffusive regimes can be described in the bead interior: free diffusion at a timescale from 10^{-6} to 2×10^{-5} s, subdiffusion from 2×10^{-5} to 10^{-4} s, and reduced free diffusion above 10^{-5} s ($D_{inf} = 62 \pm 2$ μm^2/s). The two crossover timescales linking unobstructed to reduced GFP diffusivity in the Sephacryl beads are labeled as τ_1 and τ_2. The *inset* shows a representative SEM image of a Sephacryl beads in which many submicrometer cavities are visible

level of few tens of nanometers within the nucleus suggests that a further level of regulation imparted by the intranuclear architecture on GFP motion must be active. To get further insight onto the regulation of GFP diffusion within the nucleus we used the pair correlation function (pCF) approach. pCF measures the time a particle takes to go from one location to another by correlating the intensity fluctuations at specific points on a grid independently of how many particles are in the imaging field [29, 30]. In such a way, this method provides single-molecule sensitivity in the presence of many molecules, and high (sub-micron) spatial resolution in the description of the spatial heterogeneity of the environment in terms of barriers and/or obstacles to diffusion (Fig. 5a). For instance, changes in chromatin organization can be detected if the diffusive behavior of an inert tracer like GFP is analyzed by pair correlation functions. If the chromatin is impermeable, then the molecular diffusion will appear as disconnected at the boundary of the barrier. If, conversely, the structured network is permeable, then molecular diffusion will be continuous and the delay time at the boundary is indicative of the local compaction status (Fig. 5b). In light of this, monomeric GFP transiently transfected in live cells was used as an inert tracer, in analogy with previous measurements, while Hoechst was used to label chromatin. We were able to concomitantly perform ACF and pCF analysis on the line scans acquired: this kind of experiment was conducted during the different phases of the cell cycle [31–33] (interphase and mitosis are shown here, see Fig. 6). The ACF analysis in interphase nuclei (data not shown, see Ref. [31] for details), which is local, well agrees with the observation by Dross et al. that the local diffusion coefficient of EGFP throughout the nucleus is independent of DNA density [16, 34]. The ACF carpet analysis, however, does not provide information about the translational diffusion of GFP between two different locations with respect to the DNA environment. On the contrary, by cross-correlating pairs of points in the nucleus, we are able to see that there is a dependence of the diffusive route taken by GFP on DNA density, in agreement with the observation by Wachsmuth et al. that GFP diffusion in the nucleus can be locally impeded by cellular components [34]. pCF analysis of GFP diffusion between different DNA environments in interphase nuclei shows migration paths which allow for communication, but also barriers to diffusion resulting in poor or no communication. In more detail, as shown in Fig. 6b, we found the two types of DNA density (high and low) to cause disconnect GFP molecular diffusion throughout the nucleus, where the high density DNA forms a networked channel that allows GFP to diffuse freely throughout, however with restricted ability to traverse the channel barriers to the low DNA density environment. These measurements suggest a model of two virtually disconnect DNA environments (or channels), differentiated by density, that allow continuous molecular diffusion throughout either and restricted movement in between. As comparison, we addressed the impact nuclear architecture has on GFP molecular diffusion within the mitotic nucleus of live cells. The mitotic chromatin is found to allow delayed but continuous molecular flow of GFP in and out of a high chromatin density region, which, by pCF analysis, is shown as a

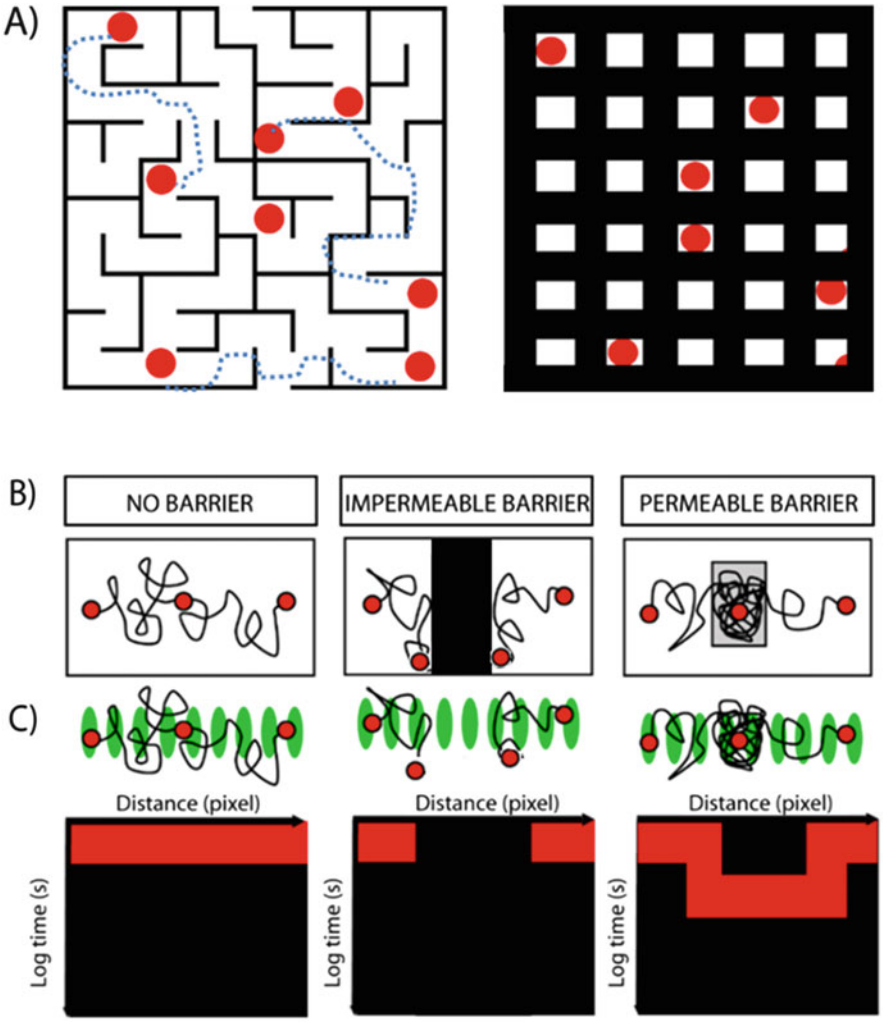

Fig. 5 The connectivity of molecular diffusion is regulated by intracellular architecture. (**a**) The intracellular landscape forms a maze, which molecules must navigate to arrive at a final destination (*left*). In live cells, unfortunately, the topography of this maze is not observed (*right*). We must extract how the intracellular landscape directs molecular flow from the diffusive route the molecules adopt within it. (**b**, **c**) Pair correlation analysis of an inert tracer can reveal the real time changes in intracellular architecture. Changes in chromatin organization can be detected at each pixel along the line scan (*green*) from pair correlation analysis of the *red* molecule diffusion along a line scan that traverses a structured network. If the chromatin is impermeable, then the molecular diffusion is disconnected at the boundary of the barrier. If, conversely, the structured network is permeable, then molecular diffusion is continuous and the delay time at the boundary is indicative of the local compaction status

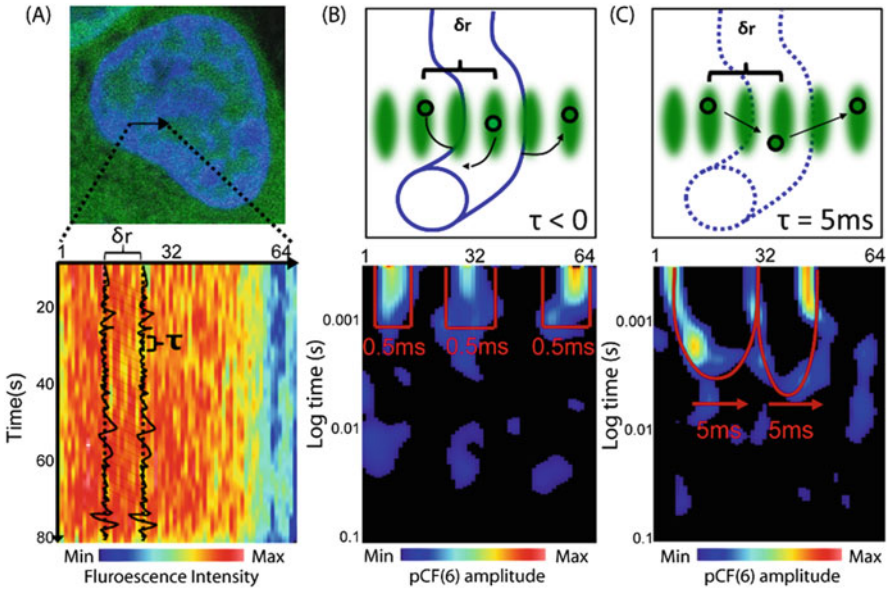

Fig. 6 Pair correlation analysis detects barriers to diffusion. (**a**) Inside the cell nucleus, molecules encounter barriers to diffusion that direct their molecular path around or throughout on a delayed timescale, depending on permeability. (**b**) A confocal line scan acquired across a fluorescent molecule's diffusive route can detect and trace the contours of barriers. (**c**) Pair correlation analysis of the molecule's arrival time along the line reveals the degree of permeability of the barrier (or if impermeable, the lack of communication)

characteristic arc shape that appears upon entry and exit (Fig. 6c). We argue that, in this case, the densely packed mitotic chromatin is acting just as a physical barrier to GFP free intranuclear diffusion. By contrast, if there is an almost complete absence of molecular flow through a region of different DNA density in interphase and yet GFP can be easily detected in both DNA environments, then how did this transit occur? One possible explanation is that the transit through a change in DNA density is statistically a rare event in time and/or space (schematic representation in Fig. 7a), which upon extensive averaging does not appear in the pCF carpet. It was thus decided to increase the probability of detecting this event (which would give rise to a positive cross-correlation) by sequentially averaging smaller time segments of our acquisitions. Notably, occasionally, in discrete blocks of time (typically around 300 ms), a "burst" of GFP molecules can travel across a DNA density barrier (Fig. 7b, c). The confinement in time of the burst also indicates that they do not depend on a fixed potential barrier to diffusion, because this fixed barrier would produce a continuous small flow instead of an intermittent one. Local variation of chromatin compaction, due, for instance, to conformational changes of the DNA, can represent a way to enable communication across regions of different DNA density. The role of DNA as a master template is not new: it was recently proposed, among others, for the regulation of the genetic and molecular flows in

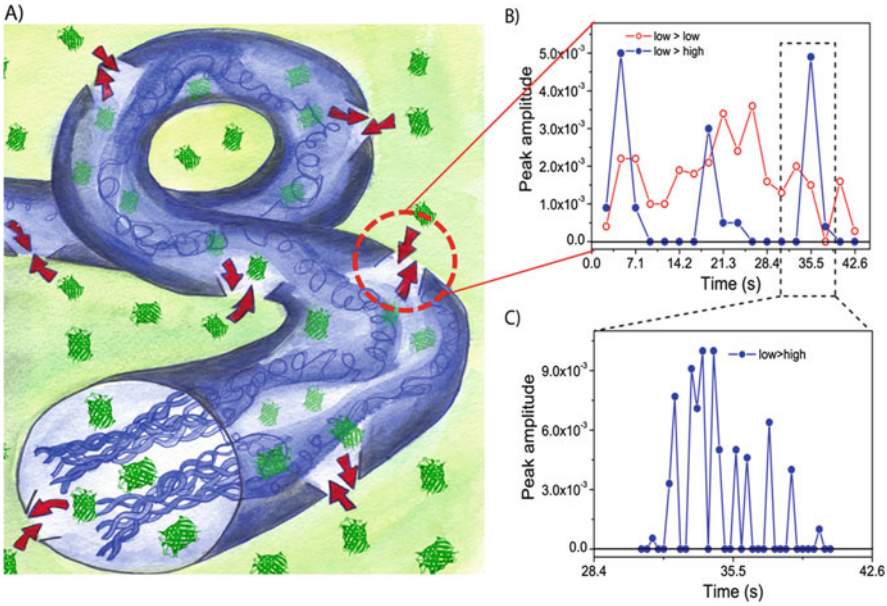

Fig. 7 Model of diffusion within the nucleus. (**a**) Schematic of monomeric GFP (*green*) diffusing throughout the high DNA density networked channel (*blue*) as well as the low DNA density surroundings (*light green*), with intermittent bursts of EGFP traversing the channel barriers (*red arrows*). (**b**) A pCF carpet column with no apparent correlation is here re-analyzed in shorter time fragments (every 5.0×10^3 lines, 2.36 s) in an attempt to detect communication between different DNA density environments. A plot of the amplitude of the pair correlation function derived for each 5.0×10^3 line segment against time (**b**, *upper panel*, *blue dots*). In the instance a time segment gives rise to a negative pCF profile (which corresponds to no communication), we report the amplitude as zero. For comparison, the same analysis is performed for a carpet column that showed positive correlation (**b**, *upper panel*, *red dots*). (**c**) Further temporal analysis of a peak reported in **b** is here carried out every 6.0×10^2 lines (300 ms) to evaluate the temporal nature of the intermittent periods of communication

bacteria [16]. In general, these data speak in favor of a very dynamic behavior of the intracellular landscape directing the diffusion of the inert tracer and provide explanation for the presence of GFP in both DNA environments, yet with no considerable molecular transfer being observed between either. It is worth noting that GFP disconnect bidirectional diffusion through a region of different DNA density could not be detected by an ensemble averaging measurement, such as FRAP, because it contains no spatial information about molecular motion. On the contrary, the pCF approach, by "tracking" single molecules as they travel from a specific location to another, can measure anisotropic diffusion, detect the presence of barriers to diffusion, and produce a map of transport. In conclusion, reported results indicate that chromatin is organized as a networked channel, which directs the diffusion of small molecules throughout and controls communication to the surrounding low DNA density environment.

3 GFP Diffusion Across the Nuclear Pore Complex: Beating the Thermal Noise!

Thus far, the diffusion features of an inert tracer (GFP) were reported and discussed in order to get insight into the mechanisms through which diffusion is regulated in the two major compartments of a cell, i.e., the cytoplasm and the nucleus. The subcellular structure deputed to put nucleus and cytoplasm in communication is the nuclear pore complex (NPC). Measurements of transport through NPCs can potentially provide valuable information on the molecular mechanisms of communication between the nucleus and the cytoplasm [35, 36]. At a first level, the possibility to study these processes in a physiological state in live cells is challenged by the very rapid transport of single molecules through the NPC. To tackle this issue, researchers have developed a variety of camera-based single particle tracking (SPT) approaches which enabled to analyze molecular transit times, trajectories, and interactions between transport receptors and model cargo molecules at the NPC [37, 38]. However, SPT measurements rely on the tracking of bright and isolated particles, and measurements must be repeated many times to provide enough statistics. Furthermore, most SPT experiments require complex experimental procedures for the molecule of interest to be produced, purified, fluorescently labeled, and introduced into the cell (e.g., by electroporation or micro-injection). Consequently, it is unclear whether the correct pore function is preserved under classical SPT experimental conditions. By contrast, the FCS-based pCF approach reported above can in principle provide information on single molecules crossing the pore, in presence of many molecules, with no need to perturb the cell. However, in this kind of measurement, the transit times of GFP-tagged molecules are typically probed over several microns across the nuclear envelope (NE) (i.e., by pCF analysis on a line-scan acquisition), thus without single-pore resolution. In other words, the contribution of many NPCs is averaged together in a single measurement (Fig. 8a) [39]. Also, because the entire NPC can perform local nanometer diffusion within the NE or follow global rearrangements of the cell (Fig. 8b) [40], it is crucial to subtract this motion if the diffusion of the molecules and the overall thermal motion of the NPC have to be distinguished. To overcome these limitations we decided to track the position of the NPC so that only the motion of the molecules relative to the entire structure is effectively measured. This feedback-based fluorescence tracking method (see schematic representation in Fig. 9), previously developed to track a particle in a chromosome [41], compensates for temperature-driven local diffusion of the large unit represented by the NPC. In this reference frame, the NPC will be stationary. The measurement is based on rapid orbiting of a laser beam around the object to be tracked, with a response time of few milliseconds and a location precision in the nanometer range. In other words, we jump onto the reference system of the pore and follow the translocation of molecules with great precision and a time resolution that is faster than the motion of the overall NPC [42, 43]. Because we are only measuring the changes in fluorescence intensity along the orbit with very high time resolution, we can determine the correlations in space

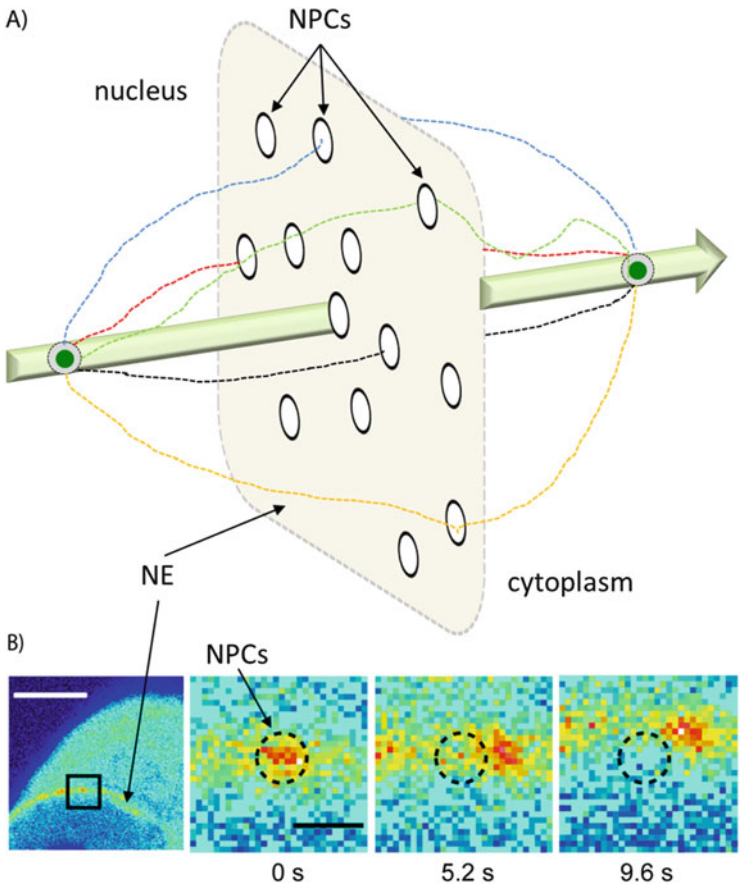

Fig. 8 GFP diffusion within nanoscopic, dynamic, subcellular structures: the need for a new technology. (**a**) Schematic representation of a typical line-scan measurement performed across the nuclear envelope. If cross-correlation between two points of the line is performed in this configuration, all the possible molecular trajectories among the two points (and passing through many NPCs) will be averaged together. (**b**) In addition, single NPCs are constantly moving within the NE, also following rearrangements of the entire envelope

and time of single molecules binding and leaving the NPC. For example, if molecules are leaving one location of the NPC and reappearing in another area of the same NPC, the intensity along the orbit will change in a time- and space-correlated way. Also, we can measure the exact location of the event and the time course of the process. To prove this principle, we show here a two-channel experiment in which we simultaneously assess Kapβ1-GFP active transport and

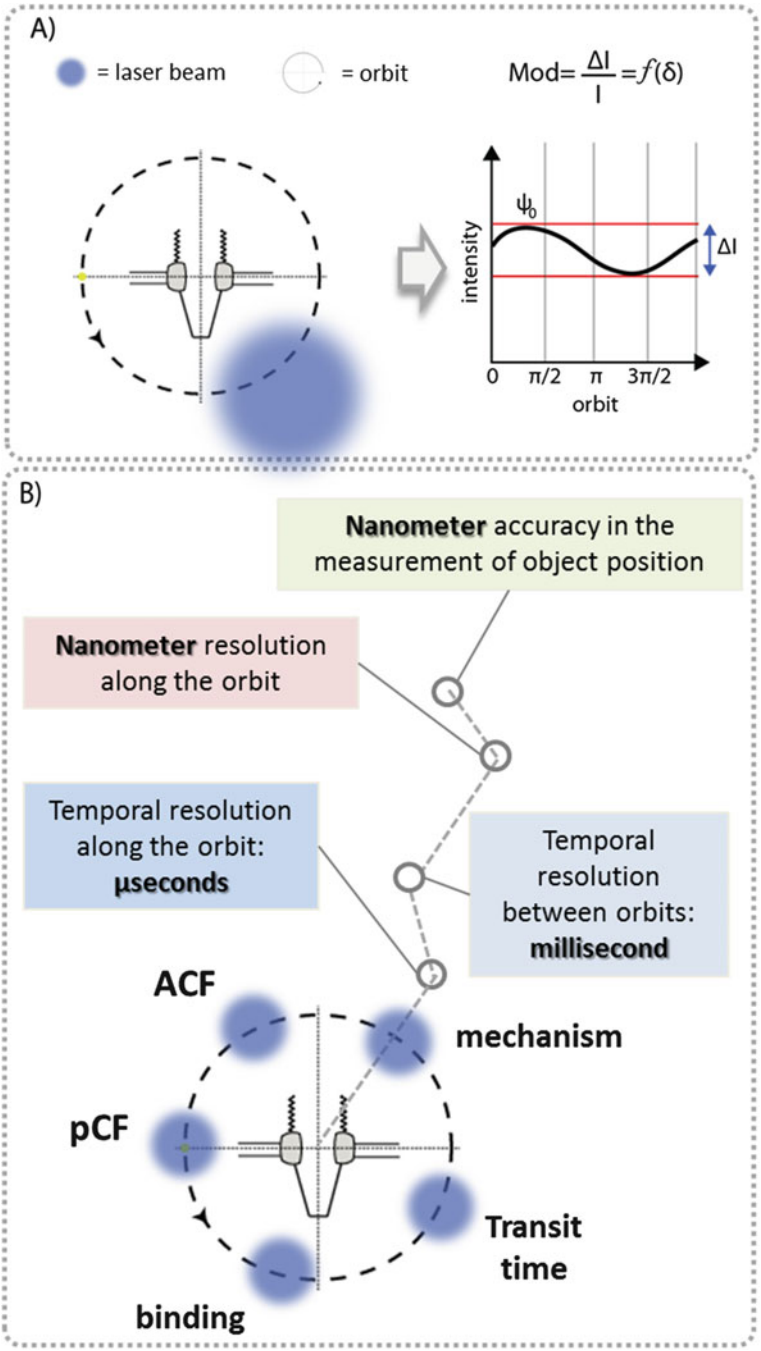

Fig. 9 The orbital-tracking principle. (**a**) Schematic representation of the feedback algorithm that guarantees orbit repositioning around the fluorescent object of interest, the nuclear pore complex

untagged mCherry unbiased diffusion through the pore (Fig. 10). Here the GFP signal is exploited to track the pore position (thanks to the specific accumulation of Kapβ1 on the NPC) while the shuttling of untagged mCherry is concomitantly recorded within the same reference system. Of note, the autocorrelation function analysis shows a "hump effect" for Kapβ1-GFP, i.e., the presence of representative correlation time for the transport of this protein across the pore (Fig. 10b, c). By contrast, the same ACF analysis reveals the absence of any specific time of correlation at the pore for untagged mCherry, as expected for a protein that is not expected to specifically interact with the pore structure (Fig. 10b, c). On this basis, we could argue that the hump effect measured through the ACF may reflect specific Kapβ1 activity at the pore. Consistent with this hypothesis, if an orbit much larger than the NPC size (e.g., with a radius of ∼1 μm) is scanned around the pore, the hump effect vanishes from the first channel, and only Kapβ1-GFP isotropic diffusion can be measured (data not shown, see [43]). Also, if a small-radius orbit is scanned far from the pore (e.g., in the nucleoplasm), only isotropic intracompartment diffusivity can be measured (data not shown, see [43]). This demonstrates that the hump is visible only in proximity to the pore: further analysis allowed us to link this effect to the action of specific nucleoporins (e.g., Nup153) capable to transporting Kapβ1-cargoes across the pore by reversible collapse/release events [42]. In summary, the combination of FCS with orbital tracking allows us extracting the characteristic correlations of transport events in the reference system of the pore, and in the presence of many molecules under physiological conditions. This information is somewhat hidden in the trajectories of isolated molecules, but it becomes evident when the fluctuation analysis is applied to many events.

4 Concluding Remarks and Future Perspectives

We would like to stress here that the use of an inert tracer, GFP, is an indispensable tool to probe the effect of the environment on molecular diffusion in live cells. Overall, the observations on GFP diffusion within cytoplasm unveiled the previously hidden connection between intracellular "nano"- and "micro"-viscosities. As postulated by Gregorio Weber more than fifty years ago in a footnote of his PhD thesis (as reported above), both of these quantities are of importance, the first in relation to diffusion processes, the second in relation to the structural organization of the cell. In our opinion, the results discussed here represent a paradigmatic shift in the way we describe protein intracellular diffusion, from the 3D reduced motion in a continuum fluid of soluble and colliding crowding agents to the unobstructed

Fig. 9 (continued) in this example. (**b**) The main features of a typical orbital-tracking measurement are reported here, together with peculiar analytical tools that can be used along the orbit and the biological quantities that can in principle be retrieved

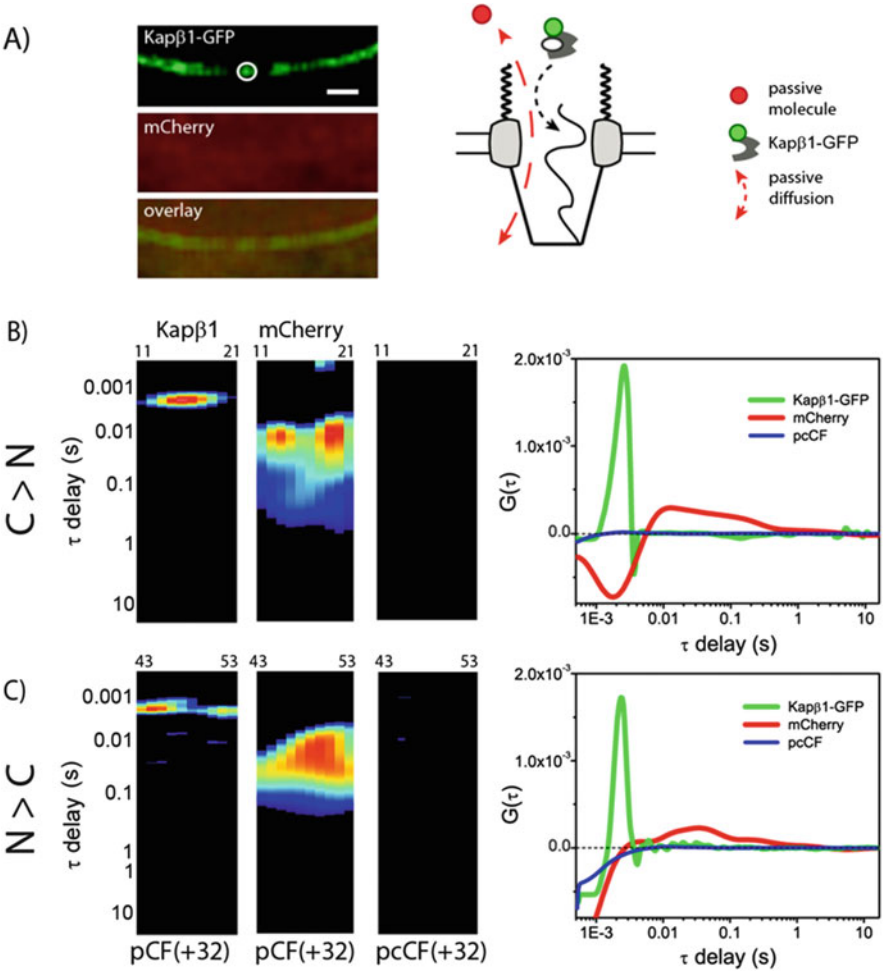

Fig. 10 Diffusion of molecules across the NPC. (**a**) Kapβ1-GFP is cotransfected with untagged mCherry (scale bar: 1 μm) (*left*). In the schematic diagram (*right*), both Kapβ1-GFP and mCherry are represented. A symmetric process must exist to account for both Kapβ1 (active) and mCherry (passive) movement across the NPC. (**b**) The pCF(32) from cytoplasm to nucleus shows a sharp distribution of Kapβ1 translocation times (*left carpet*, *green curve*) opposed to a much broader distribution of mCherry translocation times (*middle carpet*, *red curve*). The pcCF(32) shows that Kapβ1-GFP and mCherry are not translocating together from cytoplasm to nucleus (*right carpet*, *blue curve*). (**c**) The pCF and pcCF at the distance of 32 pixels from nucleus to cytoplasm reveal the symmetry of the observed behaviors: Kapβ1 rapidly translocates, independently from mCherry passive diffusion

motion in a fluid of spatially organized, impermeable macromolecular structures, similarly to what already demonstrated on the plasma membrane [21]. We speculate that such a structural organization of the cell cytoplasm may act as a "supramolecular" regulatory system, directing protein diffusion through spatially defined

paths. In this view, spatiotemporal correlation spectroscopy at tunable timescales has the potential to become a standard for sub-diffusive transport both in cells and *in cuvette*, able to cross-calibrate different experimental and theoretical approaches to crowded environments [44]. On the other hand, the observation of channeled molecular diffusion within the nucleus is in agreement with two theoretical chromatin models that were proposed based on simulation of intranuclear diffusion of inert molecules. The first is the phenomenological ICD (inter-chromosomal domain) model [45], which postulates a network of channels that enable diffusion of small molecules between chromosomal domains. The second is the MLS (multi-loop sub-compartment model) [46], which describes the interphase nucleus as being filled with chromosome territories that intermingle only moderately but allow inter- as well as intra-chromosomal transport of small molecules via obstructed diffusion. Last, we discussed the challenging perspective of studying the diffusion of molecules within subcellular, nanoscopic, dynamic cellular structures or compartments, such as the nuclear pore complex (but examples extend also to vesicles, organelles, or entire cellular protrusions). Our ability to study molecular biochemistry in such a challenging condition, in live cells, is severely hindered by the restless, rapid movement in the 3D cellular environment of these structures/compartments. State-of-the-art optical microscopy tools for delivering subcellular information at molecular resolution, in fact, fail to subtract the 3D evolution of the entire system while preserving the spatiotemporal resolution required to probe dynamic molecular events. We demonstrated that this bottleneck can be tackled by focusing an excitation light-beam in a periodic orbit around the nanostructure of interest. The recorded signal (e.g., fluorescence) can be used as feedback to localize the nanostructure position with unprecedented spatiotemporal resolution. The acquired, privileged observation point is then used to push single-molecule studies to an entirely new level. The ultimate significance of this idea goes well beyond its application to the nuclear pore case proposed here, potentially promoting a dramatic paradigm shift in the way we describe biological processes in general. A vast amount of biochemical information, in fact, is still hidden behind several dynamic intracellular nanostructures. For each target, the proposed strategy would have the potential to discriminate single-molecule behavior from the natural movement of the reference system, thus making biophysical studies feasible in one of the natural conditions of living matter at the nanoscale. For the first time, in fact, state-of-the-art imaging and analytical tools (e.g., ultrafast spatiotemporal correlation spectroscopy, spectral information, lifetime, and polarization) can be used to measure biochemical parameters (e.g., molecular dynamics, interactions, and oligomerization state) on moving, nanoscopic, reference systems, where single-molecule sensitivity, high spatiotemporal resolution, and large volume sampling are concomitantly needed in a single measurement.

In conclusion, we believe the present findings coupled with use of genetically encoded fluorescent markers pave the way to novel studies of biomolecular processes in live cells at the physiologically relevant spatiotemporal scale. Let us argue, in fact, that key processes of cell function like the kinetics of biochemical reactions, the dynamics of protein folding/unfolding, the effectiveness of target-

search processes, and intracellular signaling pathways will necessarily be regulated at the same spatiotemporal scale revealed by the use of an inert tracer, but they will be influenced by the specific interactions of their molecular components with the cellular environment.

Acknowledgments This work ideally encompasses the research conducted across several years and, as such, reflects the invaluable contribution by other people. In particular, the authors are grateful to Dr. Elizabeth Hinde and Dr. Michelle Digman who conducted the research on chromatin, Dr. Luca Lanzano who contributed to the research on the nuclear pore, and Dr. Carmine Di Rienzo who conducted the research on protein diffusion in the cell. Also, the authors acknowledge the precious contribution to research of other colleagues, including Prof. Fabio Beltram, Dr. Vincenzo Piazza, Dr. Milka Stakic, Dr. Aaron Kershner, and Prof. Judith Kimble.

The research described in this work was supported by several grants, including: the Cell Migration Consortium Grant U54 GM064346, the National Institutes of Health Grants P41-RRO3155, P41-GM103540, RO1 DK066029, P50-GM076516, MIUR under FIRB-RBAP11X42L, and Fondazione Monte dei Paschi di Siena.

References

1. Chalfie M (2009) GFP: lighting up life. Proc Natl Acad Sci U S A 106(25):10073–10080
2. Fushimi K, Verkman AS (1991) Low viscosity in the aqueous domain of cell cytoplasm measured by picosecond polarization microfluorimetry. J Cell Biol 112(4):719–725
3. Swaminathan R, Hoang CP, Verkman AS (1997) Photobleaching recovery and anisotropy decay of green fluorescent protein GFP-S65T in solution and cells: cytoplasmic viscosity probed by green fluorescent protein translational and rotational diffusion. Biophys J 72 (4):1900–1907
4. Hofling F, Franosch T (2013) Anomalous transport in the crowded world of biological cells. Rep Prog Phys 76(4):046602
5. Luby-Phelps K, Taylor DL, Lanni F (1986) Probing the structure of cytoplasm. J Cell Biol 102 (6):2015–2022
6. Seksek O, Biwersi J, Verkman AS (1997) Translational diffusion of macromolecule-sized solutes in cytoplasm and nucleus. J Cell Biol 138(1):131–142
7. Caspi A, Granek R, Elbaum M (2002) Diffusion and directed motion in cellular transport. Phys Rev E Stat Nonlin Soft Matter Phys 66(1 Pt 1):011916
8. Schwille P et al (1999) Molecular dynamics in living cells observed by fluorescence correlation spectroscopy with one- and two-photon excitation. Biophys J 77(4):2251–2265
9. Wawrezinieck L et al (2005) Fluorescence correlation spectroscopy diffusion laws to probe the submicron cell membrane organization. Biophys J 89(6):4029–4042
10. Lenne PF et al (2006) Dynamic molecular confinement in the plasma membrane by microdomains and the cytoskeleton meshwork. EMBO J 25(14):3245–3256
11. Ruprecht V et al (2011) Spot variation fluorescence correlation spectroscopy allows for superresolution chronoscopy of confinement times in membranes. Biophys J 100 (11):2839–2845
12. Hell SW (2007) Far-field optical nanoscopy. Science 316(5828):1153–1158
13. Eggeling C et al (2009) Direct observation of the nanoscale dynamics of membrane lipids in a living cell. Nature 457(7233):1159–1162
14. Hedde PN et al (2013) Stimulated emission depletion-based raster image correlation spectroscopy reveals biomolecular dynamics in live cells. Nat Commun 4:2093

15. Shusterman R et al (2004) Monomer dynamics in double- and single-stranded DNA polymers. Phys Rev Lett 92(4):048303
16. Dross N et al (2009) Mapping eGFP oligomer mobility in living cell nuclei. PLoS One 4(4), e5041
17. Di Rienzo C et al (2014) Probing short-range protein Brownian motion in the cytoplasm of living cells. Nat Commun 5:5891
18. Groner N et al (2010) Measuring and imaging diffusion with multiple scan speed image correlation spectroscopy. Opt Express 18(20):21225–21237
19. Arrio-Dupont M et al (2000) Translational diffusion of globular proteins in the cytoplasm of cultured muscle cells. Biophys J 78(2):901–907
20. Saxton MJ (1994) Anomalous diffusion due to obstacles: a Monte Carlo study. Biophys J 66 (2 Pt 1):394–401
21. Kusumi A et al (2005) Paradigm shift of the plasma membrane concept from the two-dimensional continuum fluid to the partitioned fluid: high-speed single-molecule tracking of membrane molecules. Annu Rev Biophys Biomol Struct 34:351–378
22. Di Rienzo C et al (2013) Fast spatiotemporal correlation spectroscopy to determine protein lateral diffusion laws in live cell membranes. Proc Natl Acad Sci U S A 110(30):12307–12312
23. Di Rienzo C et al (2014) From fast fluorescence imaging to molecular diffusion law on live cell membranes in a commercial microscope. J Vis Exp 92, e51994
24. Fujiwara T et al (2002) Phospholipids undergo hop diffusion in compartmentalized cell membrane. J Cell Biol 157(6):1071–1081
25. Roosen-Runge F et al (2011) Protein self-diffusion in crowded solutions. Proc Natl Acad Sci U S A 108(29):11815–11820
26. Novak IL, Kraikivski P, Slepchenko BM (2009) Diffusion in cytoplasm: effects of excluded volume due to internal membranes and cytoskeletal structures. Biophys J 97(3):758–767
27. Kuhn T et al (2011) Protein diffusion in mammalian cell cytoplasm. PLoS One 6(8), e22962
28. Cardarelli F et al (2007) In vivo study of HIV-1 Tat arginine-rich motif unveils its transport properties. Mol Ther 15(7):1313–1322
29. Digman MA, Gratton E (2009) Imaging barriers to diffusion by pair correlation functions. Biophys J 97(2):665–673
30. Hinde E, Cardarelli F (2011) Measuring the flow of molecules in cells. Biophys Rev 3 (3):119–129
31. Hinde E et al (2010) In vivo pair correlation analysis of EGFP intranuclear diffusion reveals DNA-dependent molecular flow. Proc Natl Acad Sci U S A 107(38):16560–16565
32. Hinde E et al (2012) Changes in chromatin compaction during the cell cycle revealed by micrometer-scale measurement of molecular flow in the nucleus. Biophys J 102(3):691–697
33. Hinde E et al (2011) The impact of mitotic versus interphase chromatin architecture on the molecular flow of EGFP by pair correlation analysis. Biophys J 100(7):1829–1836
34. Wachsmuth M, Waldeck W, Langowski J (2000) Anomalous diffusion of fluorescent probes inside living cell nuclei investigated by spatially-resolved fluorescence correlation spectroscopy. J Mol Biol 298(4):677–689
35. Fahrenkrog B, Aebi U (2003) The nuclear pore complex: nucleocytoplasmic transport and beyond. Nat Rev Mol Cell Biol 4(10):757–766
36. Weis K (2003) Regulating access to the genome: nucleocytoplasmic transport throughout the cell cycle. Cell 112(4):441–451
37. Yang W, Gelles J, Musser SM (2004) Imaging of single-molecule translocation through nuclear pore complexes. Proc Natl Acad Sci U S A 101(35):12887–12892
38. Yang W, Musser SM (2006) Nuclear import time and transport efficiency depend on importin beta concentration. J Cell Biol 174(7):951–961
39. Cardarelli F, Gratton E (2010) In vivo imaging of single-molecule translocation through nuclear pore complexes by pair correlation functions. PLoS One 5(5), e10475
40. Daigle N et al (2001) Nuclear pore complexes form immobile networks and have a very low turnover in live mammalian cells. J Cell Biol 154(1):71–84

41. Levi V, Ruan Q, Gratton E (2005) 3-D particle tracking in a two-photon microscope: application to the study of molecular dynamics in cells. Biophys J 88(4):2919–2928
42. Cardarelli F, Lanzano L, Gratton E (2012) Capturing directed molecular motion in the nuclear pore complex of live cells. Proc Natl Acad Sci U S A 109(25):9863–9868
43. Cardarelli F, Lanzano L, Gratton E (2011) Fluorescence correlation spectroscopy of intact nuclear pore complexes. Biophys J 101(4):L27–L29
44. Saxton MJ (2012) Wanted: a positive control for anomalous subdiffusion. Biophys J 103 (12):2411–2422
45. Cremer T et al (1993) Role of chromosome territories in the functional compartmentalization of the cell nucleus. Cold Spring Harb Symp Quant Biol 58:777–792
46. Munkel C et al (1999) Compartmentalization of interphase chromosomes observed in simulation and experiment. J Mol Biol 285(3):1053–1065

Role of the Pico-Nano-Second Temporal Dimension in STED Microscopy

Luca Lanzanò, Lorenzo Scipioni, Marco Castello, Paolo Bianchini, Giuseppe Vicidomini, and Alberto Diaspro

Abstract In the last decades, several techniques have been developed to push the spatial resolution of far-field fluorescence microscopy beyond the diffraction limit. Stimulated emission depletion (STED) microscopy is a super-resolution technique in which the targeted switching off of the fluorophores by a secondary laser beam

L. Lanzanò
Nanoscopy, Nanophysics, Istituto Italiano di Tecnologia, via Morego 30, 16163 Genoa, Italy

L. Scipioni
Nanoscopy, Nanophysics, Istituto Italiano di Tecnologia, via Morego 30, 16163 Genoa, Italy

Department of Computer Science, Bioengineering, Robotics and Systems Engineering, University of Genoa, via Opera Pia 13, 16145 Genoa, Italy

M. Castello
Department of Computer Science, Bioengineering, Robotics and Systems Engineering, University of Genoa, via Opera Pia 13, 16145 Genoa, Italy

Molecular Microscopy and Spectroscopy, Nanophysics, Istituto Italiano di Tecnologia, via Morego 30, 16163 Genoa, Italy

P. Bianchini
Nanoscopy, Nanophysics, Istituto Italiano di Tecnologia, via Morego 30, 16163 Genoa, Italy

NIC@IIT, Nikon Imaging Center, Istituto Italiano di Tecnologia, via Morego 30, 16163 Genoa, Italy

G. Vicidomini
Molecular Microscopy and Spectroscopy, Nanophysics, Istituto Italiano di Tecnologia, via Morego 30, 16163 Genoa, Italy

A. Diaspro (✉)
Nanoscopy, Nanophysics, Istituto Italiano di Tecnologia, via Morego 30, 16163 Genoa, Italy

NIC@IIT, Nikon Imaging Center, Istituto Italiano di Tecnologia, via Morego 30, 16163 Genoa, Italy

Department of Physics, University of Genoa, via Dodecaneso 33, 16146 Genoa, Italy
e-mail: alberto.diaspro@iit.it

D.M. Jameson (ed.), *Perspectives on Fluorescence: A Tribute to Gregorio Weber*,
Springer Ser Fluoresc (2016) 17: 311–330, DOI 10.1007/4243_2016_19,

results in an effective increase in optical resolution. However, to fully exploit the maximum performances of a STED microscope (effective spatial resolution achievable for a given STED beam's intensity, versatility, live-cell imaging capability, etc.) several experimental precautions have to be considered. In this respect, the temporal dimension (at the pico- and nanosecond scale) has often a central role on the overall efficiency and versatility of a STED microscope, working in pulsed or continuous-wave mode.

In pulsed STED, temporal alignment between the excitation and STED pulses has direct consequences on the maximum spatial resolution achievable by the STED microscope. In a specific pulsed STED implementation, called single wavelength two-photon excitation STED, the modulation of the temporal width of the pulse results in the use of the very same laser for excitation and depletion of the fluorophores. In continuous-wave (CW)-STED, the analysis of nanosecond fluorescence dynamics allows one to preserve the effective resolution of a STED microscope, but with a significant reduction of the illumination intensity. In this respect, we discuss two different approaches for the analysis of nanosecond dynamics in CW-STED images, namely the so-called gated-STED microscopy and Separation of Photons by LIfetime Tuning (SPLIT)-STED microscopy. Overall, these examples show that concepts developed in time-resolved fluorescence spectroscopy are important for the advancement of optical super-resolution microscopy.

Keywords CW-STED • Nanosecond dynamics • SPLIT-STED • STED • Super-resolution • Two-photon excitation

Contents

1 Introduction

Since its invention in 1908, far-field florescence microscopy has been the workhouse for many life sciences investigations [1]. Throughout the twentieth century far-field microscopy has enormously grown and all its distinctive features, such as the high sensitivity and specificity through the fluorescent tagging, the possibility to investigate the interior of living organisms, and the ability to extract quantitative

data about molecular dynamics and organizations, were continuously refined. However, the fundamental barrier, which was limiting the spatial resolution of the early far-field fluorescent microscope, was still intact at the end of the twentieth century. The diffraction barrier precluded to far-field microscopy the access to the entire sub-cellular components whose structural complexities were below around half of the light's wavelength used for the investigation (i.e., ~200 nm).

The twenty-first century opened with a fundamental microscopy revolution, the so-called resolution revolution. The beginning of the century saw the introduction of new viable concepts able to effectively overcome the diffraction barrier and push the spatial resolution of a far-field fluorescence microscope to the double-digit nanometer scale [2–6]. These techniques are usually referred to as super-resolved microscopies and their importance has been recently recognized by the assignment of the 2014 Nobel Prize in Chemistry to their inventors.

Super-resolved fluorescence microscopy techniques [7–13] can be classified based on the fundamental differences in implementation and the photo-physical mechanism used to circumvent the diffraction barrier. However, all of them rely on the same basic principle [14]: in order to resolve features closer than the diffraction limit fluorophores (defining the structures) are transiently driven into two discernible (pseudo-) states, i.e. (pseudo-) states with different spectral or temporal or any other detectable response to the illumination.

Stimulated emission depletion (STED) microscopy [10] uses two fundamental processes to transiently transfer a fluorophore from a dark to a bright state and vice versa: the excitation process transfers the fluorophore from the singlet ground-state (dark) to the singlet excited-state (bright) whereas the stimulated emission (SE) induces the opposite transition. In a typical STED microscope, a focused Gaussian beam excites all the fluorophores within a diffraction-limited spot. Successively, a focused doughnut-shaped beam, the STED beam, featuring a zero-intensity point co-aligned with the peak of the Gaussian excitation spot and a wavelength able to induce stimulated emission, quenches the excited fluorophores except those located in a tiny sub-diffraction sized region around the zero-intensity point. In order to efficiently quench fluorescence the stimulated emission process has to compete with spontaneous de-excitation, which normally occurs after few nanoseconds ($\tau_0 \sim 1$–10 ns) from the excitation event. This short time-window, together with the low cross-section of the stimulated emission process ($\sigma_{STED} \sim 10^{-17}/10^{-16}$ cm^2) [15], results in a relatively high dose of illumination intensity from the STED beam, typically in the order of 0.1–1 GW/cm^2, which might introduce side effects such as photobleaching of the fluorophores and phototoxicity for the sample.

Maximizing the performances of a STED microscope includes achieving the maximum resolution at a given STED power and reducing complexity and cost of implementation. The spatial resolution is determined by the ability of the depletion beam to silence the fluorophores located in the periphery of the diffraction-limited illumination (excitation) volume. Note that here the term "to silence" does not necessarily mean "to quench" the fluorescence. When the signal at the periphery of

the illumination volume is inhibited, only the signal in a tiny sub-diffraction volume around the center of the illumination region builds up the final image. An effective reduction of the observation volume (the region from which the signal that generates the final image is effectively collected) is obtained only if three conditions are simultaneously met, namely, the spatial, the spectral, and the temporal conditions.

The spatial condition requires that the excitation and STED beams be carefully aligned in all spatial directions. Moreover a good quality of the "zero"-intensity point of the doughnut-shaped STED focus is mandatory. The spectral condition is in most of the case only partially satisfied and requires that the STED beam induce only stimulated emission. Unfortunately, in many cases the stimulating photons can be absorbed by the fluorophores, thus exciting the fluorophores or convoying the fluorophore in some photobleaching pathway. In this chapter we will focus more deeply on the temporal condition, in particular we will explain its role in STED and we will overview the recent methods that play on the temporal condition, or more in general on the pico- nano-second temporal dimension, to enhance the performances of modern STED microscopy implementations.

Currently, the STED implementations that act on the temporal conditions to enhance the performance can be divided into two broad categories. The first class deals with all-pulsed STED implementations, namely implementations in which both the excitation and the STED beams run in pulsed mode. We can include in this class the all-pulsed STED implementations that focus on a two-photon excitation (2PE) approach. The second category is based on hybrid configurations in which the excitation beam runs in pulsed mode whilst the STED beam runs in continuous-wave.

2 All-Pulsed STED Implementation

The STED beam irradiance of 0.1–1 GW/cm^2 requested to effectively quench the fluorescence signal is most conveniently realized by focusing (ultra-)short pulsed laser beam (50–200 ps). However, another fundamental aspect for an efficient fluorescence quenching is represented by the fact that stimulating photons have to act "immediately" after the fluorophores excitation events, or better, "immediately" after the fluorophores relax to the lowest excited-state. These two conditions set the bases for one of the most used STED implementations, the so-called all-pulsed STED implementation, in which both the excitation and STED beams run in pulsed modality and are synchronized together.

2.1 Temporal Alignment and Time-Gating in All-Pulsed STED

In all-pulsed STED, ideally, the excitation and the stimulated emission act sequentially and continuously in time without overlap. Thus, temporal misalignment between the excitation and STED pulses reduces the fluorescence quenching and consequently the maximum spatial resolution achievable by the STED microscope (for a given STED beam intensity) (Fig. 1). For instance, if the depletion beam is delayed with respect to the excitation beam (Fig. 1c), the fluorophores have a non-negligible probability to spontaneously emit before having been exposed to much of the stimulating photons. Thus residual fluorescence outside the zero-intensity point of the STED beam leads to a pedestal in the effective observation volume, resulting in somewhat lower-contrast images and spatial resolution [16] (Fig. 1f).

Obviously, the straightforward solution to this problem is to precisely align the excitation and the STED beam pulses (Fig. 1b). However, practically, this solution is inefficient in condition of laser jittering or long pulse-width (>200 ps) beam. In the first case a perfect temporal alignment does not exist. In the second case, even if the temporal alignment is satisfied, a non-negligible spontaneous emission can take place during the depletion time-window, i.e. during the pulse-width.

It has been shown that a solution to temporal misalignment, laser jittering, and long pulse-width is obtained by using time-gated detection [17]. The reason for which time-gated detection helps solving the above problems is that, to obtain a resolution enhancement, it is not strictly necessary to fully quench the fluorophores at the periphery of the excitation volume, but, more generally, it is necessary to inhibit their registered signal. Roughly speaking, it is necessary to enhance the signal contrast between the situation in which the STED beam is active and the situation in which is inactive (ON-OFF switching contrast). This ON-OFF contrast is mostly described by means of the so-called depletion curve, which represents the ratio between the registered signal as given with and without the exposure to the STED beam as a function of the STED beam intensity.

In this scenario, it is important to highlight that the suppression of fluorescence depends on the number of stimulating photons to which the fluorophore is exposed while residing in the excited-state. As a consequence by collecting fluorescence signal from fluorophores that have resided into the excited-state for the entire duration of the STED beam action helps improving the switching ON-OFF contrast. This is exactly how time-gated detection works, namely, early fluorescence signal collected during the action of the STED beam is discarded and only late fluorescence signal after the STED beam action is collected.

In the case of temporal misalignment between the excitation and the STED beam pulses, the unwanted spontaneous emission obtained as consequence of the delayed STED beam action can be discarded by time-gated detection and the switching ON-OFF contrast is fully recovered (Fig. 1i). In other words, if the fluorescence signal is collected after the action of all stimulating photons (at the end of the STED

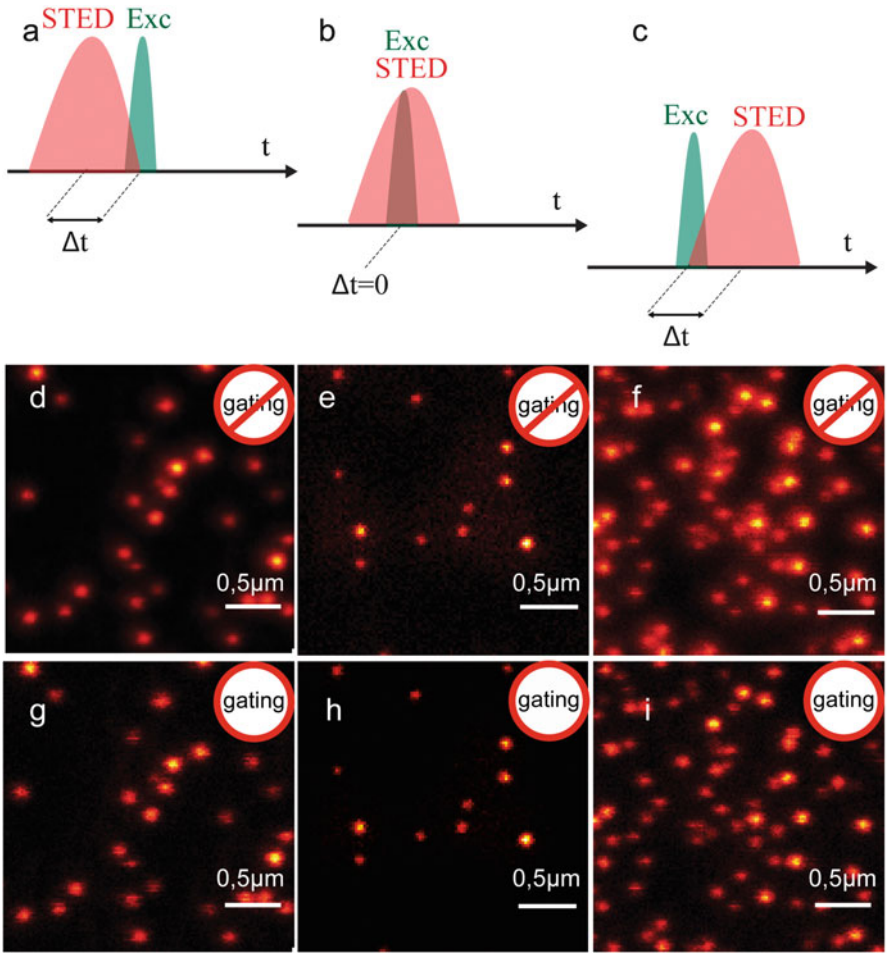

Fig. 1 In the all-pulsed STED configuration, STED inhibition depends on the time delay between the excitation beam and the STED beam. Essentially three cases are possible (**a**, **b**, **c**): the STED pulse arrives before (**a**), simultaneously (**b**), or later than the excitation pulse (**c**). In the case of time-gated detection, a more effective inhibition is obtained by collecting the fluorescence immediately after the STED beam action. We compare between STED and gated-STED imaging of 40 nm florescent beads for different time delay between the excitation and the STED pulses. In particular the pairs (**d**, **g**), (**e**, **g**), and (**f**, **i**) are representative of the cases (**a**), (**b**), and (**c**), respectively. Excitation 572/15 nm, detection 641/75 nm, depletion 720/20 nm. Excitation average power ~4 μW; STED average power ~4.2 mW. The scale bars in these images are 0.5 μm. The time-scale of the pulses in (**a**, **b**, **c**) is only symbolic and not necessarily to scale

beam pulse), then what is important is not the specific temporal distribution of the stimulating photons but only their total amount. Thus, stimulating photons can arrive few hundreds picoseconds after the excitation events (misalignment) (Fig. 1c, f, i), or be spread over few hundreds of picoseconds (long pulse-width)

(Fig. 1b, e, h) without decreasing the switching ON-OFF contrast or compromising the spatial resolution for a given STED beam power (average intensity). Obviously, time-gating cannot compensate for an early STED beam action (stimulating photons acting before fluorophores excitations take place) (Fig. 1a). But, in the case of jittering the STED beam can be slightly delayed in order to avoid any situation of early STED beam action and the time-gating can be delayed to ensure that fluorescence is collected always after the STED beam action.

As a matter of fact the introduction of time-gated detection increases the complexity of the architecture, however, the time-gated detection always consists in a post-processing of the signal collected by the detector, thus does not need any optical change of the system. Furthermore, easy and cheap solutions based on dedicated time-gated box electronics are fast emerging. It is important to remember that this type of gated-box needs relatively high temporal resolution (few hundreds of picoseconds).

The price of introducing a time-gated detection on the architecture is fully recovered by the possibility to use turn-key laser source as STED beam. Indeed, thanks to the time-gated detection, it is possible to use sub-nanosecond triggerable lasers which substantial reduce the complexity and cost of the early STED implementations based on mode-locked lasers.

2.2 Single Wavelength Two-Photon Excitation STED

Another substantial reduction of all-pulsed STED system complexity has been recently obtained implementing both the excitation beam and the STED beam with the very same laser, and the very same wavelength. This is the so-called single wavelength two-photon excitation STED [18]. This approach takes advantages of two observations: (1) for some fluorophores the two-photon excitation spectra and the stimulated emission spectra overlap, namely, it is possible to find a wavelength for which the probability to excite the fluorophore by two photon absorption and to de-excite it by stimulated emission is not negligible; (2) the two-photon excitation (instantaneous) probability is quadratic with the intensity of the beam, whilst the stimulated emission (instantaneous) probability is linear with the intensity of the beam. As a consequence by carefully controlling the pulse-width of a single-wavelength beam it is possible to alternatively induce two-photon excitation or stimulated emission. In practice, an ultra-short (femtosecond) laser beam is divided into two parts. The first part is used as excitation (two-photon excitation) beam, whilst the second part is stretched up to few hundreds picoseconds and used as STED beam. Notably, since the same laser source generates both the excitation and the STED beam the synchronization is automatically obtained, thus reducing the system complexity. On the other side, this approach can be obtained only in the context of two-photon-excitation with its advantages, such as higher penetration depth and lower phototoxicity, but also its disadvantages, such as higher photobleaching in the focal plane. Furthermore, the overlapping between the

two-photon excitation spectra and the stimulated emission spectra is obtained, thanks to the ability of exciting fluorophore to higher-order excited state, indeed, the fluorophore can be excited (two-photon excitation) also at lower wavelength (higher energy) with respect to the conventional wavelength. For example, fluorophore like the ATTO647N, which is normally excited at ~1,400 nm by two-photon-absorption, can be excited at its typical wavelength of stimulated emission, i.e. 760 nm, thanks to the excitation to a higher-order state.

3 Continuous-Wave STED Implementation

The use of the pico-nanosecond temporal dimension is especially relevant in CW-STED, where it can be used to reduce the peak power required to reach a certain sub-diffraction resolution. Indeed, it has been demonstrated that using the nanosecond fluorescence dynamics information of a time-resolved STED microscopy experiment it is possible to improve the effective resolution of STED microscopy without increasing the (peak) intensity of the STED beam [19, 20]. Two different implementations of this idea are the so-called gated-STED microscopy [20–23] and separation of photons by lifetime tuning STED (SPLIT-STED) microscopy [24]. Gated-STED and SPLIT-STED microscopy are based on the observation that the doughnut-shape of the STED beam imposes a spatial signature for the excited-state lifetime of the fluorophores within the excitation spot, i.e. the excited-state lifetime of a fluorophore changes according to its position, decreasing away from the STED zero-intensity point, reaching a minimum in the proximity of the doughnut crest where there is the maximum STED beam intensity. The two implementations share similar STED architecture, in particular, both need the access to the so-called photon-arrival time information. This is normally obtained using a pulsed laser which synchronizes the excitation events and dedicated electronics that measures the arrival time of the photons with a precision of few tens of picoseconds.

Given the photon-arrival times for each pixel the gated-STED microscope simply selects the photons within a certain time-window (time-gated detection) [20]. For this reason, it does not need the full photon-arrival-time histogram, and the expensive time-correlated-single-photon counting based-hardware can be substituted by cheaper time-gated electronics [20, 25, 26]. On the other hand, the SPLIT-STED microscope performs an explicit analysis of the temporal dynamics of fluorescence, using the full photon-arrival time histogram [24]. In order to quantify in a fast, fit-free mode, the relative contribution of a specific component at each pixel of an image, this analysis is based on the phasor approach to FLIM [27–29], a methodology originally derived from spectroscopy [30] that has found wide application in FRET [16, 31–34, 49], spectral fingerprinting [35, 36], and correlation spectroscopy [37].

3.1 Gated CW-STED Microscopy

In a continuous-wave (CW) STED microscope, the stimulated emission process opens a new de-excitation pathway for the excited fluorophore, shortening the excited-state lifetime of the fluorophore, i.e. the time that the fluorophore spends on average into the excited-state after the excitation event (Fig. 2a). Based on this principle, it has been demonstrated that using the nanosecond fluorescence dynamics information of a time-resolved STED microscopy experiment it is possible to increase the effective spatial resolution of a STED microscope without increasing the (peak) intensity of the STED beam [19, 20].

In the presence of a STED beam, the lifetime of the fluorophore decreases as $\tau_{S1} = 1/(k_0 + k_{STED})$, with (1) $k_0 = 1/\tau_0$ the rate of spontaneous de-excitation, which

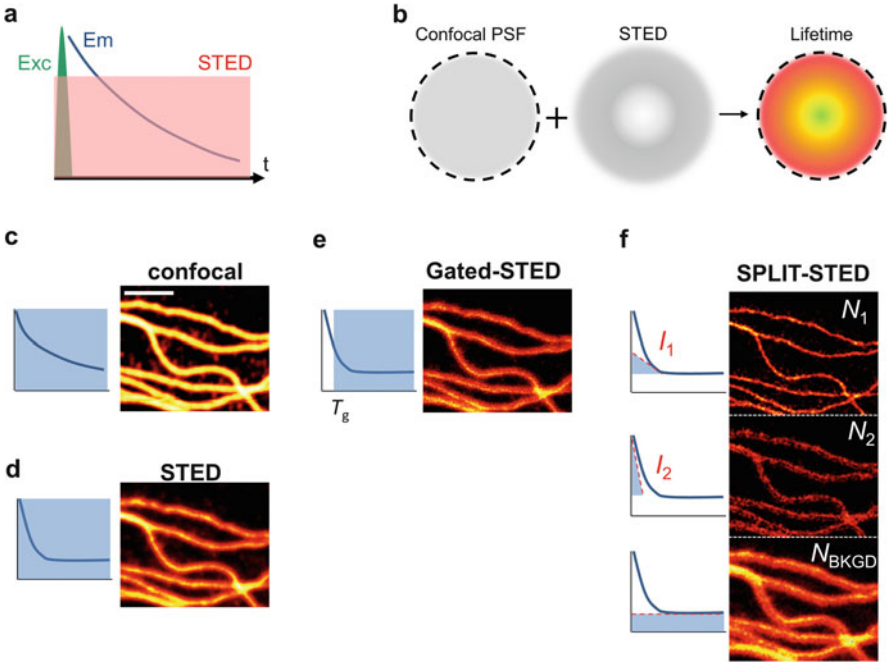

Fig. 2 (**a**) In continuous-wave (CW) STED, the stimulated emission process opens a new de-excitation pathway for the excited fluorophore, shortening the lifetime associated with the fluorescence emission. (**b**) A doughnut-shaped CW-STED beam co-aligned with a confocal spot generates a continuous distribution of dynamics within the PSF. (**c**–**f**) Time-resolved STED imaging of tubulin in fixed HeLa cells immunostained with Oregon Green 488. In the confocal (**c**) and STED (**d**) images the temporal information is ignored and all photons are used to build the images. In Gated-STED (**e**) only late photons ($T_g = 1$ ns) are used to generate a super-resolved image. In SPLIT-STED (**f**) two decay components plus the uncorrelated background are resolved to produce the associated images. The slowest component I_1 corresponds to the photons coming from the center of the PSF. The uncorrelated background is generated by Anti-Stokes emission induced by the CW-STED beam. The STED beam power was set to 40 mW. Scale bar 2 μm

is the inverse of the excited-state lifetime τ_0 in the absence of the STED beam; (2) $k_{STED} \propto I^*_{STED}$ the rate of stimulated emission, which is directly proportional to the instantaneous intensity I^*_{STED} of the STED beam [17]. As a result, the doughnut-shape of the STED beam generates a gradient of excited-state lifetimes within the excitation spot, i.e. the excited-state lifetime of a fluorophore changes according to its position (Fig. 2b). The effective excited-state lifetime decreases away from the zero-intensity point, reaching a minimum in the proximity of the doughnut crest where there is the maximum STED beam intensity.

By selecting only the photons emitted from the long-lived fluorophores, it is possible to increase the resolution of the STED system, without increasing the intensity of the STED beam. The gated-STED microscope uses a straightforward approach to select the photons from the long-lived fluorophores, which reside in the central part of the excitation volume. Given the photon-arrival times for each pixel the gated-STED microscope simply selects the photons within a certain time-window (time-gated detection) [20].

To obtain an analytical description of the temporal PSF we can make the following assumptions: (1) a Gaussian profile of the confocal PSF $h(r) = \exp(-2r^2/w^2)$, with w being the beam waist along the radial direction and $r^2 = x'^2 + y'^2$ the radial distance from the focal point ($x = 0$, $y = 0$); (2) a parabolic approximation for the doughnut-shaped STED beam $I_{STED}(r) = I_{STED}(w)r^2/w^2$, with $I_{STED}(w)$ the STED beam intensity at position $r = w$; (3) a single exponential decay rate for the unperturbed fluorophores $\gamma_0 = 1/\tau_0$, where τ_0 is the unperturbed excited-state lifetime; (4) the fluorophores are excited only at time zero ($t = 0$) and the STED beam is active during all the time course of the experiments (i.e., the STED beam is running in CW).

The instantaneous probability of stimulated emission depends linearly on the STED beam intensity:

$$\gamma_{STED}(r^2) = \gamma_0[I_{STED}(r)/I_{SAT}], \tag{1}$$

where the constant I_{SAT}, usually called saturation intensity, represents the value of intensity for which $\gamma_{STED} = \gamma_0$. The resulting radial distribution of the decay rates can be approximated by a parabolic function:

$$\begin{aligned}\gamma(r^2) &= \gamma_0 + \gamma_{STED}(r^2) = \gamma_0 + \gamma_0\left[I_{STED}(w)\left(r^2/w^2\right)/I_{SAT}\right] \\ &= \gamma_0 + \gamma_0 k_s r^2/w^2,\end{aligned} \tag{2}$$

where we have defined:

$$k_s = I_{STED}(w)/I_{SAT}. \tag{3}$$

According to this definition, k_S is the ratio between $I_{STED}(w)$ and the saturation value I_{SAT} for which the probability of decay due to SE and spontaneous emission is equal.

The time-dependent fluorescence intensity $F(x,y,t)$ at any given pixel (x,y) can be expressed as

$$F(x,y,t) = K \int e^{-\gamma(r^2)t} \rho(x',y') e^{-\frac{2r^2}{w^2}} dx'dy', \tag{4}$$

where K is a constant that depends on the quantum yield of the fluorophore, the maximum of the excitation intensity and the detection efficiency, $r^2 = (x'-x)^2 + (y'-y)^2$ and $\rho(x',y')$ is the density of fluorophores.

The point-spread-function of the CW-STED microscope can be obtained by substituting the density of fluorophores $\rho(x',y')$ with the Dirac's δ function in Eq. (4). We get the following time-dependent PSF:

$$h_{\mathrm{STED}}(r,t) = Ke^{-\gamma(r^2)t} e^{-\frac{2r^2}{w^2}} \tag{5}$$

Now, the gated-STED microscope increases the spatial resolution of a CW-STED implementation by discarding early photons, most likely generated from short-lived fluorophores located in the periphery of the detection volume, and highlighting late-photons most likely generated from long-lived fluorophores located in the center of the detection volume. For this purpose, early photons collected within a short time interval from the excitation events $[0,T_g]$ are discarded whilst late fluorescent photons in the remaining part of the excitation pulse period $[T_g,T]$ are used to generate the final image (Fig. 2e).

Integration of Equation (5) in the temporal window of detection $[T_g,T]$ leads to the point-spread-function of the gated CW-STED microscope. Assuming that the pulse interval is much longer than the excited-state lifetime of the fluorophores ($T \gg \tau_0$) we obtain

$$\begin{aligned} h_{\mathrm{gCW\text{-}STED}}(r) = \int_{T_g}^{T} h_{\mathrm{STED}}(r,t)dt = Ke^{-\frac{2r^2}{w^2}} \frac{1}{\gamma_0 + \gamma_0 k_s r^2/w^2} e^{-\left(\gamma_0 + \gamma_0 k_s r^2/w^2\right)T_g} = Ke^{-\gamma_0 T_g} \\ \times e^{-\frac{2r^2}{w^2}} \times \frac{1}{\gamma_0 + \gamma_0 k_s r^2/w^2} \times e^{-T_g \gamma_0 k_s r^2/w^2}. \end{aligned} \tag{6}$$

The PSF (Eq. (6)) immediately highlights the positive and negative aspects of the gCW-STED implementation. We can distinguish four terms: (1) a constant term that denotes the amplitude of the PSF, clearly indicating that the signal decreases exponentially with the increasing of the time-gating value T_g; (2) a Gaussian function that denotes the confocal PSF; (3) a Lorentzian function that reflects the PSF of a non-gated ($T_g = 0$) CW-STED microscope; (4) a Gaussian term that indicates the reduction of the effective PSF for increasing values of T_g.

For increasing T_g the effective PSF gets smaller and the Gaussian term dominates over the Lorentzian term, removing the PSF tails which drastically decrease the contrast, thus the effective resolution in the conventional CW-STED

microscope. The resolution of a gated CW-STED microscope theoretically increases to infinity for increasing T_g, but, unfortunately, the simultaneous reduction of the PSF's amplitude translates into a reduction of the signal-to-noise ratio (SNR) of the gated images. It is clear that a strong reduction of the SNR can cancel out the benefits of the time-gating and typically used values of T_g are only in the order of half of the excited-state lifetime τ_0. In this case the image contrast effectively improves, but the PSF's amplitude is reduced only by a factor of 0.4. In order to compensate for SNR loss in gated-STED microscopy, the usually discarded early photons can be combined with the conventional gated-STED image (late-photons) through a multi-image deconvolution algorithm [38, 39]. It is also interesting to observe that the working principle of gCW-STED microscopy can be explained also in terms similar to the gated all-pulsed STED implementations. Indeed, the suppression of fluorescence depends on the number of stimulating photons to which the fluorophore is exposed while residing in the excited-state, thus registering fluorescence only after a time T_g from the excitation event ensures that the fluorophores have been exposed to stimulating photons at least for the time T_g and switching ON-OFF contrast is optimized.

3.2 SPLIT-STED Microscopy

A radically different strategy that exploits the entire information contained in the nanosecond fluorescence dynamics of a time-resolved STED microscope is represented by SPLIT (Separation of Photons by LIfetime Tuning) microscopy.

The basic principle of SPLIT microscopy is to achieve super-resolution by an explicit separation of the different components of the fluorescent signals according to their "temporal dynamics" [24]. In this sense, SPLIT can be considered as part of a class of super-resolution methods that aim at improving spatial resolution by using differences in fluorescence dynamics [40–43]. In CW-STED, SPLIT microscopy isolates the slow fluorescence component that is most likely associated with fluorophores in the center of the effective detection volume. By using a spectroscopy point of view, the maximum achievable spatial resolution will be ultimately determined by the ability to distinguish between different temporal dynamics. In this framework the problem of increasing spatial resolution is translated into the spectroscopy problem of resolving the stimulated emission-induced variations of the fluorescence lifetime.

Starting from Eq. (4) it is possible to find an approximate, explicit expression for the temporal decay of fluorescence emitted from the center of the detection volume in a CW-STED microscope. In order to quantify the relative contribution of this component at each pixel of the image, we will describe a fit-free analysis of the fluorescence decays based on the phasor approach to FLIM [27–29].

We can rewrite Eq. (4) as

$$F(x,y,t) = K\int_0^{\infty} C\left(r^2\right)dr^2 e^{-\gamma\left(r^2\right)t} e^{-\frac{2r^2}{w^2}}, \tag{7}$$

with

$$C\left(r^2\right)dr^2 = \int_0^{2\pi} \rho(r',\phi')rdrd\phi'. \tag{8}$$

With this definition, $C(r)$ describes the effective concentration of fluorophores in a concentric ring of radius r around the pixel position. The distribution of exponential decay components is fully described in this model by the parameters γ_0 and k_S in Eq. (2). Notably, the value of k_S quantifies the relative variation of decay rate values within the PSF of the CW-STED microscope [24] (Fig. 2b). The parameter $k_S = I_{STED}(w)/I_{SAT}$ is proportional to the STED beam power and its precise value depends on the optical configuration (in particular, the shape of the excitation and STED beams) and on the properties of the sample and needs to be calibrated.

In order to find an approximate, explicit expression for the temporal decay of fluorescence emitted from the center of the detection volume, we split the integral into $n = 2$ parts:

$$F(x,y,t) = K\int_0^{r_1} C\left(r^2\right)dr^2 e^{-\gamma\left(r^2\right)t} e^{-\frac{2r^2}{w^2}} + K\int_{r_1}^{\infty} C\left(r^2\right)dr^2 e^{-\gamma\left(r^2\right)t} e^{-\frac{2r^2}{w^2}}. \tag{9}$$

We then define the i^{th} decay component $I_i(t)$ as

$$I_{\text{i}} \approx \int_{r_{\text{i-1}}}^{r_{\text{i}}} dr^2 e^{-\gamma\left(r^2\right)t} e^{-\frac{2r^2}{w^2}} \tag{10}$$

for $i = 1, 2$ and $r_{\text{j}} = 0, r_1, \infty$ for $j = 0, 1, 2$ respectively.

Taking into account the distribution of decay rates $\gamma(r^2)$ expressed by Eq. (2), we find an explicit expression for $I_{\text{i}}(t)$:

$$\begin{aligned} I_i(t) &= \int_{r_{i-1}}^{r_i} dr^2 e^{-\gamma\left(r^2\right)t} e^{-\frac{2r^2}{w^2}} \\ &\propto e^{-\gamma_0 t}\frac{1}{1+k_s\gamma_0 t/2}\left(e^{-(1+k_s\gamma_0 t/2)2r_{i-1}^2/w^2} - e^{-(1+k_s\gamma_0 t/2)2r_i^2/w^2}\right) \end{aligned} \tag{11}$$

The distance r_1 that defines the two sub-diffraction volumes can be arbitrarily chosen in such a way that

$$\int_0^T I_1(t)dt = \int_0^T I_2(t)dt. \tag{12}$$

Finally, we can write the intensity $F(x,y,t)$ at each pixel as a linear combination of components:

$$F(x,y,t) \approx K\left[C_0^1(x,y)I_1(t) + C_0^2(x,y)I_2(t)\right] \tag{13}$$

The intensity decay at each pixel is expressed as the sum of a slow and a fast decay component, associated, respectively, with the fluorophores located on the inner and outer part of the PSF (Fig. 2f). Approximating $F(x,y,t)$ as a linear combination of the decay components $I_1(t)$ and $I_2(t)$ is equivalent to ignoring variations of $C(r^2)$ inside $({r_{i-1}}^2, {r_i}^2)$.

In order to quantify in a fast, fit-free mode, the relative contribution of the component $I_1(t)$ to the total intensity $F(x,y,t)$ collected at each pixel, we make use of phasor analysis. In the phasor analysis any decay $J(t)$ is converted via a fast Fourier transform (FFT) into a pair of phasor coordinates (g,s) defined as

$$\begin{aligned} g &= \int_0^T J(t)\cos(2\pi t/T)dt \Big/ \int_0^T J(t)dt \\ s &= \int_0^T J(t)\sin(2\pi t/T)dt \Big/ \int_0^T J(t)dt \end{aligned} \tag{14}$$

where T is the pulse interval. Here we assume that $T \gg \tau_0$, thus the function $J(t)$ has already decayed to background [28]. The slow and fast decays (Fig. 2f) can be described as phasors $\mathbf{P_1} = (g_1,s_1)$ and $\mathbf{P_2} = (g_2,s_2)$ in a polar plot.

We assume that the intensity at one pixel is the sum of two components plus a term representing any uncorrelated background $F(x,y,t) = A_1(x,y)I_1(t) + A_2(x,y)I_2(t) + I_{BKGD}(x,y)$. Thus, the phasor of each pixel $\mathbf{P}(x,y) = (g_1(x,y),s_1(x,y))$ can be expressed as a linear combination of the phasors of the two components and the phasor of the background

$$\begin{aligned} g(x,y) &= \frac{\int_0^T \left[A_1(x,y)I_1(t) + A_2(x,y)I_2(t) + I_{BKGD}(x,y)\right]\cos(2\pi \mathrm{t}/\mathrm{T})d\mathrm{t}}{\int_0^T \left[A_1(x,y)I_1(t) + A_2(x,y)I_2(t) + I_{BKGD}(x,y)\right]d\mathrm{t}} \\ &= \frac{N_1(x,y)}{N(x,y)}g_1 + \frac{N_2(x,y)}{N(x,y)}g_2 \\ s(x,y) &= \frac{\int_0^T \left[A_1(x,y)I_1(t) + A_2(x,y)I_2(t) + I_{BKGD}(x,y)\right]sin(2\pi \mathrm{t}/\mathrm{T})d\mathrm{t}}{\int_0^T \left[A_1(x,y)I_1(t) + A_2(x,y)I_2(t) + I_{BKGD}(x,y)\right]d\mathrm{t}} \\ &= \frac{N_1(x,y)}{N(x,y)}s_1 + \frac{N_2(x,y)}{N(x,y)}s_2 \end{aligned} \tag{15}$$

where the total number of photons $N(x,y)$ detected at one pixel is the sum of the photons originating in the two spatial components plus the uncorrelated background $N(x,y) = N_1(x,y) + N_2(x,y) + N_{\mathrm{BKGD}}(x,y)$. The phasor of the uncorrelated background is $\mathbf{P_{BKGD}} = (0,0)$. Using vector notation we can rewrite: $\mathbf{P}(x,y) = [N_1(x,y)\,\mathbf{P}_1 + N_2(x,y)\mathbf{P}_2]/N(x,y) = f_1(x,y)\mathbf{P}_1 + f_2(x,y)\mathbf{P}_2$. This linear system of equations can be written in the form $\mathbf{P} = \mathbf{Mf}$, where $\mathbf{f} = (f_1, f_2)$ is the vector of the unknown fractional components and M_{ij} is the matrix

$$\mathbf{M} = \begin{pmatrix} g_1 & g_2 \\ s_1 & s_2 \end{pmatrix}, \tag{16}$$

which describes the two temporal decay components $I_1(t)$ and $I_2(t)$ in the phasor domain. The solution of this system is given by $\mathbf{f} = \mathbf{M}^{-1}\mathbf{P}$. The images $N_i(x,y)$ $(i = 1,2)$ of the photons emitted in each of the two sub-diffraction volumes and the image $N_{\mathrm{BKGD}}(x,y)$ of the background can be calculated as $N_{\mathrm{i}}(\mathrm{x,y}) = f_{\mathrm{i}}(x,y)N(x,y)$ and

$$N_{\mathrm{BKGD}}(x,y) = \left[1 - \sum_{i=1}^{n} f_i(x,y)\right] N(x,y). \tag{17}$$

respectively (Fig. 2f).

The super-resolved image $N_I(x,y)$ has been obtained by using a model for the STED-induced variations of fluorescence lifetime and the phasor analysis of lifetime data. The decay components $I_1(t)$ and $I_2(t)$ are calculated starting from the parameters γ_0 and k_{S} that describe the decay rate distribution. The parameter $\tau_0 = 1/\gamma_0$ depends on the specific fluorophore and can be measured from the sample. The parameter $k_{\mathrm{S}} = I_{\mathrm{STED}}(w)/I_{\mathrm{SAT}}$ is proportional to the STED beam power and its value depends on the optical configuration and on the properties of the sample. We have shown that, within the same theoretical framework, we can estimate the value of k_{S} from the very same image $F(x,y,t)$ by considering the average time-resolved decay $I(t)$ of all the pixels of an image [24]:

$$I(t) = Ae^{-\gamma_0 t}\frac{1}{1 + k_{\mathrm{s}}\gamma_0 t/2} + B \tag{18}$$

This formula is an approximation of the average STED decay, and can be obtained from Eq. (7) or Eq. (13) when equal contributions are taken into account from center and periphery. The non-exponential behavior is due to the continuous distribution of decay rates induced by the STED beam.

4 Discussion and Conclusion

Modern microscopy has access to many new dimensions, which up to few years ago were discarded due to the averaging during the registration. For example, in many scanning microscopy implementation the fluorescence signal registered from the

observation volume can be quantified not only in terms of intensity, but it also possible to measure its spectral, polarization and temporal signature. It is worth to remember that, if we are able today to connect these parameters to the photophysics and dynamics of the fluorescent molecules, we owe it to the pioneering investigations of outstanding fluorescence spectroscopists like Gregorio Weber (1916–1997). The characterization of fundamental fluorescence properties [44–46] as well as the development of new methods and probes [30, 47] has had a profound impact on the use of fluorescence spectroscopy in biochemical applications. The capability of observing these spectroscopic properties at each pixel of an image has recently opened fascinating perspectives for study of molecular processes in cells.

It is clear that all these new dimensions in microscopy carry some important information. In this chapter we have focused only on the temporal dimension and its role in super-resolution STED microscopy. We have shown that in almost any STED microscopy implementation the ability to measure the pico- nano-second temporal dynamics of the fluorescence signal, more in particular the ability to know for each fluorescence photons its delay from the fluorophore excitation event (photon-arrival time), substantially helps (1) in reducing the illumination dose of light requested to obtain a certain spatial resolution; (2) in saving complexity of the system architecture, and (3) in reducing costs.

In particular, in the case of CW-STED, the fluorescence dynamics detected at each pixel can be modeled as the heterogeneous combination of species characterized by a fluorescence lifetime that depends on the position of the fluorophores within the observation volume. In this case the lifetime heterogeneity is not the result of variations in the local environment of the probe but the result of the differences in STED intensity induced by a doughnut-shaped STED beam. In the SPLIT-STED approach we have shown that resolving this heterogeneity at each pixel, by analyzing the phase and modulation of the temporal decay, leads to a significant improvement of spatial resolution of the STED microscope. This example demonstrates that concepts developed in fluorescence spectroscopy for measurement and analysis of fluorescence lifetimes [30, 48] can find today applications in other fields and, for instance, push technical advances in optical microscopy. Now, while the manipulation of fluorescence lifetime to improve the spatial resolution of a microscope is a strategy that offers some technical advantages (e.g. reduction of the illumination intensity), one should keep in mind that one of the unique properties of fluorescence lifetime is that it can be a very sensitive indicator of the environment of a probe [47]. In this respect we believe that, in the near future, it will be of interest to join the advantages of fluorescence sensitivity to the environment and optical super-resolution to explore the biological environment at the nanoscale.

References

1. Cella Zanacchi F, Bianchini P, Vicidomini G (2014) Fluorescence microscopy in the spotlight. Microsc Res Tech 77(7):479–482
2. Diaspro A (ed) (2009) Nanoscopy and multidimensional optical fluorescence microscopy. Chapman & Hall, Boca Raton

3. Hell SW (2003) Toward fluorescence nanoscopy. Nat Biotechnol 21(11):1347–1355
4. Hell SW (2009) Microscopy and its focal switch. Nat Methods 6(1):24–32
5. Hell SW, Sahl SJ, Bates M, Zhuang X, Heintzmann R, Booth MJ, Bewersdorf J, Shtengel G, Hess H, Tinnefeld P, Honigmann A, Jakobs S, Testa I, Cognet L, Lounis B, Ewers H, Davis SJ, Eggeling C, Klenerman D, Willig KI, Vicidomini G, Castello M, Diaspro A, Cordes T (2015) The 2015 super-resolution microscopy roadmap. J Phys D Appl Phys 48(44):443001
6. Huang B, Babcock H, Zhuang X (2010) Breaking the diffraction barrier: super-resolution imaging of cells. Cell 143(7):1047–1058
7. Betzig E, Patterson GH, Sougrat R, Lindwasser OW, Olenych S, Bonifacino JS, Davidson MW, Lippincott-Schwartz J, Hess HF (2006) Imaging intracellular fluorescent proteins at nanometer resolution. Science 313(5793):1642–1645
8. Dertinger T, Colyer R, Iyer G, Weiss S, Enderlein J (2009) Fast, background-free, 3D super-resolution optical fluctuation imaging (SOFI). Proc Natl Acad Sci U S A 106(52): 22287–22292
9. Gustafsson MG (2005) Nonlinear structured-illumination microscopy: wide-field fluorescence imaging with theoretically unlimited resolution. Proc Natl Acad Sci U S A 102(37): 13081–13086
10. Hell SW, Wichmann J (1994) Breaking the diffraction resolution limit by stimulated emission: stimulated-emission-depletion fluorescence microscopy. Opt Lett 19(11):780–782
11. Hess ST, Girirajan TP, Mason MD (2006) Ultra-high resolution imaging by fluorescence photoactivation localization microscopy. Biophys J 91(11):4258–4272
12. Hofmann M, Eggeling C, Jakobs S, Hell SW (2005) Breaking the diffraction barrier in fluorescence microscopy at low light intensities by using reversibly photoswitchable proteins. Proc Natl Acad Sci U S A 102(49):17565–17569
13. Rust MJ, Bates M, Zhuang X (2006) Sub-diffraction-limit imaging by stochastic optical reconstruction microscopy (STORM). Nat Methods 3(10):793–795
14. Hell SW (2007) Far-field optical nanoscopy. Science 316(5828):1153–1158
15. Kastrup L, Hell SW (2004) Absolute optical cross section of individual fluorescent molecules. Angew Chem Int Ed Engl 43(48):6646–6649
16. Galiani S, Harke B, Vicidomini G, Lignani G, Benfenati F, Diaspro A, Bianchini P (2012) Strategies to maximize the performance of a STED microscope. Opt Express 20(7):7362–7374
17. Vicidomini G, Schonle A, Ta H, Han KY, Moneron G, Eggeling C, Hell SW (2013) STED nanoscopy with time-gated detection: theoretical and experimental aspects. PLoS One 8(1), e54421
18. Bianchini P, Harke B, Galiani S, Vicidomini G, Diaspro A (2012) Single-wavelength two-photon excitation-stimulated emission depletion (SW2PE-STED) superresolution imaging. Proc Natl Acad Sci U S A 109(17):6390–6393
19. Moffitt JR, Osseforth C, Michaelis J (2011) Time-gating improves the spatial resolution of STED microscopy. Opt Express 19(5):4242–4254
20. Vicidomini G, Moneron G, Han KY, Westphal V, Ta H, Reuss M, Engelhardt J, Eggeling C, Hell SW (2011) Sharper low-power STED nanoscopy by time gating. Nat Methods 8(7): 571–573
21. Coto Hernàndez I, d'Amora M, Diaspro A, Vicidomini G (2014) Influence of laser intensity noise on gated CW-STED microscopy. Laser Phys Lett 11(9):095603
22. Vicidomini G, Coto Hernàndez I, Diaspro A, Galiani S, Eggeling C (2015) The importance of photon arrival times in STED microscopy. In: Kapusta P, Wahl M, Erdmann R (eds) Advanced photon counting, vol 15. Springer, Berlin/Heidelberg, pp 283–301
23. Vicidomini G, Hernandez IC, d'Amora M, Zanacchi FC, Bianchini P, Diaspro A (2014) Gated CW-STED microscopy: a versatile tool for biological nanometer scale investigation. Methods 66(2):124–130
24. Lanzano L, Coto Hernandez I, Castello M, Gratton E, Diaspro A, Vicidomini G (2015) Encoding and decoding spatio-temporal information for super-resolution microscopy. Nat Commun 6:6701

25. Coto Hernàndez I, Buttafava M, Boso G, Diaspro A, Tosi A, Vicidomini G (2015) Gated STED microscopy with time-gated single-photon avalanche diode. Biomed Opt Express 6(6): 2258–2267
26. Wu X, Toro L, Stefani E, Wu Y (2015) Ultrafast photon counting applied to resonant scanning STED microscopy. J Microsc 257(1):31–38
27. Clayton AH, Hanley QS, Verveer PJ (2004) Graphical representation and multicomponent analysis of single-frequency fluorescence lifetime imaging microscopy data. J Microsc 213 (Pt 1):1–5
28. Digman MA, Caiolfa VR, Zamai M, Gratton E (2008) The phasor approach to fluorescence lifetime imaging analysis. Biophys J 94(2):L14–L16
29. Redford GI, Clegg RM (2005) Polar plot representation for frequency-domain analysis of fluorescence lifetimes. J Fluoresc 15(5):805–815
30. Weber G (1981) Resolution of the fluorescence lifetimes in a heterogeneous system by phase and modulation measurements. J Phys Chem 85(8):949–953
31. Barreiro O, Zamai M, Yanez-Mo M, Tejera E, Lopez-Romero P, Monk PN, Gratton E, Caiolfa VR, Sanchez-Madrid F (2008) Endothelial adhesion receptors are recruited to adherent leukocytes by inclusion in preformed tetraspanin nanoplatforms. J Cell Biol 183(3):527–542
32. Blaine J, Lanzano L, Giral H, Caldas Y, Levi M, Gratton E, Moldovan R, Lei T (2011) Dynamic imaging of the sodium phosphate cotransporters. Adv Chronic Kidney Dis 18(2): 145–150
33. Dobrinskikh E, Lanzano L, Rachelson J, Cranston D, Moldovan R, Lei T, Gratton E, Doctor RB (2013) Shank2 contributes to the apical retention and intracellular redistribution of NaPiIIa in OK cells. Am J Physiol Cell Physiol 304(6):C561–C573
34. Giral H, Lanzano L, Caldas Y, Blaine J, Verlander JW, Lei T, Gratton E, Levi M (2011) Role of PDZK1 protein in apical membrane expression of renal sodium-coupled phosphate transporters. J Biol Chem 286(17):15032–15042
35. Cutrale F, Salih A, Gratton E (2013) Spectral phasor approach for fingerprinting of photoactivatable fluorescent proteins Dronpa, Kaede and KikGR. Methods Appl Fluoresc 1(3): 35001
36. Fereidouni F, Bader AN, Colonna A, Gerritsen HC (2014) Phasor analysis of multiphoton spectral images distinguishes autofluorescence components of in vivo human skin. J Biophotonics 7(8):589–596
37. Ranjit S, Lanzano L, Gratton E (2014) Mapping diffusion in a living cell via the phasor approach. Biophys J 107(12):2775–2785
38. Castello M, Diaspro A, Vicidomini G (2014) Multi-images deconvolution improves signal-to-noise ratio on gated stimulated emission depletion microscopy. Appl Phys Lett 105 (23):234106
39. Coto Hernández I, Castello M, Lanzanò L, d'Amora M, Bianchini P, Diaspro A, Vicidomini G (2016) Two-photon excitation STED microscopy with time-gated detection. Sci Rep 6:19419
40. Enderlein J (2005) Breaking the diffraction limit with dynamic saturation optical microscopy. Appl Phys Lett 87(9):095105
41. Humpolickova J, Benda A, Machan R, Enderlein J, Hof M (2010) Dynamic saturation optical microscopy: employing dark-state formation kinetics for resolution enhancement. Phys Chem Chem Phys 12(39):12457–12465
42. Marsh RJ, Culley S, Bain AJ (2014) Low power super resolution fluorescence microscopy by lifetime modification and image reconstruction. Opt Express 22(10):12327–12338
43. Yao J, Shcherbakova DM, Li C, Krumholz A, Lorca RA, Reinl E, England SK, Verkhusha VV, Wang LV (2014) Reversibly switchable fluorescence microscopy with enhanced resolution and image contrast. J Biomed Opt 19(8):086018
44. Lakowicz JR, Weber G (1973) Quenching of fluorescence by oxygen. A probe for structural fluctuations in macromolecules. Biochemistry 12(21):4161–4170
45. Teale FW, Weber G (1957) Ultraviolet fluorescence of the aromatic amino acids. Biochem J 65(3):476–482

46. Weber G (1952) Polarization of the fluorescence of macromolecules. I. Theory and experimental method. Biochem J 51(2):145–155
47. Weber G, Farris FJ (1979) Synthesis and spectral properties of a hydrophobic fluorescent probe: 6-propionyl-2-(dimethylamino)naphthalene. Biochemistry 18(14):3075–3078
48. Gratton E, Jameson DM, Hall RD (1984) Multifrequency phase and modulation fluorometry. Annu Rev Biophys Bioeng 13(1):105–124
49. Giral H, Cranston D, Lanzano L, Caldas Y, Sutherland E, Rachelson J, Dobrinskikh E, Weinman EJ, Doctor RB, Gratton E, Levi M (2012) NHE3 regulatory factor 1 (NHERF1) modulates intestinal sodium-dependent phosphate transporter (NaPi-2b) expression in apical microvilli. J Biol Chem 287(42):35047–35056

Plasma Membrane DC-SIGN Clusters and Their Lateral Transport: Role in the Cellular Entry of Dengue Virus

Ken Jacobson, Laurie Betts, Ping Liu, Marc Ridilla, Aravinda de Silva, and Nancy L. Thompson

One of us (KJ) was profoundly influenced by his interactions with Professor Gregorio Weber who is rightfully the father of fluorescence in biochemistry and molecular and cell biology. Gregorio served as the outside reader on KJ's Ph.D. thesis that described the fluorescence polarization of perylene in lipid bilayer vesicles as a measure of membrane fluidity. KJ and his young family subsequently traveled to Urbana-Champaign in the summer of 1972 where he worked in the Weber laboratory at the University of Illinois interacting with the Professor and a number of people in the lab at that time, including two graduate students, Dave Jameson and Joe Lakowicz, and two postdoctoral fellows, Dick Spencer and George Mitchell. The summer in Urbana was also productive in that phase fluorimetry was used to measure the rotation of lysozyme bound to acidic phospholipid vesicles for the first time. For KJ and his family, it was a delightful experience, the benefits of which carry forward to today.

K. Jacobson (✉)
Department of Cell Biology and Physiology, University of North Carolina at Chapel Hill, Chapel Hill, NC, USA

Lineberger Comprehensive Cancer Center, University of North Carolina at Chapel Hill, Chapel Hill, NC, USA
e-mail: frap@med.unc.edu

L. Betts and P. Liu
Department of Cell Biology and Physiology, University of North Carolina at Chapel Hill, Chapel Hill, NC, USA

M. Ridilla
Department of Cell Biology and Physiology, University of North Carolina at Chapel Hill, Chapel Hill, NC, USA

Present address: Brandeis University Materials Research Science and Engineering Center, Abelson 239, MS 057, 415 South Street, Waltham, MA 02453, USA

A. de Silva
Department of Microbiology and Immunology, University of North Carolina at Chapel Hill, Chapel Hill, NC, USA

N.L. Thompson
Department of Chemistry, University of North Carolina at Chapel Hill, Chapel Hill, NC, USA

D.M. Jameson (ed.), *Perspectives on Fluorescence: A Tribute to Gregorio Weber*,
Springer Ser Fluoresc (2016) 17: 331–342, DOI 10.1007/4243_2016_2,

Abstract DC-SIGN (a single-pass transmembrane protein and C-type lectin) is a major receptor for a variety of pathogens on human dendritic cells including dengue virus (DENV), which has become a global health threat. DENV binds to cell-surface DC-SIGN and the virus/receptor complexes migrate to clathrin-coated pits where the complexes are endocytosed; during subsequent processing, the viral genome is released for replication. DC-SIGN exists on cellular plasma membranes in nanoclusters that may themselves be clustered on longer length scales that appear as microdomains in wide-field and confocal fluorescence microscopy. We have investigated the dynamic structure of these clusters using fluorescence and super-resolution imaging in addition to large-scale single particle tracking. While clusters themselves can be laterally mobile there appears to be little mobility of DC-SIGN within clusters or exchange of DC-SIGN between the clusters and the surroundings. We end this account with some outstanding issues that remain to be addressed with respect to the composition and architecture of DC-SIGN domains and some highly unusual aspects of their lateral mobility on the cell surface that may accompany and perhaps facilitate DENV infection.

Keywords DC-SIGN • Dengue virus • Lateral mobility • Membrane nanodomains • Super-resolution microscopy • TIRF microscopy

Contents

1 Introduction

Immature dendritic cells (DC) express many antigen-capture receptors and these include those of the C-type lectin family. These receptors enable DCs to bind and internalize antigen efficiently [1, 2]. One such pathogen is the mosquito-borne dengue virus (DENV), which has been recognized as a global health threat because nearly ½ billion people may be infected per year. One fifth of these develop systemic infection and out of those, 500,000 experience life-threatening symptoms

[3, 4]. DENV is a small (~50 nm) flavivirus that is bounded by a lipid membrane packed with envelope glycoproteins, termed E-proteins.

A major receptor for DENV on DCs is the C-type lectin DC-SIGN (dendritic cell-specific intercellular adhesion molecule-3-grabbing non-integrin) [5, 6]. DC-SIGN is termed a pattern-recognition receptor for microbial surfaces [7] because it recognizes glycosylation patterns, specifically mannose or fucose containing structures, expressed by glycosylated components on the surfaces of numerous virions, bacteria, yeast, and parasite species. The binding of pathogens to DC-SIGN triggers diverse immune responses [8].

DC-SIGN is a single pass, 44 kDa (without glycosylation), type II transmembrane protein. Its extracellular region contains the carbohydrate recognition domain (CRD) which is connected to the transmembrane domain by a region containing up to seven and a half repeats of a 23 amino acid helical domain. The short cytoplasmic domain contains three internalization motifs. Tetramerization of DC-SIGN, facilitated by the tandem repeats in the extracellular region, greatly enhances DC-SIGN's binding affinity to high mannose carbohydrates when compared to that of monomeric CRDs [9]. Indeed, DC-SIGN forms multimers as shown by biochemical and biophysical assays [9–11]. The structural features of DC-SIGN and a conceptualization of its binding to multivalent, pathogenic ligands are shown in Fig. 1.

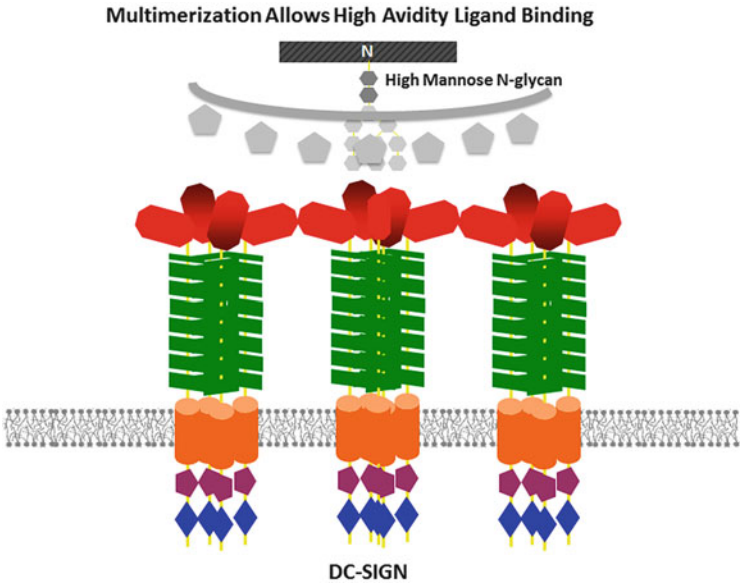

Fig. 1 Conceptualization of DC-SIGN interaction with pathogens that express mannose residues on their surface. Individual DC-SIGN proteins are depicted as clustered in tetramers in which the C-terminal portions of the ectodomains (*red*) contain the carbohydrate recognition domains (CRD) that are connected to the "neck" repeat sections (*green*). The transmembrane domains are colored *orange* and the short cytoplasmic domains containing the internalization motifs are colored in *mauve* and *blue*

Once DENV binds to cell-surface DC-SIGN clusters, the virus/receptor complexes migrate to clathrin-coated pits where the complexes are endocytosed [12]. Processing through the endosomal pathway leads to a low pH – induced fusion of the viral and endosomal membranes. This fusion event releases the viral genome into the cytoplasm for subsequent translation and replication.

DC-SIGN clusters exhibit a number of quite unusual properties in both their structure and mobility in the plasma membrane and this is the main subject of this review. These properties leave open a number of outstanding questions that are enumerated at the end.

2 Structure of DC-SIGN Clusters

Previous studies have shown that DC-SIGN on the surface of fixed DCs is organized in clusters on the nanometer scale; these studies employed transmission electron microscopy and near-field scanning optical microscopy [13, 14]. Clustering of DC-SIGN could improve binding to viral particles or bacteria by providing high-avidity platforms for these multivalent entities. Heterogeneity in the cluster size or nanoarchitecture could provide a variety of structurally different binding platforms tuned for recognizing different pathogen types.

2.1 Clusters Imaged at Light Microscope Resolution

DC-SIGN clusters imaged in wide-field or confocal microscopy show a variety of sizes ranging from the diffraction limit to over a micron in dimension (Fig. 2, left panel). Interestingly, similar sizes are seen when DC-SIGN is endogenously expressed in DCs or when it is expressed in a permanently transfected NIH 3 T3 cell line (termed MX DC-SIGN) (Fig. 2, right panel) [15].

We measured, employing total internal reflection fluorescence microscopy (TIRFM), the copy number occupancy of DC-SIGN domains [16]. Our approach was based on comparing the intensities of fluorescently labeled microdomains, in which DC-SIGN was labeled with primary monoclonal antibodies (mAbs) or expressed as GFP fusions in NIH 3 T3 cells, with those of single antibodies. In microdomains that range in dimension from the diffraction limit (slightly greater than 200 nm) to over 1 μm, the number of DC-SIGN molecules ranges from only a few to over 20 in both DCs and NIH 3 T3 cells. However, microdomains that appear at the diffraction limit typically contain only 4–8 molecules of DC-SIGN in either immature DCs or NIH 3 T3 cells. In fact, these small domains are capable of binding DENV leading to infection of host cells [12]).

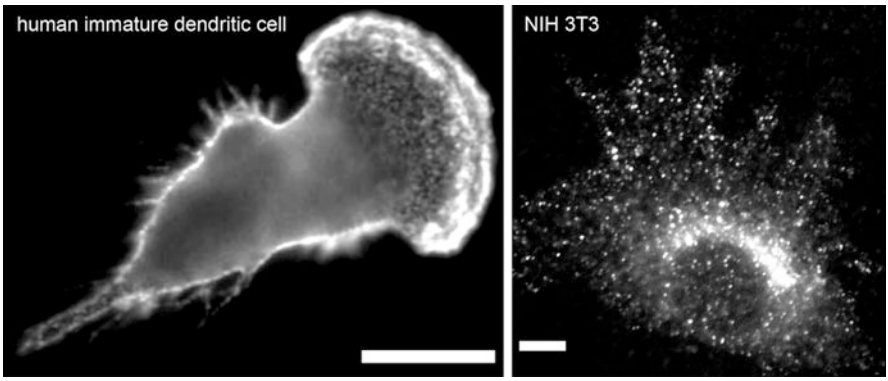

Fig. 2 DC-SIGN spontaneously forms microdomains when endogenously expressed in the plasma membranes of DCs (*left*) or permanently expressed in the plasma membranes of MX DC-SIGN cells (*right*). Indirect immunofluorescence on fixed cells. Bars = 10 μm. Reproduced by permission of the Company of Biologists

2.2 Clusters Imaged with Super-Resolution Microscopy

Larger DC-SIGN microdomains are remarkably stable [17], but the fact that inner leaflet lipid markers can diffuse through them (see below) suggests that they have an internal substructure rather than being densely packed with this C-type lectin (CTL). We therefore investigated the lateral distribution of DC-SIGN within microdomains by using a super-resolution imaging technique, Blink microscopy. Blink uses reducing/oxidizing buffers and a tuned excitation intensity to adjust the fluctuating emission of fluorophores on antibodies [18] so that only a few emit during a given image frame within the total movie acquisition time; thus, observed fluorophores are well separated in space (for single frames) so that their locations can be more precisely determined and a full map of fluorophore positions can be constructed from the movie. Blink is one type of molecular localization super-resolution microscopy.

Blink images of DC-SIGN in fixed DCs revealed a frequent presence of *several small nanodomains*, about 75 nm wide, which appeared as *single microdomains* by TIRFM (Fig. 3). Another CTL, CD206, and influenza hemagglutinin (HA) are similarly clustered in small (~80 nm diameter) nanodomains on the plasma membrane. Spatial analysis of nanodomain centroids from Blink images indicated that DC-SIGN and CD206 nanodomains are localized randomly on the plasma membrane, and two-color Blink imaging showed that these CTLs were largely restricted to separate nanodomains, despite their apparent co-localization by wide-field microscopy. By contrast, HA nanodomains are not randomly distributed, and clustered on length scales up to 1 μm.

We estimated that DC-SIGN nanodomains contain between one and three tetramers, as a lower limit, by comparing the number of Blink localizations from nanodomains and single antibodies (Fabs). Given the measured average

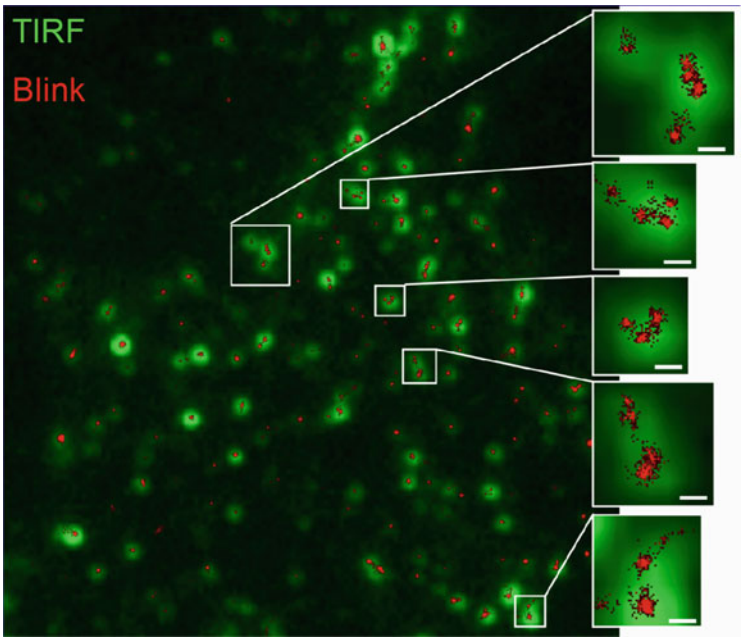

Fig. 3 Blink spatial localization super-resolution microscopy images of DC-SIGN expressing MX DC-SIGN cells. *Green* represents the TIRFM image while *red* represents the Blink image showing the centroids of DC-SIGN molecular localizations. *Insets* show magnifications of specific areas on the large image and show that more than one nanocluster is often contained within a microdomain as visualized in TIRFM images. (Bars = 100 nm)

nanodomain size and the known DC-SIGN size, the estimated DC-SIGN copy number occupancies strongly suggest that other proteins and lipids are present in nanodomains (see Figure 7 in [18], and below). Thus, the nanodomains themselves most likely possess an intricate underlying architecture.

2.3 Additional Structural Considerations

We undertook a mutational approach to investigate which domains/motifs of DC-SIGN might be responsible for clustering and how the microdomains form and remain stable [19]. Four mutants, expressed in NIH 3 T3 cells and either unlabeled or as GFP fusions, were generated for use with confocal imaging and fluorescence recovery after photobleaching (FRAP) studies to assess the existence, size, and stability of resultant microdomains. Deletion of the cytoplasmic portion had little effect on microdomain formation or stability, implying that DC-SIGN clustering is not mediated by a direct interaction with cytoskeletal structures. A point mutation preventing potential N-linked glycosylation at Asn80 also failed to reduce microdomain stability, thereby ruling out any significant contribution from

galectin–glycoprotein crosslinking in microdomain formation. By contrast, deletion of the seven and a half tandem repeats, which are thought to mediate tetramerization by forming coiled-coil α-helices, resulted in enhanced membrane diffusion and nearly complete recovery in FRAP measurements. A more profound effect – the complete loss of observable microdomains on the cell surface – was observed following removal of the CRD; the deletion mutants instead showed a diffuse and homogeneous distribution within the membrane and nearly full lateral mobility. This result suggests that the CRD might interact directly with components of the extracellular matrix or with transmembrane adaptor proteins to indirectly link to the cytoskeleton. A plausible possibility is that pathogens may compete with these putative stabilizing interactions to facilitate their attachment to DCs and more rapid movement to sites of internalization.

3 Lateral Mobility of Clusters and DC-SIGN Molecules Within Clusters

We initially found that most bright DC-SIGN clusters on DCs and NIH 3 T3 cells are apparently immobile when examined for relatively short times [15]. Moreover, FRAP measurements on these clusters revealed that little or no recovery occurred after many seconds, indicating that exchange of DC-SIGN molecules between the clusters and the surrounding membrane was minimal (Fig. 4, left panel). By contrast, recovery of a lipid probe, PM tracker, on the inner leaflet was substantial suggesting that at least some lipids could move through the DC-SIGN clusters as imaged at light microscope resolution (Fig. 4, right panel). Lateral mobility and partial or complete loss of DC-SIGN microdomains could be effected by certain mutations as described above.

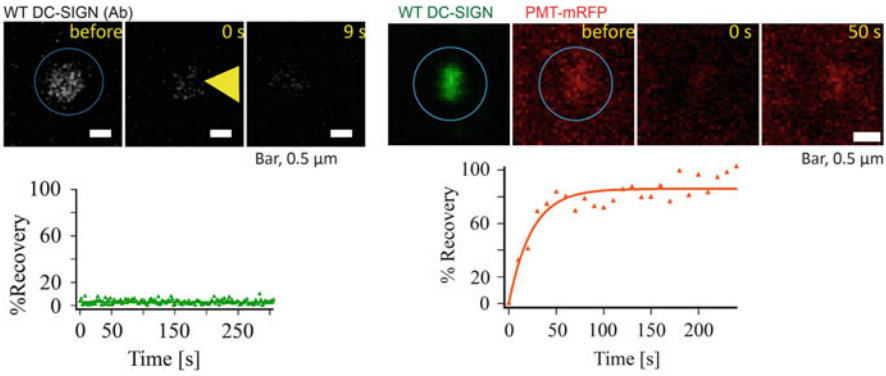

Fig. 4 Different exchange mobilities of DC-SIGN and an inner leaflet plasma membrane probe (PMT-mRFP) in the plasma membranes of MX DC-SIGN cells. *Top panels*: confocal images of the initial area followed by bleaching and recovery (times in seconds). *Bottom panels*: FRAP curves for DC-SIGN (*left panel*) and plasma membrane tracker – mRFP (*right panel*)

We investigated DC-SIGN and HA lateral mobility within membrane domains using both line scan fluorescence correlation spectroscopy and single particle tracking with defined-valency quantum dots [17]. Both techniques indicated essentially undetectable lateral mobility for DC-SIGN within microdomains. By contrast, HA retained appreciable lateral mobility within its domains on the cell surface.

More recently, we have employed u-track to investigate the mobility of both native and DENV-bound DC-SIGN clusters. U-track is a single particle tracking software package [20] that enables large numbers of clusters to be tracked simultaneously from live cell TIRFM videos. Using a moment scaling spectrum approach, particle trajectories can be divided into sub-diffusive, diffusive, and super-diffusive (likely directed) motion categories [20]. These data and their analysis have revealed some remarkable results. First, we found that many DC-SIGN clusters are laterally mobile in agreement with previous studies [21]. We believe that our earlier failure to find such mobility most probably resulted from a previous focus on brighter clusters and shorter time scales. Second, DENV binding, even only to a few DC-SIGN clusters, induces a *global* cellular response in which both DENV-loaded and DENV-unloaded DC-SIGN clusters exhibit dramatically increased lateral mobility; this is probably the result of cytoskeletal rearrangement proximate to the plasma membrane and has the possible consequence of enhancing DENV-loaded DC-SIGN cluster encounters with clathrin-coated pits [22]. Also, a small but significant fraction of DC-SIGN clusters *in the plasma membrane* undergo rapid, microtubule-based directed transport towards the cell center and the velocities are increased after dengue binding [22]. This activity may be required to bring captured pathogens from the leading margins of DCs back to the perinuclear zone for subsequent internalization and processing.

4 Outstanding Questions

Given that nanoclustering of membrane proteins appears to be a pervasive motif [23], our results for DC-SIGN raise four important questions not only for DENV virology but also for membrane biology in general.

4.1 Question 1: What Is the Architecture and Composition of DC-SIGN Clusters?

An initial statistical analysis of DC-SIGN nanodomain locations found no long-range order; i.e., no evidence against a random spatial arrangement in the membrane plane [18]. On the other hand, distinct microdomains having a large range of sizes appear at the level of light microscope resolution [15]. This range in sizes of

DC-SIGN clusters begs the question of whether a) the density of nanoclusters is in the range where individual nanoclusters convolute with the microscope point spread function to produce an apparent size distribution with a larger average size or b) there is a hierarchical, local, and "invisible" ordering of DC-SIGN nanoclusters such that they can arrange in structures that appear distinct in wide-field or confocal images. If such long-range order exists, what is the mechanism for coordinating these structures?

Proteomics (and lipidomics) will be invaluable in sorting out the molecular constituents that give rise to DC-SIGN clustering on several different length scales and whether these components of clusters are involved in pathogen recognition and/or internalization. Thus, for example, we have shown that annexin VI associates with DC-SIGN by proteomic and immunoprecipitation analysis, but knockdown of annexin VI does not affect DENV infection of DC-SIGN expressing human lymphoid cells [24]. Nevertheless, this study is a paradigm for investigating what proteins associate with DC-SIGN and how these proteins affect DC-SIGN cluster structure and pathogen recognition properties required for mediating DENV infection.

4.2 Question 2: What Is the Relationship Between DC-SIGN Cluster Size and Pathogen Processing?

DC-SIGN mediates the binding and internalization of pathogens ranging in size from small viruses like DENV to yeast. What are the structures of DC-SIGN cluster/pathogen complexes and possible structural rearrangements of the complex components during initial recognition; after binding but before internalization; during internalization; or after internalization and during intracellular pathogen processing? Forexample, we have shown by super-resolution microscopy (dSTORM) that single DENV particles can co-localize with apparent single DC-SIGN tetramers [16]. Whether or not these minimal DENV/cluster complexes can proceed to facilitate productive cellular infection is at present unknown. In another example, we have shown that DC-SIGN nanoclusters accumulate in the region of contact between DCs and yeast zymosan as a consequence of pathogen recognition [25].

Associated with this broad question is the issue of whether DC-SIGN is a complete pathogen receptor leading both to attachment and entry into host cells or whether a co-receptor(s) is involved. For DENV, the possible existence of a co-receptor is the subject of an active and ongoing controversy. Co-localization microscopy showed that both full-length DC-SIGN and DC-SIGN without its cytoplasmic tail (containing the internalization motifs) are internalized along with dengue [12]. Although the absence of the DC-SIGN cytoplasmic region reduced both dengue binding and endocytosis, cell infection was not abrogated but only reduced. Thus, DC-SIGN appears able to act in concert with a co-receptor

containing cell entry motifs. However, productive DENV entry may also occur adventitiously, employing constitutive endocytosis mechanisms all of which meet in the early endosome. It is likely that proteomic analysis (see above) will give important leads in the search for putative co-receptors that DENV may require (or sometimes employ) for cellular entry via DC-SIGN.

4.3 *Question 3: How and Why Does Global Activation of DC-SIGN Cluster Mobility Occur as Triggered by DENV?*

What is the mechanism of global activation of DC-SIGN diffusion? The enhanced mobility might in part be a consequence of pathogen-mediated release from stabilizing interactions of the CRD with pericellular matrix components, as suggested above [19]. The global character of the phenomenon suggests that transmembrane signal transduction might affect the subjacent membrane skeleton fence, a presumed regulator of lateral diffusion. Changes in lipid composition or organization are also possible, although the effect is large enough (fourfold) to suggest that membrane core modification would not alone be an adequate explanation. Is enhanced mobility after viral exposure exhibited by all membrane proteins or only a subset (e.g., solely DC-SIGN or only proteins that are clustered)? It is likely that answers to these questions will significantly advance our basic understanding of the structure and dynamics of the cortical cytoskeleton subjacent to the plasma membrane as well as interactions of plasma membrane components with the cytoskeletal and the pericellular matrix.

With respect to DENV virology, can global activation be triggered by DENV binding to its many other receptors or is it specific to binding to DC-SIGN, and what is the cell-type specificity? Does the mobility enhancement directly accelerate the DENV uptake mechanism in a biologically significant manner, or is the phenomenon primarily a reflection of another cellular event (e.g., cytoskeletal rearrangement) that occurs as an intrinsic part of the anti-viral response?

4.4 *Question 4: How Does Directed Transport of DC-SIGN Clusters in the Plane of the Plasma Membrane Occur and What Is Its Role in DENV Entry and Infection?*

What role does superdiffusion (i.e., directed transport) of DC-SIGN clusters play in pathogen processing in DCs and what is the mechanism of such unusually rapid cell-surface transport? Will understanding this phenomenon alter our current view of membrane cytoskeletal interactions?

In all, the investigation of DC-SIGN and its relation to DENV entry has proved to be a fertile ground for those interested in the continuing mysteries of the plasma membrane and its associated structures.

Acknowledgements This work was supported by NIH grant GM40402 (K.J. & N.L.T.) and RO1-AI107731 (A.M.dS.).

References

1. Banchereau J, Steinman RM (1998) Dendritic cells and the control of immunity. Nature 392:245–252
2. Weiss JM et al (1998) CD44 variant isoforms are essential for the function of epidermal Langerhans cells and dendritic cells. Cell Adhes Commun 6:157–160
3. Bhatt S et al (2013) The global distribution and burden of dengue. Nature 496:504–507
4. Katzelnick LC et al (2015) Dengue viruses cluster antigenically but not as discrete serotypes. Science 349:1338–1343
5. Geijtenbeek TB et al (2000) DC-SIGN, a dendritic cell-specific HIV-1-binding protein that enhances trans-infection of T cells. Cell 100:587–597
6. Tassaneetrithep B et al (2003) DC-SIGN (CD209) mediates dengue virus infection of human dendritic cells. J Exp Med 197:823–829
7. Cambi A, Koopman M, Figdor CG (2005) How C-type lectins detect pathogens. Cell Microbiol 7:481–488
8. Guo Y et al (2004) Structural basis for distinct ligand-binding and targeting properties of the receptors DC-SIGN and DC-SIGNR. Nat Struct Mol Biol 11:591–598
9. Bernhard OK, Lai J, Wilkinson J, Sheil MM, Cunningham AL (2004) Proteomic analysis of DC-SIGN on dendritic cells detects tetramers required for ligand binding but no association with CD4. J Biol Chem 279:51828–51835
10. Feinberg H, Guo Y, Mitchell DA, Drickamer K, Weis WI (2005) Extended neck regions stabilize tetramers of the receptors DC-SIGN and DC-SIGNR. J Biol Chem 280:1327–35
11. Tabarani G et al (2009) DC-SIGN neck domain is a pH-sensor controlling oligomerization: SAXS and hydrodynamic studies of extracellular domain. J Biol Chem 284:21229–21240
12. Liu et al (2016) Beyond attachment: roles of DC-SIGN in dengue virus infection. Traffic (in revision)
13. Cambi A et al (2004) Microdomains of the C-type lectin DC-SIGN are portals for virus entry into dendritic cells. J Cell Biol 164:145–155
14. Koopman M et al (2004) Near-field scanning optical microscopy in liquid for high resolution single molecule detection on dendritic cells. FEBS Lett 573:6–10
15. Neumann AK, Thompson NL, Jacobson K (2008) Distribution and lateral mobility of DC-SIGN on immature dendritic cells–implications for pathogen uptake. J Cell Sci 121:634–643
16. Liu P et al (2014) Low copy numbers of DC-SIGN in cell membrane microdomains: implications for structure and function. Traffic 15:179–196
17. Itano MS et al (2011) DC-SIGN and influenza hemagglutinin dynamics in plasma membrane microdomains are markedly different. Biophys J 100:2662–2670
18. Itano MS et al (2012) Super-resolution imaging of C-type lectin and influenza hemagglutinin nanodomains on plasma membranes using blink microscopy. Biophys J 102:1534–1542
19. Liu P et al (2012) The formation and stability of DC-SIGN microdomains require its extracellular moiety. Traffic 13:715–726
20. Jaqaman K et al (2008) Robust single-particle tracking in live-cell time-lapse sequences. Nat Methods 5:695–702

21. Manzo C et al (2012) The neck region of the C-type lectin DC-SIGN regulates its surface spatiotemporal organization and virus-binding capacity on antigen-presenting cells. J Biol Chem 287:38946–38955
22. Liu P et al (2015) How dengue virus enters cells via the receptor DC-SIGN. Poster presented at the American Society for Cell Biology Meeting, San Diego
23. Garcia-Parajo MF, Cambi A, Torreno-Pina JA, Thompson N, Jacobson K (2014) Nanoclustering as a dominant feature of plasma membrane organization. J Cell Sci 127:4995–5005
24. Betts L et al (2015) A proteomics study of membrane microdomains of the dengue virus attachment factor DC-SIGN reveals novel binding partners. Poster presented at American Society for Cell Biology Annual Meeting, San Diego
25. Itano MS et al (2014) Super-resolution imaging of C-type lectin spatial rearrangement within the dendritic cell plasma membrane at fungal microbe contact sites. Front Phys 2:14

Index

D.M. Jameson (ed.), *Perspectives on Fluorescence: A Tribute to Gregorio Weber*,
Springer Ser Fluoresc (2016) 17: 343–346, DOI 10.1007/978-3-319-41328-0,